

ÉCOLE DOCTORALE ED 222 Sciences Chimiques
UMR 7042 LIMA CNRS – Université de Strasbourg

THÈSE présentée par :
Maxime DONZEL

soutenue le : 7 Juin 2021

pour obtenir le grade de : **Docteur de l'université de Strasbourg**

Discipline/ Spécialité : Chimie – Chimie Organique

**Nouvelles méthodologies de synthèse
de 3-benz(o)ylménadiones et propriétés
rédox à l'origine de leur(s) mode(s)
d'action antipaludique**

THÈSE dirigée par :

Dr. DAVIOUD-CHARVET Elisabeth Directeur de Recherche CNRS, Université de Strasbourg
Dr. ELHABIRI Mourad Directeur de Recherche CNRS, Université de Strasbourg

RAPPORTEURS :

Dr. MEDEBIELLE Maurice Directeur de Recherche CNRS, Université Claude Bernard Lyon 1
Dr. SIX Yvan Chargé de Recherche CNRS, Ecole Polytechnique

AUTRES MEMBRES DU JURY :

Pr. MORAN Joseph Professeur, Université de Strasbourg
Dr. PY Sandrine Directeur de Recherche CNRS, Université Grenoble Alpes

Remerciements

Tout d'abord je souhaiterais remercier les Dr. Maurice Médebielle, Dr. Yvan Six, Pr. Joseph Moran et Dr. Sandrine Py pour avoir accepté de faire partie du jury de cette thèse et de juger mon travail.

Ensuite, tout naturellement, je remercie les Dr. Elisabeth Davioud-Charvet et Dr. Mourad Elhabiri, respectivement directeure et co-directeur de cette thèse. Elisabeth, pour m'avoir fait confiance tout le long de cette thèse et m'avoir toujours laissé libre dans mes initiatives. Merci également pour ta patience et ta bienveillance, tes conseils, toutes les idées que tu as pu me donner (dont sans doute la plus importante !), toute l'aide que tu m'as apporté au jour le jour pendant ces 3 ans et demi et surtout ta gentillesse. Mourad, merci pour toute l'aide que tu m'as apporté, très particulièrement en physico-chimie et pour comprendre les mécanismes de nos réactions, mais aussi pour les discussions toujours stimulantes que ce soit en chimie ou sur un tout autre sujet, et surtout, merci pour le café frais tous les matins !

Je voudrais ensuite remercier tous les membres de notre équipe, actuels ou passé. En premier Mickael, on a sûrement plus parlé de foot que de chimie, quand on ne regardait pas Roland-Garros ou la Coupe du Monde dans le bureau, mais tu m'as été d'une grande aide pour attaquer au mieux cette thèse. Leandro avec qui j'ai travaillé pour publier un chouette papier. Nathan, tu es arrivé comme mon stagiaire pour finalement continuer en thèse et devenir mon collègue de bureau permanent et ce fut un plaisir ! Matthieu, tu n'es pas arrivé depuis longtemps et je t'ai plus vu avec un masque que sans, mais c'était quand même un plaisir et de toute façon je dois dire du bien de toi vu que tu prends la suite de mon travail. Sans oublier Angéline qui m'a beaucoup aidé à mon arrivé dans l'équipe, Vrushrali et Bogdan les deux biologistes de l'équipe, Mouss et enfin Valérie.

Egalement, je voudrais remercier tous les stagiaires que j'ai encadrés ou qui sont passés dans le labo : les petits stagiaires de l'ECPM, Zaïd, Alizée et Mylène. Félix qui a opté pour la même stratégie de changement de bureau que moi et surtout Deniz. Tu es tombé en plein COVID et tu ne seras resté qu'une semaine au labo, mais je te remercie pour la revue qu'on a écrit ensemble (et pour les bières aussi).

Je voudrais aussi remercier tous les membres du LIMA, plus particulièrement Nicolas Kern pour les discussions et l'aide quand je me suis lancé dans la photochimie, Sabine Choppin pour m'avoir confié les TP de chimie organique, une expérience formidable, ainsi que Emeric et Matthieu pour leur aide. Enfin, Didier, peut être la personne la plus importante de toute l'unité, merci de toute ton aide, toujours précieuse.

Merci à tous les copains de Strasbourg et du jeu des vaisseaux spatiaux, Alex, Ben, Rémi, Martin (l'autre thésard) et Guillaume pour les soirées bière/bouffe (surtout en temps de COVID). Les copains de Grenoble et d'Ardèche, Thibaut, Marianne, Mathilde, le coach, Nico et tous les collègues que j'oublie. Pour finir, les copains de la maison, Aney, Nico et Kévin que je n'ai clairement pas pu assez voir pendant ces 3 ans, j'espère bien me rattraper.

Enfin je voudrais remercier du fond du coeur ma famille, mon frère et mes parents, pour m'avoir toujours soutenu tout au long de cette thèse, et de mes études en général.

UNIVERSITE DE STRASBOURG

ECOLE DOCTORALE DES SCIENCES CHIMIQUES

RESUME DE LA THESE DE DOCTORAT

Discipline : Chimie

Spécialité : Chimie Organique

Présentée par : Maxime Donzel

Titre : Nouvelles méthodologies de synthèse de 3-benz(o)ylménadiones et propriétés rédox à l'origine de leur(s) mode(s) d'action antipaludique

Unité de Recherche : UMR 7042 CNRS – Unistra – UHA, Laboratoire d’Innovation Moléculaire et Applications

Directeur de Thèse : Davioud-Charvet Elisabeth, Directeur de Recherche CNRS

Co-Directeur de Thèse : Elhabiri Mourad, Directeur de Recherche CNRS

Localisation : Equipe de chimie Bio(in)organique et médicinale, LIMA UMR7042 CNRS-Unistra-UHA, European School of Chemistry, Polymers and Materials (ECPM), 25, rue Becquerel, F-67087 Strasbourg, France

Thèse confidentielle : NON OUI

Introduction

Le paludisme est une des maladies parasitaires les plus sévères qui affecte particulièrement les populations les plus pauvres de la planète. Les projets actuels de l'équipe sont centrés sur le développement de nouveaux médicaments rédox-actifs antiparasitaires ainsi que sur la compréhension de leur mécanisme d'action. En 2011, l'équipe a découvert une nouvelle série d'agents antiparasitaires, les 3-benzylménadiques, dont le composé tête de série, appelé plasmodione, possède une importante activité antipaludique *in vitro* mais aussi des effets *in vivo* (Figure 1A.).^{1,2} La plasmodione a fait l'objet de vastes études de recherche, en chimie organique et biologique, et en parasitologie. Son profil d'activité antiplasmoidal a été investigué dans de nombreux modèles cellulaires. Le mécanisme d'action proposé fait intervenir une cascade de réactions rédox complexe, générant des métabolites actifs sur différentes cibles protéiques essentielles du globule rouge parasité. La plasmodione agit comme une prodrogue : la 3-benzoylménadione générée à partir de la plasmodione est supposée être le métabolite-clé qui entre dans un cycle rédox fatal au parasite en détruisant l'homéostasie redox des érythrocytes parasités.^{3,4} D'autres métabolites ont été également proposés pour contribuer à l'activité antipaludique de la plasmodione selon d'autres modes d'action.

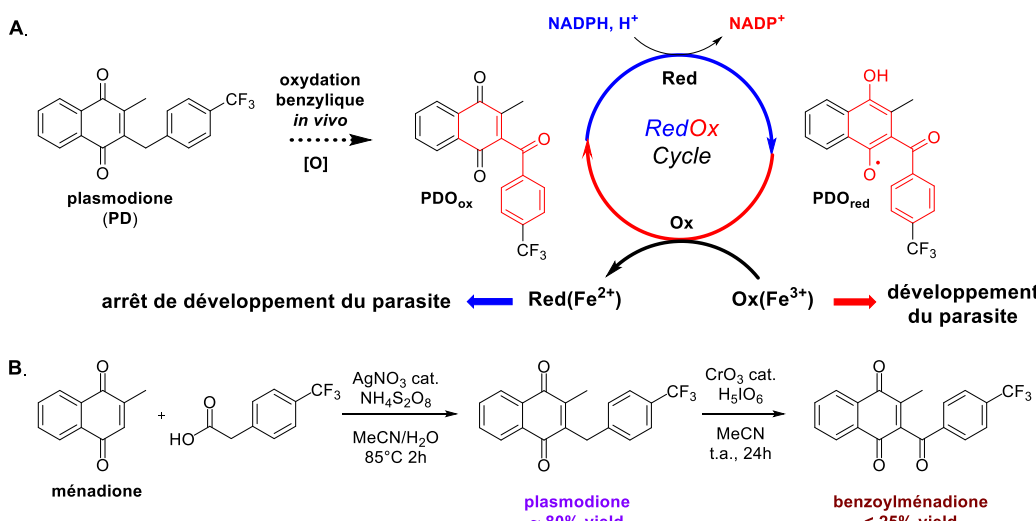


Figure 1. A. Mécanisme postulé de bioactivation de la plasmodione et B. Synthèse de la plasmodione et son métabolite actif 3-benzoylménadione.

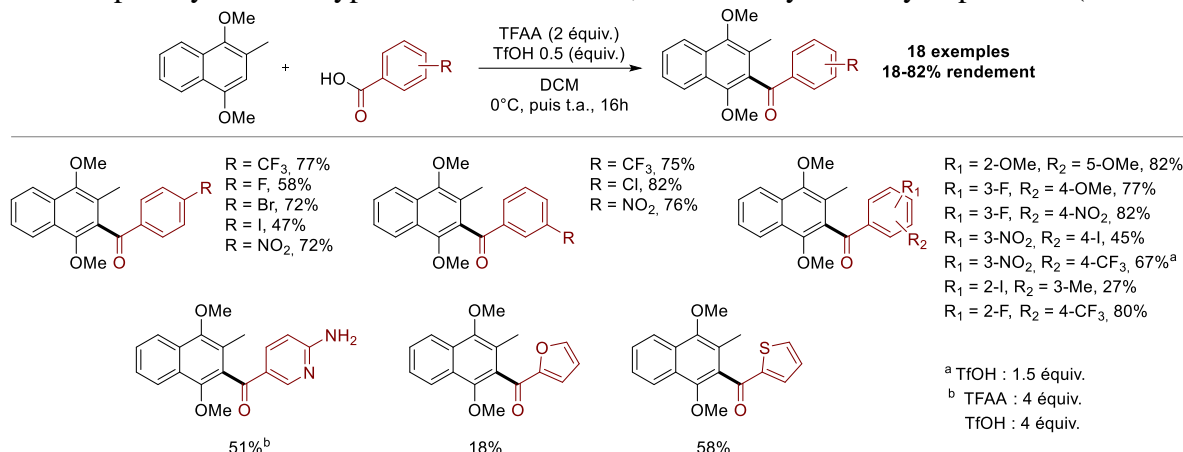
La synthèse de la plasmodione et de ses analogues, ainsi que des métabolites actifs de type 3-benzoylménadione, a été réalisée précédemment au sein du laboratoire. Celle-ci correspond à une benzylation radicalaire par décarboxylation d'acides phénylacétiques à l'aide de sels d'argent et de persulfate d'ammonium, puis à l'oxydation du carbone benzylique à l'aide de chrome(VI) et d'iode hypervalent (Figure 1B.). Bien qu'efficace, cette benzylation présentait cependant plusieurs limitations. Les acides phénylacétiques commerciaux ou faciles à synthétiser ont déjà été utilisés au sein de notre équipe et l'introduction de cycles hétéroaromatiques est très difficile voire impossible. Quant à l'oxydation benzylique, celle-ci a lieu avec de très faibles rendements et ne fonctionne pas pour tous les composés. Pour l'ensemble de ces raisons, il est apparu essentiel de mettre en place de nouvelles méthodologies de synthèse pour chacune de ces séries (benzylménadione et benzoylménadione), afin de pouvoir diversifier au mieux la substitution sur le fragment benzyle ou benzoyle de ces molécules.

Nous avons donc, au cours de ce travail de thèse, développé 3 voies de synthèse différentes pour obtenir des 3-benzoylménadiques, des 3-benzylménadiques et des analogues hétéroaromatiques de 3-benzylménadiques.

Résultats & discussion

Synthèse de nouvelles 3-benzoylménadiques polysubstituées

Nous avons tout d'abord étudié la possibilité de synthétiser des 3-benzoylménadiques diversement substituées par acylation de type Friedel-Crafts du 1,4-diméthoxy-2-méthynaphtalène (Schéma 1).



Une méthodologie de synthèse originale impliquant l'utilisation d'anhydride trifluoroacétique et d'acide triflique a été mise en place. Cette réaction fonctionne dans des conditions très douces et permet de réaliser directement l'acylation à partir d'acides benzoïques commerciaux (Schéma 1). Cette méthode a permis l'accès à des précurseurs de nouvelles 3-benzoylménadiques avec de bons rendements. Une simple étape de déprotection par oxydation démethylante à l'aide de nitrate de céryum et d'ammonium (CAN) permet ainsi d'accéder à de nouvelles 3-benzoylménadiques diversement substituées (Schéma 2).

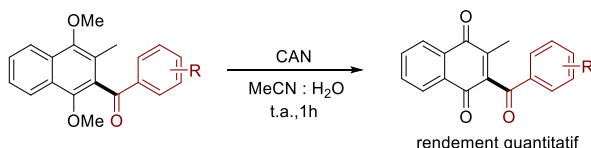


Schéma 2. Déprotection des 3-benzoylménadiques méthylées.

Les propriétés électrochimiques de ces molécules ont été par ailleurs étudiées par voltampérométrie cyclique (CV) et à ondes carrées (SWV) et ont permis d'évaluer les effets électroniques des substitutions de la partie benz(o)yle sur le cœur électro-actif 1,4-naphtoquinone et ainsi de progresser dans la compréhension des mécanismes d'actions des 3-benzoylménadiques dans l'activité antiparasitaire de la plasmodione. Un mécanisme de transfert à 1 et 2 électrons a permis de rationaliser les relations structure-propriétés rédox mesurées.

Synthèse d'outils dérivés des 3-benzoylménadiques pour la chimie-click

Par ailleurs, cette nouvelle voie de synthèse nous a permis d'accéder à des intermédiaires clés pour la synthèse d'outils pour la chimie « click », appelés PD-ABPP pour *plasmodione-derived activity-based protein profiling probes* (Figure 2).

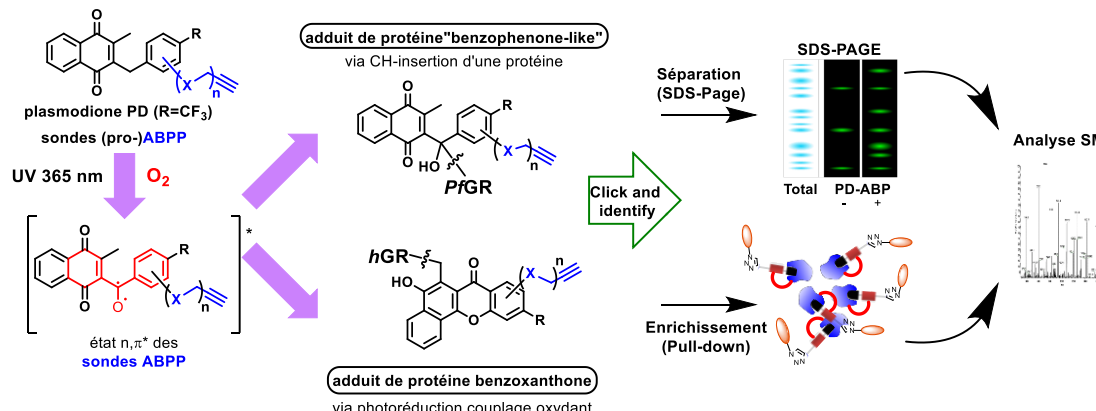


Figure 2. Photoalkylation des dérivés 3-benzoylménadiques portant une fonction alcyne.

Dans ce travail, l'objectif principal était de synthétiser trois dérivés 3-benzoylménadiones portant des fonctions alcynes impossibles à préparer par les méthodologies de synthèse développées antérieurement au sein de l'équipe. Ces outils ont été préparés pour permettre d'aider à identifier les protéines-cibles interagissant avec les 3-benzoylménadiones dans un cycle rédox à l'aide d'une approche dite « *click and fish* » particulièrement originale.⁵ En effet, une 3-benzoylménadione a la particularité de comporter un « cœur » de type benzophénone photoractif, qui, sous photoirradiation UV, est susceptible de se lier de manière covalente avec la(s) cible(s) avec lesquelles la molécule interagit au sein du parasite (Figure 1A.).⁶ Les fonctions alcynes sont ensuite capables de participer à une réaction de cyclo-addition catalysée par du cuivre(I) avec une sonde fluorescente (ou une biotine) portant une fonction azoture, permettant ainsi d'identifier et/ou d'isoler plus aisément les protéines photoalkylées avec le composé antiparasitaire (Figure 2).

A partir d'intermédiaires obtenus par réaction de Friedel & Crafts, deux analogues de la 3-benzoylménadione dérivée de la plasmodione ont ainsi été synthétisés : ils comportent chacun un halogène (I ou F) en alpha du groupe R électro-attracteur (-CF₃ ou NO₂) sur le noyau aromatique de la chaîne benzyle pour la post-fonctionnalisation. Une fonction alcyne a été directement introduite par un couplage de Sonogashira sur le premier analogue iodé tandis qu'un groupement propargyl a été introduit par substitution nucléophile sur le second analogue fluoré (Schéma 3). Un analogue de la 3-benzoylménadione portant une fonction nitro en position 4 du benzoyle a été aussi synthétisé. En effet, cette substitution par un groupement nitro a permis d'accéder au composé, en série 3-benzoylménadione, possédant l'activité antipaludique la plus puissante¹ mesurée au sein de notre équipe (Schéma 3).

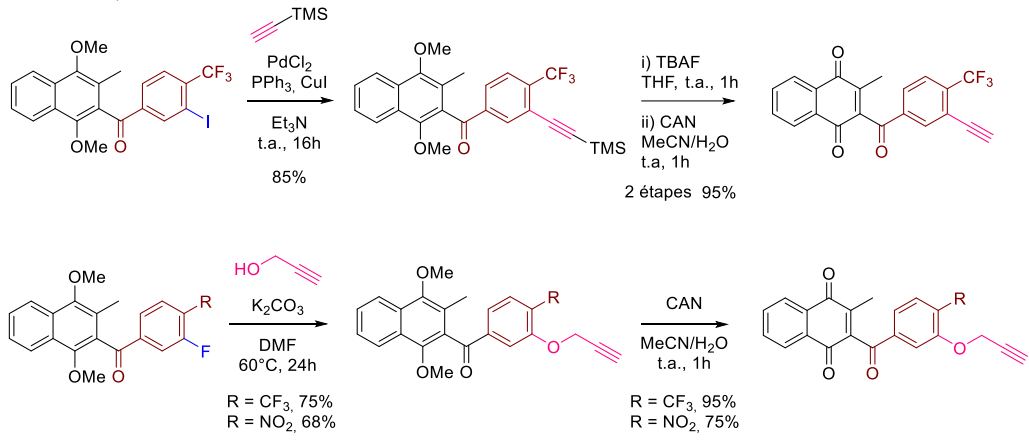


Schéma 3. Synthèse des outils chimiques dérivés de la plasmodione.

Fonctionnalisation de la ménadione avec des radicaux benzyles générés par photocatalyse

Durant la deuxième année, nous avons tenté d'appliquer la méthodologie de Friedel & Crafts pour la synthèse de 3-benzoylménadiones. Cependant les résultats obtenus n'ont pas été à la hauteur de nos attentes. Nous avons donc réfléchi à une nouvelle voie d'accès de ces 3-benzoylménadiones et nous nous sommes intéressés à la génération de radicaux par photocatalyse à partir de benzyles électrophiles simples, afin de fonctionnaliser directement le squelette ménadione (Schéma 4).

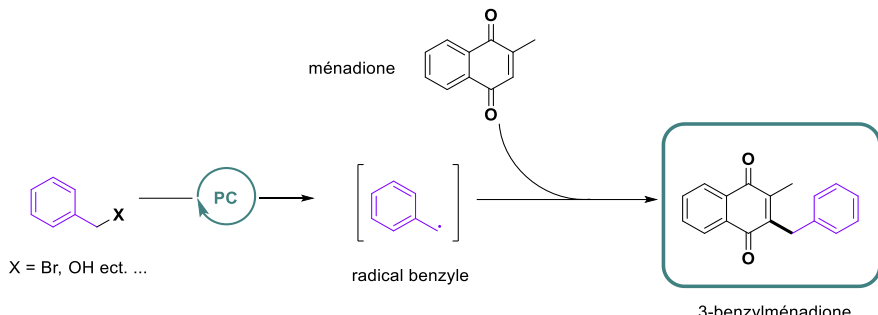


Schéma 4. Méthode envisagée pour la fonctionnalisation radicalaire de la ménadione.

Après plusieurs essais infructueux en utilisant des photocatalyseurs organométalliques, nous avons porté notre attention sur une méthode innovante décrite récemment par Melchiorre⁷ dans laquelle un catalyseur nucléophile et chromophorique est utilisé (Schéma 5). L'anion dithiocarbonyle peut former une espèce catalytique photosensible capable de réagir avec notre électrophile. Après irradiation et chauffage, la liaison C-S est coupée et le radical benzyle libéré réagit avec la ménadione.

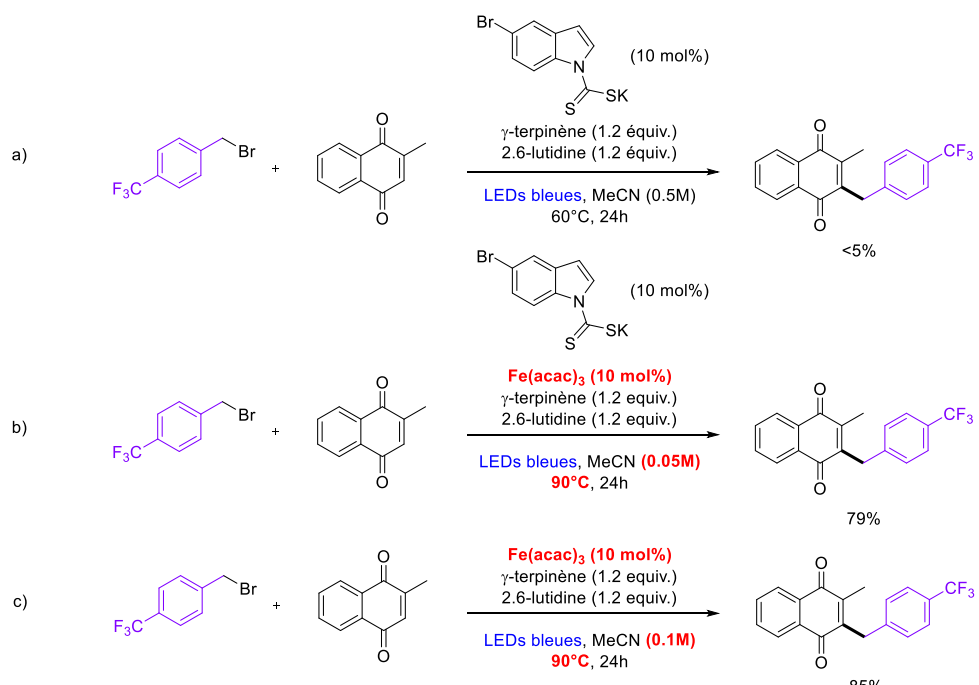


Schéma 5. Synthèse de la plasmodione par réaction radicalaire photocatalysée.

Dans les conditions décrites par Melchiorre, la plasmodione n'est obtenue qu'avec un rendement inférieur à 5% (Schéma 5.a). Après optimisation des conditions expérimentales, le rendement obtenu a été augmenté jusqu'à 79% du produit désiré. Ceci a été rendu possible grâce à l'ajout d'un catalyseur ferrique, le Fe(acac)₃ dont l'utilisation s'est inspirée du mécanisme d'action de la plasmodione (Figure 1.a. et Schéma 5.b). Dans ce mécanisme d'action (Figure 1.a.), la plasmodione oxydée est régénérée par transfert d'électron(s) de sa forme réduite vers des cibles ferriques (methemoglobin). Par ailleurs, de manière surprenante, en absence du catalyseur de Melchiorre, des conditions de réaction similaires en présence de Fe(acac)₃ conduisent à la plasmodione avec un rendement de 85% (Schéma 5.c).

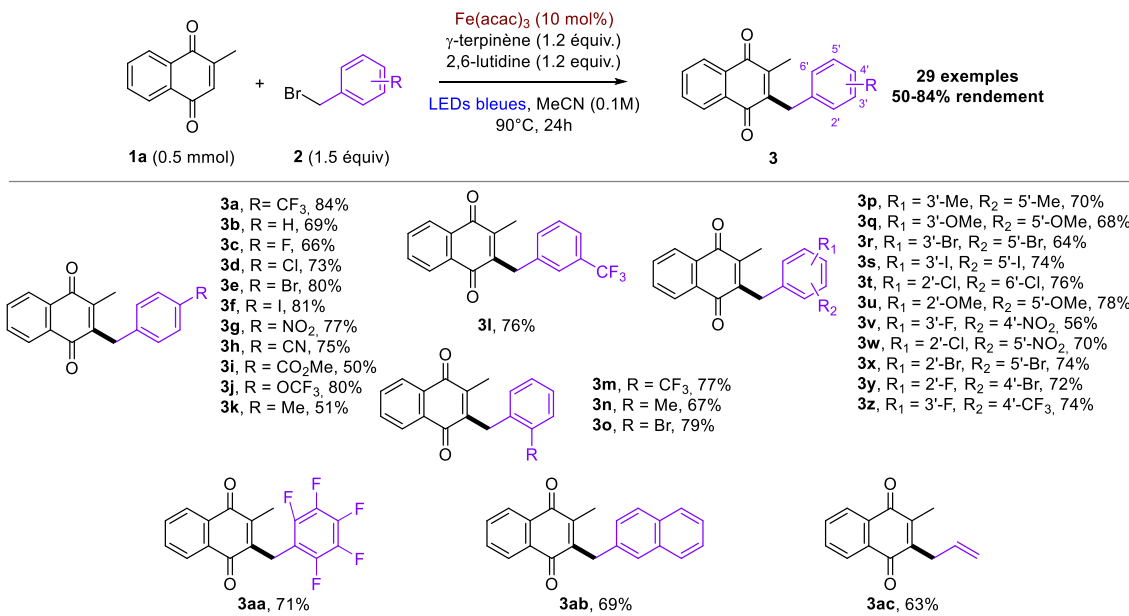


Schéma 6. Exemples de benzylation de la ménadione.

Cette réaction a été ensuite étendue à de nombreux bromures de benzyle diversement fonctionnalisés (Schéma 6). Les groupements électroattracteurs ou électrodonneurs sont tous bien tolérés ainsi qu'une substitution aux positions *ortho*, *méta* ou *para*, de l'unité benzyle (**3a-o**). De même, les rendements obtenus pour des bromures de benzyle disubstitués sont bons (**3p-z**). Il a été également possible d'introduire grâce à cette méthodologie un groupement naphtyle ou allyle (**3ab** et **3ac**).

Différentes quinones ont été par ailleurs également testées. Une modification de la substitution en position 2 de la naphtoquinone est tolérée et permet d'obtenir, avec des rendements acceptables, des 3-benzylnaphtoquinones diversement substituées en position 2 (**4a-g**). Des ménadiques fonctionnalisées en position 5 à 8 du cycle aromatique sont également compatibles avec cette réaction (**4h-j**) (Schéma 7).

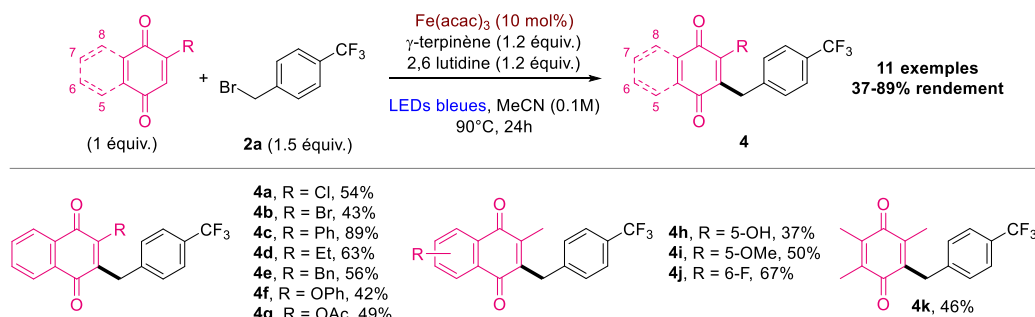


Schéma 7. Benzylation de différentes (naphto)quinones fonctionnalisées.

Des études mécanistiques ont été ensuite menées afin de mieux comprendre le mécanisme de cette réaction (Schéma 8). Nous avons tout d'abord pu démontrer que l'oxygène était indispensable pour que la réaction puisse avoir lieu, ce qui montre que ce dernier joue un rôle important. Des exemples dans la littérature montrent que la ménadione est photoréduite sous irradiation d'une lumière bleue et en présence d'un agent de transfert d'hydrogène pour former un radical semiquinone (étape 1).⁸ Ce radical semiquinone peut ensuite réagir avec l'oxygène dissous en solution pour former un ion superoxyde O₂^{•-} (étape 2),⁹ qui lui-même est ensuite capable de réduire le Fe(III) en Fe(II) (étape 3).

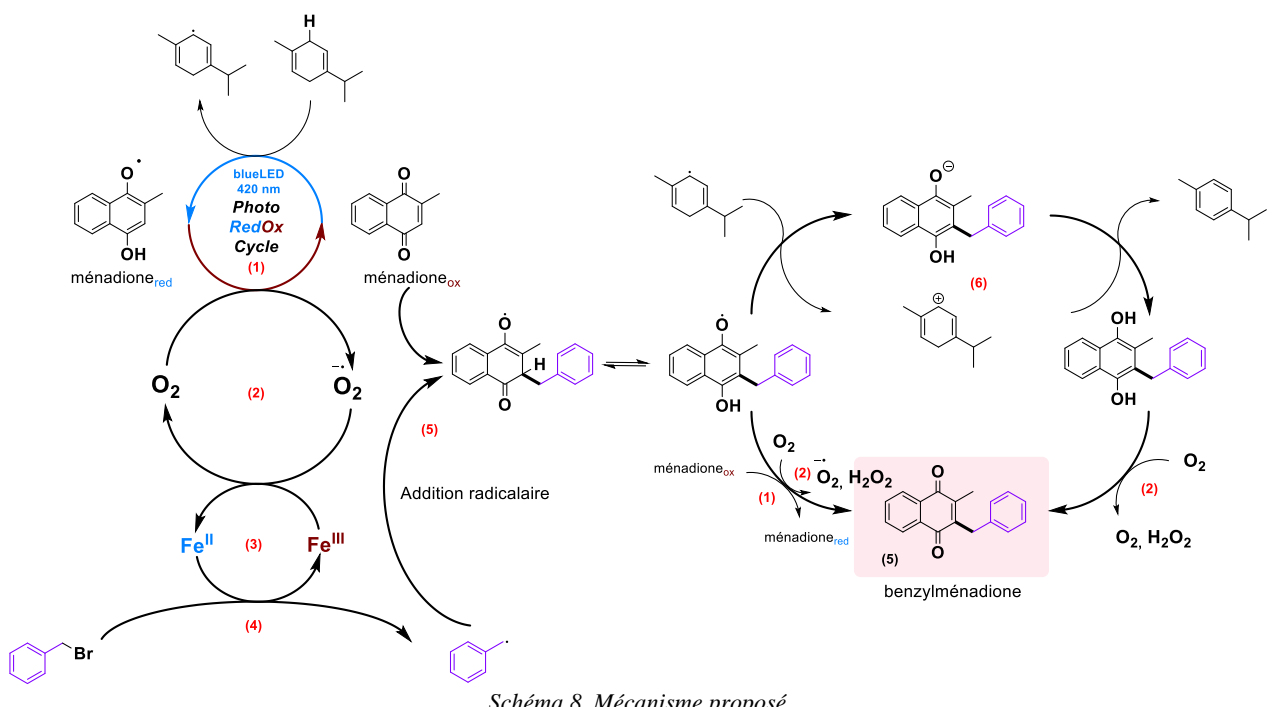


Schéma 8. Mécanisme proposé

Le Fe(II) a déjà été décrit comme étant capable de réduire la liaisons C-Br de bromures de benzyle pour former un radical benzyle (étape 4) qui peut ensuite réagir avec la ménadione pour former un nouveau radical semiquinone benzylé (étape 5).¹⁰ Ce dernier peut ensuite directement réagir avec la ménadione pour régénérer la forme radical semiquinone de celle-ci et conduire au produit final ou alors initier un autre cycle catalytique (étape 1 ou 2). Une terminaison peut également être envisagée par une réaction de transfert d'électron avec le radical terpinène pour générer après un transfert de proton la 3-benzylménadione ciblée (étape 6).

L'ensemble de mes travaux sur la méthodologie de synthèse photo-rédox de 3-benzylménadiques a été soumis dans un brevet européen (Déclaration d'invention CNRS : 11861-01).

Synthèse de benzylménadiques hétéroaromatiques par couplage de Suzuki.

Suite à l'échec lors de la synthèse de dérivés portant un cycle hétéroaromatique sur la partie benzyllique, nous avons opté pour une nouvelle stratégie. Nous nous sommes basés sur un exemple de la littérature,¹¹ dans lequel, par un couplage pallado-catalysé de Suzuki, des chlorures de benzyles sont, de manière efficace, couplés à divers acides boroniques hétéroaromatiques. Pour cela nous avons synthétisé, à partir du 1,4-diméthoxy-2-méthynaphtalène et par une réaction de chlorométhylation, le chlorure de benzyle correspondant (Schéma 9).

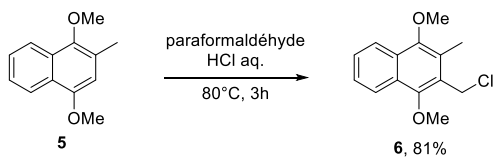


Schéma 9. Chlorométhylation du 1,4-diméthoxy-2-méthynaphtalène.

Une fois ce substrat obtenu, nous avons réussi à l'engager dans un couplage pallado-catalysé avec succès pour obtenir avec d'excellents rendements les diarylméthanes correspondants. Ces derniers ont pu par suite être très facilement déprotégés avec du CAN (Schéma 10).

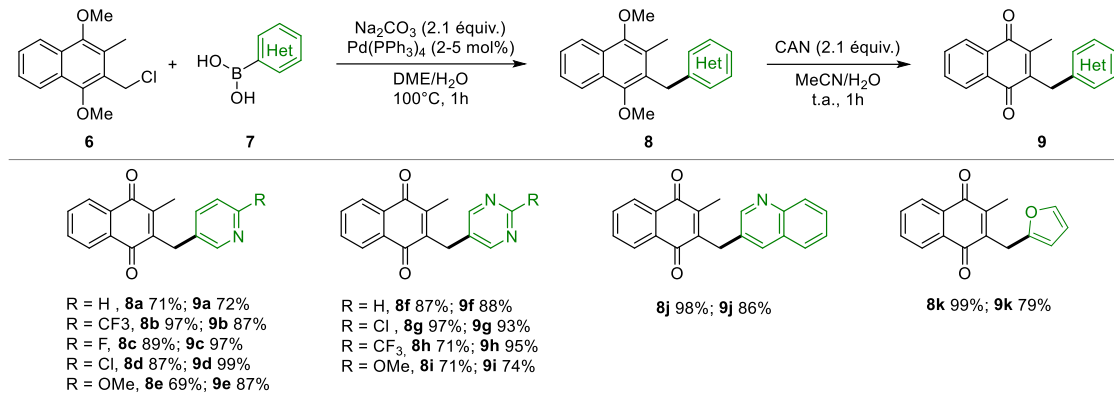


Schéma 10. Synthèse d'analogue hétéroaromatiques de 3-benzylménadiones

Les produits de couplages, des naphtoquinones protégées par des groupements méthyles, offrent des opportunités de fonctionnaliser la nouvelle partie hétéroaromatique. En effet, les ménadiones sont en général très sensibles et ne peuvent pas être utilisées dans des milieux réducteurs ou basiques. Par exemple, nous avons pu introduire par substitution nucléophile de l'adduit 2-chloropyrimidine un groupement cyano ou un brome (Schéma 11).

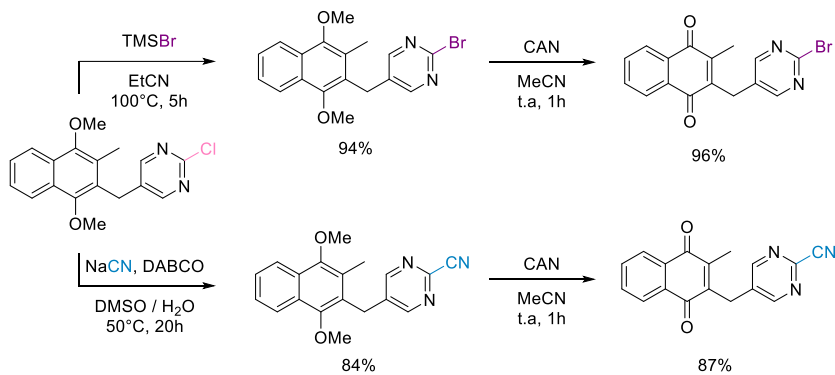


Schéma 11. Post-fonctionnalisation de la partie hétéroaromatique.

La synthèse des analogues hétéroaromatiques des 3-benzylménadiones, portant des hétérocycles pyridines, ou pyrimidines, a été soumis dans un brevet européen (Déclaration d'invention CNRS : 11861-03).

Conclusion

Durant ce travail de thèse, nous avons pu développer avec succès plusieurs nouvelles méthodologies de synthèse pour obtenir de nouvelles 3-benzylménadiones antiparasitaires, dont des analogues hétéroaromatiques originaux, ainsi que des métabolites supposés de ces dernières, les 3-benzoylménadiones.

Les 3-benzoylménadiones ont été synthétisées grâce à une réaction Friedel-Crafts revisitée permettant l'acylation, habituellement difficile, de groupement benzoyles fortement appauvris en électrons. Cette méthodologie a permis de synthétiser toute une série de 3-benzoylménadiones que nous avons étudiée par électrochimie afin de mieux comprendre l'influence de la substitution du groupement benzoyle sur les propriétés rédox de ces quinones. Grâce à cette même méthodologie, nous avons synthétisé des outils fonctionnels chimiques qui ont pu être utilisés pour identifier les protéines avec lesquelles nos composés antiparasitaires interagissent.

L'un des objectifs a été ensuite de développer une nouvelle voie de synthèse complémentaire à celles utilisées précédemment au sein de l'équipe pour préparer de nouvelles 3-benzylménadiones diversement substituées ou portant un hétérocycle. Pour cela, nous avons développé une méthodologie innovante de benzylation photocatalysée de la ménadione avec des bromures de benzyle en présence de Fe(III). Concernant les analogues hétéroaromatiques, ces derniers ont été

obtenus par couplage pallado-catalysé de Suzuki entre la chlorométhyl-ménadione protégée et des acides boroniques hétéroaromatiques.

Toutes les 3-benzylménadiques synthétisées par photocatalyse ou par couplage pallado-catalysé ont été envoyées à l'institut *Swiss Tropical and Public Health Institute* (Swiss TPH) pour déterminer leur activité contre les parasites du paludisme, *Plasmodium falciparum*.

Références bibliographiques

-
- ¹ T. Müller, L. Johann, B. Jannack, M. Brückner, D.A. Lanfranchi, H. Bauer, C. Sanchez, V. Yardley, C. Deregaucourt, J. Schrével, M. Lanzer, R.H. Schirmer, E. Davioud-Charvet, *J. Am. Chem. Soc.* **2011**, *133*, 11557-11571.
- ² K. Ehrhardt, C. Deregaucourt, A.A. Goetz, T. Tzanova, V. Gallo, P. Arese, B. Pradines, S. H. Adjalley, D. Bagrel, S. Blandin, M. Lanzer, E. Davioud-Charvet, *Antimicrob. Agents Chemother.* **2016**, *60*, 5146-5158.
- ³ M. Bielitz, D. Belorgey, K. Ehrhardt, L. Johann, D. A. Lanfranchi, V. Gallo, E. Schwarzer, F. Mohring, E. Jortzik, D. L. Williams, K. Becker, P. Arese, M. Elhabiri, E. Davioud-Charvet, *Antioxid. Redox Signal.* **2015**, *22*, 1337-1351.
- ⁴ L. Feng, D. A. Lanfranchi, L. Cotos, E. Cesar Rodo, K. Ehrhardt, A. A. Goetz, H. Zimmerman, F. Fenaille, S. Blandin, E. Davioud-Charvet, *Org. Biomol. Chem.* **2018**, *16*, 2647-2665.
- ⁵ B. P. Duckworth, D. J. Wilson, K. M. Nelson, H. I. Boshoff, C. E. Barry 3rd, C. C. Aldrich, *ACS Chem. Biol.* **2012**, *7*, 1653-1658.
- ⁶ E. Deseke, Y. Nakatani, G. Ourisson, *Eur. J. Org. Chem.* **1998**, 243-251.
- ⁷ B. Schweitzer-Chaput, M. A. Horwitz, E. Beato, P. Melchiorre, *Nat. Chem.* **2019**, *11*, 129-135.
- ⁸ H. Görner, *J. Photoch. Photobio. A*, **2004**, *165*, 215-222.
- ⁹ T. Chih, S. Y. Yeh, C. M. Wang, *J. Electroanal. Chem.* **2002**, *543*, 135-142.
- ¹⁰ D. Li, X. Shen, *Org. Biomol. Chem.* **2020**, *18*, 750-754.
- ¹¹ N. Henry, C. Enguehard-Gueiffier, I. Thery, A. Gueiffier, *Eur. J. Org. Chem.* **2008**, 4824-4827.

Liste des publications

L. Cotos, M. Donzel, M. Elhabiri, E. Davioud-Charvet. A mild and versatile Friedel-Crafts methodology for the diversity-oriented synthesis of redox-active 3-benzoylmenadiones with tuneable redox potentials. *Chem. Eur. J.* **2020**, 26, 3314-3325. doi: 10.1002/chem.201904220. Cover Feature: 26, 3192 doi: 10.1002/chem.201905613.

B. A. Cichocki,# V. Khobragade,# M. Donzel, L. Cotos, S. Blandin, C. Schaeffer-Reiss, S. Cianférani, J.-M. Strub, M. Elhabiri, E. Davioud-Charvet. A Class of Valuable (Pro-)Activity-Based Protein Profiling Probes: Application to the Redox-Active Antiplasmodial Agent, Plasmodione. *JACS^{Au}*, **2021**, Accepté le 11-03-2021, sous presse. doi: 10.1021/jacsau.1c00025.

B. A. Cichocki,# M. Donzel,# K. Heimsch,# M. Lesanavicius,# L. Feng, E. J. Montagut, K. Becker, A. Aliverti, M. Elhabiri, N. Cenas, E. Davioud-Charvet. *Plasmodium falciparum* ferredoxin-NADP⁽⁺⁾ reductase-catalyzed redox cycling of plasmodione generates both predicted key drug metabolites. Implication for antimalarial drug development. *ACS Infect. Dis.* **2021**, Accepté le 01-04-2021 sous presse. doi: 10.1021/acsinfecdis.1c00054.

les auteurs classés par ordre alphabétique ont contribué à parts égales en tant que premiers co-auteurs.

Liste des brevets

M. Donzel, M. Elhabiri, E. Davioud-Charvet «Photoredox radical benzylation process », DI CNRS: 11861-02. Réf. BET 21P0257 (EMO/KYB). Demande de brevet européen N° 21305263.2 déposée le 5 mars 2021.

Liste des présentations

27-28 Août 2018 – Barrande-Vltava 2018 - 9th French-Czech Chemistry meeting - Strasbourg Maxime Donzel, Leandro Cotos, Vrushali Khobragade, Elisabeth Davioud-Charvet. *Synthesis of clickable chemical tools to identify the activity-based flavoprotein profiling of the early antimalarial drug plasmodione*. Poster communication.

9-11 Septembre 2019 – 39th Regio Symposium - Mittelwihr Maxime Donzel, Leandro Cotos, Vrushali Khobragade, Elisabeth Davioud-Charvet. *New methodologies for the synthesis of antimalarial 3-benz(o)ylmenadiones*. Poster communication.

16 Décembre 2020 – Journée du LIMA – e-Conference (situation COVID) Maxime Donzel, Mourad Elhabiri, Elisabeth Davioud-Charvet. *New methodologies for the synthesis of antimalarial 3-benzylmenadiones*. Présentation orale.

Table des matières

Remerciements v

Résumé de thèse vii

Liste des abréviations xxi

Chapitre I. Introduction au paludisme et à la plasmodione 1

1. Le paludisme.....	3
1.1. Le cycle de vie de <i>Plasmodium falciparum</i>	5
1.2. Les traitements antipaludiques.....	6
2. La plasmodione et les 3-benzylménadiones comme candidats-médicaments antipaludiques potentiels.....	12
2.1. Les 1,4-naphtoquinones.....	12
2.2. La plasmodione.	14
2.3. Mode d'action de la plasmodione.....	15
3. Synthèse de naphtoquinones fonctionnalisées.	17
3.1. Synthèse de ménadiones fonctionnalisées.	18
3.2. Synthèse des 3-benzoylménadiones.....	23
3.3. Article 1. Mini-revue.....	25
4. Objectifs de recherche.	39

Chapitre II. Synthèse de 3-benzoylménadiones par réaction Friedel-Crafts, étude de leurs propriétés rédox et applications pour la synthèse de sondes chimiques photoréactives..... 41

1. Développement d'une nouvelle méthodologie d'acylation de Friedel-Crafts pour la synthèse de 3-benzoylménadiones.	43
1.1. Introduction.....	43
1.2. Article 2.	47
2. Applications de la méthode d'acylation de Friedel-Crafts pour la synthèse de sondes ABPP..	62
2.1. Objectifs et travaux préliminaires.	62
2.2. Article 3.	65

Chapitre III. Synthèse et oxydation des 3-benzylménadiones par des méthodes photochimiques.. 91

1. Développement d'une nouvelle méthode de benzylation des naphtoquinones.....	93
--	----

1.1.	Travaux préliminaires	93
1.2.	Article 4	99
2.	Oxydation benzylique de la plasmodione.....	113
2.1.	Travaux préliminaires	113
2.2.	Article 5	117
Chapitre IV. Synthèse d'analogues hétéroaromatiques de 3-benzylménadione		139
1.	Synthèse de 1,4-quinones portant un motif méthyl-hétéroaromatique dans la littérature..	142
1.1.	Synthèse de 2-nicotinyl-1,4-quinones.....	142
1.2.	Synthèse de la 3-(4-picolinyl)ménadione.....	143
1.3.	Introduction de cycles hétéroaromatiques à 5 chaînons.....	143
2.	Synthèse d'analogues hétéroaromatiques de la plasmodione	145
2.1.	Objectifs.....	145
2.2.	Stratégie de synthèse de di(hétéro)arylméthanes.....	145
2.3.	Application à la synthèse de dérivés hétéroaromatiques de la plasmodione	147
2.4.	Post-fonctionnalisation des intermédiaires de couplage.....	149
Conclusion générale et perspectives		151
Partie expérimentale		155
General information.....		157
Chapitre II. Experimental part.....		158
Article 2		158
Article 3		167
Chapitre III. Experimental part		173
Article 4		173
Article 5		184
Chapitre IV. Experimental part		186
Références bibliographiques.....		193

Liste des abréviations

ACT	Combinaison thérapeutique à base d'artémisinine
APTS	Acide para-toluènesulfonique
ART	Artémisinine
ATP	Adénosine triphosphate
BMD	3-Benzylménadione
BQ	Benzoquinone
CAN	Nitrate de Cérium et d'Ammonium
CQ	Chloroquine
CV	Voltampérométrie cyclique
DABCO	1,4-Diazabicyclo[2.2.2]octane
DCE	Dichloroéthane
DCM	Dichlorométhane
DDQ	2,3-dichloro-5,6-dicyano-1,4-benzoquinone
DDT	Dichlorodiphényltrichloroéthane
DHOD	Dihydroorotate déshydrogénase
DIPEA	<i>N,N</i> -Diisopropyléthylamine
DLP	Péroxyde de dilauroyle
DMA	Diméthylacétamide
DME	Diméthoxyéthane
DMF	Diméthylformamide
DMSO	Diméthylsulfoxyde
DTBP	Péroxyde de di-tert-butyle
EDA	Donneur-accepteur d'électrons
ESI	Ionisation par électronébulisation
G6PD	Glucose-6-phosphate déshydrogénase
GR	Glutathion réductase
GSH	Glutathion (réduit)
GSSG	Glutathion disulfure
HAT	Transfert d'atome d'hydrogène
Hb	Oxyhémoglobine
HBr	Acide bromhydrique
HCl	Acide chlorhydrique
HFIP	Hexafluoroisopropanol
hGR	Glutathion réductase humaine
HRMS	Spectroscopie de masse à haute résolution
IC₅₀	Concentration inhibitrice médiane
iPrOH	Isopropanol
LED	Diode électroluminescente
metHB	Méthémoglobine
NADPH	Nicotinamide adénine dinucléotide phosphate réduite
n.d	Non déterminé
nMet	<i>N</i> -acetylmethionine methyl ester
NQ	Naphtoquinone

OMS	Organisation Mondiale de la Santé
PD	Plasmodione
 PDO	3-(4-(trifluorométhyl)benzoyl)ménadione
PfFNR	Ferredoxin:NADP ⁺ oxidoreductase de <i>P. falciparum</i>
PfGR	Glutathion réductase de <i>P. falciparum</i>
PIDA	Diacétate d'iodobenzène
RMN	Résonance magnétique nucléaire
SEAr	Substitution électrophile aromatique
SET	Transfert d'un électron
SNAr	Substitution nucléophile aromatique
SWV	Voltampérométrie à ondes carrées
t.a.	Température ambiante
TBHP	Hydropéroxyde de tert-butyle
TFA	Acide trifluoroacétique
TFAA	Anhydride trifluoroacétique
TFAT	Triflate de trifluoroacétyle
TfOH	Acide triflique
THF	Tétrahydrofurane
TMSBr	Bromure de triméthylsilane
UV	Ultraviolet
XAT	Transfert d'atome d'halogène

Chapitre I. Introduction au paludisme et à la plasmodione.

1. Le paludisme

Le paludisme (ou malaria) est une maladie due à des parasites du genre *Plasmodium* transmis à l'humain par l'intermédiaire des piqûres des femelles moustiques de genre *Anopheles*. En 2019, selon l'Organisation Mondiale de la Santé (OMS), on estime à près 229 millions le nombre de cas de paludisme (contre 238 millions en 2000) ainsi que 409 000 décès (contre 736 000 en 2000). Le paludisme est endémique dans 87 pays (**Figure 1**) mais la région Afrique représente à elle seule 94% des cas recensés et des décès. Les enfants de moins de 5 ans représentent 67% des décès associés au paludisme.¹

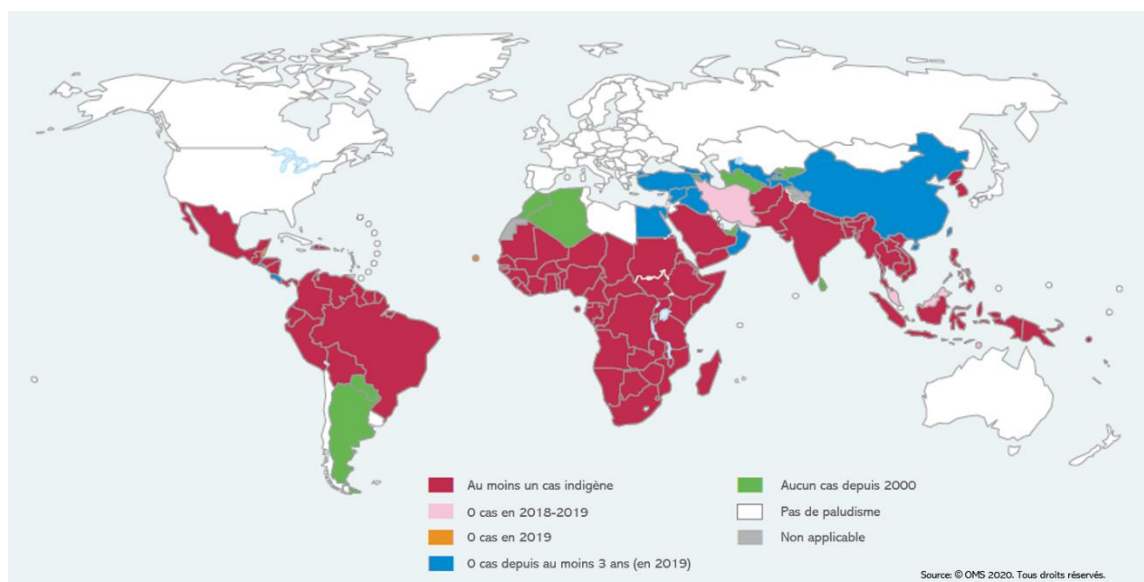


Figure 1. Présence et évolution du paludisme dans le monde en 2019. Figure traduite de la Ref. 1

Il existe 5 souches de *Plasmodium* responsables du paludisme chez les humains *P. falciparum*, *P. vivax*, *P. malariae*, *P. ovale* et *P. knowlesi*. Parmi ceux-ci, *P. falciparum* est de loin le plus dangereux, et est majoritairement présent en Afrique. En effet, ce dernier représente plus de 99% des cas de paludisme dans cette région et est responsable des cas de paludisme sévère ainsi que de complications pendant les grossesses.² *P. vivax* est la deuxième espèce parasitaire la plus représentée chez l'homme et est responsable de la majorité des cas de paludisme en Amérique du Sud. C'est aussi le parasite pour lequel la plus grande part de la population mondiale est exposée de l'Amérique centrale et du Sud, jusqu'en Asie du Sud-Est, ce qui représente plus de 2 milliards d'êtres humains.³ Les atteintes dues à *P. vivax* sont en général bénignes, mais il existe une forme latente du parasite qui, se développant dans

¹ World malaria report, 2020, Organisation Mondiale de la Santé.

² M. A. Phillips, J. N. Burrows, C. Manyando, R. H. van Huijsduijnen, W. C. Van Voorhis, T. N. C. Wells, *Nat. Rev. Dis. Primers*, 2017, 3, 17050.

³ C. A. Guerra, R. E. Howes, A. P. Patil, P. W. Gething, T. P. Van Boeckel, W. H. Temperley, C. W. Kabaria, A. J. Tatem, B. H. Manh, I. R. F. Elyazar, J. K. Baird, R. W. Snow, S. I. Hay, *Plos Neglect. Trop. Dis.* 2011, 4, e774.

le foie, peut provoquer une chronicité des symptômes. *P. ovale* et *P. malariae* sont quant à eux moins courants que les deux précédemment cités et provoquent des infections souvent bénignes. Enfin, *P. knowlesi*, initialement un parasite de macaques, s'est révélé transmissible à l'homme et peut être responsable de cas de paludisme sévère.⁴

Les groupes de personnes susceptibles d'être gravement atteintes par le paludisme sont les nourrissons, les jeunes enfants de moins de 5 ans, les femmes enceintes et de manière générale les personnes possédant un système immunitaire affaibli ou n'ayant jamais été en contact avec le parasite auparavant (voyageurs, migrants venant d'une zone non-endémique). Ceci s'explique par le fait que les résidents des zones endémiques, par exposition répétée, développent une immunité partielle envers le parasite permettant une disparition des cas sévères d'infection chez les plus de 5 ans, et à terme, une disparition des cas symptomatiques et même de la parasitémie.⁵ Cependant cette immunité est acquise au détriment d'une surmortalité chez les enfants de moins de 5 ans.¹

La chute de l'incidence du paludisme (i.e. nombre de cas pour 1 000 habitants exposés au risque de paludisme) de 80 en 2000 à 57 en 2019 ainsi que la baisse significative du nombre de décès enregistrés depuis le début des années 2000 démontrent le succès de l'effort global de lutte contre le paludisme. Ces progrès sont dus à une multitude de facteurs dont trois principaux : 1) le contrôle du vecteur de l'infection (le moustique) par utilisation d'insecticides, 2) l'emploi de moustiquaires imprégnées d'insecticides, et 3) le traitement des cas de paludisme par une combinaison thérapeutique à base d'artémisinine (ACT).⁶ Cependant, le rythme de la baisse de contamination est en diminution de façon inquiétante ces dernières années et de nouvelles souches résistantes à l'artémisinine sont apparues dans plusieurs régions d'Asie du Sud-Est il y a plus de 10 ans.^{7,8} Plus récemment, des souches résistantes à l'artémisinine ont été détectées indépendamment dans plusieurs régions d'Afrique et d'Amérique du Sud. De la même façon, une résistance des moustiques *Anopheles* envers les insecticides a commencé à émerger et bien qu'une étude de l'OMS montre que la protection engendrée par les moustiquaires imprégnées d'insecticide, grandement utilisées en Afrique, est

⁴ B. Singh, L. K. Sung, A. Matusop, A. Radhakrishnan, S. S. G. Shamsul, J. Cox-Singh, A. Thomas, D. J. Conway, *Lancet*, **2004**, 363, 1017–1024.

⁵ K. Marsh, S. Kinyanjui, *Parasite Immunol.* **2006**, 28, 51-60.

⁶ S. Bhatt, D. J. Weiss, E. Cameron, D. Bisanzio, B. Mappin, U. Dalrymple, K. E. Battle, C. L. Moyes, A. Henry, P. A. Eckhoff, E. A. Wenger, O. Briët, M. A. Penny, T. A. Smith, A. Bennett, J. Yukich, T. P. Eisele, J. T. Griffin, C. A. Fergus, M. Lynch, F. Lindgren, J. M. Cohen, C. L. J. Murray, D. L. Smith, S. I. Hay, R. E. Cibulskis, P. W. Gething, *Nature*, **2015**, 526, 207-211.

⁷ A. M. Dondorp, F. Nosten, P. Yi, D. Das, A. P. Phyo, J. Tarning, K. Lwin, F. Ariey, W. Hanpithakpong, S. J. Lee, P. Ringwald, K. Silamut, M. Imwong, K. Chotivanich, P. Lim, T. Herdman, S. S. An, S. Yeung, P. Singhasivanon, N. P. J. Day, N. Lindegardh, D. Socheat, N. J. White, *N. Engl. J. Med.* **2009**, 361, 455-467.

⁸ A. P. Phyo, S. Nkhoma, K. Stepniewska, E. A. Ashley, S. Nair, R. McGready, C. Moo, S. Al-Saai, A. M. Dondorp, K. M. Lwin, P. Singhasivanon, N. P. J. Day, N. J. White, T. J. C. Anderson, F. Nosten, *Lancet*, **2012**, 379, 1960-1966.

toujours très élevée,⁹ il est nécessaire de disposer de nouveaux outils pour lutter de manière efficace et diversifiée contre le paludisme.

1.1. Le cycle de vie de *Plasmodium falciparum*.

P. falciparum suit un cycle de vie complexe partagé entre deux espèces : le moustique et l'être humain (**Figure 2**). Le cycle commence par la morsure d'un moustique femelle *Anopheles* et l'introduction d'une forme infectieuse nommée sporozoïte dans le derme (A). Les sporozoïtes, mobiles, vont migrer jusqu'au foie (B) et chacun d'entre eux va se multiplier au sein des cellules hépatiques et former des schizontes. Après quelques jours, les cellules du foie vont se rompre et libérer dans la circulation sanguine (C) des merozoïtes, qui sont les cellules résultantes de la reproduction asexuée du parasite dans le foie. Lors de la phase sanguine, les merozoïtes vont alors envahir les globules rouges pour entamer un nouveau cycle de reproduction asexuée en passant par les stades anneaux, qui vont évoluer en stades trophozoïtes, puis schizontes et après éclatement de la cellule, en de nouveaux stades merozoïtes. Ce cycle intraérythrocytaire de *P. falciparum* dure 48 h.

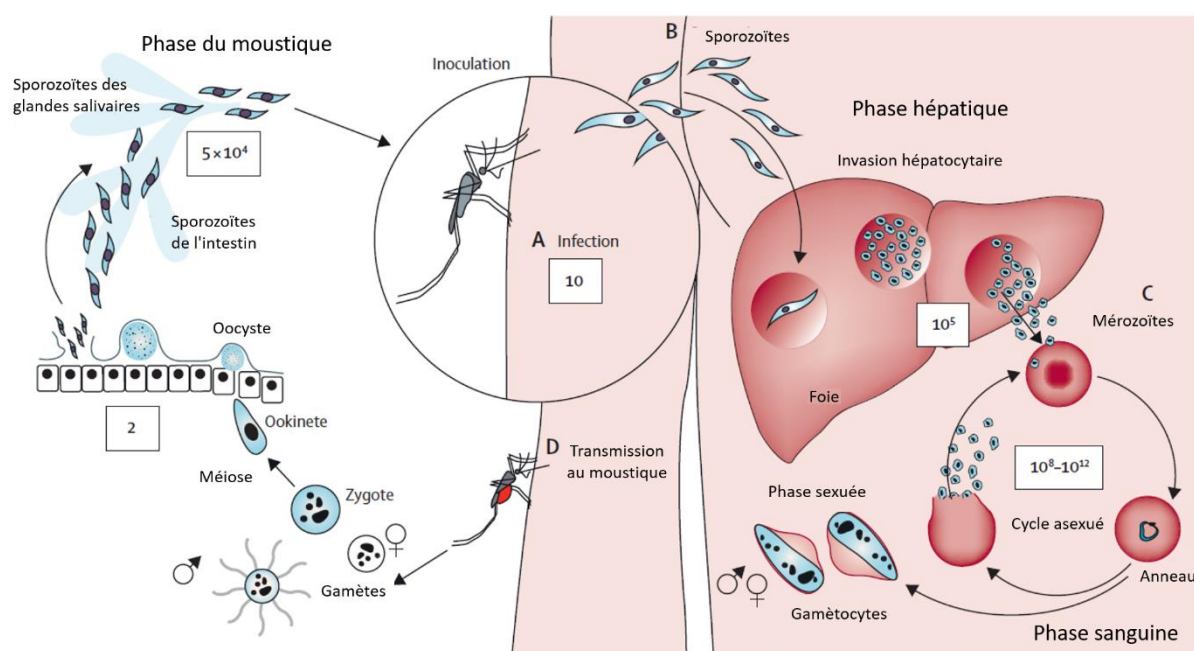


Figure 2. Cycle de vie de *P. Falciparum*. Figure copiée et traduite¹⁰.

Le nombre de parasites chez l'hôte va alors passer très rapidement de quelques milliers à plusieurs millions de stades asexués. A partir d'environ 100 millions de parasites asexués en circulation dans le sang, l'infection devient symptomatique avec l'apparition de fièvres, de courbatures, de maux de tête, évoluant en l'absence de traitement chez des personnes fragiles, vers l'inflammation du cerveau, le

⁹ Implications of insecticide resistance for malaria vector control, 2016, Organisation Mondiale de la Santé.

¹⁰ N. J. White, S. Pukrittayakamee, T. T. Hien, M. A. Faiz, O. A. Mokuolu, A. M. Dondorp, Lancet, 2014, 383, 723-735.

coma, et la mort. Lors de la phase sanguine, certains parasites vont se développer en forme sexuée, les gamétocytes, qui vont aussi évoluer du stade I au stade V. Au stade V, les gamétocytes sont matures et circulants, et peuvent se faire ingérer lors d'un repas sanguin par un moustique. Ce sont les seuls stades infectants pour le moustique.

Après ingestion des gamétocytes lors d'un repas sanguin sur un humain infecté (D). Les gamétocytes, par reproduction sexuée, vont former des zygotes, puis des ookinetes et enfin des ookystes dans les intestins du moustique. Les ookystes vont libérer des sporozoïtes qui vont migrer dans les glandes salivaires du moustique où ils pourront infecter un être humain pendant un repas sanguin pour continuer le cycle.^{2,8}

1.2. Les traitements antipaludiques.

L'armoise chinoise, *Artemisia annua*, connue en Chine depuis deux millénaires a été utilisée en médecine traditionnelle en décoction en Asie. Mais, c'est dans les années 1970, que des chercheurs chinois extraient le produit actif, baptisé *qing hao su* (artémisinine). La découverte de l'artémisinine a valu à la Chinoise, le Dr Tu Youyou, le Prix Nobel de physiologie ou médecine 2015, conjointement avec l'Irlandais William Campbell et le Japonais Satoshi Ōmura, découvreurs de l'ivermectine. En Occident, les traitements chimiothérapeutiques du paludisme ont grandement évolué depuis plus de 400 ans, de la simple écorce de quinquina broyée jusqu'aux combinaisons thérapeutiques à base d'artémisinine (ACT), traitement privilégié depuis les années 1990 et recommandé de nos jours par l'OMS.^{1,11}

Les quinoléines.

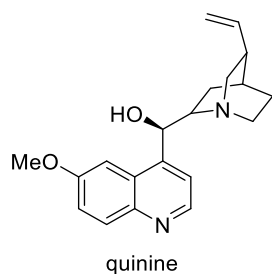
Dès le XVII^{ème} siècle, la poudre d'écorce de quinquina, un arbuste originaire d'Amérique du Sud, fut utilisée en médecine en Europe pour traiter le paludisme.¹² Ce n'est que 200 ans plus tard que la substance active de cette écorce, la quinine (**Figure 3**), fut extraite pour la première fois par Joseph Pelletier et Joseph Caventou.¹³ C'est à partir de ce moment que la production industrielle de quinine a commencé et que cette dernière a supplanté l'écorce de quinquina dans le traitement du paludisme. C'est seulement en 1945, que la première synthèse totale de la quinine a été publiée par Woodward et Doering.¹⁴

¹¹ A. R. Butler, S Khan, E. Ferguson, *J. R. Coll. Physicians Edinb.* **2010**, *40*, 172–177.

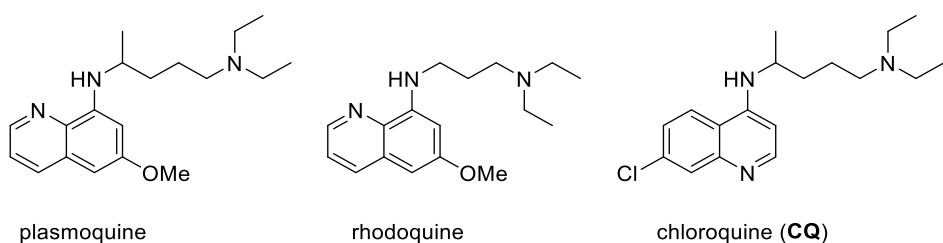
¹² J. Achan, A. O. Talisuna, A. Erhart, A. Yeka, J. K. Tibenderana, F. N. Baliraine, P. J. Rosenthal, U. D'Alessandro, *Malar. J.* **2011**, *10*, 144.

¹³ P. J. Pelletier, J. B. Caventou. *Annal. Chim. Phys.* **1820**, *15*, 289–318.

¹⁴ R. B. Woodward, W. E. Doering, *J. Am. Chem. Soc.* **1945**, *67*, 860–874.

**Figure 3.** Structure de la quinine.

L'action antipaludique de la quinine chez *P. falciparum* est particulièrement ciblée sur les érythrocytes infectés et il agit comme schizonticide. La quinine a été largement utilisée jusque durant les années 1920 où elle a peu à peu été remplacée par des quinoléines de synthèse moins coûteuses à produire et non dépendantes des cultures de quinquina.¹⁵ Ces composés de synthèse sont principalement des aminoquinoléines. On peut citer la plasmoquine ou la rhodoquine, mais le composé le plus important est certainement la chloroquine (**CQ**) qui bien que découverte pour la première fois dans les années 1930, puis écartée car jugée trop毒ique, a été finalement approuvée et largement utilisée après la seconde guerre mondiale (**Figure 4**).

**Figure 4.** Structure de la plasmoquine, de la rhodoquine et de la chloroquine.

L'élucidation du mode d'action de la **CQ** est toujours en cours. Il a été démontré que la **CQ** inhibe la détoxicification de l'hème, généré par le parasite comme sous-produit toxique formé au cours de la digestion de l'hémoglobine durant la phase sanguine de l'infection. L'hème, toxique pour le parasite, s'accumule dans la vacuole digestive du parasite, fuit dans les membranes du fait de sa lipophilicité, et participe à l'oxydation des macromolécules, menant à la mort du parasite.¹⁶

La **CQ** est restée le fer de lance de la lutte contre le paludisme pendant plus de 50 ans et a grandement contribué, avec l'insecticide dichlorodiphényltrichloroéthane (DDT), aux premières campagnes de luttes mondiales contre le paludisme. Cependant, dès les années 50, les premiers cas de résistance chez *P. falciparum* ont été identifiés sur le continent américain et en Asie du Sud-Est,¹⁷ et malgré un

¹⁵ S. R. Meshnick, M. J. Dobson, *Antimalarial Chemotherapy*, Chapitre 2, **2001**.

¹⁶ T. E. Wellem, C. V. Plowe, *J. Infect. Dis.* **2001**, 784, 770-776.

¹⁷ D. Payne, *Parasitol. Today*, **1987**, 3, 241-246.

développement lent des souches résistantes à la **CQ**, ces dernières ont peu à peu émergé sur tous les continents.¹⁸

D'autres dérivés de quinolines ont été synthétisés plus tard et utilisés comme antiparasitaires efficaces contre les souches résistantes à la **CQ**. On peut notamment citer la méfloquine et l'amodiaquine (**Figure 5**).

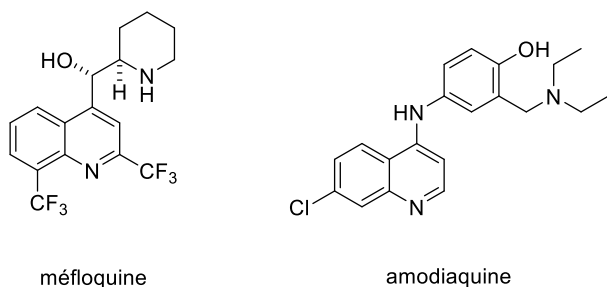


Figure 5. Structure de la méfloquine et de l'amodiaquine.

La méfloquine est couramment utilisée comme traitement préventif (prophylaxie), notamment pour des voyageurs dans des zones fortement impactées par les souches résistantes à la **CQ**. Des souches parasitaires résistantes à la méfloquine ont rapidement émergé.¹⁹ De la même façon, l'amodiaquine s'est révélée très efficace pour lutter contre les souches résistantes à la **CQ** de *Plasmodium*. Cette molécule est cependant susceptible de provoquer des effets secondaires graves chez une faible proportion de patients.²⁰

Un autre composé de synthèse important est la primaquine (**Figure 6**), un analogue de la plasmoquine.

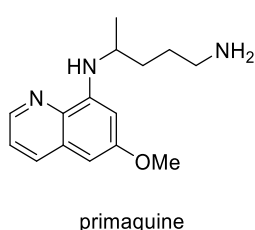


Figure 6. Structure de la primaquine.

Cette molécule décrite pour la première fois en 1946 a la particularité d'être efficace contre les schizontes dormants de *P. vivax* et *P. ovale* dans le foie et a été utilisée massivement en Asie du Sud-Est pour lutter contre *P. vivax*. Cependant la primaquine montre une grande toxicité envers les

¹⁸ R. G. Ridley, *Nature*, **2002**, 415, 686-693.

¹⁹ K. J. Palmer, S. M. Holliday, R. N. Brogden, *Drugs*, **1993**, 45, 430-475.

²⁰ P. Olliario, C. Nevill, J. LeBras, P. Ringwald, P. Mussano, P. Garner, P. Brasseur, *Lancet*, **1996**, 348, 1196-1201.

populations déficientes en glucose-6-phosphate-déhydrogénase (G6PD), distribuées dans les zones endémiques au paludisme.²¹

L'artémisinine et les combinaisons thérapeutiques à base d'artémisinine (ACT)

L'artémisinine (**ART**) est une molécule isolée de la plante *Artemisia annua*, une espèce d'armoise nommée « quinghao » en Chine. Les premiers récits attestant de l'efficacité du quinghao, sous forme de soupe ou de poudre, pour traiter les symptômes du paludisme remontent au IV^{ème} siècle. C'est pendant la guerre du Vietnam, alors que l'émergence de souches résistantes de *P. falciparum* était grandissante en Asie du Sud-Est, que la Chine a commencé à développer un programme antipaludique. Après l'échec du criblage massif de milliers de molécules, Tu Youyou s'est intéressée aux techniques de médecine traditionnelle chinoise afin d'essayer d'identifier un traitement efficace contre le paludisme. Très rapidement, les propriétés antipaludiques des extraits de quinghao ont été identifiées et attestées en 1971 conjointement par un essai clinique sur une trentaine de patients atteints par *P. falciparum* ou *P. vivax* et le traitement de singes et de rongeurs. En 1972, le composé actif de cet extrait a été isolé et nommé artémisinine (qinghaosu en chinois) et approuvé en 1986 comme médicament. L'artémisinine est une lactone sesquiterpéنية possédant un groupement endopéroxyde. Dans le même temps, divers composés hémisynthétiques de l'artémisinine, plus efficaces dans le traitement du paludisme, ont été identifiés : la dihydroartémisinine, l'artésunate et l'artémether (**Schéma 1**).

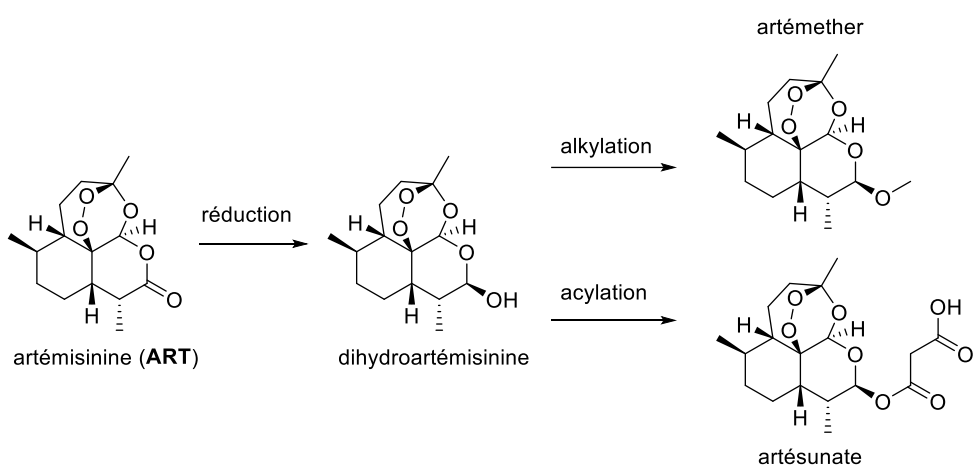


Schéma 1. Structure de l'artémisinine et de ses dérivés.

La dihydroartémisinine est considérée comme le métabolite clé de l'artémisinine *in vivo*. La réduction du pont endopéroxyde de ces composés a mené à une inhibition complète de l'activité antipaludique, indiquant que cette fonction joue un rôle clé dans le mécanisme d'action de ces composés.²²

²¹ a) E. A. Ashley, J. Recht, N. J. White, *Malar. J.* **2014**, *13*, 418; b) G. K. John, N. M. Douglas, L. von Seidlein, F. Nosten, J. K. Baird, N. J. White, R. N. Price, *Malar. J.* **2012**, *11*, 280.

²² Y. Tu, *Angew. Chem. Int. Ed.* **2016**, *55*, 10210–10226.

L'artémisinine et ses dérivés se montrent également très efficaces pour traiter les atteintes liées aux souches résistantes à la **CQ** et d'autres antipaludiques. Les dérivés de l'artémisinine sont aujourd'hui utilisés en majorité, possédant une bien meilleure biodisponibilité orale que cette dernière.

Très rapidement, les dérivés d'artémisinine ont été administrés en combinaison thérapeutique avec d'autres traitements antipaludiques (ACT). En effet, utilisés en monothérapie, les propriétés pharmacocinétiques de ces composés endoperoxides, dont le faible temps de demi-vie dans l'organisme, ont conduit à des échecs de traitements. Les ACT ont l'avantage de compenser ce faible temps de demi-vie avec d'autres molécules antipaludiques et de ralentir également l'émergence d'une résistance croisée des parasites.²³ Les ACTs sont désormais les traitements favorisés par l'OMS, l'artésunate est par exemple utilisé en combinaison avec la mèfloquine ou l'amodiaquine.

Malgré cela, une résistance aux dérivés d'artémisinine a rapidement commencé à émerger, particulièrement en Asie du Sud-Est au Cambodge.^{7, 8} Cependant, il est déjà observé que cette résistance s'étend à court terme dans d'autres régions, et tout particulièrement en Afrique, où les ACTs sont désormais utilisés communément.²⁴ Les parasites « résistants » à l'artémisinine rentrent en dormance, au stade anneau, pendant le traitement antipaludique, favorisant l'apparition de gamétocytes circulants et la transmission des parasites aux moustiques. L'OMS préconise donc de développer de nouvelles molécules tuant les anneaux dans le cycle intraérythrocytaire et les gamétocytes afin de bloquer la transmission parasitaire.²⁵

L'atovaquone.

L'atovaquone est le résultat de plusieurs décennies de recherche de nouveaux traitements antipaludiques de la classe des quinones et plus particulièrement les 2-hydroxynaphтоquinones (**Figure 7**).²⁶ Cette molécule possède une activité antipaludique contre les parasites de stades sanguins supérieure à la **CQ** ou aux dérivés d'**ARTs**.²⁷ L'atovaquone inhibe sélectivement la chaîne de transport des électrons mitochondriale du parasite sans interférer avec celle de l'hôte. Pour cela, il peut se lier au site d'oxydation de l'ubiquinol, forme réduite de la co-enzyme Q₁₀ ubiquinone, et empêche sa réoxydation. Ce cycle redox est indispensable chez le parasite pour la formation des orotates, à partir de la dihydroorotate par l'enzyme dihydroorotate déhydrogénase (DHOD), et la biosynthèse des

²³ R. T. Eastman, D. A. Fidock, *Nat. Rev. Microbiol.* **2009**, 7, 864-874.

²⁴ A. Uwimana, E. Legrand, B. H. Stokes, J.-L. Mangala Ndikumana, M. Warsame, N. Umulisa, D. Ngamije, T. Munyaneza, J.-B. Mazarati, K. Munguti, P. Campagne, A. Criscuolo, F. Ariey, M. Murindahabi, P. Ringwald, D. A. Fidock, A. Mbituyumuremyi, D. Menard, *Nat. Med.* **2020**, 26, 1602-1608.

²⁵ A. Hott, M. S. Tucker, D. Casandra, K. Sparks, D. E. Kyle, *J. Antimicrob. Chemother.* **2015**, 70, 2787-2796.

²⁶ a) A. T. Hudson, A. W. Randall, M. Fry, C. D. Ginger, B. Hill, V. S. Latter, N. McHardy, R. B. Williams, *Parasitology*, **1985**, 90, 45-55. b) L. G. Haile, J. F. Flaherty, *Ann. Pharmacother.* **1993**, 27, 1488-1494.

²⁷ K. McKeage, L. J. Scott, *Drugs*, **2003**, 63, 597-623.

pyrimidines. L'inhibition de la biosynthèse des pyrimidines, briques de départ à la synthèse de l'ADN, mène à un arrêt du développement chez les parasites.²⁸ Ce mode d'action a pu être prouvé en démontrant que des parasites transgéniques exprimant une dihydroorotate déhydrogénase (γ DHOD) de levure, qui utilise le fumarate comme co-facteur au lieu de l'ubiquinone, expriment une résistance à l'atovaquone.²⁹

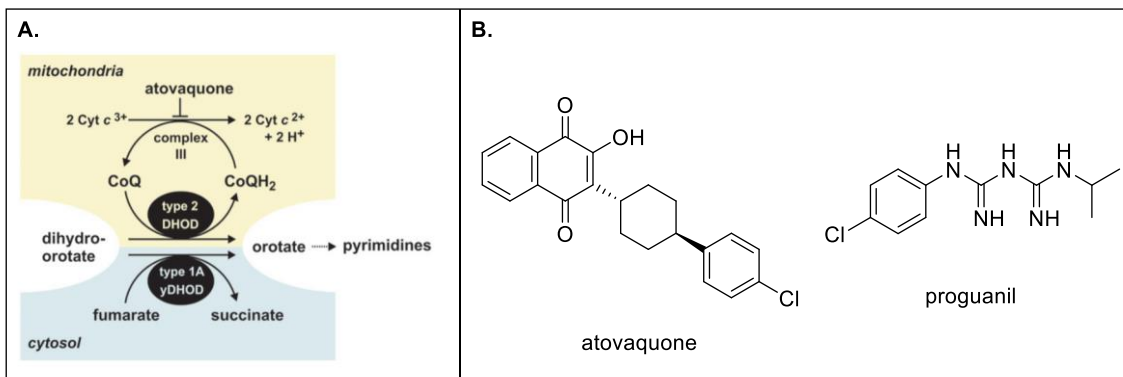


Figure 7. A. Schéma du transport d'électron mitochondrial visé par l'atovaquone chez *P. falciparum*. L'expression du gène codant pour le gène γ DHOD de levure permet au parasite de court-circuiter le transport d'électron basé sur l'ubiquinone et de devenir résistant à l'atovaquone. Schéma copié de la Ref 39. B. Structure de l'atovaquone et du proguanil.

Un an après le lancement de l'atovaquone en monothérapie, des souches de *Plasmodium* ont rapidement montré une résistance au traitement en raison de mutations sur le gène codant pour le complexe bc1 (complexe III de la chaîne de transport des électrons de la mitochondrie). Très rapidement, la recherche d'un partenaire antipaludique dans des tests de combinaison avec l'atovaquone a abouti à la sélection du proguanil, un autre antipaludique, qui montre une synergie en utilisation combinée avec l'atovaquone. C'est cette association, atovaquone-proguanil qui est utilisée exclusivement en bithérapie. Récemment, il a cependant été montré que les parasites résistants à l'atovaquone (mutés au niveau du gène bc1) ne peuvent pas se reproduire efficacement chez le moustique ce qui empêche la réplication rapide des souches résistantes à l'atovaquone chez le moustique.³⁰ En d'autres mots, la résistance à l'atovaquone bloque la transmission des parasites chez le moustique, et donc les parasites résistants à l'atovaquone ne peuvent pas être transmis à un autre mammifère ou à l'homme.

²⁸ G. L. Nixon, D. M. Moss, A. E. Shone, D. G. Laloo, N. Fisher, P. M. O'Neill, S. A. Ward, G. A. Biagini, *J. Antimicrob. Chemother.*, **2013**, 68, 977-985.

²⁹ H. J. Painter, J. M. Morrisey, M. W. Mather, A. B. Vaidya, *Nature*, **2007**, 446, 88-91.

³⁰ C. D. Goodman, J. E. Siregar, V. Mollard, J. Vega-Rodríguez, D. Syafruddin, H. Matsuoka, M. Matsuzaki, T. Toyama, A. Sturm, A. Cozijnse, M. Jacobs-Lorena, K. Kita, S. Marzuki, G. I. McFadden, *Science*, **2016**, 352, 349-353.

2. La plasmodione et les 3-benzylménadiques comme candidats-médicaments antipaludiques potentiels.

2.1. Les 1,4-naphtoquinones.

Les 1,4-naphtoquinones (**NQ**) sont une classe de composés rédox-actifs présents au sein de nombreux produits naturels et synthétiques et présentant de nombreuses activités biologiques de type anticancéreuse³¹ ou bien, comme nous avons pu le voir avec l'atovaquone, antiparasitaire.³² Cette activité biologique est très souvent reliée à leurs propriétés rédox, les **NQs** sont capables d'accepter 1 ou 2 électrons et le potentiel de réduction est grandement influencé par les substituants portés par le cœur électroactif (**Schéma 2**).³³

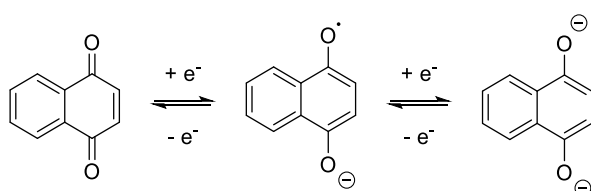


Schéma 2. Equilibre rédox des NQs.

Parmi les **NQs**, on peut notamment citer la famille des vitamines K. La vitamine K₁ et la vitamine K₂ sont des molécules naturelles synthétisées, respectivement, par les plantes et les bactéries de la flore intestinale. Quant à la vitamine K₃, aussi appelée ménadione, c'est une 1,4-naphthoquinone synthétique méthylée en position 2 (Figure 8).

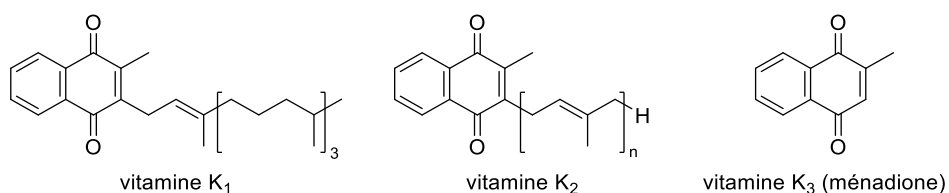


Figure 8. Structure des vitamines K.

Il a été montré que les **NQs** sont des substrats efficaces pour inhiber les glutathion réductases humaine (**hGR**) et de *P. falciparum* (**PfGR**).³⁴ Au début du projet, en 2005, l'intérêt des molécules ciblant les deux GR du globule rouge parasité était lié au fait que les globules rouges parasités montraient une concentration plus élevée en glutathion réduit (GSH) et un flux de formation très important en glutathion disulfure (GSSG) produit à cause de la digestion de l'hémoglobine de l'hôte par le parasite,

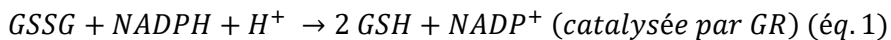
³¹ C. E. Pereyra, R. F. Dantas, S. B. Ferreira, L. P. Gomes, F. P. Silva-Jr, *Cancer Cell. Int.* **2019**, *19*, 207.

³² O. P.S. Patel, R. M. Beteck, L. J. Legoabe, *Eur. J. Med. Chem.* **2020**, *210*, 113084.

³³ P. Sidorov, I. Desta, M. Chessé, D. Horvath, G. Marcou, A. Varnek, E. Davioud-Charvet, M. Elhabiri, *ChemMedChem*, **2016**, *11*, 1339-1351.

³⁴ E. Davioud-Charvet, S. Delarue, C. Biot, B. Schwöbel, C. C. Boehme, A. Müssigbrodt, L. Maes, C. Sergheraert, P. Grellier, R. H. Schirmer, K. Becker, *J. Med. Chem.* **2001**, *44*, 4268-4276.

qui produit aussi un intense stress oxydant. Le GSSG produit est re-réduit une réaction catalysée par la **PfGR** à l'aide de NADPH (éq 1).



Cette réaction est inhibée par les **NQs** qui agissent comme des substrats subversifs de la **GR** et consomment ainsi le NADPH de la cellule (éq. 2) en présence d'oxygène moléculaire (éq. 3).³⁵



Plusieurs dérivés alkylés de la ménadione ont été ainsi synthétisés et testés comme substrats subversifs des deux **GRs**. Notamment des molécules duales portant également des motifs quinoléines pour augmenter la pénétration des molécules finales dans le parasite.^{34, 36}

Aucune toxicité accrue liée à l'inhibition de la **hGR** n'était attendue car la majorité des cellules nucléées chez l'hôte peuvent contrôler le flux GSSG/GSH, même en présence d'un inhibiteur réversible de hGR. Par contre, le globule rouge n'étant pas une cellule à noyau qui peut compenser rapidement la destruction de l'homéostasie rédox, la présence d'un inhibiteur de la **hGR** entraîne du stress oxydant, condition hostile pour le développement parasitaire. La meilleure illustration est donnée par les humains porteurs de mutations en G6PD qui ont des globules rouges qui produisent naturellement du stress oxydant du fait d'un flux plus faible en NADPH. Ces mêmes porteurs peuvent être infectés par le parasite du paludisme mais feront des accès palustres beaucoup moins importants que les porteurs du gène g6pd sain (non déficients en G6PD) car le milieu hostile induit par le stress oxydant dans leurs érythrocytes est suffisant pour ralentir la progression de l'infection parasitaire.

C'est ce raisonnement qui a été à l'origine de la stratégie de l'équipe : mimer les effets des mutations naturelles en G6PD avec des inhibiteurs des deux **GRs** qui agissent comme substrats subversifs en produisant du stress oxydant dans le globule rouge parasité mais pas dans les globules rouges sains.

³⁵ C. Biot, H. Bauer, R. H. Schirmer, E. Davioud-Charvet, *J. Med. Chem.* **2004**, 47, 5972-5983.

³⁶ W. Friebolin, B. Jannack, N. Wenzel, J. Furrer, T. Oeser, C. P. Sanchez, M. Lanzer, V. Yardley, K. Becker, E. Davioud-Charvet, *J. Med. Chem.* **2008**, 51, 1260-1277.

2.2. La plasmodione.

Suite à ce travail de prospection, mon équipe d'accueil a développé une chimie basée sur la ménadione en introduisant de la diversité structurale et a pu identifier une série de 3-benzylménadiques (**BMd**) possédant une activité antipaludique *in vitro* de l'ordre du bas nanomolaire contre *P. falciparum* (Figure 9).³⁷

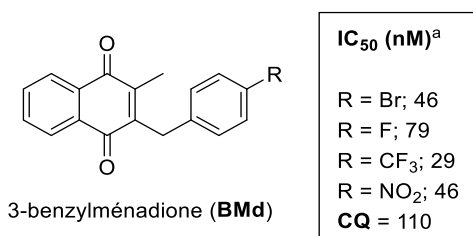


Figure 9. Structure des BMds et leur activité antipaludique *in vitro* comparée à celle de la chloroquine (CQ). ^aLes valeurs des IC₅₀ ont été calculées sur des souches de *P. falciparum* Dd2 en utilisant le test basé sur l'incorporation de ³H-hypoxanthine.

Comme nous pouvons le voir sur la Figure 9, la **BMd** fonctionnalisée par un trifluorométhyle en position *para* du groupement benzyle (i.e. 3-[4-(trifluoromethyl)benzyl]-menadione) est le composé possédant la meilleure activité *in vitro* (IC₅₀ : 29 nM). Ce composé a été nommé plasmodione (**PD**) et a été extensivement étudié par l'équipe pendant ces dernières années.

Le profil détaillé de l'activité antipaludique de **PD** sur la phase sanguine de *P. falciparum* *in vitro* a révélé : (i) une activité antipaludique importante sur la forme asexuée de *P. falciparum* sur des souches résistantes à différents médicaments (Figure 10) mais aussi sur les gamétocytes précoce, (ii) un profil toxicologique sûr pour une utilisation humaine, (iii) une activité importante contre les anneaux intra-érythrocytes, (iv) une efficacité aussi rapide que celle de l'artémisinine, (v) un faible potentiel de développement d'une résistance médicamenteuse et (vi) un effet synergique avec divers médicaments déjà sur le marché, dont la déhydroartémisinine.³⁸

³⁷ T. Müller, L. Johann, B. Jannack, M. Brückner, D. A. Lanfranchi, D. H. Bauer, C. Sanchez, V. Yardley, C. Deregnaucourt, J. Schrével, M. Lanzer, R. H. Schirmer, E. Davioud-Charvet, *J. Am. Chem. Soc.* **2011**, *133*, 11557-11571.

³⁸ K. Ehrhardt, C. Deregnaucourt, A.-A. Goetz, T. Tzanova, V. Gallo, P. Arese, B. Pradines, S. H. Adjalley, D. Bagrel, S. Blandin, M. Lanzer, E. Davioud-Charvet, *Antimicrob. Agents Chemother.* **2016**, *60*, 5146-5158.

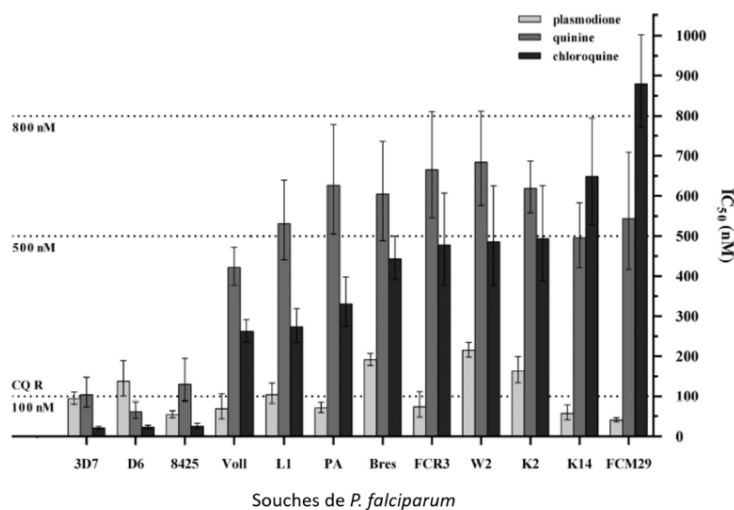


Figure 10. Activités antipaludiques in vitro de PD, la CQ et la quinine contre différentes souches résistantes de *P. falciparum* originaires d'Asie, d'Afrique et d'Amérique du Sud. Les résultats sont présentés sous forme d' IC_{50} avec un intervalle de confiance de $\pm 95\%$ pour de 3 à 5 expériences indépendantes du test basé sur l'incorporation de 3H -hypoxanthine. Figure copiée de la Ref 38.

Cependant, les tests d'activité sur *P. berghei* et le modèle murin montrent une activité modérée *in vivo*, ce qui suggère une biodisponibilité faible de la molécule, ou bien une métabolisation et élimination rapide. C'est pour ces raisons qu'il a été nécessaire de développer de nouveaux dérivés de **PD** plus adaptés.

2.3. Mode d'action de la plasmodione.

L'atovaquone et la **PD** sont toutes les deux des **NQs** avec des structures similaires mais des propriétés rédox très différentes. Il a été démontré que les deux molécules n'ont pas le même mécanisme d'action pour inhiber la croissance des parasites. Tout d'abord, contrairement à **PD** et aux dérivés de ménadiones, l'atovaquone n'est pas un bon substrat de la **GR** humaine ou de *P. falciparum*³⁹ à cause de ses potentiels redox très différents à ceux de la **PD**. La **PD** est une molécule oxydante au contraire de l'atovaquone. Cette différence de mécanisme s'accompagne aussi d'effets phénotypiques très distincts : la **PD** entraîne un retard dans la progression du cycle parasitaire sur 48 h, et ceci est accru sur 96 h : les parasites meurent en montrant des formes anneaux pycnotiques ou abbérantes (avec plusieurs noyaux) suggérant une mort par stress oxydant.⁴⁰ De plus, en utilisant les parasites transgéniques de Painter et al.,²⁹ qui expriment la γ DHOD, insensibles à l'atovaquone, les mêmes parasites restent toujours très sensibles à la **PD** dans le bas nM. Ceci suggère que la **PD** n'interagit pas avec le complexe III de la chaîne de transfert d'électrons comme le fait l'atovaquone.

³⁹ D. A. Lanfranchi, D. Belorgey, T. Müller, H. Vezin, M. Lanzer, E. Davioud-Charvet, *Org. Biomol. Chem.* **2012**, *10*, 4795-4806.

⁴⁰ K Ehrhardt, E. Davioud-Charvet, H. Ke, A. B. Vaidya, M. Lanzer, M. Deponte. *Antimicrob. Agents Chemother.* **2013**, *57*, 2114-2120.

Un mécanisme d'action impliquant les propriétés rédox de **PD** a donc été proposé sur l'hypothèse que le stress oxydant intense produit dans le globule rouge produira des réactions d'oxydation sur toute molécule exogène. La bioactivation de la **PD** a donc été proposée comme étant une cascade de réactions rédox passant par : (i) une oxydation benzylique de la **PD** vers la 3-benzoylménadione correspondante (**PDO**), (ii) la **PDO** est ensuite réduite par le couple NADPH/**PfGR** ou tout autre enzyme, (iii) la forme réduite de **PDO** est réoxydée par la méthémoglobine (metHb) et génère continuellement de l'(oxy)hémoglobine (Hb) non digestible pour le parasite, (iv) ce processus augmente également la formation de dérivés réactifs de l'oxygène provoquant des dégâts cellulaires, (v) la forme réduite de **PDO** est proposée pour former par couplage oxydatif phénolique la benzoxanthone correspondante qui inhibe la formation de beta-hématine (hémozoïne synthétique), de façon aussi puissante que la **CQ**, dans un test *in vitro* (Figure 11).⁴¹

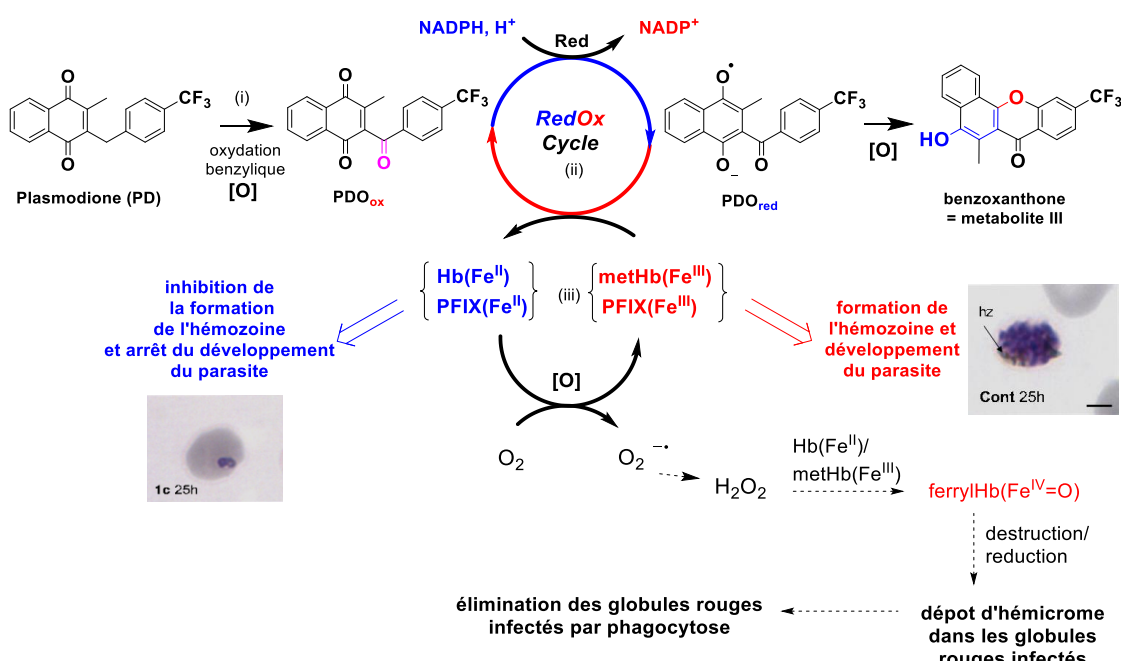


Figure 11. Mécanisme hypothétique du mode d'action de la plasmodione.

Il a également été montré que le méthyle en position C-2 du cœur ménadione et l'unité benzylique sont indispensables à l'activité antipaludique des dérivés **BMds**. Ceci renforce l'hypothèse d'une oxydation benzylique *in situ*.³⁷ Similairement, un dérivé méthylé sur les positions 2' et 6' de la chaîne benzylique perd son activité antipaludique, un tel dérivé ne pouvant pas former la benzoxanthone correspondante (résultats non publiés).

⁴¹ M. Bielitzka, D. Belorgey, K. Ehrhardt, L. Johann, D. A. Lanfranchi, V. Gallo, E. Schwarzer, F. Mohring, E. Jortzik, D. L. Williams, K. Becker, P. Arese, M. Elhabiri, E. Davioud-Charvet, *Antioxid. Redox Signal.* **2015**, 22, 1337-1352.

3. Synthèse de naphtoquinones fonctionnalisées.

La diversité structurale des **BMds** peut être divisée en 2 sous parties, la partie « Ouest » qui comprend les fonctionnalisations du cœur ménadione et la partie « Est » concernant la chaîne benzylique (**Figure 12**).

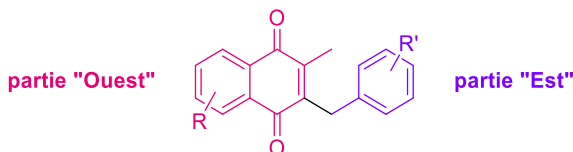


Figure 12. Partie "Ouest" et "Est" des 3-benzylménadiques.

Dans cette 3^{ème} partie, nous allons revenir sur les efforts de synthèse précédemment effectués au sein du laboratoire pour introduire de la diversité structurale, non seulement sur les **BMds** antipaludiques que ce soit pour la partie « ouest » ou « est », mais aussi sur certains métabolites supposés, dont les 3-benzoylménadiques. Enfin un article de revue a été réalisé durant cette thèse pour faire l'inventaire des réactions radicalaires d'alkylation des quinones décrites récemment dans la littérature.

Jusqu'à maintenant, la voie privilégiée pour la synthèse des **BMds** est la réaction de Kochi-Anderson, via les conditions décrites par Jacobsen et Torsell.⁴² Cette réaction de décarboxylation radicalaire à l'avantage de former efficacement la plasmodione à l'échelle multi-gramme en une seule étape à partir de la ménadione et de l'acide 4-(trifluorométhyl)phénylacétique (**Schéma 3**). Un mécanisme détaillé de cette transformation est explicité dans la revue Partie 3.3 de ce Chapitre.



Schéma 3. Synthèse de la plasmodione par la réaction de Kochi-Anderson.

Cette méthodologie a été appliquée dans le laboratoire pour la synthèse efficace de centaines de dérivés de **PD**. Cependant, tous les acides phénylacétiques complexes ne sont pas commerciaux et leur synthèse peut s'avérer fastidieuse. L'introduction directe de cycle hétéroaromatique par cette réaction s'est révélée difficile, voire impossible dans une grande majorité de cas,⁴³ alors que ces motifs présentent des propriétés physicochimiques intéressantes en chimie médicinale, incluant notamment

⁴² a) N. Jacobsen, K. Torsell, *Acta Chem. Scand.* **1973**, 27, 3211-3216. b) J. Goldman, N. Jacobsen, K. Torsell, *Acta Chem. Scand.* **1974**, 28b, 492-500. c) J. M. Anderson, J. K. Kochi, *J. Am. Chem. Soc.* **1970**, 92, 1651–1659.

⁴³ D. A. Lanfranchi, E. Cesar-Rodo, B. Bertrand, H.-H. Huang, L. Day L, L. Johann, M. Elhabiri, K. Becker, D. L. Williams, E. Davioud-Charvet, *Org. Biomol. Chem.* **2012**, 10, 6375–6387.

une solubilité accrue dans les milieux aqueux par rapport aux cycles aromatiques carbonés.^{43, 44} Un autre frein à cette synthèse est que les dérivés de ménadione commerciaux sont très peu nombreux (la ménadione et la 5-hydroxy-ménadione appelée plumbagine). La synthèse de dérivés de ménadiques fonctionnalisées a donc fait l'objet de nombreux développements au sein de l'équipe. Dans un second temps, nous nous intéresserons à la synthèse des dérivés 3-benzoylménadiques et enfin nous avons écrit une mini-revue recensant les méthodes récentes d'alkylations radicalaires de quinones.

3.1. Synthèse de ménadiques fonctionnalisées.

Au cours de ces dernières années, deux stratégies générales de synthèses ont été mises en place dans l'équipe pour obtenir un grand nombre de dérivés de la ménadione incluant des analogues azotés (**Schéma 4**).

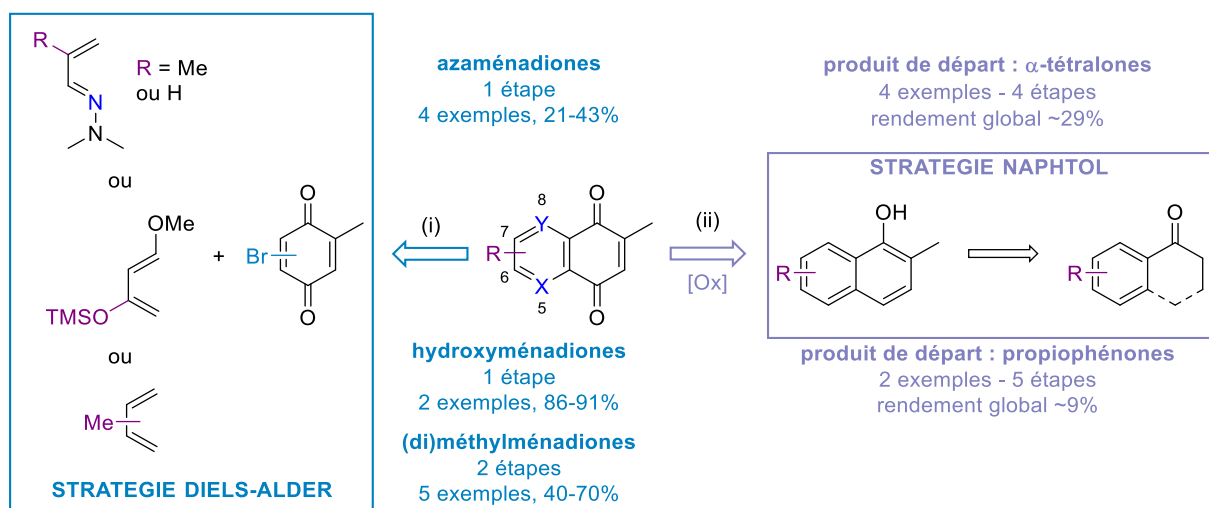


Schéma 4. Stratégies Diels-Alder et Naphtol.

Celles-ci ont été appelée stratégie « Diels-Alder/hétéro-Diels-Alder » et « Naphtol ». Comme leur nom l'indique, (i) la stratégie « Diels-Alder » repose sur une réaction de Diels-Alder entre une bromoquinone et un diène pour former en une ou deux étapes les (aza)ménadiques correspondantes et (ii) la stratégie naphtol, qui passe par un naphtol intermédiaire clé de la stratégie éponyme pour former la quinone après oxydation en *para* à partir de tétralones ou de propiophénones (**Schéma 4**).^{43,}

⁴⁵

⁴⁴ T. J. Ritchie, S. J. F. Macdonald, R. J. Young, S. D. Pickett, *Drug Discov. Today*, **2011**, *16*, 164-171.

⁴⁵ E. Cesar Rodo, L. Feng, M. Jida, K. Ehrhardt, M. Bielitz, J. Boilevin, M. Lanzer, D. L. Williams, D. A. Lanfranchi, E. Davioud-Charvet, *Eur. J. Org. Chem.* **2016**, 1982–1993.

Stratégie Diels-Alder.

La formation régiosélective de dérivés de la ménadione repose sur l'utilisation de deux méthylbenzoquinones comme diénophiles (2-bromo-5-méthylbenzoquinone et 2-bromo-6-méthylbenzoquinone).

Une synthèse précédemment décrite⁴⁶ a été optimisée dans mon équipe, au niveau des étapes de l'élimination de HBr et de diméthylamine, après cycloaddition entre la quinone halogénée et le dérivé azadiène pour obtenir les azaménadienes désirées avec des rendements modérés. L'excès d'anhydride acétique (Ac_2O) utilisé a pour but de piéger la diméthylamine formée pour éviter des réactions secondaires (**Schéma 5**).⁴²

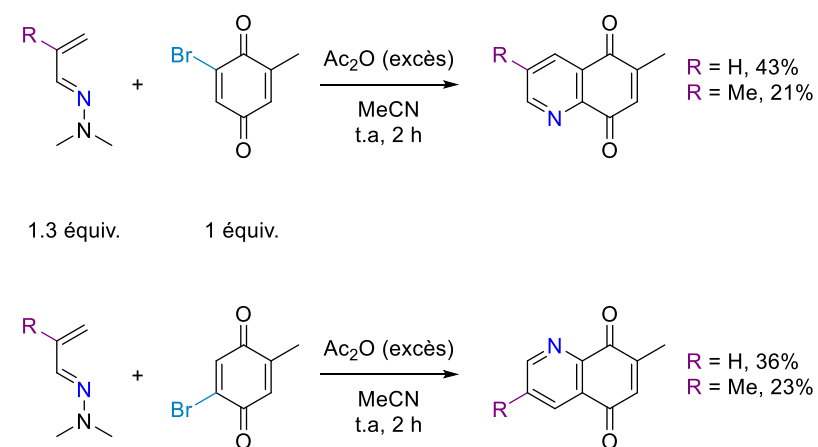


Schéma 5. Synthèse d'azaménadienes par réaction d'aza-Diels-Alder.

Le diène de Danishefsky réagit similairement avec les bromoquinones pour former en une seule étape, après cycloaddition, élimination de HBr et de méthanol, des hydroxyménadienes avec de très bons rendements (**Schéma 6**).⁴⁵ Il est à noter l'ajout de pyridine qui est capitale pour éviter la dégradation totale du cycloadduit si HBr n'est pas piégé par cette base (les autres bases participent à la dégradation de la menadione formée).

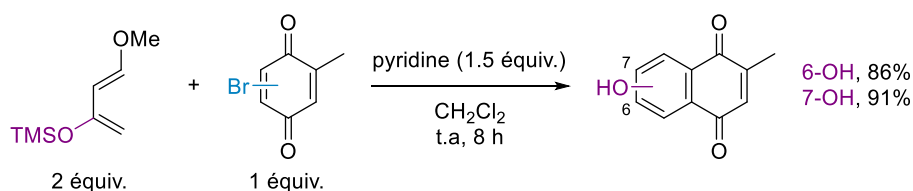


Schéma 6. Synthèse d'hydroxyménadione par réaction de Diels-Alder.

Enfin, plusieurs ménadienes mono ou diméthylées ont été obtenues en 2 étapes à partir du pipérylène, l'isoprène et du 2,3-diméthyl-1,3-butadiène qui réagissent avec les quinones bromées sous catalyse

⁴⁶ C. Morin, T. Basset, J.-C. Moutet, M. Fayolle, M. Bruckner, D. Limosin, K. Becker, E. Davioud-Charvet, *Org. Biomol. Chem.* **2008**, 6, 2731-2742.

acide pour former le cycloadduit correspondant. Ce dernier est ensuite oxydé à l'aide de DDQ pour former la ménadione méthylée correspondante (**Schéma 7**).⁴⁴

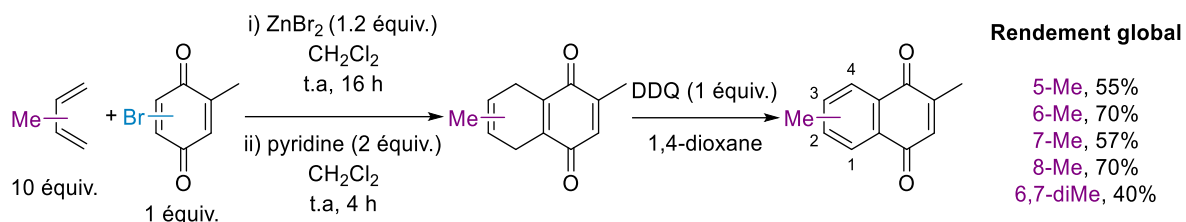


Schéma 7. Synthèse de (di)méthylménadiques par réaction de Diels-Alder.

Stratégie naphtol.

La stratégie naphtol repose sur la formation en plusieurs étapes de méthynaphhtols fonctionnalisés qui sont ensuite oxydés sélectivement en ménadiques. Pour cela, deux classes de molécules simples et commerciales ont été utilisées afin d'obtenir des ménadiques fonctionnalisées en position 6 et 7.

En partant d' α -tétralones, les méthynaphhtols correspondants sont synthétisés en 3 étapes successives via condensation du formiate d'éthyle, aromatisation de l'alcool correspondant à l'aide de DDQ et enfin réduction de l'aldéhyde vers le méthyle final. La principale limitation de cette synthèse est notamment le faible nombre d' α -tétralones commerciales (**Schéma 8**).⁴⁵

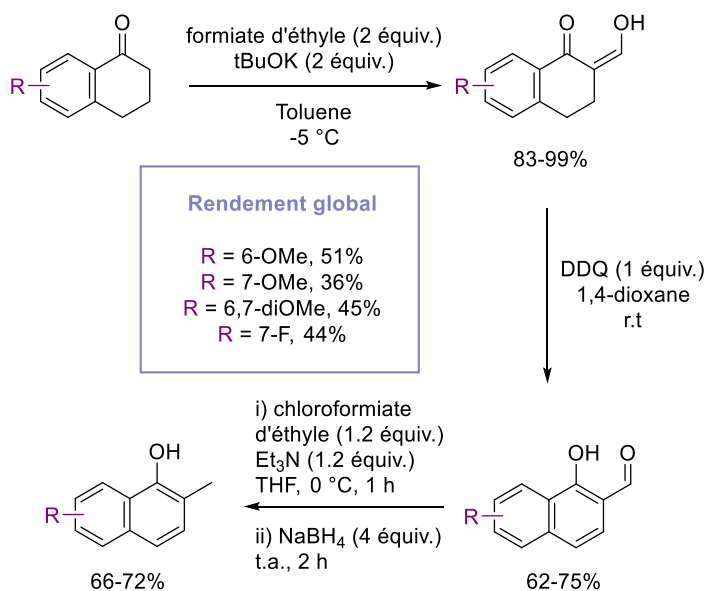


Schéma 8. Synthèse de méthynaphhtols en 3 étapes à partir d' α -tétralones.

L'autre méthode consiste à bromer des propiophénones en position α de la cétone, l'halogène étant ensuite substitué par l'éthylxanthate de potassium pour obtenir les α -xanthate propiophénones. Ces composés sont ensuite transformés en tétralones par l'intermédiaire de la procédure de Zard par la succession d'une addition radicalaire catalysée par le peroxyde de dilaurolate (DLP) et d'une cyclisation intramoléculaire. L'alcool protégé résultant est ensuite déshydraté en présence d'APTS pour former le

naphtol correspondant (**Schéma 9**). Cette synthèse permet d'obtenir sélectivement des naphtols fonctionnalisés en position C-6 ; cependant elle souffre d'un rendement très faible sur l'étape de formation de la tétralone.⁴⁵

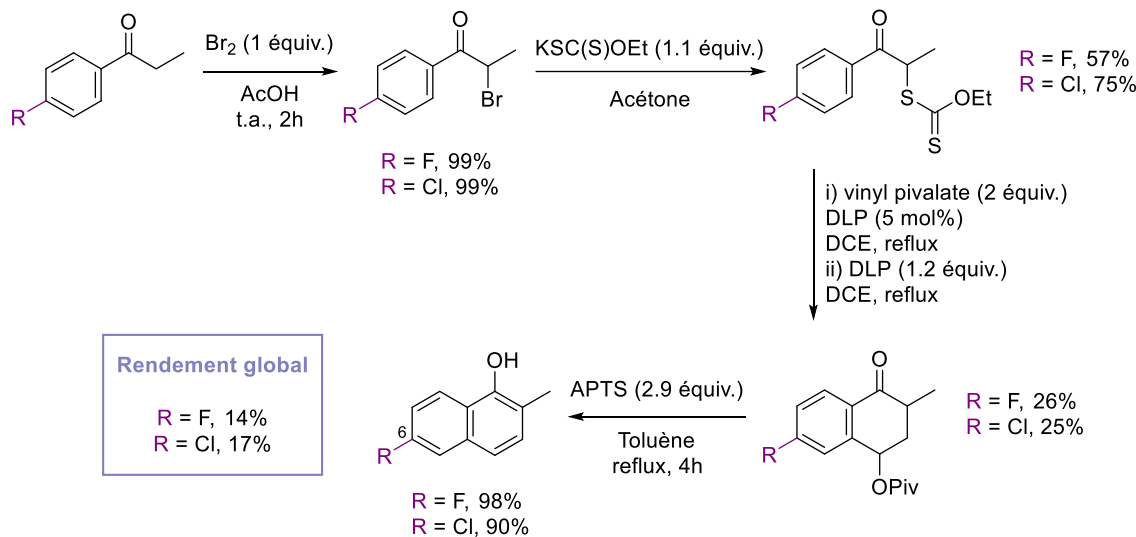


Schéma 9. Synthèse de méthynaphtols en 4 étapes à partir de 6-halogénopropiophénones.

Les naphtols synthétisés par les deux voies de synthèse sont ensuite oxydés sélectivement par le diacétate de iodobenzène (PIDA) pour former les **NQs** correspondantes (**Schéma 10**).⁴⁴

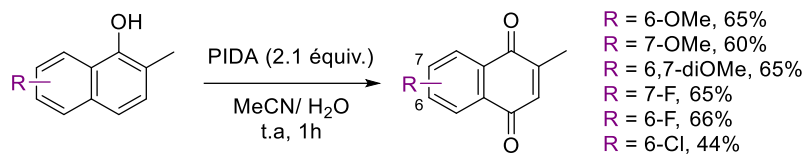


Schéma 10. Oxydation des méthynaphtols par PIDA.

Synthèse directe de 3-benzylménadiones fonctionnalisées sur la partie « ouest » et « est ».

La stratégie de formation de méthynaphtol à partir d'α-tétralones a également été exploitée pour synthétiser par une voie alternative des 3-benzylménadiones fonctionnalisées sur la partie ménadione et la partie benzyle. A partir de tétralones et via une séquence de condensation du 4-trifluorobenzaldéhyde, aromatisation et oxydation, les 1,4-naphtoquinones benzylées sont obtenues avec d'excellents rendements. Celles-ci sont ensuite méthylées par la réaction de Kochi-Anderson pour former les dérivés 3-benzylménadiones correspondants. Cette dernière étape limite cependant le rendement global de synthèse. Il s'agissait au début de cette thèse de la seule voie de synthèse vers les **BMds**, alternative à la benzylation radicalaire directe de ménadiones (**Schéma 11**).

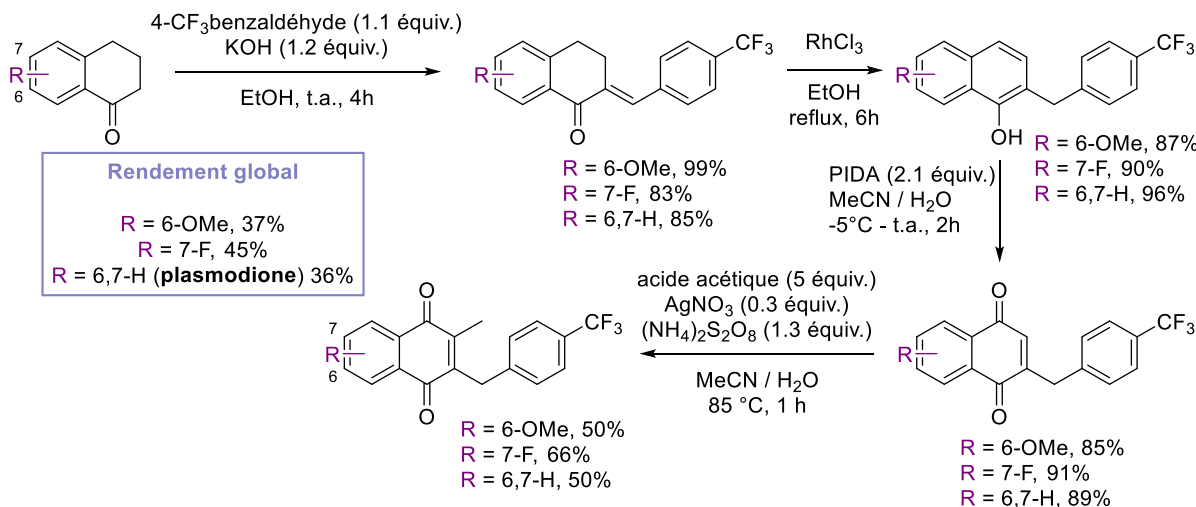


Schéma 11. Synthèse directe de dérivés de plasmodione à partir de téralones.

3-benzylménadions fonctionnalisés sur la partie « ouest », activité antipaludique et perspectives.

Les (aza)ménadions obtenues par les deux stratégies vues précédemment ont permis de synthétiser, grâce à la réaction de Kochi-Anderson, toute une série de 3-benzyl(aza)ménadions pour lesquelles l'activité antipaludique a été déterminée. L'activité des azaménadions benzylées s'est révélée très faible vis-à-vis d'une souche résistante à la chloroquine de *P. falciparum*. Cependant ces composés ont montré une activité intéressante contre le parasite *Schistosoma mansoni*.⁴³ Concernant la série de ménadions fonctionnalisées sur le cycle aromatique de la quinone, les positions 6 et 7 sont les deux positions qui tolèrent des substituants sans une grande perte d'activité antipaludique, avec notamment la 6-fluoroplasmidine qui affiche une activité semblable à celle de la PD (**Figure 13**).

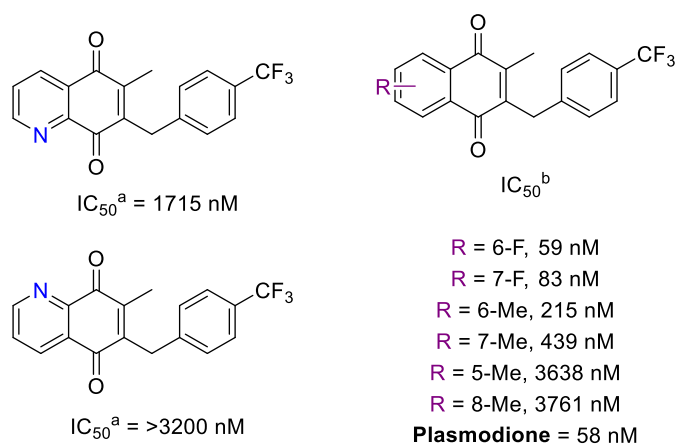


Figure 13. Sélection d' IC_{50} de dérivés de plasmodione modifiés sur la partie "ouest". ^aValeurs rapportées de la Ref 43.
^bValeurs rapportées de la Ref 45.

Ces 2 positions se révèlent également être les positions les plus intéressantes à fonctionnaliser sur les **BMds** étant donné que les 6 et 7-hydroxyplasmidine sont des métabolites supposés d'élimination *in*

vivo de la **PD** par les cytochromes P450 hépatiques.⁴⁷ Fonctionnaliser ces positions pourraient donc permettre d'obtenir un composé moins susceptible d'être éliminé rapidement de l'organisme. Des souris traitées par la **PD** éliminent la molécule majoritairement sous forme de 6-hydroxy-**PD** et de son ester glucuronide dans les urines.

Tout le travail réalisé sur la synthèse de ces substrats a donc permis de mieux identifier les structures intéressantes pour le projet médicinal de nouvelles naphtoquinones antipaludiques. En conséquence, du fait de notre intérêt poussé pour les ménadiques fonctionnalisées en position 6, une nouvelle voie de synthèse à partir de propiophénones, plus performante que celle vue précédemment, est en cours de développement au sein de notre équipe.

3.2. Synthèse des 3-benzoylménadiques.

Les 3-benzoylménadiques, métabolites supposés des **BMDs**, ont tout d'abord été synthétisés par l'oxydation benzylique des **BMDs** en présence d'acide périodique et de d'oxyde de chrome. Cette méthode a permis facilement d'obtenir les dérivés benzoyles correspondants. Cependant les rendements d'oxydation sont au mieux modérés et tous les composés ne sont pas compatibles. Nous sommes donc limités par les **BMDs** déjà accessibles.³⁷ Une autre solution envisagée a été l'addition d'un organolithien sur un chlorure de benzoyle pour former après déprotection la quinone désirée. Cependant les chlorures de benzoyles sont sensibles à l'eau et ne sont pas tous commerciaux. De plus, l'utilisation d'un organolithien pourrait limiter les fonctionnalisations compatibles avec ce couplage et les rendements obtenus par cette méthode sont très inégaux (**Schéma 12**).³³

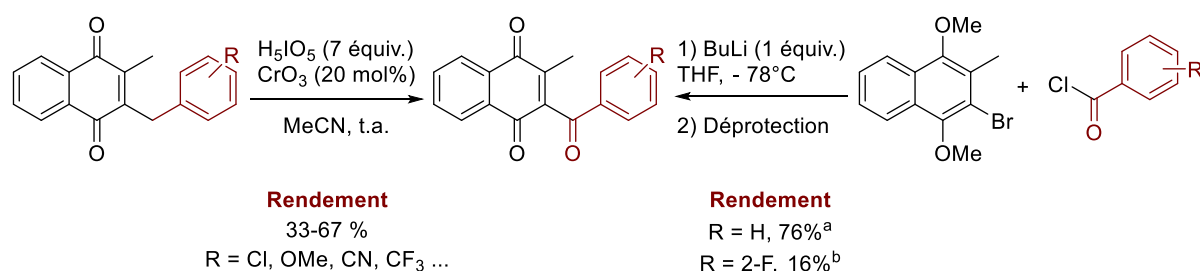


Schéma 12. Les deux voies de synthèses utilisées pour la synthèse de 3-benzoylménadiques.^a Déprotection : CAN (3 équiv.), MeCN / H₂O, t.a. ^bDéprotection : BBr₃ (1 équiv.), CH₂Cl₂, t.a.

En tant que métabolite supposé de la **PD** et des **BMDs** en général, il est important de développer une synthèse globale de 3-benzoylménadiques pour pouvoir mieux comprendre son interaction avec les cibles biologiques dans des conditions biomimétiques. Aussi, introduire de la diversité structurale sur la chaîne benzoyle nous permettrait également de mesurer les potentiels d'oxydo-reduction et les vitesses de réduction par différentes oxydo-réductases parasitaires afin d'établir des relations

⁴⁷ L. Feng, D. A. Lanfranchi, L. Cotos, E. Cesar-Rodo, K. Ehrhardt, A.-A. Goetz, H. Zimmermann, F. Fenaille, S. A. Blandin, E. Davioud-Charvet, *Org. Biomol. Chem.* **2018**, *16*, 2647-2665.

structure-activité de ces substrats subversifs. Pour les meilleurs substrats, nous pourrions ainsi synthétiser les **BMds** correspondantes pour tester l’activité antipaludique.

3.3. Article 1. Mini-revue

Recent Advances in Direct C-H Radical Alkylation of 1,4-Quinones

Maxime Donzel, Deniz Karabiyikli, Leandro Cotos, Mourad Elhabiri, Elisabeth Davioud-Charvet

Manuscript soumis

Recent Advances in Direct C-H Radical Alkylation of 1,4-Quinones

Maxime Donzel^[a], Deniz Karabiyikli^[a], Leandro Cotos^[a], Mourad Elhabiri^[a], Elisabeth Davioud-Charvet^{*[a]}

[a] M. Donzel, Deniz Karabiyikli, Dr. Leandro Cotos, Dr Mourad Elhabiri, Dr. Elisabeth Davioud-Charvet
UMR7042 Université de Strasbourg-CNRS-UHA, Laboratoire d'Innovation Moléculaire et Applications (LIMA) Team Bio(IN)organic and Medicinal Chemistry, European School of Chemistry, Polymers and Materials (ECPM), 25 Rue Becquerel, Strasbourg 67087, France
E-mail: elisabeth.davioud@unistra.fr

Abstract: 1,4-quinones display unique redox and biological properties and have multiple applications in a wide array of fields, including health. Synthesis of diversely-substituted quinone-based compounds remains difficult and usually consists of multiple step sequences. Interest in direct C-H radical alkylation of 1,4-quinones has thus continuously grown over this last decade. These reactions involve addition of carbon-centered radicals generated from radical precursors through decarboxylative alkylation, hydrogen-atom

abstraction, or by carbon-halogen bond reduction. Recent progresses in radical chemistry, including photoredox catalysis, have provided useful tools for quinone functionalization. This review describes the recent progress with these methodologies, including the new promising three-component cascade reactions involving quinones and alkenes, allowing the preparation of complex substituted 1,4-quinones in a single step.

1. Introduction

The 1,4-quinones represent an important class of ubiquitous compounds in nature, especially in plants, bacteria or fungi. This scaffold displays exhibits remarkable redox properties due to its alternating Csp^2 and Csp bonds and electron-deficient nature acting as a 1- or 2-electron reversible and efficient redox cycler. It is responsible for a wide range of biological activities in different key pathways. Among the numerous examples is the vital role of the isoprenoid quinone coenzyme Q₁₀ (also called ubiquinone)^[1] in cellular bioenergetics, serving as a main cofactor in the mitochondrial electron transport chain of eukaryotic cells through aerobic respiration and ATP production. Another example is the role of vitamin K (Figure 1)^[2] involved in the carboxylation of glutamate residues for the regulation of prominent physiological mechanisms such as blood coagulation, bone metabolism or neuroprotection.^[3]

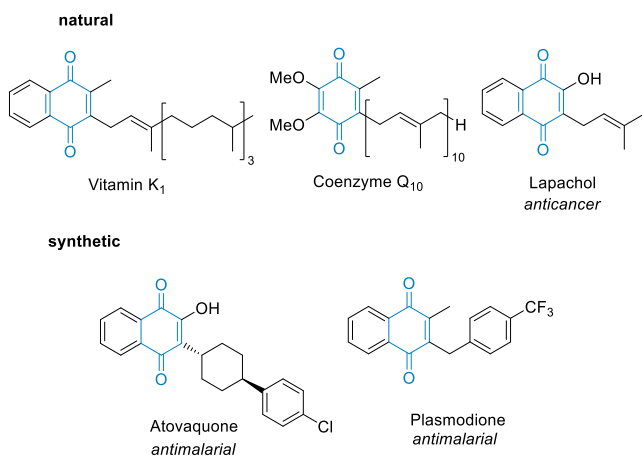


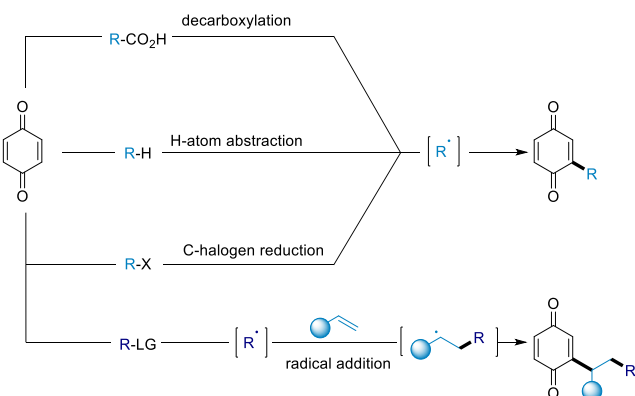
Figure 1. Natural and synthetic alkylated 1,4-quinones.

Compounds containing a quinone core also serve as important building blocks in synthetic chemistry, in various fields,^[4] most notably in medicinal chemistry. For instance, some 1,4-quinones display potent antimalarial,^[5] antibiotic or anticancer^[6] activities.

Their unique redox properties were shown essential for the design of quinoidal systems as activable fluorescent probes for biological imaging.^[7]

Radical chemistry has existed since the origins of organic chemistry, when it appeared in the early 19th century. It was historically considered uncontrollable and chaotic. However, it has slowly emerged as a major component of organic synthesis (frequently referred to the renaissance of radical chemistry)^[8] thanks to both the development of new methodologies and the elucidation of radical mechanisms. Due to the remarkable capacity of quinones to act as efficient radical acceptors,^[9] radical chemistry has become an essential field in its own right for molecular functionalization, and many synthetic processes have been described in literature in the last ten years.

In this review article, we will mainly focus on the very recent advances in quinone alkylation, since this field has been evolving very rapidly over the last few years. Arylations and other functionalization of quinones, partly based on intramolecular photoredox reactions, have been thoroughly discussed in two recent reviews, and no significant breakthroughs have been described since.^[10] For this reason, except few cases, previously reviewed alkylation processes will not be expanded in further detail in this report.



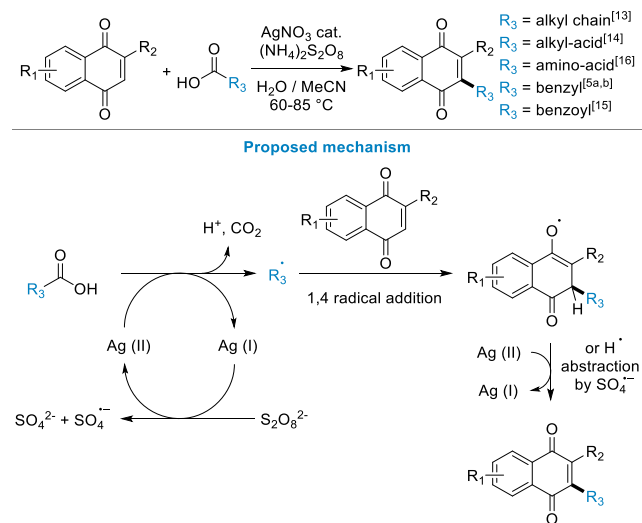
Scheme 1. Different methods of radical alkylation reviewed in this article.

Radical alkylation of quinones generally involves the addition of a carbon-centered radical generated from a radical precursor. The latter is often activated by an external agent such as a transition metal, an oxidant or a reductant. Here, we will review the formation of alkyl radicals generated from, which are currently the main three processes used for direct functionalization of quinone with carbon-centered radicals. We will also explore the broad diversity of three-component cascade reactions involving quinones and alkenes, which have been extensively developed very recently, opening the field to the preparation of complex substituted 1,4-quinones in a single step (Scheme 1).

2. Radical generation by decarboxylation

The most popular and convenient method used to functionalize quinones is the Kochi-Anderson reaction,^[11] which is a one-step decarboxylation reaction from carboxylic acids under radical conditions. It was first described by Anderson and Kochi, who demonstrated that the oxidative decarboxylation of acids by peroxydisulfate ion (i.e., persulfate) is markedly accelerated by the *in situ* generated Ag(II), making the $\text{AgNO}_3/\text{(NH}_4)_2\text{S}_2\text{O}_8$ oxidant system a prerequisite for this reaction.

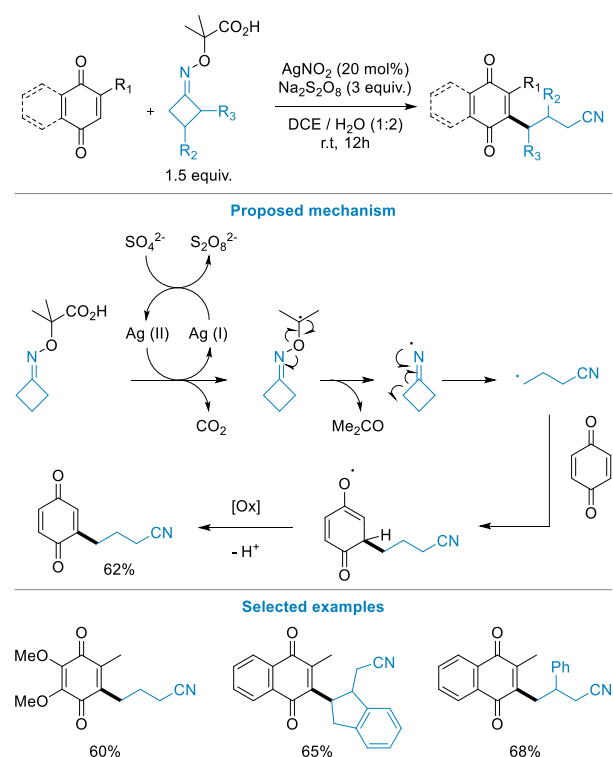
This procedure was applied for the first time to the alkylation of 1,4-quinones by Jacobsen and Torssell in the early 1970's^[12] and has since been particularly well exploited in radical alkylation of 1,4-naphthoquinones. In 1991, Zhang's group explored this reaction to synthesize a large array of vitamin K derivatives by direct radical alkylation of vitamin K₃, also known as menadione.^[13] Then, Davioud-Charvet's group applied this methodology for the introduction of various alkyl-acids and alkylamines into 2-substituted naphthoquinone scaffolds for the preparation of potential inhibitors of trypanothione reductase of *Trypanosoma cruzi*.^[14] This approach is still used by the team for the benzylation of menadione through decarboxylation of acids, leading to antimalarial 3-benzylmenadiones^[5a,b], or for the benzoylation of menadione to prepare the 3-benzoylmenadiones.^[15] In a similar approach, Dessolin and co-workers also described the direct alkylation of naphthoquinones with amino acids (Scheme 2).^[16]



Scheme 2. Alkylation of quinones via silver-catalyzed decarboxylation of acids.

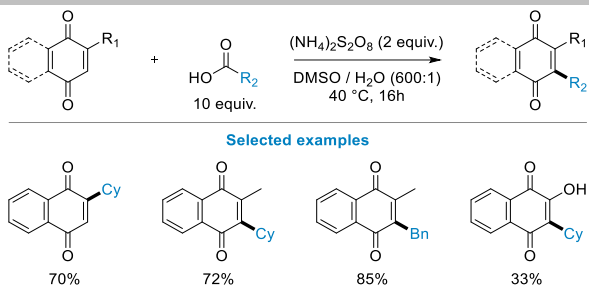
This method is still actively used and has even been revisited for the functionalization of quinones, as demonstrated by Wang's team in the gram-scale synthesis of various coenzyme Q derivatives.^[17]

Also in the same context, Xu and co-workers developed a decarboxylative cyanoalkylation of heteroarenes and quinones via iminyl radical and cyclobutyl opening at room temperature.^[18] The authors suggested a mechanism whereby, after decarboxylation catalyzed by Ag(II), acetone is released while liberating an iminyl radical, thus triggering cycle opening to form a carbon-centered radical (Scheme 3). This cyanoalkyl radical then undergoes free radical addition to the quinone, followed by oxidation, resulting in the formation of the cyanoalkylated quinone. These conditions allowed the efficient functionalization of coenzyme Q₁₀ or menadione in good yields (Scheme 3).



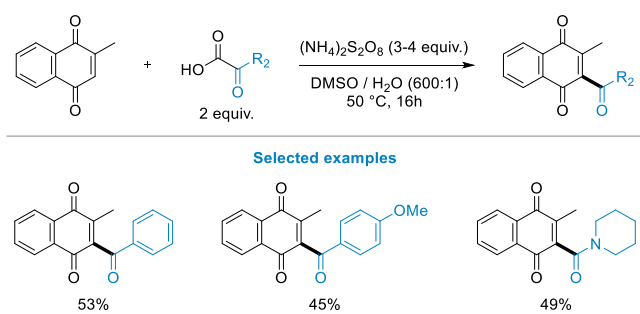
Scheme 3. Cyano-alkylation of quinones via cyclobutyl intermediate opening.

Over the last decade, radical generation by decarboxylation has been continuously revisited,^[19] including *inter alia* for the functionalization of quinones. For example, Lee and co-workers developed a silver-free Kochi-Anderson-type C-H alkylation of heteroarenes and quinones using ammonium persulfate in a mixture of water and DMSO as the sole reagent under mild temperature conditions allowing for the alkylation of various naphthoquinones including menadione and lawsone (Scheme 4).^[20]



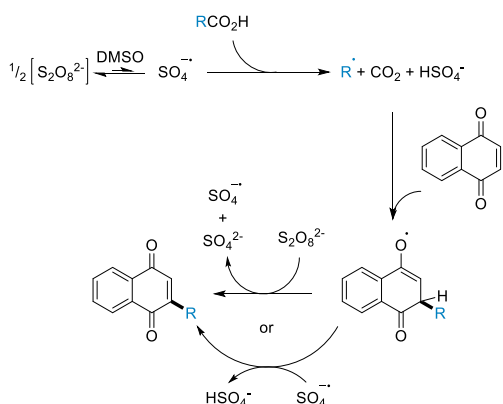
Scheme 4. Silver-free radical decarboxylation.

Subsequently, they described an acylation and carbamoylation version of this procedure.^[21] Although this reaction was shown to be efficient with heteroaromatic substrates as radical acceptors, only a few examples of quinone functionalization with moderate yields have been described (Scheme 5).



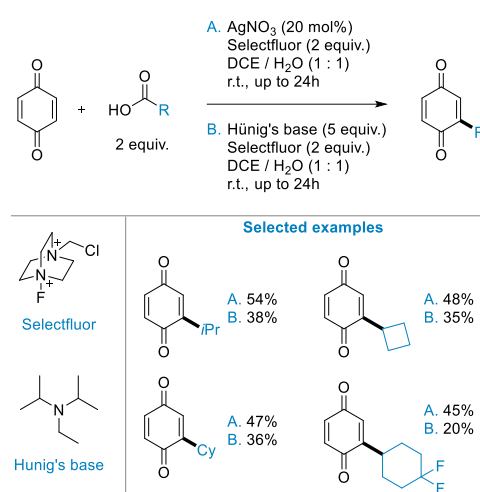
Scheme 5. Silver-free radical acylation and carbamoylation of quinones.

The authors demonstrated that under these specific conditions, $\text{SO}_4^{\cdot-}$ radicals can be generated gently in DMSO in the absence of any metal catalyst and play a crucial role in the decarboxylation process. DMSO has been shown to be essential for the reaction, as the decomposition of the persulfate ion is described as occurring much more consistently in this solvent. After decarboxylation, the radical intermediate reacts with the quinone, which after functionalization is regenerated after single-electron transfer by $\text{S}_2\text{O}_8^{2-}$ or hydrogen abstraction by $\text{SO}_4^{\cdot-}$ (Scheme 6).



Scheme 6. Proposed mechanism of the silver-free decarboxylation.

Recently, Baxter *et al.* showed that selectfluor could be used as a mild alternative to the strong oxidant ammonium persulfate.^[22] These conditions allowed the reaction to occur at room temperature and to lead to selective mono-alkylation of the highly reactive 1,4-benzoquinone with moderate to satisfactory yields (Scheme 7.A.). In comparison, the standard $\text{AgNO}_3/(\text{NH}_4)_2\text{S}_2\text{O}_8$ system applied to the same 1,4-quinone invariably leads to lower yield with a majority of polysubstituted compound. The same research team also found that the Hünig's base used as an additive under the same experimental conditions significantly improved the reactivity and even afforded the radical process without any metal additive, although leading in slightly lower yields (Scheme 7.B.).^[23]



Scheme 7. Selectfluor-mediated alkylation of 1,4-benzoquinones.

In 2020, the $\text{AgNO}_3/\text{selectfluor}$ system was used by Qing's group to introduce the CF_2OAr motif from the corresponding difluoroacetic acids in various heteroaromatic compounds and the 1,4-naphthoquinone (Scheme 8).^[24] Noteworthy, the conventional use of persulfate as an oxidant did not yield any target product, making selectfluor an useful alternative.

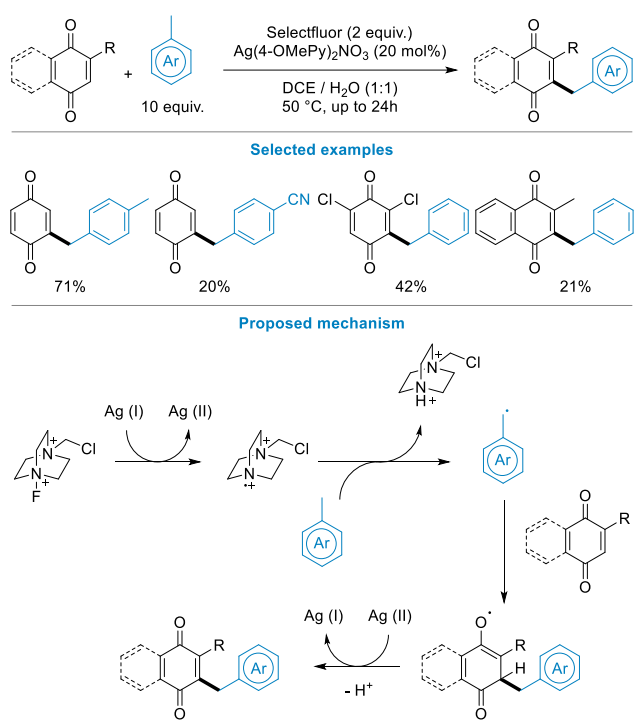


Scheme 8. Selectfluor-mediated introduction of difluoroalkylethers on 1,4-naphthoquinone.

3. Radical generation by hydrogen-atom abstraction

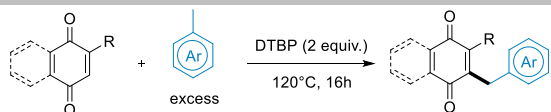
Based on previous work on decarboxylation with the $\text{Ag(I)}/\text{selectfluor}$ couple and on formation of a diazabicyclo radical dication ($\text{TEDA}^{2+}\cdot$) after 1-electron reduction or photolysis, selectfluor was shown to act as an effective hydrogen transfer agent for the generation of carbon-centered radicals to enable new bond formation.^[25] Hence, Baxter's team developed an original radical benzylation of 1,4-quinones by $\text{Csp}_3\text{-H}$ abstraction

starting from toluenes.^[26] Using this process, 1,4-benzoquinones could be mono-benzylated with good yields. However, arene bearing electron-withdrawing groups in *para*-position were found to be poor coupling partners as illustrated with menadione, which led to 3-benzylmenadione with moderate yields (Scheme 9).

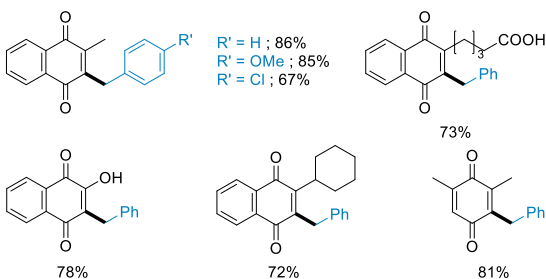


Scheme 9. Radical benzylation of quinones via Selectfluor-mediated C-H abstraction.

Quinone benzylation via a Csp^3 -H abstraction has been well explored in recent years. The early work was developed in 2014 by Duan and coworkers when they reported a copper-catalyzed benzylation of various coumarins, which turned out to be compatible with menadione.^[27] Later, inspired by this method, Wang's group developed a copper-free oxidative cross-dehydrogenative coupling between various quinones and toluenes.^[28] This reaction proceeds via di-*tert*-butyl peroxide (DTBP)-assisted hydrogen-abstraction on the benzylic Csp^3 to generate highly reactive benzyl radicals, prone to react readily with electrophilic quinones. Various quinones, including 2-substituted-1,4-naphthoquinones and substituted 1,4-benzoquinones were successfully benzylated by diversely substituted toluenes (Scheme 10). The main drawback of this process is likely the use of toluene derivatives in large excess used both as a reactant and as a solvent, limiting the scope of the reaction to cheap or easily available starting materials.

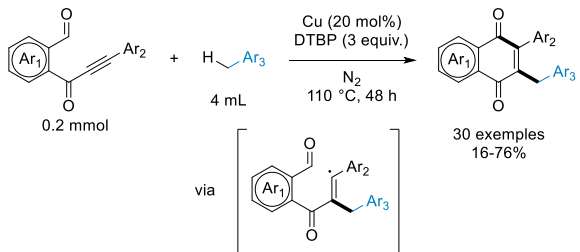


Selected examples



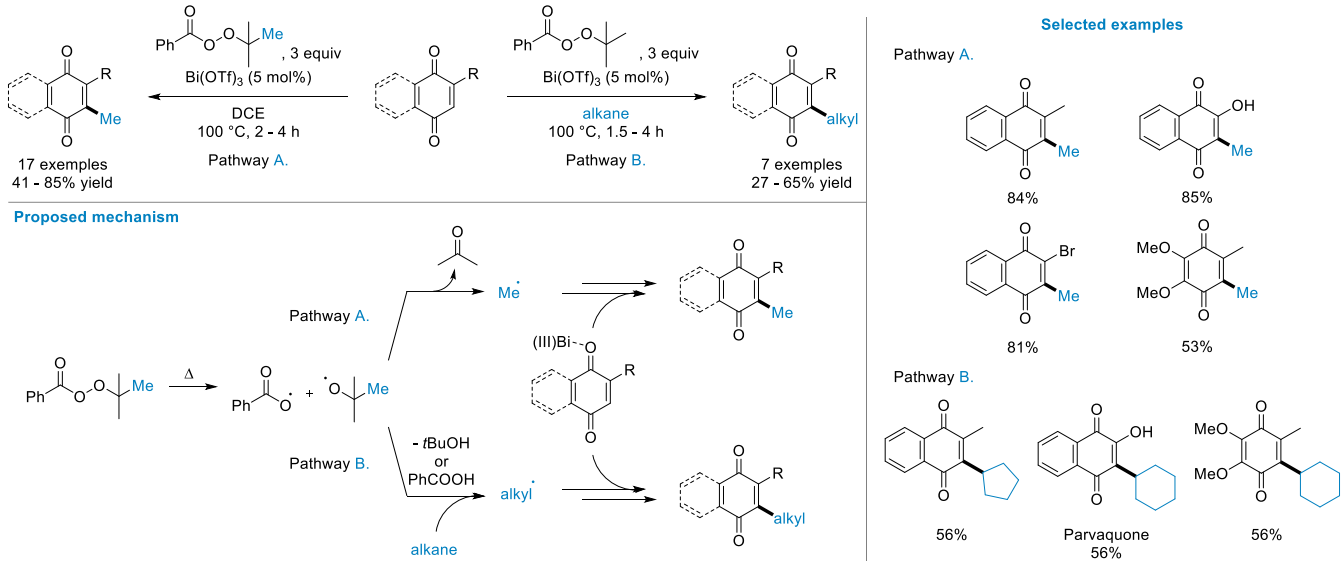
Scheme 10. Radical benzylation of quinones via DTBP-mediated C-H abstraction.

Noteworthy, a similar process was recently described for the cyclization of 2-(3-arylpropioloyl)benzaldehydes in the presence of catalytic copper powder leading to 3-benzylated 2-aryl-1,4-naphthoquinones.^[29] Strictly speaking, this process is not a direct functionalization of quinones but allows the formation of a very wide range of various 1,4-naphthoquinones in a single step (Scheme 11).



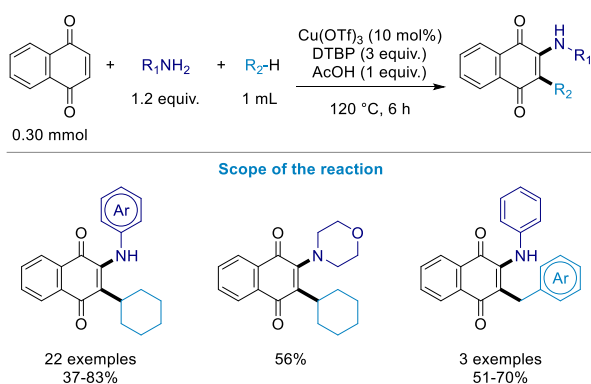
Scheme 11. Cascade radical formation of benzylated 1,4-naphthoquinones.

Obviously, radical generation by hydrogen-abstraction has not been applied to benzylation reactions only. At the end of the 20th century, Chuang's group studied a direct manganese-mediated alkylation of various 1,4-naphthoquinones with malonates.^[30] In 2016, Lee's group described a direct copper-catalyzed cycloalkylation using *tert*-butyl hydroperoxide (TBHP) as hydrogen-abstraction agent starting from cycloalkanes.^[31] Finally, Wang's team extended their benzylation method to the direct alkylation of quinones using *tert*-butyl peroxybenzoate (TBPB) and bismuth(III) trifluoromethanesulfonate as catalyst.^[32] Remarkably, they showed that TBPB could act as a radical methyl donor allowing the radical methylation of numerous bismuth-activated quinones in good yields (Scheme 12, Pathway A). On the other hand, the use of an alkane as a solvent promoted the corresponding alkylation via hydrogen-abstraction from the alkane by one of the resulting radicals of the homolytic cleavage of TBPB (Scheme 12, Pathway B).



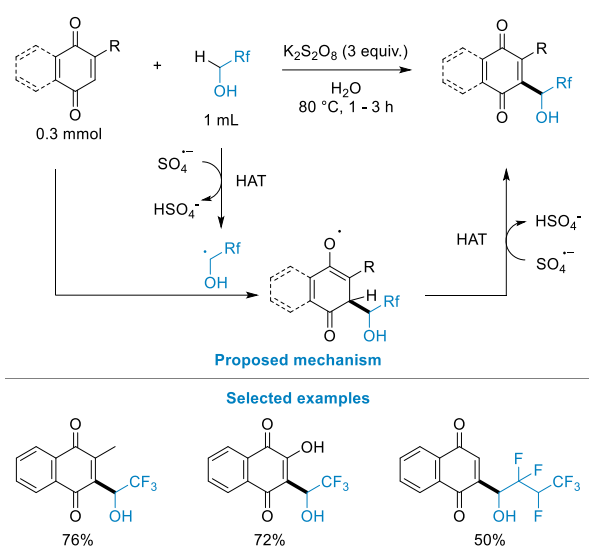
Scheme 12. Bismuth-catalyzed quinone alkylation.

This radical alkylation has been explored very recently by the same team to develop the very first direct one-pot dual amination-alkylation of 1,4-naphthoquinones.^[33] It is proposed that in the presence of a source of copper(II) as catalyst, 1,4-Michael addition of the amine occurs first, followed by 1,4-radical addition of the alkyl radical generated by DTBP (Scheme 13).



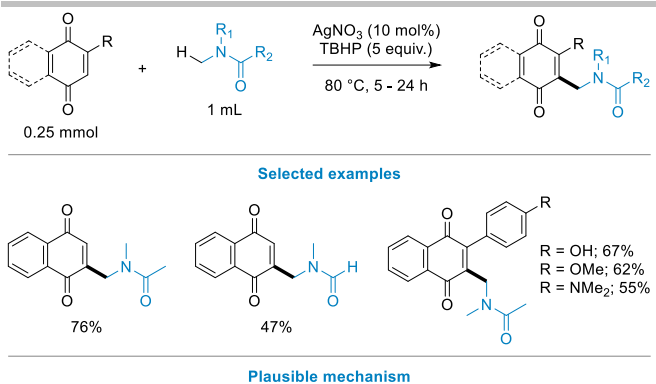
Scheme 13. Dual amination-alkylation of 1,4-naphthoquinone.

Shortly before, Liu's group found that these hydrogen abstraction methods can also be successfully applied to the coupling of fluorinated alcohols to quinones.^[34] In a heated water/polyfluorinated alcohol mixture, potassium persulfate decomposes to the sulfate radical ($\text{SO}_4^{\cdot-}$), which allows the hydrogen atom abstraction (HAT) from the polyfluorinated alcohol to generate a key radical. This latter readily reacts with the electrophilic quinone, and the corresponding radical adduct is then converted to the target quinone via a second HAT from the sulfate radical. This reaction is compatible with a large array of polyfluorinated alcohols and quinones, including menadione and lawsone (Scheme 14). The authors also showed that coumarin and chromone were also suitable radical acceptors.

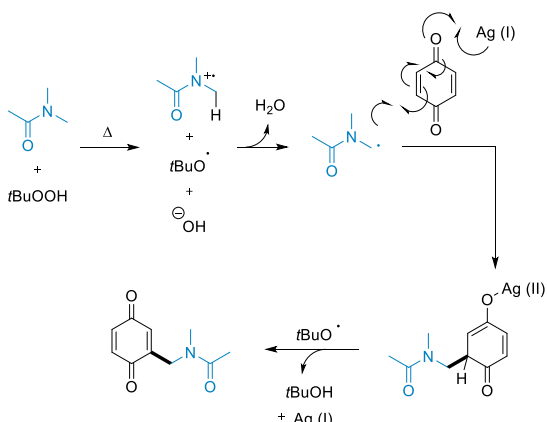


Scheme 14. Quinone functionalization with polyfluorinated alcohols.

Regarding other more diversified alkylations, Ilangovan's team, who previously published the radical opening of cyclopropanols to generate alkyl-ketone functionalized quinones,^[35] described in 2020 an original direct functionalization of quinones with dialkylamides using the $\text{AgNO}_3/\text{TBHP}$ couple.^[36] In their report, the authors postulated that the thermally generated *tert*-butoxyl radical reacted with the alkylamide, first to generate the *N*-acyliminium alkyl radical and subsequently the *N*-alkyl radical. This key radical intermediate firstly undergoes a silver-catalyzed conjugated addition to the quinone, and then the resulting radical adduct reacts again with the *tert*-butoxyl radical adduct to regenerate Ag(I) and the quinone moiety. Although a broad range of quinones were directly functionalized by dimethylacetamide (DMA), access to various dialkylamides was however rather limited (Scheme 15).

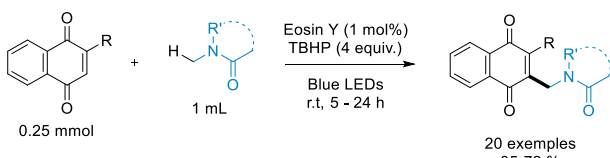


Plausible mechanism



Scheme 15. Silver-catalyzed alkylamidation of quinones.

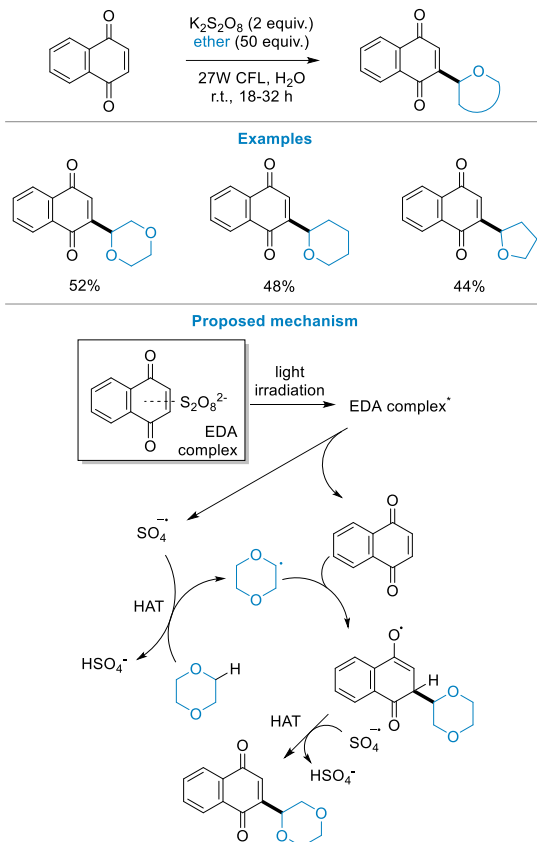
Shortly after, Ilangoan's group described a photocatalyzed version of this reaction, compatible with mono- and di-alkylamides.^[37] Eosin Y was used as a photosensitizer, generating upon blue LED photoexcitation $t\text{BuO}^{\cdot}$ via a single-electron transfer, which then undergoes HAT from the alkylamide. These conditions allowed alkylation of diversely substituted 1,4-naphthoquinones in much milder conditions with good yields (Scheme 16).



Scheme 16. Photocatalyzed alkylamidation of 1,4-naphthoquinones.

Surprisingly, in the fast-evolving groundbreaking field of photochemistry over the past decade, this was so far the only example of functionalization of a quinone by a photosensitive catalyst.^[38] Devari and Shah, however, reported in 2016 a photosensitizer-free alkylation of various electron-deficient arenes, including few examples of 1,4-naphthoquinones, with cyclic ethers in the presence of $\text{K}_2\text{S}_2\text{O}_8$ and under light-irradiation.^[39] The authors proposed the formation of an electron donor-acceptor (EDA) complex between $\text{S}_2\text{O}_8^{2-}$ and the electron-deficient arene. Upon light irradiation of this EDA complex, $\text{S}_2\text{O}_8^{2-}$ undergoes a homolytic cleavage to generate $\text{SO}_4^{\cdot-}$, which, following HAT with ethers, leads to the formation of α -oxyalkyl radicals. The latter radicals then react with the quinone and afford,

likely after HAT from $\text{SO}_4^{\cdot-}$, the alkylated naphthoquinone with moderate yield (Scheme 17).

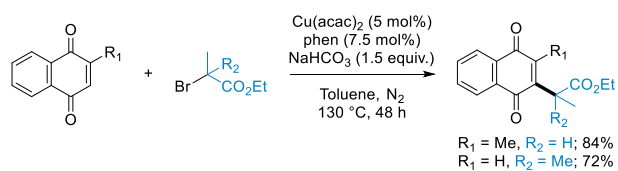


Scheme 17. Photosensitizer-free light-induced alkylation of quinones with cyclic ethers.

Furthermore, as discussed earlier, most of the described radical alkylations proceeding by HAT suffer from the use of an excess of alkyl precursors, making it difficult to functionalize quinones starting from complex or expensive adducts.

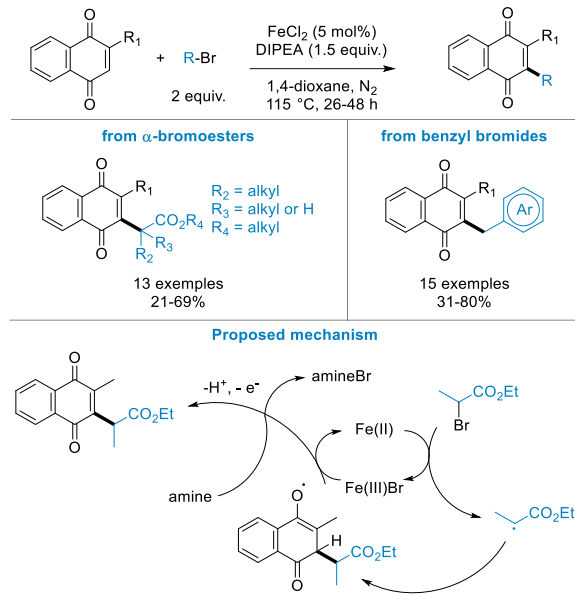
3. Radical generation by C-halogen reduction

Rare examples of alkylation of quinones by dehalogenation of a radical precursor have been reported. Particularly, Li's group described the copper-catalyzed alkylation of diverse heteroarenes, including 1,4-naphthoquinones and coumarins, with various alkyl halides.^[40] $\text{Cu}(\text{acac})_2$ and 1,10-phenanthroline (phen) were combined to form a catalytic system for the reduction of the C-Br bond and formation of the corresponding alkyl radical. Under inert atmosphere and intense heating, 1,4-naphthoquinone and menadione could be alkylated with α -bromo-esters in the presence of a base, but only two examples have been described so far (Scheme 18).



Scheme 18. Copper-catalyzed alkylation of 1,4-naphthoquinones.

Later, the same group described an iron-catalyzed version of this alkylation process with a greater scope.^[41] A Fe(II) catalyst was added to reduce the C-Br bond to form the corresponding radical species, in the presence of a base under heating, allowing the functionalization of diversely 2-substituted naphthoquinones from various α -bromoesters and benzyl bromides (Scheme 19).

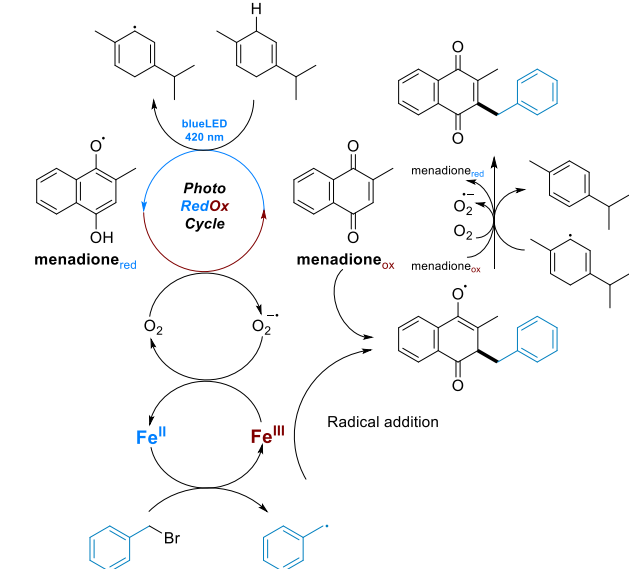


Scheme 19. Iron(II)-catalyzed alkylation of quinones.

In parallel, we have developed in our group the first Fe(III)-catalyzed benzylation of 1,4-naphthoquinones (Scheme 20).^[42] Based on previous reports about quinone photoreactivity, we proposed a mechanism where the photoreduction of the starting menadione is assisted by γ -terpinene under blue light irradiation. The resulting semiquinone radical is then re-oxidized by ambient oxygen generating superoxide anion radical continuously. This radical is known to reduce Fe(III) to Fe(II), which can then reduce the C-Br bond of benzyl bromide to generate the corresponding radical. After benzyl radical addition to menadione, the resulting benzylated semiquinone is re-oxidized by oxygen or the starting menadione to continue the redox cycle (Scheme 19). More than 40 examples of diversely substituted 1,4-naphthoquinones were synthesized with good yields.



Proposed mechanism



Scheme 20. Iron-catalyzed photoredox benzylation of quinones.

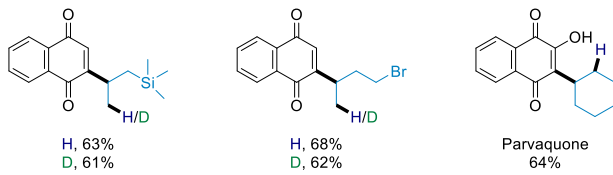
To date, these are the only examples of direct quinone alkylation by dehalogenative radical generation. However, as discussed just below, this method is beginning to be applied in three-component-reaction with quinones. It is highly likely that this field will continue to grow exponentially in the coming years, as halogenated starting materials are common building blocks and represent an important starting material in organic synthesis. However, carbon-halogen bond reduction remains difficult, especially for inactivated alkyl halides, and most of the described methods are rarely compatible with quinone redox properties (i.e., as an oxidant). Nevertheless, recent advances in the abstraction of halogen atoms (XAT) constitute very promising prospects for future development.^[43]

4. Cascade three-component alkylation

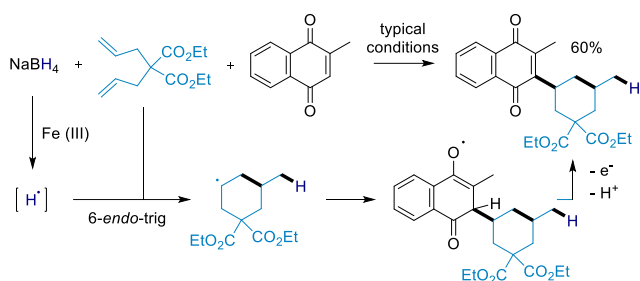
During the last decade, C-C bond construction via radical generation from starting olefins has been extensively studied. A common system used for this purpose is the couple Fe(III)/reductant.^[44] In 2019, Liu's group developed, using the $\text{Fe}(\text{NO}_3)_3 \cdot 9\text{H}_2\text{O}/\text{NaBH}_4$ couple, an efficient free radical alkylation of quinones with olefins compatible with a large array of quinones and (a)cyclic olefins, including allylsilanes.^[45] The authors demonstrated that a hydrogen radical is formed by 1-electron oxidation of NaBH_4 . This newly formed radical can then react with an olefin to form a new C-H bond and a carbon-centred radical, which in turn can then alkylate a quinone. The mechanism was suggested from a radical clock experiment where radical cyclization of a diene via a 6-endo-trig cyclization was observed (Scheme 21). Furthermore, using NaBD_4 instead of NaBH_4 led to the insertion of deuterium atom into the olefin, confirming that the reductant is indeed the H/D donor in this reaction.



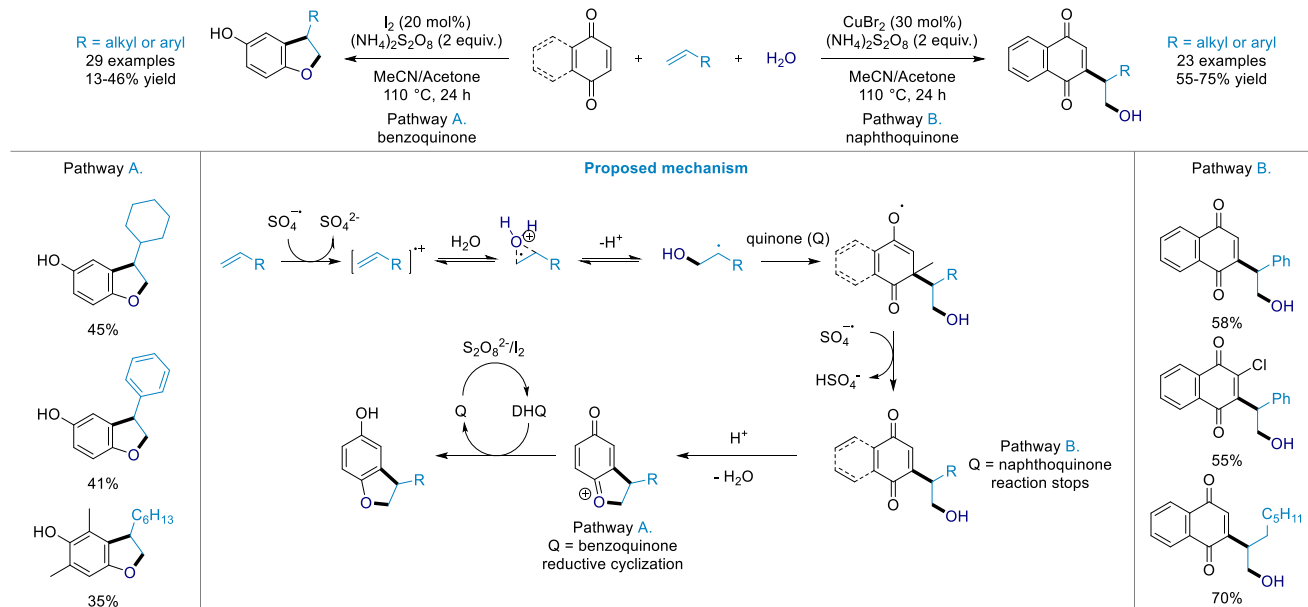
Selected examples



Radical clock experiment



Scheme 21. Cascade three-component alkylation of 1,4-naphthoquinones using the $\text{Fe}(\text{NO}_3)_3 \cdot 9\text{H}_2\text{O}/\text{NaBH}_4$ couple, with diverse (a)cyclic olefins.



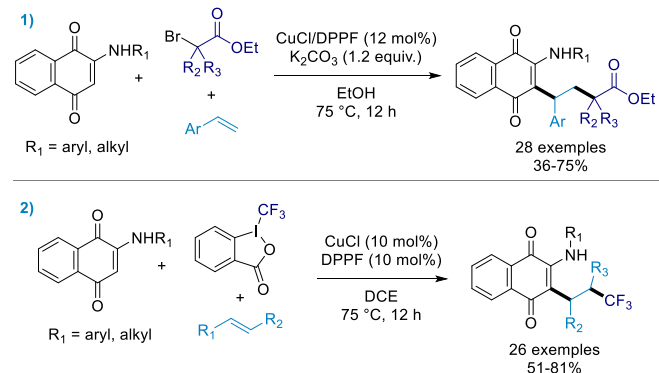
Scheme 22. Oxidative alkylation of 1,4-quinones with alkenes.

In recent years, three-component reactions have also been shown to be effective for the functionalization of 2-amino-1,4-naphthoquinones. In 2019, Zhang's group successively reported two three-component reactions allowing access to complex substituted 1,4-naphthoquinones.^[48] On one hand, α -bromocarboxylates, styrenes and 2-aminonaphthoquinones reacted in the presence of a catalytic amount of CuCl and 1,1'-bis(diphenylphosphino)ferrocene (DPPF) added as a ligand

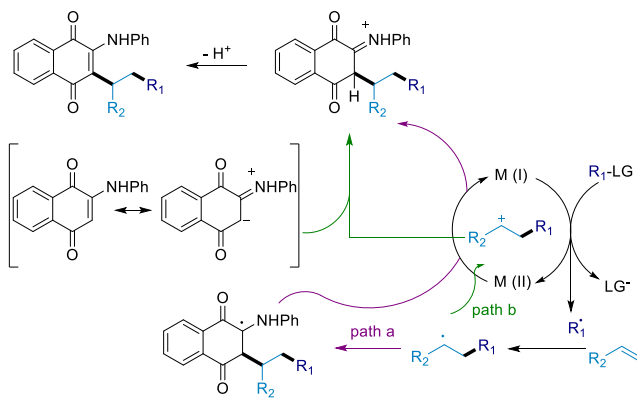
Simultaneously, Liu's team developed a synthesis of dihydroxybenzofuranes by a three-component oxyarylation of alkenes using 1,4-benzoquinones and water.^[46] This reaction proceeded in two steps. A first radical alkylation of a carbon-centred alcohol radical on a quinone generates the corresponding alcohol-bearing alkylated quinone, followed by reductive cyclization to form the dihydroxybenzofuran core (Scheme 22, Pathway A). Liu's team was able to avoid reductive cyclization by changing the experimental conditions (i.e., switching from a $(\text{NH}_4)_2\text{S}_2\text{O}_8/\text{I}_2$ system with benzoquinones to a $(\text{NH}_4)_2\text{S}_2\text{O}_8/\text{CuBr}_2$ system with naphthoquinones (Scheme 22, Pathway B).^[47] They proposed a mechanism whereby the olefin is oxidized by $\text{SO}_4^{\cdot-}$ giving the alkenyl radical cation, which reacts with water to form a bridged radical cation complex. After regio-selective opening and loss of a proton, the new carbon centre radical undergoes radical addition to the quinone. The resulting radical adduct is then oxidized by $\text{SO}_4^{\cdot-}$ to form the newly alkylated quinone. In the case of a naphthoquinone (NQ), the reaction stops there, but for a benzoquinone (BQ), the reaction continues and cyclization occurs. The authors also noted that the $(\text{NH}_4)_2\text{S}_2\text{O}_8/\text{I}_2$ mixture reduced BQ to the corresponding dihydroxyquinone which allowed the reduction of the cyclic cationic intermediate to lead to the final dihydrobenzofuran.

(Scheme, 23.1) and, on the other hand, Togni I reagent, substituted alkenes and 2-amino-1,4-naphthoquinones were involved in a reaction with AgOAc and DPPF as catalytic system (Scheme 23.2). These two reactions are proposed to proceed through the same mechanism. A first radical intermediate is generated by single-electron transfer (SET) between the metallic complex and the radical precursor. Two routes are then plausible; either this intermediate adds directly to the quinone (path A), or it

undergoes a second SET with the metallic complex to form the corresponding carbocation (path B), which can be trapped by the rearrangement product from the starting quinone. In both cases, an iminium intermediate is formed and the quinone core is regenerated by deprotonation (Scheme 23.3.). The fact that the reaction does not proceed if the amino group is replaced by an alkyl group led authors to prioritize path B, since enamine isomerization plays an important role in this path, even if, path A and direct radical alkylation cannot however be excluded.

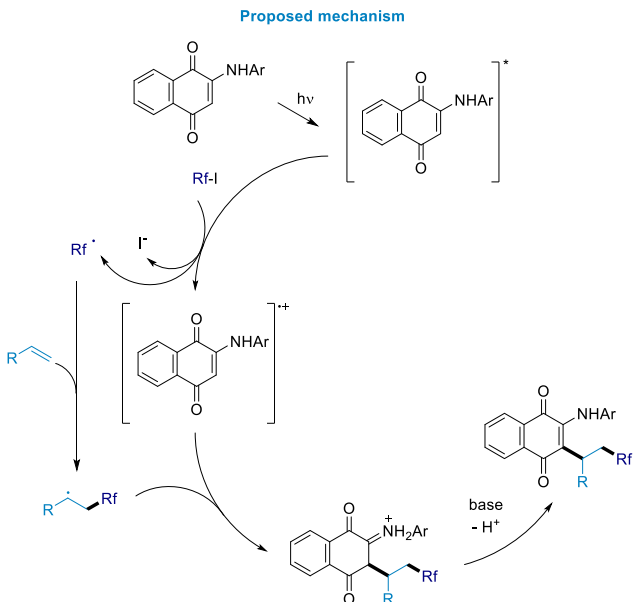
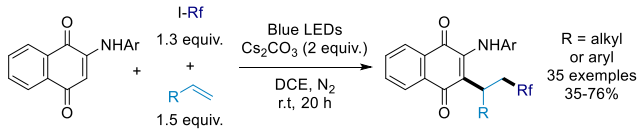


3) Proposed mechanism



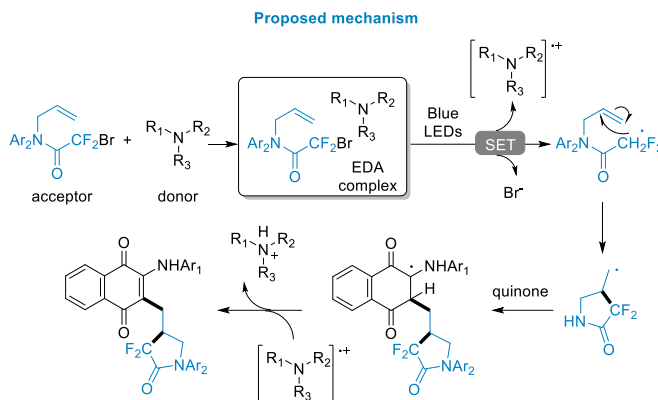
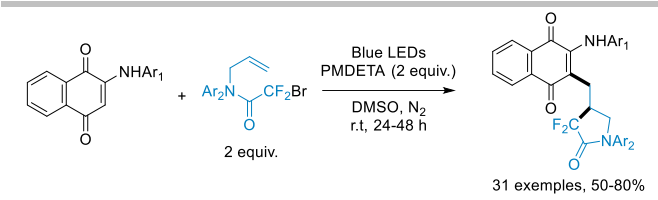
Scheme 23. Three-component alkylation of 2-amino-1,4-naphthoquinones.

Under blue-light irradiation, the cascade reaction between perfluoroalkyl iodides, alkenes and 2-amino-1,4-naphthoquinones was made possible without photocatalyst as demonstrated by Rao and co-workers.^[49] Since 2-amino-naphthoquinones absorb the blue light wavelengths and no coupling is observed between the perfluoroalkyl halide and alkenes in its absence, the authors proposed a mechanism where the quinone itself acts as a photosensitizer. Indeed, when excited with a blue LED irradiation, 2-aminonaphthoquinone is proposed to activate *in situ* the perfluoroalkyl iodide into its perfluoroalkyl radical through a SET process. Subsequent addition of the radical to the alkene leads to a carbon-centred radical, which then undergoes radical-radical coupling with the quinone radical-cation affording the targeted compound after deprotonation (Scheme 24). Although limited to 2-amino-1,4-naphthoquinones, these conditions are tolerant with various styrenes and alkyl-substituted alkenes in one side and various sized polyfluorinated alkyl chains.



Scheme 24. Photocatalyzed three-component alkylation of 2-amino-1,4-naphthoquinones.

Recently, Jin's group exploited the emerging field of electron donor-acceptor (EDA)^[50] complexes in visible-light-mediated reactions.^[51] The authors reported a tandem cyclization-arylation of inactivated alkenes with 2-amino-1,4-naphthoquinones. *N*-allyl-2-bromo-2,2-difluoroacetamides and *N,N,N',N'*-pentamethyl-diethylenetriamine (PMDETA) were demonstrated to form EDA complexes. Under blue light irradiation, a dehalogenation is observed leading to the formation of the difluoroalkyl radical which in turn undergoes intramolecular cyclization to afford a cyclic radical. This intermediate is then immediately trapped by the quinone to generate, after hydrogen abstraction from the amino radical cation, the targeted coupling product (Scheme 25).



Scheme 25. Visible-light mediated tandem cyclization-arylation of alkenes with 2-amino-1,4-naphthoquinones.

To the best of our knowledge, this constitutes, with Shah's radical alkylation with cyclic ethers (see above),^[39] the only example of quinone functionalization with EDA complexes. These two reports undoubtedly open a new field of exploration for the functionalization of quinones.

5. Conclusion

Herein, we have reviewed most of the recent advances in radical alkylation of quinones. As demonstrated by the work described in the survey, many advances have been made in recent years, opening up promising and interesting prospects despite the complexity of combining classical organic chemistry with quinones due to their unique electrochemical properties. We are convinced that this craze for the functionalization of quinones will intensify in the coming years, allowing even more breakthroughs in this field because, as we have shown, many of the methods described are still limited in diversity and efficiency but constitute a fertile ground for future discoveries.

Acknowledgements

This work was supported by the French Centre National de la Recherche Scientifique (E.D.-C.), and the University of Strasbourg (E.D.-C., M.D.), the Laboratoire d'Excellence (LabEx) ParaFrap (grant LabEx ParaFrap ANR-11-LABX-0024 to E.D.-C.), and the ANR PRC2017 (grant PlasmoPrim including the salary of the Ph.D. student M.D.).

Keywords: C-halogen reduction • C-H radical alkylation • decarboxylation • 1,4-(naphtho)quinone • H-abstraction • (photo)redox

- [1] A. Hidalgo-Gutiérrez, P. González-García, M. E. Díaz-Casado, E. Barriocanal-Casado, S. López-Herrador, C. M. Quinzi, L. C. López *Antioxidants (Basel)* **2021**, *10*(4):520.
- [2] J. Stenflo, P. Fernlund, W. Egan, P. Roepstorff, *Proc. Natl. Acad. Sci. USA* **1974**, *71*, 2730–2733.
- [3] a) G. L. Nelsetuen, T. H. Ztykovicz, J. B. Howard, *J. Biol. Chem.* **1974**, *249*, 6347–6350; b) C. Rodríguez-Olleros Rodríguez, M. Díaz Curiel, J. Osteoporos. **2019**, *2019*:2069176; c) M. Vos, G. Esposito, J. N. Edirisinghe, S. Vilain, D. M. Haddad, J. R. Slabbaert, S. Van Meensel, O. Schaap, B. De Strooper, R. Meganathan, V. A. Morais, P. Verstreken. *Science* **2012**, *336*, 1306–1310; d) B. J. Josey, E. S. Inks, X. Wen, C. J. Chou, *J. Med. Chem.* **2013**, *56*, 1007–1022.
- [4] E. J. Son, J. H. Kim, K. Kim, C. B. Park, *J. Mater. Chem. A*, **2016**, *4*, 11179–11202.
- [5] a) T. Müller, L. Johann, B. Jannack, M. Brückner, D. A. Lanfranchi, H. Bauer, C. Sanchez, V. Yardley, C. Deregnacourt, J. Schrével, M. Lanzer, R. H. Schirmer, E. Davioud-Charvet, *J. Am. Chem. Soc.* **2011**, *133*, 11557–11571; b) E. C. Rodo, L. Feng, M. Jida, K. Ehrhardt, M. Bielitz, J. Boilevin, M. Lanzer, D. L. Williams, D. A. Lanfranchi, E. Davioud-Charvet, *Eur. J. Org. Chem.* **2016**, 1982–1993; c) O. P.S. Patel, R. M. Beteck, L. J. Legoabe, *Eur. J. Med. Chem.* **2021**, *210*, 113084.
- [6] a) K. W. Wellington, *RSC Adv.* **2015**, *5*, 20309–20338; b) F. Epifano, S. Genovese, S. Fiorito, V. Mathieu, R. Kiss, *Phytochem. Rev.* **2014**, *13*, 37–49; c) R. Verma, *Anti-Cancer Agents Med. Chem.* **2006**, *6*, 489–499; d) Y. Zhang, Y.-H. Luo, X.-J. Piao, G.-N. Shen, J.-R. Wang, Y.-C. Feng, J.-Q. Li, W.-T. Xu, Y. Zhang, T. Zhang, C.-Y. Wang, C.-H. Jin, *Bioorg. Med. Chem.* **2019**, *27*, 1577–1587; e) S. N. Sunassee, C. G. L. Veale, N. Shunmoogam-Gounden, O. Osoniyi, D. T. Hendricks, M. R. Caira, J.-A. de la Mare, A. L. Edkins, A. V. Pinto, E. N. da Silva Júnior, M. T. Davies-Coleman, *Eur. J. Med. Chem.* **2013**, *62*, 98–110; f) G. Vialut, D. Grée, S. Das, J. S. Yadav, R. Grée, *Eur. J. Org. Chem.* **2011**, 1233–1241; g) V. Sanna, S. Nurra, N. Pala, S. Marceddu, D. Pathania, N. Neamat, M. Sechi, *J. Med. Chem.* **2016**, *59*, 5209–5220; h) E. M. Hodnett, C. Wongwiechintana, W. J. Dunn, P. Marrs, *J. Med. Chem.* **1983**, *26*, 570–574.
- [7] G. G. Dias, A. King, F. de Moliner, M. Vendrell, E. N. da Silva Júnior, *Chem. Soc. Rev.* **2018**, *47*, 12–27.
- [8] M. Yan, J. C. Lo, J. T. Edwards, P. S. Baran, *J. Am. Chem. Soc.* **2016**, *138*, 12692–12714.
- [9] E. T. Denisov, *Kinet. Catal.* **2006**, *47*, 662–671.
- [10] a) Y. Wang, S. Zhu, L.-H. Zou, *Eur. J. Org. Chem.* **2019**, 2179–2201; b) Y. Ando, K. Suzuki, *Chem. Eur. J.* **2018**, *24*, 15955–15964.
- [11] J. M. Anderson, J. K. Kochi, *J. Am. Chem. Soc.* **1970**, *92*, 1651–1659.
- [12] a) N. Jacobsen, K. Torsell, *Acta Chem. Scand.* **1973**, *27*, 3211–3216; b) J. Goldman, N. Jacobsen, K. Torsell, *Acta Chem. Scand.* **1974**, *28*, 492–500.
- [13] B. Liu, L. Gu, J. Zhang, *Recl. Trav. Chim. Pays-Bas* **1991**, *110*, 99–103.
- [14] L. Salmon-Chemin, E. Buisine, V. Yardley, S. Kohler, M.-A. Debreu, V. Landry, C. Sergheraert, S. L. Croft, R. L. Krauth-Siegel, E. Davioud-Charvet, *J. Med. Chem.* **2001**, *44*, 548–565.
- [15] L. Cotos, M. Donzel, M. Elhabiri, E. Davioud-Charvet, *Chem. Eur. J.* **2020**, *26*, 3314–3325.
- [16] G. Naturale, M. Lamblin, C. Commandeur, F.-X. Felpin, J. Dessolin, *Eur. J. Org. Chem.* **2012**, 5774–5788.
- [17] W.-Y. Luo, B. Lu, Y.-F. Qiu, R.-Y. Zhou, Y.-J. Hea, J. Wang, *New J. Chem.* **2020**, *44*, 8702–8704.
- [18] X. Li, X. Yan, Z. Wang, X. He, Y. Dai, X. Yan, D. Zhao, X. Xu, *J. Org. Chem.* **2020**, *85*, 2504–2511.
- [19] R. S. J. Proctor, R. J. Phipps, *Angew. Chem. Int. Ed.* **2019**, *58*, 13666–13699.
- [20] D. R. Sutherland, M. Veguillas, C. L. Oates, A.-L. Lee, *Org. Lett.* **2018**, *20*, 6863–6867.
- [21] M. T. Westwood, C. J. C. Lamb, D. R. Sutherland, A.-L. Lee, *Org. Lett.* **2019**, *21*, 7119–7123.
- [22] J. D. Galloway, D. N. Mai, R. D. Baxter, *Org. Lett.* **2017**, *19*, 5772–5775.
- [23] J. D. Galloway, R. D. Baxter, *Tetrahedron* **2019**, *75*, 130665.
- [24] X.-L. Zhu, Y. Huang, X.-H. Xu, F.-L. Qing, *Org. Lett.* **2020**, *22*, 5451–5455.
- [25] a) C. R. Pitts, S. Bloom, R. Woltonist, D. J. Auvenshine, L. R. Ryzhkov, M. A. Siegler, T. Lectka, *J. Am. Chem. Soc.* **2014**, *136*, 9780–9791; b) L.

- Niu, J. Liu, X.-A. Liang, S. Wang, A. Lei, *Nat. Commun.* **2019**, *10*, 467; c) X.-A. Liang, L. Niu, S. Wang, J. Liu, A. Lei, *Org. Lett.* **2019**, *21*, 2441–2444; d) For a review about TEDA²⁺: F. J. Aguilar Troyano, K. Merkens, A. Gómez - Suárez, *Asian J. Org. Chem.* **2020**, *9*, 992 –1007.
- [26] J. D. Galloway, D. N. Mai, R. D. Baxter, *J. Org. Chem.* **2019**, *84*, 12131–12137.
- [27] S.-L. Zhou, L.-N. Guo, X.-H. Duan, *Eur. J. Org. Chem.* **2014**, 8094–8100.
- [28] Y. Dong, J. Yang, S. He, Z.-C. Shi, Y. Wang, X.-M. Zhang, J.-Y. Wang, *RSC Adv.* **2019**, *9*, 27588–27592.
- [29] B. Zhu, H. Han, W.-K. Su, C. Yu, X. Jiang, *Adv. Synth. Catal.* **2021**, *363*, 484 – 489.
- [30] a) C.-P. Chuang, S.-F. Wang, *Tetrahedron*, **1998**, *54*, 10043–10052; b) M.-C. Jiang, C.-P. Chuang, *J. Org. Chem.* **2000**, *65*, 5409–5412.
- [31] E. R. Baral, S. H. Kim, Y. R. Lee, *Asian J. Org. Chem.* **2016**, *5*, 1134 – 1141.
- [32] J. Yang, Y. Dong, S. He, Z.-C. Shi, Y. Wang, J.-Y. Wang, *Tetrahedron*, **2019**, *75*, 130729.
- [33] J. Yang, B. Wang, Y. Zhang, S. Zhang, S. He, Z.-C. Shi, J.-Y. Wang, *Org. Biomol. Chem.* **2021**, *19*, 988–992.
- [34] J. Liu, D. Yu, Y. Yang, H. You, M. Sun, Y. Wang, X. Shen, Z.-Q. Liu, *Org. Lett.* **2020**, *22*, 4844–4847.
- [35] A. Ilangovan, S. Saravanakumar, S. Malayappasamy, *Org. Lett.* **2013**, *15*, 4968–4971.
- [36] S. Pandaram, A. Krishna T. P., A. Ilangovan, *Org. Biomol. Chem.* **2020**, *18*, 3027–3031.
- [37] P. Sakthivel, T. P. A. Krishna, A. Ilangovan, *ChemistrySelect*, **2021**, *6*, 2094 –2100.
- [38] For reviews on visible light photocatalysis: a) C. K. Prier, D. A. Rankic, D. W. MacMillan, *Chem. Rev.* **2013**, *113*, 5322–5363; b) N. A. Romero, D. A. Nicewicz, *Chem. Rev.* **2016**, *116*, 10075–10166.
- [39] S. Devariab, B. A. Shah, *Chem. Commun.* **2016**, *52*, 1490–1493.
- [40] D. Li, W.-C. Yang, *Tetrahedron Lett.* **2019**, *60*, 1792–1795.
- [41] D. Li, X. Shen, *Org. Biomol. Chem.* **2020**, *18*, 750–754.
- [42] M. Donzel, M. Elhabiri, E. Davioud-Charvet, *Manuscript submitted on April 08, 2021*.
- [43] T. Constantin, M. Zanini, A. Regni, N. S. Sheikh, F. Juliá, D. Leonori, *Science*, **2020**, *367*, 1021–1026.
- [44] J. C. Lo, D. Kim, C.-M. Pan, J. T. Edwards, Y. Yabe, J. Gui, T. Qin, S. Gutiérrez, J. Giacoboni, M. W. Smith, P. L. Holland, P. S. Baran, *J. Am. Chem. Soc.* **2017**, *139*, 2484–2503.
- [45] S. Liu, T. Shen, Z. Luo, Z.-Q. Liu, *Chem. Commun.* **2019**, *55*, 4027–4030.
- [46] G. Feng, S. Sun, G. Liu, H. Long, L. Liu, *Org. Lett.* **2018**, *20*, 7522–7525.
- [47] L. Cao, H. Long, H. Guan, Y. Bi, G. Bi, H. Huang, L. Liu, *Tetrahedron Lett.* **2019**, *60*, 1268–1271.
- [48] a) Y. Shangguan, F. Yang, H. Deng, H. Liu, Z. Liu, W. Zhuang, C. Qiao, A. Wang, Y. Xiao, C. Zhang, *J. Org. Chem.* **2019**, *84*, 10649–10657; b) Q. Wang, B. Wang, H. Deng, Y. Shangguan, Y. Lin, Y. Zhang, Z. Zhang, Y. Xiao, H. Guo, C. Zhang, *J. Org. Chem.* **2019**, *84*, 1006–1014.
- [49] L. Tang, F. Yang, Z. Yang, H. Chen, H. Cheng, S. Zhang, Q. Zhou, W. Rao, *Org. Lett.* **2021**, *23*, 519–524.
- [50] For reviews and insights on EDA complexes: a) C. G. S. Lima, T. M. Lima, M. Duarte, I. D. Jurberg, M. W. Paixão, *ACS Catal.* **2016**, *6*, 1389–1407; b) G. E. M. Crisenza, D. Mazzarella, P. Melchiorre, *J. Am. Chem. Soc.* **2020**, *142*, 5461–5476.
- [51] B. Sun, X. Shi, X. Zhuang, P. Huang, R. Shi, R. Zhu, C. Jin, *Org. Lett.* **2021**, *23*, 1862–1867.

5 points à retenir de l'article de revue.

- 1) La fonctionnalisation de quinones par voie radicalaire connaît un intérêt croissant depuis les 5 dernières années, y compris la benzylation des quinones et de la ménadione.
- 2) Les réactions de décarboxylation radicalaire de précurseurs sont encore à ce jour une des méthodes les plus efficaces pour alkyler des quinones.
- 3) Un grand intérêt est porté pour les réactions de couplage C-H entre les carbones Sp³ et les quinones par abstraction d'atome d'hydrogène (HAT). Cependant ces réactions nécessitent toujours un excès du réactant alkyle correspondant.
- 4) Générer un radical par déhalogénéation est très peu utilisé pour fonctionnaliser des quinones.
- 5) De plus en plus de réactions catalysées par la lumière visible sont développées pour alkyler des quinones.

4. Objectifs de recherche.

Les objectifs de recherche au cours de cette thèse sont multiples et sont notamment centrés sur de nouvelles méthodes de synthèse de 3-benzylménadiones et de métabolites supposés de type 3-benzoyleménadione ainsi que sur une meilleure compréhension des modes d'actions antiparasitaires de ces composés.

Ce manuscrit se découpe en 3 grands axes :

- i) Développement d'une nouvelle méthode de synthèse de 3-benzoyleménadiones afin de faciliter l'accès à des sondes chimiques photoréactives ; ii) Prouver le concept de sondes chimiques pour identifier les adduits 3-benzoyleménadiones-protéines formés sous photoirradiation UV afin de développer dans le futur des études ABPP pour étudier le profil protéomique (interactome) des 3-benz(o)yleménadiones dans les parasites vivants.
- Exploitation des propriétés photochimiques de la ménadione et des 3-benzylménadiones pour développer respectivement une nouvelle méthode de benzylation des quinones et démontrer l'oxydation benzylique des 3-benzylménadiones sous photoirradiation.
- Développement d'une méthode de synthèse pour préparer efficacement des analogues hétéroaromatiques de la plasmodione.

**Chapitre II. Synthèse de 3-benzoylménadiones par
réaction Friedel-Crafts, étude de leurs propriétés
rédox et applications pour la synthèse de sondes
chimiques photoréactives.**

1. Développement d'une nouvelle méthodologie d'acylation de Friedel-Crafts pour la synthèse de 3-benzoylménadiones.

1.1. Introduction

Ma thèse a débuté dans l'équipe quand un post-doctorant, Leandro Cotos étudiait la possibilité de développer un variant de Friedel-Crafts pour synthétiser les 3-benzoylménadiones. Pendant plusieurs mois, j'ai exemplifié les différentes conditions sous sa supervision. Puis, j'ai poursuivi la stratégie, seul, lorsque Léandro Cotos a poursuivi un autre projet sur la synthèse de fluorophores au sein de l'équipe. Dans le but de développer une méthode de synthèse générale aux 3-benzoylménadiones, métabolites supposés des 3-benzylménadiones, mais aussi d'ouvrir la voie à la synthèse d'outils chimiques dérivés de ces dernières qui sera détaillée dans la partie 2 de ce chapitre, une réaction de Friedel-Crafts entre le 1,4-diméthoxy-2-méthynaphthalène et des dérivés d'acides benzoïques a été imaginée. L'adduit de Friedel-Crafts correspondant pourrait ensuite être modifié par diverses réactions ou directement déprotégé pour obtenir les 3-benzoylménadiones (**Schéma 13**).

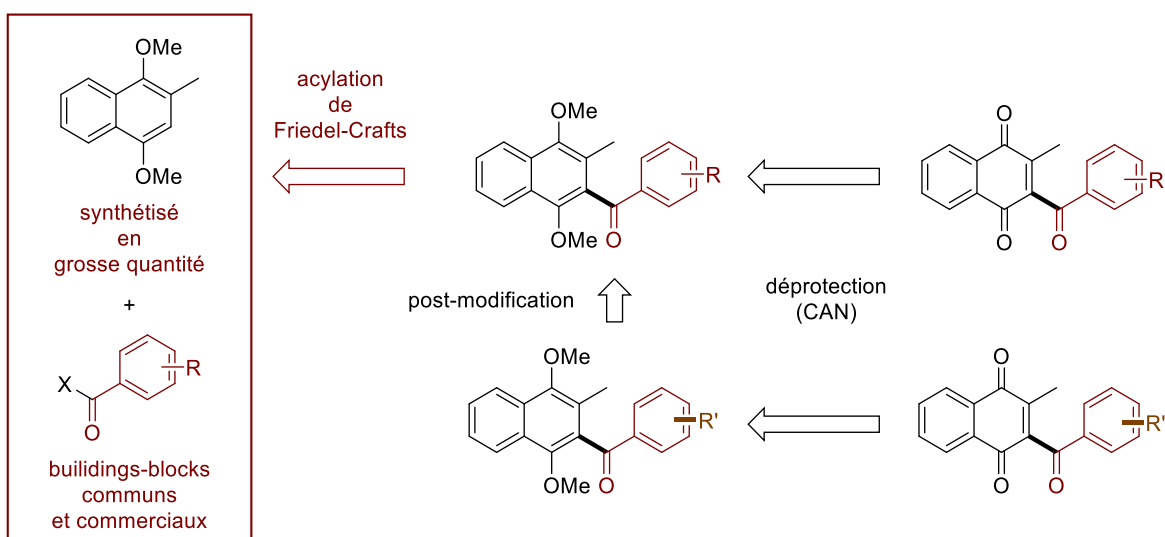


Schéma 13. Schéma rétrosynthétique imaginé pour la synthèse de 3-benzoylménadiones fonctionnalisées.

Une des conditions que nous avons fixées pour cette méthode, est que celle-ci devait être compatible avec la plus grande diversité de substituants aromatiques sur la partie benzoyle, incluant les substituants fortement électroattracteurs tels que les groupements trifluorométhyle ou nitro. Or, les réactions d'acylations de Friedel-Crafts classiques, décrites entre des chlorures d'acyles et des arènes ne fonctionnent pas ou peu avec des chlorures d'acyles benzoïques appauvris en électrons. Ceci a été confirmé avec nos essais préliminaires entre le 1,4-diméthoxy-2-méthynaphthalène et le chlorure d'acyle dérivé de l'acide 3-fluoro-4-nitrobenzoïque très appauvri en électron. Comme attendu, le produit d'acylation n'a pu être obtenu qu'en très faible quantité (14% de rendement, **Schéma 14**).

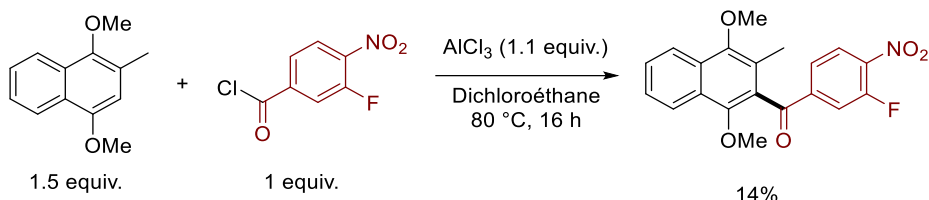


Schéma 14. Essai de réaction de Friedel & Crafts « classique » entre un chlorure d'acyle et le 1,4-diméthoxy-2-méthylnaphthalène.

D'autre part, à partir d'acides benzoïques, la méthode d'acylation assistée par le chlorure cyanurique décrite par Kangani⁴⁸ n'a donné aucun résultat à température ambiante comme rapporté et une augmentation de la température conduit à l'obtention d'un mélange complexe de produits. L'acylation de Friedel-Crafts par le couple anhydrique trifluoroacétique et acide trifluoroacétique (TFAA/TFA), déjà utilisée sur des systèmes semblables,⁴⁹ est uniquement compatible avec les acides benzoïques non appauvris en électron et aucune trace d'acylation n'a pu être observée avec des acides benzoïques nitrés (**Schéma 15**).

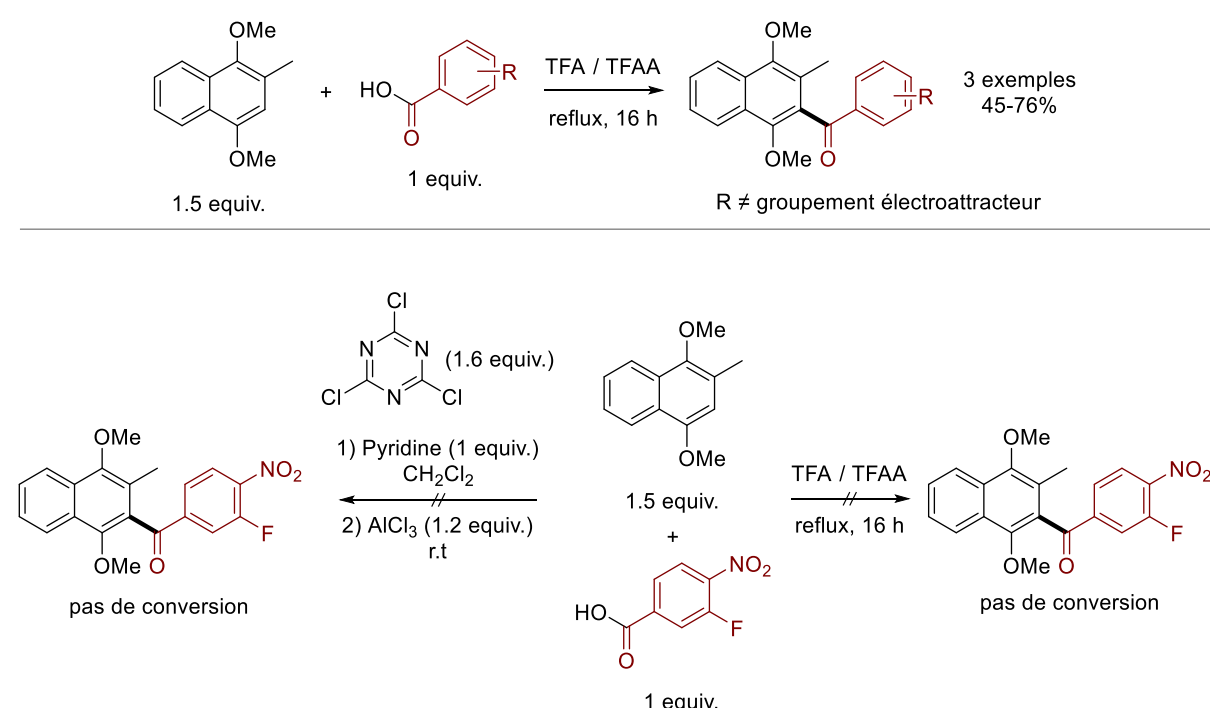


Schéma 15. Essais préliminaires d'acylation de Friedel-Crafts entre le 1,4-diméthoxy-2-méthylnaphthalène et des acides benzoïques.

Pour parer à ce défaut, nous avons réussi à mettre au point une méthode d'acylation de Friedel-Crafts compatible avec une grande variété de substituants dont des groupements fortement électroattracteurs. Cette réaction à l'avantage d'avoir lieu à température ambiante et repose sur le

⁴⁸ C. O. Kangani, B. W. Day, *Org. Lett.* **2008**, *10*, 2645-2648.

⁴⁹ a) B. S. Joshi, Q. Jiang, T. Rho, S. W. Pelletier, *J. Org. Chem.* **1994**, *59*, 8220-8232; b) M. Buccini, M. J. Piggott, *Org. Lett.* **2014**, *16*, 2490-2493.

système acide triflique et anhydride trifluoroacétique (TfOH/TFAA). Grâce à ce procédé nous avons pu accéder à une grande variété de 3-benzylménadiones difficiles d'accès. Le mécanisme proposé pour cette réaction inclut notamment la formation de l'intermédiaire triflate de trifluoroacétyle (TFAT), très réactif, permettant de former un acyle trifluoroacétate. Sous la supervision de Mourad Elhabiri, codirecteur de ma thèse, j'ai également étudié les propriétés électrochimiques de ces composés par voltampérométrie cyclique (CV) et à ondes carrées (SWV). Ceci nous a permis de proposer un mécanisme probable de réduction à 1 puis 2 électrons de ces molécules impliquant une forte influence de l'unité benzoyle (et donc de sa fonctionnalisation par divers substituants) sur les propriétés rédox du cœur électroactif, notamment sur les valeurs des potentiels de réduction à 2 e⁻, E^{2/1}, qui s'étendent sur une large gamme de potentiels rédox (500 mV) selon la substitution du groupement benzoyle (**Schéma 16**).

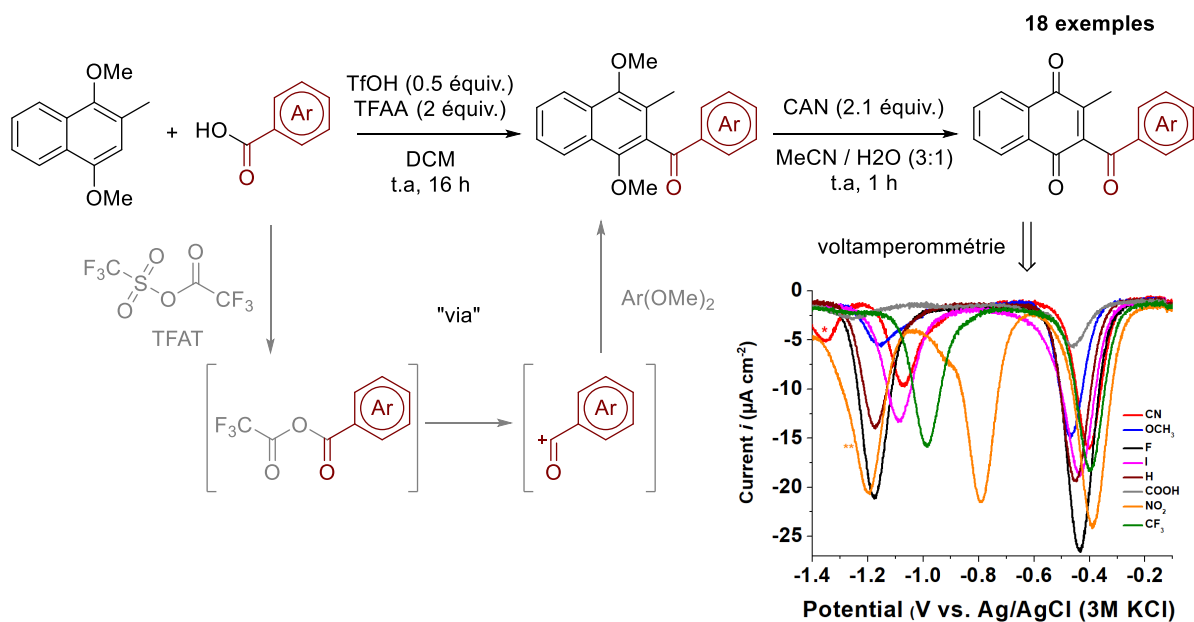


Schéma 16. Méthode d'acylation de Friedel-Crafts mise en place pour la synthèse de 3-benzylménadiones.

Cette méthodologie nous a également permis de synthétiser efficacement des sondes chimiques pour l'étude du mécanisme d'action de la plasmodione et de ses métabolites dont nous discuterons de manière détaillée dans la partie 2 de ce chapitre.

1.2. Article 2.

A Mild and Versatile Friedel–Crafts Methodology for the
Diversity-Oriented Synthesis of Redox-Active 3-
Benzoylmenadiones with Tunable Redox Potentials

Leandro Cotos, Maxime Donzel, Mourad Elhabiri, Elisabeth Davioud-Charvet

Chem. Eur. J. **2020**, 26, 3314-3325

doi: 10.1002/chem.201904220

A Mild and Versatile Friedel-Crafts Methodology for the Diversity-Oriented Synthesis of Redox-Active 3-Benzoylmenadienes with Tuneable Redox Potentials

Leandro Cotos,^[a] Maxime Donzel,^[a] Mourad Elhabiri,*^[a] and Elisabeth Davioud-Charvet,*^[a]

Abstract: A series of highly diversified 3-arylménadienes was prepared by a new Friedel-Crafts acylation variant/oxidative demethylation strategy. A mild and versatile acylation was performed between 1,4-dimethoxy-2-methylnaphthalene and various activated/deactivated benzoic and heteroaromatic carboxylic acids, in the presence of mixed trifluoroacetic anhydride and triflic acid, at room temperature and air. The 1,4-dimethoxy-2-methylnaphthalene-derived benzopheno-nes were isolated in high yield, and submitted to oxidative demethylation with cerium ammonium nitrate to produce 3-

benzoylménadienes. All 1,4-naphthoquinone derivatives were investigated as redox-active electrophores by cyclic voltammetry. The electrochemical data recorded on 3-acylated menadienes are characterized by a second redox process, the potentials of which cover a wide range of values (500 mV). These data emphasize the ability of the reached structural diversity at the 3-aryl chain of these electrophores to fine-tune their corresponding redox potentials. These properties are of significance in the context of antimalarial drug development and understanding of the mechanism of bioactivation/action.

Introduction

1,4-Naphthoquinones (NQs) are redox-active compounds widespread in all areas of life, synthesized in microorganisms and plants used in traditional medicine as secondary bioactive metabolites.^[1] They are well represented in numerous natural products with biological activities (e.g. antibiotic, anticancer, antiparasitic) and are generated in many vital metabolic processes.^[2] Structurally, the NQ core, in its oxidized form (NQ_{ox}), is responsible for its redox properties owing to its ability to accept one or two electrons. In the presence of oxygen, the resulting dihydro-naphthoquinone (NQ_{red}) can transfer 1 or 2 electrons in reactions regenerating the NQ_{ox} form, and releasing reactive oxygen species.^[3] Numerous NAD(P)H-dependent flavoproteins of the oxido-reductase family reduce NQs, and these latter were described as redox-cyclers or “subversive substrates” of these flavoenzymes^[4] (Figure 1). A well-known example is menadione (2-methyl-1,4-naphthoquinone or vitamin K3). In particular, 3-benzoylménadienes (**1**) were proven to be highly oxidative compared to the parent menadiones^[5] and proposed to be the active principles of potent antimalarial 3-benzylmenadienes.^[6] Variation of the substitution pattern at the west or east parts of the electroactive core of NQs^[2, 7, 8] modulates the electrochemical properties and thus both their biological and pharmacokinetic activities.

Benzoyl-1,4-naphthoquinones are also privileged scaffolds in medicinal chemistry.^[6, 7] From a synthetic point of view, they are valuable molecular templates in drug discovery to produce lead compounds or crucial intermediates in multistep synthesis to build complex natural products (Figure 1).^[9] As such, 2-benzoyl-NQs

have been reported as key intermediates for the synthesis of 7H-benzo[c]xanthen-7-ones,^[10] or advanced precursors to obtain the complex polycyclic 1,4-dioxygenated xanthone aglycone, IB-00208.^[9] These key moieties have also defined a smart strategy in the total 4 step-synthesis of the naturally occurring red pigment radermachol,^[11] improving the previous synthetic scheme.^[12]

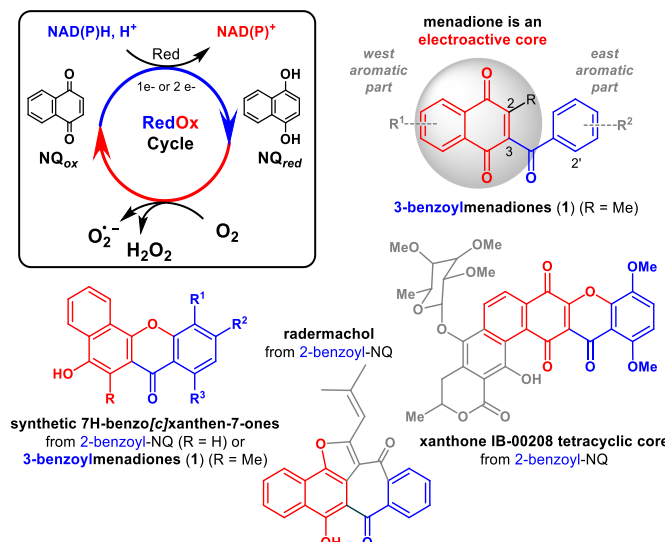
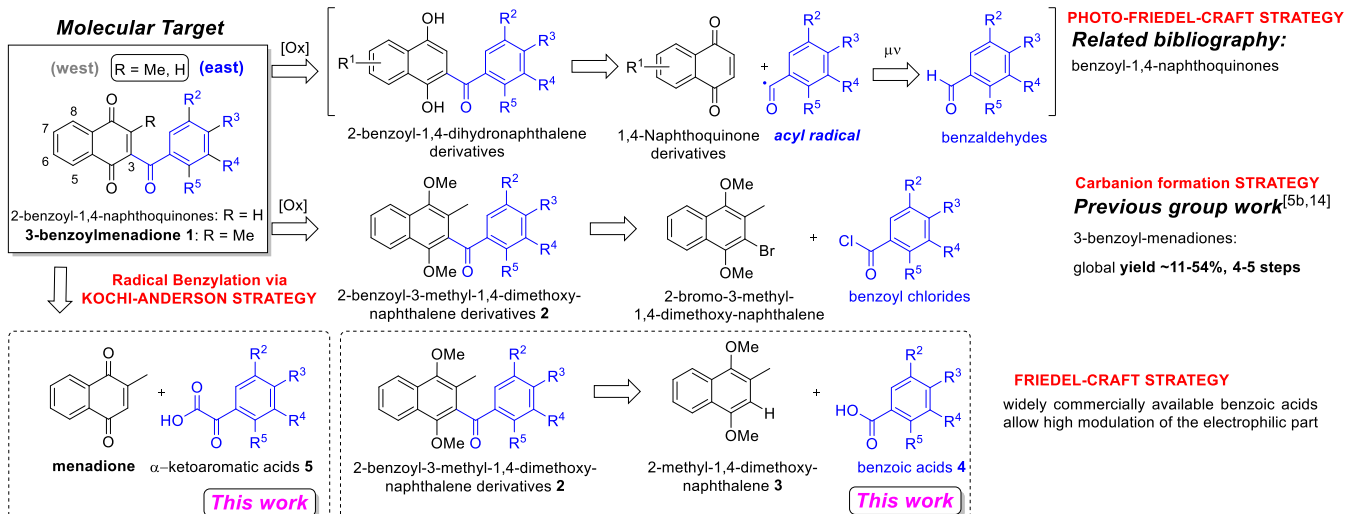


Figure 14. Natural and synthetic menadione derivatives polysubstituted at the aromatic ring including menadione (2-methyl-1,4-naphthoquinone).

[a] Dr. L. Cotos, M. Donzel, Dr. M. Elhabiri, Dr. E. Davioud-Charvet, Laboratoire d'Innovation Moléculaire et Applications (LIMA), UMR7042 CNRS-Unistra-UHA, European School of Chemistry, Polymers and Materials (ECPM), 25, rue Becquerel, F-67087 Strasbourg, France. E-mail : elhabiri@unistra.fr; elisabeth.davioud@unistra.fr



Scheme 1. Synthesis of 3-benzoylmenadione derivatives **1** ($R = \text{Me}$) starting from 1,4-dimethoxy-2-methyl-naphthalene **3** and benzoic acids **4**.

One of the strategies to build 2-benzoyl-1,4-naphthoquinone moieties is based on the generation of the 2-benzoyl-1,4-dihydro-naphthalene; this hydroquinone is readily oxidized into the target quinone moiety. Photo-Friedel-Crafts acylation of NQs with a large stoichiometric excess of aromatic aldehydes provided the 2-benzoyl-dihydro-naphthalene derivatives (Scheme 1).^[13] Previous work of the group to synthesize 3-benzoylmenadione derivatives **1** was based on the formation of a carbanion after i) bromination of the reduced and protected form of menadione, that is, the 1,4-dimethoxy-2-methylnaphthalene, ii) halogen/metal exchange, followed by iii) addition of benzoyl chloride to give 2-benzoyl-3-methyl-1,4-dimethoxy-naphthalene derivatives **2**, and finally, iv) oxidative demethylation by cerium ammonium nitrate (CAN, Scheme 1).^{[5b], [14]}

The Friedel-Crafts acylation process is widely used to synthesize benzophenones moieties (Scheme 1). From the original version^[15] based on the use of AlCl_3 in stoichiometric amount with a benzoyl chloride at high temperature, the corresponding acylium cation is formed, allowing an electrophilic aromatic substitution ($S_{\text{E}}\text{Ar}$) by the corresponding aromatic nucleophile. In this scenario, $\text{HCl}_{(\text{g})}$ and toxic aluminium metal waste are generated. Several improvements were further described, for example, solvent-free conditions made the process greener when $\text{Zn}^{[16]}$ or $\text{ZnO}^{[17]}$ are used as Lewis acids. Alternatively, use of a Brønsted acid to activate the aryl chloride was reported using a catalytic amount of the non-toxic perfluorinated acid resin Nafion-H^[18], trifluoromethanesulfonic acid (or triflic acid, TfOH)^[19] and bis(trifluoromethylsulfonylimino)-trifluoromethanesulfonic acid.^[20] Combination of Lewis and Brønsted acids was also shown to be an efficient acylation method when using benzoyl chlorides.^[21] Benzoyl chlorides are known to be substrates for benzoyl triflate generation, providing excellent acylating agents.^[22] To render the process more efficient, benzoic acids can be used as acylating reactants to avoid the use of chlorinated reagents. Methanesulfonic acid appeared in literature to perform acylations in combination with other reagents, such as Eaton's reagent (P_2O_5)^[23], alumina^[24] or graphite.^[25] Also, P_2O_5 ^[26] and the combination $\text{P}_2\text{O}_5/\text{SiO}_2$ ^[27] was applied to activated and deactivated benzoic acids, and methanesulfonic anhydride^[28] was shown to promote acylation of aryl and alkyl carboxylic acids in metal- and halogen free

conditions. Most of the cited methodologies required dry conditions, high temperatures, or pre-activation of the reagents. Nevertheless, noticeable progress has been made by using trifluoroacetic anhydride (TFAA)^[29] or trifluoroacetic acid/trifluoroacetic anhydride (TFA/TFAA),^{[11], [30]} under mild heating conditions and air moisture, to allow $S_{\text{E}}\text{Ar}$ of activated and non-strong deactivated benzoic acids, depending on the nucleophilicity strength of the aromatic compound.

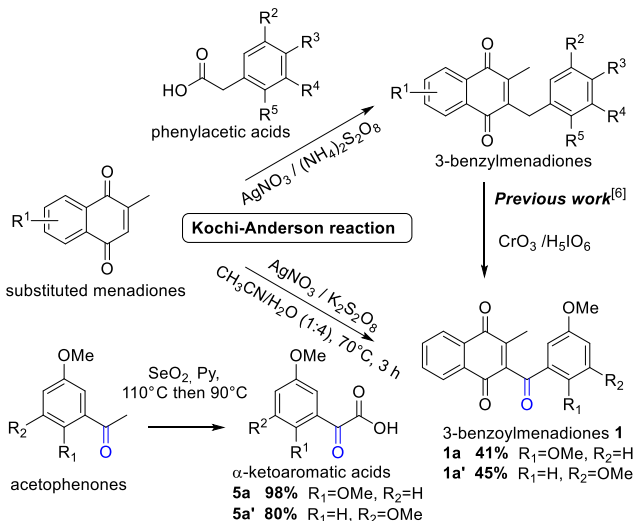
Taking the acylation of 1,4-dimethoxy-2-methylnaphthalene **3** by several activated and (strongly) deactivated benzoic/heteroaromatic carboxylic acids **4** as a model reaction to incorporate a new pattern of substitution at C-3 position of menadione, we developed a versatile Friedel-Crafts acylation variant to produce the benzophenone intermediates in mild conditions, *i.e.* air moisture and room temperature, in moderate to excellent yields (Scheme 1). In a second step, the diversified 3-benzoylmenadiones **1** were almost quantitatively produced after demethylation/oxidation with CAN. All the final compounds were evaluated in term of their electrochemical properties by cyclic voltammetry. Thus, the incorporation of the broad structural diversity in the 3-acylated chain of menadione brought new insights for the understanding of the bioactivation/action mechanisms and the structure-electroactivity relationships of this important new electrophore series at the origin of the potent antimalarial activity of 3-benzylmenadiones.

Results and Discussion

Preliminary Study

Previous strategies developed in the team to obtain polysubstituted 3-benz(o)ylmenadiones at both aromatic parts, that is, west (quinone moiety) and east (benzoic core), were based on the Kochi-Anderson reaction shown in Scheme 2.^{[6], [7b]} Phenylacetic acids in the presence of a catalytic amount of silver salt with stoichiometric excess of an oxidant (peroxodisulfate) undergo radical decarboxylation upon heating. The resulting benzyl radical specifically thus undergoes a nucleophilic radical addition to menadione core at the C-3 position, generating the corresponding 3-benzylmenadione. In the next step, 3-benzoylmenadiones **1** were produced by benzylic oxidation using $\text{CrO}_3/\text{H}_5\text{IO}_6$ reagent system.^[6]

A first straightforward pathway to synthesize 3-benzoylmenadiones **1** was investigated by a silver(I)-catalyzed decarboxylation reaction^[31] between menadione and α -ketoaromatic acids **5** according to the reaction shown in Scheme 2. To do so, starting α -keto acids **5a** and **5a'** had to be prepared, first, by a described method^[32] and were obtained with 80 and 98%, respectively. When the Kochi-Anderson reaction conditions were applied to menadione and α -ketoaromatic acids **5**, an acyl radical was generated, producing directly the 3-benzoylmenadione derivatives **1a** and **1a'** in 45% and 41% yield, respectively (Scheme 2).

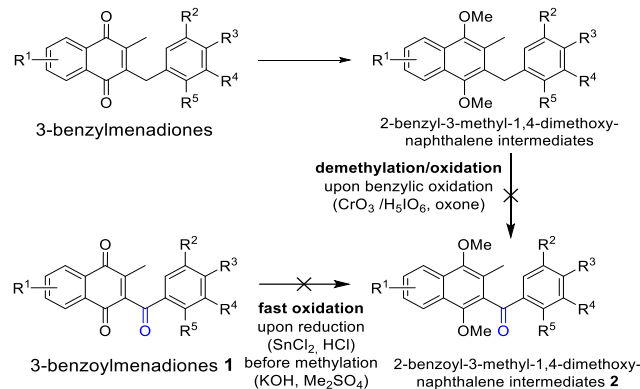


Scheme 2. Kochi-Anderson reactions used to synthesize 3-benz(o)yl-menadiones, in particular 3-benzoylmenadiones **1a** and **1a'**.

However, these strategies to build the 3-benzoylmenadione **1** core have several drawbacks that prevent them from providing a widely diversified chemical library. Phenylacetic and α -ketoaromatic acids are not widely commercially available. The synthesis of phenylacetic acids from benzaldehydes^[33] and benzoic acids^[34] are not very convenient for building a chemical library because it involves multiple steps, long reaction times, and expensive reagents with non-versatile protocols to achieve their production. In the next step, the benzylic oxidation with $\text{CrO}_3/\text{H}_5\text{IO}_6$ proceeded with low to moderate yields along with many side products and high toxicity toward the environment.^[6] In parallel, the synthesis of 3-benzoylmenadiones (e.g. **1a**, **1a'**, Scheme 2) from α -ketoaromatic acids **5** resulted in poor yields. The use of the Kochi-Anderson reaction showed incompatibilities with hydroxyl^[6] and amino^[7a] groups, and low efficiency to introduce pyridine rings.^[7a]

Firstly, the direct functionalization of the benz(o)ylmenadione skeleton has proven to be difficult due the presence of the C2 methyl group attached to the quinone moiety, which is highly base-sensitive. Secondly, the functionalization of the benz(o)ylmenadione derivatives through the 1,4-dihydro- or 1,4-dimethoxy-3-methyl-2-benz(o)yl-naphthalene intermediates was found difficult to handle (Scheme 3). On the one hand, the 1,4-dimethoxy groups of the benzyl intermediate were demethylated by using proton assistance as previously described with the benzylic oxidation using $\text{CrO}_3/\text{H}_5\text{IO}_6$ (or oxone) as reagents; thus, formation of several side products was observed (Scheme 3). On the other hand, in contact with trace oxygen (i.e. despite an argon atmosphere), the produced 2-benzoyl-1,4-

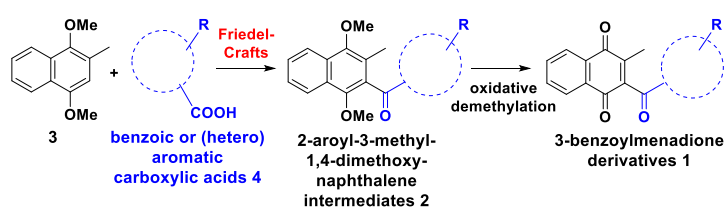
dihydro-3-methylnaphthalene intermediate was quickly oxidized into its quinone form before methylation occurred (Scheme 3).



Scheme 3. Side-reactions occurring via the 1,4-dihydro- or 1,4-dimethoxy-2-methylnaphthalene intermediates.

Preliminary Friedel-Crafts Reaction Study

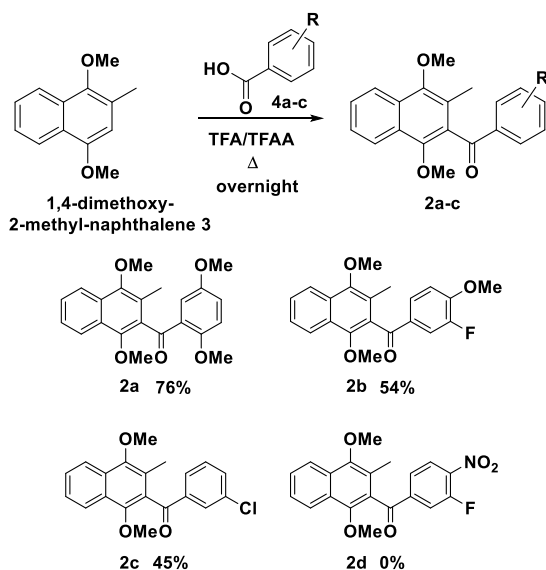
In this work, our objective was to develop a chemical library of structurally diversified electroactive 3-(hetero)arylmenadiones **1** after incorporation of polysubstituted (hetero)aromatics moieties and to modulate their redox characteristics. Diversity-oriented synthesis (DOS) implies the generation, under efficient and versatile procedures, of functionally diverse small-molecules acting as chemical modulators.^[35] In the new strategy reported herein, diversity at the east aromatic part of 3-benzoylmenadione was achieved by using a large array of readily commercially available benzoic and heteroaromatic carboxylic acids as starting materials. Benzoic acids and heteroaromatic carboxylic acids are acylating substrates for the Friedel-Crafts reaction. The west aromatic part of the 3-benzoylmenadione **1** core was introduced via its 1,4-dimethoxy-2-methylnaphthalene precursor **2** upon the Friedel-Crafts acylation. In the next step, the diversified 3-benzoylmenadiones **1** were generated upon selective oxidative demethylation using CAN (Scheme 4).



Scheme 4. Synthesis of 3-(hetero)arylmenadione derivatives **1** based on Friedel-Crafts acylation/oxidative demethylation.

The key point is the development of a Friedel-Crafts acylation reaction, which allows electrophilic aromatic substitution from activated or deactivated benzoic and heteroaromatic carboxylic acids under mild conditions, thus promoting an easy experimental protocol, for example, no air moisture-sensitive reagents, no high temperatures, activating the acylating agents *in situ*. The TFA/TFAA reagent system has been reported to be an efficient practical system to achieve the $\text{S}_{\text{E}}\text{Ar}$ under mild heating conditions, in open air with air moisture compatibility. As was reported, this methodology proceeds with non-strongly deactivated and activated benzoic acids **4** (Scheme 5), depending on the nucleophilicity of the aromatic nucleophile. Owing to the high electronic density of 1,4-dimethoxy-2-methylnaphthalene **3**, we first started the screening from activated benzoic acids **4a-c** to

generate the 2-benzoyl-3-methyl-1,4-dimethoxy-naphthalene intermediates **2a-c** with moderate to good yields (Scheme 5). The mechanism of the reaction likely proceeds through the *in situ* generation of the mixed anhydride, that is, an acyltrifluoroacetyl intermediate,^[36] formed between the benzoic acid and TFAA. This intermediate is activated by the proton of TFA to promote the formation of the corresponding acylium cation. Subsequently, S_EAr of 1,4-dimethoxy-2-methylnaphthalene **3** produced the corresponding 2-benzoyl-3-methyl-1,4-dimethoxy-naphthalene derivatives **2a-c**. Then, following oxidative demethylation by CAN, the 3-benzoylmenadiones **1** were generated in excellent yields. Notably, CAN oxidation is sensitive to the electronic density of the aromatic ring.



Scheme 5. Preliminary study on the Friedel-Crafts reaction to build 2-acylated 3-methoxy-1,4-dimethoxy-naphthalene derivatives **2a-c**.

In the 2-benzoyl-3-methyl-1,4-dimethoxy-naphthalene **2a** two pairs of 1,4-dimethoxy moieties are present. Nevertheless, the most electronically rich naphthalene moiety (west aromatic part) promotes faster oxidation than the phenyl fragment (east aromatic part), and only the desired 3-benzoylmenadione **1a** was obtained.

When the TFA/TFAA reagent mixture was applied to strongly deactivated benzoic acids, such as 3-fluoro-4-nitrobenzoic acid (**4d**), the targeted compound **2d** was not obtained (Scheme 5). Even by increasing the temperature and with longer time of reaction, the acyltrifluoroacetate intermediate was likely not formed with strongly deactivated benzoic acids, despite the presence of the electronically rich aromatic nucleophile, that is, 1,4-dimethoxy-2-methylnaphthalene. Therefore, we directed our acylation study by screening reagents able to activate (strongly) deactivated benzoic acids, such as **4d** (Scheme 5), under mild heating conditions and with air moisture, to achieve a versatile methodology.

Development of an Optimized Friedel-Crafts Variant

In very specific applied cases, the use of TfOH/TFAA in an equimolecular mixture was used in biological chemistry applications for ferrocene^[37] and (D)-biotin^[38] acylations. Surprisingly, this reagent system was never applied to perform S_EAr with deactivated aromatic carboxylic acids. Once TfOH and TFAA are combined, the strong trifluoroacetyl agent, that is,

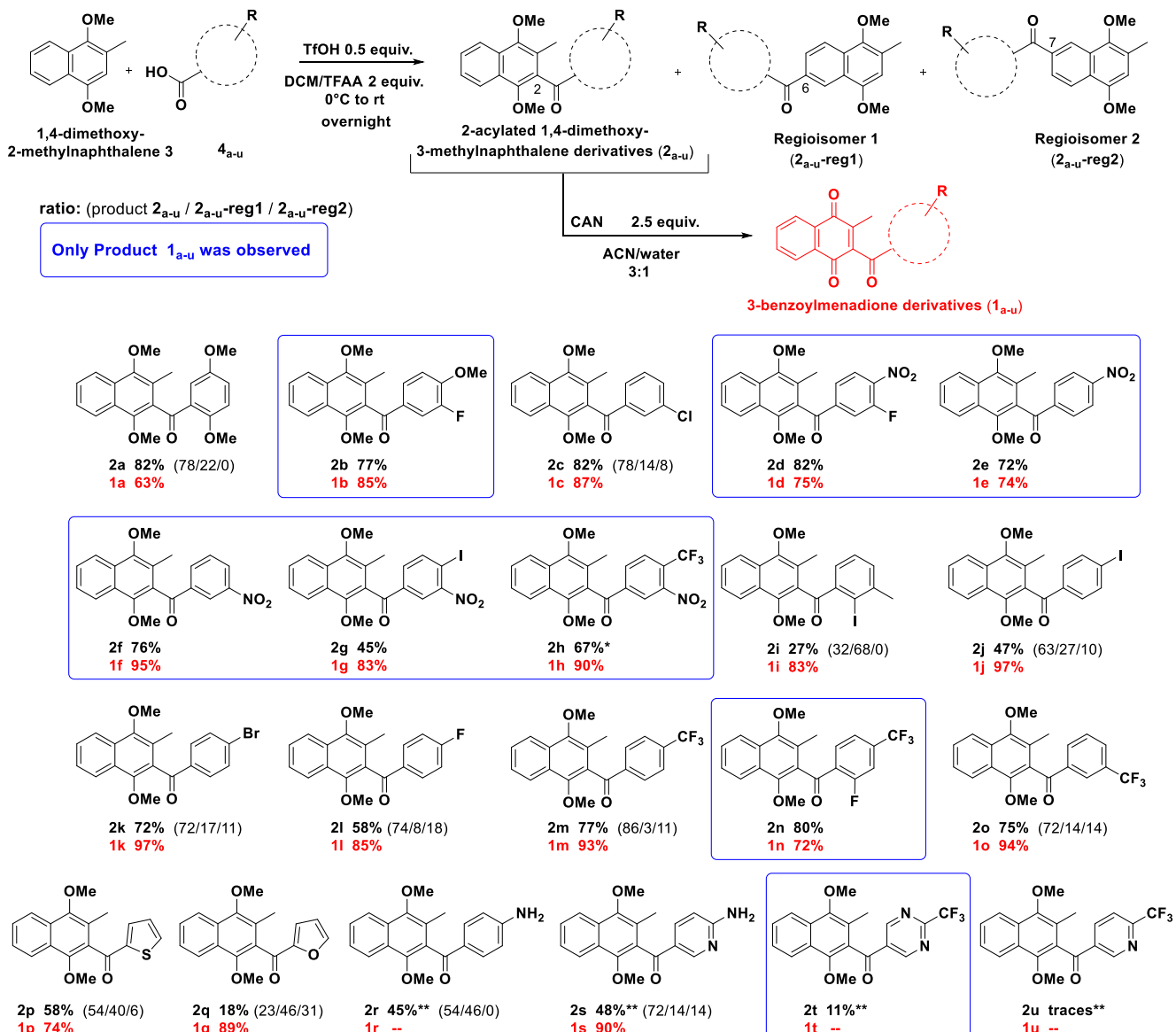
trifluoroacetyl triflate (TFAT), is assumed to be generated.^[39] We investigated the acylation of 1,4-dimethoxy-2-methylnaphthalene by 3-fluoro-4-nitrobenzoic acid and monitored the progression of the reaction by TLC upon addition of TFAA (4 mL) and TfOH (2 equiv. in 10 mL of dichloromethane) to the reaction mixture at 0°C in open air, and then the reaction was performed at room temperature without dry conditions (Table 1, entry 1).

The formation of the targeted compound was clearly evidenced after one hour of reaction, and the desired diarylketone intermediate was isolated in 73 % yield after overnight reaction at room temperature. The effect of TfOH on the acylation reaction was then investigated by adding different amounts of TfOH (Table 1, entries 1-4). A catalytic amount of TfOH (0.1 equiv.) provided the product only in trace amounts (entry 4), and the unreactive starting materials were mainly observed in the crude mixture by NMR spectroscopy. Increasing the TfOH amount up to 20% allowed the reaction to proceed, but with less than 50% conversion and in low yield (entry 4). Finally, by adding 0.5 equiv. of TfOH, full conversion was achieved and the benzophenone was isolated in 82% yield (entry 2). Reducing the quantity of TFAA up to 2 equivalents (entry 5) with the optimized TfOH amount (0.5 equiv.) afforded the product with the same yield and with a much cleaner reaction crude. Furthermore, we checked that TFAA or TFAT did not react with 1,4-dimethoxy-2-methylnaphthalene in the absence of the benzoic acid. An excess of 1.5 equiv. of 1,4-dimethoxy-2-methylnaphthalene was required toward benzoic acid because it enhanced the rate of the reaction under these conditions to observe completion of the reaction overnight. Thus, with an easy defined experimental procedure, these experimental conditions at room temperature allowed us to build a wide variety of 2-benzoyl-3-methyl-1,4-dimethoxy-naphthalene derivatives **2a-u**, including those from strongly deactivated benzoic acids, through an efficient Friedel-Crafts acylation variant (Scheme 6). In the next step, the corresponding 3-arylménadiones **1a-u** diversified at their east aromatic part were prepared following CAN oxidation with moderate to good yields (72-97%) in the majority of the cases (Scheme 6).

Table 1. Optimization of the model Friedel-Crafts reaction conditions with 1,4-dimethoxy-2-methylnaphthalene **3^[a]** and 3-fluoro-4-nitrobenzoic acid **4d^[b]**.

1,4-dimethoxy-2-methylnaphthalene 3		3-fluoro-4-nitrobenzoic acid 4d	TfOH / TFAA overnight	2d
Entry	TfOH (equiv.)	TFAA (equiv.)	Yield (%) ^[c]	
1	2	53	73	
2	0.5	53	82	
3	0.2	53	50	
4	0.1	53	trace	
5	0.5	2	82	

[a] 1.5 equiv., [b] 1.0 equiv., [c] yield after purification.



Scheme 6. Scope of the Friedel-Crafts reaction variant between 3-methyl-1,4-dimethoxy-naphthalene **3** and benzoic acids **4** with base-sensitive moieties. The ratio between the formed Friedel-Crafts products acylated at C-2, C-6 or C-7 was deduced from a regiosomeric analysis based on carbonyl signals of ¹³C NMR spectra of the reaction crude. *: 1.5 equiv. of TfOH was used and the reaction duration was 48h. **: upon addition of 4 equiv. of a mixture TfOH/TFAA (1:1). Abbrev.: The product code of the desired product is 1a-u; 1a-u-reg1 stands for regiosomer 1 (position C-6, *vide infra*), and 1a-u-reg2 for regiosomer 2 (position C-7, *vide infra*).

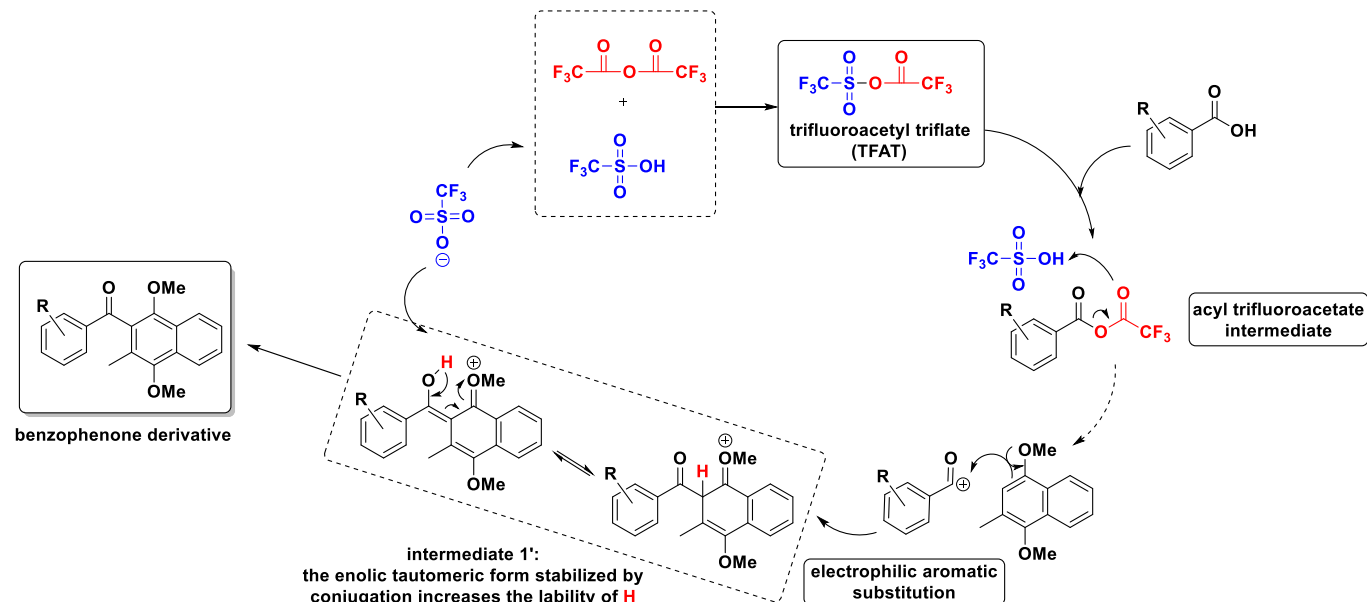
In parallel, an analysis of the regiosomers was performed by ¹³C NMR spectroscopy from the crude of the reaction to quantify their nature and the corresponding ratio formed during the acylation reaction (Scheme 6, and the Supporting Information for details from page S13) by integrating the carbonyl signals of the acylated compounds.^[40] After isolation and purification of each regiosomer from the crude of the reactions to produce **2i**, **2p**, and **2q**, it was possible to attribute the carbonyl signals of each isolated regiosomer upon their ¹³C NMR analysis. Their structures were found to correspond to the acylated products in position C-6 (regiosomer 1) or C-7 (regiosomer 2) of the 1,4-dimethoxy-2-methylnaphthalene core. The new experimental conditions led to improved (or similar) yields of the acylation products **2a-2c** with respect to the previously reported cases using the non-deactivated benzoic acids depicted in Scheme 5. In the case of **2c** with a Cl atom in the *meta* position, the yield

was improved from 45 to 82 % yield. The acylation reaction was observed to be sensitive to steric effects when a bulky group is adjacent to the carboxylic acid (*ortho*), like in the example **2i** where the desired benzophenone is obtained in low yield (27%), supporting the formation of another regiosomer isolated in 71 % yield, by acylation of the 1,4-dimethoxy-2-methylnaphthalene in position C-6. With halogens (I, Br, F) in *para*, benzophenones **2j-2k-2l** were produced in moderate to good yields (47-72-58%, respectively), with a regioselectivity of about 70%. With a Cl atom in *meta* position, the corresponding benzophenone **2c** was obtained in 82% yield with minor regiosomers. Examples with deactivated benzoic acids, incorporating strong electron-withdrawing groups (NO₂ and CF₃) in *para* or *meta*, combined or not with other functionalities (iodo or fluoro), provided excellent yields and regioselectivity. The example **2h**, where a strong deactivated benzoic acid including CF₃ (*para*) and NO₂ (*meta*),

has to be highlighted with the resulting 67% yield of the isolated benzophenone upon addition of 1.5 equivalents of TfOH, confirmed by the observation of only one carbonyl signal in the crude of the ^{13}C NMR spectrum. The use of non-activated heteroaromatic carboxylic acids, like 2-thiophene carboxylic acid or 2-furoic acid, led to acylated products **2p** and **2q** incorporating thiophene and furan moieties in the east aromatic part (Scheme 6), with moderate to low yields of the desired product. However, in both cases, that is, **2p** and **2q**, and also in the case of **2i**, the formation of regioisomers was obtained in higher proportions, probably due to steric effects. However, benzophenone **2q** was obtained with easier experimental conditions compared with the reported reaction using polyphosphoric acid at high temperature.^[41] Direct introduction of acid-sensitive moieties like amino group, pyridine and pyrimidine rings could be achieved after addition of 4 equivalents of a mixture TfOH/TFAA (1:1). Examples **2r** and **2s** incorporate an amino group in *para* in the aromatic and pyridine moieties. The excess of generated TFAT allowed the transient protection of the amino group through a trifluoroacetyl amide group. Consequently, in both cases, moderate yields were obtained with low regioselectivity. The trifluoroacetyl amide group was removed in basic conditions. A pyrimidine fragment incorporating CF_3 was introduced in product **2t** formed in 11% yield but no regioisomer was detected. With the CF_3 group in the same position located in the pyridine fragment, only traces of product **2u** were observed. Although the oxidative demethylation by CAN produced the 3-acylated menadiones **1a–1q** in 63–97% yields (Scheme 6), two nitrogen-based benzophenones (**2r–2t**) led to complex mixtures under these deprotection conditions.

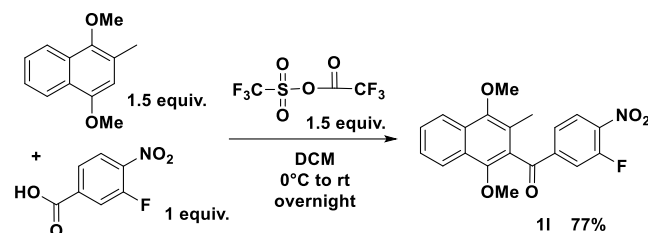
Mechanistic Insight

Based on our present results and a literature report, a possible acylation reaction pathway is depicted in Scheme 7, with the reaction between the 1,4-dimethoxy-2-methylnaphthalene and a substituted benzoic acid representative. The mechanism of the reaction is proposed to proceed through the formation of an acyltrifluoroacetyl intermediate from benzoic acid, promoted by the in situ generation of the reactive trifluoroacetyl triflate (TFAT).



Scheme 7. Putative mechanism of the Friedel-Crafts variant reaction.

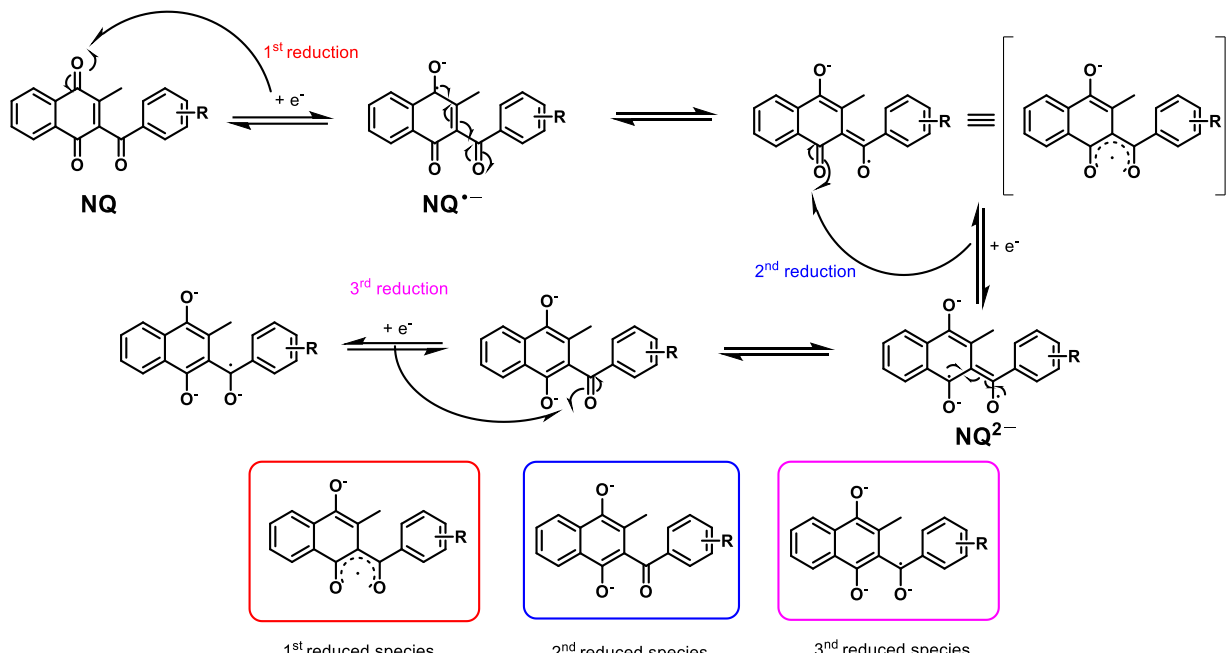
reagent, generated by mixing TfOH and TFAA. TFAT was indeed described as more reactive than TFAA.^[39] In this scenario, the acyltrifluoroacetyl intermediate might be formed for deactivated benzoic acids. During the process of trifluoroacetylation, one molecule of TfOH is produced, which, owing to its excellent proton donor properties, efficiently activates the acyltrifluoroacetate at low temperature and promotes the formation of the acylium cation, allowing the $\text{S}_{\text{E}}\text{Ar}$ of 1,4-dimethoxy-2-methylnaphthalene. Upon acylation, the intermediate **2'** (Scheme 7), which is in equilibrium with the enolic form (more stable by conjugation), is generated. The OH-enol function likely allowed the regeneration of TfOH and, then release of the targeted benzophenone derivative. In situ TFAT formation from TfOH and TFAA was supported by reacting the costly and highly unstable commercial TFAT with 1,4-dimethoxy-2-methylnaphthalene and 3-fluoro-4-nitrobenzoic acid, under the same experimental conditions of the herein described Friedel-Crafts acylation variant. The reaction afforded the desired benzophenone in 77% yield (Scheme 8).



Scheme 8. TFAT as the key reagent for Friedel-Crafts acylation of 1,4-dimethoxy-2-methylnaphthalene by the deactivated 3-fluoro-4-nitrobenzoic acid.

Redox Properties

We will herein discuss the electrochemical data of our homogenous series of 3-acylated-menadiones (Scheme 6). These redox-active compounds only differ by the substitution pattern of their aryl subunit on the east part of the molecule, thus providing evidence for the key role of this moiety (electronic and steric effects) on the redox modulation of the NQ core.



Scheme 9. Proposed mechanism for the consecutive 1-electron transfers centred on 3-benzoylmenadione derivatives.

Table 2. Electrochemical data measured using cyclic voltammetry (CV)^[a] and Square Wave Voltammetry (SWV)^[b] for all 3-benzoylmenadione derivatives examined in this work. Solvent: DMSO; $I = 0.1 \text{ M } n\text{-Bu}_4\text{PF}_6$, $v = 200 \text{ mV s}^{-1}$. ($E_{1/2}$ (V), ΔE (mV), $\Delta E_{1/2} = E^{1/2} - E^{2/2}$ (V))

Cpds	Quinone		Carbonyl group	Nitro group		$\Delta E_{1/2 - E^{2/2}}$ (V)
	$E^{1/2}(\Delta E)^{[a]}$ $E^{1/2}_{1/2}^{[b]}$ [V(mV)] ^[a] [V] ^[b]	$E^{2/2}(\Delta E)$ $E^{2/2}_{1/2}^{[b]}$ [V(mV)] ^[a] [V] ^[b]		$E^{3/2}(\Delta E)^{[a]}$ $E^{3/2}_{1/2}^{[b]}$ [V(mV)] ^[a] [V] ^[b]	$E^{4/2}(\Delta E)^{[a]}$ $E^{4/2}_{1/2}^{[b]}$ [V(mV)] ^[a] [V] ^[b]	
3-benzoyl-menadione 1 ^[5]	-0.47(92)	-1.19(72)				0.72
1a	-0.529(90) / -0.526(78) -0.505	-1.131(94) / -1.128(87) -1.106	br	-	-	0.601
1b	-0.467(90) / -0.463(73) -0.447	-1.172(88) / -1.166(73) -1.147	-1.610	-	-	0.700
1c	-0.444(88) / -0.445(73) -0.427	-1.152(92) / -1.157(82) -1.139	-1.638(85) -1.594	-	-	0.712
1d	-0.418(125) / -0.409(91) -0.469	-0.773(99) / -0.778(97) -0.755	br	-1.002(102) / -0.997(61) 0.977	-1.285(111) / -1.273(85) -1.249	0.286
1e	-0.412(92) / -0.413(77) -0.390	-0.812(96) / -0.808(77) -0.789	-1.484	-1.178(105) / -1.22 (92) -1.192	-	0.399
1f	-0.409(89) / -0.408(86) -0.385	-0.942(95) / -0.945(86) -0.914	br	-1.148(96) / -1.140(74) -1.128	-	0.533
1g	-0.419(82) / -0.422(76) -0.396	-0.948(60) / -0.938(52) -0.933	br	-1.28(86) / -1.291(67) -1.24	-	0.519
1h	-0.387(94) / -0.403(78) -0.362	-0.822(87) / -0.826(82) -0.798	-1.728	nd / -0.985(52) -0.952	-1.182(84) / -1.24(72) -1.158	0.436
1i	-0.434(80) / -0.425(76) -0.404	-1.056(76) / -1.055(70) -1.038	-1.615	-	-	0.634
1j	-0.455(90) / -0.444(77) -0.435	-1.110(96) / -1.094(77) -1.091	-1.573	-	-	0.656
1k	-0.450(88) / -0.449(64) -0.424	-1.134(92) / -1.131(73) -1.102	-1.613	-	-	0.678
1l	-0.457(90) / -0.451(74) -0.433	-1.196(92) / -1.192(80) -1.176	-1.624	-	-	0.743
1m	-0.431(87) / -0.417(80) -0.397	-1.021(86) / -1.005(80) -0.984	-1.87	-	-	0.587
1n ^[b]	$E_{1\text{red}} = -0.45$	$E_{2\text{red}} = -1.065$	nd	-	-	na
1o	-0.423(90) / -0.420(74) -0.397	-1.055(94) / -1.053(80) -1.029	-1.607	-	-	0.632
1p	-0.462(96) / -0.460(79) -0.489	-1.168(100) / -1.168(79) -1.202	-1.750	-	-	0.713
1q	-0.468(100) / -0.464(82) -0.447	-1.159(92) / -1.211(76) -1.135	-1.631 -1.577	-	-	0.691
1s	-0.488(88) / -0.485(70) -0.466	-1.093(102) / -1.117(79) -1.069	-1.953	-	-	0.603

[a] CVs and [b] SWVs measured in DMSO with 0.1 M $n\text{-Bu}_4\text{PF}_6$ electrolyte support at 25°C. $v = 200 \text{ mV s}^{-1}$; reference electrode = $\text{KCl}(3 \text{ M})/\text{Ag}/\text{AgCl}$; working electrode = glassy carbon disk of 0.07 cm^2 area. $E^{1/2}$ and $E^{2/2}$ are related to the quinone-centred redox processes, $E^{3/2}$ is related to the carbonyl benzoyl unit while $E^{4/2}$ and $E^{5/2}$ characterize the nitro-centred redox processes. br = broad. nd = not determined. na = not applicable. [b] Measured at $v = 500 \text{ mV s}^{-1}$. The values in italics correspond to measurements at 50 mV s⁻¹.

The redox potentials of the substituted 3-aryl-menadiones **1** (Table 2 and Figures S1-19 in the Supporting Information) were measured by cyclic voltammetry (CV) and square wave voltammetry (SWV, Table 2) at $23 \pm 1^\circ\text{C}$ by using a glassy carbon (GC) working electrode in DMSO solvent and tetra-*n*-butylammonium hexafluorophosphate (*n*-NBu₄PF₆) as the supporting/inert electrolyte. The electrochemical properties measured by SWV were found to be in good agreement with those measured by CV (Table 2). Furthermore, the data recorded for **1f**, **1g**, **1h** and **1a** were found to be in excellent agreement with those measured in a previous communication.^[5]

Irrespective of the substitution pattern of the aryl subunit, no alteration of the global electrochemical profile of the NQ core was observed. Two consecutive one-electron quasi-reversible waves ($E_{\text{pc}}^1 - E_{\text{pa}}^1 \sim 80-125$ mV and $E_{\text{pc}}^2 - E_{\text{pa}}^2 \sim 72-100$ mV) were systematically observed under our experimental conditions. NQ reduction indeed occurs by two successive one-electron transfers. The monoradical-anion NQ^{•-} is formed in the $E_{\text{pc}1}$ reduction step, and is then reduced to its related dihydro-naphthoquinone dianion NQ²⁻ in a second $E_{\text{pc}2}$ step. The 3-benzoylmenadiones **1a-s** examined in this work were not subjected to any inter- or intramolecular proton transfers and therefore the electrochemical properties were considered to be strictly associated to the successive formation of the two anionic reduced species.

In addition to these consecutive one-electron transfers, a third (i.e. in some cases as for **1h** and **1d**, a fourth redox wave is also observed) redox wave at potential value $E_{1/2}^3$ of about -1 to -1.2 V was also observed for the nitro-benzoyl-menadiones **1d**, **1e**, **1f**, **1g** and **1h** (Figures S4-S8, S19 in the Supporting Information and Table 2). These additional redox signals most likely result from the reduction of the nitro function.^[42] Finally, a last weak, broad and ill-defined wave was often observed at much more negative values ($E_{1/2}^3 >> -1.5$ V) and was attributed to oxidation/reduction processes centered on the benzoyl carbonyl unit (Figure 2).

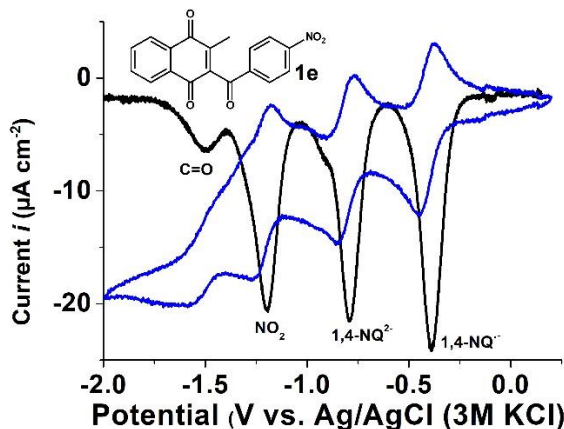


Figure 2. CV (blue) and SWV (black) profiles of **1e** (1.40 mM) measured in DMSO with 0.1 M *n*-Bu₄PF₆ electrolyte support at 25°C. $v = 50$ mV s⁻¹; reference electrode = KCl(3 M)/Ag/AgCl; working electrode = glassy carbon disk of 0.07 cm² area; auxiliary electrode = Pt wire.

Compound **1n** bearing a 2'-fluoro substituent stands in an interesting contrast with the other systems. Reduction at 1 (or 2) electrons afforded an anionic species which can rapidly trigger (at the time scale of the electrochemical experiment) a nucleophilic substitution, at the 2'-position, leading to a benzoxanthone product (Figure 1).^[10c] Increasing the voltage sweep rate up to 5

V (Figure S14 in the supporting information) indeed allowed us to evidence in the first cycle the characteristic reduction peaks of the benzoquinone unit which then faded completely in the following cycles as a result of the reaction.

Combining previously published data^[5] with the present ones, a clear relationship between the half-wave potentials of the first ($E_{1/2}^1$) and second ($E_{1/2}^2$) electrochemical processes can be proposed (Figure 3). Exceptions have been, however, observed for the 2'-substituted benzoyl-menadiones (i.e., steric effect) or proton-donor substituent such as 4'-OH.^[5] This feature suggests that the substituents borne by the benzoyl core induce sizeable electronic effects both on the NQ unit or on its one-electron reduced semi-quinone, NQ^{•-}. With respect to the first redox process ($E_{1/2}^1$) of 4'-substituted benzoyl-menadiones, the gap in potential was, however, measured to be only about 80 mV between the menadione substituted with a methoxy group^[5] in the 4' position and that substituted with a nitro group at the same position (**1e**). This likely suggests weak to no influence of the benzoyl substitution pattern on the first electron transfer of the naphthoquinone redox active core. It is noteworthy, that under its oxidized state, the NQ is poorly conjugated with its benzoyl counterpart.

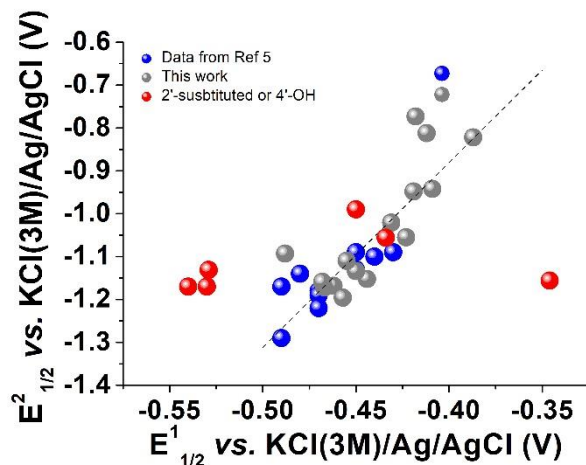


Figure 3. Variation of $E_{1/2}^2$ (V, second redox step) as a function of $E_{1/2}^1$ (V, first redox step). $v = 200$ mV s⁻¹; reference electrode = KCl(3 M)/Ag/AgCl; working electrode = glassy carbon disk of 0.07 cm² area; auxiliary electrode = Pt wire. The dashed line is only provided as a guide for the eyes. ● Data taken from ref [5]. ● Data from this present work. ● Compound with particular behaviour (e.g. 2'-substituted or 4'-OH benzoylmenadiones, see text).

By contrast, a marked impact of the 4'-benzoyl substitution can be observed on the second electron transfer leading to the dihydro-naphthoquinone dianion NQ²⁻. Interestingly, the gap in potential amounts to up 500 mV between the menadione substituted with a carboxylic group in the 4' position^[5] and that substituted with a nitro group at the same position (**1e**, Figure 4). To rationalize this behaviour, we therefore hypothesized that upon the first one electron reduction of the benzoylmenadiones, the radical is stabilized by the benzoyl carbonyl unit thus allowing electronic communication between the redox-active NQ core and the benzoyl subunit (Scheme 9). Consequently, the second one-electron transfer leading to the dihydro-naphthoquinone dianion NQ²⁻ is thus highly sensitive to the nature of the benzoyl substitution (Figure 4 and Figure S1-S19). Within this series of molecules, the presence of the benzoyl carbonyl function thus allows significant modulation over a large potential (~ 500 mV)

span for the oxidant character of the semi-quinone $\text{NQ}^{\cdot-}$ while slightly affecting that of the NQ analogue (~ 80 mV). These properties are of significant importance in the context of antimalarial drug development and understanding of the mechanism of action of the early lead plasmodione.^[6]

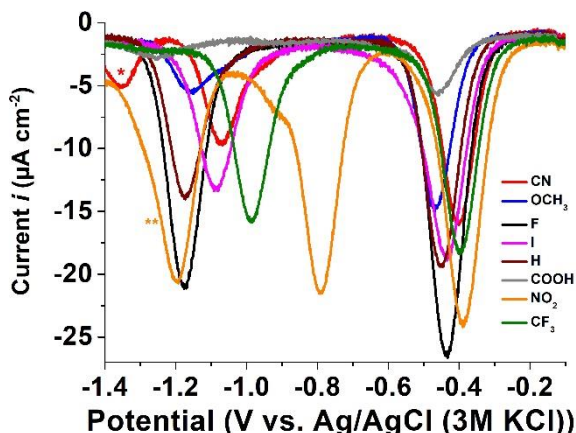
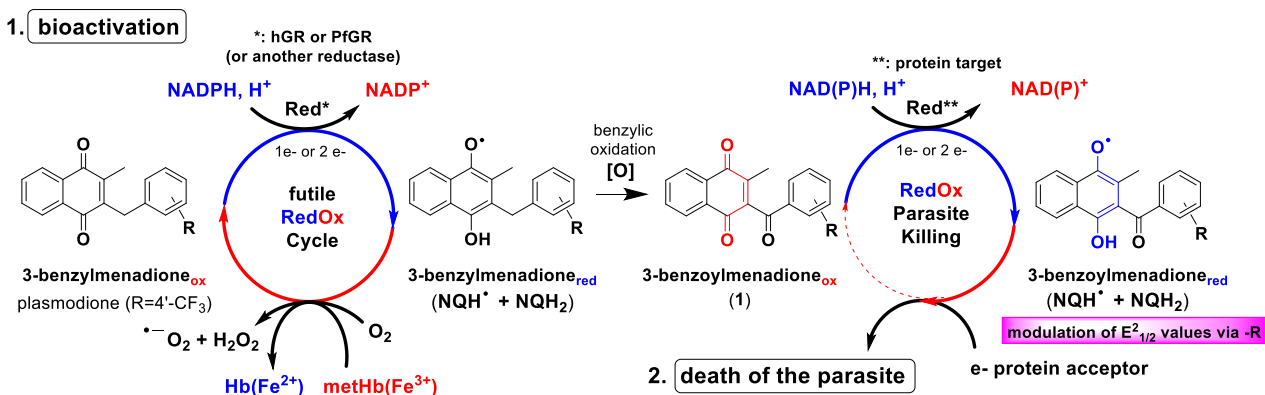


Figure 4. SWV profiles of compound cited as **3k** in ref.^[5] (1.06 mM, 4'-CN), compound cited as **3l** in ref.^[5] (1.03 mM, 4'-OCH₃), **1l** (1.38 mM, 4'-F), **1j** (1.20 mM, 4'-I), compound cited as **3h** in ref.^[5] (1.19 mM, 4'-H), compound cited as **3f** in ref.^[5] (0.94 mM, 4'-COOH), **1e** (1.40 mM, 4'-NO₂), **1m** 1.16 mM, 4'-CF₃) measured in DMSO with 0.1 M *n*-Bu₄PF₆ electrolyte support at 25°C. $v = 200$ mV s⁻¹; reference electrode = KCl(3 M)/Ag/AgCl; working electrode = glassy carbon disk of 0.07 cm² area.

Bioactivation through redox-cycling of NQ mediated by one- or two-electron transferring oxido-reductase enzymes is an oxygen-dependent process (Scheme 10).^[4-6] Under aerobic conditions, we previously showed that both major cytosolic NADPH-dependent glutathione reductases (and possibly other reductases) from *P. falciparum*-parasitized red blood cells participate in a futile redox cycle in which the production of the protonated NQH[·] species from NQ is rapidly back-oxidized to its

parent compound, NQ, at near diffusion-limited rates.^[5] Oxygen and methemoglobin(Fe³⁺), the major hemoglobin catabolite and nutrient generated in *Plasmodium* parasites, play the role of one-electron acceptors from the semi-quinone NQH[·]. Upon 1-e⁻ and 2-e⁻ reduction, NQH[·] and NQH₂ react rapidly with O₂ to regenerate the non-toxic parent prodrug, NQ, superoxide radicals and hydrogen peroxide as by-products. Therefore, our expectation is that under aerobic conditions, NQH[·] per se does not contribute significantly to killing the cells, as it has been observed for plasmidione by the absence of toxicity against various human cell lines.^[6] This bioactivation process was also reported for the anticancer quinonic mitomycin C.^[4g] It is well documented that, while the concentration of O₂ in arterial blood is approximately 13%, O₂ concentrations below 7.5% are found in most organs to which *Plasmodium*-parasitized red blood cells sequester, including the bone marrow, brain, and liver.^[4d] Therefore, in the hypoxic conditions where malaria parasites can survive, the half-life of NQH[·] might be extended, allowing it to participate in several metabolic transformations, such as the benzylic oxidation (Scheme 10). Thus, after transport to the parasitic compartment, NQH[·] can undergo further reduction by other key-protein targets to produce the toxic NQH₂ (Scheme 10). The observed parasite killing might be therefore attributable to the combined flux from both one- and two-electron reducing pathways generating the protonated NQH[·] and NQH₂ species, which undergo a series of spontaneous rearrangements (in particular, phenolic oxidative coupling to form the benzoxanthones, see structures of 7H-benzo[c]xanthen-7-ones from Figure 1).^[10c] By changing the molecular diversity at the benzoyl chain of 3-benzoylmenadiones **1a-u** our data showed that this aryl substitution can markedly alter the redox properties of the NQ electrophore and thus modulate the second one-electron transfer leading to the dihydro-naphthoquinone NQH₂ species. This toxic species resulting from 3-benzoylmenadiones **1** is likely generated in situ in parasites from the antimalarial 3-benzoylmenadione prodrugs and significantly contributes to the antimalarial activity.



Scheme 10. Proposed mechanism of action of antimalarial 3-benzoylmenadione prodrugs generating toxic 3-benzoylmenadione **1** metabolites in *P. falciparum*-parasitized red blood cells. The first one-electron transfer leading to the semi-quinone NQH[·] is proposed to be involved in the drug bioactivation (step 1.) while the second one-electron transfer leading to the dihydro-naphthoquinone NQH₂ might be responsible for parasite killing (step 2). For the sake of clarity, only the 1-e⁻ reduced NQ species were drawn. Abbrev.: hGR: human glutathione reductase; PfGR: *P. falciparum* glutathione reductase.

Conclusions

We have developed a mild and convenient Friedel-Crafts variant for acylation of 1,4-dimethoxy-2-methylnaphthalene by diversely substituted activated or deactivated benzoic and (hetero)aroyl acids, by using the TfOH/TFAA reagent system through mild conditions (room temperature, overnight, air moisture). The Friedel-Crafts reaction is a very useful reaction to prepare benzophenones derivatives, and the application of a versatile and mild protocol, suitable for any starting substituted benzoic acid, to produce diversely functionalized benzophenone derivatives in satisfactory yields, renders this reaction attractive for organic synthesis and medicinal chemistry. Thus, this new variant allowed us to obtain a broad library diversity, both in terms of molecular structure of 3-acylated menadienes and function – expressed here by tuneable $E^{1/2}$ values spanning over a broad range of redox potentials (500 mV). Because the antimalarial 3-benzylmenadienes are thought to be activated through a cascade of redox reactions via the 3-benzoylmenadienes **1**, the library diversity will allow us to subtly modulate the physico(electro)chemical properties of our lead antimalarial agents, which is a crucial step in any drug discovery program.

Experimental Section

Detailed descriptions of experimental procedures, data on product characterization including spectral data and ^1H and ^{13}C NMR spectra of all new compounds are given in the Supporting Information.

Typical Procedure for preparing 2-(2,5-dimethoxyphenyl)-2-oxoacetic acid (**5a**) or 2-(3,5-dimethoxyphenyl)-2-oxoacetic acid (**5a'**)

A round bottom flask which had been flushed with argon was charged with 2,5-dimethoxyacetophenone (5 mL, 31.6 mmol), SeO_2 (7.01 g, 63.2 mmol), and pyridine (16 mL). The solution was heated at 120 °C. The temperature gradually dropped to 90°C over 1 h and was heated for an additional 4h. The solution was concentrated by rotary evaporator until a small amount of liquid was present. The black selenium residue was rinsed several times with ethyl acetate. The combined organic layers were transferred to a separatory funnel containing 0.1 M HCl (100 mL). The aqueous layer was extracted three times with ethyl acetate. The aqueous layer was discarded, and the organic layers were combined and extracted several times with saturated aqueous NaHCO_3 . The aqueous layers were combined, adjusted to pH 1 with conc. HCl, and extracted three times with ethyl acetate. The final organic layers were dried over Na_2SO_4 and concentrated, producing the 2-(dimethoxyphenyl)-2-oxoacetic acid **5a** or **5a'**.

General procedure of the for the Silver(II)-Catalyzed Kochi-Anderson reaction between menadione and α -keto carboxylic acids

A mixture of menadione (131 mg, 0.50 mmol), 2-oxopropionic acid (133 mg, 1.51 mmol), silver(I) nitrate (34 mg, 0.20 mmol), and potassium persulfate (484 mg, 1.79 mmol) in acetonitrile (2 mL) and H_2O (6 mL) was heated at 70 °C for 3 h. The reaction mixture was diluted with ethyl acetate (100 mL), washed with water (3 x 50 mL), dried (Na_2SO_4), and concentrated in vacuum. The crude product was purified by column chromatography over silica gel (20 g; ethyl acetate/hexane, 1:15) followed by recrystallization (ethyl acetate/hexane) to give **1a** or **1a'**.

General procedure for the Friedel-Crafts acylation using the reagent mixture TFA-TFAA.

1,4-dimethoxy-2-methylnaphthalene (1.0 mmol) and 3-chlorobenzoic acid (0.66 mmol) were mixed to a solution of TFAA (2 mL). Then, TFA (1 mL) was added and the mixture was heated under reflux for overnight. When the time described for the reaction finished, the system was cold down and water (10 mL) was added steadily. At that point, ethyl acetate (3 x 50 mL) was added, and the organic layers were combined, dried over magnesium sulfate. The solid was discarded by filtration, and the excess of the solvent removed under reduced pressure. The crude was absorbed on silica gel and purified by flash chromatography by using toluene-cyclohexane as eluent system.

General procedure for the Friedel-Crafts acylation using the reagent mixture TfOH-TFAA

1,4-dimethoxy-2-methylnaphthalene (1.5 mmol) and benzoic acid (1 mmol) were dissolved in dichloromethane (0.2 M). At 0°C, TFAA (2 mmol) was added. After stirring for 10 minutes, TfOH (0.5 mmol) was added cautiously and the reaction mixture was allowed to warm up slowly to room temperature and stirred for 16h. Then, the reaction was quenched by an aqueous saturated NaHCO_3 solution and the aqueous phase was extracted three times by dichloromethane. The combined organic phases were dried over MgSO_4 and the solvent was removed under reduced pressure. The reaction crude was purified by silica gel chromatography by using a mixture of cyclohexane and toluene as eluent to afford analytically pure Friedel & Crafts products.

General procedure fo oxidative demethylation

2-Aroyl-3-methyl-1,4-dimethoxy-naphthalene derivative **2** (1 mmol) was dissolved in stirring MeCN (3 mL). Then, at room temperature, CAN (2.1 mmol) dissolved in water (2 mL) was added drop by drop. The mixture was stirred at room temperature during 1h. Then, most of the organic solvent was removed under reduced pressure and the aqueous phase was extracted three times with dichloromethane. Combined organic layers were dried over MgSO_4 and the solvent was removed under reduced pressure. Purification by silica gel chromatography was performed by using cyclohexane/EtOAc as eluent.

Acknowledgements

The authors wish to thank the ANR-PRC program (grant PlasmoPrim project, E.D.C.), the Laboratoire d'Excellence (LabEx) ParaFrap (grant LabEx ParaFrap ANR-11-LABX-0024, E.D.C.), for funding and creating a proper framework for this scientific research. The Centre National de la Recherche Scientifique (CNRS), the University of Strasbourg (UMR 7042 CNRS-Unistra-UHA), and the International Center for Frontier Research in Chemistry (ic-FRC) in Strasbourg (ic-FRC-LabEx Chimie des systèmes complexes, project entitled "Understanding the mechanisms of antimalarial redox-active substrates in *Plasmodium*-infected red blood cells: a combined physicochemical and computational approach to unveiling biological complexity") partly supported this work. M.D. thank the ANR-PRC program (grant PlasmoPrim project) for his salary.

Keywords: acylation • acyltrifluoroacetate • benzoyl • electrochemistry • Friedel-Crafts

- [2] H.Y. Qiu, P.F. Wang, H.Y. Lin, C.Y. Tang, H.L. Zhu, Y.H. Yang, *Chem. Biol. Drug Des.* **2018**, *91*, 681-690.
- [3] E.A. Hillard, F.C. de Abreu, D.C. Ferreira, G. Jaouen, M. O. Goulart, C. Amatore, *Chem. Commun.* **2008**, *23*, 2612-2628.
- [4] a) L. Salmon-Chemin, E. Buisine, V. Yardley, S. Kohler, M.A. Debreu, V. Landry, C. Sergheraert, S.L. Croft, R.L. Krauth-Siegel, E. Davioud-Charvet, *J. Med. Chem.* **2001**, *44*, 548-565; b) D. Belorgey, D.A. Lanfranchi, E. Davioud-Charvet, *Curr. Pharm. Des.* **2013**, *19*, 2512-2528.
- [5] a) M. Elhabiri, P. Sidorov, E. Cesar-Rodo, G. Marcou, D.A. Lanfranchi, E. Davioud-Charvet, D. Horvath, A. Varnek, *Chem. Eur. J.* **2015**, *21*, 3415-3424; b) P. Sidorov, I. Desta, M. Chesse, D. Horvath, G. Marcou, A. Varnek, E. Davioud-Charvet, M. Elhabiri, *ChemMedChem* **2016**, *11*, 1339-1351.
- [6] T. Müller, L. Johann, B. Jannack, M. Bruckner, D.A. Lanfranchi, H. Bauer, C. Sanchez, V. Yardley, C. Deregnaucourt, J. Schrevel, M. Lanzer, R.H. Schirmer, E. Davioud-Charvet, *J. Am. Chem. Soc.* **2011**, *133*, 11557-11571.
- [7] a) D.A. Lanfranchi, E. Cesar-Rodo, B. Bertrand, H.-H. Huang, L. Day, L. Johann, M. Elhabiri, K. Becker, D.L. Williams, E. Davioud-Charvet, *Org. Biomol. Chem.* **2012**, *10*, 6375-6387; b) E. Cesar Rodo, L. Feng, M. Jida, K. Ehrhardt, M. Bielitz, J. Boilevin, M. Lanzer, D.L. Williams, D.A. Lanfranchi, E. Davioud-Charvet, *Eur. J. Org. Chem.* **2016**, *11*, 1982-1993; c) K. Usgin, M. Jida, K. Ehrhardt, T. Müller, M. Lanzer, L. Maes, M. Elhabiri, E. Davioud-Charvet, *Molecules* **2017**, *22*:1.
- [8] a) P.C.B. Halicki, L.A. Ferreira, K.C.G. De Moura, P.F. Carneiro, K.P. Del Rio, T.D.S.C. Carvalho, M.D.C.F.R. Pinto, P.E.A. da Silva, D.F. Ramos, *Front Microbiol.* **2018**, *9*, 673. b) S.B. Vafai, E. Mevers, K.W. Higgins, Y. Fomina, J. Zhang, A. Mandinova, D. Newman, S.Y. Shaw, J. Clardy, V.K. Mootha, *PLoS One* **2016**, *11*(9):e0162686. c) C.O. Salas, M. Faundez, A. Morello, J.D. Maya, R.A. Tapia, *Curr. Med. Chem.* **2011**, *18*, 144-161.
- [9] a) J. Yang, D. Knueppel, B. Cheng, D. Mans, S.F. Martin, *Org. Lett.* **2015**, *17*, 114-117; b) D. Knueppel, J. Yang, B. Cheng, D. Mans, S.F. Martin, *Tetrahedron* **2015**, *71*, 5741-5757.
- [10] a) G.A. Kraus, J. Mengwasser, *Molecules* **2009**, *14*, 2857-2861; b) L. Johann, D.A. Lanfranchi, E. Davioud-Charvet, M. Elhabiri, *Curr. Pharm. Des.* **2012**, *18*, 3539-3566; c) M. Bielitz, D. Belorgey, K. Ehrhardt, L. Johann, D.A. Lanfranchi, V. Gallo, E. Schwarzer, F. Mohring, E. Jortzik, D.L. Williams, K. Becker, P. Arese, M. Elhabiri, E. Davioud-Charvet, *Antioxid. Redox Signal.* **2015**, *22*, 1337-51.
- [11] M. Buccini, M.J. Piggott, *Org. Lett.* **2014**, *16*, 2490-2493.
- [12] a) B.S. Joshi, Q. Jiang, T. Rho, S.W. Pelletier, *J. Org. Chem.* **1994**, *59*, 8220-8223; b) F.M. Hauser, H. Yin, *Org. Lett.* **2000**, *2*, 1045-1047.
- [13] a) M. Oelgemöller, C. Schiel, R. Frohlich, J. Mattay, *Eur. J. Org. Chem.* **2002**, *2002*, 2465-2474; b) J. Benites, D. Rios, P. Diaz, J.A. Valderrama, *Tetrahedron Lett.* **2011**, *52*, 609-611.
- [14] L. Feng, D.A. Lanfranchi, L. Cotos-Munoz, E. Cesar Rodo, K. Ehrhardt, A.-A. Goetz, H. Zimmerman, F. Fenaille, S. Blandin, E. Davioud-Charvet, *Org. Biomol. Chem.* **2018**, *16*, 2647-2665.
- [15] a) G. Kranzlein, in *Aluminium Chloride in der Organischen Chemie*, 3rd ed.; Verlag Chemie, Berlin, **1939**. b) C.A. Thomas, in *Anhydrous Aluminium Chloride in Organic Chemistry*; Rainhold: New York, 1961.
- [16] S. Paul, P. Nanda, R. Gupta, A. Loupy, *Synthesis* **2003**, *18*, 2877-2881.
- [17] M.H. Sarvari, H. Sharghi, *J. Org. Chem.* **2004**, *69*, 6953-6956.
- [18] G.A. Olah, R. Malhorta, S.C. Narang, J.A. Olah, *Synthesis* **1978**, *9*, 672-673.
- [19] a) O. Akiko, M. Katsuya, O. Hideaki, Y. Noriyuki, *Synth. Commun.* **2007**, *37*, 2701-2715; b) I.R. Butler, J.O. Morley, *J. Chem. Res. (S)* **1980**, *10*, 358-359.
- [20] A.G. Posternak, R.Yu. Garlyauskayte, L.M. Yagupolskii, *Tetrahedron Lett.* **2009**, *50*, 446-447.
- [21] a) J. Izumi, T. Mukaiyama, *Chem. Lett.* **1996**, 739-740; b) K. Shū, I. Shunsuke, *Tetrahedron Lett.* **1998**, *39*, 4697-4700.
- [22] a) F. Effenberger, G. Epple, *Angew. Chem. Int. Ed. Engl.* **1972**, *11*, 299-300; b) F. Effenberger, G. Epple, *Angew. Chem. Int. Ed. Engl.* **1972**, *11*, 300-301; c) F. Effenberger, E. Sohn, G. Epple, *Chem. Ber.* **1983**, *116*, 1195-1208.
- [23] a) J.J. Li, L.H. Mitchell, R.L. Dow, *Bioorg. Med. Chem. Lett.* **2010**, *20*, 306-308; b) Z. Wu, G. Wei, G. Lian, B. Yu, *J. Org. Chem.* **2010**, *75*, 5725-5728.
- [24] H. Sharghi, B. Kaboudin, *J. Chem. Res. (S)* **1998**, 628-629.
- [25] a) H. Sharghi, M. Hosseini-Sarvari, R. Eskandari, *Synthesis* **2006**, *12*, 2047-2052. b) Hosseini-Sarvari, M.; Sharghi, H. *Synthesis* **2004**, *12*, 2165-2168.
- [26] a) S. Grasso, G. De Sarro, A. De Sarro, N. Micale, M. Zappalà, G. Puja, M. Baraldi, C. De Micheli, *J. Med. Chem.* **2000**, *43*, 2851-2859; b) M. Zappalà, S. Grasso, N. Micale, S. Polimeni, C. De Micheli, *Synth. Commun.* **2002**, *32*, 527-533; c) M. Zappalà, A. Pellicanò, N. Micale, F.S. Menniti, G. Ferreri, G. De Sarro, S. Grasso, C. De Micheli, *Bioorg. Med. Chem. Lett.* **2006**, *16*, 167-170.
- [27] A. Zarei, A.R. Hajipour, L. Khazdooz, *Tetrahedron Lett.* **2008**, *49*, 6715-6719.
- [28] M.C. Wilkinson, *Org. Lett.* **2011**, *13*, 2232-2235.
- [29] D. Tejedor, L. Cotos, D. Marquez-Arce, M. Odriozola-Gimeno, M. Torrent-Sucarrat, F.P. Cossio, F. Garcia-Tellado, *Chem. Eur. J.* **2015**, *21*, 18280-18289.
- [30] G. Mlostoň, R. Hamera, H. Heimgartner, *Phosphorus Sulfur Silicon Relat. Elem.* **2015**, *190*, 2125-2133.
- [31] Z.-Y. Lin, Y.-L. Chen, C.-S. Lee, C.-P. Chuang, *Eur. J. Org. Chem.* **2010**, *3876-3882*.
- [32] M. C. Pirrung, R. J. Tepper, *J. Org. Chem.* **1995**, *60*, 2461-2465.
- [33] a) J. McNulty, P. Das, *Tetrahedron* **2009**, *65*, 7794-7800; b) D. Van Leusen, A.M. Van Leusen, *Org. React.* **2001**, *57*, 417-666; c) S.S. Yan, L. Zhu, J.H. Ye, Z. Zhang, H. Huang, H. Zeng, C.J. Li, Y. Lan, D.G. Yu, *Chem. Sci.* **2018**, *9*, 4873-4878; d) L.R. Cafiero, T.S. Snowden, *Org. Lett.* **2008**, *10*, 3853-3856.
- [34] a) J. Cesar, M. Sollner Dolenc, *Tetrahedron Lett.* **2001**, *42*, 7099-7102; b) T. Tsuchida, A. Kuroda, H. Nagai, M. Yoshida, T. Nakashima, K. Konuki, K. Isshiki, H. Nakamura, T. Takeuchi, *J. Antibiot.* **2003**, *56*, 38-41; c) M.B. Khaled, R.K. EI Mokadem, J.D. Weaver, *J. Am. Chem. Soc.* **2017**, *139*, 13092-13101.
- [35] W.R.J.D. Galloway, A. Isidro-Llobet, D.R. Spring, *Nature Commun.* **2010**, *1*, 1-13.
- [36] a) E.J. Bourne, M. Stacey, J.C. Tatlow, J. M. Tedder, *J. Chem. Soc.* **1951**, *718-720*; b) E.J. Bourne, M. Stacey, J.C. Tatlow, R. Worrall, *J. Chem. Soc.* **1954**, 2006-2012.
- [37] D. Plazuk, J. Zakrzewski, *Synth. Commun.* **2004**, *34*, 99-107.
- [38] D. Plazuk, J. Zakrzewski, M. Salmain, *Org. Biomol. Chem.* **2011**, *9*, 408-417.
- [39] a) T.R. Forbus Jr., J.C. Martin, *J. Org. Chem.* **1979**, *44*, 313-314. b) T.R. Forbus Jr., S.L. Taylor, J.C. Martin, *J. Org. Chem.* **1987**, *52*, 4156-4159.
- [40] D.A.L. Otte, D.E. Borchmann, C. Lin, M. Weck, K.A. Woerpel, *Org. Lett.* **2014**, *16*, 1566-1569.
- [41] R.T. Pardasani, P. Pardasani, S. Muktarawat, R. Ghosh, T. Mukherjee, *Heterocycl. Commun.* **1998**, *4*, 77-80.
- [42] a) W.H. Smith, A.J. Bard, *J. Am. Chem. Soc.* **1975**, *97*, 5203-5210; b) J. Šarlauskas, V. Miliukienė, Ž. Anusevičius, L. Misievičienė, K. Krikštopaitis, A. Nemeikaitė-Čenienė, I. Vitienė, N. Čėnas, *Chemija* **2009**, *20*, 109-115; c) J. Šarlauskas, A. Nemeikaitė-Čenienė, L. Misievičienė, K. Krikštopaitis, Ž. Anusevičius, N. Čėnas, *Acta Biochim. Pol.* **2013**, *60*, 227-231; d) O. Hammerich in *Organic electrochemistry revised and expanded*, 5th Edition, (Eds: O. Hammerich, B. Speiser) CRC Press, **2015**, Ch. 30, pp. 1149-1201.
- [43] H.A. Seow, P.G. Penketh, R.P. Baumann, A.C. Sartorelli, *Methods Enzymol.* **2004**, *382*, 221-233.
- [44] N.M. Archer, N. Petersen, M.A. Clark, C.O. Buckee, L.M. Childs, M.T. Duraisingham, *Proc. Natl. Acad. Sci. U S A* **2018**, *115*, 7350-7355.

5 points à retenir de l'article

- 1) Mise en place d'une méthode de benzoylation de Friedel & Crafts entre un arène riche en électron et des acides benzoïques portant une grande diversité de groupements électrodonneurs ou électroattracteurs.
- 2) Réaction régiosélective en l'absence d'encombrement stérique important.
- 3) Obtention d'une série de 3-benzoylménadiones après déprotection des produits de Friedel & Crafts.
- 4) Caractérisation des propriétés rédox des 3-benzoylménadiones par voltampérométrie cyclique (CV) et à ondes carrées (SWV).
- 5) Rationalisation de l'effet des substituants des unités benzoyles sur les potentiels rédox des 3-benzoylménadiones.

2. Applications de la méthode d'acylation de Friedel-Crafts pour la synthèse de sondes ABPP.

2.1. Objectifs et travaux préliminaires.

L'acylation de Friedel-Crafts vue précédemment nous a permis d'obtenir efficacement en une seule étape les précurseurs nécessaires à l'élaboration de sondes chimiques. Leur synthèse est détaillée dans l'article présenté dans la partie 2.2 de ce chapitre (**Figure 15**).

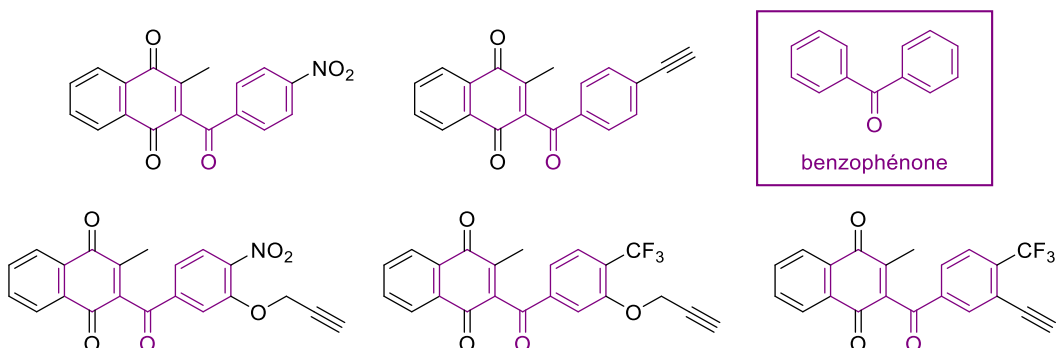


Figure 15. Structure des sondes chimiques synthétisées pour ce projet et de leur cœur "benzophénone like".

Les 3-benzoylménadiques ont la particularité de porter dans leur structure un motif « benzophénone-like », ou une vraie benzophenone après réduction des 3-benzoylménadiques en dihydronaphthoquinone. Afin de concevoir des sondes pour étudier le profil protéomique des parasites traités par les benzoylménadiques, métabolites de la **PD**, nous avons envisagé l'hypothèse selon laquelle le motif soit photoréactif, et que, sous irradiation UV, la sonde puisse se lier aux cibles avec lesquelles elle interagit. Ainsi, la fonctionnalisation de ces sondes devenait minimaliste puisqu'elle nécessitait l'introduction de fonctions alcynes seulement sur le squelette 3-benzoylménadione, sans ajout d'un motif benzophénone qui aurait pu modifier l'affinité de la 3-benzoylménadione pour sa cible. Les fonctions alcynes avaient le rôle d'étiquette pour marquer les photo-adduits par une réaction de cyclisation de type CuAAC (réaction click, ou couplage au cuivre azide-alcyne) afin d'isoler/d'enrichir les adduits par une technique dite de « click & fish ». Cette hypothèse a été validée par notre équipe et les résultats ont été publiés dans l'article présenté ci-dessous.

En plus de la synthèse des sondes chimiques, j'ai pu réaliser la preuve de concept préliminaire d'alkylation de ces dernières 3-benzoylménadiques avec un partenaire-modèle, la *N*-acetyl-méthionine methyl ester (nMet). Pour cela, nous nous sommes inspirés des travaux de l'équipe de Guy Ourisson dans lesquelles le couplage de divers acides aminés protégés et la benzophénone ont été étudiés.⁵⁰ Le mécanisme supposé de ce couplage est le suivant : la benzophénone, excitée sous photoirradiation par lumière UV, va procéder à l'abstraction d'un hydrogène (HAT) de l'acide aminé, les deux radicaux

⁵⁰ E. Deseke, Y. Nakatani, G. Ourisson, *Eur. J. Org. Chem.* **1998**, 243-251.

obtenus pouvant ensuite procéder à un couplage intramoléculaire (**Schéma 17**). Dans la réaction modèle mise au point au laboratoire, le choix du partenaire nMet s'est fait sur la réactivité connue de la méthionine, acide aminé le plus réactif au sein des protéines, pour réagir avec la benzophénone dans les études de photomarquage d'affinité ou les études ABPP.

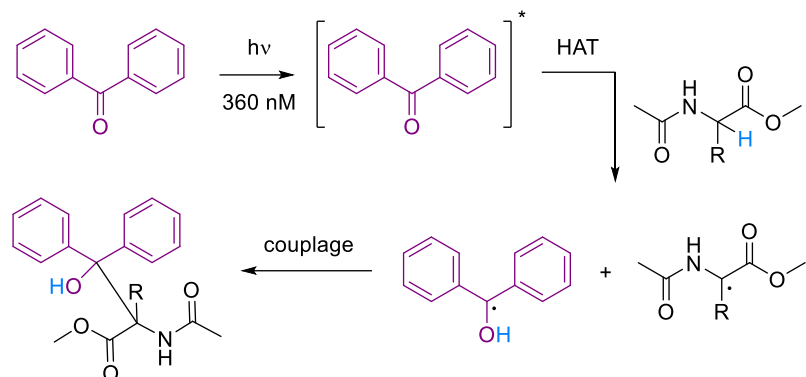
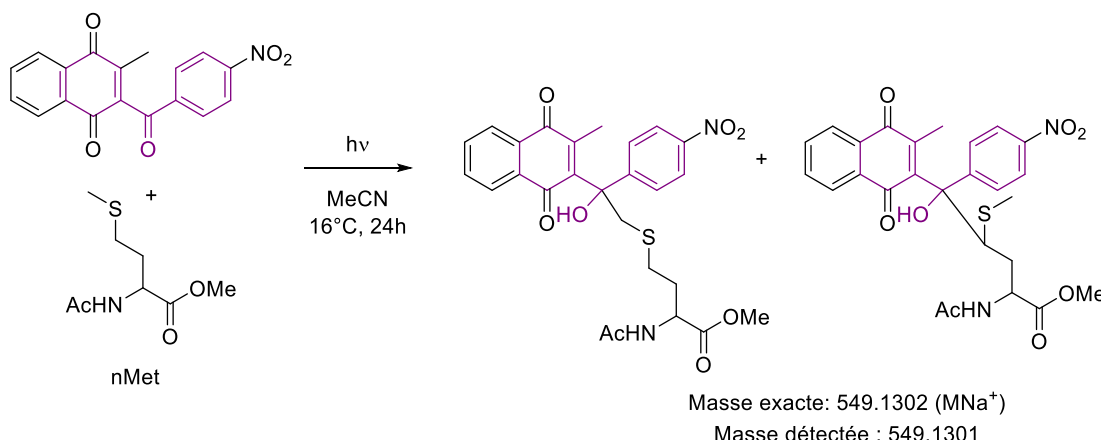


Schéma 17. Mécanisme proposé du couplage photocatalysé de la benzophénone et des acides aminés protégés.

Ainsi, nous avons pu évaluer la possibilité de réaliser ce type de couplage entre une 3-benzoylménadione et un acide aminé modèle avant de réaliser les expériences avec des protéines. Nous avons réalisé l'étude préliminaire avec la 3-benzoylménadione fonctionnalisée par un groupement nitro en position *para* du benzoyle et la méthionine protégée nMet. J'ai pu ensuite analyser les milieux réactionnels par RMN.

D'après les travaux de Guy Ourisson vus précédemment, le nMet peut être couplé avec une benzophénone sur les 2 positions en α du soufre.⁵⁰ Les réactions ont été menées dans des tubes en verre dans l'acetonitrile sous irradiation UV et pendant 24h à l'intérieur d'une armoire ventilée à 16 °C. Lors du premier essai, sous atmosphère d'air ambiant, nous n'avons observé la formation d'aucun produit de couplage (**Tableau 1**, Entrée 1), cependant la même réaction sous atmosphère d'argon nous a permis d'observer par analyse du spectre RMN des traces de nouveaux produits (**Tableau 1**, Entrée 2). Après de nombreux essais, nous avons pu déterminer qu'il était préférable de travailler en conditions diluées et avec un excès de méthionine (**Tableau 1**, Entrée 5). Les adduits de photocouplages n'ont pas été isolés, mais un produit possédant la même masse a été détecté par spectroscopie de masse haute résolution, confirmant la formation d'un adduit de 3-benzoylménadione et nMet. Ces résultats ont ensuite été repris par Bogdan Cichocki et Vrushali Khobragade, respectivement post-doctorant et doctorante dans notre laboratoire, et ont été optimisés et étendus à toutes les sondes chimiques synthétisées et à différents partenaires de la photoirradiation (peptides modèles et deux protéines modèles de type GR). Ces derniers ont pu également mettre au point les conditions de la réaction de cyclisation « click » optimisée entre les sondes alcynes et divers azotures.

Tableau 1. Essais préliminaires de couplages par photoirradiation entre une 3-benzoylménadione et un acide aminé.

Entrée	Concentration (mol/L)	nMet (équiv.)	Argon	Conversion (%) ^a
1	0,01	1	Non	n.d.
2	0,01	1	Oui	traces
3	0,1 (Saturé)	1	Oui	4
4	0,1 (Saturé)	4	Oui	10
5	0,02	5	Oui	20
6	0,02	10	Oui	15

^aLa conversion a été déterminée en comparant les intégrations des pics RMN des nouveaux produits formés et de la 3-benzoylménadione de départ.

Egalement, en étudiant l’oxydation benzylique de la plasmodione (chapitre suivant), nous nous sommes rendus compte que la photoirradiation UV, conduisait non seulement à la photoréduction de la naphtoquinone en dihydroquinone, mais aussi à l’insertion d’oxygène au sein de la chaîne benzyle. Ainsi, en partant d’une simple 3-benzylménadione portant une fonction alcyne, notre stratégie devenait extrêmement simplifiée : la photoirradiation UV d’une sonde 3-benzylménadione ‘clickable’ permet de générer une 3-benzoylménadione « clickable » dans le milieu réactionnel en présence d’un partenaire H-donneur (comme une protéine). Nos sondes 3-benzylménadione « clickables » ont été baptisées (pro-)ABPP (comme prodrogues) car elles fonctionnent comme des précurseurs de benzophénone photoréactives, utiles dans des applications ABPP pour étudier l’interactome de la PD. Dans ce travail, j’ai investigué les conditions d’oxydation benzylique d’une sonde 3-benzylménadione ‘clickable’ (molécule 11) sous photoirradiation UV et analysé les conditions optimales par RMN.

L’ensemble de ces travaux sur la conception de sondes chimiques basées sur le squelette 3-benz(o)ylménadiones a été publié dans *JACS^{AU}*.

2.2. Article 3.

A Class of Valuable (Pro-)Activity-Based Protein Profiling Probes: Application to the Redox-Active Antiplasmodial Agent, Plasmodione

Bogdan Adam Cichocki, Vrushali Khobragade, Maxime Donzel, Leandro Cotos, Stephanie Blandin, Christine Schaeffer-Reiss, Sarah Cianférani, Jean-Marc Strub, Mourad Elhabiri, Elisabeth Davioud-Charvet

JACS^{AU} accepted article, 11 Mars 2021, publié en ligne le 15 Avril 2021.

doi: 10.1021/jacsau.1c00025

A Class of Valuable (Pro-)Activity-Based Protein Profiling Probes: Application to the Redox-Active Antiplasmodial Agent, Plasmodione

Bogdan Adam Cichocki,[#] Vrushali Khobragade,[#] Maxime Donzel, Leandro Cotos, Stephanie Blandin, Christine Schaeffer-Reiss, Sarah Cianfrani, Jean-Marc Strub, Mourad Elhabiri, and Elisabeth Davioud-Charvet*



Cite This: <https://doi.org/10.1021/jacsau.1c00025>



Read Online

ACCESS |

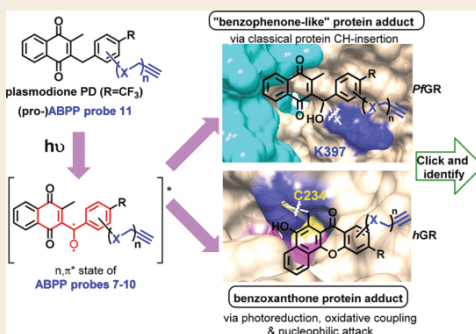
Metrics & More

Article Recommendations

Supporting Information

ABSTRACT: Plasmodione (PD) is a potent antimalarial redox-active drug acting at low nM range concentrations on different malaria parasite stages. In this study, in order to determine the precise PD protein interactome in parasites, we developed a class of (pro-)activity-based protein profiling probes (ABPP) as precursors of photoreactive benzophenone-like probes based on the skeleton of PD metabolites (PDO) generated in a cascade of redox reactions. Under UV-photolysis, we clearly demonstrate that benzylic oxidation of 3-benzylmenadione 11 produces the 3-benzoylmenadione probe 7, allowing investigation of the proof-of-concept of the ABPP strategy with 3-benzoylmenadienes 7–10. The synthesized 3-benzoylmenadienes, probe 7 with an alkyne group or probe 9 with $-NO_2$ in *para* position of the benzoyl chain, were found to be the most efficient photoreactive and clickable probes. In the presence of various H-donor partners, the UV-irradiation of the photoreactive ABPP probes generates different adducts, the expected “benzophenone-like” adducts (pathway 1) in addition to “benzoxanthone” adducts (via two other pathways, 2 and 3). Using both human and *Plasmodium falciparum* glutathione reductases, three protein ligand binding sites were identified following photolabeling with probes 7 or 9. The photoreduction of 3-benzoylmenadienes (PDO and probe 9) promoting the formation of both the corresponding benzoxanthone and the derived enone could be replaced by the glutathione reductase-catalyzed reduction step. In particular, the electrophilic character of the benzoxanthone was evidenced by its ability to alkylate heme, as a relevant event supporting the antimalarial mode of action of PD. This work provides a proof-of-principle that (pro-)ABPP probes can generate benzophenone-like metabolites enabling optimized activity-based protein profiling conditions that will be instrumental to analyze the interactome of early lead antiplasmodial 3-benzylmenadienes displaying an original and innovative mode of action.

KEYWORDS: *activity-based protein profiling, antimalarial, 3-benz(o)ylmenadione, CuAAC, electrophile, photoaffinity labeling, photoredox, quinone*



INTRODUCTION

To decipher drug modes of action (MoA), chemical strategies for functional proteomics have been developed in the recent years with the activity-based protein profiling (ABPP) being one of the most specific.¹ This unbiased and alternative methodology to identify drug or drug metabolite interactors in diverse organisms has successfully detected protein partners of miscellaneous biomolecules^{2–4} (see the pioneering work from Cravatt et al. and then from Bogyo et al., with the first reports about serine hydrolase inhibitors). ABPP allows monitoring and dissecting a drug interactome from complex proteomes in their native forms. This is achieved by the design and synthesis of small drug-activity-based probes that can react with the protein targets. The selective separation of the drug–protein adducts from the whole proteome is made possible by the

Cu(I)-catalyzed alkyne–azide cycloaddition (CuAAC) “click” reaction, also known as the seminal Huisgen reaction adapted for biological chemistry and proteomics purposes.^{5,6} The ABPP probe is based on three essential functional chemical elements: (1) a recognition group—drug/metabolite that has affinity to specific proteins defined as interactome; (2) a reactive group—either electrophilic or photoreactive feature that favors cross-linking or covalent binding of the probe to the

Received: January 22, 2021

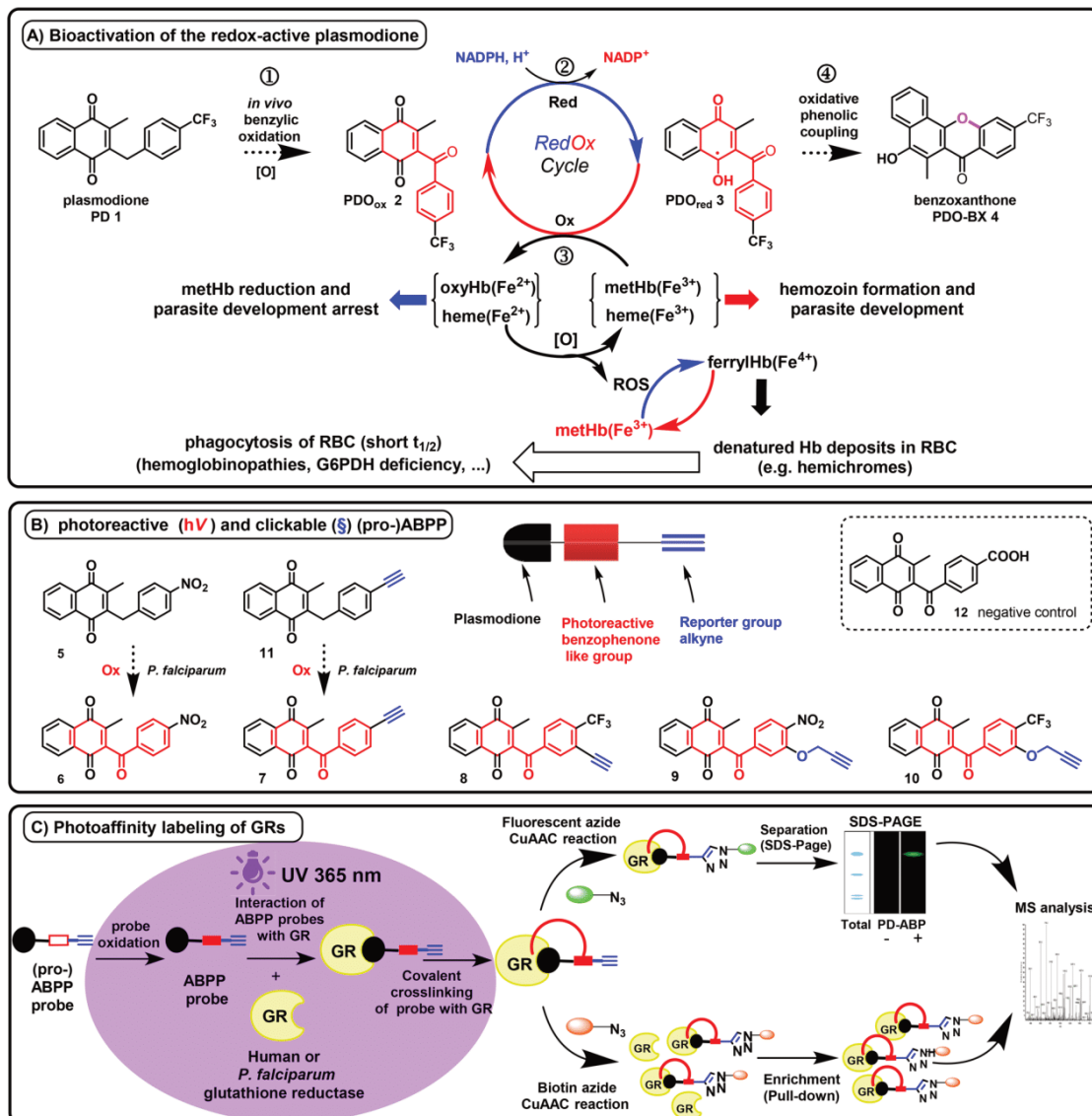


Figure 1. (A) Bioactivation of plasmodione (PD 1): Upon internalization in the parasite, plasmodione PD (1) is proposed to generate the drug metabolite PDO_{ox} (2) by benzylic oxidation (step ①), the 3-benzoylmenadione (benzoylMD), which, under its oxidized form, possesses a photoreactive benzophenone-like moiety (indicated in red). This metabolite is further reduced (step ②) and under its reduced form (3) takes part in oxidoreductase-mediated redox-cycling (step ③), leading to ROS-induced parasite death. In addition, the generation of a third metabolite, namely the benzo[*c*]xanthene-7-one (benzoxyanthone, PDO-BX) derivative (4), has been envisioned as one possible metabolite generated through an oxidative phenolic coupling reaction from the 1-electron-reduced benzoylMD (3) radical (step ④). Significantly, PDO_{red} (3) exists in different mesomeric species, but for the clarity of the scheme, only one species is shown. (B) Plasmodione-activity based probes (PD-ABPP): The common scaffold of the PD-ABPP probes 7–11 is a photoreactive 3-benzoylmenadione, functionalized by different electron-withdrawing groups in *para*-position (-CF₃ or -NO₂ or -alkyne) affecting their photoreactivity. 3-Benzylmenadienes (such as 1, 5, 11) are not photoreactive per se, while probes 6–11 in the benzoylMD series are photoreactive. (C) ABPP strategy: This approach is aimed at identifying drug activity-based protein profiling in living parasites incubated with a parent PD-ABPP precursor designed as (pro)-PD-ABPP. The (pro)-PD-ABPP probe is released upon bioactivation through the benzylic oxidation. In this paper, our aim is to showcase the proof-of-concept by starting the work from the benzoylmenadione derivatives (metabolites and ABPP probes). Upon UV irradiation, covalent cross-linking of PD-ABP to its potential targets is expected to occur. Further, a reporter click reaction between the probe-derived alkyne and the fluorescent rhodamine azide or biotin azide reveals successful cross-linking of probe to peptides and GRs as protein models, which can be analyzed by SDS PAGE and/or LC-MS/MS. Identification of the site where the ABPP probe was bound to both GRs was investigated and discussed.

target(s); (3) a reporter group/tag (e.g., alkyne or azide) enabled to react in the click reaction with a partner (e.g., azide or alkyne) that is functionalized either by a fluorophore for visualization of the drug–protein adducts or a affinity

chromatography tag for enrichment and identification of the adduct.⁷ An additional advantage in the ABPP field is the enlargement of the variety of chemical probes that trap representatives of various enzyme classes and can be utilized in

proteome studies. In the case of the flavin-dependent oxidoreductase family, the design of clickable ABPP probes was limited to the cytochrome P450,⁸ 2-oxoglutarate oxygenases,⁹ and amine oxidases.^{10,11} According to the literature, several proteomics studies have been conducted with ABPP probes for the detection of drug targets in *P. falciparum*.^{12–16}

NAD(P)H-dependent flavoenzymes from the malarial parasites have been proposed as possible targets of plasmidione, an early antimalarial lead compound (**PD**, 3-[4-(trifluoromethyl)benzyl]-menadione, **1**, Figure 1).¹⁷ Initial studies have focused on the chemical reactivity of the 3-benzylmenadione core, and of its key putative metabolites, the 3-benzoylmenadienes, which were shown *in vitro* to act as effective subversive substrates of recombinant glutathione reductases from human (*hGR*) and *P. falciparum* (*PfGR*). GR is a homodimeric NADPH-dependent FAD-containing enzyme (GR; EC 1.8.1.7) that belongs to the family of NADPH-dependent oxidoreductases. GR catalyzes the reduction of glutathione disulfide (GSSG): $\text{NADPH} + \text{H}^+ + \text{GSSG} \rightleftharpoons \text{NADP}^+ + 2 \text{GSH}$ (eq 1). According to previous studies, suicide-substrates such as fluoroM_S, a fluoromethylmenadione derivative, inactivates GSSG reduction by *hGR* but not naphthoquinone reduction, thus suggesting that napthoquinone reduction occurs at a different site than GSSG reduction, possibly near the flavin, close to the NADPH binding site, as previously postulated.¹⁸

Subversive substrates inhibit GSSG reduction activity because they are reduced by the NADPH-reduced flavin enzyme species, thus preventing electrons to flow normally from NADPH to GSSG. In the presence of natural oxidizers, for example, oxygen or methemoglobin(Fe³⁺) (metHb), naphthoquinone reduction was demonstrated to be reversible for **PD** and its key metabolite, the 3-benzoylmenadione (**PDO_{ox}** compound **2**), starting a redox-cycling process (Figure 1A). Reduced benzoylmenadienes can efficiently transfer one electron to metHb, and the redox cycle constantly regenerates the benzoylmenadione under its oxidized form at the expense of the NADPH pool.¹⁹ MetHb is a critical nutrient for *Plasmodium* crucial for its growth (e.g., at the trophozoite stage) while Hb(Fe²⁺) is not digestible.¹⁷ The shift in metHb/Hb(Fe²⁺) balance during redox-cycling results in metHb depletion and parasite growth arrest. From **PD**, the NADPH-dependent oxidoreductase-promoted redox-cycling also produces a continuous flux of reactive oxygen species (ROS) and toxic metabolites, including the reduced 3-benzoylmenadione (**PDO_{red}** compound **3**) (i.e., via 1-electron transfer) along with hemoglobin degradation catabolites identified as membrane-enriched hemicromes. The latter are known to act as biomarkers of red blood cell (RBC) senescence and to trigger early phagocytosis by macrophages. Hence, **PD** activation via **PDO**-mediated redox-cycling most likely results in the specific removal and clearance of the parasitized RBCs (pRBC).^{20,21}

Furthermore, during metHb digestion, toxic heme is released into the acidic food vacuole of the parasite. To detoxify free heme, the parasite converts it into a nontoxic insoluble hemozoin biocrystal. We previously proposed that **PD** bioactivation in pRBCs, possibly by GR, generates a key metabolite—the benzoxanthone **4** (**PDO-BX**) (Figure 1A) via a cascade of redox reactions and oxidative phenolic coupling. In turn, **PDO-BX** can firmly interact with free heme and is thus suggested to prevent heme crystallization leading to parasite death.^{17,20}

Finally, in yeast, the mitochondrial type II NADPH-dehydrogenase *Nde1*, was found to be the main target responsible for **PD** redox-cycling, with GR and two other oxidoreductases (*Mcr1* and *Lpd1*) being minor targets.²² Taken together, these observations and the current model for **PD** MoA suggest that, once generated, **PD** metabolites could (i) redox cycle with several oxidoreductases, which may vary according to parasite developmental stage, generating oxidative stress; and/or (ii) disturb key parasite processes such as hemozoin formation. Additionally, the abundance of proteins expressed in parasites is variable and depends on the parasite stages. Thus, during any ABPP study, actual drug targets expressed in traces would be difficult to distinguish from unspecific labeled but abundantly expressed proteins recovered in the HPLC MS/MS analysis. The focus of the present study was therefore to design a series of relevant and specific **PD**-ABPP probes, to define standardized conditions for their use and establish a proof-of-concept of their application with isolated proteins such as *hGR* and *PfGR* as models (Figure 1C). Here, for the first time, we report that 3-benzoylmenadienes are photoreactive and, as (pro-)activity-based protein profiling probes ((pro-)ABPP), can be used for ABPP applications.

The 3-benzoylmenadione probe generates a benzophenone-like moiety upon photoreduction, a step that mimics the reductive bioactivation drug pathway catalyzed by a flavoenzyme in the living cell.

Diversely substituted benzophenone-like and **BX** adducts were produced in the presence of different partners via original photoredox pathways that have not been previously described. The successful photoaffinity labeling of both GRs not only allowed the identification of naphthoquinone binding sites in GR structure but also revealed an alkylation process of the toxic heme by **PDO-BX**, generated upon **PD** redox-cycling with *hGR*, which is likely a relevant event contributing to **PD** MoA.

RESULTS AND DISCUSSION

Design of 3-Benzoylmenadienes as Photoreactive Probes

Our original strategy for designing the **PD**-ABPP is leveraged from the postulated MoA of **PD**.¹⁷ **PD** was suggested to act as a prodrug generating *in situ* a key metabolite, **PDO**, upon **PD** bioactivation (i.e., benzylic oxidation) (Figure 1A). Interestingly, **PDO** possesses in its structure the 2-benzoyl-1,4-naphthalenedione group that could behave as a 2-benzonaphthone precursor.²³ Therefore, we assumed that the redox-active **PD**-derived benzoylmenadione, under its reduced state, might have an intrinsic photoreactive benzophenone-like structure per se and thus permit the spontaneous covalent trapping of targets upon photoirradiation. Such probes might show high spatiotemporal control of targeted enzyme recognition/alkylation and drastically lower nonspecific binding. Interestingly, no additional bulky photoreactive group was introduced into the **PD** metabolite structure. Furthermore, the newly designed ABPP probes **7–11** (Figure 1B) were functionalized in the benz(o)yl chain, by a reporter alkyne group known to bring minimal structural and electronic perturbation.

To validate the hypothesis of the intrinsic photoreactivity properties attributed to the benzophenone-like structure, we first studied the 3-benz(o)ylmenadione derivatives in model photochemical reactions. We compared the photoreactivity of the previously reported **PD** analogue 3-benz(o)ylmenadione

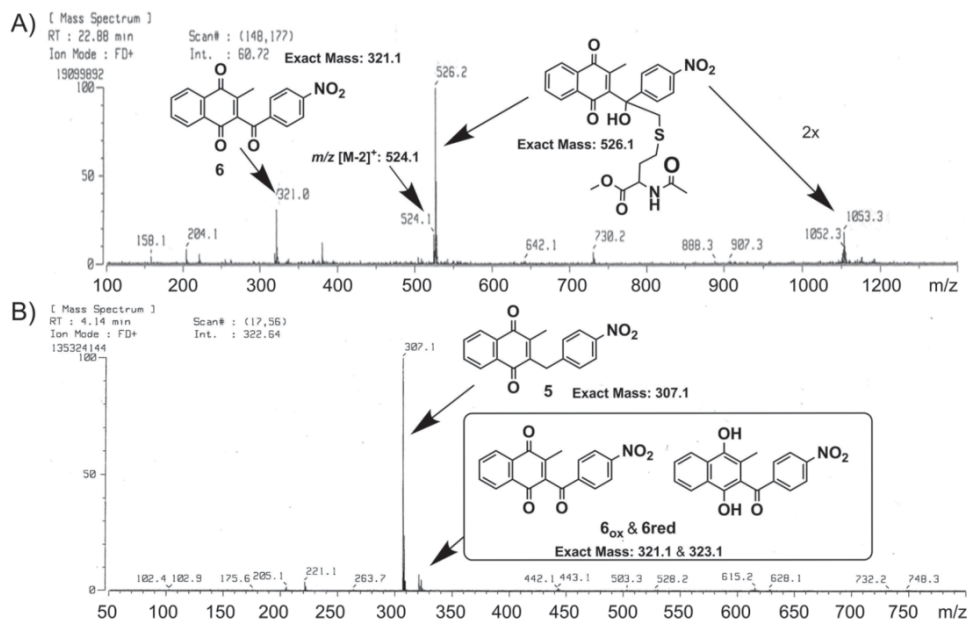
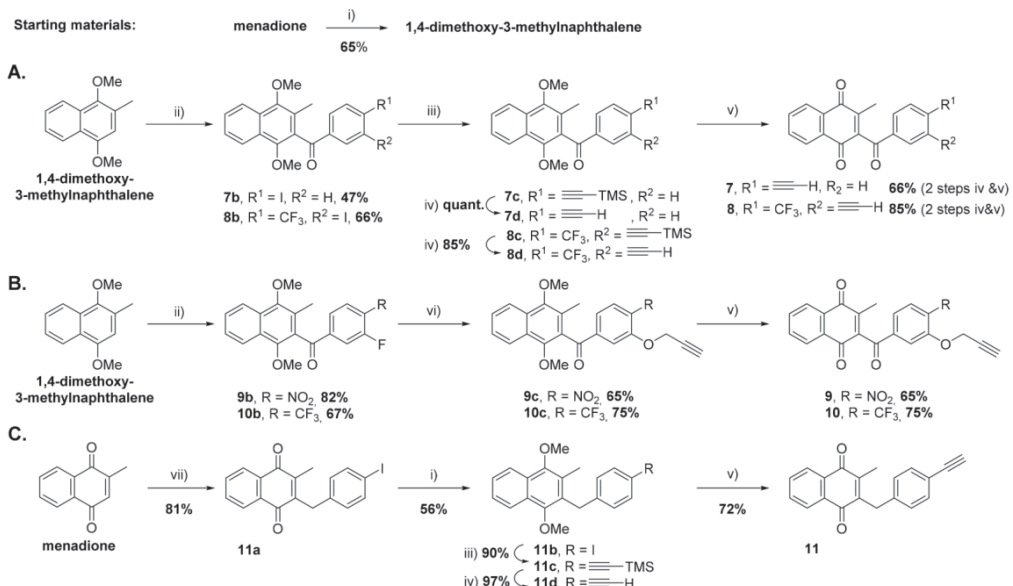


Figure 2. Mass spectrometric analysis of the photochemical reaction mixtures. Field-desorption mass spectrometry (FD-MS) analyses of the photochemical reaction mixtures of (panel A) the 3-benzoylmenadione 6 or (panel B) the 3-benzylmenadione 5 derivatives, in the presence of the diprotected methionine nMet.

Scheme 1. Synthesis of the 3-Benzoylmenadienes 7–10 (Paths A and B) through the Friedel–Crafts Reaction Variant³¹ and the 3-Benzylmenadione 11 (Path C) through the Kochi–Anderson Reaction³² ^a



^aReaction conditions: (i) 1. SnCl_2 cc HCl, EtOH, rt, 2 h, 2. Me_2SO_4 acetone, KOH, MeOH, 60 °C, 4 h; (ii) TfOH/TFAA, DCM, and A. 4-iodobenzoic acid 7a, or 3-iodo-4-(trifluoromethyl)benzoic acid 8a, B. 4-nitro-3-fluorobenzoic acid 9a, or 3-fluoro-4-(trifluoromethyl)benzoic acid 10a, 0 °C then rt, 16 h; (iii) CuI, Pd(PPh_3)₂Cl₂, NEt₃ rt, 16 h, HC ≡ C-TMS; (iv) TBAF, THF, rt, 1.5 h; (v) CAN, H₂O/MeCN, rt, 3 h; (vi) K_2CO_3 , DMF, propargylic alcohol, 60 °C, 24 h; (vii) 4-iodophenylacetic acid, AgNO₃, Na₂S₂O₈, MeCN/H₂O, reflux, 4 h.

5–6 pair¹⁷ (Figure 1B) upon photoirradiation at 350 nm (Figure 2) in comparison with benzophenone (Figure S1) to evaluate whether the keto group of the benzoyl chain is essential for photoreaction. For this, we used *N*-acetyl-methionine methyl ester (*N*-Ac-Met-OMe, shortened as nMet) as a partner model, in accordance with previous studies

demonstrating that methionine and its *N*-Ac-Met-OMe derivative are predominantly alkylated at the side-chain in α -position to the sulfur.^{24,25} The products of the photoreaction were analyzed by field desorption-mass spectrometry (FD-MS). As observed in Figure 2A, the insertion product of the 3-benzoylmenadione derivative 6 and nMet displayed a mass

peak at $m/z = 526.2$. Under the same photoirradiation conditions, the photoreactive benzophenone generated the insertion product with nMet as attested by the presence of mass peaks at $m/z = 387.2$ (M^+) and 369.2 ($M^+ - H_2O$) (Figure S1). No major insertion product was observed for the 3-benzoylmenadione derivative **5** (Figure 2B), demonstrating that the 3-benzoyl chain is essential for the photoreactivity of the benzoylmenadione derivative **6**.

Interestingly, probe **6** appears to be photochemically reactive per se, even in the absence of a reduction step in the presence of the NADPH/GR. The 3-benzoyl-dihydronaphthoquinone is likely generated by photoreduction upon photoirradiation,^{23,26} thus allowing formation of the insertion product. At first glance, we neglected the small peaks appearing at $m/z = 321.1$ and 323.1 suggesting the formation of trace photoproducts upon photoirradiation of the 3-benzoylmenadione **5**, which were finally attributed to both oxidized and reduced species of the 3-benzoylmenadione **6** (Figure 2, black box). This observation was confirmed later when we used the most photoreactive 3-benzoylmenadione ABPP probe **11** per se to investigate the generation of photoproducts upon UV-photoirradiation.

Using FD-MS under the same experimental conditions with 3-benzoylmenadienes, we were able to observe the insertion product of the benzoylmenadione **6** with a *p*-nitro-benzoyl derivative but not with benzoylmenadione **12** with a carboxylic acid group in *para*- to the benzoyl ring (data not shown). This result might be explained by the fact that the carboxylate form, which predominates in neutral aqueous solution, is not an electron-withdrawing group (EWG) but rather a donor or even neutral²⁷ group; some photochemical decarboxylations were also reported.²⁸ Thus, the promising photochemical properties of probe **6** convinced us to design the new PD-ABPP probes **7–11** (Figure 1B) functionalized by different EWGs in *para*-position of the benz(o)yl chain and an additional reporter group (i.e., alkyne prone to be reactive with azides in the click reaction). Noteworthy is that the *p*-alkyne group can be considered both as the reporter group for the CuAAC reaction but also an EWG to favor the formation of an insertion product upon photoirradiation.^{29,30}

Synthesis of Clickable 3-Benz(o)ylmenadienes as PD-ABPP Probes

Each of the 3-benzoylmenadienes alkyne derivatives **2**, **4**, **6**, and **8** was synthesized using as a key step, the Friedel–Crafts acylation, recently described by our team.³¹ Using the electron-rich 1,4-dimethoxy-2-methylnaphthalene (i.e., aromatic nucleophile) and readily available synthetic benzoic acids (**7a–10a**) (i.e., acylating agent) as starting materials, this reaction variant allowed us to prepare the corresponding 2-benzoyl-1,4-dimethoxynaphthalene intermediates (**7b–10b**) in mild conditions. These are key intermediates, to achieve, in a few additional steps the desired chemicals probes described in paths A and B (Scheme 1). The four benzoyl-1,4-dimethoxy-2-methylnaphthalenes **7b–10b** were obtained with 47%, 66%, 82% and 67% yield, respectively. It is worth mentioning that without the Friedel–Crafts reaction variant, the 3-benzoylmenadienes functionalized by an alkyne group could not have been produced easily (i.e., see the different synthetic pathways discussed previously).³¹

A Sonogashira pallado-catalyzed coupling allowed the trimethylsilane (TMS)-protected alkyne insertion, starting from the iodinated aromatic compounds **7b–8b**, to obtain

efficiently intermediates **7c–8c**. These were successively deprotected in **7d–8d**, first with TBAF and then by cerium ammonium nitrate (CAN) to afford both desired alkynated 3-benzoylmenadiones **7–8** upon oxidative demethylation. For the synthesis of alkynes **9c** and **10c**, propargyl alcohol was first submitted to a nucleophilic aromatic substitution reaction on the electron-poor fluorinated aromatic intermediates **9b** and **10b**, leading to the targeted quinones **9** and **10** after oxidative demethylation with CAN.

ABPP probe **11** in the benzylmenadione series was synthesized according to path C in a five-step route starting from the Kochi–Anderson reaction³² (Scheme 1). First, 3-benzylmenadione **11a** (80%) was produced by addition to menadione of a benzyl radical generated from 4-iodophenyl-acetic acid by decarboxylation in the presence of silver salts' catalysis and stoichiometric amounts of the $\text{Na}_2\text{S}_2\text{O}_8$ oxidant. Owing to the incompatibility of the methyl group of **11a** in basic medium, it was not possible to introduce the alkyne moiety directly on the quinone by palladium cross coupling reaction. Consequently, the benzylmenadione **11a** was first reduced with SnCl_2 in acid medium to the corresponding 2-(4-iodobenzyl)-3-methylnaphthalene-1,4-diol intermediate, which was protected (after a quick crystallization step under nitrogen) by methylation using dimethylsulfate to produce the 2-(4-iodobenzyl)-1,4-dimethoxy-3-methylnaphthalene intermediate **11b** (56%). Then, the iodo derivative **11b** was submitted to the Sonogashira pallado-cross coupling reaction, using ethynyl(trimethyl)silane in excess. This reaction successfully promoted the formation of the TMS-protected alkyne **11c** in excellent yield (90%). The TMS group was removed from **11c** by TBAF to obtain the free terminal alkyne **11d** (97%), and the 1,4-quinone moiety was recovered by oxidative demethylation following addition of CAN in acetonitrile (ACN)/water mixture to obtain in good yield (66%) the targeted 3-benzyl-[4'-alkynyl]-menadione **11**.

Standardization of the UV Cross-Linking Parameters Using PD-ABPP Probes and nMet as Partner Model

These PD-ABPP probes have been primarily designed to highlight both the binding sites and elucidate the protein interactome of PD in living cells. Additionally, considering the originally studied glutathione reductases from the pRBC unit, the reduction site of subversive substrates is a matter of debate (discussed in ref.³³), even if menadione was observed to bind to various cavities of the crystal structure of the human enzyme.³⁴ Before testing the cross-linking ability of these ABPP probes, we undertook the evaluation of their inhibition capabilities with the human GR in 1 mM GSSG reduction assays (in 2% ACN instead of 1% DMSO). We observed that the probes **7**, **8**, **9**, and **10** behaved as potent GR inhibitors, with IC_{50} values of 0.60, 0.80, 0.58, and 0.85 μM , respectively; these values are in the same range as those previously observed for **6** and **12** (0.4 and 0.7 μM , respectively).¹⁷ Thus, functionalization did not decrease the inhibitor activity in comparison to effective 3-benzoylmenadienes.

Photoreactivity of the PD-ABPPs was evaluated under the same photoreaction conditions used for the model reaction between nMet and probe **6** (vide supra). We observed that among the five PD-ABPP, the photoreaction preferably occurred with probes **6**, **7**, and **9** bearing $-\text{NO}_2$ or alkyne (strong to moderate EWG) in *para*-position in accordance with yields of starting probe consumption and photoproduct formation, calculated from the ^1H NMR spectra (Table 1,

Table 1. Photoirradiation of N-Acetyl Methionine Acid Methyl Ester (nMet) and Probes 6, 7, and 9^a

probe	δ (ppm)/signal shape for each probe and photogenerated product from ^1H NMR spectra	residual probe/formed products (ratio)
6	8.07 (dd)/8.04 (dd)	69:31
7	7.60 (dd)/7.38 (dd)	75:25
9	7.51 (dd)/7.40 (dd)	61:39

^aRatio of residual probe and formed coupling products is based on the integration of the corresponding signal in the ^1H NMR spectra of the crude reaction mixtures.

(Figures S2–S4). For probes 8, 10, and benzophenone, the ^1H NMR data did not allow the calculation of the yields of probe consumption or formed products because the signals were either too small or combined with other signals. The CF_3 group is known to be a strong EWG group, such as $-\text{NO}_2$ and even more than an alkyne group,²⁷ but the mesomeric effect, inherent to both of the latter groups, can stabilize more efficiently a ketyl radical generated by photoreduction, than the inductive effect of a $-\text{CF}_3$ group. Additionally, we determined the absorption spectrophotometric characteristics (ϵ^{\max} and λ^{\max}) of all PD-ABPP probes 7–11 along with probe 6 (Figure S5; at the photoirradiation λ of 350 nm, all the PD-ABPP probes are characterized by weak $n-\pi^*$ transitions). On the basis of these data, we can conclude that benzoylmenadione probes are photoreactive per se and can be used to covalently trap targets in an ABPP approach.

The (Pro-)ABPP Benzylmenadione Probe 11 Generates the Benzylmenadione 7 upon Photoreduction and Then Oxidation

Starting from the prior observation of the generation of trace amounts of oxidized and reduced benzylmenadione species upon photoirradiation of the parent 3-benzylmenadione, we investigated the reaction to produce the most efficient photoreactive probe 7 from the parent prodrug, the 3-benzylmenadione 11. Since it is well-known that the dihydronaphthoquinone is favorably generated via the semi-quinone by photoreduction of the naphthoquinone in isopropanol,³⁵ we submitted the benzylmenadione probe 11 to UV-irradiation in this solvent under bubbling of oxygen. After 72 h of irradiation, the formation of the corresponding 3-benzoylmenadione was clearly observed, as attested, for example, by monitoring the deshielding of the alkyne proton seen in the NMR spectra (Figures 3, S6, for the full-scale ^1H NMR spectrum). The same reaction in a 1:1 mixture of ACN and water only afforded traces of the species oxidized at the benzylic position. To overcome the poor solubility of probe 11 in both systems, a 1:1 mixture of dichloromethane and isopropanol was selected, and these conditions were shown to be optimal with a full conversion of the initial 3-benzylmenadione 11 to the 3-benzoylmenadione 7 upon photoirradiation. The aerobic benzylic oxidation mechanism likely involves intermediate hydroperoxidation.³⁶ However, the low quantity of 3-benzoylmenadione generated during the photoirradiation of 3-benzylmenadione in an ACN/water mixture prevented any detailed study on the optimization of the conditions for effective photoalkylation followed by the click reaction. This condition is not physiological, but we could demonstrate herein that naphthoquinone reduction by a flavoenzyme (e.g., both GRs) can be substituted by UV-photoactivation in the presence of oxygen. Notably, the

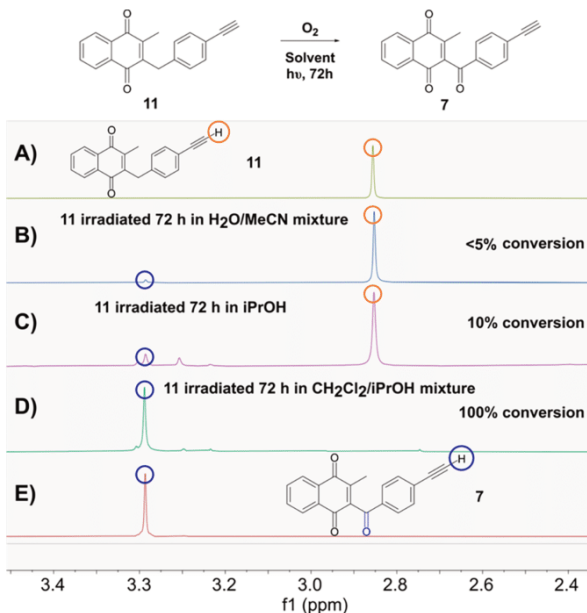


Figure 3. Overlay of the ^1H NMR spectra in the 2.8–3.4 ppm area of (A) pure probe 11 and reaction mixtures of 3-benzylmenadione probe 11 in various solvents after 72 h of UV-photoirradiation at 350 nm: (B) in a 1:1 $\text{H}_2\text{O}:\text{MeCN}$ system; (C) in iPrOH ; (D) in a 1:1 $\text{CH}_2\text{Cl}_2:\text{iPrOH}$ system; (E) pure 3-benzoylmenadione probe 7.

benzylic oxidation might occur in living cells during enzymic catalysis with flavoenzymes in a hydrophobic environment like membrane lipid bilayers or a hydrophobic protein core. For this reason, the following study was carried out using 3-benzoylmenadione-based ABPP probes (instead of 3-benzylmenadione-based ABPP probes) to optimize the methodology and strengthen the ABPP approach.

Characterization of Clickability Properties of the ABPP Probes Using Azide Models

The click (CuAAC) reaction is crucial for the analysis of complex proteomes because it allows the grafting of a pulldown-tag to the cross-link adducts. Subsequent adduct enrichment through the affinity purification enhances correct peptide identification during MS analysis. The ABPP probes 7–10 were predicted to have different click reaction reactivity depending on the position of the alkyne on the phenyl ring and the length of the linker connecting them (via $\text{O}-\text{CH}_2$ or directly attached). To assess the influence of both factors on the ABPP properties and select the best probe in model click reactions, we first evaluated the PD-ABPPs reactivity with the commercially available and fluorescent rhodamine azide (RA) (Figure S7C). RA was used to develop and improve the reaction conditions by varying Cu(I) ligands (TBTA, THPTA, or BCDA) and/or the reductants (NaASC and TCEP) that are essential for the efficiency of the CuAAC reaction (Figure S7A,B). The yields of the CuAAC reactions were determined by LC-MS analysis (Figures S8–S15).

During the development of an optimized protocol for the click reaction, we identified several factors, which surprisingly have greater than anticipated influence on the effectiveness of the click reaction with ABPP probes 7–10. Although well-known, the influence of these factors has not been sufficiently emphasized and described in the literature and has led us to

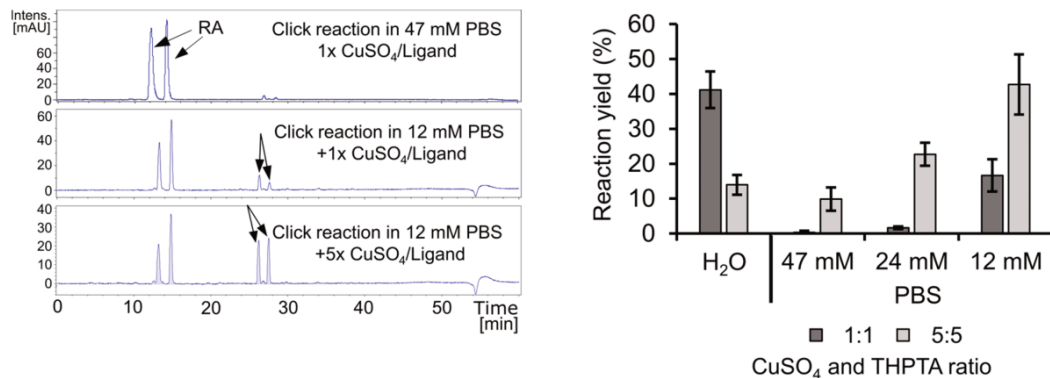


Figure 4. Phosphate buffer affects the click reaction efficiency. An increase of CuSO₄ and THPTA ratios and decrease of PBS concentrations led to a click reaction between probe 7 and RA as efficient as in pure water. Left panel: overnight click reaction of RA with probe 7 in 47 mM or 12 mM phosphate buffer. Copper-ligand preincubated mixture was added after 40 min of incubation. Copper-ligand preincubation mixture – 1:1 = 132 μ M of TCEP, CuSO₄, and THPTA; 5:5 = 132 μ M of TCEP and 660 μ M of CuSO₄ and THPTA. Chromatograms using absorption detection at 507 nm are shown. The two peaks evidenced for RA are related to both isomers in solution. Right panel: Yields of reactions determined from reactions in left panel; additional reaction data in H₂O and 24 mM PBS are shown. Reactions were analyzed by LC-MS. Total area of rhodamine absorption at 507 nm of the peaks corresponding to the product mass was measured and normalized to 24 μ M RA unreacted control. N = 3 independent experiments Error bars represent \pm SD.

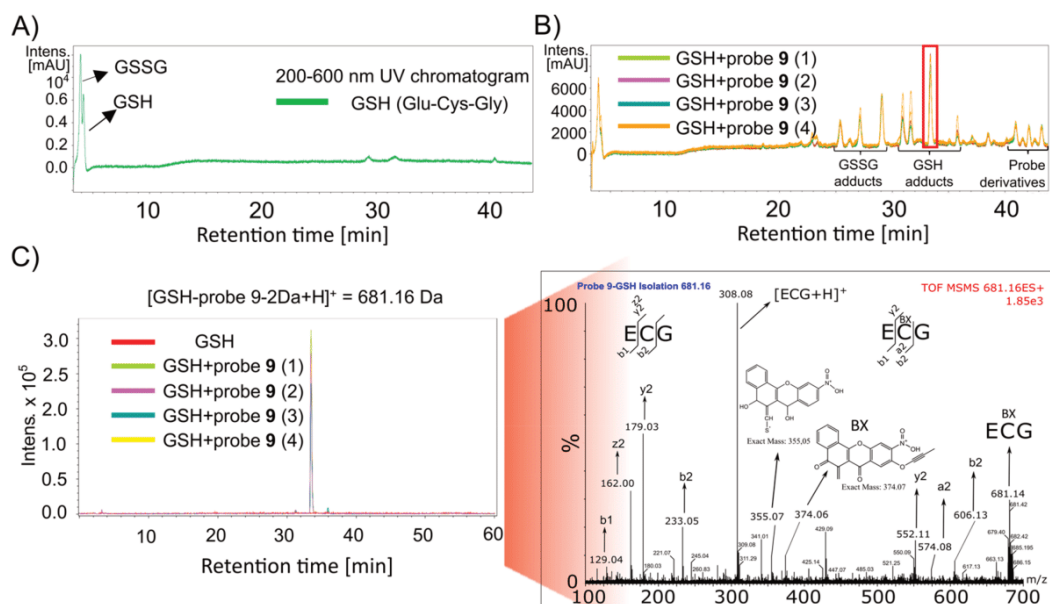


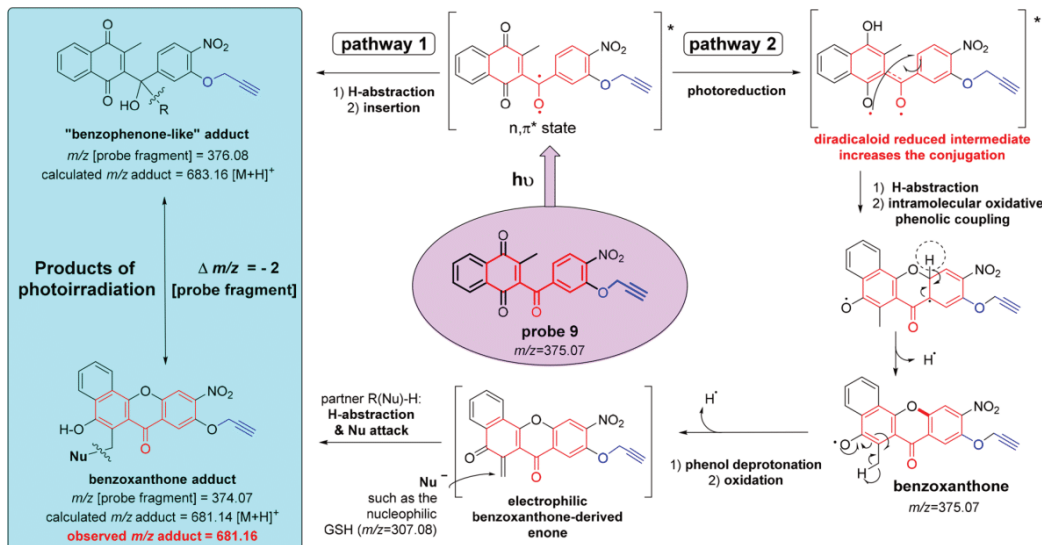
Figure 5. Probe 9 forms photoadducts with GSH in aqueous ACN conditions. (A) Chromatogram using absorption detection at 200–600 nm obtained by LC-MS analysis of reaction mixture containing GSH (3 mM) without ABPP probe upon 8 min UV irradiation. Glutathione disulfide (GSSG, RT = 4 min) is formed in the reaction by oxidation of GSH (RT = 4.25). (B) Under the conditions described in (A), 200–600 nm chromatogram is depicted after LC-MS analysis of reaction mixture containing probe 9 (600 μ M) and 3 mM GSH upon UV irradiation for 8 min ($n = 4$). Multiple peaks corresponding to different GSH and GSSG adducts (different cross-linking site, GSH and GSSG fragments, double cross-linking) are visible in the chromatograms. Peak corresponding to mass of photo-cross-linked adduct of full GSH and probe 9 is highlighted in red box (RT = 33.5 min). (C) Left panel – Extracted ion chromatogram of $m/z = 681.16$ Da from reaction in (B). Right panel – Fragmentation pattern of the selected peak in (B) spectrum showing adduct m/z at 681.16 Da. ECG – amino acid letter code of GSH. Peaks on the right side from $m/z = 308.08$ originate from probe 9-derived BX-SG fragmentation, on the left side from GSH fragmentation.

carry out a detailed fundamental investigation of each of the partners of the CuAAC reaction (vide infra). Additional observations, troubleshooting and click reaction optimization steps are described in the Supporting Information.

To improve the performance of the CuAAC reaction, we applied the generally used CuSO₄-THPTA-TCEP (copper source-ligand-reductant) trio in a 1:1:1 ratio. According to the

yield of the optimized click reaction (Figure S10B), the sequence of probe efficiency (i.e., 2 h reaction) was determined as follows: probe 7 with *p*-alkyne (58.8% yield) > probe 9 with *p*-NO₂ and *m*-O-CH₂-alkyne (12.8% yield) > probe 10 with *p*-CF₃ and *m*-O-CH₂-alkyne (2.9% yield) > probe 8 with *p*-CF₃ and *m*-alkyne (2.2% yield). The CuAAC reaction efficiency can be directly correlated with the probe structure

Scheme 2. Chemical Analysis of the Insertion Products upon Photoirradiation of the ABPP Probe 9 with Glutathione (GSH) by Mass Spectrometry^a



^aTwo pathways of photoreactivity of the benzoylmenadione were expressed through the formation of two insertion products (blue box) with nucleophilic partners.

and the resulting three factors: steric effects around the alkyne group, aqueous solubility of the probe and EWG properties of the aryl side groups (See Supporting Information, section “Click reaction optimization and troubleshooting”).

Additionally, in a click reaction with probe 7, we compared the generally used THPTA ligand with another Cu(I) ligand, the bathocuproinedisulfonic acid (BCDA)³⁷ in various conditions of the (copper source–ligand–reductant) trio both in water and in PBS buffer (Tables S1 and S2).

With this optimization study, we could conclude that phosphate ions can inhibit the CuAAC reaction and that this problem can be solved by lowering the phosphate buffer concentration and increasing copper/ligand ratio with respect to TCEP (Figure 4). Under these newly designed experimental conditions, we demonstrated that probe 7 can be clicked with an efficiency as high as in water without increasing concentrations of the reductant. BCDA is fully compatible with this click reaction conditions in PBS buffer (Table S2, R28–R30). Furthermore, it is preferred over THPTA in oxygen-free conditions.³⁸

Finally, we analyzed the click reaction of probe 7 with biotin-azide (BA), which is used to enrich tagged adducts by interaction with streptavidin. Despite changing the cosolvent of the reaction medium from DMF to ACN, the Cu(I) cycloaddition of BA had a similar pattern in triazole formation efficiency as RA (R32–39 vs R40–48; Tables S3 and S4). Thus, we conclude that our optimized click conditions are also compatible with an efficient labeling of alkynes with the biotin tag.

Using Peptide as a Model for Photoreaction

Based on nMet-PD-ABPP cross-linking data, we chose probes 7 and 9 to further explore the cross-linking ability of the ABPPs toward a peptide model. Additionally, this allowed us to determine the peptide adduct behavior (mass shift, fragmentation) during MS analysis, which is a crucial parameter to facilitate detection in proteomic analysis. The

GSH and P52C peptides were chosen as models for cross-linking. GSH was selected as a model peptide because of its commercial availability, simple structure, high solubility in water, and relevance in the context of our model approach. P52C is a 16 amino-acid-peptide covering the pseudoactive site of the trypanothione disulfide oxidoreductase from *T. cruzi*.³⁹

To assess the photoactivation of ABPPs in more physiological conditions, cross-linking with GSH or P52C was performed in a water:organic solvent mixture (H₂O:ACN, 1:1, v/v). These conditions were different from those used for the cross-linking conditions with nMet (vide supra) where pure ACN solvent was used. However, we observed that the probe solubility is significantly limited in aqueous ACN solutions (Figure S16). The observed solubility properties of the probes followed this sequence (from the less to the most soluble): probe 10 < probe 8 ≈ probe 7 < probe 9. Since probe 9 was the most water-soluble ABPP probe and displayed the highest cross-linking efficiency with nMet, we used it as a binding partner for GSH. We found that although reagent concentrations were lowered (from mM to μM), we were still able to identify a significant fraction of GSH/GSSG-probe adducts after overnight photoirradiation (Figure 5A,B).

MS/MS analysis of the most prominent product (681.16 Da, retention time (RT) = 33.5 min) revealed that this adduct has apparently lost two hydrogens (expected M-2H) compared with the initially expected mass of the photoalkylated peptide (Scheme 2, pathway 1). However, MS fragmentation of this adduct revealed no further alteration from predicted peptide fragmentation patterns (Figure 5C). Similarly, cross-link adducts have been detected for P52C (Figure S17).

A more rational explanation for the apparent loss of two hydrogen atoms of the observed probe 9-GSH adduct could stem from the second pathway (Scheme 2) upon photoirradiation of probe 9 in the presence of GSH. After photoreduction, an intramolecular process, much faster because it is entropically favored, leads to the benzoxanthone

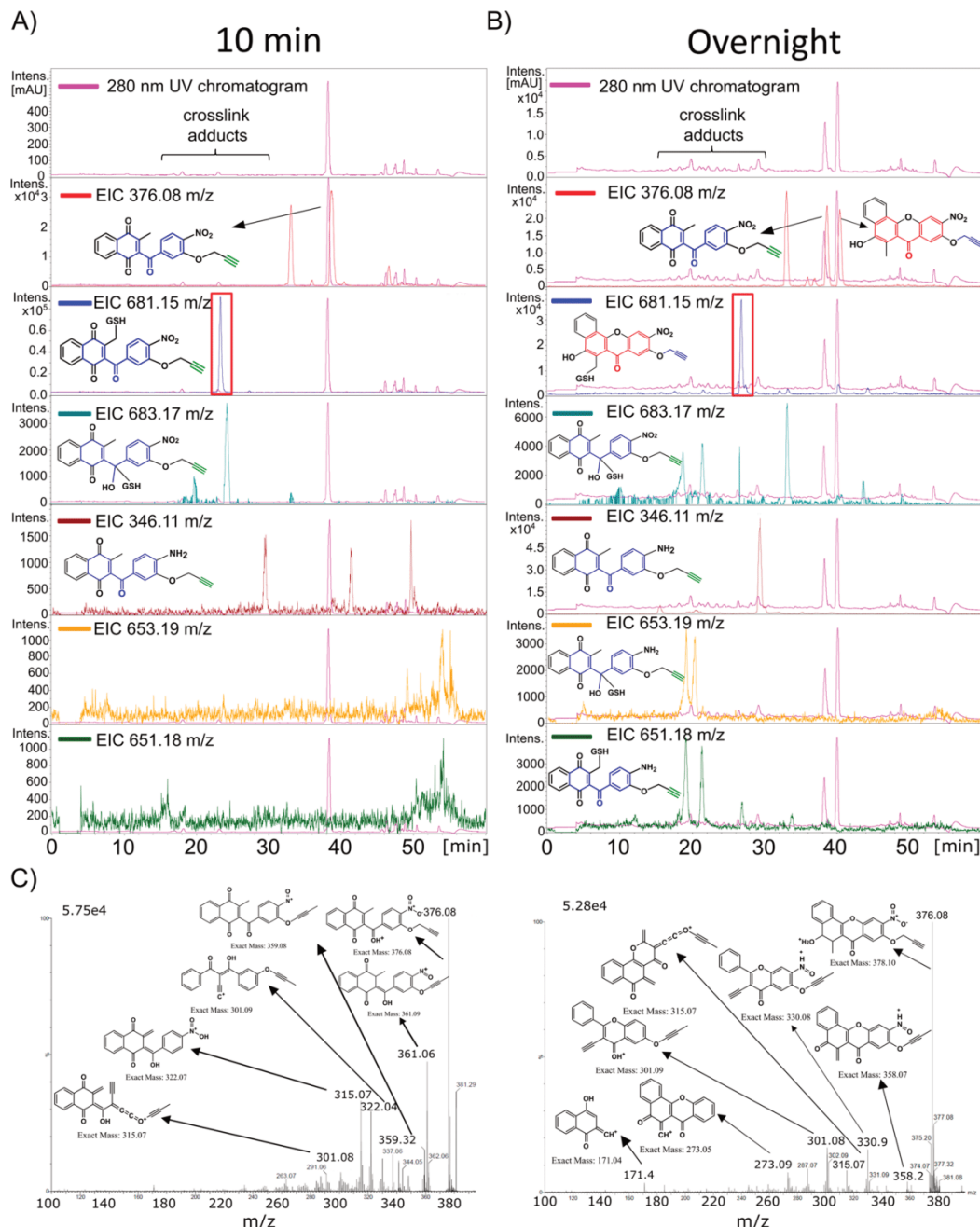


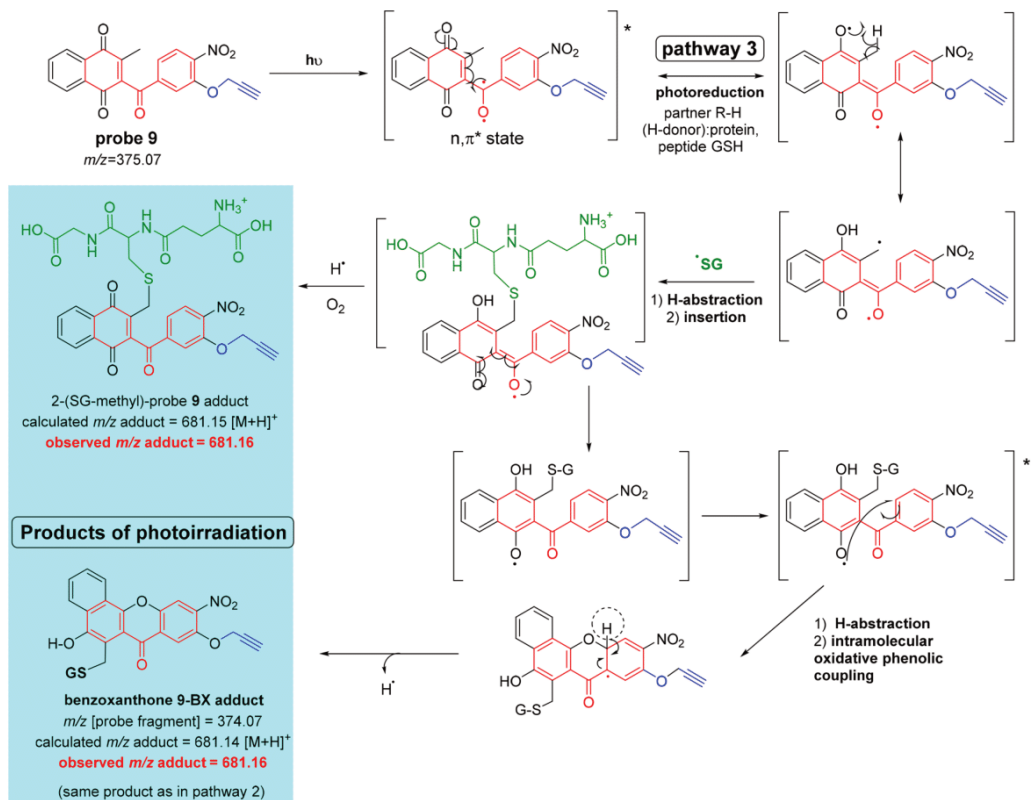
Figure 6. Photoreduction of probe 9 generates multiple probe-insertion products with GSH. (A) 280 nm UV-chromatogram overlaid with extracted ion chromatograms (EIC) corresponding to detected adduct and probe species. Reaction analyzed after 10 min of UV-irradiation with GSH and probe 9 (RT = 39 min). Red box indicates position of 2-(S-methyl) adduct peak (RT = 23 min). (B) 280 nm UV-chromatogram and EICs for an overnight photoreaction of probe 9 with GSH. Red box indicates position of 9-BX adduct (RT = 26.5 min). (C) MS/MS spectra of probe 9 peak (RT = 39 min; left panel) and 9-BX peak (RT = 40.5 min; right panel) from the reaction depicted in B).

formation. Several studies have clearly exemplified the photoreduction of quinones and subsequent intramolecular cyclization of a phenoxy radical,^{40–44} which effectively occurred in the presence of a H-donor. It is important to note that in these experiments, GSH can act as both reductant and H-donor.

Phenolate radical in position C-4 of the diradicaloid reduced intermediate promotes the intramolecular oxidative phenolic

coupling. The methyl group in *ortho* to the free phenolate radical of the resulting benzoxanthone possesses a very labile -H, which releases a benzoxanthone-derived enone owing to the favored energetically structure. The electrophilic enone undergoes Michael addition with GSH leading to the benzoxanthone adduct (theoretical m/z = 681.16) in perfect agreement with the observed mass peak at m/z = 681.16. It is worth highlighting that the initial photoirradiation of probe 6

Scheme 3. Mechanism of Formation of Both Observed Insertion Products (Blue Box) via Pathway 3 upon Photoirradiation of the ABPP Probe 9 with Glutathione^a



^aThe structure of the intermediate 2-(SG-methyl)-probe 9 adduct, formed after 10 min-irradiation, was deduced by ESI-MS/MS mass spectrometry.

with nMet did show an additional mass peak ($m/z = 524.1$), albeit with lower intensity, in the FD-MS spectrum (Figure 2A), attesting to the expression of two pathways occurring in the photochemical reaction.

Indeed, additional MS/MS analysis of the GSH adduct revealed that the generated probe fragment is benzoxanthone and that it was bound to the peptides at the sulfur atom of the cysteine residue (Figures 6C, S18). Consequently, a major formed probe species with the retention time of 40.2 min and $m/z = 376.08$ (identical to the probe 9 mass) found after photoirradiation was identified as the benzoxanthone (Figure 6B,C). This compound was not detected in the nonirradiated control (Figure S19A) or after 10 min of irradiation (Figure 6A), suggesting that prolonged photoreduction time is necessary to generate the cyclization product. Additionally, the newly found species underwent deprotonation overtime forming the predicted and reactive enone of pathway 2 ($m/z = 374.07$) (Figures S20, S21E). Incubation of synthesized PDO-BX with GSH confirmed the BX reactivity toward free thiol of GSH (Figures S22A, S22B, S23).

Interestingly, although no benzoxanthone is formed after 10 min of UV-irradiation of PD metabolite PDO_{ox} or probe 9, with GSH, the reactions also gave rise to adducts missing two hydrogen atoms (Figures 6A, S22C). MS/MS analysis identified this compound as a 2-(S-glutathionyl-substituted-methyl)-3-(benzoyl)-1,4-naphthoquinone (shortened as 2-(GS-methyl)-PDO or 2-(GS-methyl)-probe 9) (Figures

S24A, S25). Surprisingly, the 2-(SG-methyl)-9 is not present upon overnight irradiation of probe 9 and GSH, suggesting that the species is an intermediate formed in the synthesis of 9-BX-SG, according to pathway 3 (Scheme 3).

To further support our findings on the occurrence of pathways 2 and 3 occurrence, we substituted GSH in the reaction with another nucleophilic agent with a thiol group—thiophenol. LC-MS showed that already after 10 min of irradiation of PDO or probe 9, benzoxanthones as well as adducts lacking two hydrogens were formed (Figures S26, S27).

However, the suggested pathways are not mutually exclusive as a more careful LC-MS/MS analysis of the probe 9 reaction mixtures with GSH or thiophenol revealed that formation of benzophenone-like adducts occurred as well (Figures 6B, S24B, S26B, S28). Furthermore, in photoreactions, the nitro group from probe 9 was photoreduced to an amine,³⁵ which has given rise to amine-substituted benzophenone adducts and -(SG-methyl)-9 adducts (Figures 6B, S29, S30).

With that, we demonstrated that probe 9 is able to efficiently cross-link to a peptide and that the corresponding peptide-ABPP adducts can be detected by MS analysis.

Importantly, three labeling pathways were evidenced to occur in the photoirradiation experiments involving the metabolite PDO_{ox} or probe 9 and GSH, as depicted in Schemes 2 and 3. Using the LC-MS/MS approach, we were able to detect the main intermediates and products of the

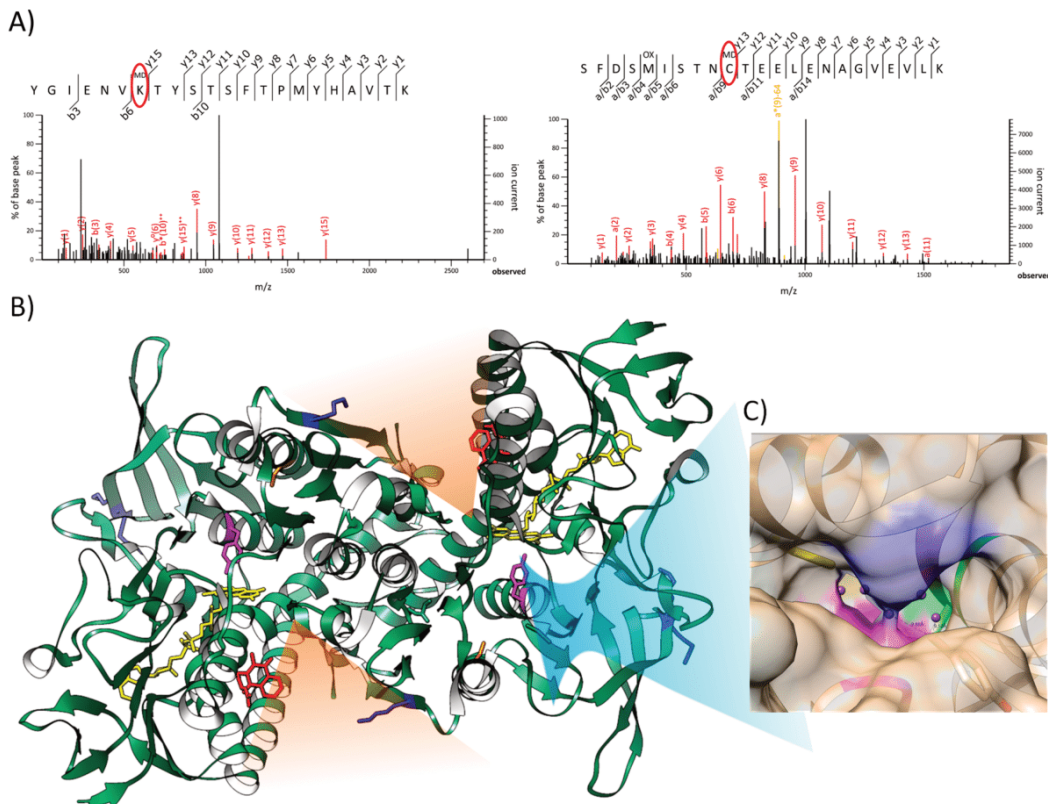


Figure 7. Probe 9 cross-links to *hGR* (A) MS/MS fragmentation pattern of identified peptides of *hGR* photoreaction mixture with probe 9. Left panel – peptide cross-linked at K397 (2893.23 Da = Y393–K416 + 9 - 18 Da; dehydration is common for benzophenone adducts). Right panel – peptide cross-linked at C234 (2874.23 + 9-BX[NH₂] Da). Red circles indicate identified cross-linking sight. (B) Left panel – position of K256–7, K397 (blue), C234 (orange), Tyr197 (pink), and FAD (yellow) have been marked on the previously reported *hGR* dimer structure cross-linked to menadione analogue (red). The substrate binding cleft leading to the catalytic disulfide bridge is visible between K397 and menadione core (orange triangle). (C) Magnification on C234 (yellow) containing the binding pocket with indicated water molecules (violet balls). Surface of A241 (blue) and H374 (pink) at pocked opening and V200 (green) in cavity is visible.

pathways: the probe, the benzophenone-like adduct, the 2-(SG-methyl)-probe adduct, the cyclized probe-BX, the probe-BX-derived enone, and the probe-BX insertion adduct.

Probe Cycling with Glutathione Reductase Generates Benzoxanthone

As for photoreduction, the benzoxanthone formation has been postulated to occur during several cycles of enzymatic (GR) 1e-reduction of PDO_{ox} (Figure 1A). However, the metabolite was only indirectly detected by electrochemical measurements of PDO derivatives due to its minor amount.³¹ To prove definitively that PDO-BX is generated by continuous redox-cycling of the drug under *hGR* catalysis, we analyzed such reaction by LC-MS/MS after 6 h of regular addition of NADPH. The BX-derived enone could be found in reactions in open air (Figures S21B, S21C) but not in the deoxidized control where redox-cycling was not possible due to the absence of oxidants like oxygen (Figure S21A). This clearly demonstrates that PDO-BX is indeed a product of PD metabolite redox-cycling (Figure 1A).

In addition, we investigated similarities in the BX formation during the redox-cycling processes during photoreduction and GR catalysis. For this, we irradiated *hGR* with probe 9 in oxygen-free conditions. Interestingly, despite the lack of oxygen, we were able to obtain 9-BX from probe 9 after 10

min of UV-irradiation with *hGR* (Figure S21D), although this was not possible in a comparable period of time when GSH was acting as a nucleophile. This demonstrates that the presence of the enzyme is enough to accelerate light-induced formation of 9-BX. Indeed, the UV-photoreduction process can mimic the reduction of naphthoquinone by NADPH-reduced enzyme in this pathway, indicating that both processes might share similarities. Generation of BX from PDO_{ox} or probe 9 was also possible in the presence of thiophenol after 10 min of photoirradiation. However, the cysteine thiol group in GSH only led to minor formation of PDO-BX even after overnight UV-irradiation (Figure S22 compared to S26). The results obtained with *hGR* upon irradiation imply that the protein cysteines might be more reactive than GSH. Alternatively, the entropic interaction between the naphthoquinone and the enzyme might play a mutual influence on each other upon transferring electrons and kinetically favor pathways 2–3 following probe binding to a cavity where the molecular environment favors BX formation.

Using Glutathione Reductase as a Model for Photoreaction

To test the ability of the probes to interact with protein targets and to understand the exact probe binding/reduction site in GR structure we studied the cross-linking pattern of an ABPP

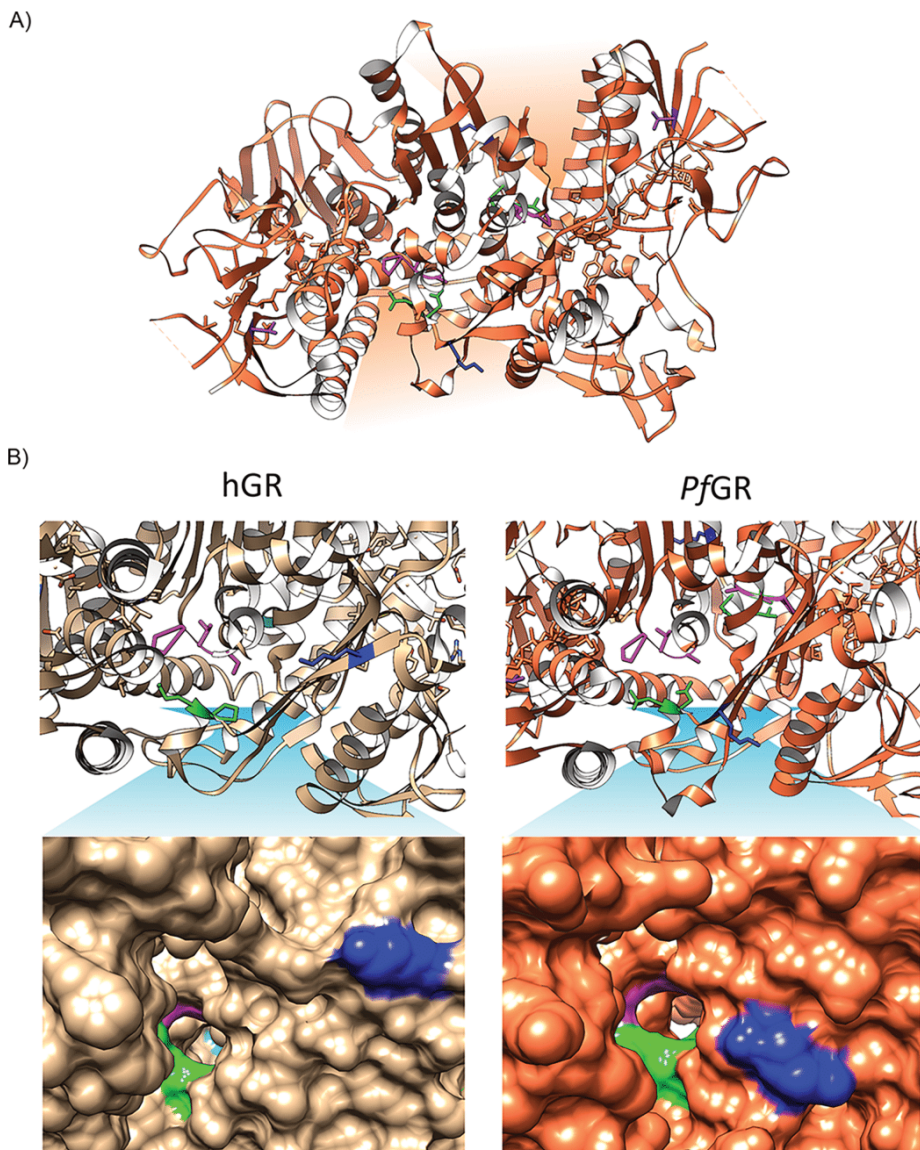


Figure 8. Probe 9 cross-links to *Pf*GR. (A) Positions of cross-linked amino acids (K415 – blue, V6 – pink) to probe 9 in the *Pf*GR structure. The substrate binding cleft leading to the catalytic disulfide bridge and interspace cavity opening is indicated by the orange triangles. (B) Images picturing the distance between cross-linked K397 in *h*GR (left panels), K415 in *Pf*GR (right panels), and the interspace cavity opening. Upper panel – amino acid positions on protein chain. Lower panels – surface density of cavity opening. Blue – cross-linked lysine; Green and violet – amino acids of the cavity opening.

probe with GR upon photoirradiation. Enzymatic inhibition assays proved that the ABPP probes series (e.g., probes 9 and 6) with a EWG (i.e., NO₂) in *para*-position to the benzoyl moiety possess the highest inhibitory potency toward *h*GR among all probes. Furthermore, considering the better solubility and photoreactivity of probe 9, we selected it as the best ABPP probe for studies with model proteins *h*GR and *Pf*GR.

Mass spectrometry analysis confirmed probe 9-*h*GR or -*Pf*GR adduct formation. Similarly to GSH cross-linking, the adduct *m/z* suggested the formation of GR-probe products such as benzophenone-type adduct (+376 Da) and 9-BX or 2-(S-methyl)-9 (+374 Da) adducts as well as species with reduced nitro group (346.11 and 344.10 Da) (Figure S31).

Importantly no significant cross-linked peptides (Mascot score >30) have been identified during MS analysis of UV-irradiated negative control BSA incubated with 9 and the UV-irradiated GRs alone.

Interestingly, the cross-linking sites associated to 9-BX or 2-(S-methyl)-9 were found in sites distinct from the active cysteines. Alkylation of GR was pinpointed at Lys residues whose intrinsically nucleophilic ϵ -amines confer important roles. Beyond cysteines, lysines represent a source for covalent probe development, and several studies on epigenetics *in vivo* have started to identify and map the Lys ligand ability of the human proteome.⁴⁵ We can assume that the highly electrophilic BX-derived enone might be attacked by the intrinsically nucleophilic lysine ϵ -amine (Scheme 3). Furthermore, Lys

cross-linking would explain why this amino acid is miscleaved after trypsin digestion in a large portion of identified peptide adducts (Figure S31). Similar cleavage blocking has been reported in MS studies when Lys is targeted by electrophiles and supports our correct identification of the adducts.⁴⁵

Analysis by MS/MS of the probe 9-cross-linked peptide adducts identified three *hGR* peptides with high confidence (Figures 7A, S31A). The identification of these adducts several times confirms that the probe 9 can be used as a photoreactive ABPP probe to bind to target proteins. The involved binding site between K255 and T257 on peptide E253-R272 is located on the exposed surface of the protein, away from the protein catalytic centers, in this apparently nonfunctional region. However, the two other identified binding sites lie in known functionally related regions.

The cross-linking position (K397) of peptide Y393–K416 does not reside in known binding pockets of *hGR* (Figure 7A,B). Interestingly, the binding locus correlates to previous enzyme kinetic analyses performed with 3-benzoylemenadienes exhibiting uncompetitive GR inhibition.¹⁷ Indeed, it is localized in the interface domain, known to mediate the dimerization of the protein. The domain is crucial for GR activity as the enzyme is not active as a monomer. Additionally, in the interface domain, at the 2-fold symmetry axis of the homodimeric protein, a cavity is present, which was reported to bind numerous GR inhibitors, such as 2-methyl-1,4-NQ (menadione),³⁴ 6-hydroxy-3-oxo-3H-xanthene-9-propionic acid,⁴⁶ a series of 10-arylisalloxazines,⁴⁷ and S-(2,4-dinitrophenyl) glutathione.⁴⁸ The cavity does not have a direct connection with the NADPH or FAD binding sites. It is linked to the external surface of the protein and to the GSSG binding site by two pairs of short channels. The channel pair openings, which are located in the catalytic center, emerge at the bottom of the V-shaped catalytic crevices in close proximity to the redox-active disulfide bridges. Significantly, in total, 41 amino acids of both subunits participate to line the GSSG binding site in *hGR*.³³ It was suggested that compounds docked in the cavity⁴⁹ could either trigger structural changes disturbing the dimer stability leading to decrease of enzyme activity or interfere with the redox potential of the flavin.

Interestingly, the amino acids of the channel opening (403-FTP MYH-408) are present in the identified peptide where K399 was alkylated by probe 9, however, separated by a distance of 19–25 Å from the identified cross-link site and 9.5–19 Å from the active Cys in the GSSG binding site. It is possible that the original interaction site does not overlap with the alkylation site especially considering the reactivity of Lys toward BX. In line, when probe 9 was cross-linked with *PfGR*, instead of *hGR*, the peptide that was identified with the highest confidence (I411–K431) (Figure S31B) is the exact homologous region of peptide Y393–K416 in *hGR* (Figure S31A). Moreover, compared with *hGR*, the suggested part cross-linked to the probe in this peptide (411-IYESKFT-417) contains a K415 to S402 substitution, which lies in proximity to the channel opening (Figure 8A,B). K415 was miscleaved during trypsin digestion indicating the exact probe modification site at this amino acid. Strikingly, the peptide sequence prior to the cavity is conserved between *PfGR* and *hGR* with a high degree of identity emphasizing the importance of this region⁴⁹ (Figure 8).

The amine generated upon nitro group reduction in the 9-BX[NH₂]-peptide S225–K247 adduct was localized on the free cysteine Cys234 lying in proximity to enzyme's catalytic

center where FAD is reduced by NADPH, especially very close to the ultraconserved tyrosine 197. Tyr197 serves as gate keeper of cofactor access to FAD because of its ability to flip and block NADPH positioning near FAD.⁵⁰

Structural analysis shows that Cys234 is part of a sizable pocket that extends into it all the way from the surface near the side chain of Ala 241 (Figure 7C). The pocket lies in a relatively accessible region, which directly interacts with a network of water molecules. Since the pocket is partly lined with nonpolar side chains, this could allow the naphthoquinone to displace the water molecules and gain access to Cys234. Trapping of the probe could additionally be bolstered by intrinsic reactivity of the 9-BX toward cysteine. In fact, Cys234 might have promoted the formation of 9-BX via pathways 2 or 3 (Schemes 2 and 3). When testing the orthologous *Plasmodium* enzyme *PfGR*, cross-linking with probe 9 did not occur at the homologous peptide, probably because of the lack of cysteine in this region in comparison to the equivalent in *hGR*. Of note, the pocket does not appear to have direct access to Tyr197 as it is additionally blocked by Val200 or Cys234 itself. Nevertheless, Cys234 and especially the surrounding cavity represent an interesting target for future PD MoA investigation. A clearer picture of its importance should be studied in the future by generating *hGR* mutants for enzyme kinetics and drug binding/reduction evaluation.

Photolabeling of *hGR* and Pull-Down of Labeled Protein Adducts

Having established the cross-linking and click conditions for the probes as well as selection of the most efficient ones for ABPP, we tested their labeling capability of proteins on *hGR*. Cross-linking with 9 and subsequent click reaction allowed for efficient RA attachment on *hGR* (Figure S32). Similarly, tagging with BA after cross-linking with 7 or 9 followed by pull-down with avidine of labeled adducts proves the ability of the probes to target and isolate proteins (Figure 9). Both

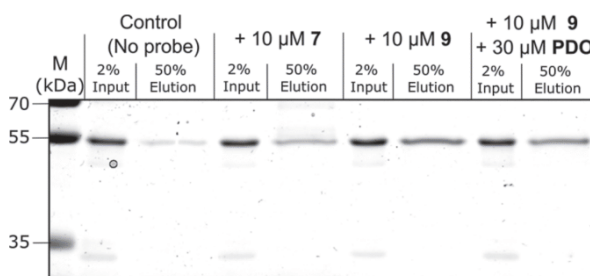


Figure 9. Pull-down of *hGR* labeled with ABPP probes 7 and 9 and clicked with biotin tag. SDS-PAGE gel stained with Coomassie is pictured. For each reaction, 2% of the reaction before pulldown and 50% of the elution after avidin binding were loaded on the gel. *hGR* is localized at the height of the 55 kDa marker band. M – marker.

tagging reactions of probe 9 with RA and BA are competitive toward nonclickable drug analogues (6 in RA and PDO in BA labeling), demonstrating the specificity of the labeling. Altogether, we evidenced that both the cross-linking and click reaction of our probes can be combined for the ABPP strategy.

The plasmodione-derived benzoxanthone is a strong electrophile with relevant meaning for the antiplasmodial plasmodione. The PDO-BX 4 has already been proposed to be a key PD metabolite (Figure 1A).^{20,21} Previously, we evidenced the

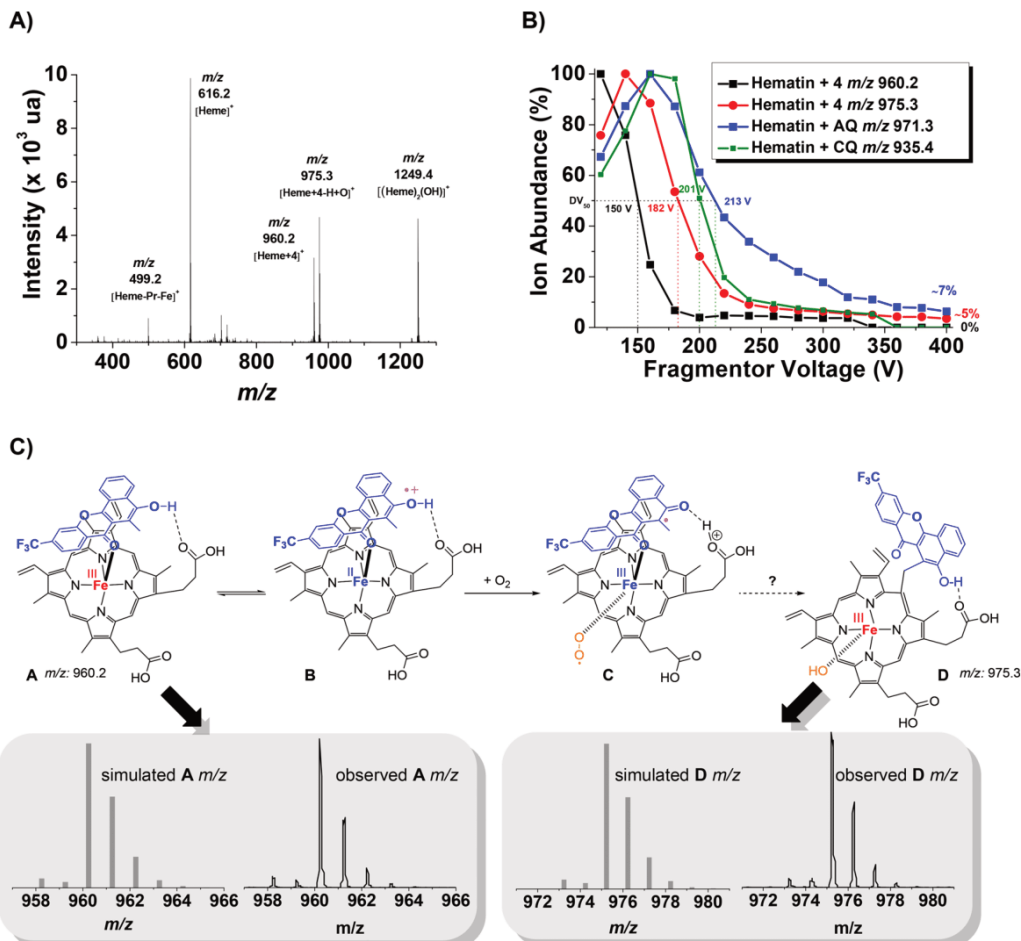


Figure 10. ESI-MS and CID-MS analysis of PDO-BX 4-heme complexes. (A) ESI mass spectrum (exit potential: 120 V) of a 1:1 mixture of 50 μM heme and 50 μM PDO-BX 4 in $\text{H}_2\text{O}/\text{CH}_3\text{CN}$ (5/95) – 1% formic acid. (B) Stability responses of the BX 4-heme (at m/z = 960.2 and at 975.3), AQ-heme (at m/z = 971.3) and CQ-heme (at m/z = 935.4) complexes obtained by CID-MS experiments. ESI-MS⁺; 120 V < fragmentor < 400 V with 20 V increments. (C) Proposed molecular structure of iron^{III}-hematin species alkylated by the BX 4 and comparison between simulated and observed mass signatures of species A and D.

formation of a PDO–hematin complex by binding titrations.²⁰ Having demonstrated the electrophilic nature of the BX 4-derived enone, we used a collision-induced dissociation tandem mass spectrometry (CID-MS) methodology to characterize the complex in detail.⁵¹ In particular, two intense PDO-BX–heme adducts at m/z = 960.2 ([heme+PDO]⁺) and m/z = 975.3 (formally [Heme+BX 4-H+O]⁺) were clearly detected (Figure 10A). The first BX 4–heme adduct at m/z = 960.2 corresponds to a π – π complex. This feature is assessed by the weak dissociation voltage DV_{50} (150 V) and the absence of a residual complex at high fragmentor voltage (Figure 10B). In addition, the π -stacking in the PDO–hematin complex might be strengthened by additional interactions such as hydrogen bonding between the propionate of the heme side chain⁵² and the phenol in PDO-BX and Fe^{III} axial coordination of the BX carbonyl unit (Figure 10C, species A). It is noteworthy that PDO-BX can be oxidized ($E_{\text{pa}} = -50$ mV and -208 mV) through its phenolic moiety and might undergo an exchange of electron(s) with the tightly bound Fe^{III} heme. The intramolecular PDO \rightarrow Fe^{III} heme 1e- transfer is favored by

hydrogen bonding⁵² and generates a carbon radical at the BX core (Figure 10C, species B).

The concomitantly formed Fe^{II} heme from species B binds O₂, and the resulting species C (Figure 10C) might be attacked by the nucleophilic α -keto carbon radical⁵³ of the tightly bound BX, ultimately leading to hematin meso-alkylation⁵⁴ by PDO-BX, as suggested from the CID-ESI-MS experiments (second adduct at m/z 975.3). It is noteworthy that the DV₅₀ value of this second PDO–heme adduct is markedly increased (+32 V), and a significant amount of the complex is observed at high fragmentor voltage, which is therefore indicative of a very stable heme adduct (~5% for PDO–heme adduct and ~7% for the antimalarial drug amodiaquine (AQ)–heme adduct used as reported reference). In this experiment (Figure 10B), the antimalarial chloroquine (CQ), known to be a reversible heme binder did not show a residual covalent adduct at high fragmentor voltage. Similarly, when probe 9 was UV-irradiated with GSH, the formed benzoxanthone was demonstrated to be reactive toward heme, when added to the reaction, leading to the generation of the adduct 9-BX–heme and its hydrated version (Figure S33). Together with the

CID-MS experiments, this proves that the previously observed PDO-BX–heme complex is covalently linked to heme through the reactive enone alkylation. The structural signature of this alkylated hematin product is tentatively proposed in species D (Figure 10C), following reaction of the quinone methide radical at the *meso*-position of the tetrapyrrole and release of a water molecule, as already demonstrated for artemisinin.⁵⁴ This suggested that the heme alkylation product has to be regarded as the result of the formation of a key carbon radical generated from a redox-active agent in redox-driven bioactivation processes and a relevant reaction to the MoA occurring in the parasite *in vivo*.

Such contribution needs more detailed investigations to understand the MoA of the redox-active lead antimalarial PD. Interestingly, the data obtained with PDO-BX are reminiscent of the hypothesized formation of xanthones to explain the potentiation of antimalarial activities of polyhydroxylated benzophenone derivatives tested in the presence of Fenton catalysts upon catalysis of redox-active metals such as Fe^{III}.^{55,56} In the present study, upon oxidative phenolic coupling of PDO_{red}, BX releases a powerful electrophile that can be attacked by the nucleophilic species present in the reaction, GSH, the terminal *ε*-amine group of lysine-like K397 in *hGR*, or heme.

Evaluation of the Antimalarial Properties of PD-ABPP

To validate the applicability of ABPPs in parasites, we then evaluated the antimalarial activity of the five newly synthesized 3-benz(o)ylmenadione-based ABPP probes (7–11, Table 2).

Table 2. IC₅₀ Values for 3-Benz(o)ylmenadione Derivatives Determined from Growth Inhibition Assays with Highly Synchronized *P. falciparum* Strain Dd2

series	compound	IC ₅₀	
		<i>P. falciparum</i> Dd2 ^{a,b} (nM)	hMRC-5 (μM) ^c
3-benzoylmenadienes	6	513 ± 287	24.0
	7	1806 ± 302	20.5
	8	2993 ± 750	25.8
	9	417 ± 222	42.2
	10	>5000	29.4
3-benzylmenadienes	11	49 ± 15	>64.0
	plasmodione	20 ± 5	>32.0 ^d

^aThree independent experiments with the SYBR green assay (mean ± SD). ^bThe *P. falciparum* Dd2 strain is sensitive to DHA (IC₅₀ DHA = 0.7 ± 0.2), to methylene blue (IC₅₀ MB = 7 ± 0.3), and resistant to chloroquine (IC₅₀ CQ = 189 ± 12). ^cToxicity values against human fibroblasts hMRC-5 were determined by using reported protocols.¹⁷

^dValue from ref 17.

The potent antimalarial activities of plasmodione 1, its nitro analogue 5 and the PDO-BX 4 were already reported.^{17,20} As previously observed and despite being the likely key metabolites of 3-benzylmenadienes, the 3-benzoylmenadienes do not display a high antimalarial activity, with an IC₅₀ of ca. 10–50-fold higher than the corresponding 3-benzylmenadienes.^{17,21} This may be explained by the very poor internalization of 3-benzoylmenadione metabolites in pRBCs when given externally. Indeed, similar to the 3-benzylmenadione metabolite PDO, probes 6–10 (Figure 1) are more polar and planar than the 3-benzylmenadienes (PD, probes 5 and 11), likely reducing their ability to be internalized in parasites, and in accordance with the same observation in the

yeast model.⁵⁷ To act as the key active principle of the prodrug PD, the metabolite has thus to be generated *in situ* in the parasite before it can efficiently cycle with NAD(P)H-dependent reductases. With respect to the ABPP properties studied in the click reaction and under photoirradiation, we observed that probes 7 and 9 are the most efficient probes to be used in photolabeling of plasmodione targets.

This result has motivated the synthesis of a first PD-ABPP, probe 11, in the 3-benzylmenadione series. Probe 11 (Figure 1) displayed an IC₅₀ value comparable to that of PD regardless of substitution of the CF₃ function at the *para*-position by an alkyne group. On the basis of our studies on the photo-reactivity and clickability of 3-benz(o)ylmenadione-based ABPP probes, probe 11 is selected for future PD interactome analysis as the most efficient prodrug in killing parasites with a similar IC₅₀ value as the value of PD and because it is expected to generate the most photoreactive probe 7 upon bioactivation in living *Plasmodium* parasites.

CONCLUSIONS

Herein, we have presented the design and the synthesis of specific (pro-)PD-ABPP probes based on the postulated MoA of the antimalarial prodrug PD. We have studied the influence of different EWGs in the 3-benzoylmenadione series on the photoreaction effectiveness of the ABPPs as well as the probes' "clickability" properties. This allowed us to select probes 7 and 9 as the most effective tools for the ABPP approach. Optimization of the ABPP methodology (e.g., click in PBS with Cu^{II}:BCDA:TCEP (5:1:1)) has been successfully demonstrated by hGR photolabeling with probe 7 or 9 and subsequent pull-down of labeled protein adducts. Interestingly, labeling of different nucleophilic amino acids in distinct regions of hGR and P_fGR will open new directions to study GR mutants of these different residues in the context of drug development. Finally, using UV-photoirradiation, we provide evidence that (pro-)ABPP probe 11 can indeed be photo-oxidized in 3-benzoylmenadione-derived ABPP probe 7. While these conditions are not physiological, this result further supports the current model for PD activation and MoA. Additionally, by correlating the efficiency of (pro-)ABPP with their antimalarial activity, we concluded that the (pro-)PD-ABPP probe 11 should be the most effective one to be used in parasite cultures to identify the PD interactome by proteomics analysis. Identifying PD targets will be essential to further optimize the properties of this compound series and to design more active and target-specific derivatives.

Beyond the investigated plasmodione-based tools, we believe that the concept of (pro-)ABPP can be further expanded as a generalizable and emerging strategy to investigate redox-active drugs with various biological properties (e.g., anticancer, antibiotic, antiviral, antiparasitic) to identify new protein targets, while noting that other warheads than menadione are also possible.

Linking drug effects from complex reactions to killing processes/targets in parasites is one of the most challenging steps when studying the MoA of any drug. When the latter is a redox-activatable prodrug it is even more difficult because a wide range of metabolites can be generated in trace amounts during redox bioactivation. One solution dealing with this quantity limit is the development ABPP probes based on already known drug metabolites, keeping in mind that the method addresses a common limitation of exogenously added probe, which does not necessarily mimic the endogenous generation of an active

principle from a prodrug in the target living cell. Therefore, to circumvent this limitation, we designed a series of photo-reactive prodrugs, which upon UV irradiation generate the same drug metabolites as those formed through redox bioactivation, and we put this concept into practice using the antimalarial agent plasmodione. Besides this applied and deep investigation about an antiplasmoidal early lead agent, we believe that understanding the various parameters influencing the CuAAC reaction, for example, Cu(I) preincubation reaction with reductant and ligand, organic solvent, reductant and ligand ratios, pH, buffer dilution, salts, counter-anions, is essential for the success of the CuAAC strategy. The interplay between these elusive factors is key in the setting up of the optimization of the CuAAC reaction, as demonstrated by our findings.

MATERIAL AND METHODS

UV-Irradiation

Reactions were irradiated either with a 365 nm light generated by a UV monochromator of 1000 W intensity for 8 to 10 min or with a 350 nm light generated by eight RPR-3500A lamps of 200 W with a Rayonet photochemical reactor overnight at a distance of 3 cm from the light source.

Irradiation Experiments for Photobenzylic Oxidation of the (Pro-)ABPP Benzylmenadione Probe 11 to Benzoylmenadione 7

First, 50 mg of 2-(4-ethynylbenzyl)-3-methylnaphthalene-1,4-dione **11** and 2 mL of the appropriate solvent were added in a tube. The mixture was agitated and bubbled with oxygen during 30 min. Then, under a positive pressure of oxygen, the tube was placed in a Rayonet photochemical reactor and irradiated at 350 nm for 72 h. The resulting mixture was extracted with dichloromethane if necessary, and the solvent was removed under reduced pressure. The reaction crude was directly analyzed by NMR spectroscopy.

Irradiation Experiments for Model Photoreaction

The photochemical reaction of *N*-acetyl-methionine methyl ester (*N*-Ac-Met-OMe, shortened as nMet) with benzophenone and benz(o)ylmenadione **6** was carried out in a pyrex tube (filter for $\lambda < 300$ nm) at a final concentration of 0.1 M at final concentration of 0.1 M in ACN. The reaction was irradiated at 5 °C for 24 h in a Rayonet reactor (at 350 nm). Finally, the reaction was analyzed by field-desorption mass spectrometry (FD-MS), as seen in Figure 2. FD-MS of the reactions was performed at Heidelberg University according to a published protocol with a JEOL JMS-700.⁵⁸

Standardization of UV Cross-Linking Parameters Using nMet

The e^{\max} and λ^{\max} of all the PD-ABPP were first analyzed by UV-vis absorption spectrophotometry in the λ region >300 nm (Figure S5). It is noteworthy to mention that the $\pi-\pi^*$ transitions are below 300 nm for all PD-ABPP probes. In addition to the intense absorption below 300 nm ($\pi-\pi^*$), the maximum of absorption $\lambda^{\max}(\pi-\pi^*$ transitions) is about 340 nm for probes **7**, **8**, **9**, **11**; 320 nm for probes **8** and **10**; and 350 nm for benzophenone with low intense absorption ($n-\pi^*$ transitions) centered at about 400 nm. For all probes, we selected 350 nm (Rayonet, 24 h) or 365 nm (1000 W λ monochromator, 2 min, at room temperature) wavelengths as the light excitation sources for studying the corresponding photoreaction because of the proximity of $\lambda^{\max}(n-\pi^*$ transitions) of the probe and the low probability of damaging the protein.

The reaction conditions are as follows: 1 equiv of PD-ABPP + 5 equiv of nMet (i.e., 100 μ L of 20 mM PD-ABPP in ACN + 100 μ L of 1000 mM PD-ABPP in ACN), with a total 200 μ L volume. The reaction mixtures were deoxygenated under strict oxygen-free conditions using argon-vacuum cycles, exposed to photoirradiation,

and then analyzed by 1 H NMR. The covalently cross-linked products were confirmed by TLC and NMR analysis.

Inhibition Potency of ABPP Probes toward Human GR

The inhibition of hGR by ABPP probes **7–10** was evaluated by using a standard GR assay¹⁷ with 100 μ M NADPH (Biomol) and 1 mM GSSG (Serva) in GR buffer (47 mM potassium phosphate buffer, 200 mM KCl, 1 mM EDTA, pH 6.9) at 25 °C in a 1 mL-cuvette using the inhibitor concentrations ranging from 0 to 2 μ M. The final concentration of ACN in the assay was 2%. Initial rates of NADPH oxidation by hGR (8 mU or 0.85 pmol) was monitored at 340 nm with a Cary 50 UV-vis absorption spectrophotometer.

Photoreaction between the ABPP Probe **9** and Thiophenol, Peptides, and Proteins as Partners

For peptide cross-linking, stock solutions of GSH (Sigma) or PS2C were prepared in 20 mM PBS at pH = 6.9. Stock solutions of PDO **2** or of probe **9** were prepared in pure ACN. For thiophenol cross-linking, the stock solution of the thiol was prepared in ACN. Then, the reaction was started by mixing 3 mM of peptide or thiophenol with 600 μ M **9** or 100 μ M **3** in a mixture of 1:1 ACN and 10 mM PBS in 200 μ L volume. The reaction mixtures were deoxygenized by seven alternative cycles of vacuum and Ar flux in an anaerobic cuvette with longer argon cycles (15s) than vacuum cycles (<6s) to avoid ACN evaporation. The mixture was photoirradiated for 10 min or overnight (O/N), and the next day the solution was analyzed by HPLC-MS.

For heme alkylation by **9-BX**, 1.5 mM heme solution in PBS was added to the reaction mixture containing GSH and probe **9** at completion. The resulting mixture was incubated for 2 h and analyzed by HPLC-MS. Hematin was generated from hemin (Sigma) by basifying the heme solution with 2 M NaOH.

In the study about cross-linked adduct formation, protein photoirradiation was performed with a mixture of 6 μ M hGR or 5 μ M PfGR (or BSA - used as negative control) with 6 μ M or 5 μ M probe **9**, respectively, in 200 μ L of 10 mM PBS buffer at pH 6.9 with 2% ACN. Probe solubility in 2% ACN was assessed spectrophotometrically with a Cary 50 absorption spectrophotometer by monitoring absorbance kinetics of decreasing ABPP probe concentrations, starting with 20 μ M (Figure S16).

In reactions with hGR and the probe, 52.5 μ M NADPH was added to initiate the redox-cycling. The reaction mixture was deoxygenized by seven alternative vacuum and Ar flux cycles (10 s each) in an anaerobic cuvette. Subsequently, the mixture was photoirradiated for 8 min, and afterward, 100 μ L of 3X Laemmli buffer was added. The next day, the samples were separated on 10% SDS-PAGE gels, stained with Coomassie solution, and destained according to published protocol.⁵⁹ Protein bands were cut out and subjected to trypsin digestion and HPLC-MS analysis.

Generation of **9-BX** from ABPP Probe **9** upon hGR Redox-Cycling

In order to generate **9-BX**, 40 μ M of probe **9** was allowed to redox-cycle with hGR and 1.44 mM NADPH. Probe **9** stock solution was prepared in DMSO and added to the reaction mixture in the presence of 2% solvent final in 47 mM PBS buffer in 200 μ L of total reaction volume. In the hemoglobin reduction assay, 80 μ M methemoglobin was mixed additionally to the reaction. Redox-cycling was started by addition of a 6 μ L-aliquot of 16 mM NADPH and 4 μ M hGR. The same amount of NADPH was added at regular 2 h-intervals for the next 6 h. A control sample was deoxygenized by seven vacuum-argon cycles before first addition of the separately deoxygenized NADPH solution.

Generation of **9-BX** from ABPP Probe **9** upon hGR Photoreduction

Probe **9** photoreduction in the presence of hGR was achieved by mixing 100 μ M of the probe in 20% ACN with 4 μ M hGR in 47 mM PBS buffer. Samples were deoxygenized by 7 alternative vacuum-Ar cycles with longer argon cycles (15s) than vacuum cycles (<6s) to

avoid ACN evaporation. The reaction was UV-irradiated for 10 min and the mixture was analyzed by HPLC-MS.

Successive Cross-Linking and Click Reaction with hGR

For hGR labeling 150 μ L of 10 μ M hGR in 12.5 mM PBS (potassium based) and 2% DMSO was UV irradiated in the presence of 10 μ M probe 7 or 9 for 10 min. The reaction was beforehand deoxygenized by seven alternative cycles of vacuum and Ar flux. In competition assays 30 μ M of probe 6 or PDO was added additionally. After a 10 min photoreduction, 3.3% DMF and 20 μ M RA or 10 μ M BA was added. The reaction was deoxygenized a second time, and 0.4% of deoxygenized SDS was added with a syringe. A click reaction was initiated by adding a 1:5:1 copper BCDA:CuSO₄:TCEP 40 min-long preincubation mixture to a final concentration ratio of 132:660:132 μ M, respectively, and final volume of 200 μ L. The reaction was incubated overnight at 30 °C. Reactions containing biotin azide (BA) were subjected to pull-down, whereas rhodamine azide (RA) reactions were mixed with 100 μ L of 3X Laemmli, heated at 60 °C, and separated by SDS-PAGE. Gel fluorescence was visualized by GelDoc EZ imager (BioRad) on a blue tray (excitation = 430–460 nm). The gel was stained by Coomassie staining after fluorescence analysis.

Biotin Pulldown

Biotin-protein adducts were pulled down by binding to avidin agarose beads (Pierce). Prior to use, the beads were washed five times with 1.5 mL of washing buffer (47 mM sodium based PBS, pH 6.9) and centrifuged at 5000g for 1 min at RT. Unspecific sites on the avidin agarose beads were blocked by incubating the beads for 1.5 h at RT with 0.5 mM BSA. Overnight click reactions were diluted with 47 mM PBS with 0.3% SDS to 1 mL of volume and incubated for 1 h with beads at RT. The suspension was washed once with washing buffer + 0.05% Tween20 and once with washing buffer + 1% SDS, as well as once with washing buffer in-between, before, and after. Subsequently, the beads were centrifuged at 4500g for 1 min at RT. Bound proteins were eluted at 96 °C for 10 min with 80 μ L of Laemmli buffer. Eluted proteins were separated on 10% SDS-PAGE gel and stained with Coomassie stain.

Protein Preparation for In-Gel Digestion

The gel pieces were successively washed with 50 μ L of 25 mM NH₄HCO₃ and 50 μ L of ACN (three times) and dehydrated with 100 μ L of ACN before reduction in the presence of 10 mM DTT in 25 mM NH₄HCO₃ (1 h at 57 °C) and alkylation in the presence of 55 mM iodoacetamide in 25 mM NH₄HCO₃. For tryptic digestion, the gel pieces were resuspended in 2× volumes of trypsin (12.5 ng/ μ L; Promega V5111) freshly diluted in 25 mM NH₄HCO₃ and incubated overnight at 37 °C. The digested peptides were then extracted from the gel in a buffer containing 34.9% H₂O, 65% ACN, and 0.1% HCOOH, and the excess of ACN was removed by evaporation and peptides analyzed by nanoLC-MS/MS.

NanoLC-MS/MS Analysis

Peptide digests analysis was performed on a nanoACQUITY Ultra-Performance-LC (Waters, Milford, MA, U.S.A.) coupled to a TripleTOF 5600+ mass spectrometer (Sciex, Framingham, U.S.A.). The samples were trapped on a 20 × 0.18 mm, 5 μ m Symmetry C18 precolumn (Waters Corp.), and the peptides were separated on a nanoEase M/Z Peptide BEH C18 Column, 130 Å, 1.7 μ m, 75 μ m × 150 mm (Waters). The solvent system consisted of 0.1% formic acid in water (solvent A) and 0.1% formic acid in ACN (solvent B). Trapping was performed during 3 min at 5 μ L/min with 99% of solvent A and 1% of solvent B. Elution was performed at a flow rate of 300 nL/min, using 1–40% gradient (solvent B) over 35 min at 60 °C followed by 65% (solvent B) over 5 min. The mass spectrometer was operated in positive mode, with the following settings: ion spray voltage floating (ISVF) 2300 V, curtain gas (CUR) 25 psi, interface heater temperature (IHT) 75 °C, ion source gas 1 (GS1) 2 psi, declustering potential (DP) 100 V. Information-dependent acquisition (IDA) mode was used with top 5 MS/MS scans. The MS scan had an accumulation time of 250 ms on m/z [400–1250] range and

the MS/MS scans 100 ms m/z [150–1600] range in high sensitivity mode. Switching criteria were set to ions with charge state of 2–4 and an abundance threshold of more than 150 counts, and exclusion time was set at 12 s. IDA rolling collision energy script was used for automatically adapting the CE. Mass calibration of the analyzer was achieved using peptides from digested BSA. The complete system was fully controlled by AnalystTF 1.6 (AB Sciex).

Protein Identification

Mass data collected during nanoLC-MS/MS were searched using a local Mascot server (Matrix Science, London, U.K.) against an in-house-generated protein database composed of protein sequences of hGR, PfGR and BSA using an in-house database generation toolbox (<https://msda.unistra.fr>). Searches were performed with selected modification (on each 20 encoded proteinogenic amino acids either +375.07 Da (9 or 9-BX), +374.07 Da (9 - 1 Da), +373.06 Da (9-BX) +357.06 Da (9 - H₂O), +356.06 Da (9-BX - OH), +358.07 Da (9 - OH), +345.10 Da (9-NH₂), 343.08 Da (9-BX-NH₂) or +327.09 Da (9-NH₂ - H₂O), trypsin was selected as the enzyme, carbamidomethylation of cysteine (+57 Da) and oxidation of methionine (+16 Da) were set as variable modifications, three miscleavages were tolerated and mass tolerances on precursor, and fragment ions of 20 ppm and 0.07 Da were used, respectively. Modified peptides were manually validated. Selected peptides binding sites were visualized, and distances were calculated on hGR (PDB ID: 3GRS; 2GHS) and PfGR (PDB ID: 1ONF) structure models using Chimera software.⁶⁰

HPLC-MS Analysis

LC/MS analyses were performed using an Agilent 1100 series LC coupled to a MicrOTOF-Q (Bruker Daltonics, Bremen, Germany) or to a maXis II Q-TOF mass spectrometer (Bruker). The mass spectrometer was operated in positive mode with a capillary voltage of 4500 V. Acquisitions were performed on the mass range of 200–1850 m/z . Calibration was performed using the singly charged ions produced by a solution of Tune mix (G1969–85000, Agilent, U.S.A.). Data analysis was performed by using Compass DataAnalysis 4.3 (Bruker Daltonics). A cross-linking reaction mixture containing GSH and PDO 2 (or probe 9) was directly analyzed onto a HPLC connected to MicrOTOF-Q. Compounds were separated on a XBridge Peptide BEH C18 column (300 Å, 3.5 μ m, 2.1 mm × 250 mm) column. The gradient was generated at a flow rate of 250 μ L/min using 0.1% trifluoroacetic acid (TFA) in water for mobile phase A and ACN containing 0.08% TFA for mobile phase B at 60 °C. Phase B was increased from 5 to 85% in 45 min.

MS Fragmentation of Collected Fractions

Adducts synthesized in photoreactions and selected for fragmentation were purified by HPLC into specific fractions. Fragmentation of compounds and standards was performed on a hybrid electrospray quadrupole time-of-flight mass spectrometer MS (Synapt G2 HDMS, Waters, Manchester, U.K.) coupled to an automated chip-based nanoelectrospray device (Triversa Nanomat, Advion Biosciences, Ithaca, U.S.A.) operating in the positive ion mode. The MS analysis was performed on the Synapt G2 HDMS instrument with external calibration using the singly charged ions produced by an ES-TOF tuning mix (G1969–85000, Agilent, U.S.A.). The nanoelectrospray device (Triversa Nanomat) was set at 1.5 kV on capillary, and the pressure of the nebulizer gas was 0.55 psi. Selected ions were fragmented with a collision energy ranging from 5 to 40 eV until sufficient fragmentation was achieved.

Collision-Induced Dissociation-Electrospray Mass Spectrometry Measurements

Electrospray mass spectra of heme complexes were obtained with a Bruker Daltonics MicroTOF spectrometer (Bruker Daltonik GmGmbH, Bremen, Germany) equipped with an orthogonal electrospray (ESI) interface. Calibration was performed using Tuning mix (Agilent Technologies). CID experiments⁵¹ were performed with a capillary exit (cone voltage) ranging from 120 to 400 V with 20 V increments.⁶¹ Stock solution of hematin ([Fe^{III}PPIX (OH)₂]³⁺ or [Fe^{III}PPIX (OH)]²⁺) was freshly prepared from hemin (ferriproto-

porphyrin chloride, $[\text{Fe}^{\text{III}}\text{PPIX}(\text{Cl})]^{2+}$) just before use in 50% ammonia. Stock solution of benzoxanthone BX 4 (5 mM) was prepared in ACN, while chloroquine (CQ, 2.91 mM) and amodiaquine (AQ, 2.28 mM) were prepared in water. Hematin and the substrate (4 or CQ or AQ) were mixed together in $\text{CH}_3\text{CN}/\text{H}_2\text{O}$ (50:50 v:v) in order to obtain equimolar concentrations of 100 μM . Prior to analyses, the samples were further diluted at 50 μM in ACN/ $\text{H}_2\text{O}/\text{HCOOH}$ (50:50:1 v:v:v). The sample solutions were then introduced into the spectrometer source with a syringe pump (Harvard type 55 1111; Harvard Apparatus Inc., South Natick, MA, U.S.A.) with a flow rate of 5 $\mu\text{L}\cdot\text{min}^{-1}$. Stability responses of the heme-drug adducts obtained by ESI-CID experiments were drawn.

Antimalarial Activity

Antimalarial activity is represented by IC_{50} , the concentration of biomolecule at which half of the parasites are killed. The antimalarial activity of PD-ABPP was evaluated on asexual parasite stages of the chloroquine-resistant Dd2 strain of *P. falciparum*. Highly synchronised young rings (0-3h old)^{62,63} were treated for 72 h with various concentrations of PD-ABPP. For this, mature schizonts of highly synchronous parasite cultures were separated using 60% percoll gradient and the mature segmented schizonts were incubated for 3 hours for reinvasion. Remaining mature stages were then killed with 5% sorbitol and parasitemia adjusted to 0.5% in 1.5% haematocrit. Each inhibitor was analysed in a three-fold serial dilution in duplicates in three independent experiments and PD was used as a control. Parasite replication was assessed by fluorescent SYBR green staining of parasitic DNA as previously described.^{64,65} After 72 hours, the parasites were frozen at -80 °C overnight, followed by thawing and the DNA stained by SYBR green and the fluorescence measured on a plate reader (Promega) at 591 nm wavelength. For each well, the signal before adding SYBR green was subtracted to the signal with SYBR green to eliminate compound fluorescence. The percentage of surviving parasites compared to controls was determined as follows: $(\text{Fluo}_X - \text{Fluo}_{\text{diRBC}}) / (\text{Fluo}_{\text{DMSO}} - \text{Fluo}_{\text{diRBC}}) * 100$ where Fluo_X and $\text{Fluo}_{\text{DMSO}}$ are the mean fluorescence signals of parasites incubated with compound X or DMSO as a control, and $\text{Fluo}_{\text{diRBC}}$, the mean fluorescence signal of infected parasites exposed to high drug concentrations that kill them all to account for DNA of the starting parasites in each well (0.5% parasitemia). IC_{50} values were calculated using Prism (GraphPad, log(inhibitor) vs normalized response – Variable slope). Control parasitemia at T0 and T72 was determined by microscopic analysis of Giemsa stained blood smears to verify parasite stages and multiplication factor.

■ ASSOCIATED CONTENT

Supporting Information

The Supporting Information is available free of charge at <https://pubs.acs.org/doi/10.1021/jacsau.1c00025>.

Detailed experimental procedures, spectroscopic data, NMR and mass spectrometry analyses of the new compounds 7–11 and of various partners-probes adducts ([PDF](#))

■ AUTHOR INFORMATION

Corresponding Author

Elisabeth Davioud-Charvet – Université de Strasbourg–CNRS–UHA, UMR7042, Laboratoire d’Innovation Moléculaire et Applications (LIMA), Team Bio(IN)organic and Medicinal Chemistry, European School of Chemistry, Polymers and Materials (ECPM), 67087 Strasbourg, France; [orcid.org/0000-0001-7026-4034](#); Email: elisabeth.davioud@unistra.fr

Authors

Bogdan Adam Cichocki – Université de Strasbourg–CNRS–UHA, UMR7042, Laboratoire d’Innovation Moléculaire et Applications (LIMA), Team Bio(IN)organic and Medicinal Chemistry, European School of Chemistry, Polymers and Materials (ECPM), 67087 Strasbourg, France

Vrushali Khobragade – Université de Strasbourg–CNRS–UHA, UMR7042, Laboratoire d’Innovation Moléculaire et Applications (LIMA), Team Bio(IN)organic and Medicinal Chemistry, European School of Chemistry, Polymers and Materials (ECPM), 67087 Strasbourg, France

Maxime Donzel – Université de Strasbourg–CNRS–UHA, UMR7042, Laboratoire d’Innovation Moléculaire et Applications (LIMA), Team Bio(IN)organic and Medicinal Chemistry, European School of Chemistry, Polymers and Materials (ECPM), 67087 Strasbourg, France

Leandro Cotos – Université de Strasbourg–CNRS–UHA, UMR7042, Laboratoire d’Innovation Moléculaire et Applications (LIMA), Team Bio(IN)organic and Medicinal Chemistry, European School of Chemistry, Polymers and Materials (ECPM), 67087 Strasbourg, France

Stephanie Blandin – Université de Strasbourg–CNRS–UHA, UMR7042, Laboratoire d’Innovation Moléculaire et Applications (LIMA), Team Bio(IN)organic and Medicinal Chemistry, European School of Chemistry, Polymers and Materials (ECPM), 67087 Strasbourg, France

Christine Schaeffer-Reiss – Laboratoire de Spectrométrie de Masse BioOrganique, Université Strasbourg, CNRS, IPHC UMR 7178, F-67000 Strasbourg, France

Sarah Cianfranì – Laboratoire de Spectrométrie de Masse BioOrganique, Université Strasbourg, CNRS, IPHC UMR 7178, F-67000 Strasbourg, France; [orcid.org/0000-0003-4013-4129](#)

Jean-Marc Strub – Laboratoire de Spectrométrie de Masse BioOrganique, Université Strasbourg, CNRS, IPHC UMR 7178, F-67000 Strasbourg, France

Mourad Elhabiri – Université de Strasbourg–CNRS–UHA, UMR7042, Laboratoire d’Innovation Moléculaire et Applications (LIMA), Team Bio(IN)organic and Medicinal Chemistry, European School of Chemistry, Polymers and Materials (ECPM), 67087 Strasbourg, France; [orcid.org/0000-0001-6371-7533](#)

Complete contact information is available at: <https://pubs.acs.org/10.1021/jacsau.1c00025>

Author Contributions

[#](B.A.C., V.K.) These authors contributed equally

Notes

The authors declare no competing financial interest.

■ ACKNOWLEDGMENTS

This work was supported by the French Centre National de la Recherche Scientifique (E.D.-C., M.E. and S.A.B.), the Institut National de la Santé et de la Recherche Médicale (S.A.B.), the University of Strasbourg (E.D.-C., C.S., S.C., J.-M.S., and S.A.B., IDEX grant for the plasmoClick project, postdoctoral salary for B.C.), the French Proteomic Infrastructure (ProFI; ANR-10-INBS-08-03), the Laboratoire d’Excellence (LabEx) ParaFrap (grant LabEx ParaFrap ANR-11-LABX-0024 to E.D.-C. and S.A.B., Ph.D. doctoral salary for V.K.), the ANR PRC2017 (grant PlasmoPrim including the salary of the Ph.D.

student M.D.), the Fondation pour la Recherche en Chimie (grant Innovation for the FluoPlasmo project, postdoctoral salary for L.C.), and the ERC Starting Grant N°260918 (S.A.B.). The authors are indebted to Tobias Müller for preliminary 3-benzoylmenadione 6-nMet photoirradiation experiments, and both master M2 students, Alba Zugasti and Joan Guillem Mayans, for synthesizing the first batch of probes 7 and 11, respectively. They also thank Romain Ruppert (UMR 7177 CNRS-Strasbourg University, Laboratory of Controlled Ligand Architectures in Coordination chemistry-CLAC) and Jean-Pierre Sauvage (Institute of Supramolecular Science and Engineering-ISIS, UMR 7006 CNRS-Strasbourg University, Laboratory of Inorganic Chemistry) for fruitful discussion about BCDA solubility, and Alexandre Specht (UMR 7199 CNRS-Strasbourg University, Chemical Biology group) for making available the high-intensity 1000W UV monochromator. Katja Becker (Biochemistry and Molecular Biology, Interdisciplinary Research Centre, Justus Liebig Giessen University) is acknowledged for welcoming V.K. for 2 months in the frame of the COST Action CM1307.

■ REFERENCES

- (1) Galmozzi, A.; Dominguez, E.; Cravatt, B. F.; Saez, E. Application of Activity-Based Protein Profiling to Study Enzyme Function in Adipocytes. In *Methods in Enzymology*; Academic Press: San Diego, 2014; pp 151–169.
- (2) Whitby, L. R.; Obach, R. S.; Simon, G. M.; Hayward, M. M.; Cravatt, B. F. Quantitative Chemical Proteomic Profiling of the in Vivo Targets of Reactive Drug Metabolites. *ACS Chem. Biol.* **2017**, *12*, 2040–2050.
- (3) Liu, Y.; Patricelli, M. P.; Cravatt, B. F. Activity-Based Protein Profiling: The Serine Hydrolases. *Proc. Natl. Acad. Sci. U. S. A.* **1999**, *96*, 14694–14699.
- (4) Yoo, E.; Schulze, C. J.; Stokes, B. H.; Onguka, O.; Yeo, T.; Mok, S.; Gnädig, N. F.; Zhou, Y.; Kurita, K.; Foe, I. T.; Terrell, S. M.; Boucher, M. J.; Cieplak, P.; Kumpornsin, K.; Lee, M. C. S.; Linington, R. G.; Long, J. Z.; Uhlemann, A. C.; Weerapana, E.; Fidock, D. A.; Bogyo, M. The Antimalarial Natural Product Salinopostin A Identifies Essential α/β Serine Hydrolases Involved in Lipid Metabolism in *P. Falciparum* Parasites. *Cell Chem. Biol.* **2020**, *27*, 143–157.
- (5) Rostovtsev, V. V.; Green, L. G.; Fokin, V. V.; Sharpless, K. B. A Stepwise Huisgen Cycloaddition Process: Copper(I)-Catalyzed Regioselective “Ligation” of Azides and Terminal Alkynes. *Angew. Chem., Int. Ed.* **2002**, *41*, 2596–2599.
- (6) Lewis, W. G.; Magallon, F. G.; Fokin, V. V.; Finn, M. G. Discovery and Characterization of Catalysts for Azide-Alkyne Cycloaddition by Fluorescence Quenching. *J. Am. Chem. Soc.* **2004**, *126*, 9152–9153.
- (7) Parker, C. G.; Pratt, M. R. Click Chemistry in Proteomic Investigations. *Cell* **2020**, *180*, 605–632.
- (8) Wright, A. T.; Song, J. D.; Cravatt, B. F. A Suite of Activity-Based Probes for Human Cytochrome P450 Enzymes. *J. Am. Chem. Soc.* **2009**, *131*, 10692–10700.
- (9) Rotili, D.; Altun, M.; Kawamura, A.; Wolf, A.; Fischer, R.; Leung, I. K. H.; MacKeen, M. M.; Tian, Y. M.; Ratcliffe, P. J.; Mai, A.; Kessler, B. M.; Schofield, C. J. A Photoreactive Small-Molecule Probe for 2-Oxoglutarate Oxygenases. *Chem. Biol.* **2011**, *18*, 642–654.
- (10) Burke, A. A.; Barrows, L.; Solares, M. J.; Wall, A. D.; Jakobsche, C. E. Bifunctional Molecular Probes for Activity-Based Visualization of Quinone-Dependent Amine Oxidases. *Chem. - Eur. J.* **2018**, *24*, 17681–17685.
- (11) Krysiak, J. M.; Kreuzer, J.; Macheroux, P.; Hermetter, A.; Sieber, S. A.; Breinbauer, R. Activity-Based Probes for Studying the Activity of Flavin-Dependent Oxidases and for the Protein Target Profiling of Monoamine Oxidase Inhibitors. *Angew. Chem., Int. Ed.* **2012**, *51*, 7035–7040.
- (12) Penarete-Vargas, D. M.; Boisson, A.; Urbach, S.; Chantelauze, H.; Peyrottes, S.; Fraisse, L.; Vial, H. J. A Chemical Proteomics Approach for the Search of Pharmacological Targets of the Antimalarial Clinical Candidate Albitiazolium in Plasmodium Falciparum Using Photocrosslinking and Click Chemistry. *PLoS One* **2014**, *9*, No. e113918.
- (13) Wright, M. H.; Clough, B.; Rackham, M. D.; Rangachari, K.; Brannigan, J. A.; Grainger, M.; Moss, D. K.; Bottrill, A. R.; Heal, W. P.; Broncel, M.; Serwa, R. A.; Brady, D.; Mann, D. J.; Leatherbarrow, R. J.; Tewari, R.; Wilkinson, A. J.; Holder, A. A.; Tate, E. W. Validation of N-Myristoyltransferase as an Antimalarial Drug Target Using an Integrated Chemical Biology Approach. *Nat. Chem.* **2014**, *6*, 112–121.
- (14) Wang, J.; Zhang, C. J.; Chia, W. N.; Loh, C. C. Y.; Li, Z.; Lee, Y. M.; He, Y.; Yuan, L. X.; Lim, T. K.; Liu, M.; Liew, C. X.; Lee, Y. Q.; Zhang, J.; Lu, N.; Lim, C. T.; Hua, Z. C.; Liu, B.; Shen, H. M.; Tan, K. S. W.; Lin, Q. Haem-Activated Promiscuous Targeting of Artemisinin in Plasmodium Falciparum. *Nat. Commun.* **2015**, *6*, 10111.
- (15) Ismail, H. M.; Barton, V. E.; Panchana, M.; Charoensutthivarakul, S.; Biagini, G. A.; Ward, S. A.; O'Neill, P. M. Corrigendum: A Click Chemistry-Based Proteomic Approach Reveals That 1,2,4-Trioxolane and Artemisinin Antimalarials Share a Common Protein Alkylation Profile. *Angew. Chem., Int. Ed.* **2016**, *55*, 10548.
- (16) Lubin, A. S.; Rueda-Zubiaurre, A.; Matthews, H.; Baumann, H.; Fisher, F. R.; Morales-Sanfrutos, J.; Hadavizadeh, K. S.; Nardella, F.; Tate, E. W.; Baum, J.; Scherf, A.; Fuchter, M. J. Development of a Photo-Cross-Linkable Diaminoquinazoline Inhibitor for Target Identification in Plasmodium Falciparum. *ACS Infect. Dis.* **2018**, *4*, 523–530.
- (17) Müller, T.; Johann, L.; Jannack, B.; Brückner, M.; Lanfranchi, D. A.; Bauer, H.; Sanchez, C.; Yardley, V.; Deregnaucourt, C.; Schrével, J.; Lanzer, M.; Schirmer, R. H.; Davioud-Charvet, E. Glutathione Reductase-Catalyzed Cascade of Redox Reactions to Bioactivate Potent Antimalarial 1,4-Naphthoquinones—a New Strategy to Combat Malarial Parasites. *J. Am. Chem. Soc.* **2011**, *133*, 11557–11571.
- (18) Bauer, H.; Fritz-Wolf, K.; Winzer, A.; Kühner, S.; Little, S.; Yardley, V.; Vezin, H.; Palfey, B.; Schirmer, R. H.; Davioud-Charvet, E. A Fluoro Analogue of the Menadione Derivative 6-[2'-(3'-Methyl)-1',4'-Naphthoquinolyl]Hexanoic Acid Is a Suicide Substrate of Glutathione Reductase. Crystal Structure of the Alkylated Human Enzyme. *J. Am. Chem. Soc.* **2006**, *128*, 10784–10794.
- (19) Sidorov, P.; Desta, I.; Chessé, M.; Horvath, D.; Marcou, G.; Varnek, A.; Davioud-Charvet, E.; Elhabiri, M. Redox Polypharmacology as an Emerging Strategy to Combat Malarial Parasites. *ChemMedChem* **2016**, *11*, 1339–1351.
- (20) Bielitzka, M.; Belorgey, D.; Ehrhardt, K.; Johann, L.; Lanfranchi, D. A.; Gallo, V.; Schwarzer, E.; Mohring, F.; Jortzik, E.; Williams, D. L.; Becker, K.; Arese, P.; Elhabiri, M.; Davioud-Charvet, E. Antimalarial NADPH-Consuming Redox-Cyclers as Superior Glucose-6-Phosphate Dehydrogenase Deficiency Copycats. *Antioxid. Redox Signaling* **2015**, *22*, 1337–1351.
- (21) Feng, L.; Lanfranchi, D. A.; Cotos, L.; Cesar-Rodo, E.; Ehrhardt, K.; Goetz, A. A.; Zimmermann, H.; Fenaille, F.; Blandin, S. A.; Davioud-Charvet, E. Synthesis of Plasmodione Metabolites and 13C-Enriched Plasmodione as Chemical Tools for Drug Metabolism Investigation. *Org. Biomol. Chem.* **2018**, *16*, 2647–2665.
- (22) Mounkoro, P.; Michel, T.; Blandin, S.; Golinelli-Cohen, M. P.; Davioud-Charvet, E.; Meunier, B. Investigating the Mode of Action of the Redox-Active Antimalarial Drug Plasmodione Using the Yeast Model. *Free Radical Biol. Med.* **2019**, *141*, 269–278.
- (23) Oelgemöller, M.; Schiel, C.; Fröhlich, R.; Mattay, J. The “Photo-Friedel-Crafts Acylation” of 1,4-Naphthoquinones. *Eur. J. Org. Chem.* **2002**, *2002*, 2465.
- (24) Deseke, E.; Nakatani, Y.; Ourisson, G. Intrinsic Reactivities of Amino Acids towards Photoalkylation with Benzophenone - A Study Preliminary to Photolabelling of the Transmembrane Protein Glycophorin A. *Eur. J. Org. Chem.* **1998**, *1998*, 243–251.

- (25) Wittelsberger, A.; Thomas, B. E.; Mierke, D. F.; Rosenblatt, M. Methionine Acts as a "Magnet" in Photoaffinity Crosslinking Experiments. *FEBS Lett.* **2006**, *580*, 1872–1876.
- (26) Mitchell, L. J.; Lewis, W.; Moody, C. J. Solar Photochemistry: Optimisation of the Photo Friedel-Crafts Acylation of Naphthoquinones. *Green Chem.* **2013**, *15*, 2830–2842.
- (27) Hansch, C.; Leo, A.; Taft, R. W. A Survey of Hammett Substituent Constants and Resonance and Field Parameters. *Chem. Rev.* **1991**, *91*, 165–195.
- (28) Cosa, G. Photodegradation and Photosensitization in Pharmaceutical Products: Assessing Drug Phototoxicity. In *Pure Appl. Chem.*; Walter de Gruyter GmbH, 2004; Vol. 76, pp 263–275.
- (29) Bizier, N. P.; Wackerly, J. W.; Braunstein, E. D.; Zhang, M.; Nodder, S. T.; Carlin, S. M.; Katz, J. L. An Alternative Role for Acetylenes: Activation of Fluorobenzenes toward Nucleophilic Aromatic Substitution. *J. Org. Chem.* **2013**, *78*, 5987–5998.
- (30) Chen, Y.; Wu, Y.; Henklein, P.; Li, X.; Hofmann, K. P.; Nakanishi, K.; Ernst, O. P. A Photo-Cross-Linking Strategy to Map Sites of Protein-Protein Interactions. *Chem. - Eur. J.* **2010**, *16*, 7389–7394.
- (31) Cotos, L.; Donzel, M.; Elhabiri, M.; Davioud-Charvet, E. Cover Feature: A Mild and Versatile Friedel-Crafts Methodology for the Diversity-Oriented Synthesis of Redox-Active 3-Benzoylmenadienes with Tunable Redox Potentials (*Chem. Eur. J.* 15/2020). *Chem. - Eur. J.* **2020**, *26*, 3192–3192.
- (32) Anderson, J. M.; Kochi, J. K. Silver (I)-Catalyzed Oxidative Decarboxylation of Acids by Peroxydisulfate. The Role of Silver (II). *J. Am. Chem. Soc.* **1970**, *92*, 1651–1659.
- (33) Salmon-Chemin, L.; Buisine, E.; Yardley, V.; Kohler, S.; Debreu, M. A.; Landry, V.; Sergheraert, C.; Croft, S. L.; Krauth-Siegel, R. L.; Davioud-Charvet, E. 2- and 3-Substituted 1,4-Naphthoquinone Derivatives as Subversive Substrates of Trypanothione Reductase and Lipoamide Dehydrogenase from *Trypanosoma cruzi*: Synthesis and Correlation between Redox Cycling Activities and in Vitro Cytotoxicity. *J. Med. Chem.* **2001**, *44*, 548–565.
- (34) Karplus, P. A.; Pai, E. F.; Schulz, G. E. A Crystallographic Study of the Glutathione Binding Site of Glutathione Reductase at 0.3-nm Resolution. *Eur. J. Biochem.* **1989**, *178*, 693–703.
- (35) Görner, H. Photoreduction of Nitro-1,4-Naphthoquinones in Solution. *J. Photochem. Photobiol., A* **2011**, *224*, 135–140.
- (36) Bao, K.; Li, F.; Liu, H.; Wang, Z.; Shen, Q.; Wang, J.; Zhang, W. Activated Carbon for Aerobic Oxidation: Benign Approach toward 2-Benzoylbenzimidazoles and 2-Benzoylbenzoxazoles Synthesis. *Sci. Rep.* **2015**, *5*, 10360.
- (37) Blair, D.; Diehl, H. Bathophenanthrolinedisulphonic Acid and Bathocuproinedisulphonic Acid, Water Soluble Reagents for Iron and Copper. *Talanta* **1961**, *7*, 163–174.
- (38) Hong, V.; Udit, A. K.; Evans, R. A.; Finn, M. G. Electrochemically Protected Copper(I)-Catalyzed Azide-Alkyne Cycloaddition. *ChemBioChem* **2008**, *9*, 1481–1486.
- (39) Moutiez, M.; Quéméneur, E.; Sergheraert, C.; Lucas, V.; Tartar, A.; Davioud-Charvet, E. Glutathione-Dependent Activities of *Trypanosoma cruzi* P52 Makes It a New Member of the Thiol:Disulphide Oxidoreductase Family. *Biochem. J.* **1997**, *322*, 43–48.
- (40) Ando, Y.; Suzuki, K. Photoredox Reactions of Quinones. *Chem-Eur. J.*; Wiley-VCH Verlag October 26, 2018; pp 15955–15964.
- (41) Ando, Y.; Matsumoto, T.; Suzuki, K. Intramolecular Photoredox Reaction of Naphthoquinone Derivatives. *Synlett* **2017**, *28*, 1040–1045.
- (42) Porhun, V. I.; Rakimov, A. I. Mechanism of the Photochemical Reactions of Substituted Benzoquinones. *Russ. J. Gen. Chem.* **2011**, *81*, 890–912.
- (43) Belin, C.; Béarnais-Barbry, S.; Bonneau, R. Mechanism of Photocyclization of Substituted Phenylbenzoquinones. *J. Photochem. Photobiol., A* **2001**, *139*, 111–124.
- (44) Marquardt, R.; Grandjean, S.; Bonneau, R. Competition between Intersystem Crossing and Intramolecular Electron Transfer in Substituted Benzoquinones. *J. Photochem. Photobiol., A* **1992**, *69*, 143–153.
- (45) Hacker, S. M.; Backus, K. M.; Lazear, M. R.; Forli, S.; Correia, B. E.; Cravatt, B. F. Global Profiling of Lysine Reactivity and Ligandability in the Human Proteome. *Nat. Chem.* **2017**, *9*, 1181–1190.
- (46) Savvides, S. N.; Karplus, P. A. Kinetics and Crystallographic Analysis of Human Glutathione Reductase in Complex with a Xanthene Inhibitor. *J. Biol. Chem.* **1996**, *271*, 8101–8107.
- (47) Schönleben-Janas, A.; Kirsch, P.; Mittl, P. R. E.; Schirmer, R. H.; Krauth-Siegel, R. L. Inhibition of Human Glutathione Reductase by 10-Arylisalloxazines: Crystallographic, Kinetic, and Electrochemical Studies. *J. Med. Chem.* **1996**, *39*, 1549–1554.
- (48) Krauth-Siegel, R. L.; Arscott, L. D.; Schönleben-Janas, A.; Schirmer, R. H.; Williams, C. H. Role of Active Site Tyrosine Residues in Catalysis by Human Glutathione Reductase. *Biochemistry* **1998**, *37*, 13968–13977.
- (49) Sarma, G. N.; Savvides, S. N.; Becker, K.; Schirmer, M.; Schirmer, R. H.; Karplus, P. A. Glutathione Reductase of the Malarial Parasite Plasmodium Falciparum: Crystal Structure and Inhibitor Development. *J. Mol. Biol.* **2003**, *328*, 893–907.
- (50) Berkholz, D. S.; Faber, H. R.; Savvides, S. N.; Karplus, P. A. Catalytic Cycle of Human Glutathione Reductase Near 1 Å Resolution. *J. Mol. Biol.* **2008**, *382*, 371–384.
- (51) Muñoz-Durango, K.; Maciuk, A.; Harfouche, A.; Torijano-Gutiérrez, S.; Jullian, J. C.; Quintin, J.; Spelman, K.; Mouray, E.; Grellier, P.; Figadère, B. Detection, Characterization, and Screening of Heme-Binding Molecules by Mass Spectrometry for Malaria Drug Discovery. *Anal. Chem.* **2012**, *84*, 3324–3329.
- (52) Xu Kelly, J.; Winter, R.; Riscoe, M.; Peyton, D. H. A Spectroscopic Investigation of the Binding Interactions between 4,5-Dihydroxyxanthone and Heme. *J. Inorg. Biochem.* **2001**, *86*, 617–625.
- (53) Bunte, J. O.; Heilmann, E. K.; Hein, B.; Mattay, J. Cyclizations of Silyl Enol Ether Radical Cations- The Cause of the Stereoselectivity. *Eur. J. Org. Chem.* **2004**, *2004*, 3535–3550.
- (54) Robert, A.; Benoit-Vical, F.; Claparols, C.; Meunier, B. The Antimalarial Drug Artemisinin Alkylates Heme in Infected Mice. *Proc. Natl. Acad. Sci. U. S. A.* **2005**, *102*, 13676–13680.
- (55) Winter, R. W.; Cornell, K. A.; Johnson, L. L.; Ignatushchenko, M.; Hinrichs, D. J.; Riscoe, M. K. Potentiation of the Antimalarial Agent Rufigallol. *Antimicrob. Agents Chemother.* **1996**, *40*, 1408–1411.
- (56) Winter, R. W.; Ignatushchenko, M.; Ogundahunsi, O. A. T.; Cornell, K. A.; Oduola, A. M. J.; Hinrichs, D. J.; Riscoe, M. K. Potentiation of an Antimalarial Oxidant Drug. *Antimicrob. Agents Chemother.* **1997**, *41*, 1449–1454.
- (57) Mounkoro, P.; Michel, T.; Golinelli-Cohen, M. P.; Blandin, S.; Davioud-Charvet, E.; Meunier, B. A Role for the Succinate Dehydrogenase in the Mode of Action of the Redox-Active Antimalarial Drug, Plasmodione. *Free Radical Biol. Med.* **2021**, *162*, 533–541.
- (58) Gross, J. H.; Nieth, N.; Linden, H. B.; Blumbach, U.; Richter, F. J.; Tauchert, M. E.; Tompers, R.; Hofmann, P. Liquid Injection Field Desorption/Ionization of Reactive Transition Metal Complexes. *Anal. Bioanal. Chem.* **2006**, *386*, 52–58.
- (59) Simpson, R. J. Staining Proteins in Gels with Coomassie Blue. *Cold Spring Harb. Protoc.* **2007**, *2007*, pdb.prot4697.
- (60) Pettersen, E. F.; Goddard, T. D.; Huang, C. C.; Couch, G. S.; Greenblatt, D. M.; Meng, E. C.; Ferrin, T. E. UCSF Chimera - A Visualization System for Exploratory Research and Analysis. *J. Comput. Chem.* **2004**, *25*, 1605–1612.
- (61) Mishra, E.; Worlinsky, J. L.; Gilbert, T. M.; Brückner, C.; Ryzhov, V. Erratum: Axial Imidazole Binding Strengths in Porphyrinoid Cobalt(III) Complexes as Studied by Tandem Mass Spectrometry. *J. Am. Soc. Mass Spectrom.* **2012**, *23*, 1428–1439.
- (62) Witkowski, B.; Amarasingha, C.; Khim, N.; Sreng, S.; Chim, P.; Kim, S.; Lim, P.; Mao, S.; Sopha, C.; Sam, B.; Anderson, J. M.; Duong, S.; Chuor, C. M.; Taylor, W. R.; Suon, S.; Mercereau-Puijalon, O.; Fairhurst, R. M.; Menard, D. Novel Phenotypic Assays for the Detection of Artemisinin-Resistant Plasmodium falciparum

Malaria in Cambodia: In-Vitro and Ex-Vivo Drug-Response Studies. *Lancet Infect. Dis.* **2013**, *13*, 1043–1049.

(63) Ariey, F.; Witkowski, B.; Amaratunga, C.; Beghain, J.; Langlois, A. C.; Khim, N.; Kim, S.; Duru, V.; Bouchier, C.; Ma, L.; Lim, P.; Leang, R.; Duong, S.; Sreng, S.; Suon, S.; Chuor, C. M.; Bout, D. M.; Ménard, S.; Rogers, W. O.; Genton, B.; Fandeur, T.; Miotto, O.; Ringwald, P.; Le Bras, J.; Berry, A.; Barale, J. C.; Fairhurst, R. M.; Benoit-Vical, F.; Mercereau-Puijalon, O.; Ménard, D. A Molecular Marker of Artemisinin-Resistant Plasmodium Falciparum Malaria. *Nature* **2014**, *505*, 50–55.

(64) Beez, D.; Sanchez, C. P.; Stein, W. D.; Lanzer, M. Genetic Predisposition Favors the Acquisition of Stable Artemisinin Resistance in Malaria Parasites. *Antimicrob. Agents Chemother.* **2011**, *55*, 50–55.

(65) Smilkstein, M.; Sriwilaijaroen, N.; Kelly, J. X.; Wilairat, P.; Riscoe, M. Simple and Inexpensive Fluorescence-Based Technique for High-Throughput Antimalarial Drug Screening. *Antimicrob. Agents Chemother.* **2004**, *48*, 1803–1806.

5 points à retenir de l'article

- 1) Des 3-benzoylménadiones portant une fonction alcyne ont été synthétisées par l'acylation de Friedel-Crafts développée précédemment comme étape clé.
- 2) Le couplage croisé entre les 3-benzoylménadiones photoréactives et des acides aminés modèles a été réalisé.
- 3) La réaction « click » avec les 3-benzoylménadiones portant une fonction alcyne a été optimisée.
- 4) Les 3-benzoylménadiones ont été photoalkylées par les deux **GRs** modèles (**PfGR** et **hGR**).
- 5) Des sites d'interactions covalentes des 3-benzoylménadiones ont été identifiés chez ces 2 enzymes, selon 3 voies d'alkylation différentes, via la formation d'adduits classiques de type benzophénone, soit de type benzoxanthone, avec les peptides modèles ou les deux **GRs** modèles.

**Chapitre III. Synthèse et oxydation des 3-
benzylménadiones par des méthodes photochimiques.**

1. Développement d'une nouvelle méthode de benzylation des naphtoquinones.

1.1. Travaux préliminaires.

Après le succès de la benzoylation par la réaction de Friedel-Crafts, l'objectif suivant a été de réaliser cette fois-ci une benzylation de Friedel-Crafts pour fonctionnaliser rapidement le 1,4-diméthoxy-2-méthynaphthalène et former, après la déprotection oxydante avec CAN, les **BMDs**. Nous avons d'abord voulu essayer les conditions précédemment concluantes de l'acylation entre le 1,4-diméthoxy-2-méthynaphthalène et un alcool benzylique, dans l'espoir que celles-ci permettent de réaliser des alkylations efficaces. Cependant, aucune conversion n'a été obtenue par cette méthode (**Schéma 18**).

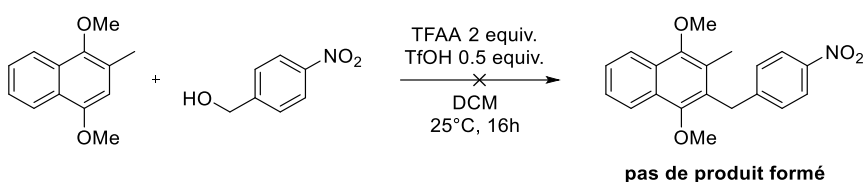


Schéma 18. Tentative de benzylation par réaction de Friedel & Crafts selon les conditions de Cotos et. Al.

Après avoir essayé sans succès d'adapter les travaux de Li pour une alkylation directe des quinones,⁵¹ et de Bode⁵² pour la synthèse de 3-benzylINQs, nous nous sommes intéressés aux travaux de l'équipe de Joseph Moran sur une réaction de Friedel-Crafts catalysée par l'acide triflique (TfOH) entre des arènes et des alcools benzyliques très désactivés dans l'hexafluoroisopropanol (HFIP) (**Schéma 19. A**).⁵³ Bien que prometteuse et malgré nos nombreux travaux d'optimisation, nous n'avons pas réussi à adapter cette procédure de sorte à obtenir les produits désirés avec des rendements satisfaisants. Nous nous sommes très vite aperçus que les adduits benzylés étaient inséparables du 1,4-diméthoxy-2-méthynaphthalène de départ par chromatographie et que nous devions réaliser la déprotection par le CAN directement sur le produit brut de la réaction afin d'obtenir directement la 3-benzylménadione déprotégée.

Le 1,4-diméthoxy-2-méthynaphthalène étant un arène riche en électrons, la réaction s'est révélée non sélective pour la position 3 et sujette à la polyfonctionnalisation. De plus, les conditions optimales pour une conversion totale sont très variables en fonction de la substitution de l'alcool benzylique. Avec un groupement *para*-trifluorométhyle, 5 min au micro-onde à 100 °C se sont révélés nécessaires, alors qu'avec un groupement *para*-fluoro, moins électroattracteur, la réaction a lieu à température ambiante en moins de 2h. Aucune condition réactionnelle n'a pu être mise en place pour obtenir la

⁵¹ X.-L. Xu, Z. Li, *Angew. Chem. Int. Ed.* **2017**, *56*, 8196–8200.

⁵² G. Schäfer, J. W. Bode, *Angew. Chem. Int. Ed.* **2011**, *50*, 10913–10916.

⁵³ V. D. Vuković, E. Richmond, E. Wolf, J. Moran, *Angew. Chem. Int. Ed.* **2017**, *56*, 3085–3089.

benzylation à partir de l'alcool 4-nitrobenzyle. De plus, malgré nos efforts, le rendement global des 2 étapes n'a jamais dépassé les 34% (**Schéma 19.B**).

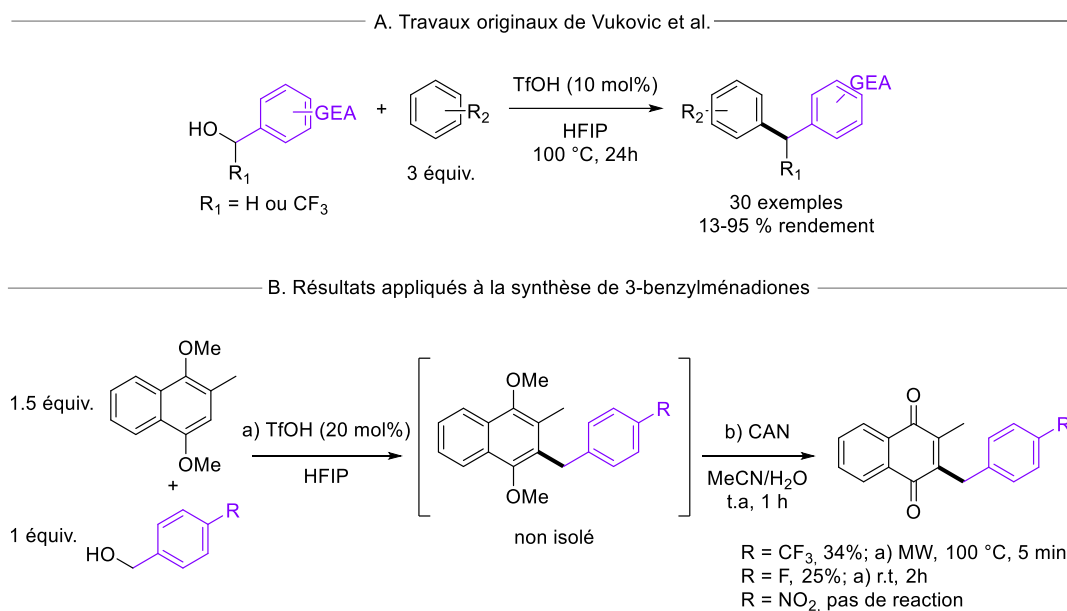


Schéma 19. Benzylation de Friedel-Crafts catalysée par l'acide triflique dans l'HFIP.

Pour toutes ces raisons, la voie Friedel-Crafts ne pouvait pas nous permettre d'obtenir une synthèse robuste d'une large variété de 3-benzylménadiones et elle a donc été abandonnée. Nous nous sommes par conséquent orientés vers une benzylation radicalaire, plus sélective, et qui a longtemps fait ses preuves avec les conditions de décarboxylation de Kochi-Anderson. L'objectif était donc de trouver de nouvelles conditions pour générer un radical benzyle à partir d'un précurseur différent des acides phénylacétiques, mais aussi si possible, un précurseur facilement accessible et peu onéreux (**Schéma 20**).

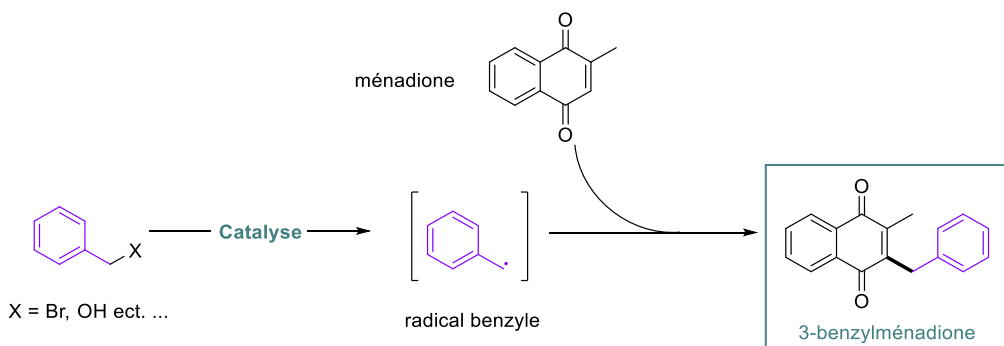


Schéma 20. Méthode envisagée pour la benzylation radicalaire de la ménadione.

Les alcools benzyliques remplissant aisément ces conditions, nous nous sommes d'abord intéressés aux conditions décrites par Ukaji pour la génération de radicaux benzyles à partir de ces derniers en

présence de manganèse et d'un complexe de titane⁵⁴. Cependant, nous avons très vite remarqué que, les fortes conditions réductrices de cette réaction ne menaient qu'à une réduction partielle de la ménadione et aucune trace de ménadione benzylée.

Un autre précurseur commun de radicaux alkyles sont les composés halogénés. Avec le renouveau de la catalyse photoredox depuis la fin des années 2000,⁵⁵ plusieurs réactions de benzylation radicalaire photocatalysées à partir d'halogénures de benzyle ont été décrites.⁵⁶ Les réactions photocatalytiques les plus communes sont celles pour lesquelles un photocatalyseur organométallique⁵⁷ (complexes d'iridium ou de ruthénium) ou organique⁵⁸ peut, après photoirradiation, être un médiateur des transferts d'électrons entre des molécules qui ne réagiraient pas en temps normal. Malheureusement, plusieurs essais ont été menés sur un système incluant la ménadione et le bromure de 4-(trifluorométhyl)benzyle avec divers photocatalyseurs organométalliques et aucune trace de la plasmodione désirée ne fut détectée. Similairement à la réaction impliquant les alcools benzyliques, nous avons remarqué la présence d'espèce hydroquinone de la ménadione.

Désireux de trouver une manière plus douce et compatible avec la ménadione pour générer des radicaux benzyliques nous avons remarqué les travaux de Paolo Melchiorre et son équipe portant sur la benzylation de divers accepteurs de radicaux par photocatalyse.⁵⁹ L'utilisation d'un chromophore nucléophile comme catalyseur permet de générer un intermédiaire benzylique photosensible après une réaction de substitution nucléophile. Sous photoirradiation, la liaison carbone-soufre est coupée par rupture homolytique et un radical benzyle libre est formé. Ce dernier peut ensuite réagir avec divers électrophiles. Le groupement partant peut non seulement être un halogène mais aussi un groupement mésylate ou trifluoroacétate (**Schéma 21**).

⁵⁴ T. Suga, S. Shimazu, Y. Ukaji, *Org. Lett.* **2018**, 20, 7846–7850.

⁵⁵ a) D. A. Nicewicz, D. W. C. MacMillan, *Science*, **2008**, 322, 77–80; b) M. A. Ischay, M. E. Anzovino, J. Du, T. P. Yoon, *J. Am. Chem. Soc.* **2008**, 130, 12886–12887; c) J. M. R. Narayanan, J. W. Tucker, C. R. J. Stephenson, *J. Am. Chem. Soc.* **2009**, 131, 8756–8757.

⁵⁶ Exemples sélectionnés: a) H.-W. Shih, M. N. Vander Wal, R. L. Grange, D. W. C. MacMillan, *J. Am. Chem. Soc.* **2011**, 132, 13600–13603; b) J. Dong, X. Lyu, Z. Wang, X. Wang, H. Song, Y. Liua, Q. Wang, *Chem. Sci.* **2019**, 10, 976–982; c) E. B. McLean, V. Gauchot, S. Brunen, D. J. Burns, Ai-Lan Lee, *Chem. Commun.* **2019**, 55, 4238–4241; d) G. Park, S. Y. Yi, J. Jung, E. J. Cho, Y. You, *Chem. Eur. J.* **2016**, 22, 17790 – 17799; e) E. Arceo, I. D. Jurberg, A. Alvarez-Fernández, P. Melchiorre, *Nat. Chem.* **2013**, 5, 750–756.

⁵⁷ C. K. Prier, D. A. Rankic, D. W. MacMillan, *Chem. Rev.* **2013**, 113, 5322–5363.

⁵⁸ N. A. Romero, D. A. Nicewicz, *Chem. Rev.* **2016**, 116, 10075–10166.

⁵⁹ B. Schweitzer-Chaput, M.A. Horwitz, E. Beato, P. Melchiorre, *Nat. Chem.* **2019**, 11, 129–135.

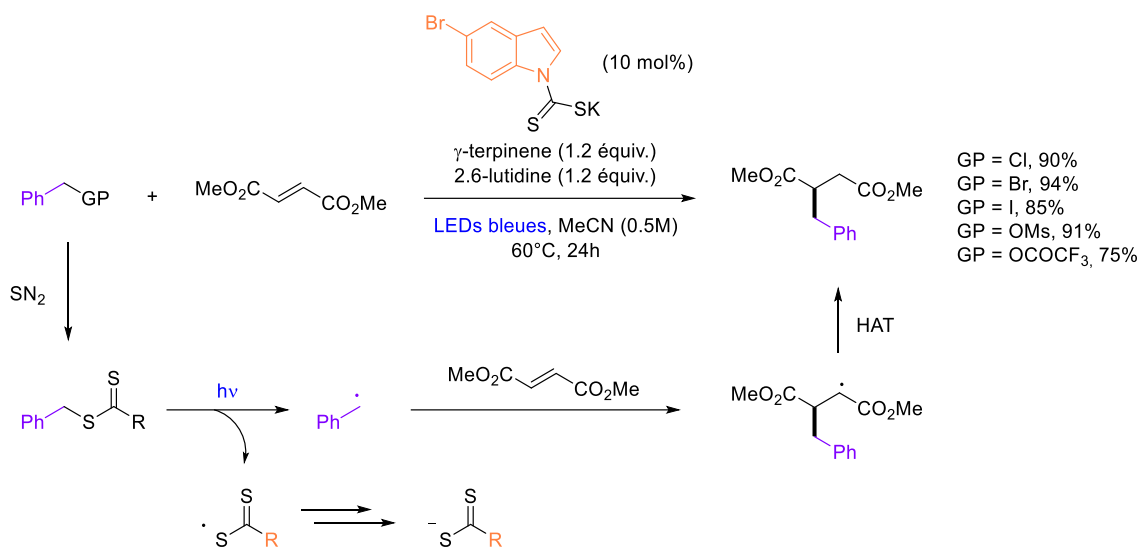


Schéma 21. Benzylation radicalaire catalysée par un nucléophile chromophorique.

Dans les conditions décrites par Melchiorre, la plasmodione n'est obtenue qu'avec un rendement inférieur à 5% (Schéma 22.a). Après optimisation des conditions expérimentales, le rendement obtenu a été augmenté jusqu'à 79% de produit désiré. Ceci a été possible grâce à l'ajout d'un catalyseur ferrique, le $\text{Fe}(\text{acac})_3$, dont l'utilisation s'est inspirée du mécanisme d'action de la plasmodione (Schéma 22.b). Par ailleurs, à notre grande surprise, en absence du catalyseur de Melchiorre, des conditions de réaction similaires en présence de $\text{Fe}(\text{acac})_3$ conduisent à la plasmodione avec un rendement de 85% après optimisation (Schéma 22.c).

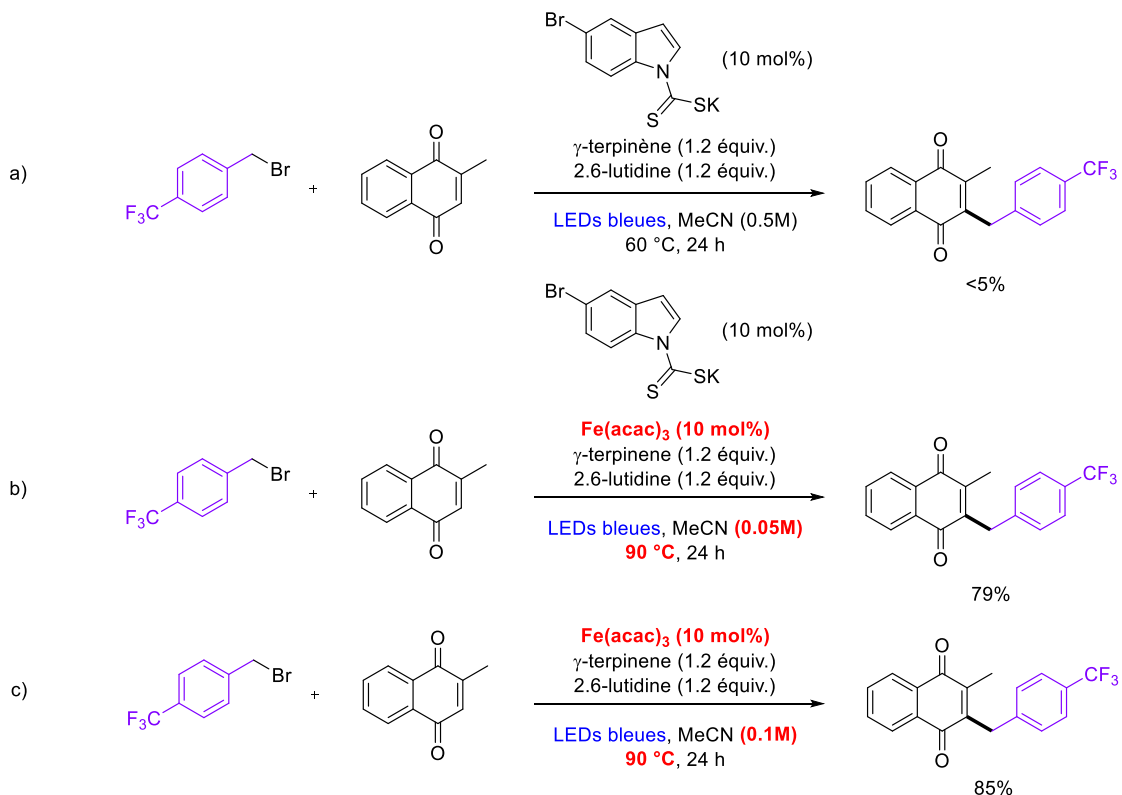


Schéma 22. Résultats préliminaires de benzylation photorédox.

Cette réaction a pu être exemplifiée avec divers bromures de benzyles et diverses 1,4-naphtoquinones. Des études mécanistiques ont également été menées nous permettant de proposer un mécanisme pour lequel les propriétés photorédox de la ménadione, le fer(III) et l'oxygène jouent un rôle clé (**Schéma 23**).

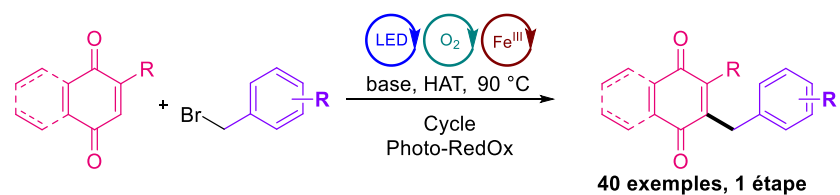


Schéma 23. Schéma général de la benzylation photorédox des quinones.

1.2. Article 4.

A Bioinspired Photoredox Benzylation of Quinones

Maxime Donzel, Mourad Elhabiri, Elisabeth Davioud-Charvet

Manuscript soumis

A Bioinspired Photoredox Benzylation of Quinones

Maxime Donzel, Mourad Elhabiri, Elisabeth Davioud-Charvet*

Université de Strasbourg–CNRS–UHA UMR7042, Laboratoire d’Innovation Moléculaire et Applications (LIMA) Team Bio(IN)organic and Medicinal Chemistry, European School of Chemistry, Polymers and Materials (ECPM), 25 Rue Becquerel, Strasbourg 67087, France

ABSTRACT: 3-Benzylmenadienes were obtained in good yields by using a blue light-induced photoredox process in the presence of Fe(III), oxygen and γ -terpinene acting as a HAT agent. This methodology is compatible with a wide variety of diversely substituted 1,4-naphthoquinones as well as various cheap, readily available benzyl bromides with excellent functional group tolerance. The benzylation mechanism was investigated and supports a three-step radical cascade with the key involvement of photogenerated superoxide anion radical.

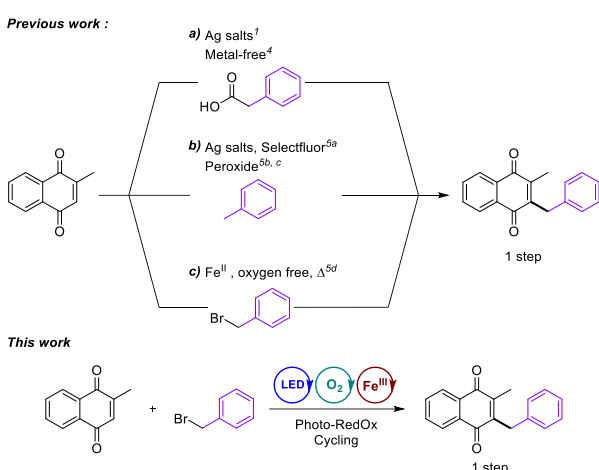
Quinones have recently shown a re-gaining interest in medicinal chemistry, particularly in the field of drug discovery for new treatments against neglected tropical parasitic diseases such as malaria. In particular, an early lead 3-benzylmenadiene named plasmodione (i.e., 3-[4-(trifluoromethyl)benzyl]menadiene) has shown potent and valuable antiplasmoidal activities against several *Plasmodium falciparum* strains *in vitro* and in *Plasmodium berghei*-infected mouse model.¹ In recent years, our team has developed new synthetic methodologies^{2a,b} to introduce structural and functional diversity for reaching more active^{2c} and water-soluble^{2d} antiparasitic analogues, or to prepare putative metabolites^{2b,e} to investigate the mechanism of action of these drug candidates^{1b,2f}. Based on a Kochi-Anderson radical decarboxylation of acids^{3a-c}, the former extensively investigated synthetic route to build 3-benzylmenadienes suffered from the use of silver salts and peroxodisulfate and was limited by the availability of phenylacetic acids used as starting materials.^{1a,3d,e} Since, Lee’s group developed an elegant silver-free alkylation of quinones (Scheme 1a)⁴ and a growing interest in benzylated quinones, including plasmodione, has emerged, as evidenced by the synthetic procedures recently described by several groups from substituted toluenes by free-radical generation via hydrogen-atom abstraction using the selectfluor/Ag(I) pair^{5a} or peroxides (Scheme 1b)^{5b,c}. Finally, when carrying out the work described here, Li *et al.* concomitantly demonstrated that benzyl radicals could be generated at high temperature in the presence of iron(II) and a base to further react with quinones or coumarins (Scheme 1c)^{5d}.

Our initial goal was to overcome the limitations and drawbacks of silver-catalyzed radical benzylation. To increase the chemical space available around this promising scaffold of benzylated quinones, it appeared essential to develop a simple, robust and efficient strategy to generate, by an eco-friendly process, benzyl radicals from cheap and easily available precursors such as benzyl bromides. The latter are common building blocks in organic chemistry, widely available and known for their ability to generate after reduction of the C-Br bond benzyl radical intermediates^{5d,6}, especially in the emerging field of photoredox catalysis.⁷

To this purpose, we first investigated classical benzyl radical generation via transition metal catalyzed photoredox process.^{7c,8} However, all attempts failed because these reactions take place

under reducing conditions, which are not compatible with the requirement of keeping menadione under its oxidized state. Then, we considered the original work described by Melchiorre and his team.⁹

Scheme 1. Reported benzylation reactions of quinones and this work.



In this report, after an initial nucleophilic substitution on the electrophilic C-Br position of a benzyl bromide, the newly formed C-S bond was cleaved under blue light irradiation and mild heating to generate a benzyl radical, which can readily react with a radical acceptor. These conditions were first applied to menadione **1a** acting as a radical acceptor and 4-trifluoromethylbenzyl bromide **2a** to form the targeted model plasmodione **3a**. Detailed NMR analysis of the crude mixture showed the formation of **3a** with a low yield (5%), together with the starting material under its oxidized (**1a**) and reduced (hydroquinone) states (Table 1, Entry 1). Despite this low yield, this encouraged us to further optimize the experimental conditions. With the purpose to limit hydroquinone formation, we were inspired by the putative mechanism of action of plasmodione in *P. falciparum*-parasitized red blood cells (Figure 1), whereby reduced naphthoquinone is continuously re-oxidized by methemoglobin (FeIII) (metHb(Fe^{III})) at the expense of NADPH.^{1a,2f} Consequently, we introduced an

iron(III) source to constantly catalyze the *in situ* re-oxidation of the hydroquinone into the quinone species **1a**. After optimization, the target **3a** plasmodione was successfully obtained with 79% isolated yield (Table 1, Entry 2).

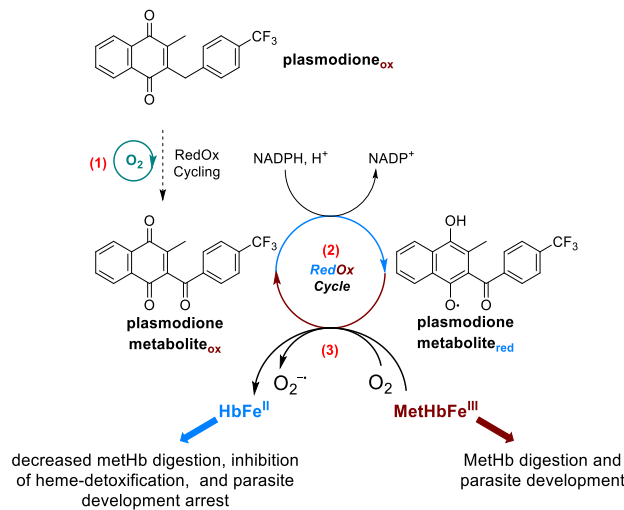


Figure 1. Bioactivation of plasmodione upon internalization in the parasite: plasmodione is proposed to enter into an oxidoreductase-mediated redox-cycle in the course of which it is metabolized in its key 3-benzoylmenadione metabolite (step 1). Under its oxidized form, plasmodione metabolite is reduced (step 2), while under its reduced form, it takes part in oxidoreductase-mediated redox-cycling (step 3) leading to decreased methemoglobin (metHb) digestion, inhibition of heme-detoxification, and ROS-induced parasite death.

Table 1. Optimization the experimental conditions of the benzylation reaction of menadione **1a**^a

Entry	Modificatio n	Catalysts (10 mol%)	Concentration (mol.L ⁻¹)	Yield 3a ^b (%)
1	60°C	Catalyst 1 ^c	0.5	<5 ^d
2	-	Fe(acac) ₃ / Catalyst 1 ^c	0.05	79
3	-	Fe(acac) ₃	0.05	73
4	-	Fe(acac)₃	0.1	84
5	-	FeCl ₃ .6H ₂ O	0.1	70
6	-	Fe(ClO ₄) ₃ .H ₂ O	0.1	65
7	-	FeCl ₂	0.1	67
8	HE ^e vs. γ- terpinene	Fe(acac) ₃	0.1	72
9	Argon atm.	Fe(acac) ₃	0.1	<5 ^d
10	2a ^f vs. 2a	Fe(acac) ₃	0.1	79
11	2a ^g vs. 2a	Fe(acac) ₃	0.1	39

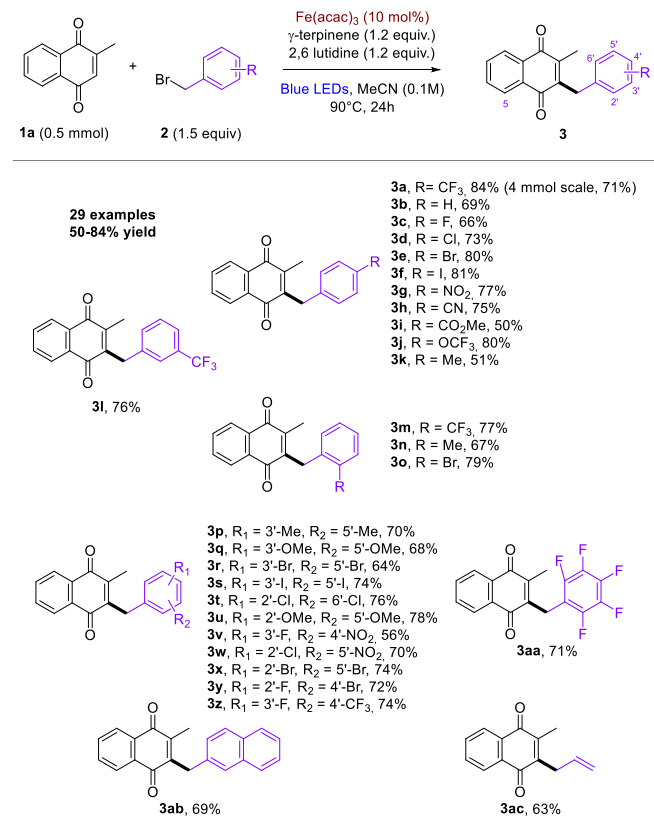
^aReaction conditions: **1a** (1.0 equiv, 0.5 mmol), **2a** (1.5 equiv), 2,6-lutidine (1.2 equiv.), γ-terpinene (1.2 equiv.), Cat. in CH₃CN at 90°C under blue light irradiation during 24h. ^bIsolated yield

^cCatalyst 1 = potassium 5-bromo-1H-indole-1-carbodithioate.

^dDetermined by ¹H NMR. ^eHE = Hantzsch ester = Diethyl 2,6-dimethyl-1,4-dihydropyridine-3,5-dicarboxylate. ^f**2a**' = 4-trifluoromethylbenzyl iodide. ^g**2a**" = 4-trifluoromethylbenzyl chloride.

Several conditions were modified to study their effects and to optimize the parameters of the reaction. We first demonstrated that the nucleophilic organic catalyst (catalyst 1) was not necessary for the reaction to proceed (Table 1, entry 3). In its absence, the target compound **3a** was still obtained with an excellent yield of 73% (versus 81%). Afterwards, the concentration was increased up to 0.1 M to achieve a very satisfactory yield of 84% (Table 1, Entry 4). The iron(III) source can be substituted by any other ferric source such as Fe(III) chloride or Fe(III) perchlorate and even Fe(II) chloride with, however, slightly lower yields (Table 1, Entry 5-7). For chloride Fe(II), partial oxidation into iron(III) species in solution likely occurs during the reaction. On the other hand, Hantzsch ester (HE) also appears to be a suitable hydrogen-atom transfer (HAT) agent (Table 1, Entry 8). Finally, ambient oxygen was found to play a critical role since nearly no targeted product **3a** was obtained under strict oxygen-free conditions (Table 1, Entry 9). Absence of catalyst, light, γ-terpinene or base led to very low yields between 0 and 20% of conversion (See SI for experimental details). Finally, benzyl iodide **2a**' was also shown to react with menadione **1a** with a comparable yield of 79%, as much as benzyl chloride **2a**"', though with a lower yield, thus widening the possibilities in many synthetic applications (Table 1, Entry 10-11).

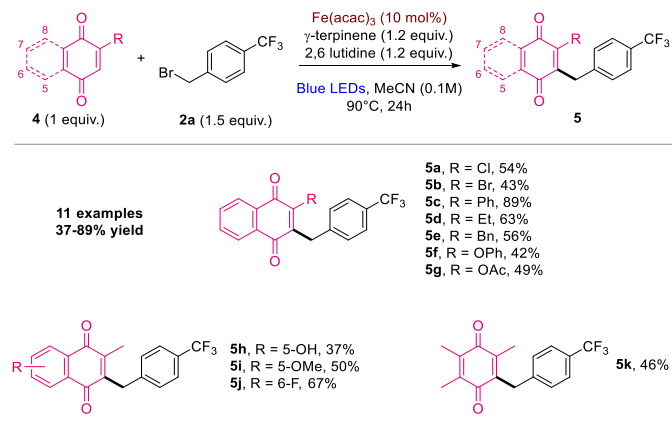
Scheme 2. Scope of benzyl bromides with optimized conditions (Table 1, entry 3)



Following this optimization stage, we then investigated the scope of this reaction (Scheme 2). First, we demonstrated that the trifluoromethyl substitution was well tolerated both in the *meta*, *ortho* or *para* positions (76-84%, **3a**, **3l**, **3m**). Plasmodione **3a** was also produced in 1 gram scale with good yield demonstrating that this reaction can be scaled up to larger quantities. Various and numerous substitutions have been shown to be compatible with this reaction leading to moderate to good yields in *para* position (**3a**-**3k**). Mono (**3m**-**o**, **3u**, **3w**,

3x, 3y) or di-substitution (**3t**) in the *ortho*-position (steric interactions) does not seem to be a major drawback. On the other hand, a wide variety of poly-substituted benzyl radicals have been also successfully incorporated into menadione (**3p-3ab**). Finally, we observed that allyl bromide could also be a suitable substrate of this reaction, affording the allylated menadione **3ac** with satisfying yield (63%) under the same experimental conditions. Then, we evaluated its compatibility with the varied substitution pattern of the quinone unit **4** (Scheme 3). 2-Substitution in 1,4-naphthoquinone was found to be well tolerated with moderate to good yields (**5a-g**). Substitution on the aromatic naphthoquinone ring was also found to be compatible with this reaction, as demonstrated by the successful preparation of the benzyl derivatives with moderate to good yields when starting from plumbagin (**5h**), its methyl derivative (**5i**) or the 6-fluoro-menadione (**5j**).

Scheme 3. Scope of 1,4-quinones with optimized conditions (Table 1, entry 3)

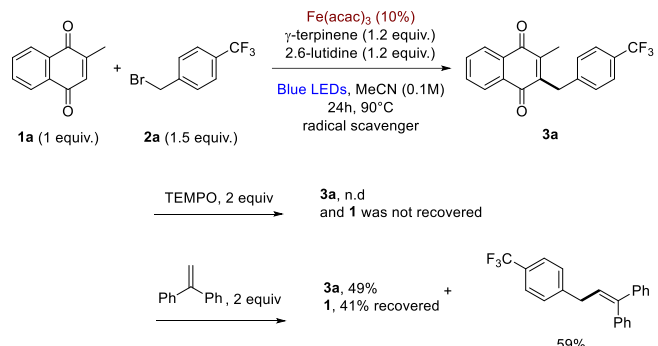


To get a deeper insight into the understanding of the mechanism of the reaction, absorption spectrophotometry and several control experiments were carried out with the model reaction involving **1a** and **2a**. The radical nature of the reaction was assessed by trapping the corresponding radical intermediates, using several radical scavengers. The reaction was completely inhibited with TEMPO since no trace of the desired 3-benzylmenadione was detected. In addition, complete degradation of the starting menadione was observed. More interestingly, reaction with 1,1-diphenylethylene as radical scavenger afforded the targeted 3-benzylmenadione with a much lower yield together with the trapped benzyl radical adduct. These data support the fact that benzyl radicals are most likely the key intermediates involved in the reaction mechanism (Scheme 4A). In the process described by Melchiorre and his coworkers⁹, the reactive radical species was generated by a homolytic cleavage of the C-S bond, which was formed after the initial nucleophilic substitution between catalyst 1 and the benzyl bromide. In the absence of this catalyst, the successful conversion to the targeted product suggests that a completely different pathway takes place during the photoreaction. During the optimization (Table SI-2, entry 2, Table SI-6, entry 2, Table SI-7, entry 9 in the SI), we noticed that both light and iron(III) were essential for the reaction to occur. Alternatively, the absence of a base, HAT agent or oxygen-free atmosphere significantly alters the reaction but quantifiable amounts of the targeted benzylated compounds were still observed. The role of γ -terpinene as HAT agent was thus investigated. The reaction was thus run in parallel with different concentrations of γ -terpinene. This demonstrates that the isolated yields do not linearly vary with the γ -terpinene concentration. A sub-stoichiometric amount of this reactant (0.5 equiv) can still efficiently lead to a satisfactory yield of 71%, while its absence

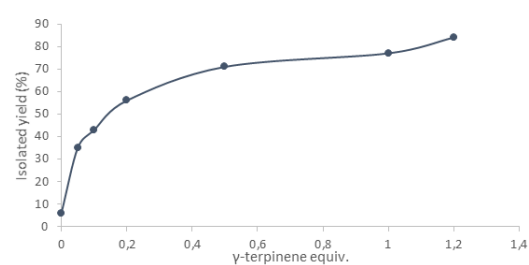
only afforded traces of the targeted compound (~5%). Even a catalytic amount (5%) is quite efficient, affording 35% of yield. This demonstrates that γ -terpinene is essential and enhances the reactivity of the reaction (Scheme 4B).

Scheme 4. Selected mechanistic studies.

A. Radical trap experiments



B. γ -terpinene influence on the reaction yield^[a].



C. Photocatalytic reaction using iPrOH both as solvent and HAT agent.

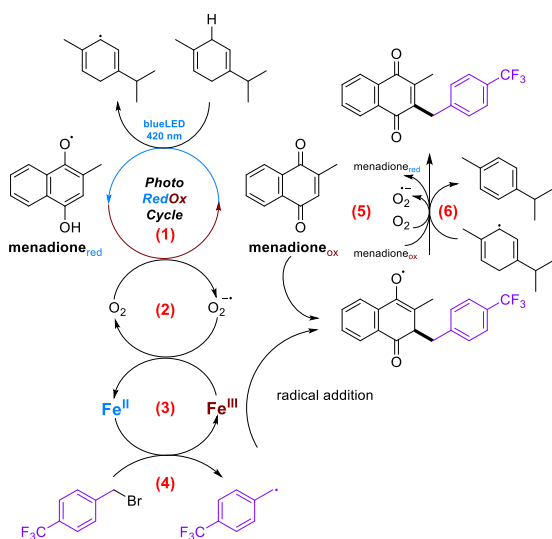


^aReaction conditions: **1a** (1.0 equiv, 0.5 mmol), **2a** (1.5 equiv), 2,6-lutidine (1.2 equiv.), γ -terpinene, $\text{Fe}(\text{acac})_3$ (10 mol%), in CH_3CN at 90°C under blue light irradiation during 24h.

Previous reports¹⁰ have established that quinones, including menadione, can be photo-reduced under light irradiation in the presence of a HAT agent, usually a protic solvent such as isopropanol (iPrOH). Under blue LED irradiation (420-470 nm), a triplet state species is generated and can be quenched by H-donor molecules to afford the semiquinone radical species. Absorption spectrophotometric demonstrated that menadione can be photoactivated by blue LED irradiation thus confirming our hypothesis. In contrary, the final 3-benzylmenadione **3a** seems not to be involved in such photo-reducing process, as we showed that it did not react under the same conditions (See Figures S1-S7 in SI for details). As already reported by our group with the NADPH/glutathione reductase/MetHb system, semiquinone radicals can reduce $\text{Fe}(\text{III})$ species into $\text{Fe}(\text{II})$ ones to reinstate the quinone molecule. In aerated media, these semiquinone radicals can alternatively generate superoxide $\text{O}_2^{\cdot-}$ radicals.^{3e,11} To support this hypothesis, we set up a model reaction, where iPrOH plays the role of both the solvent and HAT agent in the absence of γ -terpinene (Scheme 4C). Very interestingly, in addition to the expected nucleophilic substitution of iPrOH on benzyl bromide, the benzylated menadione was isolated with a yield of 38%. It is important to mention that the same reaction conducted in the absence of γ -terpinene in CH_3CN afforded only traces of **3a** (Table SI-5, entry 2) thus confirming the key role of iPrOH as a HAT agent. To account for these observations, we propose a putative

reaction mechanism based on successive redox cycles (Scheme 5).

Scheme 5. Putative mechanism of the reaction.



Under blue light irradiation, menadione is excited into its triplet state and quenched by γ -terpinene (HAT) to afford semiquinone radical in solution (step 1). This radical can thus react in a redox cycle with oxygen (i.e., under anaerobic conditions, the reaction did not take place, Table 1, entry 8) to afford menadione and superoxide radical. O_2^- is well known to reduce metallic complexes^{3c,12}, even in natural medium^{12d} (step 2), which can in turn reduce the C-Br bond of the benzyl bromide to afford the corresponding benzyl radical (step 3). Once this radical generated, addition to menadione takes place to lead to a benzylated semi-quinone radical (step 4). This new radical species can thus react with menadione (or with O_2) to lead to the targeted benzylated menadione (step 5). The semiquinone or O_2^- radicals generated during this latter step can be involved in new catalytic cycles (step 2 or 3). Semi-quinone intermediate could also be quenched by γ -terpinene radical in a SET reaction to generate after proton transfer the targeted benzylated quinone (step 6). This was supported by the fact that p-cymene was always recovered in the reaction mixtures of benzylated quinones as observed by NMR (Scheme SI-3 in the SI). Direct photoreduction of $Fe(acac)_3$ under light irradiation could not be totally excluded, and this process has already been reported in the literature.¹³ However, control reactions clearly showed that benzyl bromide was not consumed (e.g., by-products of benzyl radical formation by $Fe(acac)_3$ photoreduction) in the absence of quinone or with a different radical acceptor. Such direct photoreduction process usually occurs via a ligand-to-metal-charge transfer (LMCT) absorption and does not require oxygen contribution.^{12d, 13} In our system, the absence of oxygen inhibits the menadione benzylation reaction, and different iron sources such as $FeCl_3$, displaying markedly different LMCT absorptions, have been shown to be suitable catalysts for the benzylation reaction.

In conclusion we have developed a convenient, robust and straightforward iron(III) catalyzed photo-redox benzylation of naphthoquinones under blue LED irradiation. A wide variety of polysubstituted benzyl radicals generated from various halides can be efficiently introduced to diversely substituted 1,4-(naphtho)quinones with good yields, thanks to a redox cycle involving the photoreduced (naphtho)quinone, oxygen and ferric complexes. To the best of our knowledge, this is the first time that the photoreactivity of quinone is exploited for its intermolecular functionalization¹⁴ in a catalytic process.

ASSOCIATED CONTENT

Supporting Information

Detailed screenings of the photochemical reactions, studies of the reaction mechanism, description of the experimental procedures, characterization of the product including spectrophotometric absorption data and 1H and ^{13}C NMR spectra of all new compounds are given in the Supporting Information. The Supporting Information is available free of charge on the ACS Publications website.

AUTHOR INFORMATION

Corresponding Author

* E-mail: elisabeth.davioud@unistra.fr

Notes

The authors declare no conflict of interest.

ACKNOWLEDGMENT

The authors wish to thank the ANR-PRC program (grant PlasmoPrim project, E.D.C.), the Laboratoire d'Excellence (LabEx) ParaFrap (grant LabEx ParaFrap ANR-11-LABX-0024, E.D.C.), for funding and creating a proper framework for this scientific research, and for M. D.'s salary.

REFERENCES

- (1) (a) Müller, T.; Johann, L.; Jannack B.; Brückner, M.; Lanfranchi, D. A.; Bauer, D. H.; Sanchez, C.; Yardley, V.; Deregaucourt, C.; Schrével, J.; Lanzer, M.; Schirmer, R. H.; Davioud-Charvet, E. *J. Am. Chem. Soc.* **2011**, *133*, 11557-71. (b) Ehrhardt, K.; Deregaucourt, C.; Goetz, A.-A.; Tzanova, T.; Pradines, B.; Adjalley, S. H.; Blandin, S.; Bagrel, D.; Lanzer, M.; Davioud-Charvet, E. *Antimicrob. Agents Chemother.* **2016**, *60*, 5146-58. (c) For a recent review on antimalarial application of quinones: Patel, O. P. S.; Betek, R. M.; Legoabe, L. J.; *Eur. J. Med. Chem.* **2021**, *210*, 113084.
- (2) (a) Cesar Rodo, E.; Feng, F.; Jida, M.; Ehrhardt, K.; Bielitz, M.; Boilevin, J.; Lanzer, M.; Williams, D. L., Lanfranchi, D. A., Davioud-Charvet, E. *Eur. J. Org. Chem.* **2016**, *11*, 1982–1993. (b) Cotos, L.; Donzel, M.; Elhabiri, M.; Davioud-Charvet, E. *Chem. Eur. J.* **2020**, *26*, 3314-3325. (c) Urgin, K.; Jida, M.; Ehrhardt, K.; Müller, T.; Lanzer, M.; Maes, L.; Davioud-Charvet, E.; *Molecules*, **2017**, *22*, 161, 1-32. (d) Lanfranchi, D. A.; Cesar-Rodo, E.; Bertrand, B.; Huang, H-H.; Day, L.; Johann, L.; Elhabiri, M.; Becker, K.; Williams, D. L.; Davioud-Charvet, E. *Org. Biomol. Chem.* **2012**, *10*, 6375–6387. (e) Feng, L.; Lanfranchi, D. A.; Cotos, L.; Cesar, E.; Ehrhardt, K.; Goetz, A.-A.; Zimmerman, H.; Fenaille, F.; Blandin, S.; Davioud-Charvet, E. *Org. Biomol. Chem.* **2018**, *16*, 2647 - 2665. (f) Bielitz, M.; Belorgey, D.; Ehrhardt, K.; Johann, L.; Lanfranchi, D. A.; Gallo, V.; Schwarzer, E.; Mohring, F.; Jortzik, E.; Williams, D. L.; Becker, K.; Arese, P.; Elhabiri, M.; Davioud-Charvet, E. *Antioxid. Redox Signal.* **2015**, *22*, 1337-51.
- (3) (a) Jacobsen, N.; Torsell, K. *Acta Chem. Scand.* **1973**, *27*, 3211-3216. (b) Goldman, J.; Jacobsen, N.; Torsell, K. *Acta Chem. Scand.* **1974**, *28b*, 492-500. (c) Anderson, J. M.; Kochi, J. K. *J. Am. Chem. Soc.* **1970**, *92*, 1651–1659. (d) Salmon-Chemin, L.; Lemaire, A.; De Freitas, S.; Deprez, B.; Sergheraert, C.; Davioud-Charvet, E. *Bioorg. Med. Chem. Lett.* **2000**, *10*, 631-635. (e) Salmon-Chemin, L.; Buisine, E.; Yardley, V.; Kohler, S.; Debreu, M. A.; Landry, V.; Sergheraert, C.; Croft, S.; Krauth-Siegel, L.; Davioud-Charvet, E. *J. Med. Chem.* **2001**, *44*, 548-565.
- (4) Sutherland, D. R.; Veguillas, M.; Oates, C. L.; Lee, A-L.; *Org. Lett.* **2018**, *20*, 6863-6867.
- (5) (a) Galloway, J. D.; Mai, D. N.; Baxter, R. D. *J. Org. Chem.* **2019**, *84*, 12131–12137. (b) Zhou, S-L.; Guo, L-N.; Duan, X.-H. *Eur. J. Org. Chem.* **2014**, 8094-8100. (c) Dong, Y.; Yang, J.; He, S.; Shi, Z.-C.; Wang, Y.; Zhang, X.-M.; Wang, J.-Y. *RSC Adv.* **2019**, *9*, 27588-27592. (d) Li, D.; Shen, X. *Org. Biomol. Chem.* **2020**, *18*, 750-754.
- (6) Ramesh, N.; Prakash, C.; Sureshbabu, R.; Dhayalan, V.; Mohanakrishnan, A. K. *Tetrahedron*, **2008**, *64*, 2071-2079.

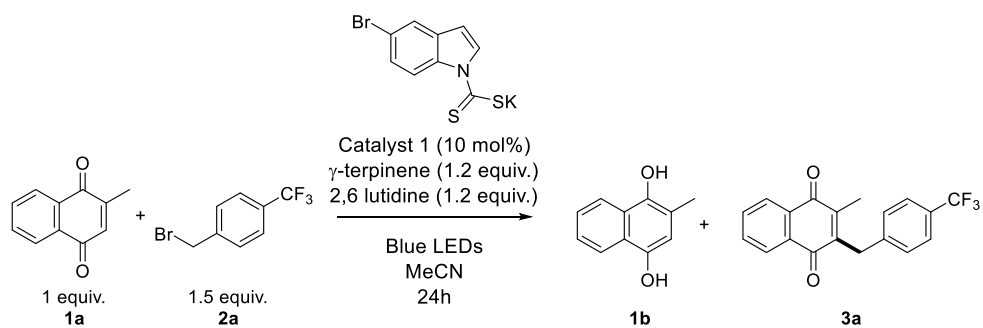
- (7) (a) Hironaka, K.; Fukuzumi, S.; Tanaka, T. *J. Chem. Soc., Perkin Trans. 2*, **1984**, 1705–1709. (b) Kern, J.-M.; Sauvage, J.-P. *J. Chem. Soc., Chem. Commun.* **1987**, 546–548. (c) Shih, H. W.; Vander Wal, M. N.; Grange, R. L.; MacMillan, D. W. *J. Am. Chem. Soc.* **2010**, 132, 13600–13603 (d) Arceo, E.; Jurberg, I. D.; Alvarez-Fernández, A.; Melchiorre, P.; *Nat. Chem.* **2013**, 5, 750–756. (e) Prier, C. K.; Rankic, D. A.; MacMillan, D. W. *Chem. Rev.* **2013**, 113, 5322–5363.
- (8) (a) McLean, E. B.; Gauchot, V.; Brunen, S.; Burns, D. J.; Lee, A.-L. *Chem. Commun.* **2019**, 55, 4238–4241. (b) Park, G.; Yi, S. Y.; Jung, J.; Cho, E. J.; You, Y. *Chem. Eur. J.* **2016**, 22, 17790–17799.
- (9) Schweitzer-Chaput, B.; Horwitz, M. A.; Beato, E.; Melchiorre, P. *Nat. Chem.* **2019**, 11, 129–135.
- (10) (a) Görner, H. *J. Photochem. Photobiol. A: Chem.* **2004**, 165, 215–222. (b) Görner, H. *Photochem. Photobiol. Sci.* **2004**, 3, 71–78. (c) Görner, H. *J. Photochem. Photobiol. A*. **2011**, 224, 135–140.
- (11) Chih, T.; Yeh, S. Y.; Wang, C. M.; *J. Electroanal. Chem.* **2003**, 543, 135–142.
- (12) (a) For a review on superoxide radical: Hayyan, M.; Hashim, M. A.; Al Nashef, I. M. *Chem. Rev.* **2016**, 116, 3029–3085. (b) Voelker, B. M.; Sedlak, D. L. *Mar. Chem.* **1995**, 50, 93–102. (c) Nunoshiba, T.; Obata, F.; Boss, A. C.; Oikawa, S.; Mori, T.; Kawanishi, S.; Yamamoto, K. *J. Biol. Chem.* **1999**, 274, 34832–34837. (d) Lueder, U.; Jørgensen, B. B.; Kapplerab, A.; Schmidt, C.; *Environ. Sci.: Processes Impacts*, **2020**, 22, 12–24.
- (13) Lang, K.; Luňák, S. *Photochem. Photobiol. Sci.* **2002**, 1, 588–591
- (14) For a review on intramolecular photoredox reaction of quinones: Ando, Y.; Suzuki, K. *Chem. Eur. J.* **2018**, 24, 15955–15964.

Optimization tables (extract from the supporting information)

General procedure for optimization and control reactions.

In a 10 mL sealable tube, **1a**, **2a**, reactants and catalyst(s) were dissolved in acetonitrile (5 mL). The tube was sealed, placed under blue light irradiation, and heated up at the given temperature during 24h under air atmosphere unless otherwise stated. After completion, the mixture was allowed to cool down at room temperature and was partitioned between ethyl acetate (10 mL) and aqueous 1M HCl (10 mL). The aqueous layer was extracted once with 10 mL ethyl acetate and the reunited organic layers were washed with brine and dried with MgSO₄. The solvent was removed and if NMR analysis showed more than 20% conversion the crude was purified by silica gel chromatography to obtain pure benzylated quinone.

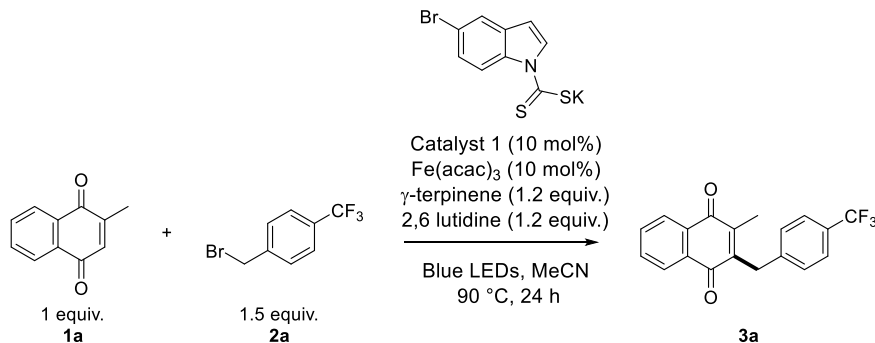
Table SI-1: Initial screening



Entry	Concentration (mol.l ⁻¹)	Temperature (°C)	Additive	Atmosphere	Ratio ^[b] 1a : 1b : 3a
1 ^[c]	0.5	60	-	Argon	55 : 45 : traces
2	0.5	60	-	Air	55 : 41 : 5
3	0.1	60	-	Air	29 : 54 : 17
4	0.05	70	-	Air	18 : 64 : 18
5	0.05	70	Fe(acac) ₃ 10 mol%	Air	78 : 0 : 22
6	0.05	90	Fe(acac) ₃ 10 mol%	Air	19 : 0 : 81 ^[c]

[a] Reactions Conditions: **1a** (1.0 equiv., 0.25 mmol), **2a** (1.5 equiv.), γ -terpinene (1.2 equiv.), 2,6-lutidine (1.2 equiv.), Catalyst 1 (10 mol%) in acetonitrile under blue light irradiation during 24h. [b] Ratio between **1a**, **1b** and **3a** were determined by ¹H NMR on the crude of the reaction [c] Original conditions described by Schweitzer-Chaput et al.⁵⁹ [d] Isolated yield: 79%.

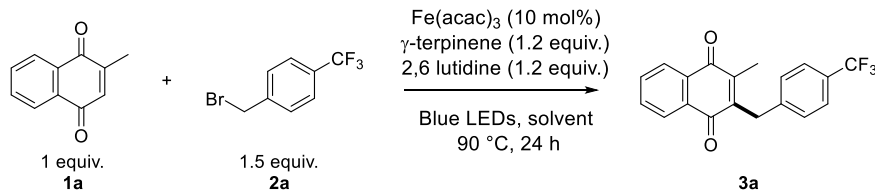
Table SI-2: Second screening



Entry	Variation from standard procedure ^[a]	3a Isolated yield (%)
1	none	79
2	No light	n.d.
3	Menadiol 1b versus menadione 1a	55
4	FeCl ₂ .6H ₂ O versus Fe(acac) ₃	63
5	No catalyst 1	73
6	No catalyst 1, Concentration 0.1M	84

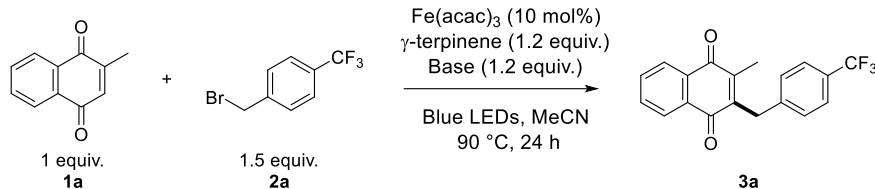
[a] Reactions Conditions: **1a** (1.0 equiv., 0.5 mmol), **2a** (1.5 equiv.), γ -terpinene (1.2 equiv.), 2,6-lutidine (1.2 equiv.), Catalyst 1 (10 mol%) in acetonitrile (0.05M) under blue light irradiation during 24h. n.d : not detected.

Table SI-3: Solvent screening



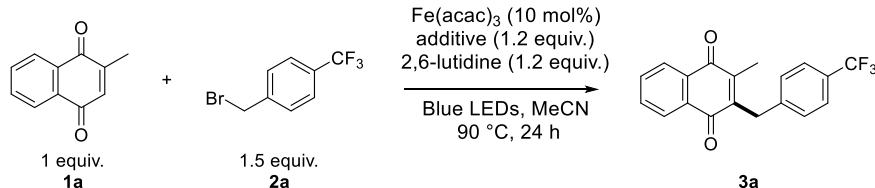
Entry	Solvent	3a Isolated yield (%)
1	Acetonitrile	84
2	Dichloroethane	59
3	Toluene	36
4	Hexafluoroisopropanol (HFIP)	54
5	Dimethylformamide (DMF)	35
6	Acetonitrile : Water (10 : 1)	n.d.

Reactions Conditions: **1a** (1.0 equiv, 0.5 mmol), **2a** (1.5 equiv), γ -terpinene (1.2 equiv.), 2,6-lutidine (1.2 equiv.), Fe(acac)₃ (10 mol%) in a solvent (0.1M) under blue light irradiation during 24h. n.d: not detected.

Table SI-4: Base screening

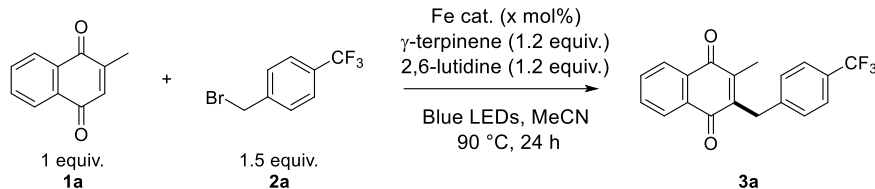
Entry	Base	3a Isolated yield (%)
1	2,6-lutidine	84
2	none	23
3	2,4,6-collidine	73
4	N,N-Diisopropylethylamine (DIPEA)	31
5	K ₂ CO ₃	n.d.

Reactions Conditions: **1a** (1.0 equiv., 0.5 mmol), **2a** (1.5 equiv.), γ -terpinene (1.2 equiv.), base (1.2 equiv.), Fe(acac)₃ (10 mol%) in acetonitrile (0.1M) under blue light irradiation during 24h. n.d: not detected.

Table SI-5: Additive screening

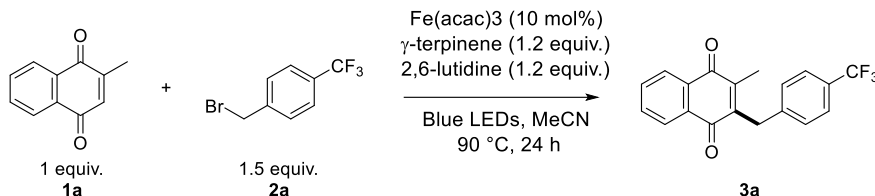
Entry	Additive	3a Isolated yield (%)
1	γ -terpinene (1.2 equiv.)	84
2	none	<5% ^[a]
3	γ -terpinene (0.05 equiv.)	35
4	γ -terpinene (0.1 equiv.)	43
5	γ -terpinene (0.2 equiv.)	56
6	γ -terpinene (0.5 equiv.)	71
7	γ -terpinene (1 equiv.)	77
8	Hantzsch's ester	65

[a] determined by ¹H NMR. Reactions Conditions: **1a** (1.0 equiv., 0.5 mmol), **2a** (1.5 equiv.), additive, 2,6-lutidine (1.2 equiv.), Fe(acac)₃ (10 mol%) in acetonitrile (0.1M) under blue light irradiation during 24h.

Table SI-6: Iron catalyst screening

Entry	Fe catalyst	3a Isolated yield (%)
1	Fe(acac) ₃ (10 mol%)	84
2	none	n.d
3	FeCl ₃ .6H ₂ O	70
4	Fe(ClO ₄) ₃ .H ₂ O	72
5	Fe(NO ₃) ₃ .9H ₂ O (10 mol%)	18
6	Ferrocene (10 mol%)	Traces ^[a]
7	FeCl ₂ (10 mol%)	67
8	Fe(acac) ₃ (5 mol%)	80
9	Fe(acac) ₃ (2 mol%)	46
10	Fe(acac) ₃ (20 mol%)	49

[a] determined by ¹H NMR. Reactions Conditions: 1a (1.0 equiv., 0.5 mmol), 2a (1.5 equiv., 0.75 mmol), γ -terpinene (1.2 equiv.), 2,6-lutidine (1.2 equiv., 0.3 mmol), Fe cat. (10 mol%) in acetonitrile (0.1M) under blue light irradiation during 24h. n.d: not detected.

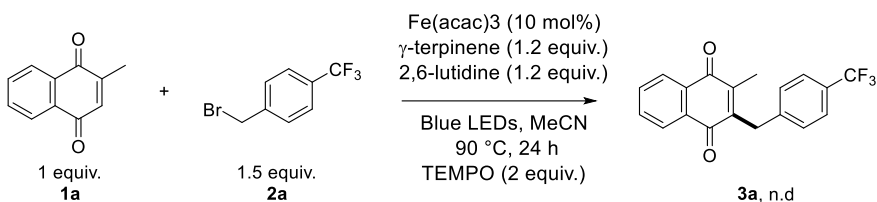
Table SI-7: Other parameters and controls

Entry	Deviations from standard conditions	3a Isolated yield (%)
1	none	84
2	2a' versus 2a ^[a]	79
3	2a'' versus 2a ^[b]	39
4	Argon atmosphere	<10 ^[c]
5	Oxygen atmosphere	35
6	48h	85
7	70°C	<20 ^[c]
8	100°C	82
9	No light	n.d
10	4 mmol scale, 0.2M	71
11	Propan-2-ol versus acetonitrile, no γ -terpinene	38

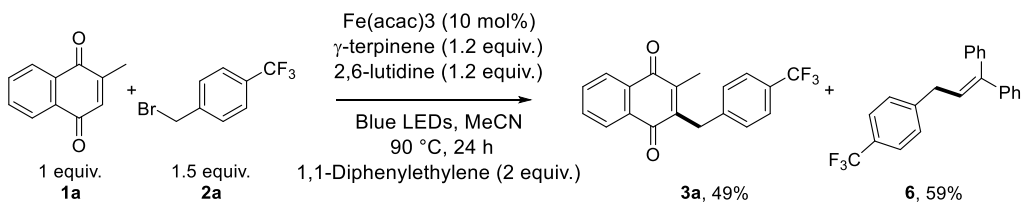
[a] 2a' = 4-trifluoromethylbenzyl iodide. [b] 2a'' = 4-trifluoromethylbenzyl chloride. [c] determined by ¹H NMR. Reactions Conditions: 1a (1.0 equiv, 0.5 mmol), 2a (1.5 equiv, 0.75 mmol), γ -terpinene (1.2 equiv.), 2,6-lutidine (1.2 equiv), Fe(acac)₃ (10 mol%) in acetonitrile (0.1M) under blue light irradiation during 24h. n.d: not detected.

Mechanistic studies.

Radical trap experiments



According to the general procedure with 2 equiv. of 2,2,6,6-Tetramethylpiperidine 1-oxyl. Analysis of the crude mixture showed complete destruction of starting materials.

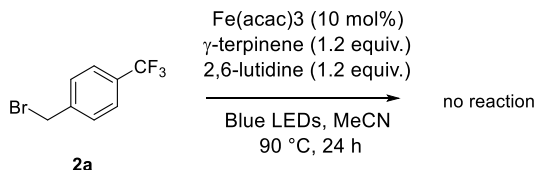


According to the general procedure with 2 equiv. of 1,1-diphenylethylene. Purification by silica gel chromatography (toluene: cyclohexane as eluant, gradient starting from 100% cyclohexane and up to 100% toluene) of the crude mixture afforded 81 mg of **3a** (49% yield), 101 mg of **6** (59% yield) and 35 mg of remaining **1a**. Yields were calculated regarding **1a**.

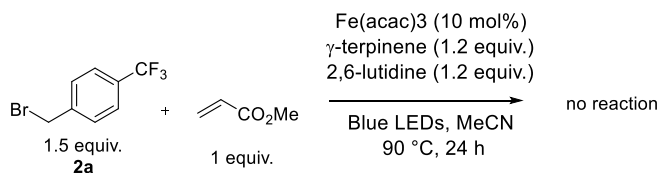
6 is a translucent oil. **1H NMR** (400 MHz, CDCl₃) δ 7.43 (d, J = 8.0 Hz, 2H), 7.33 – 7.05 (m, 12H), 6.12 (t, J = 7.6 Hz, 1H), 3.41 (d, J = 7.6 Hz, 2H). **19F NMR** (377 MHz, CDCl₃) δ -62.31.

Control reactions.

In order to assess that quinone as reactant is mandatory for the reaction to occur, several controls reaction were run in its absence or with a different radical acceptor.

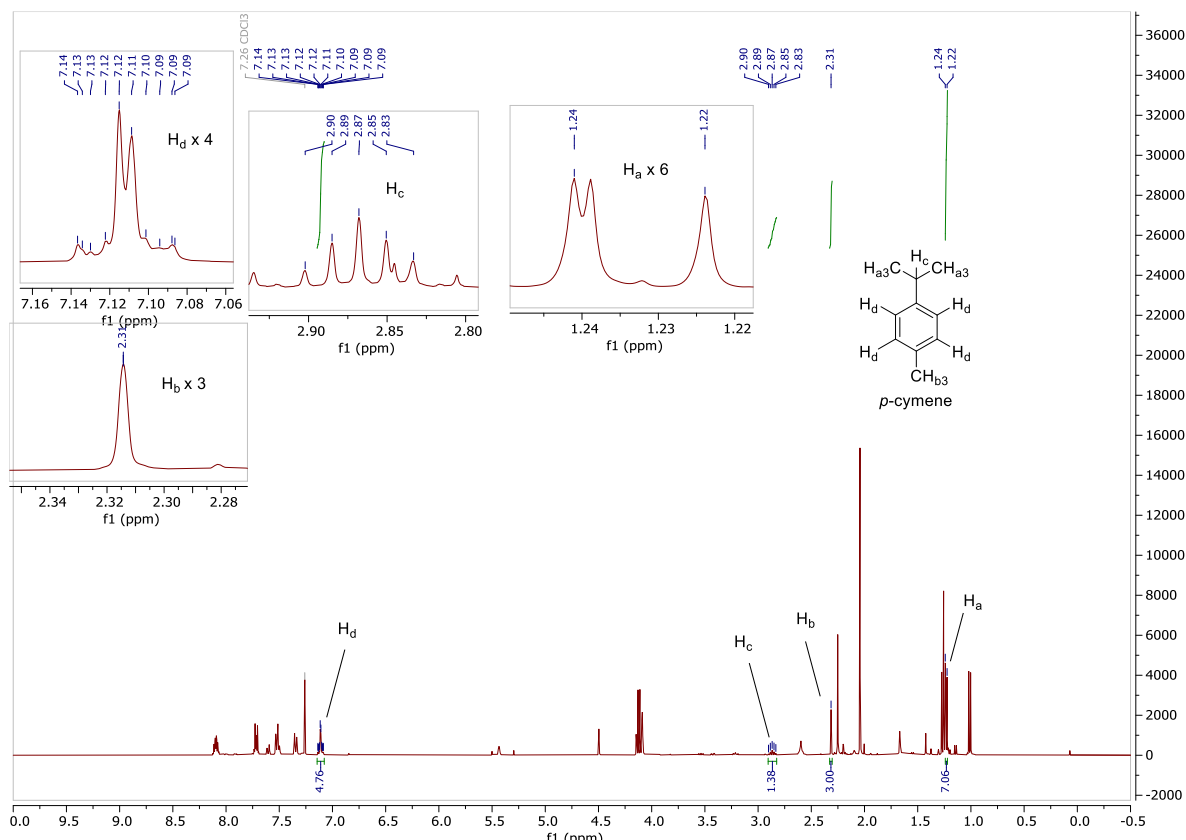


Scheme SI-1. Reaction without menadione.



Scheme SI-2. Reaction with methyl acrylate as radical acceptor.

NMR Spectra of the crude reaction mixture.



Scheme SI-3. NMR spectra of the crude of the reaction in optimized conditions.

Analysis of the NMR spectra of the crude reaction mixture showed the formation of *p*-cymene from the starting γ -terpinene.

Absorption spectrophotometric data.

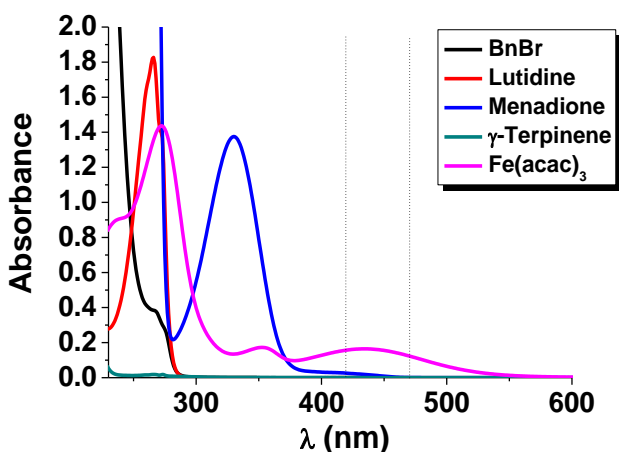


Figure S1. Absorption spectrophotometric spectra of all the reactants involved in the photoredox benzylation of menadione. [Menadione] = [Lutidine] = [BnBr] = [γ -Terpinene] = 0.5 mM; [Fe(acac)₃] = 0.05 mM. Solvent: CH₃CN; T = 25 °C; Blue LED (420-470 nm). This measurement evidenced that only menadione and Fe(acac)₃ absorb this blue electromagnetic radiation.

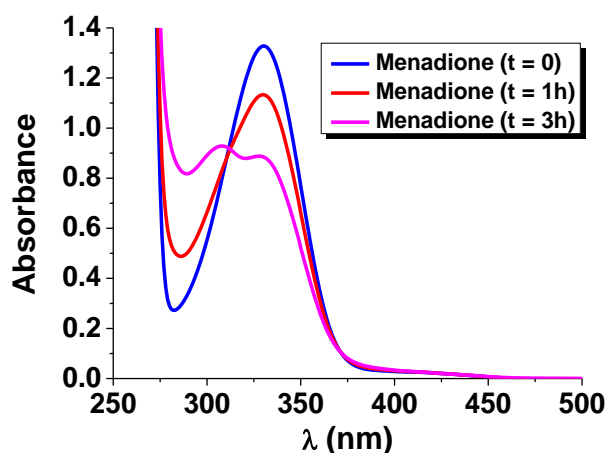


Figure S2. Absorption spectrophotometric variation recorded for menadione (0.5 mM) upon blue-LED photoirradiation for t = 0 hour, 1 hour and 3 hours. Solvent: CH₃CN; T = 25 °C; Blue LED (420-470 nm). This measurement revealed that menadione can be activated upon photoirradiation by a blue LED.

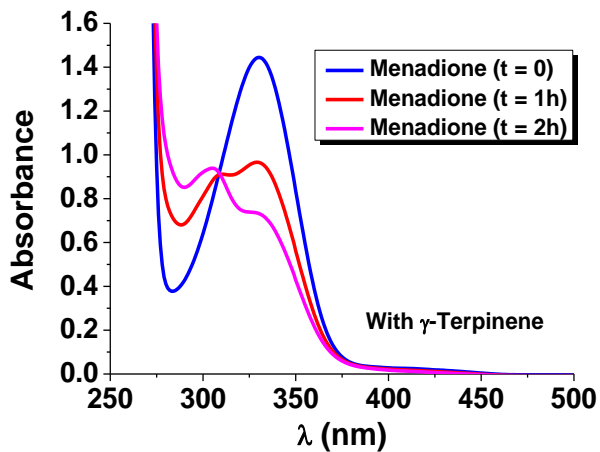


Figure S3. Absorption spectrophotometric variation recorded for menadione (0.5 mM) in the presence of γ -terpinene (0.5 mM) upon blue-LED photoirradiation for $t=0$ hour, 1 hour and 3 hours. Solvent: CH_3CN ; $T=25\text{ }^\circ\text{C}$; Blue LED (420-470 nm). This measurement revealed that menadione can be activated upon photoirradiation by a blue LED and this process is improved with a proton donor such as γ -terpinene.

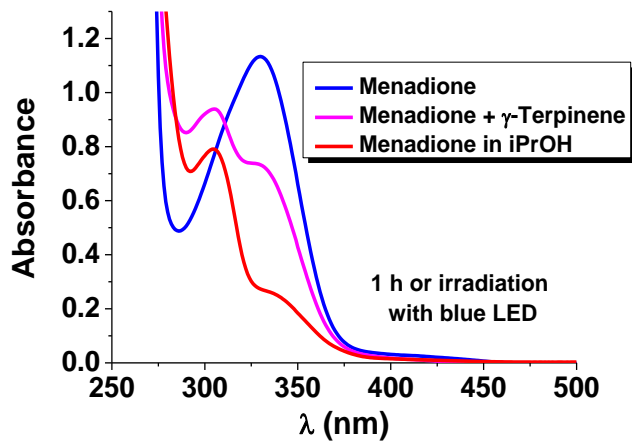


Figure S5. Absorption spectrophotometric spectra recorded for menadione (0.5 mM) in CH_3CN (alone in blue or with γ -terpinene in pink) and in isopropanol (in red) upon blue-LED photoirradiation after 1 hour of photoirradiation. $T=25\text{ }^\circ\text{C}$; Blue LED (420-470 nm). This measurement revealed that menadione is more efficiently activated upon photoirradiation by a blue LED in isopropanol (used as solvent).

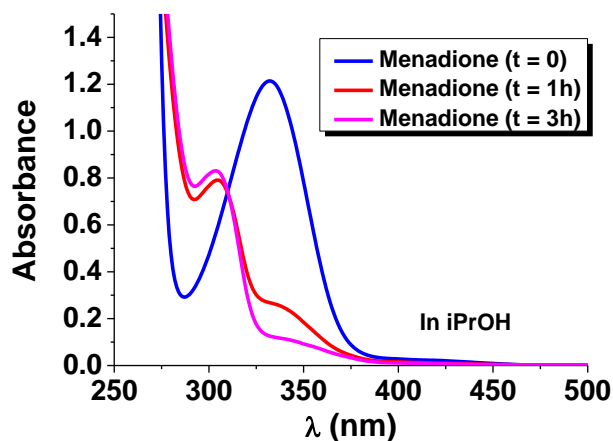


Figure S4. Absorption spectrophotometric variation recorded for menadione (0.5 mM) in isopropanol upon blue-LED photoirradiation for $t=0$ hour, 1 hour and 3 hours. Solvent: iPrOH ; $T=25\text{ }^\circ\text{C}$; Blue LED (420-470 nm). This measurement revealed that menadione can be activated upon photoirradiation by a blue LED and this process is improved with a proton donor such as iPrOH (used as solvent).

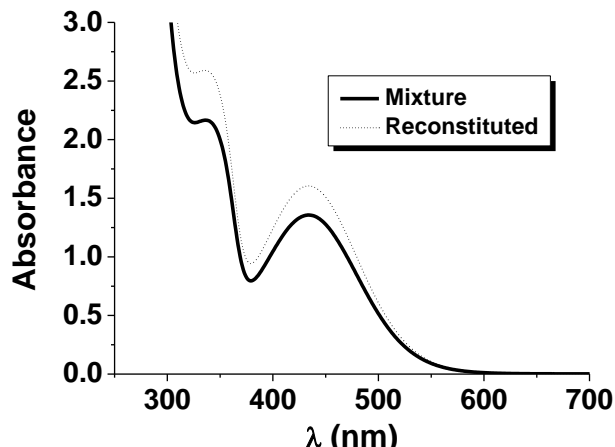


Figure S6. Absorption spectrophotometric spectrum of a mixture of all the reactants involved in the photoredox benzylolation of menadione compared to the sum of all individual spectra. [Menadione] = [Lutidine] = [BnBr] = [γ -Terpinene] = [Fe(acac)₃] = 0.5 mM. Solvent: CH_3CN ; $T=25\text{ }^\circ\text{C}$; Blue LED (420-470 nm). Within the experimental errors, no significant change in the absorption pattern could be observed, demonstrating that no reaction occurred in the absence of blue LED photoactivation.

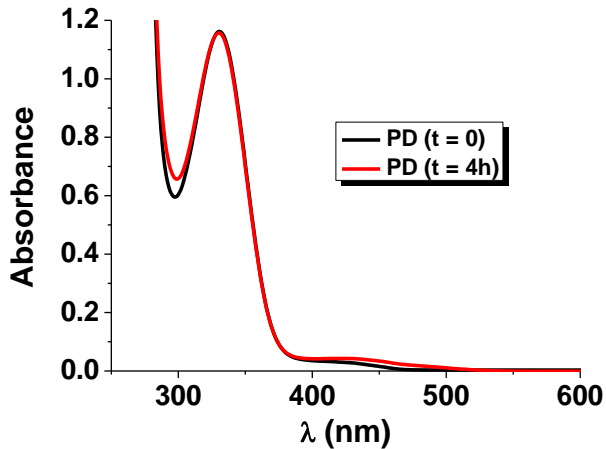


Figure S7. Absorption spectrophotometric variation recorded for plasmodione PD **3a** (0.5 mM) upon blue-LED photoirradiation for $t = 0$ hour and 4 hours. Solvent: CH_3CN ; $T = 25^\circ\text{C}$; Blue LED (420-470 nm). This measurement revealed that **3a** could not be efficiently photoactivated in contrast to what has been observed for menadione.

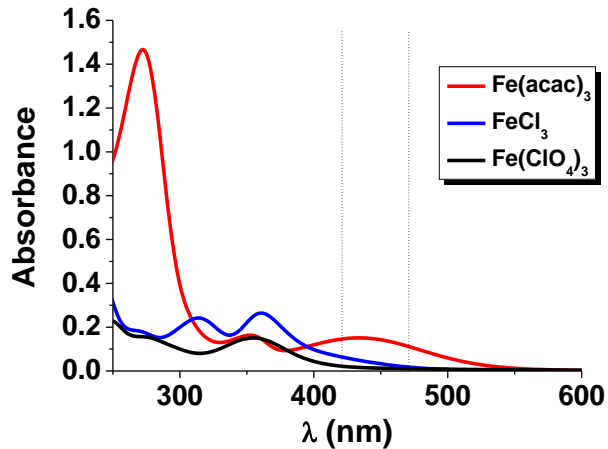


Figure S8. Absorption spectrophotometric spectra of iron(III) sources tested in the photoredox benzylation of menadione. $[\text{Fe}(\text{ClO}_4)_3] = [\text{FeCl}_3] = [\text{Fe}(\text{acac})_3] = 0.05$ mM; Blue LED (420-470 nm). Solvent: CH_3CN ; $T = 25^\circ\text{C}$. This measurement evidenced that not all iron(III) species absorb significantly in the 420-470 nm spectral range (Blue LED) while showing interesting reactivity in the photoredox process.

5 points à retenir de l'article

- 1) Une nouvelle réaction catalysée par le fer(III) et la lumière bleue a été développée pour synthétiser efficacement en une seule étape des naphtoquinones benzylées à partir de bromures de benzyle.
- 2) La réaction tolère un grand nombre de substituants sur le cycle benzylique et la naphtoquinone.
- 3) Les réactions de contrôle ont montré que le mécanisme réactionnel impliquait certainement des radicaux et que la présence d'oxygène, de lumière et d'un donneur d'hydrogène étaient indispensables.
- 4) Un mécanisme impliquant plusieurs cycles rédox a été proposé.
- 5) C'est le premier exemple de fonctionnalisation intermoléculaire d'une quinone reposant sur sa photoréactivité.

2. Oxydation benzylique de la plasmodione.

2.1. Travaux préliminaires.

Lors d'une analyse de routine par spectrométrie de masse de la plasmodione synthétisée par la méthode de benzylation photorédox vue précédemment, nous avions remarqué la présence de traces de la forme oxydée 3-benzoylménadione, indétectable dans un spectre RMN. Deux hypothèses se sont alors offertes à nous, soit la plasmodione est oxydée lentement sous sa forme solide, soit les conditions de la réaction photochimique avec les LED bleues permettent de générer en petite quantité la 3-benzoylménadione dérivée de la **PD**. Afin de valider la seconde hypothèse, nous avons placé la plasmodione dans les conditions exactes de la benzylation photorédox (**Schéma 24**). L'analyse du spectre RMN du milieu réactionnel de cette réaction nous a révélé qu'en effet, des traces de plasmodione oxydée en position benzylique ont été formées.

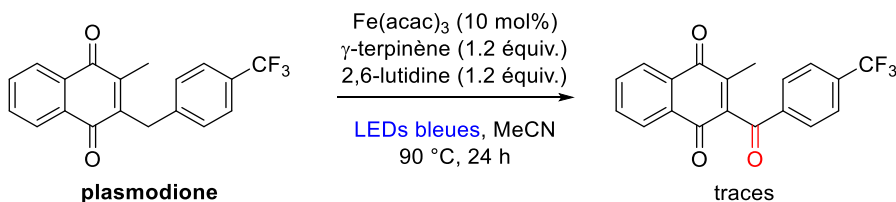


Schéma 24. Tentative d'oxydation benzylique de la plasmodione dans les conditions de benzylation photorédox.

Nous avons alors voulu améliorer la conversion de cette oxydation benzylique en faisant l'hypothèse que la photoirradiation suivi de la formation de l'intermédiaire semiquinone radical par abstraction d'hydrogène d'un donneur est une étape clé de cette transformation (**Schéma 25**).

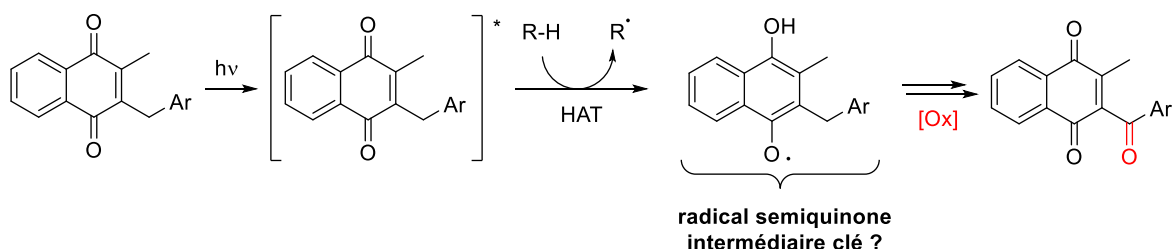
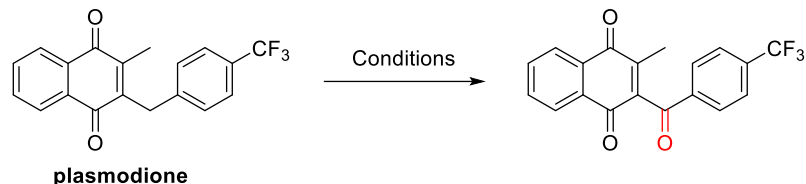


Schéma 25. Mécanisme hypothétique de la formation d'un intermédiaire clé pour l'oxydation benzylique des 3-benzylménadiques.

Plusieurs paramètres ont alors été modifiés. La base a d'abord été retirée (**Tableau 2**, Entrée 2), puis, étant donné que contrairement à la ménadione, nous avions montré précédemment que la plasmodione n'est pas photoactivée efficacement par la lumière bleue (**Figure 16**), une lampe UV irradiant à 360 nm a été utilisée à basse température, sans pour autant fournir le composé recherché autrement que sous forme de traces (**Tableau 2**, Entrée 3). Nous avons alors remplacé le système de solvant et donneur d'hydrogène MeCN/γ-terpinène par l'isopropanol (iPrOH) décrit pour jouer à la fois le rôle de solvant et de donneur d'hydrogène dans la formation de radicaux semiquinones par

photoirradiation.⁶⁰ Avec ce nouveau solvant, nous avons pu observer la formation de plasmodione oxydée dans des proportions quantifiables et de manière plus notable sous irradiation UV ($\gamma = 360$ nm) à 16 °C (Tableau 2, Entrée 4 et 5). La source de fer(III) a également été supprimée pour finalement observer 26% de conversion.

Tableau 2. Travaux préliminaires d'optimisation de l'oxydation benzylique photocatalysée de la plasmodione.



Entrée	Conditions	Conversion (%) ^a
1	2,6-lutidine (1.2 équiv.), γ -terpinène (1.2 équiv.) Fe(acac) ₃ (10 mol%), MeCN, LEDs bleues, 90 °C, 24 h	traces ^b
2	γ -terpinène (1.2 équiv.), Fe(acac) ₃ (10 mol%) MeCN, LEDs bleues, 90 °C, 72h	traces ^b
3	γ -terpinène (1.2 équiv.), Fe(acac) ₃ (10 mol%) MeCN, lampe UV, 16 °C, 72 h	traces ^b
4	Fe(acac) ₃ (10 mol%), iPrOH, LEDs bleues 90 °C, 72 h	<5
5	Fe(acac) ₃ (10 mol%), iPrOH, lampe UV, 16 °C, 72 h	17
6	iPrOH, lampe UV, 16 °C, 72 h	26

^aLa conversion a été déterminée en comparant les intégrations des pics RMN de la 3-benzoylménadione formée et de la plasmodione. ^bLa formation de la 3-benzoylménadione est détectée mais non quantifiable.

⁶⁰ a) H. Görner, *J. Photochem. Photobiol. A: Chem.* **2004**, 165, 215-222. b) H. Görner, *Photochem. Photobiol. Sci.* **2004**, 3, 71-78. c) H. Görner, *J. Photochem. Photobiol. A.* **2011**, 224, 135-140.

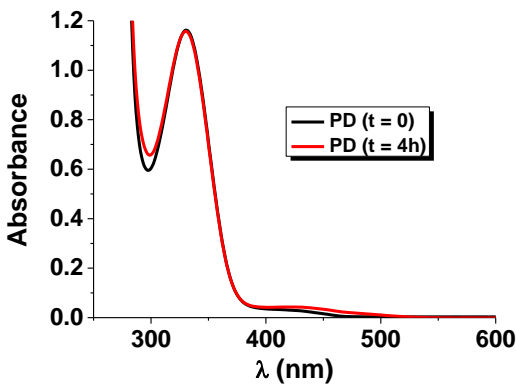


Figure 16. Variation de l'absorption spectrophotométrique de PD mesurée après photoirradiation par des LEDs bleues à $t = 0$ et $t = 4$ h. Solvent : Acétonitrile ; $T = 25\text{ }^{\circ}\text{C}$; LEDs bleues (420-470 nm). Cette mesure montre que PD ne peut pas être photoactivée efficacement par la lumière bleue.

Nous avons pu par la suite vérifier que conduire cette réaction sous atmosphère d’oxygène permettait d’augmenter le rendement d’oxydation et que cette méthode pouvait s’appliquer à diverses 3-benzylménadiones, notamment celles comportant une fonction alcyne (voir également Chapitre II. Partie 2), ou une 3-benzylménadione très encombrée par la présence de deux groupes méthyles en 2' et 6' de la chaîne benzyle. Dans le même temps, Bogdan Cichocki a pu également prouver que la plasmodione pouvait être oxydée dans des milieux biologiques par l’intermédiaire de la ferrédoxine-NADP⁺ oxidoréductase de *P. falciparum* (*PfFNR*). Ces résultats combinés confirment pour la première fois la possibilité d’une oxydation benzylique de **PD** dans des conditions biomimétiques. Nous avons ainsi proposé un mécanisme d’oxydation benzylique de la **PD** pour lequel la génération du radical benzyl semiquinone se révèle être crucial.

L’ensemble de ces travaux a été publié dans un article du journal *ACS Infectious Diseases* en collaboration avec trois autres équipes au niveau Européen situées dans les universités de Vilnius, Milan et Giessen. Mes travaux sur l’oxydation benzylique photocatalysée et les travaux de Bogdan Cichocki sur l’oxydation benzylique catalysée par *PfFNR* y sont présentés.

Kim Heimsch et Katja Becker ont démontré que la **PD** avait un effet oxydant sur l’apicoplaste du parasite. La production induite de stress oxydant dans l’apicoplaste du parasite, organelle où est localisée l’enzyme *PfFNR*, a été mesurée par imagerie en temps réel à l’Université de Giessen, dans les parasites transgéniques vivants, traités à la plasmodione exprimant la roGFP sous le contrôle de la glutarédoxine de l’apicoplaste. Enfin, Mindaugas Lesanavičius et Narimantas Cenas ont étudié la capacité de la **PD**, de ses métabolites supposés et d’un grand nombre de 3-benzoylménadiones, à être substrats subversifs vis-à-vis de *PfFNR* en mesurant l’activité naphtoquinone réductase de l’enzyme. J’ai moi-même eu la chance, lors d’un séjour de deux semaines dans leur laboratoire à Vilnius de découvrir les méthodes de mesures d’activité enzymatique de *PfFNR* envers les quinones, et des mesures de réduction des benzoylménadiones en présence d’ascorbat.

2.2. Article 5.

Plasmodium falciparum Ferredoxin-NADP(+) Reductase-Catalyzed Redox Cycling of Plasmidione Generates Both Predicted Key Drug Metabolites. Implication for Antimalarial Drug Development

Bogdan Cichocki,[#] Maxime Donzel,[#] Kim Heimsch,[#] Mindaugas Lesanavicius,[#] Liwen Feng, Enrique Jose Montagut, Katja Becker, Alessandro Aliverti, Mourad Elhabiri, Narimantas Cenas, Elisabeth Davioud-Charvet

ACS Infectious Diseases, Article accepté le 01 avril, publié en ligne le 15 avril 2021

doi: 10.1021/acsinfecdis.1c00054[#] co-1er auteurs

***Plasmodium falciparum* Ferredoxin-NADP⁺ Reductase-Catalyzed Redox Cycling of Plasmodione Generates Both Predicted Key Drug Metabolites: Implication for Antimalarial Drug Development**

Bogdan Adam Cichocki,^{1,#} Maxime Donzel,^{1,#} Kim C. Heimsch,^{2,#} Mindaugas Lesanavičius,^{3,#} Liwen Feng,¹ Enrique Jose Montagut,¹ Katja Becker,² Alessandro Aliverti,⁴ Mourad Elhabiri,¹ Narimantas Čėnas,³ Elisabeth Davioud-Charvet,^{*,1}

authors ranked by alphabetical order contributed equally as first co-authors

* Correspondence E-mail Address: elisabeth.davioud@unistra.fr

1 Université de Strasbourg–CNRS–UHA UMR7042, Laboratoire d'Innovation Moléculaire et Applications (LIMA), Team Bio(IN)organic and Medicinal Chemistry, European School of Chemistry, Polymers and Materials (ECPM), 25 Rue Becquerel, F-67087 Strasbourg, France.

2 Justus Liebig University Giessen, iFZ - Research Centre for Biosystems, Land Use and Nutrition, Department of Biochemistry and Molecular Biology, Heinrich-Buff-Ring 26-32, 35392 Giessen, Germany

3 Department of Xenobiotics Biochemistry, Institute of Biochemistry of Vilnius University, Saulėtekio 7, LT-10257 Vilnius, Lithuania

4 Department of Biosciences, Università degli Studi di Milano, via Celoria 26, I-20133 Milano, Italy.

ABSTRACT: Plasmodione (PD) is a potent antimalarial redox-active 3-benzyl-menadione acting at low nanomolar range concentrations on different malaria parasite stages. Specific bioactivation of PD was proposed to occur via a cascade of redox reactions starting from one electron-reduction, then benzylic oxidation, leading to generation of several key metabolites including the benzylic alcohol (PD-bzol, for PD benzhydrol) and the 3-benzoylmenadione (PDO for PD oxide). In this study, we showed that benzylic oxidation of PD is closely related to the formation of a benzylic semiquinone radical, which can be produced under two conditions: UV-photolysis, or catalyzed by *P. falciparum* apicoplast ferredoxin-NADP⁺ reductase (PfFNR) redox cycling in the presence of oxygen and the parent PD. Electrochemical properties of both PD metabolites were investigated in DMSO and in water. The single-electron reduction potential values of PD, PD-bzol, PDO and a series of 3-benzoylmenadienes were determined according to ascorbate oxidation kinetics. These compounds possess enhanced reactivity towards PfFNR as compared with model quinones. Optimal conditions were set up to obtain the best conversion of the starting PD to corresponding metabolites. UV-irradiation of PD in isopropanol under positive oxygen pressure led to an isolated yield of 31% PDO through the transient semiquinone species formed in a cascade of reactions. In the presence of PfFNR, PDO and PD-bzol could be observed during long lasting redox cycling of PD continuously fueled by NADPH regenerated by an enzymatic system. Finally, we observed and quantified the effect of PD on the production of oxidative stress in the apicoplast of transgenic 3D7^[Api-roGFP2-hGrx1] *P. falciparum* parasites by using the described genetically encoded glutathione redox sensor hGrx1-roGFP2 methodology. The observed fast reactive oxygen species (ROS) pulse released in the apicoplast is proposed to be mediated by PD redox cycling catalyzed by PfFNR.

KEYWORDS: apicoplast, benzylic oxidation, electrochemistry, ferredoxin-NADP⁺ reductase, plasmodione, redox cycling

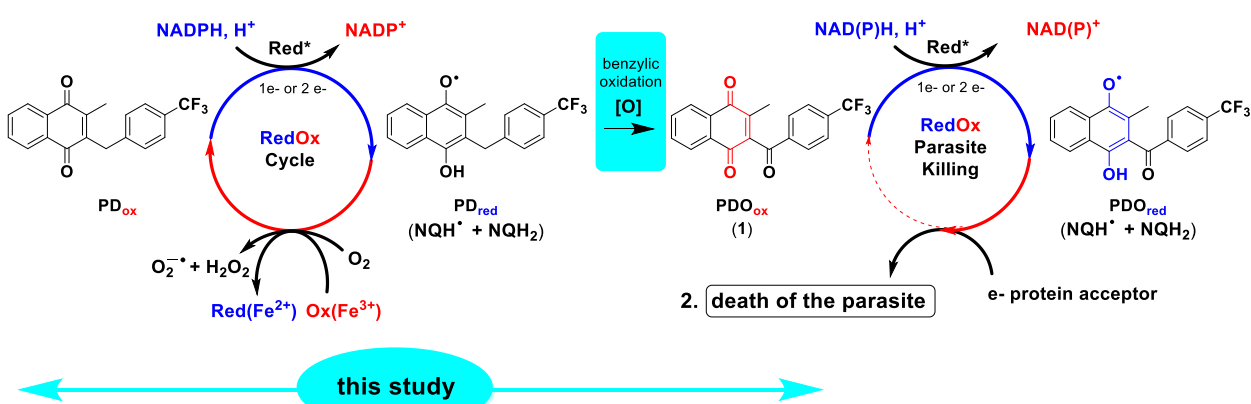
The vulnerability of protozoan parasites to oxidative stress implies that various prooxidant compounds could be potential antiparasitic agents.¹ One of the approaches in this direction is the inhibition of physiological activity of parasite antioxidant flavoenzymes responsible for maintaining the reducing milieu, or even the conversion of these antioxidant enzymes into prooxidant ones. The concept of subversive substrate (turncoat inhibitor or redox-cycler) of various disulfide oxido-reductases was established in 1988² when 2-methyl-1,4-naphthoquinone (menadione) derivatives were observed to oxidize NADPH in the presence of oxygen and the flavoenzyme trypanothione reductase (TR). In these reactions, redox cycling of menadione derivatives, accompanied by superoxide (O_2^-) formation, was evidenced. Thereafter, several groups have subsequently extended this concept to nitroheteroaromatics and various 1,4-naphthoquinones (NQ)³⁻⁵ and developed these chemical series with the objective to introduce a broad structural diversity on the redox-active cores.⁶⁻⁹ Following these investigations on TR to develop antitrypanosomal drugs, Schirmer's group evidenced that the potent antimarial dye, methylene blue, acts as an effective redox-cycler of various NADPH-dependent disulfide reductases including both glutathione reductases (GR) from humans (*hGR*) and *Plasmodium falciparum* (*PfGR*).¹⁰ However, because of the relatively low rate of quinone- and nitroreductase reactions of GR and TR, further efforts were directed to study other parasite oxidoreductases. Among those, given the data available, *P. falciparum* ferredoxin:NADP⁺ oxidoreductase (*PfFNR*) was found to possess the highest activity in redox cycling reactions with xenobiotics.¹¹⁻¹³ This FAD-dependent enzyme catalyzes NADPH-dependent reduction of FeS-protein ferredoxin (*PfFd*), and, like other flavoenzymes, e.g. dehydrogenases-electron transferases, transforms two-electron transfer into a single-electron one.¹⁴ Apart from high xenobiotic reductase activity of *PfFNR*, the importance of this enzyme is determined by its location in parasite apicoplast.^{15,16} The apicoplast was demonstrated to be essential for parasite survival,¹⁷ its structural or

functional disruption resulting in a “delayed death” phenotype.¹⁸

This emerging strategy in redox medicinal chemistry has only been validated when the effect of redox-active compounds on flavoenzymes was accompanied by an impact on the viability of the target cells, the trypanosomes⁸ or malaria parasites.^{19,20} Later on, a proof-of-concept was established with the discovery of plasmidione (PD, Figure 1), a 3-[4-(trifluoromethyl)benzyl]-menadione exerting potent antimarial effects in the low nanomolar range.^{21,22} Detailed enzymic kinetics^{9,21,23} and physico-chemical studies²⁴⁻²⁷ have demonstrated that not only the kinetics of reduction of redox cycler, but also of re-oxidation of its reduced form is essential, to continuously fuel the redox-cycle at the expense of the reducing power of the living cell (Scheme 1).²⁸

The chemical mechanism of action of PD has been investigated in depth by some of us over the past few years, starting from the hypothesis that PD is a prodrug, which is activated in malaria parasites through a cascade of redox reactions. First, we have identified the redox states of GR responsible for the reduction of menadione-derived subversive substrates.²³ Then, we identified the antimarial early lead agent PD, and proposed that, after reduction in the parasitized red blood cells (pRBC), PD is expected to be oxidized at the benzylic position into the corresponding benzoyl metabolite, abbreviated as PDO (for PD oxide) (Figure 1, Scheme 1, see also Figure 2 in Ref.²¹). Furthermore, we synthesized various compound pairs of structurally diverse PD/PDO derivatives and characterized the kinetics of re-oxidation of PD/PDO reduced forms, in the half reaction essential to continuously fuel the redox-cycle at the expense of NADPH (Scheme 1).^{21,26,27} In these studies, we demonstrated by enzymatic studies²¹ using both recombinant GRs of pRBC and methemoglobin (Fe^{3+}) – as well as by electrochemistry^{27,28} – that PDO is an effective subversive substrate of *hGR* and *PfGR*, and more oxidant than the parent PD prodrug.

1. bioactivation *: flavoenzymes: yeast NDH and SDH, human GR, or *P. falciparum* GR and FNR



Scheme 1. Proposed Mechanism of Action of the Antimalarial Early-Lead Plasmidione Prodrug Generating Toxic Metabolites in *P. falciparum*-Parasitized Red Blood Cells (pRBCs).

A one-electron (e⁻) transfer leading to the semiquinone NQH[·] (or a two-e⁻ transfer leading to the dihydro-quinone (NQH₂) is proposed to be involved in the drug bioactivation (step 1), which can be catalyzed in enzymic assays in vitro by several relevant flavoenzymes of pRBC, including *hGR* (human glutathione reductase), *PfGR* (*P. falciparum* glutathione reductase), or *PfFNR* (*P. falciparum* ferredoxin-NADP⁺ reductase (this work)). For the sake of clarity, only the one-e⁻-reduced NQH[·] species was drawn in the developed structures. In step 2, we previously demonstrated that the second one-electron transfer leading to the dihydro-naphthoquinone dianion NQ₂[·] is highly sensitive to the nature of the benzoyl substitution (p-CF₃ in PDO vs diverse substituted 3-benzoylmenadienes).²⁹ This second step is thought to be responsible for the parasite killing.

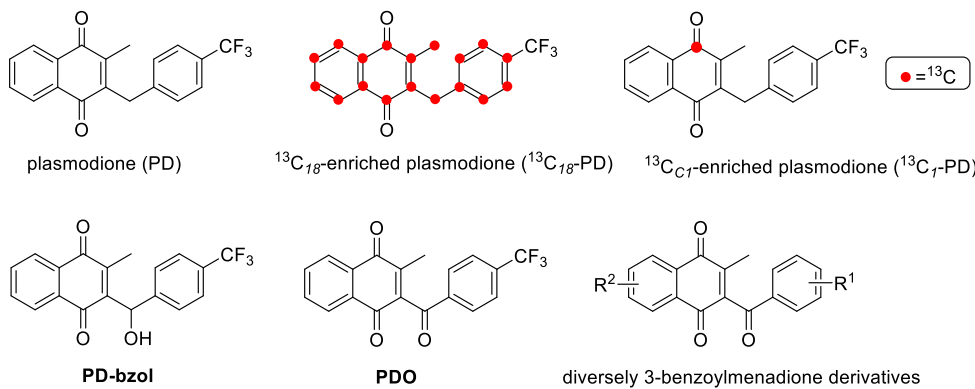


Figure 1. Structures of the chemical tools investigated in this study: the antimalarial plasmodione (**PD**) and both $^{13}\text{C}_{18/1}$ -enriched representatives ($^{13}\text{C}_{18}\text{-PD}$ and $^{13}\text{C}_1\text{-PD}$), its two metabolites (**PD-bzol** and **PDO**), and diversely substituted 3-benzoylmenadione derivatives.

Although we have demonstrated that PD can be chemically oxidized to PDO under harsh conditions²¹ we have tried, for many years, to evidence the formation of PDO from PD under quasi-physiological or biomimetic conditions. To this end, three isotopically ^{13}C -enriched PD and six putative PD metabolites, including its benzylic alcohol (PD-bzol for PD-benzhydrol, Figure 1) and PDO, were also synthesized and studied for their antimalarial effects.³⁰ However, the challenge was to oxidize PD under reducing conditions, a requirement that is only possible in an enzymatic catalytic cycle, a photochemical reaction, or an electrochemical cell. In parallel, we started to investigate the interactome of the antimalarial lead PD, using activity-based protein profiling (ABPP)-based probes and mass spectrometry analysis of the probe-protein adducts.³¹ In particular, we demonstrated that the UV-photoirradiation of a PD-based ABPP probe led to their photo-oxidoreduction, first through NQ photoreduction and then by benzylic oxidation via oxygen insertion. Concomitantly, we used various yeast strains as model cells to study their sensitivity to PD and to decipher the mode of action (MoA) of PD by taking into consideration the power of genetic engineering in yeasts^{32,33} and *Plasmodium* parasites.³⁴ We found that PD is a potent inhibitor of yeast aerobic respiratory growth.³² Genetic and biochemical analyses showed that flavoenzymes of the mitochondrial respiratory chain, NADH-dehydrogenase (NDH) and succinate dehydrogenase (SDH) play a key role in PD activity.^{32,33}

Among the important family of flavoenzymes, there are not many representative members from *P. falciparum*, which were expressed in *E. coli* and described in enzyme kinetics. Because of a shortage of relevant studies on these catalyzed redox reactions using electron-acceptors, we have been using the recombinant *PfFNR* characterized by high capability of redox-cycling in the presence of quinones as substrates¹² to study the possible PD bio-activation and -transformation.

Plastidic-type members of the structural family of plant-type ferredoxin:NADP⁺ oxidoreductase (FNR) are typically found in cyanobacteria and vegetal organisms.¹⁶ FNRs are FAD-dependent dehydrogenases/electron-transferases that, in conjunction with their respective partner ferredoxin (Fd), an iron-sulfur protein, participate in the exchange of reducing equivalents between the NADP⁺/NADPH couple and a variety of physiological electron transporters.³⁵ Starting from 2001,³⁶ plastidic-type FNRs and Fds were identified and found to be expressed in the apicoplast, a Phylum-specific organelle homologous to algal plastids.³⁷ Among the two groups of FNRs, *P. falciparum* FNR and Fd

are phylogenetically related to root-type FNRs and their redox potentials are suited to support a physiological electron flow from NADPH the final electron acceptor(s) via *PfFd* reduction.¹⁴ In particular, the redox couple was shown to fuel with reducing power the non-mevalonate pathway for the biosynthesis of isoprenoid precursors.³⁸ A backward electron flow from reduced *PfFd* to NADP⁺ via *PfFNR* is unfeasible, due to highly unfavorable redox potentials of the iron-sulfur and FAD prosthetic groups of the respective proteins.^{14,39} In addition, it is also possibly involved in the biogenesis of the clusters of the apicoplast iron-sulfur proteins, as well as in other housekeeping functions of the organelle.⁴⁰ Similarly, because of their metabolic role(s) it is not surprising that *PfFNR* and *PfFd* recently turned out to be both essential as demonstrated by saturation mutagenesis.¹⁷

Herein, we report a multidisciplinary approach based on electrochemistry, chemical reactivity, biochemistry, and analytical chemistry, to evaluate the properties and the substrate capacities of PD, its two metabolites PD-bzol and PDO (Figure 1) and various 3-benzoylmenadienes in *PfFNR*-catalyzed reactions. Furthermore, we demonstrated that the benzylic oxidation of PD could be achieved in the presence of oxygen under UV-photoirradiation, or under *PfFNR* catalysis at high rate of redox cycling. The structure of the formed metabolites, PD-bzol or/and PDO was confirmed by NMR spectroscopy and liquid chromatography coupled to mass spectrometry (LC-MS). In addition, the use of two isotopically ^{13}C -enriched PD allowed us to unambiguously assign the exact molecular and fragment masses of the generated PD metabolites. Finally, the effect of PD on the production of ROS in the apicoplast of transgenic 3D7[¹Api-roGFP2-hGrx1] parasites was visualized by using the described genetically encoded glutathione redox sensor hGrx1-roGFP2 methodology.⁴¹

RESULTS AND DISCUSSION

Redox potentials of plasmodione and its metabolites

The cytotoxicity/therapeutic activity of quinones frequently stems from their single-electron reduction by flavin-dependent dehydrogenases-electrontransferases, such as NADPH: cytochrome P-450 reductase or ferredoxin:NADP⁺ oxidoreductase, which initiate the redox cycling of their anion-radicals with the subsequent formation of O₂^{•-} and other activated oxygen species.⁴² In most cases, the single-electron reduction of quinones by above enzymes follows an ‘outer-sphere’ electron transfer model,⁴³ which is characterized by linear or parabolic

dependence of $\log(k)$ from the redox potential of quinone/semiquinone couple (single-electron reduction midpoint potential, E^1 , or E^1_7 at pH 7.0) (Ref.⁴⁴, and references therein). In turn, if quinones act mainly through the oxidative stress, their cytotoxicity increases with their E^1_7 .^{42,44} Thus, E^1_7 is an important parameter for the analysis of activity of new quinone-based drugs.

The electrochemical properties of the key redox-active triad, PD, PD-bzol and PDO, have been first examined in DMSO (0.1M NBu₄PF₆, $v = 200$ mV/s) by cyclic (CV) and square wave (SWV) voltammetry (Figures S1-S9).²⁷ In both systems, two consecutive one-electron quasi-reversible waves can be observed (Figure 2). The monoradical-anion NQ⁻ is formed in the first reduction step, and subsequently reduced to its related dihydro-naphthoquinone dianion NQ²⁻ in a second step. For PDO, an additional ill-defined reduction wave was observed at

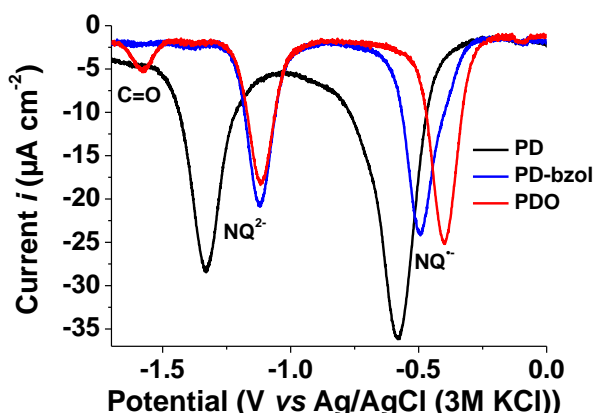


Figure 2. SWV Spectra of the PD (1.59 mM), PD-bzol (1.40 mM) and PDO (1.39 mM) triad. Solvent: DMSO; $I = 0.1$ M NBu₄PF₆; $v = 200$ mV s⁻¹. Reference electrode = KCl(3M)/Ag/AgCl; working electrode = glassy carbon disk of 0.07 cm² area; auxiliary electrode = Pt wire.

much more negative values ($E^{1/2} = -1.58$ V vs. KCl(3M)/Ag/AgCl) that is related to benzoyl carbonyl unit. As far as the first electron transfer process is concerned, PD was found to be the less oxidant derivative ($E^{1/2} = -0.58$ V vs. KCl(3M)/Ag/AgCl), while PDO is the most oxidant one ($E^{1/2} = -0.40$ V vs. KCl(3M)/Ag/AgCl). PD-bzol ($E^{1/2} = -0.49$ V vs. KCl(3M)/Ag/AgCl) is intermediate between the PD and PDO compounds. Benzylic oxidation anodically shifts the half-wave potential $E_{1/2}$ of the two redox waves by about 200 mV ($E^{1/2} = -0.58$ V for PD and -0.40 V vs. KCl(3M)/Ag/AgCl for PDO, $\Delta E^{1/2} = 210$ mV and $E^{2/2} = -1.33$ V for PD and -1.12 V vs. KCl(3M)/Ag/AgCl for PDO, $\Delta E^{2/2} = 210$ mV). This suggests that the benz(o)yl substitution has the same electronic effects both on the NQ unit or on its 1-electron reduced semiquinone, NQ⁻. PD-bzol stands in an interesting contrast with a much stronger effect on the 1-electron reduced semiquinone NQ⁻ than on

NQ likely due to formation of a strong intramolecular hydrogen bond between the benzylic alcohol and the negatively charged semiquinone (semiNQ) subunit. Due to their insufficient solubility in aqueous medium, the midpoint potentials (E^1_7) of quinone/hydroquinone couple of PD, PD-bzol and PDO were determined from CVs of surface-modified electrodes (Figure S10) at pH 7. Regardless of the system considered, the CVs of PD, PD-bzol and PDO correspond to quasi-reversible waves of two-electron transfer. PD and PDO are characterized by E^1_7 of -0.08 V and 0.03 V vs. NHE, and by apparent rate constants of electrochemical reactions of adsorbed compounds (k_s) of 0.59 s⁻¹ and 0.42 s⁻¹, respectively. The E^1_7 of PD is more negative than that of menadione, -0.03 V,^{45,46} due to the electron-donating character of 3-benzyl substituent. Furthermore, as observed in DMSO, the presence of the 3-benzoyl substituent renders the 1,4-NQ more oxidant by about 110 mV. Similarly to the first redox process in DMSO, the redox reactions of PD-bzol take place at potentials intermediate between those of PD and PDO, but, interestingly, are characterized by two redox pairs, $E^1_7 = 0.03$ V vs. NHE ($k_s = 1.1$ s⁻¹), and $E^1_7 = -0.03$ V vs. NHE (Figure S10). As suggested above, hydrogen bonding between the NQ carbonyl and the secondary alcohol can be proposed to explain this peculiar behavior.

Due to instability of quinone radicals in aqueous medium, their values of E^1_7 are obtained mainly using a pulse-radiolysis technique.⁴⁷ However, in our case this approach is hampered by insufficient solubility of PD and related 3-benzoylmenadione derivatives. Thus, we have used an alternative approach of rough estimation of E^1_7 according to the rates of O₂ consumption during quinone-mediated ascorbate oxidation (Ref.⁴⁸ and references therein). In the presence of quinones with available $E^1_7 \leq -0.10$ V, the rate of oxygen consumption is characterized by a linear log (k) vs E^1_7 relationship. The data obtained in this study (Table 1) closely matches previous results,⁴⁸ and were described by a well defined linear correlation:

$$\log k = (2.818 \pm 0.172) + (11.663 \pm 0.728) E^1_7 \quad (r^2 = 0.966) \quad (1)$$

This enables one to calculate the unavailable E^1_7 values for PD derivatives ($E^1_{7(\text{calc})}$, Table 1). Since the differences between the experimentally determined E^1_7 values and $E^1_{7(\text{calc})}$ do not exceed ± 0.03 V (Table 1), the latter values are considered to be realistic.

The data obtained herein demonstrate that due to the electron-donating character of the 3-benzyl substituent, $E^1_{7(\text{calc})}$ of PD is more negative than that of menadione **14** (2-CH₃-1,4-NQ) (Table 1). The presence of electron accepting 3-benzoyl substituent increases E^1_7 of PDO, which becomes close to that of 1,4-NQ **12** (Table 1). The E^1_7 value of PD-bzol is intermediate between those of PD and PDO (Table 1). Among the 4'-substituted PDO derivatives, their $E^1_{7(\text{calc})}$ sequence closely matches the σ_p values of substituents⁴⁹: **5** (-NO₂, $\sigma_p = 0.78$) \geq PDO (-CF₃, $\sigma_p = 0.54$) $>$ **6** (-C≡CH, $\sigma_p = 0.23$) \geq **7** (-Br, $\sigma_p = 0.23$) (Table 1) in agreement with reported values.²⁷

Table 1. Rate constants (k) of ascorbate oxidation by quinones and 3-benz(o)ylmenadione derivatives, their experimentally determined $E^{1/2}$ values,⁴⁷ and $E^{1/2}$ values calculated according to Equation (1) ($E^{1/2}_{\text{calcd.}}$).

PD	PD-bzol	PDO	1
2	3	4	5
6	7	8	
Quinone	k ($\text{M}^{-1}\text{s}^{-1}$)	$E^{1/2}$ (V)	$E^{1/2}_{\text{calcd.}}$ (V)
PD	0.30 ± 0.02	-	-0.286 ± 0.024
PD-bzol	1.17 ± 0.36		-0.236 ± 0.024
PDO	4.62 ± 0.99	-	-0.185 ± 0.019
1	1.12 ± 0.13	-	-0.238 ± 0.022
2	0.43 ± 0.07	-	-0.273 ± 0.023
3	2.89 ± 0.46	-	-0.202 ± 0.020
4	4.75 ± 0.53	-	-0.183 ± 0.017
5	5.60 ± 0.53	-	-0.169 ± 0.018
6	1.10 ± 0.2	-	-0.238 ± 0.022
7	0.81 ± 0.14	-	-0.249 ± 0.022
8	13.9 ± 1.9	-	-0.144 ± 0.018
5-OH-1,4-Naphthoquinone 9	53.5 ± 6.7	-0.09	-0.093 ± 0.017
5,8-(OH) ₂ -1,4-Naphthoquinone 10	48.9 ± 5.2	-0.11	-0.097 ± 0.016
9,10-Phenanthrene quinone 11	15.2 ± 0.9	-0.12	-0.14 ± 0.017
1,4-Naphthoquinone 12	15.9 ± 1.4	-0.15	-0.139 ± 0.017
(CH ₃) ₃ -1,4-Benzoquinone 13	16.5 ± 1.8	-0.17	-0.137 ± 0.018
2-CH ₃ -1,4-Naphthoquinone 14	2.38 ± 0.5	-0.20	-0.209 ± 0.021
(CH ₃) ₄ -1,4-Benzoquinone 15	0.3 ± 0.05	-0.26	-0.286 ± 0.024
1,8-(OH) ₂ -9,10-Anthraquinone 16	0.136 ± 0.02	-0.30	-0.316 ± 0.025
1,4-(OH) ₂ -9,10-Anthraquinone 17	0.091 ± 0.009	-0.33	-0.331 ± 0.026
2-OH-1,4-Naphthoquinone 18	0.018 ± 0.003	-0.41	-0.391 ± 0.029

In turn, the formation of H-bonds of quinone carbonyl groups with 5(8)-OH substituents increases $E^1_{7\text{(calc.)}}$ of 1,4-NQs (Table 1).⁴⁷ This phenomenon is evidenced by an increase of $E^1_{7\text{(calc.)}}$ of 5-OH-substituted 3-benzoylmenadione **8** with respect to the unsubstituted analogue **7** (Table 1).

3-Benzoyl menadione reductase activity of *PfFNR*

Based on our data, *PfFNR* may play a central role in the reductive activation of prooxidant xenobiotics relevant for malaria chemotherapy.¹³ The steady-state kinetic parameters of *PfFNR*-catalyzed reduction of PD derivatives, *i.e.* the apparent catalytic constants ($k_{\text{cat}(\text{app})}$) and

the bimolecular rate constants (or catalytic efficiency constants, k_{cat}/K_m) for the oxidants at fixed NADPH concentration are given in Table 2. The quinone-dependent enzymatic NADPH oxidation is accompanied by the superoxide dismutase (SOD)-sensitive reduction of added cytochrome *c* (cyt *c*) (Table 2), which points to the single-electron character of quinone reduction, accompanied by redox cycling and O_2^\cdot formation. Both Michaelis-Menten and Lineweaver-Burk plots for the *PfFNR*-catalyzed reduction of the 3-benzoyl menadione PDO are shown in Figure S11. In both case, no deviation was observed from both types of plots.

Table 2. $E^1_{7\text{(calc.)}}$ values of PD derivatives and model quinones, their reduction rate constants in *PfFNR*-catalyzed reactions, relative cytochrome *c* reduction rates $v_i(\text{cyt } c)/v_i(\text{NADPH})$ and their sensitivity to 100 U/ml superoxide dismutase (SOD), and calculated $\log D$ values.

Compound	$E^1_{7\text{(calc.)}}$ (V)	Reactivity with <i>PfFNR</i>		$v_i(\text{cyt } c)/v_i(\text{NADPH})$ (%)	Inhibition by SOD (%)	$\log D$
		k_{cat} (s^{-1})	k_{cat}/K_m ($\text{M}^{-1}\text{s}^{-1}$)			
PD	-0.286±0.024	2.6	1.44×10^5	146	94	4.74
PD-bzol	-0.236±0.024	5.8	1.25×10^6	195	48	3.67
PDO	-0.185±0.019	4.3	9.96×10^5	195	46	4.11
1	-0.238±0.022	3.1	5.97×10^5	169	52	4.25
2	-0.273±0.023	12.3	4.95×10^5	180	19	2.92
3	-0.202±0.020	12	9.4×10^5	193	30	2.92
4	-0.183±0.017	10.2	8.21×10^5	164	75	3.17
5	-0.169±0.018	6.4	2.34×10^6	182	31	3.17
6	-0.238±0.022	13.3	8.3×10^5	186	28	3.38
7	-0.249±0.022	5.6	2.2×10^6	195	36	4.0
8	-0.144±0.018	12.7	1.8×10^6	192	19	4.28
5-OH-1,4-naphthoquinone 9^a	-0.093±0.017	35.7	1.1×10^6			1.82
5,8-(OH) ₂ -1,4-naphthoquinone 10^a	-0.097±0.016	25.0	4.1×10^5			2.17
1,4-Naphthoquinone 12^a	-0.139±0.017	16.9	3.1×10^5			1.5
2-CH ₃ -1,4-naphthoquinone 14^a	-0.209±0.021	26.5	2.6×10^5	190	50	1.89
(CH ₃) ₄ -1,4-benzoquinone 15^a	-0.286±0.024	33.1	7.2×10^4			2.61
2-OH-1,4-naphthoquinone 16^a	-0.391±0.029	2.6	9.8×10^3			-0.7

^a: Reaction rate constants taken from Ref.¹³

One may note that the coupled cyt *c* reduction by high-potential PDO derivatives is less sensitive to SOD in

comparison with low-potential ones like PD (Table 2). This is because high potential semiquinones, being engaged in a

redox equilibrium with the O_2/O_2^- couple, will yield a lower amount of O_2^- as compared with low-potential semiquinones. Thus, the reduction of cyt *c* mediated by quinones with higher $E^{1/2}_{\text{calc.}}$ should be less sensitive to the action of SOD.⁵⁰

The reactivity of *PfFNR* towards model quinones ($\log k_{\text{cat}}/K_m$) exhibits linear dependence with their $E^{1/2}$.¹³ Interestingly, the reactivity of most 3-benz(o)ylmenadione derivatives is much higher than that of the model benzoquinone and NQs with similar $E^{1/2}_{\text{calc.}}$ values (Figure 3).

The nature of this phenomenon deserves further studies. One of the possible reasons may be the high lipophilicity of these 3-benz(o)ylmenadione derivatives ($\log D$), in most cases significantly exceeding that of model quinones (Table 1).

Indeed, the most solvent-accessible portion of the flavin ring system in *PfFNR*, *i.e.*, its dimethyl-benzene moiety as well its protein microenvironment, which includes residues Leu102, Tyr159, Val315 and Tyr315, possess a clear hydrophobic character.⁵¹

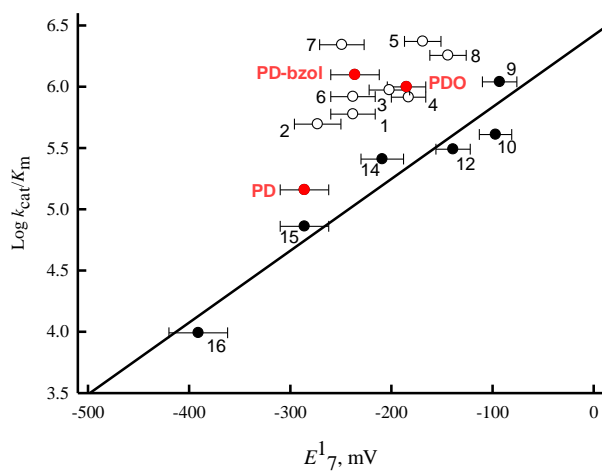


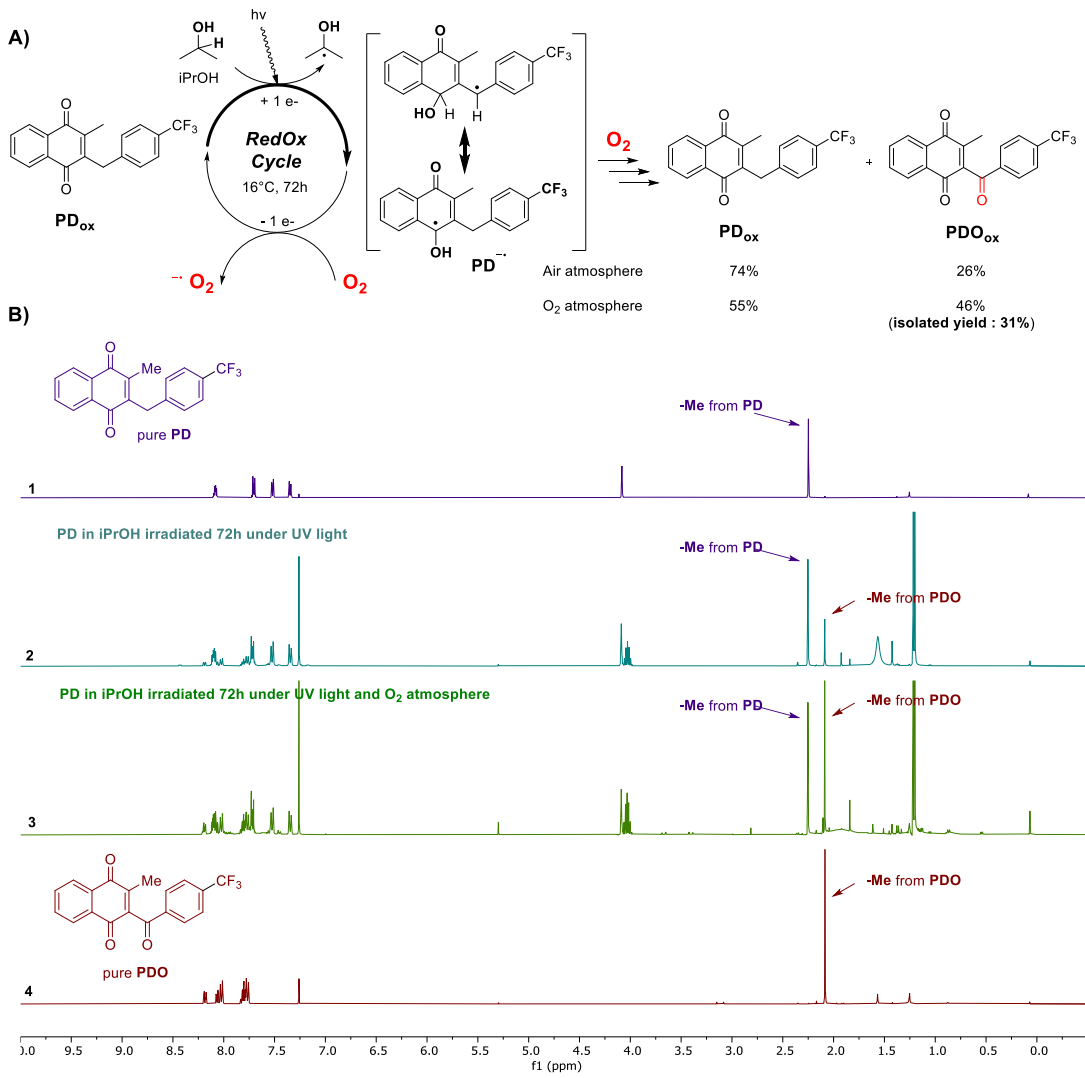
Figure 3. Relationship between the reactivity of *PfFNR*

towards PD, PD-bzol, PDO, PDO derivatives **1-8**, and model quinones **9-16**, and their $E^{1/2}_{\text{calc.}}$ values. The numbers of compounds are taken from Table 2. The straight line represents the best linear fit of data related only to model quinones **9,10,12,14-16**.

Also, while FNRs are highly specific for the $\text{NADP}^+/\text{NADPH}$ couple, they are able to reduce a large variety of non-physiological electron acceptors, of biological, organic and inorganic nature. At variance with other plastidic-type FNRs, which display high-turnover numbers, *PfFNR* has a particularly low k_{cat} in the physiological reaction.¹⁴ This is mainly due to an impaired electron transfer from the reduced enzyme to the protein partner. Because neither the stability of the *PfFNR-PfFd* complex nor the K_m of the enzyme for *PfFd* are particularly hampered in comparison to other FNRs, a possible explanation could be the poor thermodynamic stabilization of FAD semiquinone observed in *PfFNR*,¹⁴ as compared to other plastidic FNRs. Interestingly, *PfFd* was previously shown to stimulate quinone reductase activity of *PfFNR* providing an alternative pathway of quinone reduction via reduced *PfFd*.¹³

Photo-catalyzed benzylic oxidation of PD to PDO

To gain a better understanding of the mechanism of benzylic oxidation of PD to PDO in the presence of oxygen we mimicked, with a simple system, the redox cycle responsible of this reaction. UV-photoreduction of quinones in 2-propanol (iPrOH, or isopropanol) is known to generate, among other species, semiquinone radicals.⁵²



C)

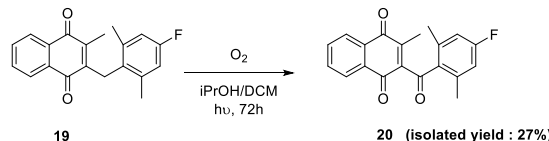


Figure 4. Photo-catalyzed oxidation of PD to PDO and of the bulky 3-benzylmenadione **19** to the corresponding 3-benzoylmenadione **20**. A) The reaction with PD was performed in iPrOH under two distinct conditions: in open air or in oxygen atmosphere. B) Overlay of the ¹H NMR spectra in the 0-10 ppm area of pure PD (spectrum 1), reaction mixtures of PD after 72 h UV-photoirradiation at 350 nm in iPrOH: under air atmosphere (spectrum 2), or in O₂ atmosphere (spectrum 3); and pure 3-benzoylmenadione PDO (spectrum 4). C) Photooxidation of 3-benzylmenadione **19** to the 3-benzoylmenadione **20** in iPrOH/DCM mixture. PD^{•-} stands for one electron-reduced PD semiquinone species.

Upon UV irradiation, PD is photo-excited and the generated excited triplet state of the quinone is quenched by iPrOH (H atom donor) to form the anionic semiNQ radical. This gives the advantage to provide an artificial way to generate the targeted radical species, which is essential for the formation of the benzylic oxidation product, i.e. PDO from PD (Figure 4A). Under air atmosphere and after 72 h of irradiation at 350 nm we observed a significant conversion of PD to PDO (ratio 74/26) without any major side product (Figure 4B, ¹H NMR spectra 1 to 4). The same reaction performed under a positive pressure of oxygen led to an even better conversion of the starting PD to the oxidized PDO (ratio 55/45) and an isolated yield of 31%. These observations confirm that PD can be oxidized through the transient anionic semiNQ species in a cascade of reactions leading to the observed PDO. A putative mechanism is proposed in Scheme 2.

With this new methodology well established, we then applied it to obtain the bulky 3-benzoylmenadione **20**, which could not be easily obtained by other methods. This allowed us to determine if steric hindrance could be a limiting factor for benzylic photooxidation. A slight modification was however necessary, especially to solubilize the starting material by adding dichloromethane (DCM) as a co-solvent. We observed that starting 3-benzylmenadione **19** was totally consumed after 72 h irradiation, but with a significant amount of degradation products. The target product **20** was isolated with a modest yield of 27% (Figure 4C).

PfFNR catalyzes the benzylic oxidation of plasmodione

During long lasting redox cycling turnover of *PfFNR* in the presence of PD, NADPH and oxygen, we raised the question on the possibility of benzylic oxidation of PD to PD-bzol and/or PDO. To validate whether *PfFNR* indeed generates PDO during PD redox cycling, we analyzed by LC-ESI-MS a reaction mixture of PD and *PfFNR* subjected to redox cycling by repetitive addition of NADPH. As shown in Figure 5 we could clearly detect the formation of increasing amount of reduced PDO species, PDO_{red}, generated from PD, from 30 min to 2 h incubation with *PfFNR* (Figures 5A and 5B). However, this transformation was observed only when *PfFNR* was present (Figure S12). Noteworthy is the fact that these experiments are much longer than the steady-state kinetic assays for reduction of PDO derivatives by *PfFNR* for 5-7 min. Importantly, no PDO formation was evidenced when as the catalyst *hGR* was present in the reaction (Figure S13).

Furthermore, we found that the presence of cyt *c* in the reaction significantly increased the rate of PDO_{red} formation. With its prosthetic heme group (Fe³⁺ center), it may additionally accept electrons from the reduced PD during redox cycling. By re-oxidizing the reduced PD species, cyt *c* accelerates *PfFNR*-catalyzed redox cycling, which is responsible for PD reduction to semiquinone. To further test whether *PfFNR* is able to generate PDO, we repeated the experiments using an NADPH-regenerating system based on glucose-6-phosphate dehydrogenase (G6PD), glucose-6-phosphate and NADP⁺, to redox-cycle PD continuously. This ensures the generation of a constant flux of NADPH, which more closely resembles physiological conditions compared to the repetitive addition of high concentrations of NADPH.

Additionally, to support metabolite identification during LC-MS PD was mixed in reaction with the isotopically-heavier PD (1/1), namely the ¹³C_{18/1}-PD, ¹³C-enriched either at all carbon atoms except at the CF₃ group (the 10 step-long

total synthesis was reported earlier³⁰) or the ¹³C_{*J*}-PD, which is ¹³C-enriched at carbon-1 position. During MS analysis these heavier ¹³C_{18/1}-PD versions generate, compared to the original compound, a mass shift corresponding to the degree of ¹³C-enrichment ($\Delta m/z = +18$ or $+1$), which increases the confidence of identification (Scheme S2).

When the PD / ¹³C-enriched PD (1/1) mixture was introduced in the redox cycling reaction with *PfFNR* fueled by the G6PD system, we evidenced both anticipated reduced PD metabolite species in reaction: the reduced PD-bzol, PD-bzol_{red} with a retention time (RT) of 40.5 min, which is believed to be the second metabolite during the formation of PDO (Scheme 2), was detected in addition to PDO_{red} (Figure 6). This finding directly confirms the formation of the active PD-bzol and PDO metabolites from PD during enzymatic cycling. Importantly, the same metabolites were detected for both ¹³C-enriched drugs as well as the non-enriched drug (Figure 6 and Scheme S2). Analysis of the chromatography peaks indicate that 5 to 10% of PD is already converted after 2 hours.

Interestingly, PD-bzol_{ox}, ($[M+H]^+ = 347.09$) but not PDO_{red} ($[M+H]^+ = 347.09$), loses 18 Da fragment during MS analysis (Figures 6 and S14) indicating that the fragment [M-18] can unambiguously be used to assign the presence of PD-bzol. Of note, the lack of fragment [M-18] in the MS spectrum of the species at RT = 41.9 min indicates that the identified compound with $m/z = 346.08$ is the diprotonated reduced PDO_{red} (exact mass = 346.08), and not the oxidized PD-bzol_{ox} (exact mass = 346.08), with which it shares an identical exact mass and RT (Figure S14). In the same vein, the use of PD / ¹³C_{18/1}-enriched PD mixture (1/1) in cycling reaction makes it possible to differentiate at RT = 41.9 min between the m/z pair PD-bzol_{ox}, ($[M+H]^+ = 347.09$) and PDO_{red} ($[M+H]^+ = 347.09$), although traces of the -18 Da fragment can be detected ($[M-18+H]^+ = 329.09$ for the PD-bzol - H₂O fragment and 330.10 for ¹³C_{*J*}-enriched PD-bzol - H₂O fragment) indicating that also the PD-bzol might be formed in minor amounts as well (Figure 6A and Scheme S2). While PD / ¹³C₁₈-enriched PD (1/1) mixture generates three m/z peaks at RT = 40.5 min, 331.09, 349.14, and 367.16 (Figure 6B and Scheme S2), LC-MS analysis allowed us to respectively assign the mass peaks to m/z PD-bzol_{red} - H₂O fragment ($[M-18+H]^+ = 331.09$), m/z PD-bzol_{red} ($[M+H]^+ = 349.10$) merged with m/z ¹³C₁₈-enriched PD-bzol_{red} - H₂O fragment ($[M-18+H]^+ = 349.15$), and m/z ¹³C₁₈-enriched PD-bzol_{red} ($[M+H]^+ = 367.16$). Because the loss of 18 Da could be attributed to both the loss of H₂O during MS analysis and the ¹³C₁₈ enrichment at 18 carbons (see the previously observed merged m/z peak at 349.14), we could conclude on the right assignment in the experiment using PD / ¹³C_{*J*}-enriched PD (1/1) mixture (Figure 6C and Scheme S2). In the MS spectra of the chromatography peak at RT = 40.5 min were observed the peaks at m/z 331.09, 332.09, 349.11, and 350.11, assigned to the four generated species: PD-bzol_{red} - H₂O fragment ($[M-18+H]^+ m/z = 331.09$), ¹³C_{*J*}-enriched PD-bzol_{red} - H₂O fragment ($[M-18+H]^+ m/z = 332.10$), PD-bzol_{red} ($[M+H]^+ m/z = 349.10$), and ¹³C_{*J*}-enriched PD-bzol_{red} ($[M+H]^+ m/z = 350.11$, and its Na⁺ adduct ($[M+Na]^+ m/z = 371.10$).

It is important to state here that the identified reduced PD metabolite species are not an artifact of the MS analysis. Not only they have different RTs compared to the controls, i.e. the pure oxidized PD-bzol_{ox} and PDO_{ox}, but also the controls were not reduced in the source of the MS spectrometer. In other words, the PD-bzol_{ox} and PDO_{ox} reduction is due to the *PfFNR*-catalyzed reaction. This important observation demonstrates that the major

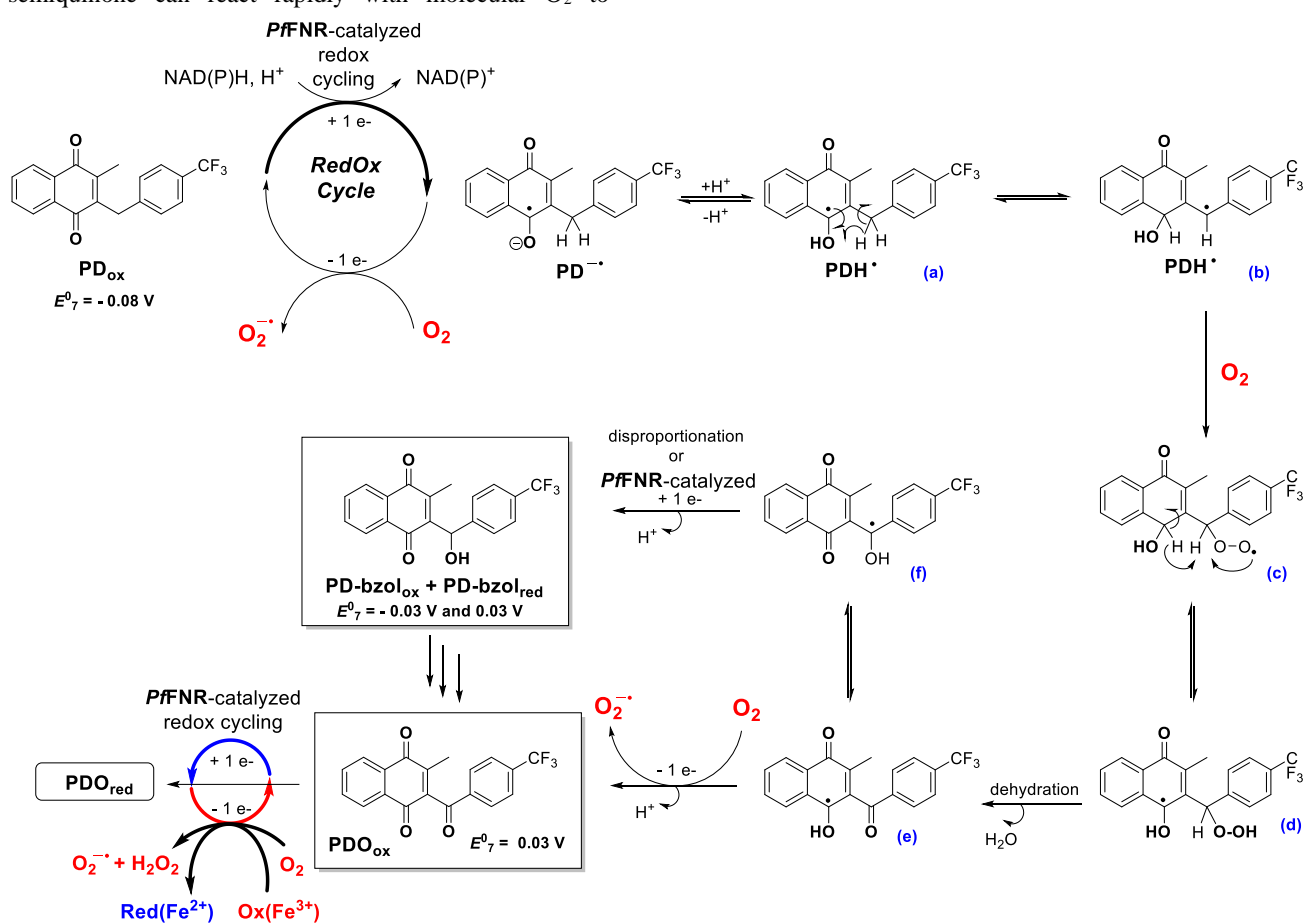
PD-bzol and PDO metabolites are predominantly present as reduced species in the presence of potent reductants like the NADPH-reduced *Pf*FNR. This situation is similar with that of methylene blue, which mainly exists as leucomethylene blue *in vivo*.

Proposed Mechanism of benzylic oxidation through redox cycling in the presence of oxygen

Scheme 2 displays the proposed mechanism of aerobic benzylic oxidation of PD, under redox cycling, to its corresponding benzhydrol (PD-bzol) and 3-benzoylmenadione (PDO) metabolites. Although less effective than with PDO ($E_{1/2} = -0.40$ V vs. KCl(3M)/Ag/AgCl in DMSO or $E^0 = 0.03$ V vs. NHE in water), PD can undergo an one-electron transfer to lead to semiNQ species PD^\bullet ($E_{1/2} = -0.58$ V vs. KCl(3M)/Ag/AgCl in DMSO or $E^0 = -0.08$ V vs. NHE in water) under NADPH-dependent reducing flavoenzyme catalysis (e.g., both GR, *Pf*FNR in this work).

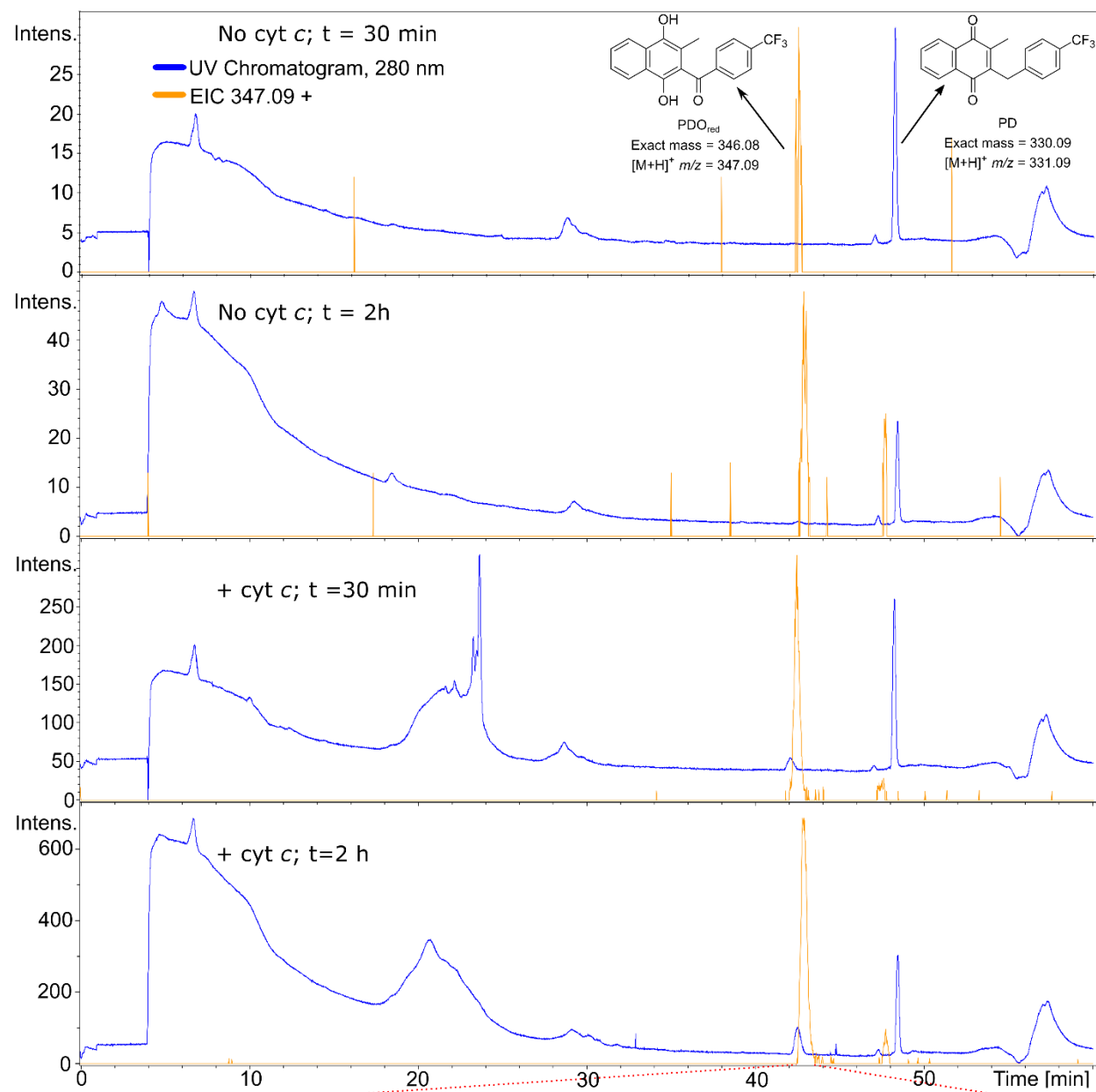
Flavoenzymes, e.g. *Pf*FNR in this work, act as biocatalysts that initiate the redox cycling cascade leading to formation of both PD-bzol and PDO. The one electron-reduced PD^\bullet semiquinone can react rapidly with molecular O_2 to

regenerate PD_{ox} and superoxide radicals O_2^\bullet . In aqueous solutions, the anionic PD^\bullet semiquinone undergoes protonation releasing a protonated PDH^\bullet (Scheme 2, species a). PDH^\bullet is then proposed to be submitted to tautomerization leading to the corresponding stable benzylic radical (Scheme 2, species b). The resulting carbon-centered radical is anticipated to be readily trapped by dioxygen to give the peroxy radical (Scheme 2, species c). Tautomerization (Scheme 2, species d) and subsequent dehydration leads to the PDO^{*} semiquinone species (Scheme 2, species e) that can rapidly react with O_2 to generate the PDO metabolite and O_2^\bullet . Interestingly, the one-electron reduced PDO semiquinone can also tautomerize into the stable C-centered benzylic alcohol radical (Scheme 2, species f). The radical intermediate f can then, either be reduced in *Pf*FNR redox cycling, or disproportionate into $\text{PD-bzol}_{\text{red}} + \text{PD-bzol}_{\text{ox}}$, respectively. The proposed mechanism pathway (Scheme 2), initiated by one electron-reduction of the NQ core thus relies on key benzylic radical (species b) and the C-centered radical (species f), for the generation of PDO and PD-bzol metabolites, via oxygen scavenging/tautomerization/disproportionation.



Scheme 2. Proposed mechanism of the aerobic *Pf*FNR-catalyzed benzylic oxidation of plasmodione, to the corresponding benzhydrol (PD-bzol) and 3-benzoylmenadione (PDO), via the formation of the semiquinone radical PD^\bullet , upon one electron-reduction, and its protonated radical species PDH^\bullet . PD^\bullet stands for one electron-reduced PD semiquinone species.

A)



B)

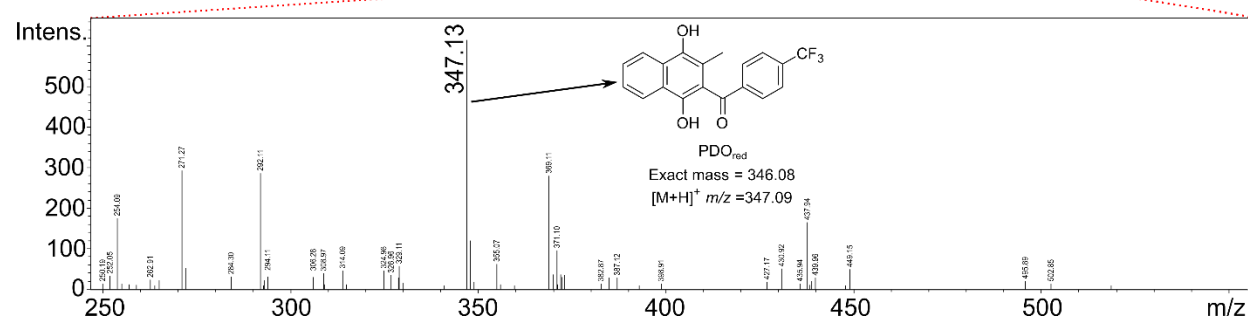


Figure 5. Redox cycling of PD by *Pf*FNR produces PDO_{red}. The reaction mixture consisting of 100 μM PD, and 2 μM *Pf*FNR was incubated with 200 μM NADPH and complemented every 15 min by another 200 μM NADPH. After 30 min and 2 h the reaction was analyzed by HPLC-MS. (A) Upper panels – 280 UV chromatograms overlaid with extracted ion chromatograms (EIC) of reaction mixtures after 30 min or 2 h, with or without addition of cyt c, evidenced the formation of PDO_{red}. (B) Bottom panel – MS spectrum of the chromatography peak corresponding to the mass of PDO_{red} at RT = 42 min, after 2 h of the reaction reaction in the presence of cyt c.

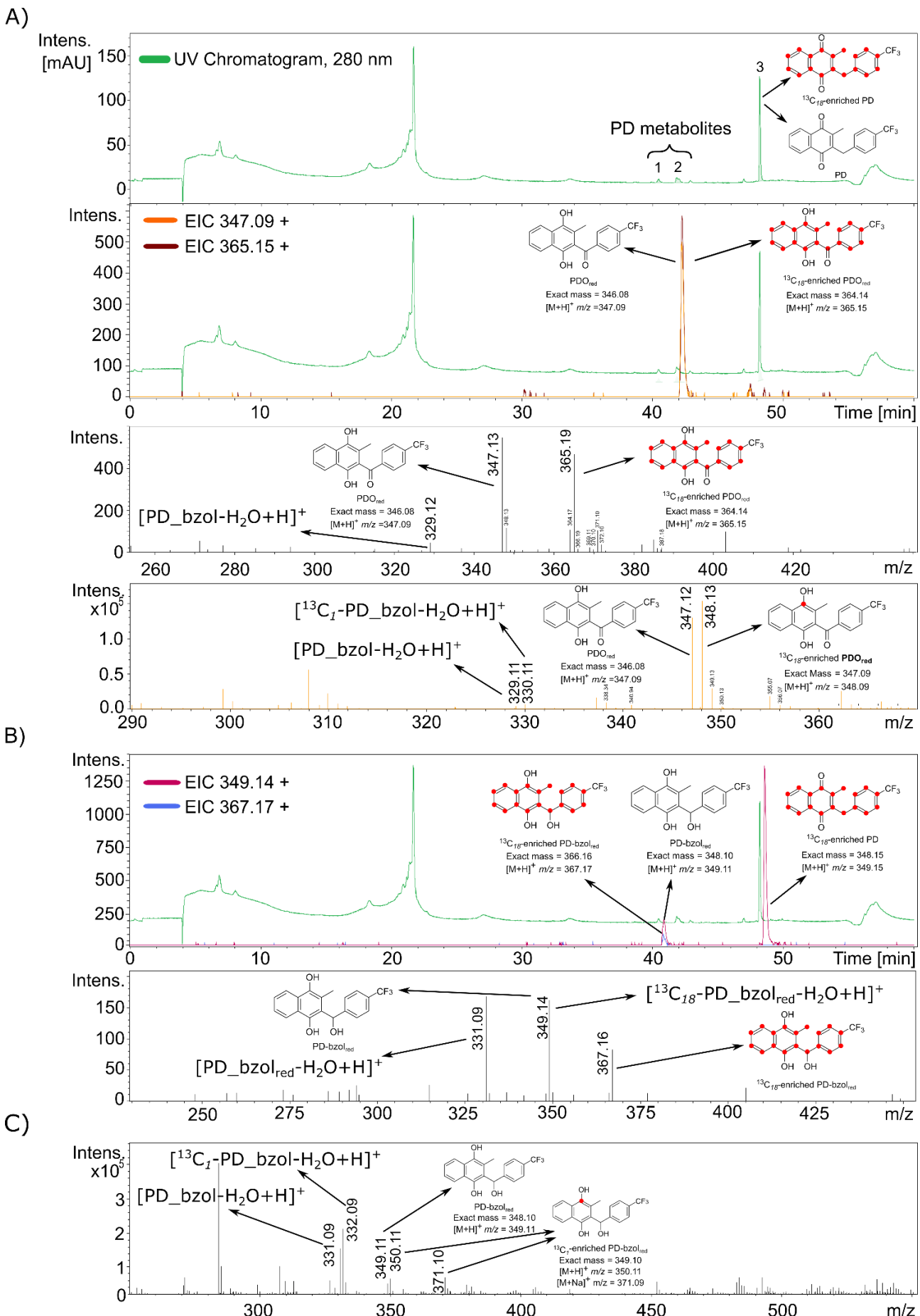


Figure 6. Redox cycling of PD catalyzed by *Pf*FNR produces reduced PD metabolites, oxidized at the benzylic position. A) Upper panel – 280 nm UV chromatogram of the reaction mixture: 25 μ M PD and 25 μ M of $^{13}\text{C}_{18}$ -enriched PD (1/1) were mixed and incubated with 2 μ M *Pf*FNR and NADPH. NADPH was generated by a G6PD recycling system from 1 mM glucose-6-phosphate and 20 μ M NADP $^+$. After 2 h the reaction mixture was analyzed by HPLC-MS. HPLC traces showed three peaks of interest: peaks 1 and 2 were assigned to PD metabolites ; peak 3 to PD. Traces 1 and 2 – PD metabolite traces, trace 3 – PD. Middle panel – extracted ion chromatograms (EIC)

corresponding to the masses of PDO_{red} and ¹³C₁₈-enriched PDO_{red} (RT = 42 min). Lower panels – MS spectra corresponding to the chromatography peak at RT = 41.9 min from the redox cycling reaction with PD/¹³C₁₈-PD or PD/¹³C₁-PD. B) Extracted ion chromatogram of the reaction mixtures in A) for the masses corresponding to the PD-bzol_{red}, ¹³C₁₈-enriched PD-bzol_{red} species and ¹³C₁₈-enriched PD (RT = 40.5 min). Lower panel – MS spectrum of the chromatography peak at RT = 40.5 min. C) MS spectrum of the chromatography peak at RT = 40.5 min from a redox cycling reaction mixture as in A and B) with enriched ¹³C₁-PD instead of ¹³C₁₈-PD.

These two PD metabolites are essential in the antimalarial action of the parent PD, in particular because of their high redox cycling potential and likely generation in parasite and specifically apicoplast where *PfFNR* is located. The mechanism and the intrinsic level of redox cycling of quinones by various flavoenzymes, including *PfFNR*,¹³ has been investigated in Čenáš's laboratory and by other groups for many years. For instance, the intrinsic reactivity of *PfFNR* for redox cycling of menadione is by far much more important for *PfFNR* than for *PfGR* or *PfNDH2*.¹² The redox cycling of PD is thought to amplify the rate of formation of the semiquinone NQ[·], the key intermediate to activate oxygen allowing benzylic oxidation of PD to occur, hence generating both PD metabolites, PD-bzol and PDO, in effective amount. For many years investigations on PD mode of action were performed by using the model based on both recombinant human and *P. falciparum* GRs and hemoglobin to mimick the redox cycling of PDO occurring in pRBCs. Since several studies have shown that rings – a parasitic stage where both partners (GR, metHb) of the redox-cycling might not be the major proteins – are more sensitive to PD than trophozoites²². Also, the studies on the mode of action of PD in yeasts revealed that more relevant flavoenzymes from the mitochondrial electron transport could be more plausible protein targets involved in PD's MoA and explain the redox-cycling generating PDO from PD.^{32,33} In the present study *PfFNR* is shown to generate both PD-bzol and PDO from PD during redox-cycling. All these studies are aimed at demonstrating a chemical reactivity of PD/PDO, more than identifying the exact targets of PD in each parasitic stage. This last objective, which is challenging, will hopefully be reached through our PD-ABPP strategy³¹ in the future.

Plasmodione leads to an oxidizing effect on the apicoplast

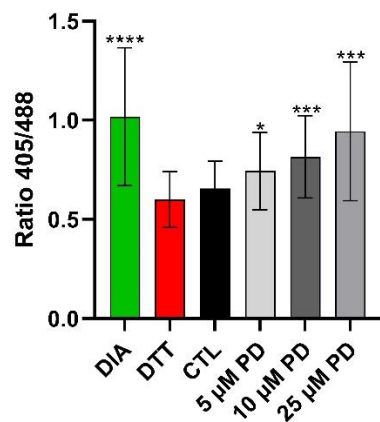
To investigate whether PD leads to a specific oxidizing effect on the apicoplast, we used the genetically encoded ratiometric redox-biosensor hGrx1-roGFP2 (human glutaredoxin 1 fused to oxidation-reduction sensitive green fluorescent protein) targeted to the apicoplast of *P. falciparum*. For this purpose, 3D7 *P. falciparum* parasites were episomally transfected with pARL1a^(+/-)-[ACP-roGFP2-hGrx1] (referred to herein as 3D7^[Api-roGFP2-hGrx1]).⁴¹ Confocal life-cell imaging was performed after PD treatment using different concentration and incubation times. After short (5 min) and mid-term (4 h) incubation, low micromolar concentrations of PD led to a significant oxidizing effect in the apicoplast (Figures 7A and 7B). The degree of oxidation (OxD) increased after short-term incubation with rising concentrations (5 μM PD, OxD = 34.8% ± 8.7%; 10 μM PD, OxD = 51.5% ± 9.6%; 25 μM PD, OxD = 69.3% ± 11.4%, given are mean values with SEM). Increase in OxD was even more pronounced after mid-term incubation with 39.1% ± 4.9% for 1 μM PD, 73.7% ± 5.0% for 5 μM PD, and 87.8% ± 5.8% OxD after incubation with 10 μM PD. Long-term (24 h) incubations with 50 nM or 100 nM PD, respectively, showed no significant effects (Figure 7C). OxD increased just slightly by 6.3% ± 8.2% and 9.9% ± 11.2%, respectively. However, long-term treatment with 1 μM and 5 μM PD lead to overoxidation of the parasites (data not shown). This

indicates that after 24 h, either the parasites have overcome the treatment (with lower PD concentrations, meaning much lower generated PDO amounts) or the redox balance has decompensated.

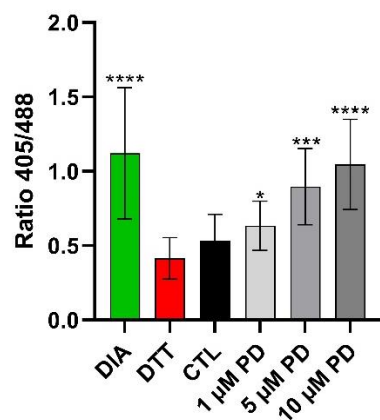
It is noteworthy to mention that the PD effect on the glutathione redox potential in the cytosol of intact living pRBCs²⁸ using the developed genetically encoded real-time fluorescent biosensor (hGrx1-roGFP2) was also analyzed after 5 min, 4 h, and 24 h of incubation.⁵³ However, in comparison, ratio changes were observed to influence the cytosolic redox potential only after 4 h incubation with 0.5 μM (10 x IC₅₀) to 5 μM (100 x IC₅₀) PD, and were not significant after 5 min incubation with up to 100 μM PD (2,000 x IC₅₀). The data obtained here demonstrates a decisively faster effect of PD on oxidizing redox potential in apicoplast than in cytosol of living cells.

Furthermore, previous observations made from the analysis of the morphology of synchronized parasite cultures during 46 h of incubation with PD have evidenced a short delay in the growth of PD-treated parasites, suggesting that the parasitic cycle was slightly retarded.³⁴ *PfFNR* is localized in the apicoplast. As compounds that kill *P. falciparum* by targeting the apicoplast usually exhibit a delayed death phenotype,¹⁸ we visualized a specific oxidizing effect on the apicoplast, shortly after PD internalization, by using the genetically encoded ratiometric redox-biosensor hGrx1-roGFP2 targeted to the apicoplast of *P. falciparum*. Therefore, we can conclude that *PfFNR*-catalyzed redox cycling of PD through the production of PD-bzol and PDO may interfere with the electron transfer system of apicoplast, which participates in the biosynthesis of isoprenoids crucial for parasite survival. However, *PfFNR* might not be the sole flavoenzyme responsible for PD bioactivation and the rapid killing of parasite. Other mitochondrial target, like NDH and SDH,^{32,33} might redox cycle PD metabolites once generated from PD in living cells. More studies will be necessary in the future to demonstrate that the observed slight parasitic cycle retardation is consistent with an apicoplast target like *PfFNR*, or that the potent antiplasmoidal potency of PD might be associated with its redox cycling activity on *PfFNR* and other mitochondrial flavoenzyme targets like *PfSDH*. Both *PfFNR* and *PfFd* recently turned out to be both essential for parasite survival.¹⁷ As *PfFNR* is highly specific for NADPH, it is prone to reduce a large variety of non-physiological one-electron-acceptors in competition with *PfFd* as *PfFNR* substrates.

A 5 min Incubation



B 4 h Incubation



C 24 h Incubation

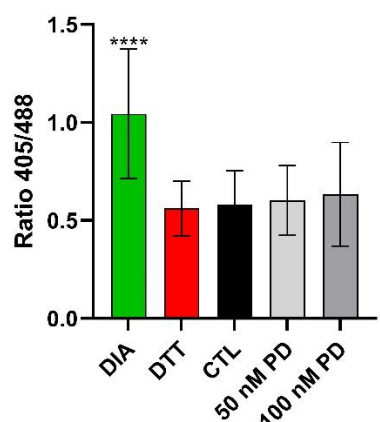


Figure 7. Effect of plasmodione incubation on the glutathione-dependent redox milieu of the apicoplast after short-term (A), mid-term (B), or long-term (C) incubation. DIA, DTT and CTL stand for diamide, dithiothreitol and control, respectively. (A) Shown are the 405nm/488nm fluorescence ratio after short-term (5 min) drug exposure experiments. 3D7^[Api-roGFP2-hGrx1] *P. falciparum* parasites were treated with 5 μM, 10 μM, or 25 μM PD for 5 min. (B) Shown are the 405nm/488nm fluorescence ratio after mid-term (4 h) drug exposure experiments. 3D7^[Api-roGFP2-hGrx1] *P. falciparum* parasites were treated with 1 μM, 5 μM, or 10 μM PD for 4 h. (C) Shown are the 405nm/488nm fluorescence ratio after long-term (24 h) drug exposure experiments. 3D7^[Api-roGFP2-hGrx1] *P. falciparum* parasites were treated with 50 nM or 100 nM PD for 24 h. Asterisks indicate significant differences, *p<0.05, **p<0.01, ***p<0.001, ****p<0.0001. Significance was calculated using GraphPadPrim8. Effects were tested in three independent experiments via CLSM, 10 parasites each were evaluated.

Noteworthy is to mention here the structural similarity between atovaquone and PD, both being 1,4-naphthoquinones. However, we previously showed that i) both compounds do not have redox potential values in the same range, in accordance with the fact that atovaquone is not oxidant and prone to be reduced by the model GRs⁵⁴; ii) PD and its metabolites are not or are weak inhibitors of yeast complex III of the mitochondrial electron transport chain³², in contrast to atovaquone, which inhibits both yeast and *P. falciparum* bc1 complex of the mitochondrial electron transfer chain. In the case of the observed weak inhibition, e.g. by the 6-hydroxy-PD, the metabolite does not share the atovaquone binding site in the bc1 complex.³² Also, transgenic *P. falciparum* parasites rendered resistant to atovaquone by expressing the yeast dihydroorotate dehydrogenase remained sensitive towards PD.³⁴

CONCLUSION

The *Pf*FNR/*Pf*Fd couple has been proposed to be a promising target for novel antimalarial drugs, whose mechanism of action could be based on the inhibition of the enzyme, the destabilization of protein-protein interaction, or even the diversion of the electron flow away from the iron-sulfur protein.¹⁵ The latter strategy is particularly attractive, due to the mentioned low efficiency of *Pf*Fd in accepting electrons from the partner. Artificial electron-acceptor substrates of *Pf*FNR have been identified in different class of compounds, including chemicals that undergoes redox cycling in the presence of O₂,¹³ and here in this manuscript with the antimalarial early-lead PD. This observation is particularly relevant, since an attempt to sabotage the electron flow from *Pf*FNR to *Pf*Fd could indeed result, in addition to the diversion of electrons from their physiological route, to the disruption of the redox balance in the apicoplast through the rise of oxidative stress. In this work, the resulting ROS production in the apicoplast was indeed observed in transgenic parasites overexpressing the genetically encoded ratiometric redox-biosensor hGrx1-roGFP2 targeted to the apicoplast. Thus, more attention will be given in the future to the studies investigating the impact of PD effect on specific pathways expressed in the apicoplast from malaria parasites.

METHODS

Chemicals. PD and PD-bzol synthesis was previously described in Ref.^{21,30}, respectively. PDO and 3-benzoylmenadione analogues **1–8** were synthesized by a recently described Friedel-Crafts reaction variant.²⁹ The synthetic route (Scheme S1), the protocols, the chemical analysis, and NMR spectra of 3-benz(o)ylmenadione **19** and **20** are described in the supporting information. In Table 2, logD values of 3-benzoylmenadione analogues **1–8** and model NQ **9–18** were calculated with logD predictor, (<https://chemaxon.com>).

Enzymes. Recombinant *P. falciparum* ferredoxin:NADP⁺ oxidoreductase (*Pf*FNR) was prepared as previously described,¹⁴ and its concentration was determined spectrophotometrically according to $\epsilon_{454} = 10.0 \text{ mM}^{-1} \text{ cm}^{-1}$. Recombinant human glutathione reductase was purified according to reported protocol⁵⁵ and had a specific activity of 100.4 U/mg. Cytochrome *c* from bovine heart, bovine superoxide dismutase, glucose-6-phosphate dehydrogenase from *Leuconostoc mesenteroides*, NADPH, and other compounds were obtained from Sigma-Aldrich (St. Louis, MO, USA), and used as received unless specified. All kinetic experiments were carried out spectrophotometrically using a PerkinElmer Lambda 25 UV–VIS apparatus (PerkinElmer, Waltham, MA, USA) in 0.1 M phosphate-KOH buffer, pH 7.0, containing 1.0 mM EDTA, at 25 °C. The steady-state parameters of the reactions, the catalytic constants ($k_{\text{cat}(\text{app})}$) and the bimolecular rate constants (or catalytic efficiency constants, k_{cat}/K_m) for the oxidants at the fixed concentration of 100 μM NADPH, were obtained by fitting the kinetic data to a hyperbolic equation using SigmaPlot 2000, version 11.0 (SPSS Inc., Chicago, IL, USA), which correspond to the reciprocal intercepts and slopes of Lineweaver-Burk plots, $[E]_T/v_0$ vs. $1/[{\text{oxidant}}]$, respectively, where v_0 is the initial reaction rate, and $[E]_T$ is the total enzyme concentration. k_{cat} represents the number of molecules of NADPH oxidized by a single active center of the enzyme per second, under substrate saturating condition. The rates of *Pf*FNR-catalyzed NADPH oxidation in the presence of quinones were determined using the value $\epsilon_{340} = 6.2 \text{ mM}^{-1} \text{ cm}^{-1}$. These rates were corrected for the intrinsic NADPH-oxidase activity of the enzyme, determined as 0.12 s⁻¹. In separate experiments, in which 50 μM cyt *c* was included in the reaction mixture, its quinone-mediated reduction was measured using the value $\epsilon_{550} = 20 \text{ mM}^{-1} \text{ cm}^{-1}$. The rates of oxygen consumption during the reactions were monitored using a Clark electrode (Rank Brothers Ltd., Bottisham, UK), assuming that initial oxygen concentration is 250 μM. The bimolecular rate constants of ascorbate oxidation by quinones (k), expressed as $k = v_0/[\text{quinone}][\text{ascorbate}]$ (Ref.⁴⁸, and references therein) were calculated from the initial rates of O₂ consumption in the presence of 1.0 mM ascorbate and various concentrations of quinones. The statistical analysis was performed using Statistica, ver. 4.3 (Statsoft, Toronto, CA).

Electrochemistry. In DMSO: The redox potentials of the PD (1.59 mM), PD-bzol (1.40 mM) and PDO (1.39

mM) were also evaluated by using cyclic (CV) and square wave voltammetries (SWV) in DMSO.^{56–58} The experiments were carried out at room temperature in solutions containing 0.1 of M tetra-*n*-butylammonium hexafluorophosphate⁵⁹ with a Voltalab 50 potentiostat/galvanostat (Radiometer Analytical MDE15 polarographic stand, PST050 analytical voltammetry and CTV101 speed control unit) controlled by the Voltamaster 4 electrochemical software. A three-electrode cell (10 mL) composed of a glassy carbon disk (GC, $s = 0.07 \text{ cm}^2$) set into a Teflon rotating tube as a working electrode, a Pt wire as a counter electrode, and KCl(3 M)/Ag/AgCl reference electrode (+210 mV vs NHE) was used in this study.⁶⁰ Prior any measurement, the surface of the GC electrode was freshly polished with 0.3 μm aluminium oxide suspension (Escil) on a silicon carbide abrasive sheet of grit 800/2400 and then washed with water and dried with paper towel. The PD, PD-bzol or PDO solutions were vigorously stirred and purged with O₂-free (Sigma Oxiclear cartridge) argon for 15 minutes before the voltammetry experiment was initiated. The cell was then maintained under argon during the measurement. For the CV measurements, the voltage sweep rate was varied from 50 to 300 mV s⁻¹ and several cyclic voltammograms were recorded from +0.5 V to -2.2 V. Peak potentials were measured at a scan rate of 200 mV s⁻¹ unless otherwise indicated. Redox potentials were determined from oxidation and reduction potentials. The corresponding square-wave voltammetric parameters⁶¹ were used: pulse height (ΔE_p), 50 mV; pulse width (t_{step}), 50 ms; step potential (E_{step}), 5 mV, step amplitude, 1 mV; scan rate, 20 mV s⁻¹; start, +0.1 V, end, -2.0 V. In aqueous media: cyclic voltammograms were also recorded in aqueous solutions using a Parstat 2273 (PAR) potentiostat in 0.1 M K-phosphate pH 7.0, at 25 °C under anaerobic conditions, obtained by purging the solutions with Ar for 20 min. Glassy carbon (GC) working electrode (PAR, diameter 2.5 mm), Ag/AgCl/3.0 M KCl (+210 mV vs. NHE) reference electrode, and auxiliary Pt wire electrode (56 mm²) were used in a standard three-electrode device. The GC electrode was polished with a suspension of corundum abrasive and rinsed with deionized water. Subsequently, 2.0 μL of 5.0 mM compound solution in DMSO were applied on the surface of GC electrode and evaporated in vacuum. The midpoint potentials of PD derivatives (E_7^0) are equal to the half-sum of reduction and oxidation peaks in CVs, E_p^{red} and E_p^{ox} , respectively. The apparent rate constants of electrochemical reactions of adsorbed compounds (k_s) were calculated according to a reported method⁶² at potential scan rates of 0.005 – 1.0 V/s.

Photo-benzylic oxidation. Irradiation experiments for photo-benzylic oxidation of PD to PDO. In a tube was added 1 mmol of PD and 2.5 mL of 2-propanol. The mixture was stirred and bubbled with oxygen for 30 min. Then, under air atmosphere or a positive pressure of oxygen, the tube was placed in a ventilated shelf of a Rayonet photochemical reactor at 16 °C and irradiated at 350 nm for 72 h. The solvent was removed under reduced pressure and the reaction crude was directly analyzed by NMR spectroscopy. Ratio between

PD and PDO were calculated by integrating the -CH₃ (Me) proton signals of PD and PDO (Figure 4B).

The crude product of the assay conducted in an oxygen atmosphere assay was purified by silica gel chromatography using toluene as eluent to afford the isolated PDO with 31% yield: ¹H NMR (400 MHz, CDCl₃) δ 8.23 - 8.13 (m, 1H), 8.10 - 8.04 (m, 1H), 7.91 - 7.65 (m, 4H), 2.09 (s, 3H). Analytical data are in agreement with those previously described.²¹

Plasmodione redox cycling with PfFNR. To catalyze redox cycling of PD and/or ¹³C-enriched PD by PfFNR or hGR, 50 μM of PD was mixed with 200 μM NADPH in a total volume of 200 μL and final DMSO concentration of 10 % in 47 mM PBS buffer. In case the reaction was sped up by cyt c, 25 μM of the hemoprotein was added. The reaction was started by addition of 2 μM of PfFNR or hGR and sustained by subsequent addition of 200 μM of NADPH (in 4 μL) every 15 min for 2 h. Reactions were incubated in glass tubes and 24 °C for the time of redox cycling.

For G6PD-sustained redox cycling 20 μM NADP⁺ and 10 mM glucose-6-phosphate were added instead of NADPH. The reaction was started by addition of G6PD (10 U/ml) and collected after 2 h 15 min incubation at 24 - 37 °C. Collected samples (from NADPH and G6PD cycling) were diluted with DMSO to a 30 % solvent concentration.

LC/MS analyses were performed using an Agilent 1100 series LC coupled to a MicroTOF-Q (Bruker Daltonics, Bremen, Germany). hGR cycling reaction with G6PD was analyzed with the same LC system coupled to maXis II Q-TOF mass spectrometer (Bruker). The mass spectrometer operated with a capillary voltage of 4,500 V in positive mode. Acquisitions were performed on the mass range *m/z* 200-1850. Calibration was performed using the singly charged ions produced by a solution of Tune mix (G1969-85000, Agilent, U.S.A.). Compounds were separated on a Xbridge Peptide BEH C18 column (300 Å, 3.5 μm, 2.1 mm X 250 mm) column. The gradient was generated at a flow rate of 250 μL/min, at 60 °C by mixing two mobile phases. Phase A consisted of 0.1 % trifluoroacetic acid (TFA) in water and phase B of 0.08 % TFA in ACN. Phase B was increased from 5 to 85% in 45 min. Data analysis was performed by using Compass DataAnalysis 4.3 (Bruker Daltonics).

P. falciparum cell culture. 3D7^[Api-roGFP2-hGrx1] *P. falciparum* parasites were cultured with slight modifications according to the reported protocol.⁶³ Parasites were cultured in RPMI medium (RPMI 1640 medium supplemented with 2.1 mM L-glutamine, 25 mM Hepes, 0.5% Albumax, 0.2 mM hypoxanthine, 9 mM glucose, and 22 μg/ml gentamycin) at 3.3% hematocrit, using A⁺ red blood cells (RBCs). 37 °C and a gaseous mixture consisting of 3% O₂, 3% CO₂, and 94% N₂ were used for culture conditions. Parasites were synchronized using 5% Sorbitol according to the reported procedure.⁶⁴

Confocal life cell imaging. Short-term PD incubations (5 min) were performed on *P. falciparum* trophozoite-stage treated with 5 μM, 10 μM, or 25 μM PD. Mid-term (4 h) incubations were performed on young

trophozoite-stage parasites with 1 μM, 5 μM, or 10 μM PD. For long-term (24 h) incubations, young ring-stage parasites were treated with 50 nM, 100 nM, 1 μM or 5 μM PD, respectively. For controls mock-treated parasites (0.2 – 0.5% DMSO) were used, as well as fully oxidized (0.2%-0.5% DMSO + 1 mM DIA) and fully reduced parasites (0.2%-0.5% DMSO + 10 mM DTT). The incubation times for DMSO treatment matched the different PD incubation times; the DIA and DTT incubation time was 5 min, respectively. After 4 h and 24 h incubations, free cysteines were blocked with 2 mM NEM for 15 min. Trophozoite-stage parasites were magnetically enriched.⁶⁵ For short-term drug exposure experiments trophozoite-stage parasites were magnetically enriched first and then incubated with 5 μM, 10 μM or 25 μM PD for 5 min. Measurements were performed without NEM-blocking. Parasites were diluted in a pre-warmed Ringers' solution and seeded on poly-L-lysine coated μ-slides VI (Ibidi, Martinsried, Germany). Life-cell imaging was performed as described⁴¹ at a Leica confocal system TCS SP5 inverted microscope equipped with the objective (HCX PL APO 63.0 x 1.30 GLYC 37°C UV) and a 37°C temperature chamber.⁴¹ Argon laser power was set to 20%, the smart Gain was set to 222.0 V and the smart offset was 12.3%. Fully reduced (10 mM DTT) and fully oxidized (1 mM DIA) parasites were used to calibrate the microscope. Data was analyzed using Leica LAS AF software. The degree of Oxidation (OxD) was calculated as follows:

$$\text{OxD} = \frac{\text{R-R}_{\text{red}}}{\frac{\text{L}_{488\text{ox}}}{\text{L}_{488\text{red}}}(\text{R}_{\text{ox}}-\text{R})+(\text{R}-\text{R}_{\text{red}})}$$

where R represents the ratio of the fluorescence intensity measured at 405 nm and 488 nm ($\text{R} = \frac{405 \text{ nm}}{488 \text{ nm}}$); R_{red} and R_{ox} describes the ratio of the fluorescence intensities of fully reduced or fully oxidized parasites; L_{488ox} is the fluorescence intensity at 488 nm for fully oxidized parasites; L_{488red} is the fluorescence intensity at 488 nm for fully reduced parasites.⁶⁶ Graphs were plotted using GraphPadPrism8.

ASSOCIATED CONTENT

Supporting Information

Procedures and additional data: The methods for the synthesis and physico-chemical analyses used to study the investigated compounds, the NMR data of new compounds **19** and **20**, the LC-MS data of PD metabolites analysed are available in the Supporting Information. This material is available free of charge on the ACS Publications website at doi:

AUTHOR INFORMATION

Corresponding Author

* E-mail: elisabeth.davioud@unistra.fr (E.D.C.).

Author Contributions

[#] B.A. C., M. D., K.C. H. and M. L. ranked by alphabetical order contributed equally as first co-

authors to this article. M. D. and E.J. M. performed the synthesis of the derivatives **19** and **20**. M. L. and M. D. measured the *Pf*FNR kinetics in the presence of 3-benz(o)ylmenadiones. L. F. synthetized the ¹³C_{18/1}-enriched PD. B.A.C. carried out all metabolic studies with PD and ¹³C_{18/1}-enriched PD in *Pf*FNR assays and analyzed PD metabolites by LC-MS. N. Č. and E. D. C. supervised the project about *Pf*FNR kinetics. K. C. H. and K. B. designed the hGrx1-roGFP experiment in the parasite assays *in cellulo*. A. A. provided the recombinant *Pf*FNR protein and specifically contributed in writing his part on FNR/Fd couple in the apicoplast pathway. M. E., N. Č. and E. D.-C. analyzed the data and wrote the manuscript. All authors edited the manuscript.

Notes

The authors declare no competing financial interest.

ACKNOWLEDGMENTS

The article is dedicated to Professor Dr. Jonathan Vennerstrom's for his 65th birthday. This work was partly supported by the Laboratoire d'Excellence ParaFrap (grant LabEx ParaFrap ANR-11-LABX-0024 (E. D.-C.), the joint PHC Gilibert project between France and Lithuania (N. Č. and E. D.-C.; grant N° 42124UH), and the International Center for Frontier Research in Chemistry in Strasbourg for the salary of B.A.C for 1 month to complete this study (E. D.-C. and M. E., ic-FRC-Innovation 2018 project entitled FluoPlasmo). E. D.-C. and B.A. C. are indebted to LSMBO, IPHC, for opening the mass spectrometry platform for LC-MS analysis of benzylic oxidation products and to Nathan Trometer for his valuable help in acquiring electrochemical experimental data.

REFERENCES

- (1) Vannerstrom, J. L., and Eaton, J. W. (1988) Oxidants, oxidant drugs, and malaria. *J. Med. Chem.* 31, 1269-1277.
- (2) Henderson, G. B., Ulrich, P., Fairlamb, A. H., Rosenberg, I., Pereira, M., Sela, M., Cerami, A. (1988) "Subversive" substrates for the enzyme trypanothione disulfide reductase: alternative approach to chemotherapy of Chagas disease. *Proc. Natl. Acad. Sci. U S A* 85, 5374-5378.
- (3) Jockers-Scherübl, M. C., Schirmer, R. H., Krauth-Siegel, R. L. (1989) Trypanothione reductase from *Trypanosoma cruzi*. Catalytic properties of the enzyme and inhibition studies with trypanocidal compounds. *Eur. J. Biochem.* 180, 267-272.
- (4) Čenáš, N. K., Arscott, D., Williams, C. H. Jr, Blanchard, J. S. (1994) Mechanism of reduction of quinones by *Trypanosoma congoense* trypanothione reductase. *Biochemistry* 33, 2509-2515.
- (5) Belorgey, D., Lanfranchi, D. A., Davioud-Charvet, E. (2013) 1,4-Naphthoquinones and others NADPH-dependent glutathione reductase-catalyzed redox cyclers as antimalarial agents. *Curr. Pharm. Des.* 19, 2512-2528.
- (6) Blumenstiel, K., Schöneck, R., Yardley, V., Croft, S. L., Krauth-Siegel, R. L. (1999) Nitrofuran drugs as common subversive substrates of *Trypanosoma cruzi* lipoamide dehydrogenase and trypanothione reductase. *Biochem Pharmacol.* 58, 1791-1799.
- (7) Salmon-Chemin, L., Lemaire, A., De Freitas, S., Deprez, B., Sergheraert, C., Davioud-Charvet, E. (2000) Parallel synthesis of a library of 1,4-naphthoquinones and automated screening of potential inhibitors of trypanothione reductase from *Trypanosoma cruzi*. *Bioorg. Med. Chem. Lett.* 10, 631-635.
- (8) Salmon-Chemin, L., Buisine, E., Yardley, V., Kohler, S., Debreu, M.A., Landry, V., Sergheraert, C., Croft, S. L., Krauth-Siegel, L. R., Davioud-Charvet, E. (2001) 2- and 3-substituted-1,4-naphthoquinone derivatives as subversive substrates of trypanothione reductase and lipoamide dehydrogenase from *Trypanosoma cruzi*: synthesis and correlation between redox cycling activities and *in vitro* cytotoxicity. *J. Med. Chem.* 44, 548-565.
- (9) Biot, C., Bauer, H., Schirmer, R. H. H. Davioud-Charvet, E. (2004) 5-Substituted tetrazoles as bioisosters of carboxylic acids. Bioisosterism and mechanistic studies on glutathione reductase inhibitors as antimalarials. *J. Med. Chem.* 47, 5972-5983.
- (10) Buchholz, K., Schirmer, R. H., Eubel, J. K., Akoachere, M. B., Dandekar, T., Becker, K., Gromer, S. (2008) Interactions of methylene blue with human disulfide reductases and their orthologues from *Plasmodium falciparum*. *Antimicrob Agents Chemother.* 52, 183-191.
- (11) Grellier, P., Marozienė, A., Nivinskas, H., Šarlauskas, J., Aliverti, A., Čenáš, N. (2010) Antiplasmodial activity of quinones: roles of aziridinyl substituents and the inhibition of *Plasmodium falciparum* glutathione reductase. *Arch Biochem Biophys.* 494, 32-39.
- (12) Marozienė, A., Lesanavičius, M., Davioud-Charvet, E., Aliverti, A., Grellier, P., Šarlauskas, J., Čenáš, N. (2019) Antiplasmodial Activity of Nitroaromatic Compounds: Correlation with Their Reduction Potential and Inhibitory Action on *Plasmodium falciparum* Glutathione Reductase. *Molecules* 24(24), 4509.
- (13) Lesanavičius, M., Aliverti, A., Šarlauskas J., Čenáš N. (2020) Reactions of *Plasmodium falciparum* Ferredoxin:NADP⁺ Oxidoreductase with Redox Cycling Xenobiotics: A Mechanistic Study. *Int. J. Mol. Sci.* 21(9), 3234.
- (14) Balconi, E., Pennati, A., Crobu, D., Pandini, V., Cerutti, R., Zanetti, G., Aliverti, A. (2009) The Ferredoxin-NADP⁺ Reductase/Ferredoxin Electron Transfer System of *Plasmodium falciparum*. *FEBS J.* 276, 3825-3836.
- (15) Seeber, F., Aliverti, A., Zanetti, G. (2005) The plant-type ferredoxin-NADP⁺ reductase/ferredoxin redox system as a possible drug target against apicomplexan human parasites. *Curr. Pharm. Design* 11, 3159-3172.
- (16) Aliverti, A., Pandini, V., Pennati, A., de Rosa, M., Zanetti, G. (2008) Structural and functional diversity

- of ferredoxin-NADP⁺ reductases. *Arch. Biochem. Biophys.* 474, 283–291.
- (17) Zhang, M., Wang, C., Otto, T. D., Oberstaller, J., Liao, X., Adapa, S. R., Udenze, K., Bronner, I. F., Casandra, D., Mayho, M., Brown, J., Li, S., Swanson, J., Rayner, J. C., Jiang, R. H. Y., Adams, J. H. (2018) Uncovering the essential genes of the human malaria parasite *Plasmodium falciparum* by saturation mutagenesis. *Science* 360(6388):eaap7847.
- (18) Fichera, M. E., and Roos, D. S. (1997) A plastid organelle as a drug target in apicomplexan parasites. *Nature* 390, 407–409.
- (19) Vennerstrom, J. L., Makler, M. T., Angerhofer, C. K., Williams, J. A. (1995) Antimalarial dyes revisited: xanthenes, azines, oxazines, and thiazines. *Antimicrob Agents Chemother.* 39, 2671–2677.
- (20) Färber, P. M., Arscott, L.D., Williams, C. H. Jr, Becker, K., Schirmer, R. H. (1998) Recombinant *Plasmodium falciparum* glutathione reductase is inhibited by the antimalarial dye methylene blue. *FEBS Lett.* 422, 311–314.
- (21) Müller, T., Johann, L., Jannack, B., Brückner, M., Lanfranchi, D. A., Bauer, H., Sanchez, C., Yardley, V., Deregnaucourt, C., Schrével, J., Lanzer, M., Schirmer, R. H., Davioud-Charvet, E. (2011) Glutathione reductase-catalyzed cascade of redox reactions to bioactivate potent antimalarial 1,4-naphthoquinones – A new strategy to combat malarial parasites. *J. Am. Chem. Soc.* 133, 11557–11571.
- (22) Ehrhardt, K., Deregnaucourt, C., Goetz, A.-A., Tzanova, T., Pradines, B., Adjalley, S. H., Blandin, S., Bagrel, D., Lanzer, M., Davioud-Charvet, E. (2016) The redox-cycler plasmodione is a fast acting antimalarial lead compound with pronounced activity against sexual and early asexual blood-stage parasites. *Antimicrob. Agents Chemother.* 60, 5146–5158.
- (23) Bauer, H., Fritz-Wolf, K., Winzer, A., Kühner, S., Little, S., Yardley, V., Vezin, H., Palfey, B., Schirmer, H., Davioud-Charvet E. (2006) A fluoro analogue of the menadione derivative 6-[2'-(3'-Methyl)-1',4'-naphthoquinolyl] hexa-noic acid is a suicide substrate of glutathione reductase. Crystal structure of the alkylated human enzyme. *J. Am. Chem. Soc.* 128, 10784–10794.
- (24) Blank, O., Davioud-Charvet, E., Elhabiri, M. (2012) Interactions of the antimalarial drug methylene blue with methemoglobin and heme targets in *Plasmodium falciparum*: A physico-biochemical study. *Antioxid. Redox Signal.* 17, 544–554.
- (25) Johann, L., Lanfranchi, D. A., Davioud-Charvet, E., Elhabiri, M. (2012) A Physico-Biochemical Study on Potential Redox-Cyclers as Antimalarial and Antischistosomal Drugs. *Curr. Pharm. Des.* 18, 3539–3566.
- (26) Elhabiri, M., Sidorov, P., Cesar-Rodo, E., Marcou, G., Lanfranchi, D. A., Davioud-Charvet, E., Horvath, D., Varnek, A. (2015) Electrochemical properties of substituted 2-methyl-1,4-naphthoquinones: redox behavior predictions. *Chem. Eur. J.*, 21, 3415–3424.
- (27) Sidorov P., Desta I., Chessé M., Horvath D., Marcou G., Varnek A., Davioud-Charvet E., Elhabiri M. (2016) Redox polypharmacology is an emerging strategy to combat malarial parasites. *ChemMedChem.* 11, 1339–1351.
- (28) Bielitz, M., Belorgey, D., Ehrhardt, K., Johann, L., Lanfranchi, D. A., Gallo, V., Schwarzer, E., Mohring, F., Jortzik, E., Williams, D. L., Becker, K., Arese, P., Elhabiri, M., Davioud-Charvet E. (2015) Antimalarial NADPH-consuming redox-cyclers as superior G6PD deficiency copycats. *Antioxid. Redox Signal.* 22, 1337–1351.
- (29) Cotos, L., Donzel, M., Elhabiri, M., Davioud-Charvet, E. (2020) A mild and versatile Friedel-Crafts methodology for the diversity-oriented synthesis of redox-active 3-benzoylmenadienes with tuneable redox potentials. *Chem. Eur. J.* 26, 3314–3325.
- (30) Feng L., Lanfranchi D. A., Cotos L., Cesar Rodo E., Ehrhardt K., Goetz, A.-A., Zimmerman H., Fenaille F., Blandin S., Davioud-Charvet E. (2018) Synthesis of plasmodione metabolites and ¹³C-enriched plasmodione as chemical tools for drug metabolism investigation. *Org. Biomol. Chem.* 16, 2647 - 2665.
- (31) Cichocki, B., Khobragade, V., Donzel, M., Cotos, L., Blandin, S., Schaeffer-Reiss, C., Cianfréani, S., Strub, J.-M., Elhabiri, M., Davioud-Charvet, E. (2021) A class of valuable (pro-)activity-based protein profiling probes: application to the redox-active antiplasmoidal agent, plasmodione. *JACS^{Au}*, in press. doi: 10.1021/jacsau.1c00025.
- (32) Mounkoro, P., Michel, T., Blandin, S., Golinelli-Cohen, M. P., Davioud-Charvet, E., Meunier, B. (2019) Investigating the mode of action of the redox-active antimalarial drug plasmodione using the yeast model. *Free Radic. Biol. Med.* 141, 269–278.
- (33) Mounkoro, P., Michel, T., Golinelli-Cohen, M.-P., Blandin, S., Davioud-Charvet, E., Meunier, B. (2021) A role for the succinate dehydrogenase in the mode of action of the redox-active antimalarial drug, plasmodione. *Free Radic Biol Med.* 162, 533–541.
- (34) Ehrhardt, K., Davioud-Charvet, E., Ke, H., Vaidya, A., Lanzer, M., Deponte, M. (2013) The mitochondrial electron transport chain is dispensable for the antimalarial activities of methylene blue and the lead 1,4-naphthoquinone 2-[4-(trifluoromethyl)benzyl]-menadione. *Antimicrob. Agents Chemother.* 57, 2114–2120.
- (35) Hanke, G., and Mulo, P. (2013) Plant type ferredoxins and ferredoxin-dependent metabolism. *Plant Cell Environ.* 36, 1071–1084.
- (36) Vollmer, M., Thomsen, N., Wiek, S., Seeber, F. (2001) Apicomplexan parasites possess distinct nuclear-encoded, but apicoplast-localized, plant-type ferredoxin-NADP⁺ reductase and ferredoxin. *J. Biol. Chem.* 276, 5483–5490.
- (37) Janouskovec, J., Horák, A., Oborník, M., Lukes, J., Keeling, P. J. (2010) A common red algal origin of the apicomplexan, dinoflagellate, and heterokont plastids. *Proc. Natl. Acad. Sci. U.S.A.* 107, 10949–10954.
- (38) Rohrich, R. C., Englert, N., Troschke, K., Reichenberg, A., Hintz, M., Seeber, F., Balconi, E., Aliverti, A., Zanetti, G., Kohler, U., Pfeiffer, M.,

- Beck, E., Jomaa, H., Wiesner, J. (2005) Reconstitution of an apicoplast-localised electron transfer pathway involved in the isoprenoid biosynthesis of *Plasmodium falciparum*. *FEBS Lett.* 579, 6433-6438.
- (39) Kimata-Ariga Y, Kurisu G, Kusunoki M, Aoki S, Sato D, Kobayashi T, Kita K, Horii T, Hase T (2007) *J Biochem* 141, 421-8.
- (40) Seeber, F., and Soldati-Favre, D. (2010) Metabolic pathways in the apicoplast of Apicomplexa. *Int. Rev. Cell Mol. Biol.* 281, 161–228.
- (41) Mohring, F., Rahbari, M., Zechmann, B., Rahlfs, S., Przyborski, J., Meyer, A. J., Becker, K. (2017) Determination of glutathione redox potential and pH value in subcellular compartments of malaria parasites. *Free Radical Biol. Med.* 104, 104-117.
- (42) O'Brien, P. J. (1991) Molecular mechanisms of quinone cytotoxicity. *Chem.-Biol. Interact.* 80, 1-41.
- (43) Marcus, R., and Sutin, N. (1985) Electron transfers in chemistry and biology. *Biochim. Biophys. Acta, Rev. Bioenerg.* 811, 265-322.
- (44) Nemeikaitė-Čenienė, A., Šarlauskas, J., Anusevičius, Ž., Nivinskas, H., Čenėnas, N. (2003) Cytotoxicity of RH1 and related aziridinylbenzoquinones: involvement of activation by NAD(P)H:quinone oxidoreductase (NQO1) and oxidative stress. *Arch. Biochem. Biophys.* 416, 110-118.
- (45) Bailey, S. I., and Ritchie I. M. (1985) A cyclic voltammetric study of the aqueous electrochemistry of some quinones. *Electrochim. Acta* 30, 3-12.
- (46) Patriarche, G. J., and Lingane, J. J. (1970) *Anal. Chim. Acta* 49, 241-246.
- (47) Wardman, P. (1989) Reduction potentials of one-electron couples involving free radicals in aqueous solution. *J. Phys. Chem. Ref. Data* 18, 1637-1755.
- (48) Marožienė, A., Nemeikaitė-Čenienė, A., Čenėnas, N. (2011) Studies of quinone cytotoxicity mechanisms: determination of quinone/semiquinone redox couple potential according to quinone-mediated ascorbate oxidation kinetics. *Chemija* 22, 162-166.
- (49) Hansch, C., Leo, A., Taft, R.W. (1991) A survey of Hammett substituent constants and resonance and field parameters. *Chem. Rev.* 91, 165-195.
- (50) Butler, J., and Hoey, B.M. (1986) The apparent inhibition of superoxide dismutase activity by quinones. *J. Free Radicals Biol. Med.* 2, 77-81.
- (51) Milani, M., Balconi, E., Aliverti, A., Mastrangelo, E., Seeber, F., Bolognesi, M., Zanetti, G. (2007) Ferredoxin-NADP⁺ reductase from *Plasmodium falciparum* undergoes NADP⁺-dependent dimerization and inactivation: functional and crystallographic analysis. *J. Mol. Biol.* 367, 501-513.
- (52) Görner, H. J. (2004) Photoreactions of 2-methyl-5-isopropyl-1,4-benzoquinone. *J. Photochem. Photobiol. A*, 165, 215-222.
- (53) Kasozi D., Mohring F., Rahlfs S., Meyer A. J., Becker K. (2013) Real-time imaging of the intracellular glutathione redox potential in the malaria parasite *Plasmodium falciparum*. *PLoS Pathog.* 9(12):e1003782.
- (54) Lanfranchi, D. A., Belorgey, D., Müller, T., Vezin, H., Bauer, H., Lanzer, M., Davioud-Charvet, E. (2012) Exploring the trifluoromenadione core as a template to design antimalarial redox-active agents interacting with glutathione reductase. *Org. Biomol. Chem.* 10, 4795-4806.
- (55) Nordhoff, A., Bücheler, U. S., Werner, D., Schirmer R. H. (1993) Folding of the four domains and dimerization are impaired by the Gly446-->Glu exchange in human glutathione reductase. Implications for the design of antiparasitic drugs. *Biochemistry* 32, 4060-4066.
- (56) Kolthoff, I. M. (1993) Theory and practice. In *Treatise on analytical chemistry: Thermal methods*, 2nd revised ed., Part 1, Vol. 13, John Wiley & Sons, New York, United States.
- (57) Ashnagar, A., Bruce, J. M., Dutton, P. L., Prince, R. C. (1984) One- and two-electron reduction of hydroxy-1,4-naphthoquinones and hydroxy-9,10-anthraquinones. The role of internal hydrogen bonding and its bearing on the redox chemistry of the anthracycline antitumour quinones. *Biochim. Biophys. Acta, Gen. Subj.* 801, 351-359.
- (58) Tsierkezos, N. G. (2007) Cyclic Voltammetric Studies of Ferrocene in Nonaqueous Solvents in the Temperature Range from 248.15 to 298.15 K. *J. Sol. Chem.* 36, 289-302.
- (59) Izutsu, K. *Electrochemistry in Nonaqueous Solutions*, Wiley-VCH, Weinheim, Germany, 2002.
- (60) Sawyer, D. T., Sobkowiak, A., Roberts, J. L. *Electrochemistry for Chemists*, Wiley New York, 1995.
- (61) Mirceski, V., Komorsky-Lovric, S., Lovric, M. *Square-Wave Voltammetry: Theory and Application*, Springer-Verlag Berlin Heidelberg, 2007.
- (62) Laviron E. (1979) General expression of the linear potential sweep voltammogram in the case of diffusionless electrochemical systems. *J. Electroanal. Chem.* 101, 19-28.
- (63) Trager, W., and Jensen, J. B. (1976) Human malaria parasites in continuous culture. *Science* 193, 673-675.
- (64) Lambros, C., and Vanderberg, J. P. (1979) Synchronization of *Plasmodium falciparum* erythrocytic stages in culture. *J. Parasitol.* 65, 418-420.
- (65) Ribaut, C., Berry, A., Chevalley, S., Reybier, K., Morlais, I., Parzy, D., Nepveu, F., Benoit-Vical, F., Valentin A. (2008) Concentration and purification by magnetic separation of the erythrocytic stages of all human Plasmodium species. *Malar J.* 7, 45. doi: 10.1186/1475-2875-7-45.
- (66) Schuh, A. K., Rahbari, M., Heimsch, K. C., Mohring, F., Gabryszewski, S. J., Weder, S., Buchholz, K., Rahlfs, S., Fidock, D. A., Becker, K. (2018) Stable integration and comparison of hGrx1-roGFP2 and sfroGFP2 redox probes in the malaria parasite *Plasmodium falciparum*. *ACS Infect. Dis.* 4, 1601-1612.

5 points à retenir de l'article

- 1) La *PfFNR* a été identifiée comme une cible potentielle de la plasmodione chez *P. falciparum*.
- 2) Les 3-benzoylménadiones sont de meilleurs substrats de *PfFNR* que la plasmodione.
- 3) L'oxydation benzylique de la plasmodione a pu être mimée par un système photochimique, impliquant d'abord une photoréduction de la **NQ** en semiquinone radical.
- 4) L'incubation de plasmodione avec la *PfFNR* permet de générer les métabolites proposés de cette molécule, les espèces réduites du benzhydrol et de la 3-benzoylménadione.
- 5) La plasmodione génère du stress oxydant dans l'apicoplaste du parasite, là où est localisée la *PfFNR*.

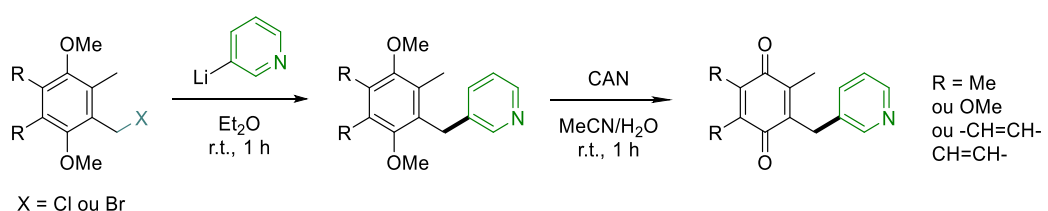
**Chapitre IV. Synthèse d'analogues hétéroaromatiques
de 3-benzylménadiones**

1. Synthèse de 1,4-quinones portant un motif méthyl-hétéroaromatique dans la littérature.

Suite à l'échec de la réaction photorédox pour l'insertion de motifs hétéroaromatiques, nous avons opté pour une nouvelle stratégie. La synthèse de quinones portant ce type de motifs a été très peu décrite dans la littérature et ces dernières ne sont pas généralisées à un large spectre de quinones ou de cycles hétéroaromatiques.

1.1. Synthèse de 2-nicotinyl-1,4-quinones.

En 1991, une équipe de Takeda Pharmaceutical (anciennement Takeda Chemical Industry) a publié la synthèse de nombreuses quinones portant un groupement 3-picolinyle.⁶¹ Parmi celles-ci, on peut citer la synthèse de la 3-(3-picolinyl)ménadione, l'une des molécules que nous avons ciblée. Cette équipe a inséré un groupement bromométhyl ou chlorométhyl en position 3 pour réaliser un couplage direct avec une 3-pyridine lithiée (**Schéma 26**).



Malheureusement, seul le rendement de couplage entre le lithien et le chlorure de 2,5-diméthoxy-3,4,6-benzyle a été communiqué par les auteurs (76% de rendement). Cette synthèse n'a cependant jamais été reproduite à ce jour. Habituellement, les organolithiens sont des intermédiaires utilisés pour introduire différents métaux (B, Sn, Si ...). Le couplage direct entre un organolithien et un dérivé halogéné a été très peu décrit notamment à cause de la très haute réactivité et de la non-stabilité de ces intermédiaires métalliques et nécessite d'être catalysé par un métal de transition.⁶² Durant la dernière décennie, bien que le couplage direct d'organolithien ait été remis au goût du jour par Feringa,⁶³ les exemples de couplage croisé entre un organolithien et un halogénure de benzyle restent très rares et s'accompagnent de faibles rendements.⁶⁴ Aucun autre exemple de couplage croisé direct entre une pyridine lithiée et un halogénure de benzyle n'a été publié à ce jour.

⁶¹ S. Ohkawa, S. Terao, Z.-I. Terashita, Y. Shibouta, K. Nishikawa, *J. Med. Chem.* **1991**, 34, 267-276.

⁶² S.-I. Murahashi, M. Yamamura, K.-I. Yanagisawa, N. Mita, K. Hondo, *J. Org. Chem.* **1979**, 44, 2408-2417.

⁶³ a) M. Giannerini, M. Fañanas-Mastral, B. L. Feringa, *Nat. Chem.* **2013**, 5, 667-672; b) V. Hornillos, M. Giannerini, C. Vila, M. Fañanas-Mastral, B. L. Feringa, *Org. Lett.* **2013**, 15, 5114-5117; c) E. B. Pinxterhuis, M. Giannerini, V. Hornillos, B. L. Feringa, *Nat. Commun.* **2016**, 7, 11698.

⁶⁴ Z. Jia, Q. Liu, X.-S. Peng, H. N. C. Wong, *Nat. Commun.* **2016**, 7, 10614.

1.2. Synthèse de la 3-(4-picolinyl)ménadione.

Il existe un seul exemple dans la littérature d'insertion d'un groupement 4-picolinyle sur une quinone. Cette dernière a été réalisée dans notre laboratoire. Dans le cadre des premières études sur la PD et ses analogues, la 3-(4-picolinyl)ménadione a été synthétisée (**Schéma 27**).⁴³

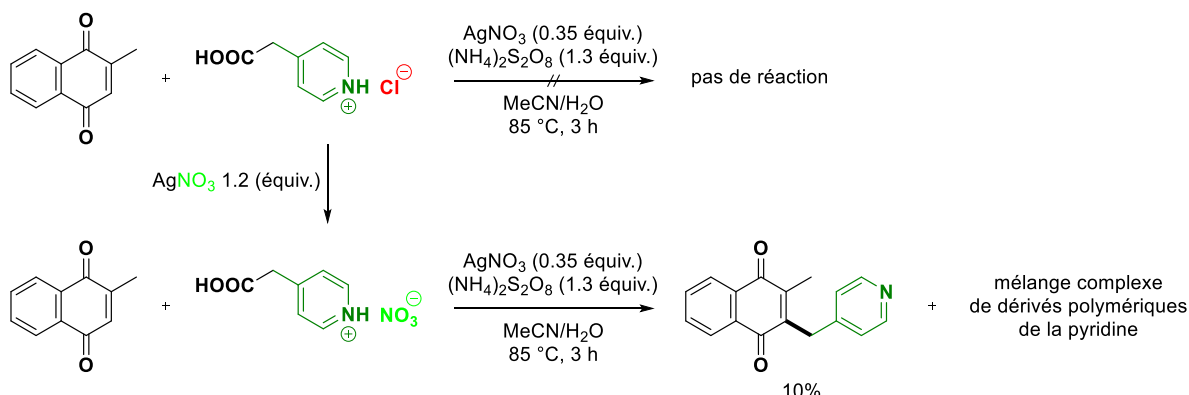


Schéma 27. Stratégie de synthèse de la 3-(4-picolinyl)ménadione par la réaction de Kochi-Anderson.

La réaction classique de Kochi-Anderson a tout d'abord été essayée mais fut un échec, probablement à cause d'un empoisonnement du nitrate d'argent par l'acide chlorhydrique, car en effet l'acide 4-picidylacétique hydrochlorique a été utilisé. Pour s'affranchir de ce problème, les auteurs ont réalisé l'échange d'anion entre le chlorure et un anion nitrate. Le meilleur rendement obtenu a été de 10%, et cela malgré diverses tentatives d'optimisation. Cela peut s'expliquer par des réactions concurrentes entre l'alkylation radicalaire sur la quinone et celle sur la pyridine de départ (via la réaction de Minisci) comme le montre la détection d'un mélange polymérique complexe dérivé de la pyridine comme produit principal de réaction.

1.3. Introduction de cycles hétéroaromatiques à 5 chaînons

Similairement à l'introduction de groupements picolinyles, les exemples d'insertion de cycles hétéroaromatiques à 5 chaînons, en lieu et place de pyridines, sont peu nombreux dans la littérature. Cependant il existe tout de même quelques exemples intéressants comme par exemple Carreño et al. qui ont décrit l'addition 1,2 d'acides boroniques dérivés de quinones protégées sur divers aldéhydes aromatiques.⁶⁵ Grâce à une catalyse au rhodium, une série de diarylméthanols ont pu être obtenus avec de bons rendements. L'introduction du 2-thiophenecarboxaldéhyde et du 1-méthylindole-2-carboxaldéhyde a ainsi été réalisée. Ces derniers peuvent ensuite être facilement déprotégés à l'aide

⁶⁵ M. Veguillas, J. Rojas-Martín, M. Ribagorda, M. C. Carreño, *Org. Biomol. Chem.* **2017**, *15*, 5386–5394.

du CAN pour obtenir les quinones correspondantes. A noter que les auteurs ont aussi développé une synthèse en *one pot* de ces quinones (**Schéma 28**).

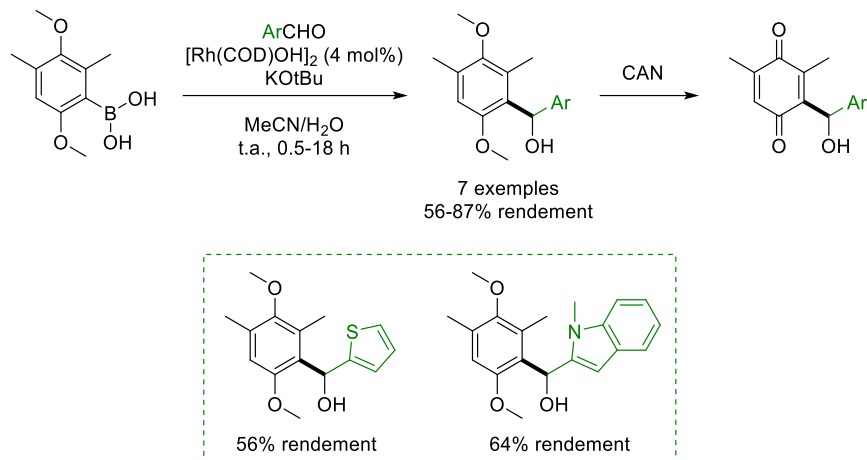


Schéma 28. Synthèse de diarylméthanols précurseurs de quinones fonctionnalisées.

Les diarylméthanols intermédiaires ou les quinones finales pourraient être soumises à une désoxygénéation afin d'obtenir les diarylméthanes désirés.⁶⁶

Enfin, récemment, pendant l'écriture de ce manuscrit, l'équipe de Jiang a décrit la synthèse de 2-aryl-3-benzylnaphthoquinones par une réaction cascade catalysée au cuivre à partir de divers toluènes et de 2-(3-arylpropioloyl)benzaldéhydes (**Schéma 29**).⁶⁷

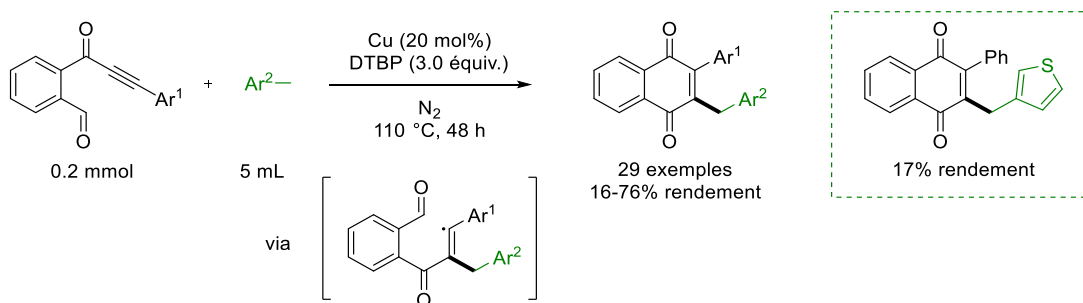


Schéma 29. Synthèse de 2-aryl-3-benzylménadiques par réaction cascade.

Divers toluènes ont pu être oxydés à l'aide de *di-tert-butyl peroxide* pour former le radical benzyllique qui va s'additionner sur l'alcyne en α de la cétone pour former un intermédiaire qui va permettre la cyclisation pour former la nouvelle 1-4-naphthoquinone benzylée. Cette réaction a pu être réalisée avec divers toluènes substitués mais aussi avec le 3-méthylthiophène. Cependant le produit désiré n'a été obtenu qu'avec un rendement de 17%.

⁶⁶ Exemples sélectionnés: a) D. N. Kursanov, Z. N. Parnes, N. M. Loim, *Synthesis*, **1974**, 9, 633-651; b) M. L. Yao, A. B. Pippin, G. W. Kabalka, *Tetrahedron Lett.* **2010**, 51, 853-855; c) S. Chandrasekar, I. Karthikeyan, G. Sekar, *RSC Adv.* **2015**, 5, 58790–58797.

⁶⁷ B. Zhu, H. Han, W.-K. Su, C. Yu, X. Jiang, *Adv. Synth. Catal.* **2021**, 363, 484 – 489.

Bien qu'élégante, cette réaction possède le défaut d'utiliser les analogues de toluène en très large excès (utilisé en tant que solvant), ce qui rend l'introduction de composés complexes impossible ou très onéreuse. De plus, la substitution de l'alcyne est limitée aux aryles ce qui rend impossible la synthèse de dérivés de la ménadione pour lesquels ce substituant devrait être un méthyle pour observer l'activité antiplasmodiale de la plasmodione.

2. Synthèse d'analogues hétéroaromatiques de la plasmodione

2.1. Objectifs

Actuellement, il n'existe pas dans la littérature de méthode conventionnelle et universelle de synthèse de 1,4-quinones reliées par un méthylène à un cycle hétéroaromatique. Au sein de notre laboratoire, seul un exemple d'analogue de la plasmodione portant un cycle pyridine a été synthétisé avec un très faible rendement.⁴³

Un des objectifs de cette thèse était donc de trouver un moyen efficace d'introduire des cycles hétéroaromatiques efficacement pour former une large variété d'analogues de 3-benzylménadione. Pour cela, nous devions trouver une méthode de synthèse applicable à un large spectre d'aryles hétéroaromatiques mais également de substituants variés pour accroître au maximum la librairie d'analogues de la **PD**, notamment les équivalents pyridine et pyrimidine trifluorométhylés (**Figure 17**).

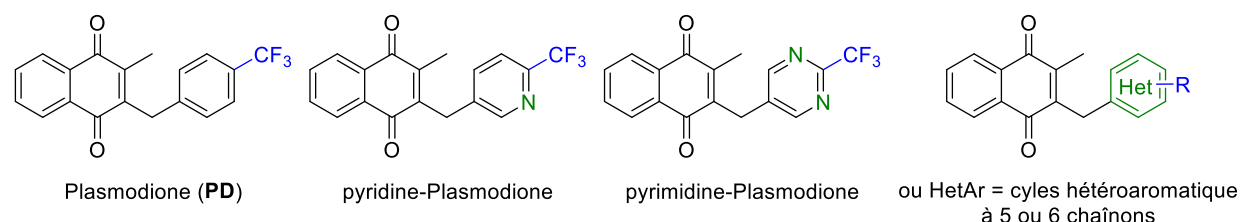


Figure 17. Analogues de PD visés par ce projet.

Comme nous l'avons vu précédemment, très peu d'exemples de telles quinones ont été décrits. Notamment, aucun des exemples recensés dans la littérature ne fait mention d'hétérocycles fonctionnalisés ou encore de pyrimidines.

Il a donc été nécessaire de mettre au point une synthèse efficace qui permette d'accéder à tous ces composés le plus aisément possible.

2.2. Stratégie de synthèse de di(hétéro)arylméthanes.

Etant donné l'échec de toute fonctionnalisation de la ménadione avec des substrats hétéroaromatiques par voie radicalaire, que ce soit par la réaction de Kochi-Anderson ou bien par benzylation photorédox, nous avons choisi de fonctionnaliser directement un dérivé de la ménadione protégé pour former un diarylméthane qui pourra ensuite être déprotégé avec CAN (**Schéma 30**).

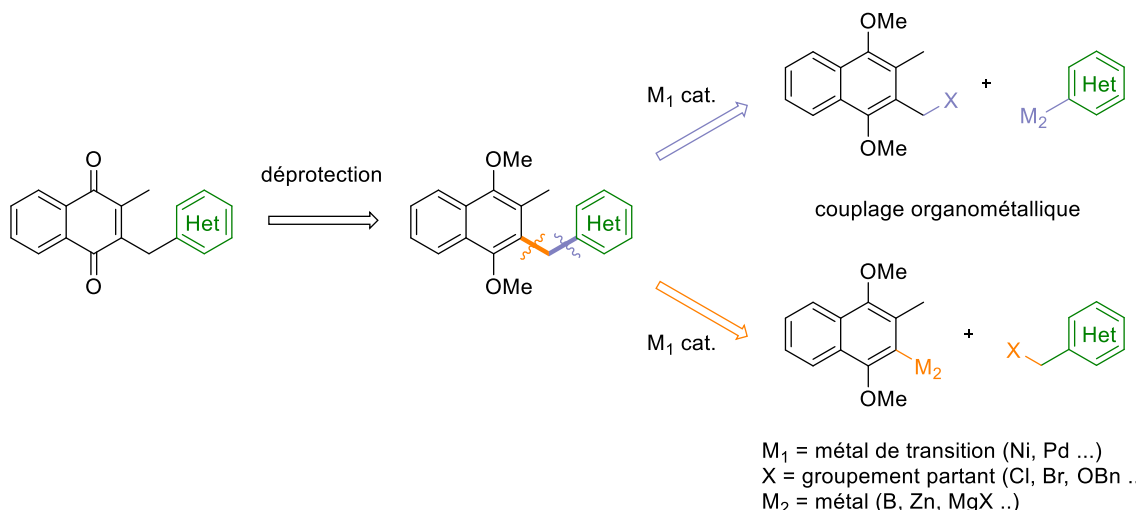


Schéma 30. Stratégie couplage/déprotection envisagée.

Une des méthodes les plus courantes pour accéder à des diarylméthanes est un couplage entre un cycle aromatique organométallique et un benzyle portant un groupement partant. La synthèse de diarylméthanes par ce type de couplages croisés organométalliques a été très largement explorée dans la littérature. Par exemple des couplages de type Suzuki-Miyaura ont été décrits entre des acides boroniques aromatiques et des halogénures de benzyles,⁶⁸ des acétates de benzyle,⁶⁹ des carbonates de benzyle⁷⁰ ou encore des phosphates de benzyle.⁷¹ Divers couplages catalysés au cuivre entre des réactifs de Grignard et des halogénures de benzyle⁷² ou des phosphates de benzyle⁷³ ont été décrit tout autant que les couplages de type Negishi⁷⁴ ou Stille⁷⁵ utilisant des organozinciques ou organostannanes comme intermédiaires organométalliques.

De notre côté, nous nous sommes particulièrement intéressés à un exemple décrit par l'équipe de Gueiffier,⁷⁶ dans lequel des halogénures de benzyles sont, par un couplage pallado-catalysé de Suzuki, couplés efficacement avec divers acides boroniques aromatiques et surtout hétéroaromatiques (**Schéma 31**).

⁶⁸ a) S. Langle, M. Abarbri, A. Duchêne, *Tetrahedron Lett.* **2003**, 44, 9255–9258; b) L. Chahen, H. Doucet, M. Santelli, *Synlett*, **2003**, 11, 1668–1672; c) S. M. Nobre, A. L. Monteiro, *Tetrahedron Lett.* **2004**, 45, 8225–8228.

⁶⁹ R. Kuwano, M. Yokogi, *Chem. Commun.* **2005**, 5899–5901.

⁷⁰ R. Kuwano, M. Yokogi, *Org. Lett.* **2005**, 7, 945–947.

⁷¹ M. McLaughlin, *Org. Lett.* **2005**, 7, 4875–4878.

⁷² Y.-Y. Ku, R. R. Patel, D. P. Sawick, *Tetrahedron Lett.* **1996**, 37, 1949–1952.

⁷³ C. C. Kofink, P. Knochel, *Org. Lett.* **2006**, 8, 4121–4124.

⁷⁴ a) M. Amatorea, C. Gosmini, *Chem. Commun.* **2008**, 5019–5021; b) R. B. Bedford, M. Huwea, M. C. Wilkinson, *Chem. Commun.* **2009**, 600–602.

⁷⁵ a) T. Z. Nichele, A. L. Monteiro, *Tetrahedron Lett.* **2007**, 48, 7472–7475; b) M. Ohsumi, R. Kuwano, *Chem. Lett.* **2008**, 37, 796–797.

⁷⁶ N. Henry, C. Enguehard-Gueiffier, I. Thery, A. Gueiffier, *Eur. J. Org. Chem.* **2008**, 4824–4827.

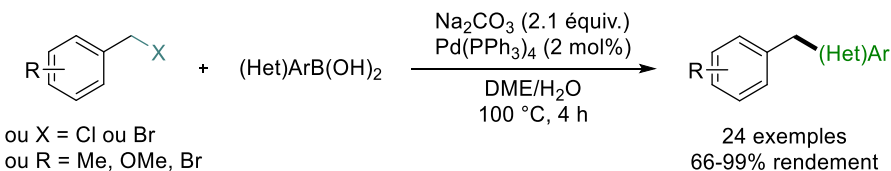


Schéma 31. Synthèse de diarylméthanes par Gueffier.

De manière intéressante, ces conditions permettent le couplage de divers chlorures de benzyle portant des groupements donneurs comme le groupe méthoxyle. Une grande variété d'acides boroniques aromatiques et hétéroatomiques sont également tolérés, incluant les groupements désirés 3-pyrimidinyles et 4-pyridine, ou bien encore un furane. Si le chlorure de benzyle ou l'acide phénylboronique porte un atome de brome comme substituant, le couplage benzyl-aryl est alors favorisé au détriment du couplage aryl-aryl, ce qui peut ouvrir la perspective de post-fonctionnalisations après le couplage, comme démontré par Gueffier lors de la double arylation monotope de chlorures de benzyle bromés avec de très bons rendements (**Schéma 32**).

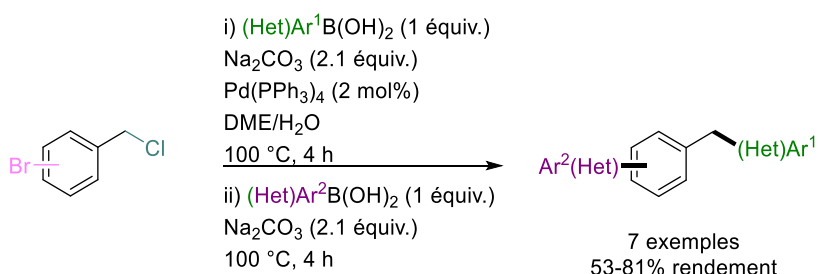


Schéma 32. Double arylation monotope de chlorure de benzyles par Gueffier

2.3. Application à la synthèse de dérivés hétéroatomatiques de la plasmodione.

Dans le but d'adapter le couplage décrit par Gueffier à la synthèse d'analogues hétéroatomatiques de la **PD**, nous avons voulu introduire un méthyle halogéné sur la ménadione ainsi que sur le 1,4-diméthoxy-2-methylnaphthalène. Bien que la plupart de ces molécules aient déjà été synthétisées par le passé, les protocoles décrits impliquaient l'utilisation d'acide chlorhydrique gazeux⁷⁷ ou bien d'acide bromhydrique en solution dans l'acide acétique⁷⁸ accompagné d'une source de formaldéhyde. HCl gazeux n'étant pas pratique à manipuler ou à générer *in situ*, nous avons décidé d'utiliser une solution aqueuse d'HCl concentrée à la place d'un gaz anhydre pour chlorométhyler le 1,4-diméthoxy-2-methylnaphthalène. Le produit attendu a été obtenu avec un très bon rendement. En substituant l'acide chlorhydrique par de l'acide bromhydrique aqueux, l'anologue bromé fut également synthétisé

⁷⁷ B. H. Lipshutz, S.-K. Kim, P. Mollard, K. L. Stevens, *Tetrahedron*, **1998**, 54, 1241-1253.

⁷⁸ G. Rotthier, D. Cappoen, Q. T. Nguyen, T. A. Dang Thi, V. Mathys, V. T. Nguyen, K. Huygen, L. Maes, P. Cosb, K. A. Tehrani, *Org. Biomol. Chem.* **2016**, 14, 2041–2051.

avec succès. Enfin les conditions utilisées se sont également avérées adaptées à l'halogènométhylation de la ménadione avec encore une fois de très bons rendements (**Schéma 33**).

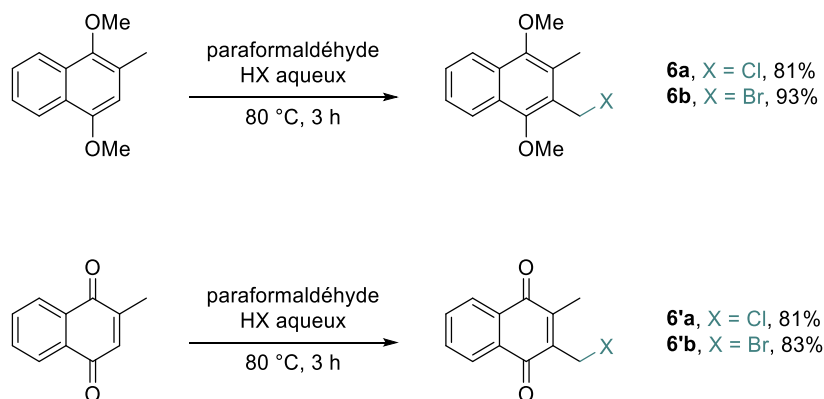


Schéma 33. Halogènométhylation du 2-méthyl-1,4-diméthoxynaphthalène et de la ménadione.

Une fois ces substrats préparés, nous avons désiré les engager dans un couplage pallado-catalysé pour tenter d'obtenir les produits de couplage correspondants. Pour cela, nous avons choisi comme acide boronique modèle l'acide 4-pyridinylboronique **7a**. Le produit attendu serait donc une ménadione portant un groupement 4-picolinyle en position 3. Ce substrat est à ce jour le seul qui ait été déjà synthétisé dans le laboratoire par la réaction de Kochi-Anderson mais avec un rendement de seulement 10%. Nous avons donc essayé d'engager chacun des produits précédemment synthétisés dans les mêmes conditions que celles décrites par Gueffier avec cependant une charge catalytique en Pd(0) un peu plus importante (5 mol% au lieu de 2 mol%) (**Schéma 34**).

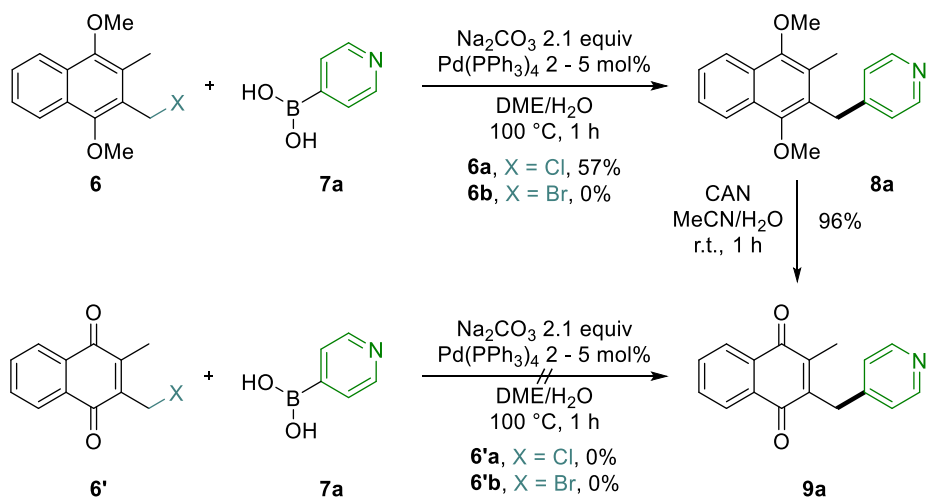


Schéma 34. Premiers essais de couplage benzyle-hétéroaryle.

Le diméthoxynaphthalène chloré **6a** est le seul à avoir réagi avec succès avec l'acide boronique correspondant pour donner le produit de couplage attendu avec un rendement encourageant de 57%. La réaction avec l'anologue bromé **6b** a quant à elle conduit à un mélange complexe ne comportant pas le produit de couplage désiré. Concernant les dérivés des ménadiques (**6'a-b**), ces derniers ont

entièrement été dégradés dans ces conditions de réactions. Ensuite, le diméthoxynaphthalène portant un groupement 4-picolinyle **8a** a pu être facilement déprotégé avec le CAN pour obtenir la quinone correspondante **9a** (**Schéma 34**).

Satisfaits de la compatibilité de ce couplage pour former des ménadiones, nous avons décidé de le tester pour insérer divers groupements 3-picolinyles fonctionnalisés nous intéressants (**Schéma 35**). L'introduction d'une 3-pyridine (**8b**) a été réalisée avec succès avec un rendement de 71%. Les analogues trifluorométhyle, halogénés et méthoxy ont également pu être couplé avec d'excellents rendements (**8c-8f**). De la même façon, des pyrimidines (**8g-8j**) et la quinoline (**8k**) se sont également révélés compatibles. Enfin, l'acide 2-furane-boronique a réagi quantitativement avec le chlorure de benzyle correspondant (**8l**). Tous ces adduits ont ensuite pu être déprotégés à l'aide du CAN pour obtenir les ménadiones fonctionnalisées (**9b-9l**).

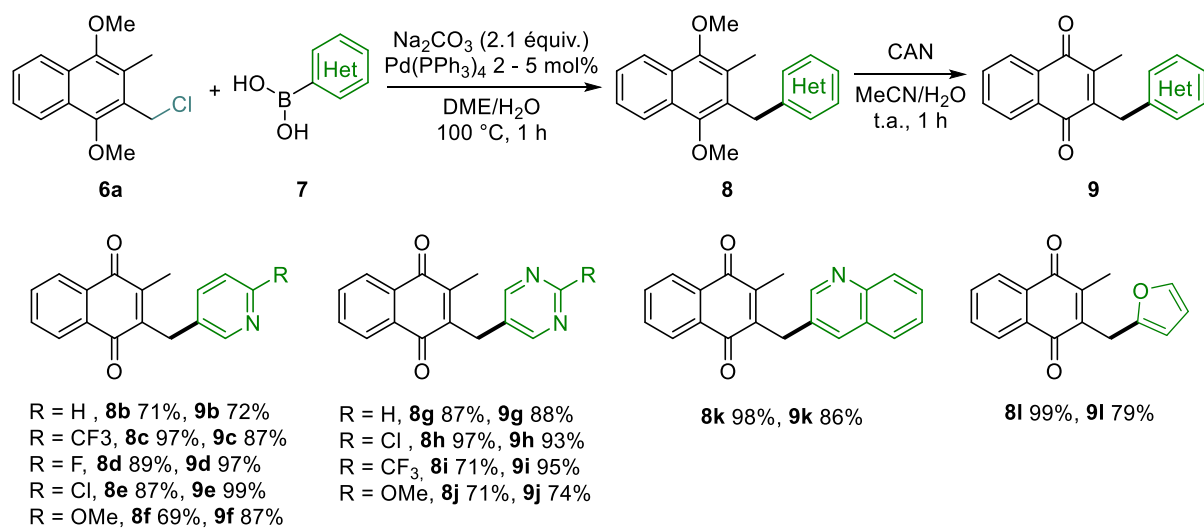


Schéma 35. Synthèse d'analogues hétéroaromatiques de la Plasmodione par couplage pallado-catalysé.

Il est également prévu au sein de l'équipe de développer de nouveaux exemples de telles ménadiques avec d'autres cycles hétéroaromatiques mais aussi en faisant varier la substitution du cycle aromatique de la quinone.

2.4. Post-fonctionnalisation des intermédiaires de couplage

Les produits de couplages, des naphtoquinones protégées par des groupements méthoxyles, offrent des opportunités de fonctionnaliser la nouvelle partie hétéroaromatique. En effet, les ménadiques sont en général très sensibles et ne peuvent être utilisées dans des milieux réducteurs ou basiques. Par exemple, nous avons pu ainsi introduire efficacement par substitution nucléophile de l'adduit 2-

chloropyrimidine **8h**, un atome de brome⁷⁹ ou bien un groupement nitrile⁸⁰ grâce à des procédures adaptées de la littérature (**Schéma 36**).

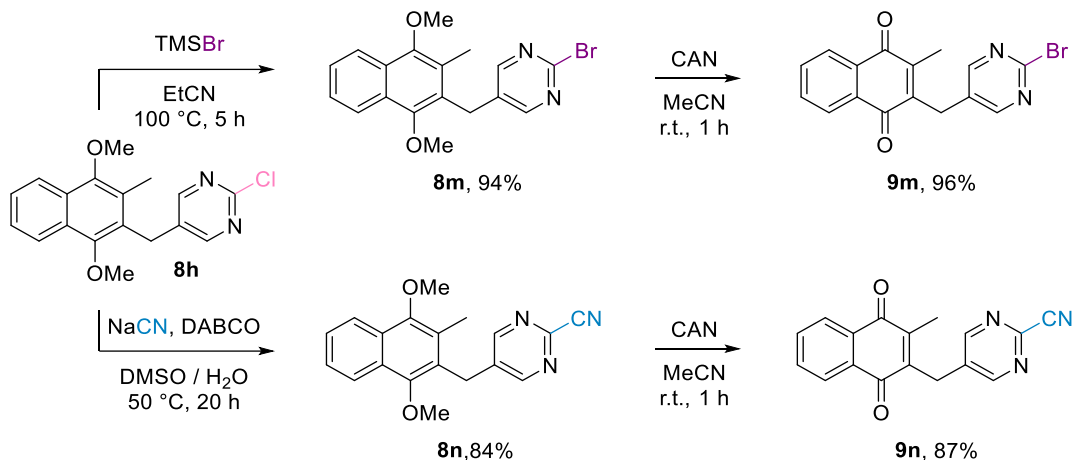


Schéma 36. Bromation et cyannation du dérivé 2-chloropyrimidine.

Nous nous sommes également intéressés à fonctionnaliser le dérivé 2-fluoropyridine **8d**. En effet, Hartwig a décrit comment fonctionnaliser efficacement ce type de composés par substitution nucléophile aromatique (S_NAr) avec de nombreux nucléophiles.⁸¹ Nous avons pu grâce à cette méthode, introduire notamment un groupement 3-oxétanol dans des conditions douces (Schéma 37). Les oxétanes sont des groupements fortement représentés dans la conception de molécules à visée thérapeutique. Par exemple, on peut citer le taxol avec son cycle oxétane qui confère à la molécule finale des propriétés physico-chimiques intéressantes comme par exemple une augmentation très significative de la solubilité dans l'eau.⁸²

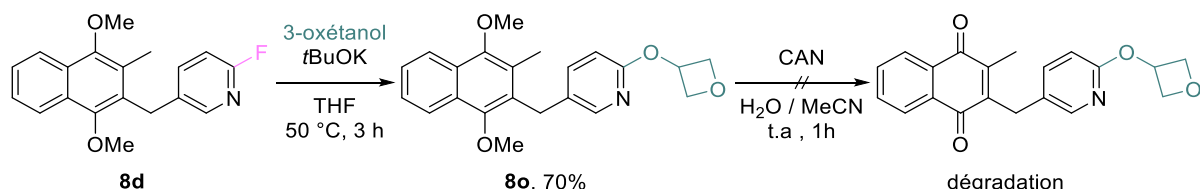


Schéma 37. Introduction d'un groupement 3-oxétane.

Malheureusement, la déprotection du substrat obtenu n'a pas mené à la quinone souhaitée mais à un produit de dégradation inconnu. Par manque de temps, nous n'avons pu optimiser cette étape ou introduire d'autres groupements. Cependant, cette réaction constitue une preuve de concept de modification de cet intermédiaire et sera explorée au sein de l'équipe à l'avenir.

⁷⁹ M. Schlosser, F. Cottet, *Eur. J. Org. Chem.* **2002**, 4181-4184.

⁸⁰ J. Šturala, S. Boháčová, J. Chudoba, R. Metelková, R. Cibulka, *J. Org. Chem.* **2015**, 80, 2676–2699.

⁸¹ P. S. Fier, J. F. Hartwig, *J. Am. Chem. Soc.* **2014**, 136, 10139–10147.

⁸² J. A. Bull, R. A. Croft, O. A. Davis, R. Doran, K. F. Morgan, *Chem. Rev.* **2016**, 116, 12150–12233.

Conclusion générale et perspectives

Au cours de ce travail de thèse, mon principal objectif a été de développer des méthodologies de synthèse innovantes pour accéder à une grande variété de naphtoquinones dérivées de la plasmodione antipaludique.

Dans un premier temps, mes efforts se sont concentrés sur le développement d'une réaction de Friedel-Crafts entre la ménadione protégée et une grande série d'acides benzoïques diversement substitués en présence d'acide triflique et d'anhydride trifluoroacétique. Les adduits acylés obtenus sont aisément déprotégés par l'intermédiaire du CAN permettant d'accéder aux 3-benzoylménadiques correspondantes. Cette réaction tolère une grande variété de substituants, notamment des groupements électroattracteurs et certains acides benzoïques hétéroaromatiques. Nous avons en outre étudié les potentiels rédox de cette large série de molécules pour rationaliser l'influence des fonctions portées par le cycle benzoyle. Ces travaux de synthèse ont été menés en collaboration avec Leandro Cotos, post-doctorant au sein de notre équipe.

Cette méthodologie nous a ensuite permis de synthétiser efficacement des sondes chimiques ABPP qui ont été utilisées avec succès pour identifier les sites actifs des 3-benzoylménadiques sur les deux glutathion réductases *hGR* et *PfGR*.

Dans un second temps, nous avons cherché à mettre au point une alternative à la réaction de Kochi-Anderson pour la benzylation de la ménadione. Cet objectif a été atteint par le développement d'une benzylation radicalaire photocatalysée de quinones à partir de bromure de benzyles. Nous avons également mené une étude mécanistique détaillée afin de comprendre le mécanisme de réaction qui implique, en plus d'une source de lumière bleue, un catalyseur ferrique et un donneur d'hydrogène. De plus, nous avons démontré que l'irradiation des naphtoquinones conduit à leur photoreduction en espèce semiquinone favorisée si la réaction est réalisée dans l'isopropanol.

Cette étude nous a également permis de mieux comprendre la photoréactivité des naphtoquinones et de démontrer la preuve de concept d'une oxydation benzylique photocatalysée de la plasmodione, après photoréduction, simplement en présence d'oxygène dans un solvant protique. La formation de la plasmodione réduite à un électron sous la forme radical semiquinone semble un intermédiaire clé. Bogdan Cichocki, post-doctorant au sein de notre équipe, a par ailleurs montré que cette oxydation pouvait être également catalysée par la *PfFNR*.

Enfin, l'un des objectifs historique du laboratoire était d'introduire un cycle hétéroaromatique sur la partie benzylique. Toutes les tentatives s'étaient soldées par des échecs ou avaient conduit à des rendements très faibles, incluant également la benzylation photorédox développée dans ce travail de thèse. Ces analogues hétéroaromatiques ont finalement pu être obtenus en quelques étapes grâce à un couplage palladio-catalysé de Suzuki.

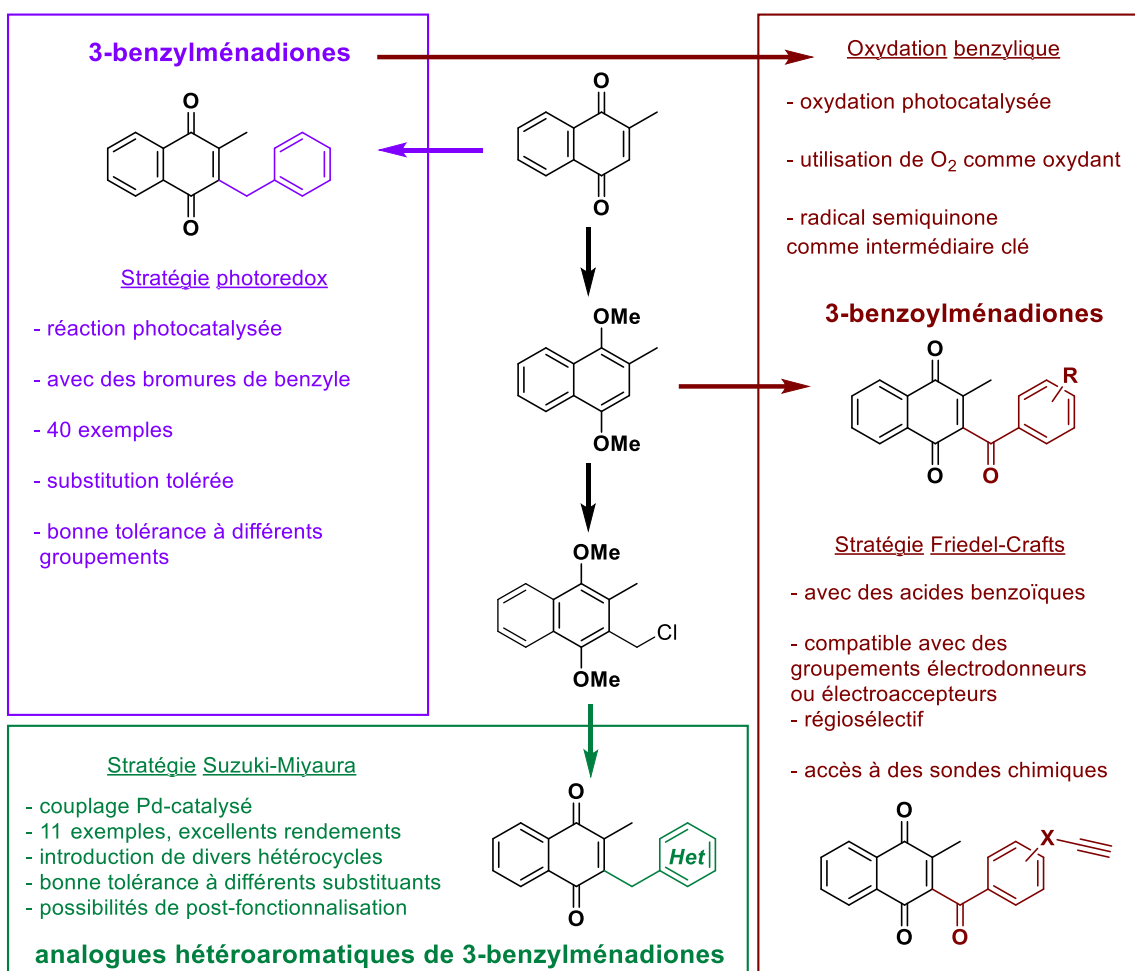


Figure 18. Les différentes méthodologies développées au cours de cette thèse.

Tous les dérivés de plasmodione synthétisés durant mon travail de thèse ont été envoyés au Swiss Tropical and Public Health Institute à Bâle en Suisse pour l'analyse de leur activité antiparasitaire, en particulier antipaludique.

Les méthodologies de synthèse développées sont actuellement utilisées par Matthieu Roignant, post doctorant, pour étendre la chimiothèque des 3-benzylménadiones (hétéroaromatiques), notamment à partir de ménadiones substituées.

Partie expérimentale

General information.

Ces parties sont rédigées en anglais, car extraites des Supporting Information de chaque article.

Solvents and reagents: Commercially available starting materials were purchased from Sigma-Aldrich, ABCR GmbH & Co. KG, Alfa Aesar, and Apollo Scientific and were used without further purification. Solvents were obtained from Sigma-Aldrich and LPCR. All reactions were performed in standard glassware. Thin Layer Chromatography (TLC) were used to monitor reactions (*vide infra*). Crude mixtures were purified by flash column chromatography. The latter were performed using silica gel 60 (230-400 mesh, 0.040-0.063 mm) purchased from E. Merck. Automatic flash chromatographies were carried out in a Biotage Puriflash apparatus with UV-Vis detection at 254 nm (unless otherwise specified). Monitoring and primary characterization of products were achieved by Thin Layer Chromatography on aluminum sheets coated with silica gel 60 F254 purchased from E. Merck. Eluted TLC's were revealed under UV (325 nm and 254 nm) and with chemicals. Analytical TLC was carried out on pre-coated Sil G-25 UV₂₅₄ plates from Macherey Nagel. Flash chromatography was performed using silica gel G60 (230–400 mesh) from E. Merck.

Nuclear Magnetic Resonance (NMR): The Nuclear Magnetic Resonance (NMR) spectra were recorded by a *Bruker avance 400* apparatus (¹H NMR 400 MHz, ¹³C NMR 100 MHz) at the ECPM. All chemical shifts (δ) are quoted in parts per million (ppm). The chemical shifts are referred to the used partial deuterated NMR solvent (for CDCl₃: ¹H NMR, 7.26 ppm and ¹³C NMR, 77.00 ppm). The coupling constants (J) and the non equivalence (Δv) are given in Hertz (Hz). Resonance patterns are reported with the following notations: br (broad), s (singlet), d (doublet), t (triplet), q (quartet), m (multiplet), dd (doublet of doublets), AB (AB system), (ABX) (AB system of an ABX) and A₂B₂ (A₂B₂ aromatic system). In addition, the following acronyms will be used: C=O carbonyl group; C_q: quaternary carbon; CH₂: secondary carbon; CH₃: methyl group.

Microanalyses: Microanalyses were obtained at "Service de Microanalyses" at the Institut de Chimie de Strasbourg.

Mass spectrometry: Mass spectra (ESI-MS) were obtained on a microTOF LC spectrometer (Bruker Daltonics, Bremen). High Resolution Mass (HRMS) spectra were measured and fitted with calculated data.

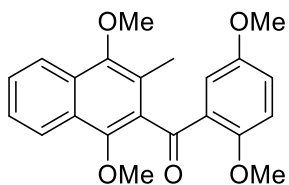
Melting point: Melting points were determined on a Büchi melting point apparatus and were not corrected.

Chapitre II. Experimental part.

Article 2.

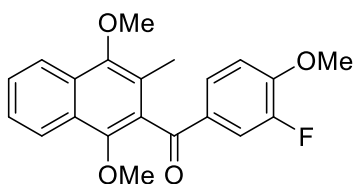
Friedel-Crafts adducts characterization.

(1,4-dimethoxy-3-methylnaphthalen-2-yl)(2,5-dimethoxyphenyl)methanone (2a)



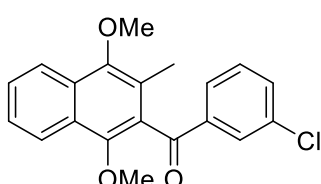
82% Yield, white solid. **mp:** 126 °C. **¹H NMR (400 MHz, Chloroform-d)** δ: 8.09-8.12 (m, 1H), 8.01-8.04 (m, 1H), 7.46-7.56 (m, 2H), 7.35 (d, *J* = 3.2 Hz, 1H), 7.07 (dd, *J* = 9.0, 3.04 Hz, 1H), 6.88 (d, *J* = 9.0 Hz, 1H), 3.90 (s, 3H), 3.79 (s, 3H), 3.77 (s, 3H), 3.50 (s, 3H), 2.29 (s, 3H). **¹³C NMR (100 MHz, Chloroform-d)** δ: 196.22, 154.10, 153.47, 150.06, 148.35, 134.25, 128.96, 128.64, 127.09, 126.64, 125.56, 123.78, 122.60, 122.26, 120.88, 114.94, 114.08, 63.17, 61.43, 56.42, 55.82, 12.76. **Elemental analysis** calcd.: 72.12%C. 6.05%H. Found: 71.91%C. 6.07%H. **HRMS (ESI)** calcd. for C₂₂H₂₃O₅: 367.164. Found: 367.152 (MH⁺).

(1,4-dimethoxy-3-methylnaphthalen-2-yl)(3-fluoro-4-methoxyphenyl)methanone (2b)



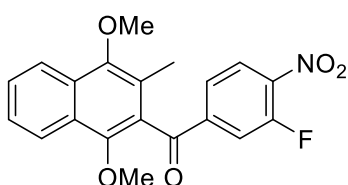
77% Yield, white solid. **mp:** 127 °C. **¹H NMR (400 MHz, Chloroform-d)** δ: 8.13-8.15 (m, 1H), 8.06-8.09 (m, 1H), 7.67 (dd, *J* = 11.7, 2.04 Hz, 1H), 7.51 – 7.60 (m, 3H), 6.94 (t, *J* = 8.3 Hz, 1H), 3.93 (s, 3H), 3.91 (s, 3H), 3.82 (s, 3H), 2.23 (s, 3H). **¹³C NMR (100 MHz, Chloroform-d)** δ: 195.15 (d, *J* = 1.99 Hz), 152.53 (d, *J* = 10.9 Hz), 150.97, 152.21 (d, *J* = 246.97 Hz), 150.44, 149.10, 130.78 (d, *J* = 5.00 Hz), 130.64, 129.35, 127.49 (d, *J* = 3.1 Hz), 127.15, 127.11, 126.05, 123.54, 122.52 (d, *J* = 19.9 Hz), 116.52 (d, *J* = 18.0 Hz), 112.44 (d, *J* = 1.67 Hz), 63.60, 61.53, 56.31, 12.72. **¹⁹F NMR (376 MHz, Chloroform-d)** δ: -134.00 (dd, *J* = 11.6, 8.0 Hz). **HRMS (ESI)** calcd. for C₂₁H₂₀FO₄: 355.1340. Found: 355.1323 (MH⁺).

(3-chlorophenyl)(1,4-dimethoxy-3-methylnaphthalen-2-yl)methanone (2c)

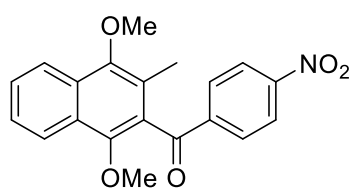


82% Yield, white solid. **mp:** 113 °C. **¹H NMR (400 MHz, Chloroform-d)** δ: 8.15-8.17 (m, 1H), 8.07-8.10 (m, 1H), 7.88 (d, *J* = 7.88 Hz, 1H), 7.68 (t, *J* = 0.46 Hz, 1H), 7.53 – 7.62 (m, 3H), 7.35-7.39 (m, 1H), 3.92 (s, 3H), 3.82 (s, 3H), 2.24 (s, 3H). **¹³C NMR (100 MHz, Chloroform-d)** δ: 196.16, 150.49, 149.30, 138.88, 135.08, 133.60, 130.28, 130.05, 129.47, 129.11, 127.79, 127.23, 127.07, 126.09, 123.38, 122.60, 122.43, 63.57, 61.51, 12.72. **Elemental analysis** calcd.: 70.49%C. 5.03%H. Found: 70.24%C. 5.05%H. **HRMS (ESI)** calcd. for C₂₀H₁₈ClO₃: 341.0939. Found: 341.0918 (MH⁺). Calcd for (C₂₀H₁₇ClO₃)₂Na: 703.1625. Found: 703.1564 (2MNa⁺).

(1,4-dimethoxy-3-methylnaphthalen-2-yl)(3-fluoro-4-nitrophenyl)methanone (2d)

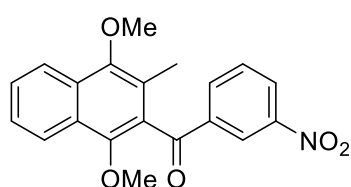


82% Yield, orange solid. **mp:** 120 °C. **¹H NMR (400 MHz, Chloroform-d)** δ: 8.15-8.17 (m, 1H), 8.05 – 8.10 (m, 2H), 7.78 (dd, *J* = 10.84, 1.68 Hz, 1H), 7.70-7.72 (m, 1H), 7.61-7.65 (m, 1H), 7.55-7.59 (m, 1H), 3.93 (s, 3H), 3.80 (s, 3H), 2.24 (s, 3H). **¹³C NMR (100 MHz, Chloroform-d)** δ: 194.76 (d, *J* = 1.06 Hz), 155.44 (d, *J* = 264.9 Hz), 150.84, 149.82, 142.84 (d, *J* = 6.2 Hz), 140.08 (d, *J* = 8.4 Hz), 129.87, 128.95, 127.74, 126.95, 126.55(d, *J* = 2.6 Hz), 126.42, 125.20 (d, *J* = 4.3 Hz), 123.20, 122.57(d, *J* = 0.9 Hz), 119.00, 18.79, 63.69, 61.60, 12.72. **¹⁹F NMR (376 MHz, Chloroform-d)** δ: -116.05 (dd, *J* = 10.9, 6.9 Hz). **Elemental analysis** calcd.: 3.79%N. 65.04%C. 4.37%H. Found: 3.79%N. 65.54%C. 4.57%H. **HRMS (ESI)** calcd. for C₂₀H₁₇FNO₅: 370.1085. Found: 370.1072 (MH⁺).

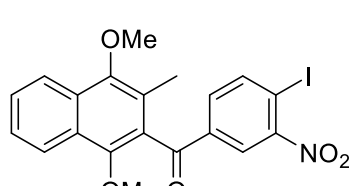
(1,4-dimethoxynaphthalen-2-yl)(4-nitrophenyl)methanone (2e)

72% Yield, yellow solid. **mp:** 107 °C. **¹H NMR (400 MHz, Chloroform-d)** δ: 8.29 (d, *J* = 9.0 Hz, 2H), 8.15-8.17 (m, 1H), 8.05-8.09 (m, 1H), 8.01 (d, *J* = 9.0 Hz, 2H), 7.60-7.64 (m, 1H), 7.53-7.58 (m, 1H), 3.93 (s, 3H), 3.80 (s, 3H), 2.24 (s, 3H). **¹³C NMR (100 MHz, Chloroform-d)** δ: 195.87, 150.75, 150.59, 149.65, 141.72, 130.36 (2C), 129.74, 129.66, 127.56, 127.03, 126.31, 123.93 (2C), 123.29, 122.58, 122.52, 63.64, 61.58, 12.75. **Elemental analysis** calcd.: 3.99%N.

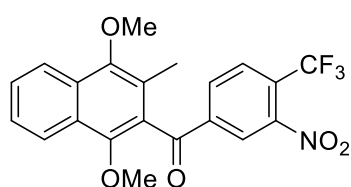
68.37%C. 4.88%H. Found: 3.92%N. 68.65%C. 4.90%H. **HRMS (ESI)** calcd. for C₂₀H₁₈NO₅: 352.1179. Found: 352.1161 (MH⁺).

(1,4-dimethoxy-3-methylnaphthalen-2-yl)(3-nitrophenyl)methanone (2f)

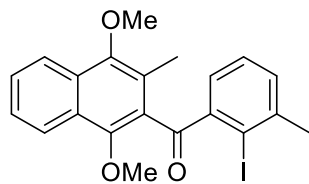
76% Yield, yellow solid. **mp:** 136 °C. **¹H NMR (400 MHz, Chloroform-d)** δ: 8.71 (t, *J* = 1.8 Hz, 1H), 8.43 (ddd, *J* = 8.2, 2.3, 1.1 Hz, 1H), 8.15-8.18 (m, 1H), 8.13 (dt, *J* = 7.9, 1.3 Hz, 1H), 8.05-8.08 (m, 1H), 7.54 – 7.68 (m, 3H), 3.93 (s, 3H), 3.80 (s, 3H), 2.24 (s, 3H). **¹³C NMR (100 MHz, Chloroform-d)** δ: 195.31, 150.82, 149.69, 148.70, 138.76, 135.12, 129.99, 129.80, 129.49, 127.80, 127.59, 127.08, 126.34, 123.99, 123.32, 122.64, 122.57, 63.70, 61.62, 12.81. **HRMS (ESI)** calcd. for C₂₀H₁₈NO₅: 352.1179. Found: 352.1179 (MH⁺).

(1,4-dimethoxy-3-methylnaphthalen-2-yl)(4-iodo-3-nitrophenyl)methanone (2g)

45% Yield, white solid. **mp:** 123°C. **¹H NMR (400 MHz, Chloroform-d)** δ: 8.29 (d, *J* = 1.9 Hz, 1H), 8.15 (d, *J* = 8.4 Hz, 1H), 8.12 (d, *J* = 8.2 Hz, 1H) 8.06 (d, *J* = 8.3 Hz, 1H), 7.54-7.64 (m, 3H), 3.92 (s, 3H), 3.79 (s, 3H), 2.24 (s, 3H). **¹³C NMR (100 MHz, Chloroform-d)** δ: 194.62, 153.55, 150.81, 149.71, 142.62, 138.24, 133.13, 129.80, 128.92, 127.64, 126.97, 126.35, 125.28, 123.23, 122.59, 122.52, 93.05, 63.68, 61.58, 12.76. **HRMS (ESI)** calcd. for C₂₀H₁₇INO₅: 478.014597. Found: 478.013648 (MH⁺).

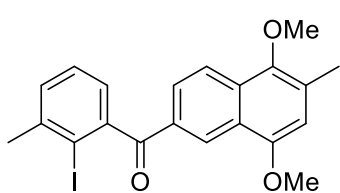
(1,4-dimethoxy-3-methylnaphthalen-2-yl)(3-nitro-4-(trifluoromethyl)phenyl)methanone (2h)

The experimental procedure applied to **1o** was modified by using TfOH:TFAA (1.5 equiv.: 2 equiv.), following the same experimental reaction for 48 hours; 67% Yield, yellow solid. **mp:** 116 °C. **¹H NMR (400 MHz, Chloroform-d)** δ: 8.37 (s, 1H), 8.17 (d, *J* = 8.32 Hz, 1H), 8.04 – 8.11 (m, 2H), 7.91 (d, *J* = 8.0 Hz, 1H), 7.62-7.66 (m, 1H), 7.55-7.59 (m, 1H), 3.93 (s, 3H), 3.80 (s, 3H), 2.25 (s, 3H). **¹³C NMR (100 MHz, Chloroform-d)** δ: 194.10, 150.97, 150.01, 148.62, 141.33, 133.57 (q, *J* = 5.4 Hz), 132.93, 130.02, 128.76 (q, *J* = 5.2 Hz), 128.51, 127.88, 127.07 (q, *J* = 34.3 Hz), 126.94, 126.49, 125.04, 123.23, 122.60 (d, *J* = 0.55 Hz), 121.53 (q, *J* = 272.4 Hz), 63.73, 61.61, 12.75. **¹⁹F NMR (376 MHz, Chloroform-d)** δ: -60.23. **Elemental analysis** calcd.: 3.34%N. 60.15%C. 3.85%H. Found: 3.45%N. 60.41%C. 3.96%H. **HRMS (ESI)** calcd. for C₂₁H₁₇F₃NO₅: 420.1053. Found: 420.1030 (MH⁺).

(1,4-dimethoxy-3-methylnaphthalen-2-yl)(2-iodo-3-methylphenyl)methanone (2i)

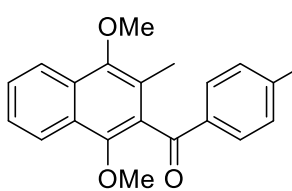
27 % Yield, light yellow solid. **mp:** 167 °C. **¹H NMR (400 MHz, Chloroform-d)** δ: 8.11-8.13 (m, 1H), 8.01-8.04 (m, 1H), 7.56-7.60 (m, 1H), 7.48-7.52 (m, 1H), 7.37 (dd, *J* = 6.72, 0.64 Hz, 1H), 7.15-7.21 (m, 2H), 3.91 (s, 3H), 3.80 (s, 3H), 2.58 (s, 3H), 2.37 (s, 3H). **¹³C NMR (100 MHz, Chloroform-d)** δ: 198.34, 150.55, 150.47, 144.06, 143.54, 132.79, 131.14, 129.88, 128.82, 127.62, 127.47, 127.07, 126.00, 124.72, 122.88, 122.45, 99.73, 64.01, 61.51, 29.94, 13.11. **Elemental analysis** calcd.:

56.52%C. 4.29%H. Found: 56.42%C. 4.54%H. **HRMS (ESI)** calcd. for C₂₁H₂₀IO₃: 447.0452. Found: 447.0435 (MH⁺).

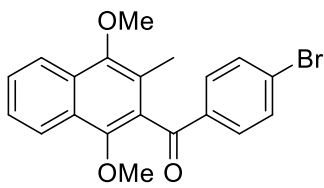
(5,8-dimethoxy-6-methylnaphthalen-2-yl)(2-iodo-3-methylphenyl)methanone (2i-reg1)

71% Yield, light yellow solid. **mp:** 168 °C. **¹H NMR (400 MHz, Chloroform-d)** δ: 8.59 (d, $J = 1.36$ Hz, 1H), 8.08 (d, $J = 8.84$ Hz, 1H), 8.01 (dd, $J = 8.8, 1.72$ Hz, 1H), 7.32 – 7.39 (m, 2H), 7.07 – 7.13 (m, 1H), 6.63 (s, 1H), 3.91 (s, 3H), 3.86 (s, 3H), 2.54 (s, 3H), 2.46 (s, 3H). **¹³C NMR (100 MHz, Chloroform-d)** δ: 197.80, 152.79, 146.96, 146.08, 142.62, 131.73, 130.98, 130.37, 130.12, 127.83, 127.60, 126.00, 125.39, 124.29, 122.19, 107.78, 98.83, 61.32, 55.63, 28.76, 16.63.

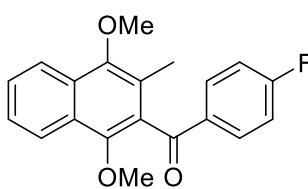
HRMS (ESI) calcd. for C₂₁H₂₀IO₃: 447.045169. Found: 447.043259. (MH⁺).

(1,4-dimethoxy-3-methylnaphthalen-2-yl)(4-iodophenyl)methanone (2j)

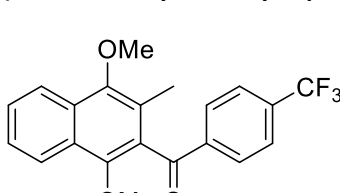
47% Yield, white solid. **mp:** 133 °C. **¹H NMR (400 MHz, Chloroform-d)** δ: 8.14 (d, $J = 8.24$ Hz, 1H), 8.07 (d, $J = 7.92$ Hz, 1H), 7.82 (d, $J = 8.5$ Hz, 2H), 7.61 – 7.52 (m, 4H), 3.91 (s, 3H), 3.80 (s, 3H), 2.22 (s, 3H). **¹³C NMR (100 MHz, Chloroform-d)** δ: 196.75, 150.49, 149.26, 138.09 (2C), 136.59, 130.83 (2C), 130.34, 129.43, 127.21, 127.09, 126.09, 123.45, 122.60, 122.43, 102.18, 63.59, 61.54, 12.74. **HRMS (ESI)** calcd. for C₂₀H₁₈IO₃: 433.029519. Found: 433.027541 (MH⁺).

(4-bromophenyl)(1,4-dimethoxy-3-methylnaphthalen-2-yl)methanone (2k)

72% Yield, white solid. **mp:** 111 °C. **¹H NMR (400 MHz, Chloroform-d)** δ: 8.13-8.15 (m, 1H), 8.06-8.09 (m, 1H), 7.71 (d, $J = 8.7$ Hz, 2H), 7.62-7.52 (m, 4H), 3.91 (s, 3H), 3.81 (s, 3H), 2.22 (s, 3H). **¹³C NMR (100 MHz, Chloroform-d)** δ: 196.42, 150.50, 149.24, 136.06, 132.08 (2C), 130.98 (2C), 130.38, 129.43, 129.13, 127.21, 127.09, 126.10, 123.44, 122.59, 122.43, 63.59, 61.54, 12.74. **HRMS (ESI)** calcd. for C₂₀H₁₈BrO₃: 385.0434. Found: 385.0409. (MH⁺).

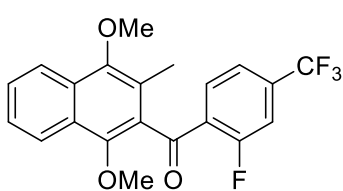
(1,4-dimethoxy-3-methylnaphthalen-2-yl)(4-fluorophenyl)methanone (2l)

58% Yield, beige solid. **mp:** 98 °C. **¹H NMR (400 MHz, Chloroform-d)** δ: 8.13-8.15 (m, 1H), 8.06-8.08 (m, 1H), 7.85 – 7.90 (m, 2H), 7.52 – 7.61 (m, 2H), 7.09 – 7.14 (m, 2H), 3.91 (s, 3H), 3.82 (s, 3H), 2.22 (s, 3H). **¹³C NMR (100 MHz, Chloroform-d)** δ: 195.83, 166.17 (d, $J = 254.39$ Hz), 150.46, 149.11, 133.78 (d, $J = 2.8$ Hz), 132.23 (2C) (d, $J = 9.5$ Hz), 130.64, 129.37, 127.14, 127.12 (d, $J = 3.3$ Hz), 126.06, 123.45, 122.58, 122.41, 115.91 (2C) (d, $J = 21.9$ Hz), 63.59, 61.53, 12.72. **¹⁹F NMR (376 MHz, Chloroform-d)** δ: -104.00 ppm. **HRMS (ESI)** calcd. for C₂₀H₁₈FO₃: 325.123449. Found: 325.121356 (MH⁺).

(1,4-dimethoxy-3-methylnaphthalen-2-yl)(4-(trifluoromethyl)phenyl)methanone (2m)

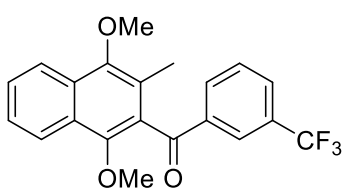
77% Yield, beige solid. **mp:** 76 °C. **¹H NMR (400 MHz, Chloroform-d)** δ: 8.14 (d, $J = 8.2$ Hz, 1H), 8.07 (d, $J = 7.92$ Hz, 1H), 7.97 (d, $J = 8.1$ Hz, 2H), 7.82 (d, $J = 8.5$ Hz, 2H), 7.62-7.52 (m, 2H), 3.91 (s, 3H), 3.80 (s, 3H), 2.22 (s, 3H). **¹³C NMR (100 MHz, Chloroform-d)** δ: 196.48, 150.62, 149.47, 139.91, 134.82 (q, $J = 32.5$ Hz), 130.15, 129.76 (2C), 129.58, 127.37, 127.08, 126.20, 125.81 (q, $J = 3.7$ Hz) (2C), 123.56 (q, $J = 271.2$ Hz), 123.40, 122.59, 122.48, 63.63, 61.57, 12.75. **¹⁹F NMR (376 MHz, Chloroform-d)** δ: -63.14. **HRMS (ESI)** calcd. for C₂₁H₁₈F₃O₃: 375.120256. Found: 375.119447. (MH⁺).

(1,4-dimethoxy-3-methylnaphthalen-2-yl)(2-fluoro-4-(trifluoromethyl)phenyl)methanone (2n)



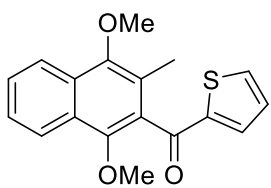
80% Yield, white solid, **mp**: 85 °C. **¹H NMR (400 MHz, Chloroform-d)** δ: 8.14 (d, *J* = 8.4 Hz, 1H), 8.04 (d, *J* = 8.2 Hz, 1H), 7.89 (ddd, *J* = 8.2, 7.2, 1.0 Hz, 1H), 7.60 (dt, *J* = 7.6, 1.0 Hz, 1H), 7.55 – 7.48 (m, 2H), 7.40 (d, *J* = 10.3 Hz, 1H), 3.92 (s, 3H), 3.79 (s, 3H), 2.33 (s, 3H). **¹³C NMR (100 MHz, Chloroform-d)** δ: 193.34, 161.12 (d, *J* = 259.5 Hz), 150.66, 149.98 (d, *J* = 1.18 Hz), 136.08 (qd, *J* = 33.4, 8.3 Hz), 132.00 (d, *J* = 1.29 Hz), 131.52, 129.86, 129.78, 127.52, 126.98, 126.12, 123.33 (d, *J* = 0.4 Hz), 122.68 (qd, *J* = 271.3, 2.4 Hz), 122.62, 122.49, 121.16 (p, *J* = 3.8 Hz), 114.54 (dq, *J* = 25.2, 3.7 Hz), 63.70, 61.68, 12.87. **¹⁹F NMR (376 MHz, Chloroform-d)** δ: -63.31, -110.03 (dd, *J* = 10.3, 7.3 Hz). **HRMS (ESI)** calcd. for C₂₁H₁₇F₄O₃: 393.110834. Found: 393.109752 (MH⁺).

(1,4-dimethoxy-3-methylnaphthalen-2-yl)(3-(trifluoromethyl)phenyl)methanone (2o)



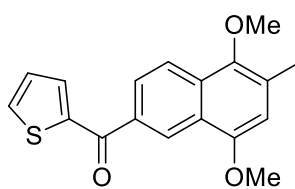
75% Yield, light yellow solid. **mp** : 88 °C. **¹H NMR (400 MHz, Chloroform-d)** δ : 8.25 (s, 1H), 8.18 (d, *J* = 8.2 Hz, 1H), 8.09 (d, *J* = 8.3 Hz, 1H), 7.93 (d, *J* = 7.8 Hz, 1H), 7.84 (d, *J* = 7.8 Hz, 1H), 7.54 – 7.64 (m, 3H), 3.93 (s, 3H), 3.83 (s, 3H), 2.25 (s, 3H). **¹³C NMR (100 MHz, Chloroform-d)** δ: 196.09, 150.60, 149.46, 137.85, 133.04, 131.41 (q, *J* = 32.7 Hz), 130.01, 129.99 (q, *J* = 3.5 Hz), 129.59, 129.40, 127.33, 127.09, 126.16, 125.71 (q, *J* = 3.8 Hz), 123.62 (q, *J* = 270.9 Hz), 123.35, 122.61, 122.47, 63.59, 61.60, 12.74. **¹⁹F NMR (376 MHz, Chloroform-d)** δ: -62.73. **Elemental analysis** calcd. 67.38%C. 4.58%H. Found: 67.49%C. 4.67%H. **HRMS (ESI)** calcd. for C₂₁H₁₈F₃O₃: 375.1203. Found: 375.1189 (MH⁺).

(1,4-dimethoxy-3-methylnaphthalen-2-yl)(thiophen-2-yl)methanone (2p)



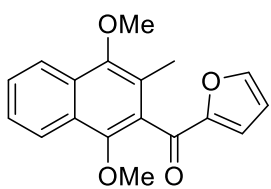
58% Yield, beige solid. **mp**: 119 °C. **¹H NMR (400 MHz, Chloroform-d)** δ: 8.12-8.14 (m, 1H), 8.08-8.10 (m, 1H), 7.73 (dd, *J* = 4.9, 1.2 Hz, 1H), 7.51-7.61 (m, 2H), 7.38 (dd, *J* = 3.8, 1.2 Hz, 1H), 7.08 (dd, *J* = 4.9, 3.8 Hz, 1H), 3.91 (s, 3H), 3.88 (s, 3H), 2.30 (s, 3H). **¹³C NMR (100 MHz, Chloroform-d)** δ: 189.30, 150.31, 149.27, 144.87, 135.27, 135.13, 130.99, 129.39, 128.38, 127.16(2C), 125.99, 123.54, 122.70, 122.36, 63.84, 61.50, 12.74. **HRMS (ESI)** calcd. for C₁₈H₁₇O₃S: 313.089292. Found: 313.087667 (MH⁺).

(5,8-dimethoxy-6-methylnaphthalen-2-yl)(thiophen-2-yl)methanone (2p-reg1)

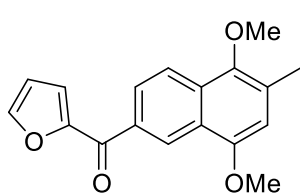


27% Yield, brown solid. **mp**: 132 °C. **¹H NMR (400 MHz, Chloroform-d)** δ: 8.77 (d, *J* = 1.7 Hz, 1H), 8.12 (d, *J* = 7.52 Hz, 1H), 7.98 (dd, *J* = 8.72, 1.8 Hz, 1H), 7.73-7.74 (m, 2H), 7.20 (dd, *J* = 4.8, 4.0 Hz, 1H), 6.68 (s, 1H), 3.98 (s, 3H), 3.88 (s, 3H), 2.49 (s, 3H). **¹³C NMR (100 MHz, Chloroform-d)** δ: 188.14, 152.49, 146.90, 143.98, 134.73, 133.91, 133.82, 130.37, 129.11, 127.96, 126.00, 125.32, 124.02, 122.13, 107.74, 61.36, 55.68, 16.55. **HRMS (ESI)** calcd. for C₁₈H₁₇O₃S: 313.087998. Found: 313.089292 (MH⁺).

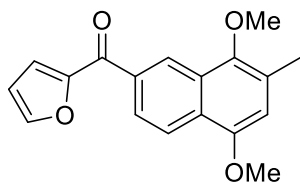
(1,4-dimethoxy-3-methylnaphthalen-2-yl)(thiophen-2-yl)methanone (2q)



18% Yield, Brown solid. **mp**: 117 °C. **¹H NMR (400 MHz, Chloroform-d)** δ: 8.12-8.14 (m, 1H), 8.07-8.10 (m, 1H), 7.68 (dd, *J* = 1.6, 0.8 Hz, 1H), 7.51-7.61 (m, 2H), 6.96 (d, *J* = 3.4 Hz, 1H), 6.53 (dd, *J* = 3.2, 1.7 Hz, 1H), 3.90 (s, 3H), 3.87 (s, 3H), 2.29 (s, 3H). **¹³C NMR (100 MHz, Chloroform-d)** δ: 184.20, 153.18, 150.29, 149.83, 147.76, 130.06, 129.53, 127.24, 127.12, 125.98, 123.75, 122.70, 122.39, 120.98, 112.57, 63.92, 61.49, 12.61. **HRMS (ESI)** calcd. for C₁₈H₁₆KO₄: 335.068017. Found: 335.065996 (M⁺ K⁺).

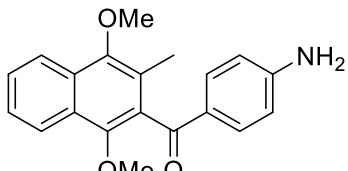
(5,8-dimethoxy-6-methylnaphthalen-2-yl)(furan-2-yl)methanone (2q-reg1)

33% Yield, Brown solid. **mp:** 117 °C. **¹H NMR (400 MHz, Chloroform-d)** δ: 8.89 (d, *J* = 1.3 Hz, 1H), 8.11 (d, *J* = 8.8 Hz, 1H), 8.05 (dd, *J* = 8.8, 1.7 Hz, 1H), 7.74-7.75 (m, 1H), 7.28 (dd *J* = 3.52, 0.56 Hz, 1H), 6.67 (s, 1H), 6.62 (dd, *J* = 3.52, 1.6 Hz, 1H), 3.99 (s, 3H), 3.87 (s, 3H), 2.48 (s, 3H). **¹³C NMR (100 MHz, Chloroform-d)** δ: 182.50, 152.57, 152.52, 146.95, 146.91, 133.13, 130.51, 129.28, 125.87, 125.50, 124.12, 122.03, 120.42, 112.14, 100.70, 61.33, 55.69, 16.56. **HRMS (ESI)** calcd. for C₁₈H₁₇O₄: 297.112997. Found: 297.112135 (MH⁺).

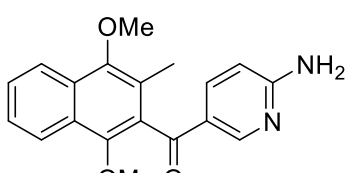
(5,8-dimethoxy-7-methylnaphthalen-2-yl)(furan-2-yl)methanone (2q-reg2)

12 % Yield, brown solid. **¹H NMR (400 MHz, Chloroform-d)** δ: 8.31 (dd, *J* = 7.9, 1.8 Hz, 1H), 7.55 (d, *J* = 1.6 Hz, 1H), 7.40-7.46 (m, 1H), 6.62-6.66 (m, 2H), 6.41 (dd *J* = 3.44, 1.6 Hz, 1H), 3.97 (s, 3H), 3.52 (s, 3H), 2.38 (s, 3H). **¹³C NMR (100 MHz, Chloroform-d)** δ: 185.98, 153.64, 151.40, 146.46, 146.36, 133.87, 126.93, 126.62, 125.92, 125.27, 123.78(2C), 118.34, 111.91, 107.82, 60.83, 55.65, 16.69. **HRMS (ESI)** calcd. for C₁₈H₁₇O₄: 297.112135. Found: 297.113495 (MH⁺).

The experimental procedure applied to the acid sensitive moieties as amino group or heteroaromatic carboxylic acids **4r-u**, pyridine, pyrimidine, was modified, by changing the proportions of the reagents, *i.e.* 4 equiv. of the mixture TfOH/TFAA (1:1), following the same experimental procedure.

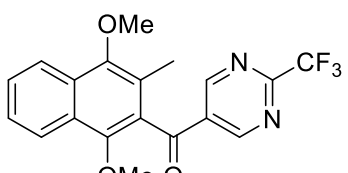
(4-aminophenyl)(1,4-dimethoxy-3-methylnaphthalen-2-yl)methanone (2r)

54% Yield, oil yellow. **¹H NMR (400 MHz, Chloroform-d)** δ: 8.11-8.13 (m, 1H), 8.06-8.09 (m, 1H), 7.66 (d, *J* = 8.2 Hz, 2H), 7.49-7.58 (m, 2H), 6.58 (d, *J* = 7.8 Hz, 2H), 3.97 (s, 2H), 3.90 (s, 3H), 3.83 (s, 3H), 2.23 (s, 3H). **¹³C NMR (100 MHz, Chloroform-d)** δ: 195.23, 151.86, 150.16, 148.72, 132.24(2C), 131.65, 129.01, 127.80, 127.16, 126.72, 125.76, 123.81, 122.58, 122.25, 113.80 (2C), 63.44, 61.43, 12.71. **HRMS (ESI)** calcd. for C₂₀H₂₀NO₃: 322.143770. Found: 322.145541 (MH⁺).

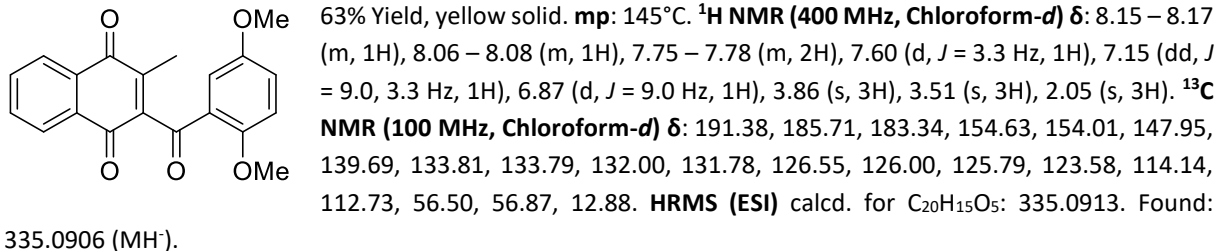
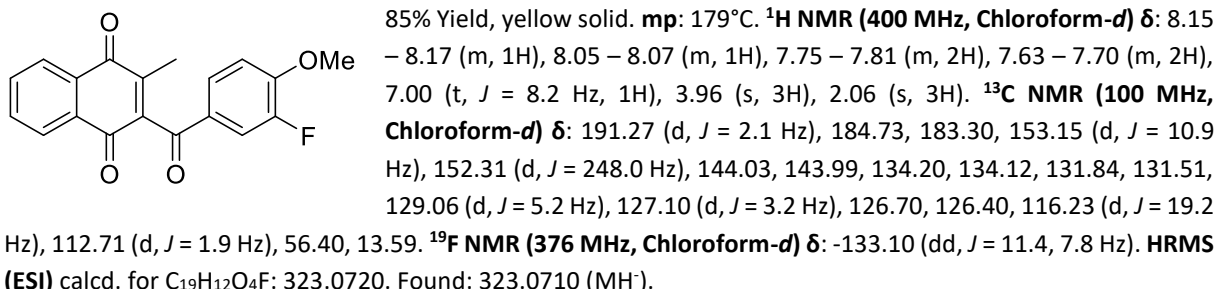
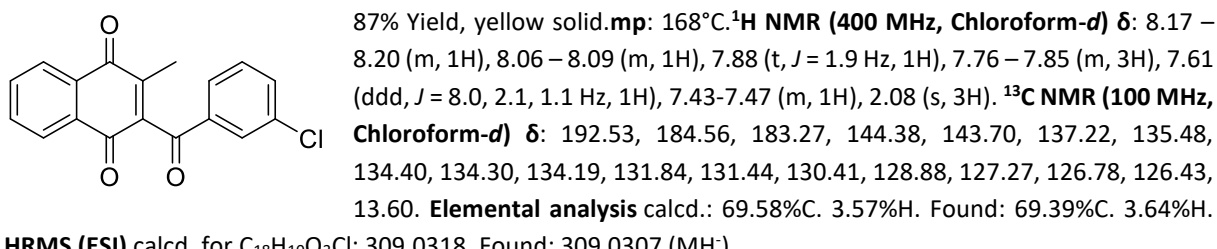
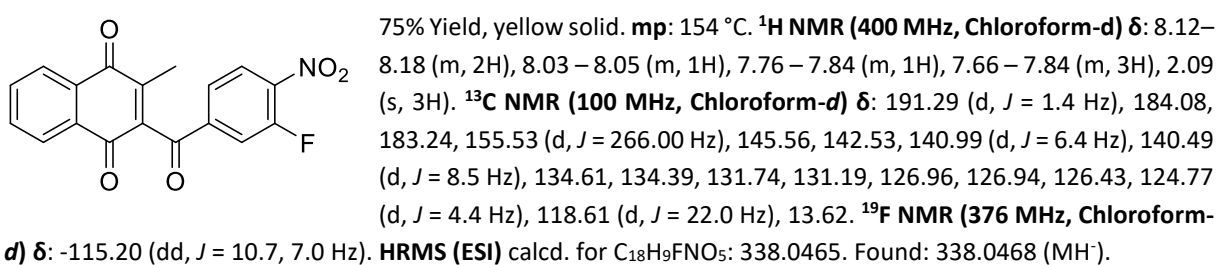
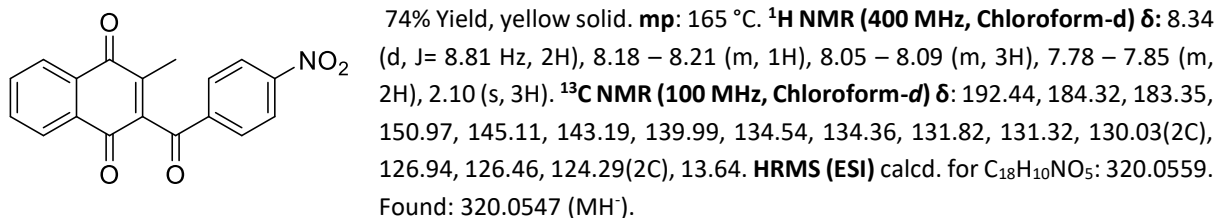
(6-aminopyridin-3-yl)(1,4-dimethoxy-3-methylnaphthalen-2-yl)methanone (2s)

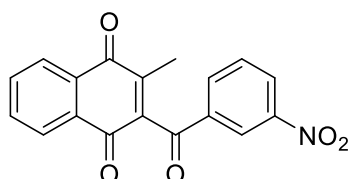
48% Yield, beige solide. **mp:** 178 °C. **¹H NMR (400 MHz, Chloroform-d)** δ: 8.43 (d, *J* = 2 Hz, 1H), 8.11-8.12 (m, 1H), 8.05-8.08 (m, 1H), 7.94 (dd, *J* = 7.0, 2.3 Hz, 1H), 7.55-7.59(m, 1H), 7.50-7.54 (m, 1H), 6.46 (dd, *J* = 8.7, 0.6 Hz, 1H), 5.15 (s, 2H), 3.90 (s, 3H), 3.83 (s, 3H), 2.24 (s, 3H). **¹³C NMR (101 MHz, Chloroform-d)** δ: 194.44, 161.41, 153.03, 150.40, 149.00, 138.49, 130.66, 129.25, 127.15, 127.00, 125.94, 124.27, 123.53, 122.59, 122.34, 107.84, 63.56, 61.48, 12.73.

HRMS (ESI) calcd. for C₁₉H₁₉N₂O₃: 323.1390. Found: 323.1380 (MH⁺).

(1,4-dimethoxy-3-methyl-1,4-dihydronaphthalen-2-yl)(2-(trifluoromethyl)pyrimidin-5 yl)methanone (2t)

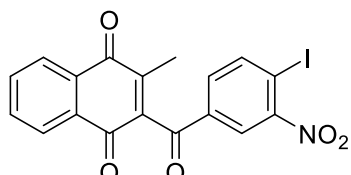
11% Yield, white solid. **mp:** 116 °C. **¹H NMR (400 MHz, Chloroform-d)** δ: 9.23 (s, 2H), 8.16 (d, *J* = 8.3 Hz, 1H), 8.06 (d, *J* = 8.2 Hz, 1H), 7.63-7.67 (m, 1H), 7.55-7.60 (m, 1H), 3.93 (s, 3H), 3.78 (s, 3H), 2.30 (s, 3H). **¹³C NMR (100 MHz, Chloroform-d)** δ: 193.56, 158.80 (2C), 158.75 (q, *J* = 37.1 Hz), 151.20, 150.50, 131.19, 130.31, 128.20, 127.85, 126.92, 126.63, 123.29, 122.64 (2C), 119.21 (q, *J* = 274.2 Hz), 63.75, 61.65, 12.77. **¹⁹F NMR (376 MHz, Chloroform-d)** δ: -70.45. **HRMS (ESI)** calcd. for C₁₉H₁₆F₃N₂O₃: 335.0913. Found: 377.110753 (MH⁺).

Oxydative demethylation adducts characterization.**2-(2,5-dimethoxybenzoyl)-3-methylnaphthalene-1,4-dione (1a)****2-(3-fluoro-4-methoxybenzoyl)-3-methylnaphthalene-1,4-dione (1b)****2-(3-chlorobenzoyl)-3-methylnaphthalene-1,4-dione (1c)****2-(3-fluoro-4-nitrobenzoyl)-3-methylnaphthalene-1,4-dione (1d)****2-methyl-3-(4-nitrobenzoyl)naphthalene-1,4-dione (1e)**

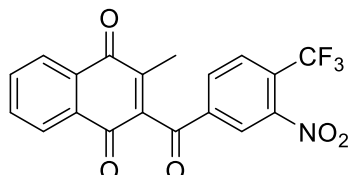
2-methyl-3-(3-nitrobenzoyl)naphthalene-1,4-dione (1f)

95% Yield, yellow solid. **mp:** 204 °C. **¹H NMR (400 MHz, Chloroform-d)** δ: 8.67 (t, *J* = 1.8 Hz, 1H), 8.49 (ddd, *J* = 8.2, 2.3, 1.1 Hz, 1H), 8.23–8.26 (m, 1H), 8.19 – 8.21 (m, 1H), 8.05 – 8.07 (m, 1H), 7.77 – 7.85 (m, 2H), 7.72 – 7.75 (m, 1H), 2.11 (s, 3H). **¹³C NMR (100 MHz, Chloroform-d)** δ: 191.86, 184.31, 183.36, 148.71, 145.23, 143.01, 137.10, 134.45, 134.34 (2C), 131.84, 131.33, 130.40, 128.53, 126.95, 126.48, 123.80, 13.68. **HRMS (ESI)** calcd. for C₁₈H₁₀NO₅: 320.056446.

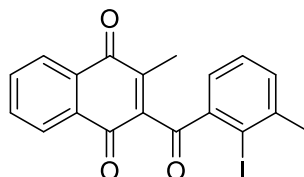
Found: 320.057033 (MH⁺).

2-(4-bromobenzoyl)-3-methylnaphthalene-1,4-dione (1g)

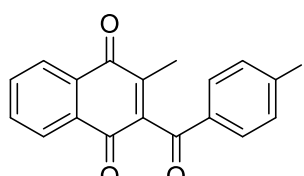
83% Yield, yellow solid. **mp:** 210 °C. **¹H NMR (400 MHz, Chloroform-d)** δ: 8.26 (d, *J* = 1.6 Hz, 1H), 8.20 (d, *J* = 8.2 Hz, 1H), 8.14–8.16 (m, 1H), 8.02–8.04 (m, 1H), 7.76–7.82 (m, 2H), 7.72 (dd, *J* = 1.7, 8.2 Hz, 1H), 2.08 (s, 3H). **¹³C NMR (100 MHz, Chloroform-d)** δ: 191.31, 184.15, 183.23, 153.55, 145.43, 143.09, 142.55, 136.60, 134.53, 134.32, 132.29, 131.76, 131.23, 126.90, 126.43, 125.02, 94.16, 13.66. **HRMS (ESI)** calcd. for C₁₈H₉INO₅: 445.9531. Found: 445.9517.

2-methyl-3-(3-nitro-4-(trifluoromethyl)benzoyl)naphthalene-1,4-dione (1h)

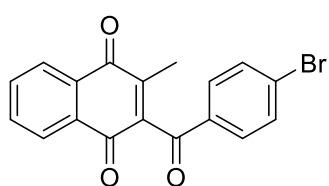
90% Yield, orange solid. **mp:** 143 °C. **¹H NMR (400 MHz, Chloroform-d)** δ: 8.33 (d, *J* = 1.2 Hz, 1H), 8.16 – 8.20 (m, 2H), 8.03 – 8.06 (m, 1H), 7.98 (d, *J* = 8.2 Hz, 1H), 7.78 – 7.85 (m, 2H), 2.12 (s, 3H). **¹³C NMR (100 MHz, Chloroform-d)** δ: 190.97, 184.01, 183.32, 148.75, 146.07, 142.19, 139.69, 134.72, 134.46, 131.77, 131.16, 130.16, 129.14 (q, *J* = 5.1 Hz), 127.88 (q, *J* = 34.5 Hz), 127.03, 126.48, 124.84, 121.35 (q, *J* = 272.6 Hz), 13.70. **HRMS (ESI)** calcd. for C₁₉H₉F₃NO₅: 388.0433. Found: 388.0450 (MH⁺). **¹⁹F NMR (376 MHz, Chloroform-d)** δ: -60.31.

2-(2-iodo-3-methylbenzoyl)-3-methylnaphthalene-1,4-dione (1i)

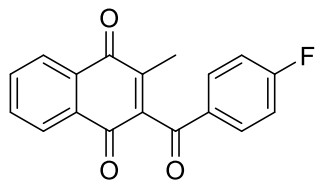
83% Yield, yellow solid. **mp:** 158 °C. **¹H NMR (400 MHz, Chloroform-d)** δ: 8.13 – 8.15 (m, 1H), 8.03 – 8.05 (m, 1H), 7.73 – 7.79 (m, 2H), 7.40–7.42 (m, 1H), 7.26 – 7.34 (m, 2H), 2.56 (s, 3H), 2.16 (s, 3H). **¹³C NMR (100 MHz, Chloroform-d)** δ: 195.08, 185.02, 183.31, 145.05, 144.51, 143.78, 141.45, 134.15, 134.12, 133.46, 131.83, 131.45, 128.65, 127.95, 126.64, 126.39, 99.75, 29.85, 13.70. **HRMS (ESI)** calcd. for C₁₉H₁₂IO₃: 414.9831. Found: 414.9818 (MH⁺).

2-(4-iodobenzoyl)-3-methylnaphthalene-1,4-dione (1j)

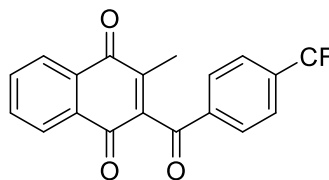
97 %Yield, yellow solid. **mp:** 184 °C. **¹H NMR (400 MHz, Chloroform-d)** δ: 8.14 – 8.16 (m, 1H), 8.03 – 8.05 (m, 1H), 7.86 (d, *J* = 8.52 Hz, 2H), 7.74–7.81 (m, 2H), 7.60 (d, *J* = 8.52 Hz, 2H), 2.05 (s, 3H). **¹³C NMR (100 MHz, Chloroform-d)** δ: 193.02, 184.57, 183.25, 144.25, 143.75, 138.41 (2C), 134.93, 134.24, 134.14, 131.80, 131.42, 130.26 (2C), 126.71, 126.37, 103.04, 13.56. **HRMS (ESI)** calcd. for C₁₈H₁₁IKO₃: 440.938450. Found: 440.941059 (MK).

2-(4-bromobenzoyl)-3-methylnaphthalene-1,4-dione (1k)

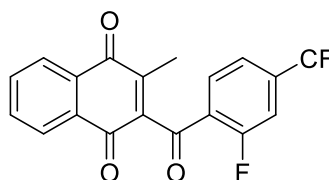
97% Yield, yellow solid. **mp:** 170 °C. **¹H NMR (400 MHz, Chloroform-d)** δ: 8.16 – 8.18 (m, 1H), 8.05 – 8.08 (m, 1H), 7.76 – 7.82 (m, 4H), 7.64 (d, *J* = 8.7 Hz, 2H), 2.06 (s, 3H). **¹³C NMR (100 MHz, Chloroform-d)** δ: reported. **HRMS (ESI)** calcd. for C₁₈H₁₀O₃Br: 352.9813. Found: 352.9797 (MH⁺).

2-(4-fluorobenzoyl)-3-methylnaphthalene-1,4-dione (1l)

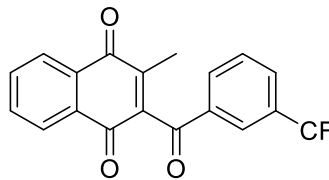
85% Yield, yellow solid. **mp:** 168 °C. **¹H NMR (400 MHz, Chloroform-d)** δ: 8.16 – 8.19 (m, 1H), 8.06 – 8.08 (m, 1H), 7.92 – 7.97 (m, 2H), 7.76 – 7.82 (m, 2H), 7.15 – 7.20 (m, 2H), 2.07 (s, 3H). **¹³C NMR (100 MHz, Chloroform-d)** δ: 192.03, 184.69, 183.34, 166.55 (d, *J* = 257.6 Hz), 144.07 (d, *J* = 6.9 Hz), 134.21 (d, *J* = 9.4 Hz) (2C), 132.25 (d, *J* = 2.9 Hz), 131.97, 131.88, 131.86, 131.50, 131.68 (d, *J* = 35.77 Hz), 126.75, 126.43, 116.39 (d, *J* = 22.1 Hz) (2C), 13.60. **¹⁹F NMR (376 MHz, Chloroform-d)** δ: -102.17. **HRMS (ESI)** calcd. for C₁₈H₁₀O₃F: 293.0614. Found: 293.0609 (MH⁺).

2-methyl-3-(4-(trifluoromethyl)benzoyl)naphthalene-1,4-dione (1m)

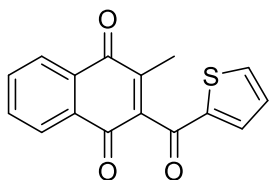
93% Yield, yellow solid. **mp:** 154 °C. **¹H NMR (400 MHz, Chloroform-d)** δ: 8.17 – 8.20 (m, 1H), 8.05 – 8.08 (m, 1H), 8.02 (d, *J* = 8.12 Hz, 2H), 7.76 – 7.84 (m, 4H), 2.08 (s, 3H). **¹³C NMR (100 MHz, Chloroform-d)** δ: 192.89, 184.49, 183.34, 144.66, 143.59, 138.26, 135.55 (q, *J* = 32.6 Hz), 134.40, 134.26, 131.84, 131.40, 129.39 (2C), 126.84, 126.43, 126.16 (q, *J* = 3.7 Hz) (2C), 123.36 (d, *J* = 271.3 Hz), 13.60. **¹⁹F NMR (376 MHz, Chloroform-d)** δ: -63.28. **HRMS (ESI)** calcd. for C₁₉H₁₀O₃F₃: 343.0582. Found: 343.0576 (MH⁺).

2-(2-fluoro-4-(trifluoromethyl)benzoyl)-3-methylnaphthalene-1,4-dione (1n)

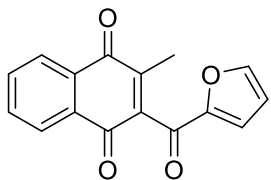
72% Yield, orange solid. **mp:** 135 °C. **¹H NMR (400 MHz, Chloroform-d)** δ: 8.14 – 8.20 (m, 2H), 8.02-8.05 (m, 1 H), 7.74-7.81(m, 2 H), 7.59 (d, *J* = 8.1 Hz, 1H), 7.36 (d, *J* = 10.6 Hz, 1H), 2.13 (s, 3H). **¹³C NMR (101 MHz, Chloroform-d)** δ: 189.24, 184.82, 183.30 (d, *J* = 2.7 Hz), 161.68 (d, *J* = 259.47 Hz), 145.00, 143.56 (d, *J* = 3.02 Hz), 137.2 (qd, *J* = 33.95, 8.7 Hz), 134.30, 134.13, 131.85, 131.55 (d, *J* = 1.3 Hz), 131.31, 127.48 (d, *J* = 10.8 Hz), 126.77, 126.21, 122.50 (qd, *J* = 274.17, 2.45 Hz), 121.71 (p, *J* = 3.7 Hz), 114.55 (dq, *J* = 28.3, 3.83 Hz), 13.19. **¹⁹F NMR (376 MHz, Chloroform-d)** δ: -63.31, -110.03. **HRMS (ESI)** calcd. for C₁₉H₉O₃F₄: 361.0488. Found: 361.0491 (MH⁺).

2-methyl-3-(3-(trifluoromethyl)benzoyl)naphthalene-1,4-dione (1o)

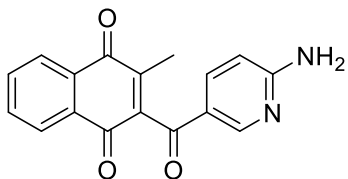
94% Yield, yellow solid. **mp:** 155 °C. **¹H NMR (400 MHz, Chloroform-d)** δ: 8.18 – 8.20 (m, 2H), 8.04 – 8.08 (m, 2H), 7.88 – 7.90 (m, 1H), 7.74 – 7.84 (m, 2H), 7.65 (t, *J* = 7.8 Hz, 1H), 2.09 (s, 3H). **¹³C NMR (100 MHz, Chloroform-d)** δ: 192.55, 184.49, 183.32, 144.69, 143.47, 136.26, 134.39, 134.26, 132.36, 131.87 (d, *J* = 33.1 Hz), 131.85, 131.42, 130.81 (q, *J* = 3.5 Hz), 129.80, 126.85, 126.46, 125.59 (q, *J* = 3.8 Hz), 123.58 (dd, *J* = 271.0 Hz), 13.63. **¹⁹F NMR (376 MHz, Chloroform-d)** δ: -62.84. **Elemental analysis** calcd.: 66.28%C. 3.22%H. Found: 66.00%C. 3.31%H. **HRMS (ESI)** calcd. for C₁₉H₁₀O₃F₃: 343.0582. Found: 343.0591 (MH⁺).

2-methyl-3-(thiophene-2-carbonyl)naphthalene-1,4-dione (1p)

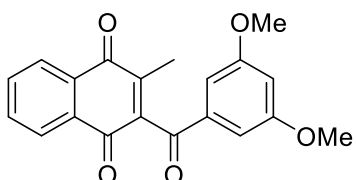
74% Yield, yellow solid. **mp:** 157 °C. **¹H NMR (400 MHz, Chloroform-d)** δ: 8.15 – 8.17 (m, 1H), 8.07 – 8.09 (m, 1H), 7.77 – 7.80 (m, 3H), 7.58 (d, *J* = 4.84 Hz, 1H), 7.15 (d, *J* = 4.3 Hz, 1H), 2.12 (s, 3H). **¹³C NMR (100 MHz, Chloroform-d)** δ: 185.20, 184.90, 182.93, 144.05, 143.88, 142.98, 136.08, 134.86, 134.17 (2C), 131.80, 131.52, 128.63, 126.69, 126.45, 13.80. **Elemental analysis** calcd.: 68.07%C. 3.57%H. Found: 68.41%C. 3.85%H. **HRMS (ESI)** calcd. for C₁₆H₉O₃S: 281.0272. Found: 381.0265 (M⁺).

2-(furan-2-carbonyl)-3-methylnaphthalene-1,4-dione (1q)

89% Yield, yellow solid. **mp:** 157 °C. **¹H NMR (400 MHz, Chloroform-d)** δ: 8.14 – 8.16 (m, 1H), 8.16 – 8.09 (m, 1H), 7.75 – 7.80 (m, 2H), 7.64 (dd, *J* = 1.6, 0.6 Hz, 1H), 7.27 (dd, *J* = 3.8, 0.8 Hz, 1H), 6.60 (dd, *J* = 3.7, 1.7 Hz, 1H), 2.11 (s, 3H). **¹³C NMR (100 MHz, Chloroform-d)** δ: 184.87, 182.89, 180.66, 125.06, 147.99, 144.52, 143.04, 134.11 (2C), 131.80, 131.52, 126.67, 126.37, 120.04, 112.97, 13.50. **HRMS (ESI)** calcd. for C₁₆H₉O₄: 265.0506. Found: 265.0500.

2-(6-aminonicotinoyl)-3-methylnaphthalene-1,4-dione (1s)

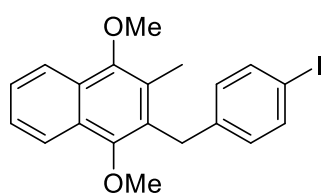
90% Yield, red solid. **mp:** 184 °C. **¹H NMR (400 MHz, Chloroform-d)** δ: 8.50 (s, 1H), 8.15 – 8.17 (m, 1H), 8.06 – 8.08 (m, 1H), 8.03 (dd, *J* = 8.72, 2.3 Hz, 1H), 7.74-7.81 (m, 2 H), 6.54 (d, *J* = 8.8 Hz, 1H), 5.10 (s, 2H), 2.08 (s, 3H). **¹³C NMR (100 MHz, Chloroform-d)** δ: 190.44, 184.90, 183.36, 161.67, 152.92, 143.94, 143.89, 137.91, 134.14, 134.09, 131.86, 131.58, 126.68, 126.41, 123.13, 108.30, 13.65. **HRMS (ESI)** calcd. for C₁₇H₁₃N₂O₃: 293.0926. Found: 293.0923 (M⁺).

Kochi-Anderson adduct characterization.**2-(3,5-dimethoxybenzoyl)-3-methylnaphthalene-1,4-dione (1a')**

45% Yield, yellow solid. **¹H NMR (400 MHz, Chloroform-d)** δ: 8.13-8.16 (m, 1H), 8.03-8.06(m, 1H), 7.72-7.81 (m, 2H), 7.03 (d, *J*= 3.04 Hz, 1H), 6.69 (t, *J*=3.0 Hz, 1H), 3.81 (s, 3H), 3.21 (s, 3H). **¹³C NMR (100 MHz, Chloroform-d)** δ: 193.37, 184.72, 183.25, 161.20, 144.24, 143.80, 137.48, 134.14, 134.06, 131.83, 131.50, 126.65, 126.37, 106.91, 106.49 (2C), 55.63(2C), 13.57. One aromatic signal is overlapped in the aromatic region. **HRMS (ESI)** calcd. for C₂₀H₁₅O₅: 336.0998. Found: 336.1005 (M⁺).

Article 3.**General procedure of reduction and protection of menadione and 3-benzyl-menadione derivatives.**

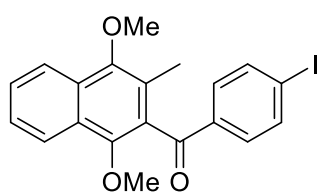
All the experiments were carried out under argon (Ar) atmosphere. Menadione or 3-benzyl-menadione derivatives (1 equiv., 7.47 mmol) was suspended in ethanol (29.1 mL). Then, stannous chloride (3 equiv.) was dissolved in HCl (8 equiv.), added dropwise to the previous solution at room temperature and the mixture was stirred for 2 h. During the reduction process, the formation of a white solid is observed. The solvent was removed in vacuum and the solid was washed with distilled water and filtrated, quickly to avoid the re-oxidation in open air. Subsequently, the resulting crude product was dissolved in acetone (36.4 mL) under Ar atmosphere. At that point, dimethyl sulfate (3 equiv.) was added, the system was heated up to 60 °C. KOH (5 equiv.) dissolved in methanol (16.6 mL) was added dropwise to the previous solution and the reaction was left to proceed at the same temperature for 4h. Once the time described for the reaction finished, KOH (7.94 equiv.) in 30 mL H₂O was added to quench the reaction. The crude of the reaction was obtained, after several extractions with DCM (5x35 mL), dried over MgSO₄ and finally concentrated. The pure compound was isolated after purification by column chromatography (DCM/ Cyclohexane, 1:1 to 7:3).

2-(4-iodobenzyl)-1,4-dimethoxy-3-methylnaphthalene (11b)

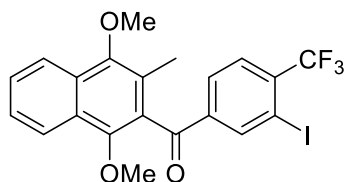
Starting with **11a** Yield 56%; translucent oil. **¹H NMR (CDCl₃, 400 MHz) δ** 8.12–8.06 (m, 2H), 7.54 (d, *J* = 8.3 Hz, 2H), 7.52–7.47 (m, 2H), 6.87 (d, *J* = 8.5 Hz, 2H), 4.21 (s, 2H), 3.86 (s, 3H), 3.83 (s, 3H), 2.24 (s, 3H). **¹³C NMR (CDCl₃, 100 MHz) δ** 150.57, 150.44, 140.22, 137.39, 130.20, 128.42, 128.05, 127.16, 126.81, 125.87, 125.53, 122.46, 122.24, 90.89, 62.31, 61.41, 32.30, 12.65. **HRMS (ESI) m/z** calcd for C₂₀H₁₉IO₂: 418.0424. Found: 418.0413 (M+H⁺).

General procedure for the Friedel-Craft acylation based on TfOH-TFAA mixture of reagent.

1,4-Dimethoxy-2-methylnaphthalene (1.5 mmol) and benzoic acid (1 mmol) were dissolved in dichloromethane (0.2 M). At 0 °C, TFAA (2 mmol) was added. After stirring for 10 min, TfOH (0.5 mmol) was cautiously added and the reaction mixture was allowed to warm up slowly to room temperature and stirred for 16 h. Then, the reaction was quenched with an aqueous saturated NaHCO₃ solution and the aqueous phase was extracted three times with dichloromethane. The combined organic phases were dried over MgSO₄ and the solvent was removed under reduced pressure. The reaction crude was purified by silica gel chromatography by using a mixture of cyclohexane and toluene as eluent to afford analytically pure Friedel–Crafts products.

(1,4-dimethoxy-3-methylnaphthalen-2-yl)(4-iodophenyl)methanone (7b)

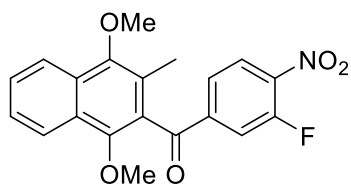
Yield 47%; white solid. m.p: 133–134 °C. **¹H NMR (CDCl₃, 400 MHz) δ** 8.14 (d, *J* = 8.24 Hz, 1H), 8.07 (d, *J* = 7.9 Hz, 1H), 7.82 (d, *J* = 8.5 Hz, 2H), 7.61 – 7.52 (m, 4H), 3.91 (s, 3H), 3.80 (s, 3H), 2.22 (s, 3H). **¹³C NMR (CDCl₃, 100 MHz) δ** 196.75, 150.49, 149.26, 138.09 (2C), 136.59, 130.83 (2C), 130.34, 129.43, 127.21, 127.09, 126.09, 123.45, 122.60, 122.43, 102.18, 63.59, 61.54, 12.74. **HRMS (ESI) calcd. for** C₂₀H₁₈IO₃: 433.0295. Found: 433.0275 (M+H⁺).

(1,4-dimethoxy-3-methylnaphthalen-2-yl)(3-iodo-4-(trifluoromethyl)phenyl)methanone (8b)

Yield 66%; white solid. **m.p:** 90–91 °C. **¹H NMR (CDCl₃, 400 MHz) δ** 8.54 (s, 1H), 8.17–8.15 (m, 1H), 8.08–8.06 (m, 1H), 7.80 – 7.77 (m, 1H), 7.70 (d, *J* = 8.2 Hz, 1H), 7.64–7.60 (m, 1H), 7.58–7.54 (m, 1H), 3.93 (s, 3H), 3.80 (s, 3H), 2.23 (s, 3H). **¹⁹F NMR (CDCl₃, 376 MHz) δ** -63.22. **¹³C NMR (CDCl₃, 100 MHz) δ** 195.19, 150.72, 149.65, 142.05, 140.52, 137.5 (q, *J* = 31.0 Hz), 129.75, 129.47, 129.09,

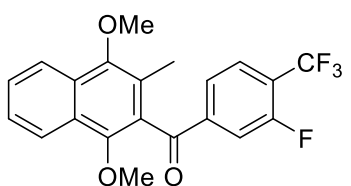
127.99 (q, $J = 6.0$ Hz), 127.55, 127.04, 126.29, 123.30, 122.65, 122.53, 122.36 (q, $J = 272$ Hz), 91.37(q, $J = 1.81$ Hz), 63.69, 61.60, 12.79. **HRMS (ESI)** calcd. for $C_{21}H_{17}F_3IO_3$: 501.0169. Found: 501.0184 ($M+H^+$).

(1,4-dimethoxy-3-methylnaphthalen-2-yl)(3-fluoro-4-nitrophenyl)methanone (9b)



Yield 82%; orange solid. **m.p:** 120 °C. **1H NMR (CDCl₃, 400 MHz)** δ 8.15-8.17 (m, 1H), 8.05 – 8.10 (m, 2H), 7.78 (dd, $J = 10.8$ Hz, 1.68 Hz, 1H), 7.70-7.72 (m, 1H), 7.61-7.65 (m, 1H), 7.55-7.59 (m, 1H), 3.93 (s, 3H), 3.80 (s, 3H), 2.24 (s, 3H). **^{13}C NMR (CDCl₃, 100 MHz)** δ 194.76 (d, $J = 1.06$ Hz), 155.44 (d, $J = 264.9$ Hz), 150.84, 149.82, 142.84 (d, $J = 6.2$ Hz), 140.08 (d, $J = 8.4$ Hz), 129.87, 128.95, 127.74, 126.95, 126.55(d, $J = 2.6$ Hz), 126.42, 125.20 (d, $J = 4.3$ Hz), 123.20, 122.57(d, $J = 0.9$ Hz), 119.00, 18.79, 63.69, 61.60, 12.72. **^{19}F NMR (CDCl₃, 376 MHz)** δ: -116.05 (dd, $J = 10.9, 6.9$ Hz). **HRMS (ESI)** calcd. for C₂₀H₁₇FNO₅: 370.1085. Found: 370.1072 ($M+H^+$).

(1,4-dimethoxy-3-methylnaphthalen-2-yl)(3-fluoro-4-(trifluoromethyl)phenyl)methanone (10b)

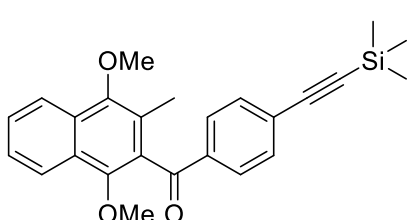


Yield 67%; yellowish oil. **1H NMR (CDCl₃, 500 MHz)** δ 8.16 (d, $J = 8.3$ Hz, 1H), 8.07 – 8.06 (m, 1H), 7.71-7.65 (m, 3H), 7.64-7.61 (m, 1H), 7.58-7.54 (m, 1H), 3.93 (s, 3H), 3.81 (s, 3H), 2.23 (s, 3H). **^{19}F NMR (CDCl₃, 376 MHz)** δ: -61.85 (d, $J = 12.7$ Hz), -112.51 – -112.74 (m). **^{13}C NMR (CDCl₃, 126 MHz)** δ: 195.29 (d, $J = 1.3$ Hz), 160.04 (dq, $J = 259.11, 2.0$ Hz), 150.74, 149.63, 142.37 (d, $J = 6.4$ Hz), 129.74, 129.52, 127.87 (q, $J = 4.4$ Hz), 127.60, 127.06, 126.36, 125.03 (d, $J = 3.6$ Hz), 123.31, 122.79 (dq, $J = 12.8, 33.2$ Hz), 122.60 (d, $J = 7.2$ Hz), 122.11 (q, $J = 273.5$ Hz), 117.34, 117.17, 63.73, 61.64, 12.77. **HRMS (ESI)** calcd. for C₂₁H₁₇F₄O₃: 393.1108. Found: 393.1107 ($M+H^+$).

General procedure to achieve the Sonogashira cross coupling reaction.

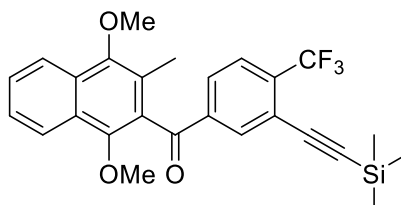
The experiments were performed under Argon and dry conditions. Triethylamine (14 mL) was added to benzoyldimethoxy-iodine derivative (1 equiv., 1 mmol) at room temperature. Subsequently, were added in the following order dichlorobis(triphenylphosphine)palladium(II) (0.06 equiv, 0.06 mmol), copper iodide (0.01 equiv, 0.01 mmol) and ethynyl(trimethyl)silane (3 equiv., 3.0 mmol). The solution darkens to brown, and was stirred at room temperature overnight. The reaction was quenched with a 1:1 brine:H₂O mixture and the crude of the reaction was extracted three times with Et₂O. The combined organic extracts were dried over Na₂SO₄, filtered through celite, and concentrated in vacuum to obtain the pure product by flash chromatography using as a mixture of eluents, cyclohexane: EtOAc.

(1,4-dimethoxy-3-methylnaphthalen-2-yl)(4-((trimethylsilyl)ethynyl)phenyl)methanone (7c)



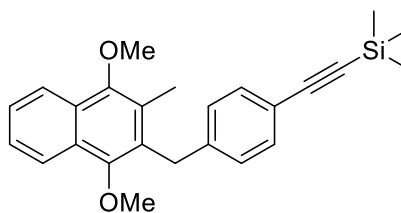
Yield 99%; **1H NMR (CDCl₃, 400 MHz)** δ 8.14 (d, 1H, $J = 8.2$ Hz), 8.07 (d, 1H, $J = 8.3$ Hz), 7.78 (d, 2H, $J = 8.5$ Hz), 7.61-7.57 (m, 1H), 7.55-7.50 (m, 3H), 7.510 (d, 2H, $J = 8.6$ Hz), 3.91 (s, 3H), 3.80 (s, 3H), 2.20 (s, 3H), 0.250 (s, 9H). **^{13}C NMR (CDCl₃, 100 MHz)** δ 195.67, 149.42, 148.25, 135.59, 131.21, 129.67, 128.40, 128.32, 127.59, 126.14 (CH + C_q), 125.03, 122.53, 121.64, 121.41, 103.08, 97.56, 62.54, 60.53, 11.75 (CH₃), -1.21. **HRMS (ESI)** calcd. For C₂₅H₂₇O₃Si: 403.1724. Found: 403.1715 ($M+H^+$).

(1,4-dimethoxy-3-methylnaphthalen-2-yl)(4-(trifluoromethyl)-3 ((trimethylsilyl)ethynyl) phenyl)methanone (8c)



Yield 85%; beige solid. **m.p:** 124-125 °C. **¹H NMR (CDCl₃, 400 MHz)** δ 8.17 (d, *J* = 8.2 Hz, 1H), 8.08 (d, *J* = 8.2 Hz, 1H), 8.05 (s, 1H), 7.81 (d, *J* = 8.2 Hz, 1H), 7.71 (d, *J* = 8.2 Hz, 1H), 7.64-7.60 (m, 1H), 7.58-7.54 (m, 1H), 3.93 (s, 3H), 3.80 (s, 3H), 2.23 (s, 3H), 0.24 (s, 9H). **¹⁹F NMR (CDCl₃, 376 MHz)** δ -62.88. **¹³C NMR (CDCl₃, 100 MHz)** δ 195.91, 150.65, 149.60, 139.57, 136.00 (q, *J* = 30.6 Hz), 134.49, 129.83, 129.67, 128.79, 127.45, 127.09, 126.47 (q, *J* = 5.1 Hz), 126.23, 123.41, 122.91 (q, *J* = 272.2 Hz), 122.67, 122.51, 122.37 (q, *J* = 1.9 Hz), 102.72, 99.46, 63.61, 61.58, 12.77, -0.55. **HRMS (ESI)** calcd. For C₂₆H₂₆F₃O₃Si: 471.1598. Found: 471.1591 (M+H⁺).

((4-((1,4-dimethoxy-3-methylnaphthalen-2-yl)methyl)phenyl)ethynyl)trimethylsilane (11c)

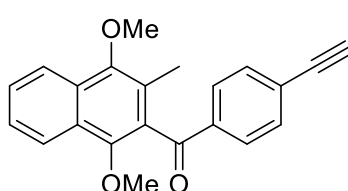


Yield 90%; light brown solid. **m.p:** 110-111 °C. **¹H NMR (CDCl₃, 400 MHz)** δ 8.13-8.08 (m, 2H), 7.54-7.49 (m, 2H), 7.35 (d, *J* = 8.3 Hz, 2H), 7.05 (d, *J* = 8.1 Hz, 2H), 4.27 (s, 2H), 3.86 (s, 3H), 3.82 (s, 3H), 2.22 (s, 3H), 0.24 (s, 9H). **¹³C NMR (CDCl₃, 100 MHz)** δ 150.58, 150.40, 141.23, 132.03, 128.58, 128.02, 128.00, 127.16, 126.94, 125.82, 125.49, 122.46, 122.22, 120.52, 105.15, 93.55, 62.30, 61.37, 32.33, 13.02, -0.03. **HRMS (ESI)** calcd. For C₂₅H₂₈LiO₂Si: 395.2014. Found: 395.2006 (M+Li⁺).

General procedure of alkyne trimethylsilyl (TMS) deprotection.

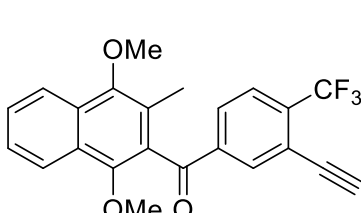
The TMS-protected alkyne derivate (1 equiv., 1.0 mmol) was dissolved in THF (6 mL). Then a solution of TBAF (2.3 equiv, 2.3 mmol) in THF (3 mL) was added dropwise to the original solution, and the reaction was stirred during 1.5 h at room temperature. The reaction was quenched with NH₄Cl (20 mL) and extracted with ether (3 x 10 mL). The organic layers were combined, dried on MgSO₄ and concentrated in vacuum without heating. Flash-chromatography on silica gel (cyclohexane: AcOEt).

(1,4-dimethoxy-3-methylnaphthalen-2-yl)(4-ethynylphenyl)methanone (7d)

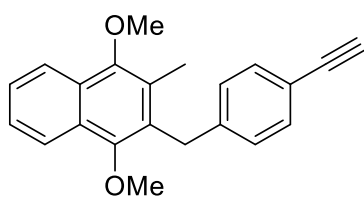


Yield 99%; **¹H NMR (CDCl₃, 400 MHz)** δ 8.14 (d, *J* = 8.3 Hz, 1H), 8.07 (d, *J* = 8.2 Hz, 1H), 7.81 (d, *J* = 8.4 Hz, 2H), 7.61-7.52 (m, 4H), 3.91 (s, 3H), 3.81 (s, 3H), 3.25 (s, 1H), 2.22 (s, 3H). **¹³C NMR (CDCl₃, 100 MHz)** δ 196.66, 150.47, 149.26, 136.99, 132.45, 130.58, 129.43, 129.36, 127.54, 127.18, 127.12, 126.07, 123.50, 122.62, 122.43, 82.83, 80.64, 63.58, 61.54, 12.75. **HRMS (ESI)** calcd. For C₂₂H₁₈NaO₃: 353.1140. Found: 353.1148 (M+Na⁺).

(1,4-dimethoxy-3-methylnaphthalen-2-yl)(3-ethynyl-4-(trifluoromethyl)phenyl) methanone (8d)



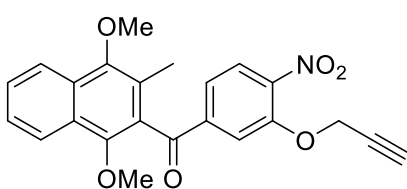
Yield 88%; beige solid. **m.p:** 121-122 °C. **¹H NMR (CDCl₃, 400 MHz)** δ 8.15-8.17 (m, 1H), 8.09 (s, 1H), 8.08 – 8.06 (m, 1H), 7.87 (dd, *J* = 8.2, 0.9 Hz, 1H), 7.75 (d, *J* = 8.2 Hz, 1H), 7.64-7.60 (m, 1H), 7.58-7.54 (m, 1H), 3.93 (s, 3H), 3.80 (s, 3H), 3.39 (s, 1H), 2.23 (s, 3H). **¹⁹F NMR (CDCl₃, 376 MHz)** δ -62.71. **¹³C NMR (CDCl₃, 100 MHz)** δ 195.73, 150.70, 149.62, 139.68, 136.00 (q, *J* = 31.1 Hz), 135.26, 129.71, 129.67, 129.26, 127.50, 127.06, 126.56 (q, *J* = 4.9 Hz), 126.27, 123.35, 122.82 (q, *J* = 272.0 Hz), 122.65, 122.53, 121.32 (q, *J* = 2.1 Hz), 84.21, 78.56, 63.65, 61.59, 12.76. **HRMS (ESI)** calcd. For C₂₃H₁₇F₃LiO₃: 405.1285. Found: 405.1275 (M+Li⁺).

2-(4-ethynylbenzyl)-1,4-dimethoxy-3-methylnaphthalene (11d)

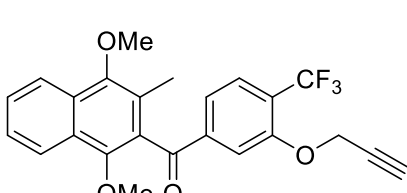
Yield 97%; brown oil. **¹H NMR (CDCl₃, 400 MHz) δ** 7.82–7.94 (m, 2H), 7.23–7.32 (m, 2H), 7.13 (d, *J* = 8.1 Hz, 4H), 6.84 (d, *J* = 8.1 Hz, 2H), 4.03 (s, 2H), 3.62 (s, 3H), 3.58 (s, 3H), 2.78 (s, 1H), 2.00 (s, 3H) **¹³C NMR (101 MHz, CDCl₃) δ** 150.76, 150.59, 141.72, 132.35, 128.65, 128.26, 128.21, 127.33, 127.05, 126.01, 125.67, 122.63, 122.40, 119.67, 83.85, 76.81, 62.45, 61.55, 32.88, 12.82. **HRMS (ESI)** calcd. For C₂₂H₂₀LiO₂: 323.1618. Found: 323.1612 (M+Li⁺).

General procedure to achieve the propargylic alcohol Nucleophilic aromatic substitution.⁸³

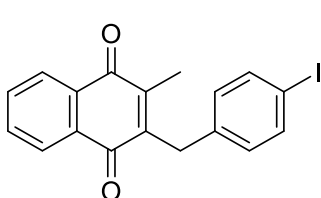
All the experiments were carried out under Ar atmosphere. **1,4-Dimethoxy-2-methylnaphthalene-benzoyl alkyne** (1 equiv., 1.00 mmol) was dissolved in DMF (5 mL). Propargyl alcohol (4 equiv., 4 mmol) and K₂CO₃ (6 equiv., 6 mmol) were added, in the described order. The system was heat up to 60 °C and stirred for 24 h at the same temperature. Once the time described for the reaction was finished, the system was cooled down to room temperature (without external agent). Then Et₂O was added and the organic phase was washed with water. Aqueous phase was extracted 3 times with Et₂O. The organic layers were combined, washed with brine, dried over MgSO₄ and the solvent was removed under vacuum. Purification was performed by silica gel chromatography using Cyclohexane:EtOAc as eluent 95:5 up to 80:20.

(1,4-dimethoxy-3-methylnaphthalen-2-yl)(4-nitro-3-(prop-2-yn-1-yloxy)phenyl) methanone (9c)

Yield 65%; yellow oil. **¹H NMR (CDCl₃, 400 MHz) δ** 8.16 – 8.15 (m, 1H), 8.07–8.05 (m, 1H), 7.83 (d, *J* = 1.6 Hz, 1H), 7.81 (d, *J* = 8.3 Hz, 1H), 7.63–7.60 (m, 1H), 7.58–7.53 (m, 1H), 7.44 (dd, *J* = 8.3, 1.6 Hz, 1H), 4.84 (d, *J* = 2.4 Hz, 2H), 3.92 (s, 3H), 3.81 (s, 3H), 2.49 (t, *J* = 2.4 Hz, 1H) 2.24 (s, 3H). **¹³C NMR (101 MHz, CDCl₃) δ** 195.57, 150.65, 150.59, 149.63, 143.22, 141.09, 129.69, 129.61, 127.52, 127.05, 126.29, 125.73, 123.26, 122.75, 122.56, 122.52, 115.53, 77.53, 76.46, 63.67, 61.57, 57.41, 12.76. **HRMS (ESI)** calcd. for C₂₃H₁₉LiNO₆: 412.1367. Found: 412.1355 (M+Li⁺).

(1,4-dimethoxy-3-methylnaphthalen-2-yl)(3-(prop-2-yn-1-yloxy)-4(trifluoromethyl) phenyl)methanone (10c)

Yield 75%; light yellow oil. **¹H NMR (CDCl₃, 400 MHz) δ** 8.16–8.14 (m, 1H), 8.08 – 8.05 (m, 1H), 7.76 (s, 1H), 7.66 (d, *J* = 7.7 Hz, 1H), 7.61–7.53 (m, 2H), 7.39 (d, *J* = 7.9 Hz, 1H), 7.39 (d, *J* = 8.0 Hz, 1H), 4.81 (d, *J* = 2.4 Hz, 2H), 3.92 (s, 3H), 3.82 (s, 3H), 2.47 (t, *J* = 2.4 Hz, 1H), 2.24 (s, 3H). **¹⁹F NMR (CDCl₃, 376 MHz) δ** -62.73. **¹³C NMR (126 MHz, DMSO) δ** 195.87, 155.52, 150.20, 149.15, 141.52, 129.98, 129.18, 128.38 (d, *J* = 5.7 Hz), 127.89, 126.75, 126.66, 123.28 (d, *J* = 248.0 Hz), 123.03, 122.72, 122.69, 122.50, 122.08 (d, *J* = 6.2 Hz), 113.06, 79.53, 78.15, 63.49, 61.64, 56.75, 12.76. **HRMS (ESI)** calcd. for C₂₄H₂₀F₃O₄: 429.1308. Found: 429.1309 (M+H⁺).

Synthesis of 2-(4-iodobenzyl)-3-methylnaphthalene-1,4-dione (11a) through Kochi-Anderson Reaction.

Menadione (1 equiv., 5.81 mmol) and 4-iodophenylacetic acid (2 equiv., 12.2 mmol) were dissolved in a mixture 3:1 acetonitrile (173 mL) and water (58 mL). The mixture was heated to 85 °C and silver nitrate (0.35 equiv., 2.03 mmol) was added. Then, ammonium persulfate (1.3 equiv., 7.55 mmol) was dissolved in a mixture ACN: water (3:1) and added dropwise. The reaction was stirred for 4.5 h at 85 °C. ACN was removed by reduced pressure, ethyl acetate was added, and

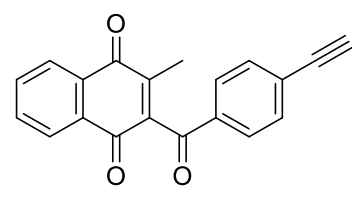
⁸³ S. Raeppe, F. Raeppe, J. Suffert, *Synlett*, **1998**, 7, 794–796.

the organic phase was washed with water several times. The organic phase was dried over Mg_2SO_4 and the solid was removed by filtration. The excess of the liquid was removed by reduced pressure, and the crude of the reaction was purified by flash chromatography (eluent: toluene). Yellow crystals were obtained and recrystallized in pure *n*-hexane to obtain the pure product. Yield 81%; yellow crystals. **m.p:** 130–131 °C. **1H NMR (CDCl₃, 400 MHz)** δ 8.11–8.06 (m, 2H), 7.73–7.68 (m, 2H), 7.58 (d, *J* = 78.4 Hz), 6.98 (d, *J* = 8.4 Hz, 2H), 3.97 (s, 2H), 2.23 (s, 3H). **^{13}C NMR (CDCl₃, 100 MHz)** δ 185.2, 184.53, 144.7, 144.59, 137.75, 137.68, 133.58, 132.07, 131.92, 130.62, 126.49, 126.34, 91.65, 32.01, 13.3 ppm. **HRMS (ESI)** calcd. for C₁₈H₁₃IKO₂: 426.9592. Found: 426.9577 (M+K⁺).

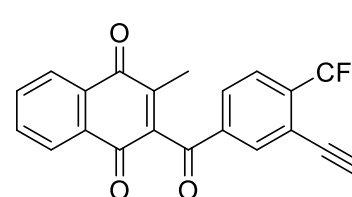
General procedure of oxidative demethylation of 3-benzyl-menadione derivatives.

The 1,4-dimethoxy-2-methyl-3-benzyl-naphthalene derivative (1 equiv., 1 mmol) was dissolved in ACN (24 mL) water (8 mL), cerium ammonium nitrate CAN (2.5 equiv., 2.5 mmol) was added portion wise at room temperature to give a yellow-orange solution. The reaction mixture was stirred for 3 h. ACN was removed under reduced pressure and the residue was extracted with DCM (2x), the organic layers were washed with brine (1x) and dried over Na₂SO₄. A flash chromatography was performed (cyclohexane:EtOAc 99.8:0.2 to 90:10).

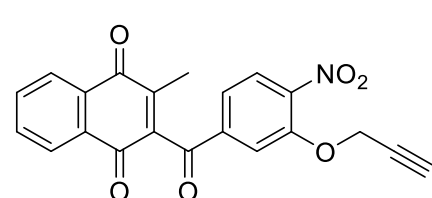
2-(4-ethynylbenzoyl)-3-methylnaphthalene-1,4-dione (7)

 Yield: 66%; yellow solid. **1H NMR (CDCl₃, 400 MHz)** δ: 8.18–8.16 (m, 1H), 8.08–8.06 (m, 1H), 7.87 (d, *J* = 8.6 Hz, 2H), 7.82–7.75 (m, 2H), 7.60 (d, *J* = 8.7 Hz, 2H), 3.29 (s, 1H), 2.06 (s, 3H). **^{13}C NMR (CDCl₃, 400 MHz)** δ: 192.91, 184.68, 183.34, 144.23, 143.99, 135.29, 134.26, 134.17, 132.73, 131.87, 131.50, 128.97, 128.40, 126.76, 126.44, 82.54, 81.33, 8.85. **HRMS (ESI)** calcd. for C₂₀H₁₂NaO₃ 323.0679. Found: 323.0672 (M+Na⁺)

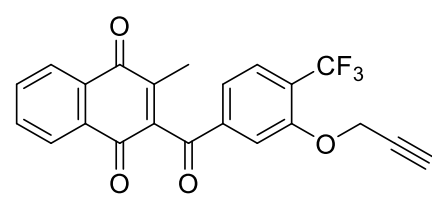
2-(3-ethynyl-4-(trifluoromethyl)benzoyl)-3-methylnaphthalene-1,4-dione (8)

 Yield 96%; pale yellow solid. **m.p:** 148–149 °C. **1H NMR (CDCl₃, 400 MHz)** δ: 8.20 – 8.18 (m, 1H), 8.09 (s, 1H), 8.08 – 8.06 (m, 1H), 7.95 (d, *J* = 8.2 Hz, 1H), 7.84 – 7.77 (m, 3H), 3.44 (s, 1H), 2.09 (s, 3H). **^{19}F NMR (CDCl₃, 376 MHz)** δ - 62.86. **^{13}C NMR (CDCl₃, 100 MHz)** δ 192.26, 184.39, 183.29, 144.99, 143.17, 138.06, 136.71 (q, *J* = 31.3 Hz), 134.87, 134.48, 134.32, 131.84, 131.36, 128.65, 126.90 (q, *J* = 4.8 Hz), 126.90, 126.48, 122.63 (q, *J* = 273.1 Hz), 121.79 (q, *J* = 2.1 Hz) 84.77, 78.23, 13.62. **HRMS (negative ESI)** calcd. for C₂₁H₁₀O₃F₃: 367.0582. Found: 367.0591 (M-H⁺)⁻

2-methyl-3-(4-nitro-3-(prop-2-yn-1-yloxy)benzoyl)naphthalene-1,4-dione (9)

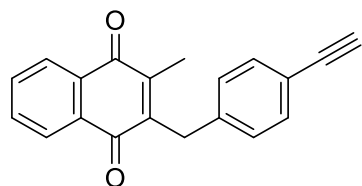
 Yield 65%; yellow solid. **m.p:** 167–168 °C. **1H NMR (CDCl₃, 400 MHz)** δ: 8.20 – 8.18 (m, 1H), 8.08 – 8.06 (m, 1H), 7.89 (d, *J* = 1.6 Hz, 1H), 7.86 (d, *J* = 8.3 Hz, 1H), 7.85 – 7.78 (m, 2H), 7.51 (dd, *J* = 8.3 Hz, 1.6 Hz, 1H) 4.91 (d, *J* = 2.4 Hz, 2H), 2.57 (t, *J* = 2.4 Hz, 1H), 2.10 (s, 3H). **^{13}C NMR (CDCl₃, 100 MHz)** δ: 192.12, 184.34, 183.24, 150.84, 144.97, 143.68, 143.17, 139.23, 134.53, 134.36, 131.81, 131.35, 126.94, 126.44, 126.04, 122.32, 115.03, 77.89, 76.39, 57.51, 13.66. **HRMS (ESI)** calcd. for C₂₁H₁₄NO₆: 376.0816. Found: 376.0823 (M+H⁺).

2-methyl-3-(3-(prop-2-yn-1-yloxy)-4-(trifluoromethyl)benzoyl)naphthalene-1,4-dione (10)

 Yield 64%; yellow solid. **m.p:** 177–178 °C. **1H NMR (CDCl₃, 400 MHz)** δ 8.20 – 8.17 (m, 1H), 8.08 – 8.06 (m, 1H), 7.84 – 7.77 (m, 3H), 7.69 (d, *J* = 8.1, 1H), 7.47 (d, *J* = 8.0, 1H), 4.87 (d, *J* = 2.4 Hz, 2H), 2.53 (t, *J* = 2.4 Hz, 2H), 2.09 (s, 3H). **^{19}F NMR (377 MHz, CDCl₃)** δ -62.90. **^{13}C NMR (CDCl₃, 100 MHz)** δ 192.72, 184.50, 183.28, 156.05 (q, *J* = 1.5 Hz), 144.61, 143.57, 139.56, 134.41, 134.28, 131.84, 131.43, 128.15 (q, *J* =

5.1 Hz), 126.87, 126.43, 124.62 (q, J = 31.67 Hz), 122.65 (q, J = 271.4 Hz), 122.10, 112.70, 77.05, 56.74, 13.63. **HRMS (ESI)** calcd. for $C_{22}H_{14}F_3O_4$: 399.0839. Found: 399.0836 ($M+H^+$).

2-(4-ethynylbenzyl)-3-methylnaphthalene-1,4-dione (11)



Yield 72%; yellow solid. **m.p:** 146–147 °C. **1H NMR (CDCl₃, 400 MHz)** δ 8.10–8.07 (m, 2H), 7.73–7.69 (m, 2H), 7.39 (d, J = 8.2 Hz, 2H), 7.18 (d, J = 8.2 Hz, 2H), 4.03 (s, 2H), 3.03 (s, 1H), 2.23 (s, 3H) ppm; **^{13}C NMR (CDCl₃, 100 MHz)** δ 185.21, 184.53, 144.74, 144.65, 138.96, 133.55, 132.39, 132.07, 131.93, 128.56, 126.49, 126.32, 120.22, 83.40, 77.05, 32.35, 13.30. **HRMS** calcd. for $C_{20}H_{14}KO_2$: 325.0625. Found: 325.0618 ($M+K^+$).

Irradiation experiments for photo-benzylic oxidation of the (pro-) ABPP benzylmenadione probe 11 to benzoylmenadione 7.

In a tube was added 50 mg of 2-(4-ethynylbenzyl)-3-methylnaphthalene-1,4-dione **11** and 2 mL of the appropriate solvent. The mixture was agitated and bubbled with oxygen during 30 min. Then, under a positive pressure of oxygen, the tube was placed in a Rayonet photochemical reactor and irradiated at 350 nm for 72 h. The resulting mixture was extracted with dichloromethane if necessary and the solvent was removed under reduced pressure. The reaction crude was directly analyzed by NMR spectroscopy.

Chapitre III. Experimental part.

Article 4.

Synthesis of precursors.

2a, 2b, 2i, 2b, 2q and 2ab were obtained from commercial sources. **2f, 2i** and **2aa** were obtained from radical bromination of commercial toluenes according to a published procedure.⁸⁴ **2c, 2d, 2e, 2g, 2h, 2j, 2k, 2r, 2s, 2u, 2v, 2w, 2x, 2y** and **2z** were obtained either from the commercial benzaldehydes, reduced by sodium borohydride, or directly from the commercial benzyl alcohols, and then brominated by triphenylphosphine/dibromide,⁸⁵ triphenylphosphine/tetrabromomethane⁸⁶ or potassium tribromide.⁸⁷ **2t** was synthetized according to a published procedure starting from the commercially available p-toluidine.⁸⁸

4-trifluoromethylbenzyl iodide **2a'** was obtained from nucleophilic substitution on **2a**.⁸⁹ 4-trifluoromethylbenzyl chloride was obtained from commercial source.

All spectral data were in accordance with published data.

1a, 4b, 4h and **4k** were obtained from commercial sources.

4a,⁹⁰ **4c**,⁹¹ **4d**,⁹² **4e**,⁹² **4f**,⁹³ **4g**,⁹⁴ **4i**,⁹⁵ **4j**⁴⁵ were synthetized according to published procedures.

All spectral data were in accordance with published data.

General procedure for the photocatalytic benzylation of quinones.

In a 10 mL tube, quinone (0.5 mmol), benzyl bromide (0.75 mmol) and Fe(acac)₃ (10%) were dissolved in Acetonitrile (5 mL). The mixture was stirred and 2,6-lutidine (0.6 mmol) and γ-terpinene (0.6 mmol) were added successively. The tube was sealed, placed under blue light irradiation and heated up at 90°C during 24h. After completion, the mixture was allowed to cool down at room temperature and was partitioned between ethyl acetate (10 mL) and aqueous 1M HCl (10 mL). The aqueous layer was extracted once with 10 mL ethyl acetate and the reunited organic layers were washed with brine and dried with MgSO₄. The solvent was removed and the crude was purified by silica gel chromatography to obtain pure benzylated quinone.

⁸⁴ R. Das, M. Kapur, *J. Org. Chem.* **2017**, *82*, 1114-1126.

⁸⁵ P. A. Champagne, J. Pomarole, M. Thérien, Y. Benhassine, S. Beaulieu, C. Y. Legault, J. Paquin, *Org. Lett.* **2013**, *15*, 2210-2213.

⁸⁶ A. L. Gill, M. Frederickson, A. Cleasby, S. J. Woodhead, M. G. Carr, A. J. Woodhead, M. T. Walker, M. S. Congreve, L. A. Devine, D. Tisi, M. O'Reilly, L. C. A. Seavers, D. J. Davis, J. Curry, R. Anthony, A. Padova, C. W. Murray, R. A. E. Carr, H. Jhoti, *J. Med. Chem.* **2005**, *48*, 414-426.

⁸⁷ L. Feng, K. Lv, M. Liu, S. Wang, J. Zhao, X. You, S. Li, J. Cao, H. Guo, *Eur. J. Med. Chem.* **2012**, *55*, 125-136.

⁸⁸ Y. Miura, T. Issiki, Y. Ushitan, Y. Teki, K. Itoh, *J. Mater. Chem.* **1996**, *6*, 1745-1750.

⁸⁹ D. F. J. Caputo, C. Arroniz, A. B. Durr, J. J. Mousseau, A. F. Stepan, S. J. Mansfield, E. A. Anderson. *Chem. Sci.* **2018**, *9*, 5295-5300.

⁹⁰ J. Su, Y. Zhang, M. Chen, W. Li, X. Qin, Y. Xie, L. Qin, S. Huang, M. Zhang, *Synlett.* **2019**, *30*, 630-634.

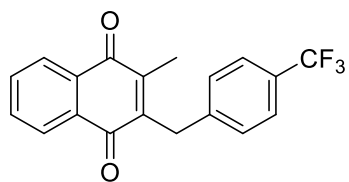
⁹¹ Z. She, Y. Shi, Y. Huang, Y. Cheng, F. Song, J. You. *ChemComm*, **2014**, *50*, 13914-13916.

⁹² A. Bunge, H.-J. Hamann, E. McCalmont, J. Liebscher, *Tetrahedron Lett.* **2009**, *50*, 4629-4632.

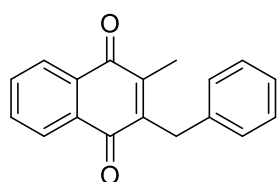
⁹³ M. L. Bolognesi, F. Lizzi, R. Perozzo, R. Brun, A. Cavalli, *Bioorg. Med. Chem. Lett.* **2008**, *18*, 2272-2276.

⁹⁴ R. B. Smith, C. Canton, N. S. Lawrence, C. Livingstone, J. Davis, *New. J. Chem.* **2006**, *30*, 1718-1724.

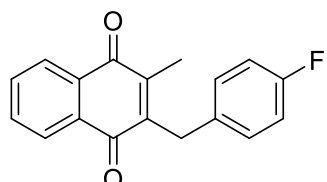
⁹⁵ K. Rajendra Prasad, K. Suresh Babu, R. Ranga Rao, G. Suresh, K. Rekha, J. Madhusudana Murthy, P. Usha Rani, J. Madhusudana Rao, *Med. Chem. Res.* **2012**, *21*, 578-583.

Product characterization.**2-methyl-3-(4-(trifluoromethyl)benzoyl)naphthalene-1,4-dione (3a)**

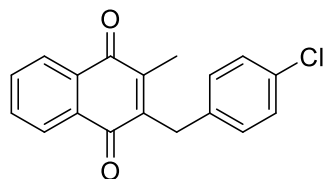
According to the general procedure, menadione and 4-trifluoromethylbenzyl bromide were used. After chromatography on silica gel (Cyclohexane:Toluene = 1:1, UV), 139 mg (0.42 mmol, 84% yield) of **3a** were isolated as a yellow solid. **m.p:** 70-71°C. **¹H NMR (500 MHz, Chloroform-d)** δ 8.13 – 8.02 (m, 2H), 7.74 – 7.65 (m, 2H), 7.52 (d, *J* = 8.1 Hz, 2H), 7.35 (d, *J* = 8.0 Hz, 2H), 4.08 (s, 2H), 2.25 (s, 3H). **¹⁹F NMR (471 MHz, Chloroform-d)** δ -62.45. **¹³C NMR (126 MHz, Chloroform-d)** δ 185.22, 184.60, 144.99, 144.51, 142.34, 133.78, 133.76, 132.19, 132.01, 129.01, 128.94 (q, *J* = 32.3 Hz), 126.64, 126.51, 125.70 (q, *J* = 3.8 Hz), 124.26 (q, *J* = 271.8 Hz), 32.47, 13.47. **HRMS (ESI)** calculated for C₁₉H₁₄F₃O₂: 331.0940. Measured: 331.0949 (MH⁺).

2-benzyl-3-methylnaphthalene-1,4-dione (3b)

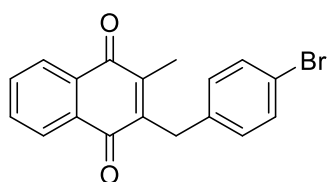
According to the general procedure, menadione and benzyl bromide were used. After chromatography on silica gel (Cyclohexane:Toluene = 4:6, UV), 90 mg (0.34 mmol, 69% yield) of **3b** were isolated as a yellow solid. **m.p:** 105-106°C. **¹H NMR (400 MHz, Chloroform-d)** δ 8.14 – 8.03 (m, 2H), 7.70 (dd, *J* = 5.7, 3.3 Hz, 2H), 7.44 – 6.92 (m, 5H), 4.04 (s, 2H), 2.25 (s, 3H). **¹³C NMR (101 MHz, Chloroform-d)** δ 185.53, 184.79, 145.48, 144.57, 138.19, 133.63, 133.60, 132.27, 132.18, 128.79, 128.73, 126.62, 126.56, 126.41, 32.55, 13.41. **HRMS (ESI)** calculated for C₁₈H₁₅O₂: 263.1067. Measured: 263.1072 (MH⁺).

2-(4-fluorobenzyl)-3-methylnaphthalene-1,4-dione (3c)

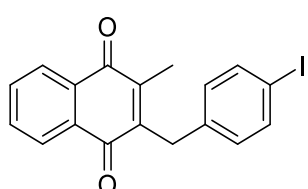
According to the general procedure, menadione and 4-fluorobenzyl bromide were used. After chromatography on silica gel (Cyclohexane:Toluene = 3:7, UV), 93 mg (0.33 mmol, 66% yield) of **3c** were isolated as a yellow solid. **m.p:** 114-115°C. **¹H NMR (400 MHz, Chloroform-d)** δ 8.15 – 8.04 (m, 2H), 7.76 – 7.66 (m, 2H), 7.22 – 7.16 (m, 2H), 7.00 – 6.90 (m, 2H), 4.00 (s, 2H), 2.25 (s, 3H). **¹⁹F NMR (377 MHz, Chloroform-d)** δ -116.52 – -116.64 (m). **¹³C NMR (126 MHz, Chloroform-d)** δ 185.40, 184.72, 161.62 (d, *J* = 244.7 Hz), 145.23, 144.49, 133.81 (d, *J* = 3.3 Hz), 133.66, 132.20, 132.09, 130.17 (d, *J* = 7.8 Hz), 126.59, 126.43, 115.56 (d, *J* = 21.3 Hz), 31.77, 13.37. **HRMS (ESI)** calculated for C₁₈H₁₄FO₂: 281.0972. Measured: 281.0987 (MH⁺).

2-(4-chlorobenzyl)-3-methylnaphthalene-1,4-dione (3d)

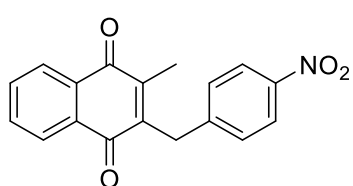
According to the general procedure, menadione and 4-chlorobenzyl bromide were used. After chromatography on silica gel (Cyclohexane:Toluene = 4:6, UV), 109 mg (0.37 mmol, 73% yield) of **3d** were isolated as a yellow solid. **m.p:** 132-133°C. **¹H NMR (400 MHz, Chloroform-d)** δ 8.28 – 7.95 (m, 2H), 7.70 (m, 2H), 7.25 – 7.20 (m, 2H), 7.19 – 7.13 (m, 2H), 3.99 (s, 1H), 2.24 (s, 1H). **¹³C NMR (101 MHz, Chloroform-d)** δ 185.36, 184.69, 144.97, 144.68, 136.66, 133.72, 132.41, 132.22, 132.08, 130.07, 128.89, 126.63, 126.48, 31.98, 13.43. **HRMS (ESI)** calculated for C₁₈H₁₄ClO₂: 297.0677. Measured: 297.0684 (MH⁺).

2-(4-bromobenzyl)-3-methylnaphthalene-1,4-dione (3e)

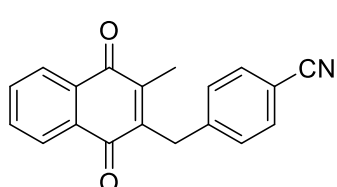
According to the general procedure, menadione and 4-bromobenzyl bromide were used. After chromatography on silica gel (Cyclohexane:Toluene = 4:6, UV), 137 mg (0.402 mmol, 80% yield) of **3e** were isolated as a yellow solid. **m.p:** 123–124°C. **¹H NMR (400 MHz, Chloroform-d)** δ 8.19 – 8.01 (m, 2H), 7.70 (m, 2H), 7.44 – 7.35 (m, 2H), 7.16 – 7.04 (m, 2H), 3.97 (s, 2H), 2.24 (s, 3H). **¹³C NMR (101 MHz, Chloroform-d)** δ 185.34, 184.68, 144.88, 144.71, 137.20, 133.72, 132.21, 132.07, 131.85, 130.45, 126.63, 126.48, 120.44, 32.05, 13.44. **HRMS (ESI)** calculated for C₁₈H₁₄BrO₂: 341.0172. Measured: 341.0180 (MH⁺).

2-(4-iodobenzyl)-3-methylnaphthalene-1,4-dione (3f)

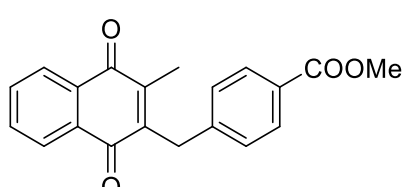
According to the general procedure, menadione and 4-iodobenzyl bromide were used. After chromatography on silica gel (Cyclohexane:Toluene = 4:6, UV), 158 mg (0.407 mmol, 81% yield) of **3f** were isolated as a yellow solid. **m.p:** 121–122°C. **¹H NMR (400 MHz, Chloroform-d)** δ 8.18 – 7.99 (m, 2H), 7.79 – 7.64 (m, 2H), 7.60 – 7.47 (m, 2H), 7.03 – 6.86 (m, 2H), 3.97 (s, 2H), 2.24 (s, 3H). **¹³C NMR (101 MHz, Chloroform-d)** δ 185.35, 184.69, 144.86, 144.74, 137.91, 137.84, 133.73, 132.23, 132.08, 130.78, 126.65, 126.50, 91.81, 32.17, 13.46. **HRMS (ESI)** calculated for C₁₈H₁₄IO₂: 389.0033. Measured: 389.0043 (MH⁺).

2-methyl-3-(4-nitrobenzyl)naphthalene-1,4-dione (3g)

According to the general procedure, menadione and 4-nitrobenzyl bromide were used. After chromatography on silica gel (Cyclohexane:Ethyl acetate = 9:1, UV), 118 mg (0.38 mmol, 77% yield) of **3g** were isolated as a yellow solid. **m.p:** 153–154°C. **¹H NMR (400 MHz, Chloroform-d)** δ 8.09 – 7.96 (m, 4H), 7.70 – 7.60 (m, 2H), 7.38 – 7.28 (m, 2H), 4.06 (s, 2H), 2.19 (s, 3H). **¹³C NMR (101 MHz, Chloroform-d)** δ 185.08, 184.53, 146.83, 145.97, 145.31, 143.96, 133.95, 133.90, 132.18, 131.94, 129.53, 126.71, 126.63, 124.05, 32.64, 13.59. **HRMS (ESI)** calculated for C₁₈H₁₄NO₄: 308.0917. Measured: 308.0923 (MH⁺).

4-(3-methyl-1,4-dioxo-1,4-dihydronaphthalene-2-carbonyl)benzonitrile (3h)

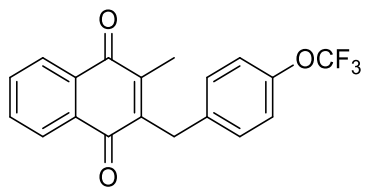
According to the general procedure, menadione and 4-cyannobenzyl bromide were used. After chromatography on silica gel (Toluene, UV), 108 mg (0.38 mmol, 75% yield) of **3h** were isolated as a yellow solid. **m.p:** 161–162°C. **¹H NMR (400 MHz, Chloroform-d)** δ 8.15 – 8.01 (m, 2H), 7.82 – 7.66 (m, 2H), 7.63 – 7.50 (m, 2H), 7.41 – 7.30 (m, 2H), 4.08 (s, 2H), 2.24 (s, 3H). **¹³C NMR (101 MHz, Chloroform-d)** δ 185.11, 184.55, 145.22, 144.04, 143.85, 133.91, 133.86, 132.60, 132.18, 131.95, 129.49, 126.68, 126.60, 118.88, 110.62, 32.82, 13.55. **HRMS (ESI)** calculated for C₁₉H₁₄NO₂: 288.1019. Measured: 288.1033 (MH⁺).

methyl 4-((3-methyl-1,4-dioxo-1,4-dihydronaphthalen-2-yl)methyl)benzoate (3i)

According to the general procedure, menadione and methyl 4-(bromomethyl)benzoate were used. After chromatography on silica gel (Toluene, UV), 80 mg (0.25 mmol, 50% yield) of **3i** were isolated as a yellow solid. **m.p:** 111–112°C. **¹H NMR (400 MHz, Chloroform-d)** δ 8.12 – 8.06 (m, 2H), 7.95 – 7.91 (m, 2H), 7.74 – 7.68 (m, 2H), 7.29 (d, J = 8.5 Hz, 2H), 4.08 (s, 2H), 3.88 (s, 3H), 2.23 (s, 3H). **¹³C NMR (101 MHz,**

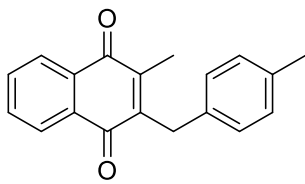
Chloroform-d) δ 185.30, 184.63, 166.98, 145.00, 144.68, 143.61, 133.75, 132.23, 132.06, 130.11, 128.70, 128.57, 126.66, 126.51, 52.18, 32.65, 13.48. **HRMS (ESI)** calculated for C₂₀H₁₇O₄: 321.1121. Measured: 321.1108 (MH⁺).

2-methyl-3-(4-(trifluoromethoxy)benzyl)naphthalene-1,4-dione (3j)



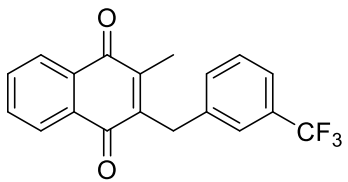
According to the general procedure, menadione and 4-trifluoromethoxybenzyl bromide were used. After chromatography on silica gel (Cyclohexane:Toluene = 4:6, UV), 138 mg (0.4 mmol, 80% yield) of **3j** were isolated as a yellow solid. **m.p:** 65–66°C. **¹H NMR (400 MHz, Chloroform-d)** δ 8.12 – 8.05 (m, 2H), 7.71 (dd, J = 5.8, 3.3 Hz, 2H), 7.30 – 7.22 (m, 2H), 7.11 (dt, J = 7.7, 1.0 Hz, 2H), 4.03 (s, 2H), 2.26 (s, 3H). **¹⁹F NMR (377 MHz, Chloroform-d)** δ -57.93. **¹³C NMR (101 MHz, Chloroform-d)** δ 185.36, 184.71, 147.93 (q, J = 2.0 Hz), 144.90, 144.74, 136.92, 133.75, 132.24, 132.09, 130.04, 129.18, 128.37, 126.65, 126.51, 120.59 (d, J = 256.9 Hz), 31.96, 13.46. **HRMS (ESI)** calculated for C₁₉H₁₄F₃O₃: 347.0890. Measured: 347.0870 (MH⁺).

2-methyl-3-(4-methylbenzyl)naphthalene-1,4-dione (3k)



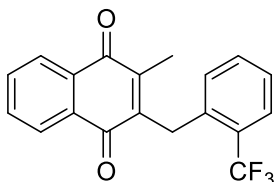
According to the general procedure, menadione and 4-methylbenzyl bromide were used. After chromatography on silica gel (Cyclohexane:Toluene = 4:6, UV), 71 mg (0.26 mmol, 51% yield) of **3k** were isolated as a yellow solid. **m.p:** 135–136 °C. **¹H NMR (500 MHz, Chloroform-d)** δ 8.08 (m, 2H), 7.69 (m, 2H), 7.13 (d, J = 8.2 Hz, 2H), 7.07 (d, J = 8.1 Hz, 2H), 4.00 (s, 2H), 2.29 (s, 3H), 2.25 (s, 3H). **¹³C NMR (126 MHz, Chloroform-d)** δ 185.59, 184.83, 145.68, 144.36, 136.13, 135.09, 133.59, 133.55, 132.26, 132.21, 129.47, 128.62, 126.60, 126.38, 32.14, 21.12, 13.39. **HRMS (ESI)** calculated for C₁₉H₁₇O₂: 277.1223. Measured: 277.1227 (MH⁺).

2-methyl-3-(3-(trifluoromethyl)benzyl)naphthalene-1,4-dione (3l)

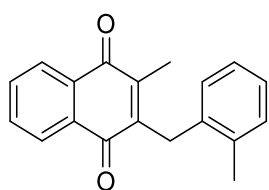


According to the general procedure, menadione and 3-trifluoromethylbenzyl bromide were used. After chromatography on silica gel (Cyclohexane:Toluene = 4:6, UV), 126 mg (0.38 mmol, 76% yield) of **3l** were isolated as a yellow solid. **m.p:** 92–93 °C. **¹H NMR (400 MHz, Chloroform-d)** δ 8.09 (m, 2H), 7.71 (m, 2H), 7.53 – 7.34 (m, 4H), 4.08 (s, 2H), 2.25 (s, 3H). **¹⁹F NMR (377 MHz, Chloroform-d)** δ -62.58. **¹³C NMR (101 MHz, Chloroform-d)** δ 185.13, 184.48, 144.86, 144.37, 139.05, 133.64, 132.09, 131.94, 131.92, 131.91, 130.97 (q, J = 32.2 Hz), 129.11, 126.55, 126.39, 125.32 (q, J = 3.9 Hz), 124.04 (q, J = 272.4 Hz), 123.40 (q, J = 3.8 Hz), 32.29, 13.35. **HRMS (ESI)** calculated for C₁₉H₁₄F₃O₂: 331.0940. Measured: 331.0936 (MH⁺).

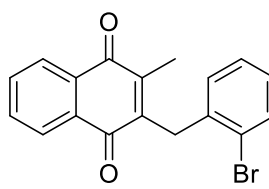
2-methyl-3-(2-(trifluoromethyl)benzyl)naphthalene-1,4-dione (3m)



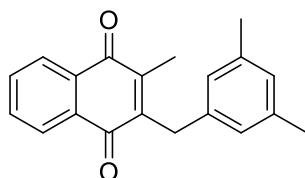
According to the general procedure, menadione and 2-trifluoromethylbenzyl bromide were used. After chromatography on silica gel (Cyclohexane:Toluene = 4:6, UV), 127 mg (0.38 mmol, 77% yield) of **3m** were isolated as a yellow solid. **m.p:** 106–107°C. **¹H NMR (400 MHz, Chloroform-d)** δ 8.28 – 8.01 (m, 2H), 7.78 – 7.72 (m, 2H), 7.70 (d, J = 7.3 Hz, 1H), 7.36 (t, J = 7.1 Hz, 1H), 7.30 (t, J = 7.3 Hz, 1H), 6.96 (d, J = 7.6 Hz, 1H), 4.25 (s, 2H), 2.11 (s, 3H). **¹⁹F NMR (377 MHz, Chloroform-d)** δ -60.90. **¹³C NMR (101 MHz, Chloroform-d)** δ 185.13, 184.50, 146.42, 144.36, 136.75, 133.83, 133.81, 132.36, 132.23, 132.10, 128.69 (q, J = 29.9 Hz), 128.29, 126.77, 126.60, 126.56, 126.44 (q, J = 5.8 Hz), 124.70 (q, J = 273.8 Hz), 28.79 (q, J = 2.6 Hz), 13.23. **HRMS (ESI)** calculated for C₁₉H₁₄F₃O₂: 331.0940. Measured: 331.0930 (MH⁺).

2-methyl-3-(2-methylbenzyl)naphthalene-1,4-dione (3n)

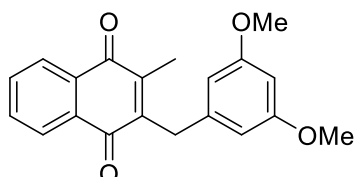
According to the general procedure, menadione and 2-methylbenzyl bromide were used. After chromatography on silica gel (Cyclohexane:Toluene = 4:6, UV), 92 mg (0.33 mmol, 67% yield) of **3n** were isolated as a yellow solid. **m.p:** 61-62 °C. **¹H NMR (400 MHz, Chloroform-d)** δ 8.15 – 8.11 (m, 1H), 8.11 – 8.06 (m, 1H), 7.77 – 7.67 (m, 2H), 7.20 (dd, *J* = 7.3, 1.6 Hz, 1H), 7.11 (td, *J* = 7.4, 1.5 Hz, 1H), 7.04 (td, *J* = 7.6, 1.6 Hz, 1H), 6.84 (dd, *J* = 7.6, 1.3 Hz, 1H), 3.97 (s, 2H), 2.45 (s, 3H), 2.16 (s, 3H). **¹³C NMR (101 MHz, Chloroform-d)** δ 185.32, 184.58, 145.65, 145.49, 136.39, 136.14, 133.65, 133.61, 132.38, 132.26, 130.47, 126.73, 126.68, 126.51, 126.47, 126.27, 29.70, 20.12, 13.36. **HRMS (ESI)** calculated for C₁₉H₁₇O₂: 277.1223. Measured: 277.1224 (MH⁺).

2-(2-bromobenzyl)-3-methylnaphthalene-1,4-dione (3o)

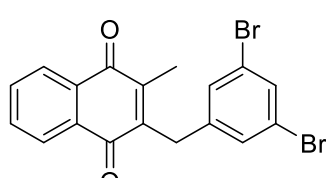
According to the general procedure, menadione and 2-bromobenzyl bromide were used. After chromatography on silica gel (Cyclohexane:Toluene = 4:6, UV), 134 mg (0.39 mmol, 79% yield) of **3o** were isolated as a yellow solid. **m.p:** 102-103°C. **¹H NMR (400 MHz, Chloroform-d)** δ 8.19 – 7.99 (m, 2H), 7.79 – 7.64 (m, 2H), 7.59 (dd, *J* = 8.0, 1.4 Hz, 1H), 7.15 (td, *J* = 7.5, 1.4 Hz, 1H), 7.06 (td, *J* = 7.6, 1.8 Hz, 1H), 6.92 (dd, *J* = 7.6, 1.8 Hz, 1H), 4.13 (s, 2H), 2.13 (s, 3H). **¹³C NMR (101 MHz, Chloroform-d)** δ 185.20, 184.51, 146.04, 144.73, 137.49, 133.75, 133.72, 133.05, 132.32, 132.15, 128.77, 128.12, 127.73, 126.72, 126.52, 124.84, 32.83, 13.45. **HRMS (ESI)** calculated for C₁₈H₁₄BrO₂: 341.0172. Measured: 341.0181 (MH⁺).

2-(3,5-dimethylbenzyl)-3-methylnaphthalene-1,4-dione (3p)

According to the general procedure, menadione and 3,5-dimethylbenzyl bromide were used. After chromatography on silica gel (Cyclohexane:Toluene = 4:6, UV), 101 mg (0.35 mmol, 70% yield) of **3p** were isolated as a yellow solid. **m.p:** 108-109°C. **¹H NMR (400 MHz, Chloroform-d)** δ 8.15 – 8.00 (m, 2H), 7.70 (dd, *J* = 5.8, 3.3 Hz, 2H), 7.02 – 6.63 (m, 3H), 3.96 (s, 2H), 2.26 (s, 6H), 2.25 (s, 3H). **¹³C NMR (101 MHz, Chloroform-d)** δ 185.64, 184.85, 145.65, 144.54, 138.31, 138.00, 133.60, 133.56, 132.32, 132.25, 128.26, 126.67, 126.47, 126.39, 32.39, 21.44, 13.45. **HRMS (ESI)** calculated for C₂₀H₁₉O₂: 291.1380. Measured: 291.1377 (MH⁺).

2-(3,5-dimethoxybenzyl)-3-methylnaphthalene-1,4-dione (3q)

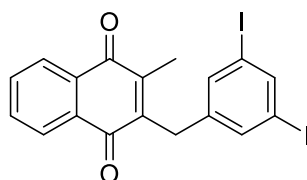
According to the general procedure, menadione and 3,5-dimethoxybenzyl bromide were used. After chromatography on silica gel (Cyclohexane:Ethyl Acetate = 95:5, UV), 110 mg (0.34 mmol, 68% yield) of **3q** were isolated as a yellow solid. **m.p:** 133-134 °C. **¹H NMR (400 MHz, Chloroform-d)** δ 8.17 – 7.99 (m, 2H), 7.74 – 7.65 (m, 2H), 6.37 (d, *J* = 2.2 Hz, 2H), 6.29 (t, *J* = 2.2 Hz, 1H), 3.97 (s, 2H), 3.75 (s, 6H), 2.24 (s, 3H). **¹³C NMR (101 MHz, Chloroform-d)** δ 185.46, 184.72, 161.04, 145.09, 144.78, 140.42, 133.61, 133.59, 132.27, 132.17, 126.63, 126.40, 106.97, 98.14, 55.39, 32.64, 13.42. **HRMS (ESI)** calculated for C₂₀H₁₉O₄: 323.1278. Measured: 323.1287 (MH⁺).

2-(3,5-dibromobenzyl)-3-methylnaphthalene-1,4-dione (3r)

According to the general procedure, menadione and 3,5-dibromobenzyl bromide were used. After chromatography on silica gel (Cyclohexane:Toluene = 1:1, UV), 135 mg (0.32 mmol, 64% yield) of **3r** were isolated as a yellow solid. **m.p:** 151-152°C. **¹H (400MHz, Chloroform-d)** δ 8.11 (m, 2H), 7.75-7.71 (m, 2H), 7.51 (t, *J* = 1.8 Hz, 1H), 7.30 (m, 2H), 3.91 (s, 2H), 2.23 (s, 3H). **¹³C NMR (126 MHz,**

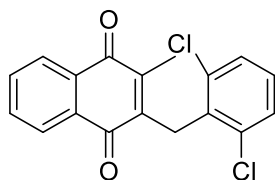
Chloroform-d) δ 185.17, 184.47, 145.27, 143.88, 142.07, 133.88, 133.86, 132.45, 132.22, 131.98, 130.49, 126.77, 126.61, 123.25, 32.00, 13.59. **HRMS (ESI)** calculated for $C_{18}H_{13}Br_2O_2$: 418.9277. Measured: 418.9290 (MH^+).

2-(3,5-diiodobenzyl)-3-methylnaphthalene-1,4-dione (3s)



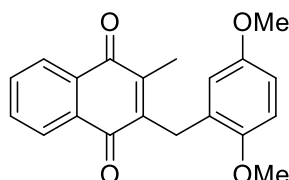
According to the general procedure, menadione and 3,5-diiodobenzyl bromide were used. After chromatography on silica gel (Cyclohexane:Toluene = 1:1, UV), 191 mg (0.37 mmol, 74% yield) of **3s** were isolated as a yellow solid. **m.p:** 176–177°C. **¹H NMR (400 MHz, Chloroform-d)** δ 8.12 (m, 2H), 7.88 (t, J = 1.8 Hz, 1H), 7.72 (m, 2H), 7.53–7.50 (m, 2H), 3.91 (s, 2H), 2.23 (s, 3H). **¹³C NMR (126 MHz, Chloroform-d)** δ 185.17, 184.45, 145.21, 143.90, 143.50, 142.27, 136.92, 133.86, 133.83, 132.22, 131.98, 126.76, 126.59, 95.20, 31.73, 13.61. **HRMS (ESI)** calculated for $C_{18}H_{13}I_2O_2$: 514.9000. Measured: 514.8989 (MH^+).

2-(2,6-dichlorobenzyl)-3-methylnaphthalene-1,4-dione (3t)



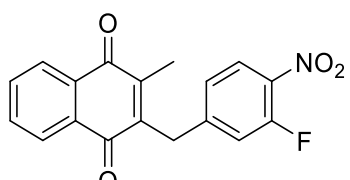
According to the general procedure, menadione and 2,6-dichlorobenzyl bromide were used. After chromatography on silica gel (Cyclohexane:Toluene = 4:6, UV), 126 mg (0.38 mmol, 76% yield) of **3t** were isolated as a yellow solid. **m.p:** 203–204 °C. **¹H NMR (400 MHz, Chloroform-d)** δ 8.21 – 7.99 (m, 2H), 7.75 – 7.63 (m, 2H), 7.30 (d, J = 8.0 Hz, 2H), 7.15 – 7.08 (m, 1H), 4.37 (s, 2H), 2.04 (s, 3H). **¹³C NMR (101 MHz, Chloroform-d)** δ 185.12, 184.12, 144.58, 144.47, 135.92, 135.46, 133.63, 133.53, 132.24, 132.20, 128.58, 128.30, 126.77, 126.43, 29.48, 12.85. **HRMS (ESI)** calculated for $C_{18}H_{13}Cl_2O_2$: 331.0287. Measured: 331.0280 (MH^+).

2-(2,5-dimethoxybenzyl)-3-methylnaphthalene-1,4-dione (3u)

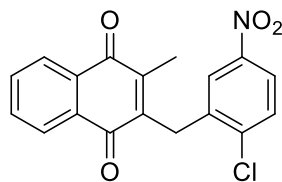


According to the general procedure, menadione and 2,5-dimethoxybenzyl bromide were used. After chromatography on silica gel (Toluene, UV), 128 mg (0.39 mmol, 78% yield) of **3u** were isolated as a yellow solid. **m.p:** 148–149 °C. **¹H NMR (400 MHz, Chloroform-d)** δ 8.14 – 8.01 (m, 2H), 7.80 – 7.61 (m, 2H), 6.78 (d, J = 8.8 Hz, 1H), 6.69 (dd, J = 8.8, 3.1 Hz, 1H), 6.62 (d, J = 3.0 Hz, 1H), 4.00 (s, 2H), 3.80 (s, 3H), 3.69 (s, 3H), 2.17 (s, 3H). **¹³C NMR (101 MHz, Chloroform-d)** δ 185.54, 184.73, 153.68, 151.67, 145.57, 145.13, 133.54, 133.47, 132.38, 132.37, 127.78, 126.61, 126.38, 116.36, 111.28, 111.05, 56.10, 55.78, 26.85, 13.18. **HRMS (ESI)** calculated for $C_{20}H_{19}O_4$: 323.1278. Measured: 323.1286 (MH^+).

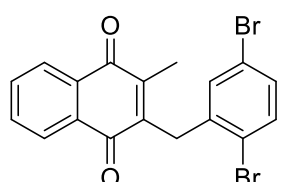
2-(3-fluoro-4-nitrobenzyl)-3-methylnaphthalene-1,4-dione (3v)



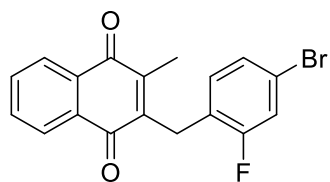
According to the general procedure, menadione and 4-nitro-3-fluorobenzyl bromide were used. After chromatography on silica gel (Cyclohexane:Toluene = 4:6, UV), 91 mg (0.28 mmol, 56% yield) of **3v** were isolated as a yellow solid. **m.p:** 140–141 °C. **¹H NMR (400 MHz, Chloroform-d)** δ 8.16 – 8.05 (m, 2H), 7.99 (dd, J = 8.7, 7.7 Hz, 1H), 7.82 – 7.65 (m, 2H), 7.22 – 7.11 (m, 2H), 4.10 (s, 2H), 2.26 (s, 3H). **¹⁹F NMR (377 MHz, Chloroform-d)** δ -116.59 (m). **¹³C NMR (101 MHz, Chloroform-d)** δ 184.92, 184.41, 155.82 (d, J = 265.6 Hz), 147.72 (d, J = 8.0 Hz), 145.58, 143.24, 135.94, 134.07, 133.99, 132.16, 131.85, 126.73 (d, J = 4.0 Hz), 126.56 (d, J = 2.5 Hz), 124.80, 124.76, 118.48 (d, J = 21.3 Hz), 32.58 (d, J = 1.4 Hz), 13.63. **HRMS (ESI)** calculated for $C_{18}H_{13}FNO_4$: 326.0823. Measured: 326.0802 (MH^+).

2-(2-chloro-5-nitrobenzyl)-3-methylnaphthalene-1,4-dione (3w)

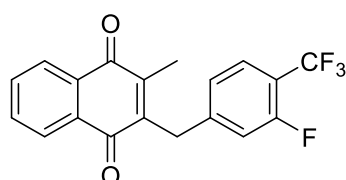
According to the general procedure, menadione and 2-chloro-5-nitrobenzyl bromide were used. After chromatography on silica gel (Cyclohexane:Toluene = 4:6, UV), 119 mg (0.35 mmol, 70% yield) of **3w** were isolated as a yellow solid. **m.p:** 172–173°C. **¹H NMR (400 MHz, Chloroform-d)** δ 8.15 – 8.12 (m, 1H), 8.10 – 8.05 (m, 1H), 8.03 (dd, *J* = 8.8, 2.7 Hz, 1H), 7.85 (d, *J* = 2.7 Hz, 1H), 7.79 – 7.68 (m, 2H), 7.57 (d, *J* = 8.7 Hz, 1H), 4.17 (s, 2H), 2.19 (s, 3H). **¹³C NMR (101 MHz, Chloroform-d)** δ 184.78, 184.32, 146.87, 146.61, 142.79, 141.06, 137.96, 134.01, 133.95, 132.24, 131.92, 130.58, 126.77, 126.72, 123.97, 122.87, 30.49, 13.61. **HRMS (ESI)** calculated for C₁₈H₁₃ClNO₄: 342.0528. Measured: 342.0529 (MH⁺).

2-(2,5-dibromobenzyl)-3-methylnaphthalene-1,4-dione (3x)

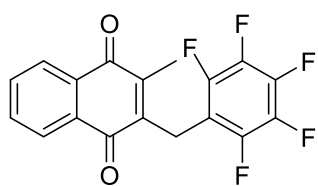
According to the general procedure, menadione and 2,5-dibromobenzyl bromide were used. After chromatography on silica gel (Cyclohexane:Toluene = 4:6, UV), 156 mg (0.37 mmol, 74% yield) of **3x** were isolated as a yellow solid. **m.p:** 126–127°C. **¹H NMR (400 MHz, Chloroform-d)** δ 8.22 – 8.02 (m, 2H), 7.83 – 7.67 (m, 2H), 7.45 (d, *J* = 8.5 Hz, 1H), 7.20 (dd, *J* = 8.5, 2.4 Hz, 1H), 7.00 (d, *J* = 2.3 Hz, 1H), 4.09 (s, 2H), 2.14 (s, 3H). **¹³C NMR (101 MHz, Chloroform-d)** δ 185.04, 184.37, 146.38, 143.84, 139.75, 134.36, 133.87, 132.31, 132.06, 131.56, 131.26, 126.82, 126.64, 123.48, 121.75, 32.81, 13.57. **HRMS (ESI)** calculated for C₁₈H₁₃Br₂O₂: 418.9277. Measured: 418.9279 (MH⁺).

2-(4-bromo-2-fluorobenzyl)-3-methylnaphthalene-1,4-dione (3y)

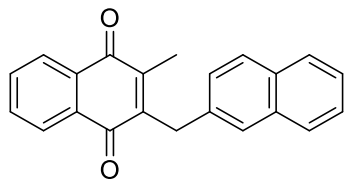
According to the general procedure, menadione and 4-bromo-2-fluorobenzyl bromide were used. After chromatography on silica gel (Cyclohexane:Toluene = 4:6, UV), 129 mg (0.36 mmol, 72% yield) of **3y** were isolated as a yellow solid. **m.p:** 108–109°C. **¹H NMR (500 MHz, Chloroform-d)** δ 8.13 – 8.00 (m, 2H), 7.81 – 7.58 (m, 2H), 7.21 (dd, *J* = 9.6, 2.0 Hz, 1H), 7.16 (dd, *J* = 8.3, 2.0 Hz, 1H), 7.06 (t, *J* = 8.1 Hz, 1H), 3.98 (s, 2H), 2.21 (s, 3H). **¹⁹F NMR (471 MHz, Chloroform-d)** δ -113.57 (*t*, *J* = 8.7 Hz). **¹³C NMR (126 MHz, Chloroform-d)** δ 185.19, 184.55, 160.70 (*d*, *J* = 250.3 Hz), 145.45, 143.75, 133.75, 132.22, 132.07, 131.74 (*d*, *J* = 4.9 Hz), 127.65 (*d*, *J* = 3.6 Hz), 126.64, 126.54, 124.31 (*d*, *J* = 15.7 Hz), 120.53 (*d*, *J* = 9.6 Hz), 119.17 (*d*, *J* = 25.6 Hz), 25.52 (*d*, *J* = 3.1 Hz), 13.21 (*d*, *J* = 2.7 Hz). **HRMS (ESI)** calculated for C₁₈H₁₃BrFO₂: 359.0077. Measured: 359.0065 (MH⁺).

2-(3-fluoro-4-(trifluoromethyl)benzyl)-3-methylnaphthalene-1,4-dione (3z)

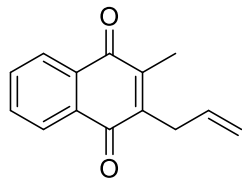
According to the general procedure, menadione and 3-fluoro-4-trifluoromethylbenzyl bromide were used. After chromatography on silica gel (Cyclohexane:Toluene = 4:6, UV), 129 mg (0.37 mmol, 74% yield) of **3z** were isolated as a yellow solid. **m.p:** 85–86 °C. **¹H NMR (500 MHz, Chloroform-d)** δ 8.16 – 8.00 (m, 2H), 7.81 – 7.66 (m, 2H), 7.50 (t, *J* = 7.7 Hz, 1H), 7.12 (dd, *J* = 8.1, 1.2 Hz, 1H), 7.09 – 7.02 (m, 1H), 4.07 (s, 2H), 2.25 (s, 3H). **¹⁹F NMR (471 MHz, Chloroform-d)** δ -61.20 (*d*, *J* = 12.2 Hz), -114.07 (*td*, *J* = 12.0, 7.3 Hz). **¹³C NMR (126 MHz, Chloroform-d)** δ 185.08, 184.50, 159.97 (*dq*, *J* = 256.4, 2.1 Hz), 145.36, 145.30, 143.80, 133.93, 133.88, 132.19, 131.94, 127.45 (*qd*, *J* = 4.4, 2.1 Hz), 126.71, 126.61, 124.32 (*d*, *J* = 3.5 Hz), 122.71 (*q*, *J* = 272.0 Hz), 117.05 (*d*, *J* = 21.0 Hz), 116.72 (*qd*, *J* = 33.2, 12.3 Hz), 32.36, 13.53. **HRMS (ESI)** calculated for C₁₉H₁₃F₄O₂: 349.0846. Measured: 349.0836 (MH⁺).

2-methyl-3-((perfluorophenyl)methyl)naphthalene-1,4-dione (3aa)

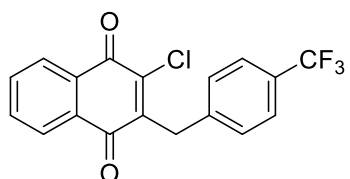
According to the general procedure, menadione and 2,3,4,5,6-pentafluorobenzyl bromide were used. After chromatography on silica gel (Cyclohexane:Toluene = 4:6, UV), 125 mg (0.35 mmol, 71% yield) of **3aa** were isolated as a yellow solid. **m.p:** 103–104 °C. **¹H NMR (400 MHz, Chloroform-d)** δ 8.09 – 8.04 (m, 1H), 8.03 – 7.98 (m, 1H), 7.75 – 7.63 (m, 2H), 4.03 (s, 2H), 2.24 (s, 3H). **¹⁹F NMR (471 MHz, Chloroform-d)** δ -141.23 – -141.33 (m), -156.45 (t, *J* = 20.9 Hz), -162.22 – -162.38 (m). **¹³C NMR (126 MHz, Chloroform-d)** δ 184.78, 183.76, 145.54, 145.41 (dm, *J* = 247.0 Hz), 141.96, 140.15 (dm, *J* = 252.7 Hz), 138.81 – 136.39 (dm, *J* = 251.8 Hz), 133.83, 133.80, 132.08, 131.85, 126.57, 126.56, 112.13 (td, *J* = 17.5, 4.1 Hz), 21.01, 13.04. **HRMS (ESI)** calculated for C₁₈H₁₀F₅O₂: 353.0595. Measured: 353.0573 (MH⁺).

2-methyl-3-(naphthalen-2-ylmethyl)naphthalene-1,4-dione (3ab)

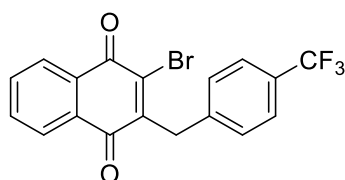
According to the general procedure, menadione and 2-(bromomethyl)naphthalene were used. After chromatography on silica gel (Cyclohexane:Toluene = 4:6, UV), 107 mg (0.34 mmol, 69% yield) of **3ab** were isolated as a yellow solid. **m.p:** 109–110 °C. **¹H NMR (400 MHz, Chloroform-d)** δ 8.20 – 8.04 (m, 2H), 7.85 – 7.67 (m, 5H), 7.64 – 7.60 (m, 1H), 7.51 – 7.34 (m, 3H), 4.21 (s, 2H), 2.29 (s, 3H). **¹³C NMR (101 MHz, Chloroform-d)** δ 185.55, 184.85, 145.37, 144.81, 135.68, 133.68, 133.65, 132.32, 132.30, 132.22, 128.48, 127.74, 127.68, 127.27, 126.93, 126.69, 126.46, 126.26, 125.70, 32.72, 13.50. **HRMS (ESI)** calculated for C₂₂H₁₆KO₂: 351.0782. Measured: 351.0806 (MK⁺).

2-allyl-3-methylnaphthalene-1,4-dione (3ac)

A variant from the general procedure was performed. In a 10 mL tube, quinone (0.5 mmol), allyl bromide (1 mmol) and Fe(acac)₃ (10%) were dissolved in Acetonitrile (5 mL). The mixture was stirred and 2,6-lutidine (0.6 mmol) and γ -terpinene (0.6 mmol) were added successively. The tube was sealed, placed under blue light irradiation and heated up at 90°C during 24h. After completion, the mixture was allowed to cool down at room temperature and was partitioned between ethyl acetate (10 mL) and aqueous 1M HCl (10 mL). The aqueous layer was extracted once with 10 mL ethyl acetate and the reunited organic layers were washed with brine and dried with MgSO₄. The solvent was removed and the crude was purified by silica gel chromatography (Cyclohexane:Ethyl Acetate = 95:5, UV) to obtain 72 mg (0.34 mmol, 68%) of **3ac** as an orange solid. **m.p:** 67–68°C. **¹H NMR (500 MHz, Chloroform-d)** δ 8.11 – 8.03 (m, 2H), 7.75 – 7.60 (m, 2H), 5.83 (ddt, *J* = 17.1, 10.1, 6.3 Hz, 1H), 5.15 – 5.01 (m, 2H), 3.41 (dd, *J* = 6.3, 0.7 Hz, 2H), 2.19 (s, 3H). **¹³C NMR (126 MHz, Chloroform-d)** δ 185.37, 184.38, 144.41, 144.40, 133.57, 133.53, 133.32, 132.27, 132.20, 126.50, 126.40, 116.76, 31.05, 12.73. **HRMS (ESI)** calculated for C₁₄H₁₃O₂: 213.0910. Measured: 213.0909 (MH⁺).

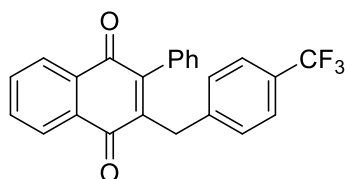
2-chloro-3-(4-(trifluoromethyl)benzyl)naphthalene-1,4-dione (5a)

According to the general procedure, 2-chloronaphthalene-1,4-dione and 4-trifluoromethylbenzyl bromide were used. After chromatography on silica gel (Cyclohexane:Toluene = 4:6, UV), 95 mg (0.27 mmol, 54% yield) of **5a** were isolated as a yellow solid. **m.p:** 160–161 °C. **¹H NMR (500 MHz, Chloroform-d)** δ 8.19 – 8.15 (m, 1H), 8.11 (m, 1H), 7.81 – 7.72 (m, 2H), 7.54 (d, *J* = 8.4 Hz, 2H), 7.49 (d, *J* = 8.3 Hz, 2H), 4.23 (s, 3H). **¹⁹F NMR (471 MHz, Chloroform-d)** δ -62.54. **¹³C NMR (126 MHz, Chloroform-d)** δ 182.41, 177.83, 145.66, 144.37, 140.89, 134.59, 134.36, 131.63, 131.43, 129.66, 129.39 (q, *J* = 32.6 Hz), 127.47, 127.37, 125.75 (q, *J* = 3.7 Hz), 124.23 (q, *J* = 272.3 Hz), 33.91. **HRMS (ESI)** calculated for C₁₈H₁₁ClF₃O₂: 351.0394. Measured: 351.0403 (MH⁺).

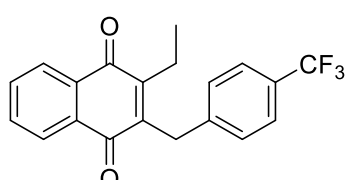
2-bromo-3-(4-(trifluoromethyl)benzyl)naphthalene-1,4-dione (5b)

According to the general procedure, 2-bromonaphthalene-1,4-dione and 4-trifluoromethylbenzyl bromide were used. After chromatography on silica gel (Cyclohexane:Toluene = 4:6, UV), 84 mg (0.21 mmol, 43% yield) of **5b** were isolated as a yellow solid. **m.p:** 126–127 °C. **¹H NMR (400 MHz, Chloroform-d)** δ 8.19 – 8.15 (m, 1H), 8.14 – 8.08 (m, 1H), 7.85 – 7.70 (m, 2H), 7.59 – 7.48 (m, 4H), 4.29 (s, 2H). **¹⁹F NMR (377 MHz, Chloroform-d)** δ -62.56. **¹³C NMR (101**

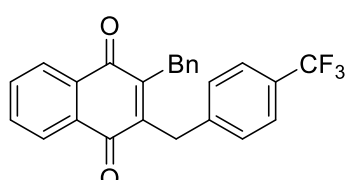
MHz, Chloroform-d) δ 181.82, 177.83, 149.18, 140.75, 140.54, 134.54, 134.34, 131.50, 131.23, 129.61, 129.05 (q, *J* = 36.5 Hz), 127.81, 127.47, 125.72 (q, *J* = 3.8 Hz), 124.24 (q, *J* = 272.0 Hz), 36.91. **HRMS (ESI)** calculated for C₁₈H₁₁BrF₃O₂: 394.9889. Measured: 394.9886 (MH⁺).

2-phenyl-3-(4-(trifluoromethyl)benzyl)naphthalene-1,4-dione (5c)

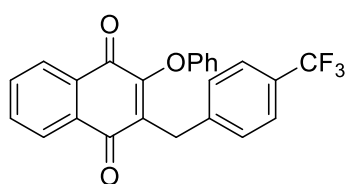
According to the general procedure, 2-phenylnaphthalene-1,4-dione and 4-trifluoromethylbenzyl bromide were used. After chromatography on silica gel (Cyclohexane:Toluene = 1:1, UV), 175 mg (0.45 mmol, 89% yield) of **5c** were isolated as an orange solid. **m.p:** 93–94 °C. **¹H NMR (500 MHz, Chloroform-d)** δ 8.22 – 8.04 (m, 2H), 7.76 (m, 2H), 7.55 – 7.39 (m, 5H), 7.25 – 7.16 (m, 2H), 7.14 – 7.06 (m, 2H), 3.97 (s, 2H). **¹⁹F NMR (471 MHz, Chloroform-d)** δ -62.44. **¹³C NMR (126 MHz, Chloroform-d)** δ 185.32, 184.63, 147.74, 145.05, 142.76, 134.13, 133.98, 133.22, 132.14, 129.22, 129.13, 129.04, 128.79 (q, *J* = 32.4 Hz), 128.55, 126.85, 126.67, 125.46 (q, *J* = 3.8 Hz), 124.29 (q, *J* = 271.8 Hz), 33.40. **HRMS (ESI)** calculated for C₂₄H₁₆F₃O₂: 393.1097. Measured: 393.1117 (MH⁺).

2-ethyl-3-(4-(trifluoromethyl)benzyl)naphthalene-1,4-dione (5d)

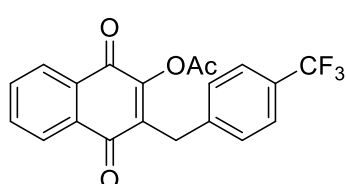
According to the general procedure, 2-ethylnaphthalene-1,4-dione and 4-trifluoromethylbenzyl bromide were used. After chromatography on silica gel (Cyclohexane:Toluene = 1:1, UV), 108 mg (0.31 mmol, 63% yield) of **5d** were isolated as an orange solid. **m.p:** 77–78 °C. **¹H NMR (500 MHz, Chloroform-d)** δ 8.15 – 7.99 (m, 2H), 7.78 – 7.65 (m, 2H), 7.52 (d, *J* = 8.0 Hz, 2H), 7.34 (d, *J* = 8.0 Hz, 2H), 4.09 (s, 2H), 2.72 (q, *J* = 7.6 Hz, 2H), 1.09 (t, *J* = 7.5 Hz, 3H). **¹⁹F NMR (471 MHz, Chloroform-d)** δ -62.44. **¹³C NMR (126 MHz, Chloroform-d)** δ 185.12, 184.90, 150.21, 143.78, 142.81, 133.80, 133.75, 132.35, 132.05, 128.93 (q, *J* = 32.4 Hz), 128.89, 126.59, 126.50, 125.69 (q, *J* = 3.7 Hz), 124.29 (q, *J* = 271.9 Hz), 32.08, 21.08, 13.61. **HRMS (ESI)** calculated for C₂₀H₁₆F₃O₂: 345.1097. Measured: 345.1099 (MH⁺).

2-benzyl-3-(4-(trifluoromethyl)benzyl)naphthalene-1,4-dione (5e)

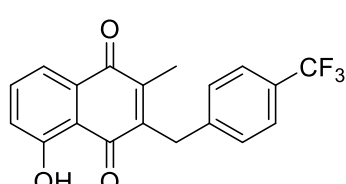
According to the general procedure, 2-benzylnaphthalene-1,4-dione and 4-trifluoromethylbenzyl bromide were used. After chromatography on silica gel (Cyclohexane:Toluene = 4:6, UV), 113 mg (0.28 mmol, 56% yield) of **5e** were isolated as a yellow solid. **m.p:** 93–94 °C. **¹H NMR (500 MHz, Chloroform-d)** δ 8.17 – 8.01 (m, 2H), 7.83 – 7.66 (m, 2H), 7.48 (d, *J* = 8.1 Hz, 2H), 7.27 – 7.12 (m, 7H), 4.13 (s, 2H), 4.10 (s, 2H). **¹⁹F NMR (471 MHz, Chloroform-d)** δ -62.45. **¹³C NMR (126 MHz, Chloroform-d)** δ 185.15, 185.09, 146.78, 145.46, 142.18, 137.80, 133.97, 133.93, 132.13, 132.06, 128.97, 128.96 (q, *J* = 32.6 Hz), 128.90, 128.60, 126.78, 126.67, 125.66 (q, *J* = 3.9 Hz), 124.26 (q, *J* = 272.1 Hz), 32.63, 32.61. **HRMS (ESI)** calculated for C₂₅H₁₈F₃O₂: 407.1253. Measured: 407.1286 (MH⁺).

2-phenoxy-3-(4-(trifluoromethyl)benzyl)naphthalene-1,4-dione (5f)

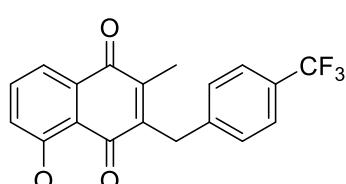
According to the general procedure, 2-phenoynaphthalene-1,4-dione and 4-trifluoromethylbenzyl bromide were used. After chromatography on silica gel (Cyclohexane:Toluene = 1:1, UV), 85 mg (0.21 mmol, 42% yield) of **5f** were isolated as a yellow solid. **m.p:** 156–157 °C. **¹H NMR (500 MHz, Chloroform-d)** δ 8.22 – 8.11 (m, 1H), 8.02 – 7.94 (m, 1H), 7.75 (td, *J* = 7.5, 1.5 Hz, 1H), 7.71 (td, *J* = 7.5, 1.5 Hz, 1H), 7.52 – 7.43 (m, 4H), 7.35 – 7.29 (m, 2H), 7.15 – 7.08 (m, 1H), 6.94 – 6.88 (m, 2H), 4.08 (s, 2H). **¹⁹F NMR (471 MHz, Chloroform-d)** δ -62.44. **¹³C NMR (126 MHz, Chloroform-d)** δ 184.89, 179.76, 157.14, 153.96, 142.20, 136.68, 134.39, 134.05, 131.97, 131.31, 129.90, 129.85, 128.99 (q, *J* = 32.4 Hz), 126.83, 126.77, 125.57 (q, *J* = 3.8 Hz), 124.30 (q, *J* = 272.0 Hz), 123.70, 116.36, 29.77. **HRMS (ESI)** calculated for C₂₄H₁₆F₃O₃: 409.1046. Measured: 409.1030 (MH⁺).

1,4-dioxo-3-(4-(trifluoromethyl)benzyl)-1,4-dihydropnaphthalen-2-yl acetate (5g)

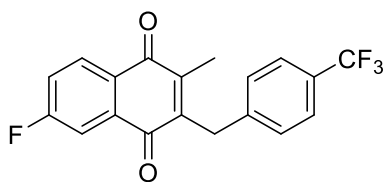
According to the general procedure, 1,4-dioxo-1,4-dihydropnaphthalen-2-yl acetate and 4-trifluoromethylbenzyl bromide were used. After chromatography on silica gel (Cyclohexane:Toluene = 1:9, UV), 91 mg (0.24 mmol, 49% yield) of **5g** were isolated as an orange solid. **m.p:** 120–121 °C. **¹H NMR (500 MHz, Chloroform-d)** δ 8.16 – 8.04 (m, 2H), 7.77 – 7.70 (m, 2H), 7.53 (d, *J* = 8.1 Hz, 2H), 7.41 (d, *J* = 8.4 Hz, 2H), 3.97 (s, 2H), 2.41 (s, 3H). **¹⁹F NMR (471 MHz, Chloroform-d)** δ -62.49. **¹³C NMR (126 MHz, Chloroform-d)** δ 184.23, 178.17, 167.91, 151.94, 141.44, 136.75, 134.47, 134.22, 131.91, 130.93, 129.41, 129.20 (q, *J* = 32.4 Hz), 127.01, 126.88, 125.71 (q, *J* = 3.8 Hz), 124.23 (q, *J* = 272.0 Hz), 30.12, 20.52. **HRMS (ESI)** calculated for C₂₀H₁₃F₃NaO₄: 397.0658. Measured: 397.0658 (MNa⁺).

5-hydroxy-2-methyl-3-(4-(trifluoromethyl)benzyl)naphthalene-1,4-dione (5h)

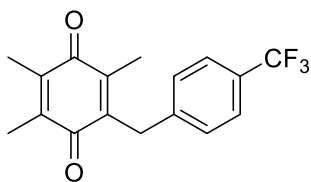
According to the general procedure, Plumbagin and 4-trifluoromethylbenzyl bromide were used. After chromatography on silica gel (Cyclohexane:Toluene = 4:6, UV), 64 mg (0.185 mmol, 37% yield) of **5h** were isolated as an orange solid. **m.p:** 124–125 °C. **¹H NMR (500 MHz, CDCl₃)** δ 12.06 (s, 1H), 7.64 – 7.49 (m, 4H), 7.35 (d, *J* = 8.0 Hz, 2H), 7.22 (dd, *J* = 8.2, 1.3 Hz, 1H), 4.07 (s, 2H), 2.24 (s, 3H). **¹⁹F NMR (471 MHz, CDCl₃)** δ -62.46. **¹³C NMR (126 MHz, CDCl₃)** δ 189.70, 184.40, 161.47, 146.41, 144.30, 141.99, 136.35, 132.15, 129.10 (q, *J* = 32.4 Hz), 128.94, 125.78 (q, *J* = 3.8 Hz), 124.23, 124.22 (q, *J* = 272.1 Hz), 119.26, 114.92, 31.85, 13.59. **HRMS (ESI)** calculated for C₁₉H₁₄F₃O₃: 347.0890. Measured: 347.0910 (MH⁺).

5-methoxy-2-methyl-3-(4-(trifluoromethyl)benzyl)naphthalene-1,4-dione (5i)

According to the general procedure, 5-methoxy-2-methylnaphthalene-1,4-dione and 4-trifluoromethylbenzyl bromide were used. After chromatography on silica gel (Cyclohexane:Toluene = 4:6, UV), 90 mg (0.25 mmol, 50% yield) of **5i** were isolated as an orange solid. **m.p:** 136–137 °C. **¹H NMR (400 MHz, Chloroform-d)** δ 7.76 (dd, *J* = 7.6, 1.1 Hz, 1H), 7.64 (dd, *J* = 8.5, 7.7 Hz, 1H), 7.50 (d, *J* = 8.1 Hz, 2H), 7.35 (d, *J* = 7.9 Hz, 2H), 7.27 (d, *J* = 8.5 Hz, 1H), 4.05 (s, 2H), 3.99 (s, 3H), 2.19 (s, 3H). **¹⁹F NMR (377 MHz, Chloroform-d)** δ -62.45. **¹³C NMR (101 MHz, Chloroform-d)** δ 185.52, 183.83, 159.72, 146.18, 142.65, 142.61, 134.86, 134.44, 129.07, 128.80 (q, *J* = 32.5 Hz), 125.63 (q, *J* = 3.6 Hz), 124.26 (q, *J* = 271.8 Hz), 119.84, 119.30, 117.69, 56.59, 32.67, 13.20. **HRMS (ESI)** calculated for C₂₀H₁₅F₃KO₃: 399.0605. Measured: 399.0635 (MK⁺).

6-fluoro-2-methyl-3-(4-(trifluoromethyl)benzyl)naphthalene-1,4-dione (5j)

According to the general procedure, 6-fluoro-2-methylnaphthalene-1,4-dione and 4-trifluoromethylbenzyl bromide were used. After chromatography on silica gel (Cyclohexane:Toluene = 1:1, UV), 116 mg (0.33 mmol, 67% yield) of **5j** were isolated as a yellow solid. **m.p:** 105–105°C. **¹H NMR (500 MHz, Chloroform-d)** δ 8.13 (dd, *J* = 8.6, 5.2 Hz, 1H), 7.72 (dd, *J* = 8.5, 2.7 Hz, 1H), 7.55 – 7.48 (m, 2H), 7.40 – 7.30 (m, 3H), 4.08 (s, 2H), 2.26 (s, 3H). **¹⁹F NMR (471 MHz, Chloroform-d)** δ -62.49, -102.18 (td, *J* = 8.4, 5.3 Hz). **¹³C NMR (126 MHz, Chloroform-d)** δ 183.82, 183.45, 166.05 (d, *J* = 257.1 Hz), 145.18, 144.58 (d, *J* = 1.8 Hz), 141.98, 134.48 (d, *J* = 7.8 Hz), 129.73 (d, *J* = 8.9 Hz), 128.97 (q, *J* = 32.3 Hz), 128.90, 128.69 (d, *J* = 3.3 Hz), 125.66 (q, *J* = 3.8 Hz), 124.13 (q, *J* = 271.9 Hz), 120.90 (d, *J* = 22.5 Hz), 113.26 (d, *J* = 23.5 Hz), 32.41, 13.41. **HRMS (ESI)** calculated for C₁₉H₁₃F₄O₂: 349.0846. Measured: 349.0835 (MH⁺).

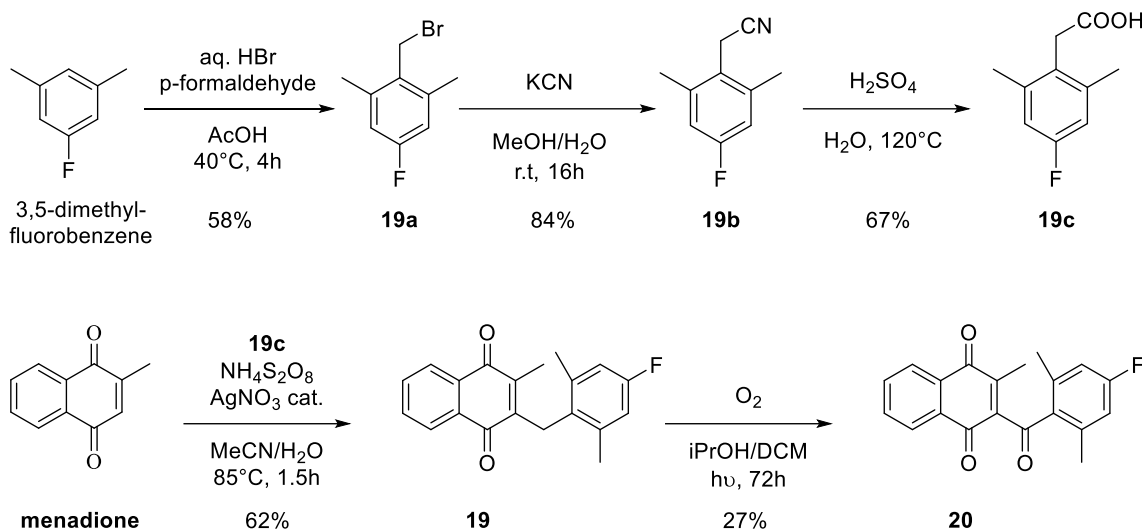
2,3,5-trimethyl-6-(4-(trifluoromethyl)benzyl)cyclohexa-2,5-diene-1,4-dione (5k)

According to the general procedure, 2,3,5-trimethylbenzoquinone and 4-trifluoromethylbenzyl bromide were used. After chromatography on silica gel (Cyclohexane:Toluene = 4:6, UV), 71 mg (0.23 mmol, 46% yield) of **5k** were isolated as a yellow solid. **m.p:** 74–75°C. **¹H NMR (500 MHz, CDCl₃)** δ 7.51 (d, *J* = 8.1 Hz, 2H), 7.29 (d, *J* = 8.0 Hz, 2H), 3.91 (s, 2H), 2.10 (s, 3H), 2.03 (d, *J* = 1.4 Hz, 3H), 2.01 (d, *J* = 1.5 Hz, 3H). **¹⁹F NMR (471 MHz, CDCl₃)** δ -62.45. **¹³C NMR (126 MHz, CDCl₃)** δ 187.66, 186.98, 142.60, 141.92, 141.67, 141.01, 140.64, 128.96, 129.31 – 128.39 (q, *J* = 32.5 Hz), 125.64 (q, *J* = 3.9 Hz), 124.29 (q, *J* = 271.8 Hz), 32.14, 12.97, 12.57, 12.55. **HRMS (ESI)** calculated for C₁₇H₁₆F₃O₂: 309.1097. Measured: 309.1096 (MH⁺)

Article 5.

Synthesis of the 3-benz(o)ylmenadiones **19** and **20**.

Cette synthèse de la molécule **19** a été réalisée par Enrique J. Montagut, étudiant Master M2, en 2015, et co-auteur de la publication.



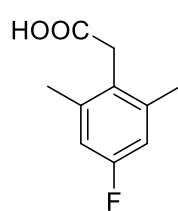
Scheme 5-S1. Synthetic route to synthesize both 3-benz(o)ylmenadione derivatives **19** and **20** with two methyl groups in the aromatic ring.

2-(bromomethyl)-5-fluoro-1,3-dimethyl benzene (**19a**)

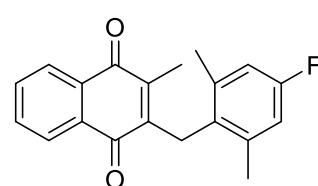
A mixture of 3,5-dimethylfluorobenzene (1 equiv., 39.9 mmol), paraformaldehyde (2.65 equiv., 105 mmol), HBr (6.65 equiv., 265 mmol) and AcOH (110 mL) was stirred 4 hours at 40°C. After that the reaction mixture was diluted with water (150 mL) and extracted with petroleum ether (3x70 mL), then dried over Na₂SO₄, filtered, and concentrated under vacuum. The crude product was purified by flash chromatography with silica gel in toluene affording **19a**: 58% yield, as white crystals. **mp:** 73-74°C. **¹H NMR (400 MHz, CDCl₃) δ** 6.75 (d, *J* = 9.3 Hz, 1H), 4.53 (s, 1H), 2.41 (s, 3H). **¹³C NMR (101 MHz, CDCl₃) δ** 162.38 (d, *J* = 247.5 Hz), 140.17 (d, *J* = 8.5 Hz), 130.09 (d, *J* = 3.0 Hz), 115.22 (d, *J* = 21.0 Hz), 28.81, 19.55 (d, *J* = 1.8 Hz). **¹⁹F NMR (376 MHz, CDCl₃) δ** -113.72. Elemental analysis: C 49.97%, H 4.65% (calcd. C 49.8%, H 4.64%).

2-(4-fluoro-2,6-dimethylphenyl) acetonitrile (**19b**)

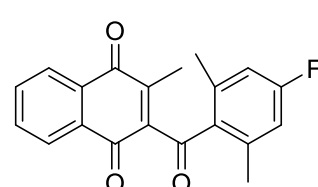
To a stirring solution of **19a** (9.2 mmol, 1 equiv.) in MeOH:Water (80 mL, 1:1) was added KCN (12 mmol, 1.3 equiv.) and the reaction mixture was stirred overnight at RT. The crude product was diluted with ice/water (30mL) and extracted with AcOEt. The organic layer was washed with brine, dried over MgSO₄ and concentrated under reduced pressure. The crude product was purified by flash chromatography Cyhex/AcOEt from 1:0 to 9:1, gradually, to afford **19b**: 84% yield, isolated as white crystals. **mp:** 74-75°C. **¹H NMR (400 MHz, CDCl₃) δ** 6.79 (d, *J* = 9.2 Hz, 2H), 3.60 (s, 2H), 2.39 (s, 6H). **¹³C NMR (101 MHz, CDCl₃) δ** 162.12 (d, *J* = 246.6 Hz), 139.16 (d, *J* = 8.4 Hz), 123.33 (d, *J* = 3.1 Hz), 117.17 (d, *J* = 1.8 Hz), 115.41 (d, *J* = 21.3 Hz), 20.36 (d, *J* = 1.8 Hz), 17.40. **¹⁹F NMR (376 MHz, CDCl₃) δ** -114.75. Elemental analysis: C 73.35%, N 8.73%, H 6.18% (calcd. C 73.60%, N 8.58%, H 6.18%).

2-(4-fluoro-2,6-dimethylphenyl) acetic acid (19c)

To a cold solution of sulfuric acid (7.5 mL) and H₂O (10 mL) was added **19b** (3.06 mmol) and then the mixture was heated to reflux (120°C) until TLC analysis showed total consumption of the starting material. The reaction mixture was diluted with water and AcOEt, the layers separated, and the aqueous phase extracted with AcOEt. The combined organic layers were washed with water and brine, dried over MgSO₄ and evaporated. Crystallization in hexane was performed in order to eliminate any impurity and afford **19c**: 67% yield, isolated as white crystals. **m.p.**: 165–166°C. **¹H NMR** (400 MHz, CDCl₃) δ 6.76 (d, *J* = 9.3 Hz, 1H), 3.67 (s, 1H), 2.31 (s, 2H). **¹³C NMR** (101 MHz, CDCl₃) δ 177.15, 161.63 (d, *J* = 244.8 Hz), 139.59 (d, *J* = 8.3 Hz), 126.71 (d, *J* = 3.0 Hz), 114.86 (d, *J* = 20.9 Hz), 34.48, 20.56 (d, *J* = 1.8 Hz). **¹⁹F NMR** (376 MHz, CDCl₃) δ -116.42. **HRMS ESI**: *m/z* [M-H]⁺ 181.0653 (calcd. *m/z* C₁₀H₁₀O₂F: 181.0670).

2-[(4-fluoro-2,6-dimethylphenyl)methyl]-3-methyl-1,4-dihydronaphthalene-1,4-dione (19)

Menadione (0.37 mmol, 1 eq) was dissolved in 11 mL of MeCN:H₂O (3:1). To this solution **19c** (0.55 mmol, 1.5 equiv.) was added at room temperature in one portion and then the mixture was heated at 85°C. At this point, AgNO₃ (0.13 mmol, 0.35 equiv.) was added, and then (NH₄)₂S₂O₈ was added dropwise as a solution (0.5 mmol, 1.35 equiv., dissolved in 2 mL of MeCN:H₂O (3:1)). The mixture was heated for 1.5 hours at 85 °C. MeCN was evaporated and then DCM was added to extract the crude of the reaction. The combined organic layers were dried over MgSO₄. The DCM was removed under reduced pressure and the crude of the reaction was purified by flash chromatography using toluene as eluent to give the product **19**: 62% yield, isolated as a yellow crystal. **mp**: 169–170°C. **¹H NMR** (400 MHz, CDCl₃) δ 8.08 – 7.86 (m, 2H), 7.73 – 7.46 (m, 2H), 6.64 (d, *J* = 9.4 Hz, 2H), 3.95 (s, 2H), 2.20 (s, 4H), 1.91 (s, 2H). **¹³C NMR** (101 MHz, CDCl₃) δ 185.15, 184.64, 161.00 (d, *J* = 243.8 Hz), 145.64, 144.41, 138.98 (d, *J* = 7.9 Hz), 133.66, 133.58, 132.21, 132.13, 131.67 (d, *J* = 3.2 Hz), 126.73, 126.40, 115.03 (d, *J* = 20.5 Hz), 27.89, 21.31 (d, *J* = 1.7 Hz), 12.59. **¹⁹F NMR** (376 MHz, CDCl₃) δ -118.03. **HRMS-ESI**: *m/z* [M+H]⁺: 309.1284 (calcd. *m/z* C₂₀H₁₈F₁O₂: 309.1285).

2-(4-fluoro-2,6-dimethylbenzoyl)-3-methylnaphthalene-1,4-dione (20)

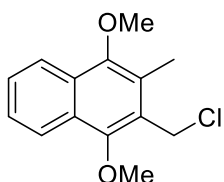
In a tube was added 130 mg (1 eq., 0.422 mmol) of **19**, 2 mL of 2-propanol and 4 mL of DCM. The mixture was agitated and bubbled with oxygen during 30 min. Then, under oxygen atmosphere, the tube was placed in a Rayonet photochemical reactor in a ventilated shelf at 16°C and irradiated at 350 nm for 72h. The solvent was removed under reduced pressure and the resulting crude was purified by silica gel chromatography using toluene as eluent to afford isolated **20** with 27% yield. **mp**: 152–153°C. **¹H NMR** (500 MHz, CDCl₃) δ 8.14 – 8.07 (m, 1H), 8.04 – 7.93 (m, 1H), 7.87 – 7.54 (m, 2H), 6.77 (d, *J* = 9.2 Hz, 2H), 2.35 (s, 6H), 2.22 (s, 3H). **¹³C NMR** (126 MHz, CDCl₃) δ 198.05, 185.56, 183.19, 163.17 (d, *J* = 251.0 Hz), 146.01, 144.27, 139.38 (d, *J* = 8.8 Hz), 136.07 (d, *J* = 3.0 Hz), 134.44, 134.26, 131.82, 131.49, 126.70, 126.63, 115.79 (d, *J* = 21.1 Hz), 20.93 (d, *J* = 1.6 Hz), 13.64. **¹⁹F NMR** (471 MHz, CDCl₃) δ -110.34 (t, *J* = 9.3 Hz). **HRMS-ESI**: *m/z* [M+Na]⁺: 345.0908 (calcd. *m/z* C₂₀H₁₅FNaO₃: 345.0879).

Chapitre IV. Experimental part

Synthesis of precursors.

Heteroarylboronic acids **2** and reactants were purchased from commercial sources, such as Fluorochem, Sigma-Aldrich and Alfa Aesar. 1,4-dimethoxy-2-methylnaphthalene was synthetized according to a previously published method.³⁷

2-(chloromethyl)-1,4-dimethoxy-3-methylnaphthalene (6a)

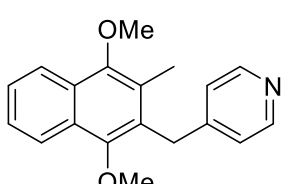


1,4-dimethoxy-2-methylnaphthalene (1 equiv., 4 g, 19.8 mmol), paraformaldehyde (5 equiv., 3.13 g, 2.89 mL, 98.9 mmol) and 37% aqueous HCl (50 mL) were heated at 80°C during 2h. The mixture was cooled down, diluted with water and extracted three times with EtOAc. The reunited organic layers were washed with brine, dried over MgSO₄ and the solvent was removed under reduced pressure. The crude oil was purified by silica gel chromatography using 8:2 Cyclohexane:Toluene as eluant system to afford 4.086 g (81% yield) of 2-(chloromethyl)-1,4-dimethoxy-3-methylnaphthalene as a colorless oil which crystallized on standing. **¹H NMR (400 MHz, CDCl₃)** δ 8.17 – 8.00 (m, 2H), 7.64 – 7.41 (m, 2H), 4.92 (s, 2H), 4.04 (s, 3H), 3.89 (s, 3H), 2.54 (s, 3H).

General procedure for the Suzuki coupling between 2-(chloromethyl)-1,4-dimethoxy-3-methylnaphthalene and heteroarylboronic acid.

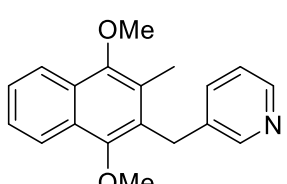
General conditions are a modification of a previously published procedure.⁷⁶ In a sealable tube, 2-(chloromethyl)-1,4-dimethoxy-3-methylnaphthalene **6a** (1 equiv), the corresponding heteroarylboronic acid **7** (1.2 equiv) and sodium carbonate (2.1 equiv) were dissolved in a 2:1 mixture of dimethoxyethane:water (0.15M). The mixture was bubbled 30min with argon, and then tetrakis(triphenylphosphine)palladium (2-5 mol%) was added at once. The tube was sealed and the mixture was heated 1h at 100°C under stirring. The mixture was then, allowed to cool down to room temperature, diluted with water and extracted three times with ethyl acetate. Reunited organic layers were washed with brine, dried over magnesium sulfate and the solvent was removed under reduced pressure to afford a crude which was purified on silica gel chromatography using the adequate eluant system to afford the corresponding coupling product **8**.

4-((1,4-dimethoxy-3-methylnaphthalen-2-yl)methyl)pyridine (8a)

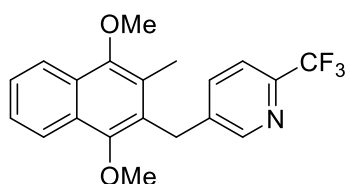


5 mol% Pd(PPh₃)₄, Eluant Cyclohexane:Ethyl acetate (1:1). **¹H NMR (400 MHz, CDCl₃)** δ 8.52 – 8.40 (m, 2H), 8.23 – 7.97 (m, 2H), 7.68 – 7.40 (m, 2H), 7.14 – 6.99 (m, 2H), 4.26 (s, 2H), 3.86 (s, 3H), 3.83 (s, 3H), 2.23 (s, 3H).

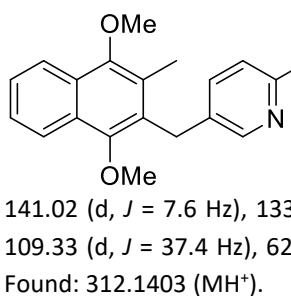
3-((1,4-dimethoxy-3-methylnaphthalen-2-yl)methyl)pyridine (8b)



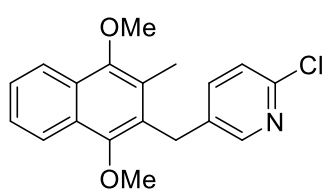
5 mol% Pd(PPh₃)₄, Eluant Cyclohexane:Ethyl acetate (1:1), yellowish solid, 71% yield. **m.p :** 105–106 °C. **¹H NMR (500 MHz, CDCl₃)** δ 8.50 (dd, *J* = 2.3, 1.0 Hz, 1H), 8.41 (dd, *J* = 4.8, 1.6 Hz, 1H), 8.12 – 8.04 (m, 2H), 7.63 – 7.42 (m, 2H), 7.39 – 7.32 (m, 1H), 7.13 (ddd, *J* = 7.8, 4.8, 0.9 Hz, 1H), 4.25 (s, 2H), 3.86 (s, 3H), 3.85 (s, 3H), 2.26 (s, 3H). **¹³C NMR (126 MHz, CDCl₃)** δ 150.75, 150.70, 149.92, 147.50, 136.08, 135.67, 128.28, 128.00, 127.30, 126.64, 126.12, 125.77, 123.55, 122.60, 122.43, 62.45, 61.58, 30.28, 12.83. **HRMS (ESI)** calcd. for C₁₉H₂₀NO₂: 294.1489. Found: 294.1490 (MH⁺).

5-((1,4-dimethoxy-3-methylnaphthalen-2-yl)methyl)-2-(trifluoromethyl)pyridine (8c)

5 mol% Pd(PPh₃)₄, Eluant Cyclohexane:Ethyl acetate (9:1), translucid oil, 97% yield. **¹H NMR (500 MHz, CDCl₃)** δ 8.64 (d, *J* = 1.4 Hz, 1H), 8.16 – 8.04 (m, 2H), 7.61 – 7.46 (m, 4H), 4.31 (s, 2H), 3.87 (s, 3H), 3.86 (s, 3H), 2.26 (s, 3H). **¹³C NMR (101 MHz, CDCl₃)** δ 150.81, 150.77, 150.08, 145.99 (q, *J* = 34.6 Hz), 139.66, 136.79, 128.42, 127.24, 127.05, 126.29, 126.17, 125.88, 122.55, 121.78 (q, *J* = 273.7 Hz), 120.31 (q, *J* = 2.7 Hz), 62.33, 61.50, 30.13, 12.77. **¹⁹F NMR (471 MHz, CDCl₃)** δ -67.68. **HRMS (ESI)** calcd. for C₂₀H₁₉F₃NO₂: 362.1362. Found: 362.1368 (MH⁺).

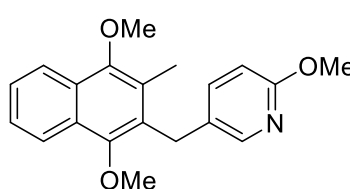
5-((1,4-dimethoxy-3-methylnaphthalen-2-yl)methyl)-2-fluoropyridine (8d)

2 mol% Pd(PPh₃)₄, Eluant Cyclohexane:Ethyl acetate (9:1), white solid, 89% yield. **m.p :** 120-121 °C. **¹H NMR (400 MHz, CDCl₃)** δ 7.94 – 7.70 (m, 3H), 7.40 – 7.19 (m, 3H), 6.54 (ddd, *J* = 8.4, 3.1, 0.6 Hz, 1H), 3.98 (s, 1H), 3.63 (s, 3H), 3.61 (s, 3H), 2.03 (s, 3H). **¹⁹F NMR (377 MHz, CDCl₃)** δ -72.09 (d, *J* = 8.0 Hz). **¹³C NMR (101 MHz, CDCl₃)** δ 162.42 (d, *J* = 237.2 Hz), 150.78, 150.65, 146.98 (d, *J* = 14.4 Hz), 141.02 (d, *J* = 7.6 Hz), 133.65 (d, *J* = 4.5 Hz), 128.33, 127.92, 127.29, 126.39, 126.21, 125.84, 122.59, 122.46, 109.33 (d, *J* = 37.4 Hz), 62.43, 61.58, 29.38 (d, *J* = 1.5 Hz), 12.78. **HRMS (ESI)** calcd. for C₁₉H₁₉FNO₂: 312.1394. Found: 312.1403 (MH⁺).

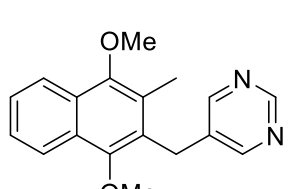
2-chloro-5-((1,4-dimethoxy-3-methylnaphthalen-2-yl)methyl)pyridine (8e)

5 mol% Pd(PPh₃)₄, Eluant Cyclohexane:Ethyl acetate (9:1), white solid, 87% yield. **m.p :** 123-124 °C. **¹H NMR (400 MHz, CDCl₃)** δ 8.19 (dd, *J* = 2.6, 0.8 Hz, 1H), 8.07 – 7.91 (m, 2H), 7.51 – 7.38 (m, 2H), 7.26 (dd, *J* = 8.2, 2.5 Hz, 1H), 7.08 (dd, *J* = 8.2, 0.7 Hz, 1H), 4.13 (s, 2H), 3.78 (s, 3H), 3.77 (s, 3H), 2.18 (s, 3H). **¹³C NMR (101 MHz, CDCl₃)** δ 150.80, 150.72, 149.55, 149.22, 138.71, 135.12, 128.38, 127.56, 127.28, 126.34, 126.27, 125.88, 124.18, 122.60, 122.48, 62.46, 61.60, 29.57, 12.82.

HRMS (ESI) calcd. for C₁₉H₁₉ClNO₂: 328.1099. Found: 328.1102 (MH⁺).

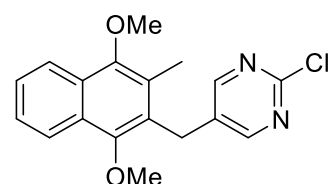
5-((1,4-dimethoxy-3-methylnaphthalen-2-yl)methyl)-2-methoxypyridine (8f)

2 mol% Pd(PPh₃)₄, Eluant Cyclohexane:Ethyl acetate (95:5), translucid oil, 69% yield. **¹H NMR (400 MHz, CDCl₃)** δ 8.14 – 8.04 (m, 2H), 8.02 – 7.94 (m, 1H), 7.58 – 7.44 (m, 2H), 7.32 (dd, *J* = 8.5, 2.6 Hz, 1H), 6.61 (dd, *J* = 8.6, 0.7 Hz, 1H), 4.16 (s, 2H), 3.89 (s, 3H), 3.85 (s, 3H), 3.85 (s, 3H), 2.28 (s, 3H). **¹³C NMR (101 MHz, CDCl₃)** δ 162.80, 150.63, 150.59, 146.04, 138.87, 128.68, 128.57, 128.16, 127.33, 126.73, 125.98, 125.67, 122.57, 122.39, 110.72, 62.43, 61.55, 53.41, 29.37, 12.75. **HRMS (ESI)** calcd. for C₂₀H₂₂NO₃: 324.1594. Found: 324.1617 (MH⁺).

5-((1,4-dimethoxy-3-methylnaphthalen-2-yl)methyl)pyrimidine (8g)

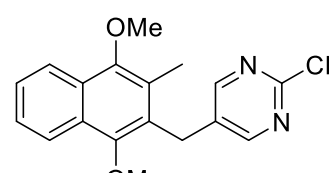
5 mol% Pd(PPh₃)₄, Eluant Cyclohexane:Ethyl acetate (1:1), beige solid, 87% yield. **m.p :** 104-105 °C. **¹H NMR (500 MHz, CDCl₃)** δ 9.04 (s, 1H), 8.54 (s, 2H), 8.13 – 7.98 (m, 2H), 7.61 – 7.41 (m, 2H), 4.22 (s, 2H), 3.88 (s, 3H), 3.86 (s, 3H), 2.29 (s, 3H). **¹³C NMR (126 MHz, CDCl₃)** δ 156.91, 156.77, 150.91, 150.80, 133.90, 128.49, 127.29, 126.68, 126.40, 125.99, 122.62, 122.52, 62.46, 61.66, 28.10, 12.92. **HRMS (ESI)** calcd. for C₁₈H₁₉N₂O₂: 295.1441. Found: 295.1450 (MH⁺).

2-chloro-5-((1,4-dimethoxy-3-methylnaphthalen-2-yl)methyl)pyrimidine (8h)



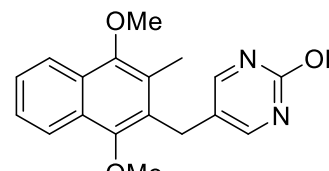
2 mol% Pd(PPh_3)₄, Eluant Cyclohexane:Ethyl acetate (8:2), white solid, 97% yield.
m.p : 88–89 °C. **$^1\text{H NMR}$ (400 MHz, CDCl_3)** δ 8.43 (s, 2H), 8.13 – 8.00 (m, 2H), 7.61 – 7.43 (m, 2H), 4.18 (s, 2H), 3.88 (s, 3H), 3.85 (s, 3H), 2.29 (s, 3H). **$^{13}\text{C NMR}$ (101 MHz, CDCl_3)** δ 159.40, 150.96, 150.73, 132.58, 128.54, 127.23, 126.50, 126.22, 126.05, 125.67, 122.59, 122.52, 62.42, 61.63, 27.32, 12.90. **HRMS (ESI)** calcd. for $\text{C}_{18}\text{H}_{18}\text{ClN}_2\text{O}_2$: 329.1051. Found: 329.1054 (MH^+).

5-((1,4-dimethoxy-3-methylnaphthalen-2-yl)methyl)-2-(trifluoromethyl)pyrimidine (8i)



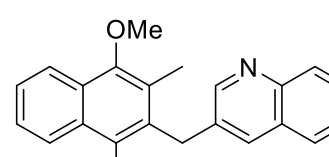
2 mol% Pd(PPh_3)₄, Eluant Cyclohexane:Ethyl acetate (8:2), white solid, 71% yield. **$^1\text{H NMR}$ (400 MHz, CDCl_3)** δ 8.70 (s, 2H), 8.23 – 7.97 (m, 2H), 7.68 – 7.33 (m, 2H), 4.28 (s, 2H), 3.90 (s, 3H), 3.86 (s, 3H), 2.30 (s, 3H). **$^{19}\text{F NMR}$ (377 MHz, CDCl_3)** δ -70.15. **$^{13}\text{C NMR}$ (101 MHz, CDCl_3)** δ 157.63, 154.88 (q, $J = 36.8$ Hz), 151.03, 150.81, 136.39, 128.63, 127.24, 126.58, 126.11, 125.86, 125.59, 122.60, 122.55, 119.78 (q, $J = 275.1$ Hz), 62.39, 61.65, 28.03, 12.93. **HRMS (ESI)** calcd. for $\text{C}_{19}\text{H}_{18}\text{F}_3\text{N}_2\text{O}_2$: 363.1315. Found: 363.1307 (MH^+).

2-((2-methoxypyrimidin-5-yl)methyl)-3-methylnaphthalene-1,4-dione (8j) :



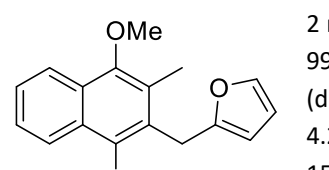
2 mol% Pd(PPh_3)₄, Eluant Cyclohexane:Ethyl acetate (60:40), translucent oil, 71% yield. **3j** was isolated with an unknown inseparable compound and was used in the next step without any further purification. **$^1\text{H NMR}$ (400 MHz, CDCl_3)** δ 8.31 (s, 2H), 8.18 – 7.95 (m, 2H), 7.60 – 7.44 (m, 2H), 4.13 (s, 2H), 3.95 (s, 3H), 3.88 (s, 3H), 3.85 (s, 3H), 2.30 (s, 3H). **HRMS (ESI)** calcd. for $\text{C}_{19}\text{H}_{20}\text{N}_2\text{NaO}_3$: 347.1366. Found: 347.1357 (MNa^+).

3-((1,4-dimethoxy-3-methylnaphthalen-2-yl)methyl)quinoline (8k)



5 mol% Pd(PPh_3)₄, Eluant Cyclohexane:Ethyl acetate (7:3), yellowish solid, 97% yield. **m.p :** 91–92 °C. **$^1\text{H NMR}$ (500 MHz, CDCl_3)** δ 8.92 (d, $J = 2.3$ Hz, 1H), 8.17 – 8.10 (m, 2H), 8.07 (dd, $J = 8.4, 1.0$ Hz, 1H), 7.69 – 7.59 (m, 3H), 7.58 – 7.50 (m, 2H), 7.46 (ddd, $J = 8.1, 6.7, 1.2$ Hz, 1H), 4.44 (s, 2H), 3.87 (s, 6H), 2.29 (s, 3H). **$^{13}\text{C NMR}$ (126 MHz, CDCl_3)** δ 151.95, 150.90, 150.77, 146.96, 133.87, 133.49, 129.24, 128.85, 128.36, 128.30, 127.90, 127.58, 127.38, 126.73, 126.19, 125.81, 122.69, 122.46, 62.58, 61.61, 30.50, 12.89. **HRMS (ESI)** calcd. for $\text{C}_{23}\text{H}_{22}\text{NO}_2$: 344.1645. Found: 344.1659 (MH^+).

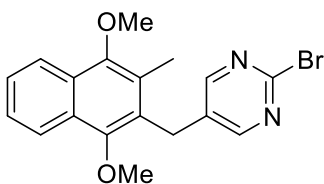
2-((1,4-dimethoxy-3-methylnaphthalen-2-yl)methyl)furan (8l):



2 mol% Pd(PPh_3)₄, Eluant Cyclohexane:Ethyl acetate (99:1 up to 98:2), translucent oil, 99% yield. **$^1\text{H NMR}$ (400 MHz, CDCl_3)** δ 8.19 – 8.03 (m, 2H), 7.62 – 7.46 (m, 2H), 7.34 (dd, $J = 1.8, 0.9$ Hz, 1H), 6.27 (dd, $J = 3.2, 1.9$ Hz, 1H), 5.85 (dq, $J = 3.2, 1.1$ Hz, 1H), 4.27 (s, 2H), 3.92 (s, 3H), 3.90 (s, 3H), 2.41 (s, 3H). **$^{13}\text{C NMR}$ (101 MHz, CDCl_3)** δ 154.30, 150.68, 150.37, 141.15, 128.18, 127.29, 127.06, 126.87, 125.98, 125.54, 122.62, 122.31, 110.37, 105.90, 62.63, 61.46, 26.34, 12.45. **HRMS (ESI)** calcd. for $\text{C}_{18}\text{H}_{19}\text{O}_3$: 283.1329. Found: 283.1334 (MH^+).

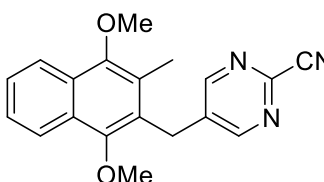
Post-functionnalization of Suzuki coupling adducts.**2-bromo-5-((1,4-dimethoxy-3-methylnaphthalen-2-yl)methyl)pyrimidine (8m) :**

Conditions derived from a previously published procedure.⁷⁹ To a solution of **3h** (1 equiv., 150 mg, 0.456 mmol) in propionitrile (1.5 mL) was added trimethylbromosilane (2 equiv., 139 mg, 0.12 mL, 0.912 mmol). A white



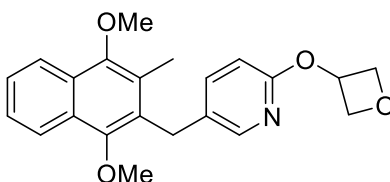
precipitate appeared. The mixture was heated at reflux 5 h and allowed to cool down to room temperature. The mixture was treated with an aqueous saturated sodium bicarbonate solution. The aqueous layer was extracted three times with ethyl acetate, the reunited organic layers were washed with brine, dried over MgSO₄ and the solvent was removed under reduced pressure. The product was purified by silica gel chromatography was performed using 95:5 Toluene:Ethyl Acetate as eluant system to afford 160 mg (94% yield) of **3m** as a translucent solid. **m.p:** 99–100 °C. **¹H NMR (500 MHz, CDCl₃) δ** 8.37 (s, 2H), 8.11 – 7.98 (m, 2H), 7.65 – 7.47 (m, 2H), 4.16 (s, 2H), 3.88 (s, 3H), 3.85 (s, 3H), 2.29 (s, 3H). **¹³C NMR (126 MHz, CDCl₃) δ** 159.33, 150.97, 150.80, 150.74, 133.07, 128.55, 127.23, 126.52, 126.13, 126.07, 125.67, 122.61, 122.54, 62.44, 61.66, 27.39, 12.92. **HRMS (ESI)** calcd. for C₁₈H₁₈BrN₂O₂: 373.0546. Found: 373.0552 (MH⁺).

5-((1,4-dimethoxy-3-methylnaphthalen-2-yl)methyl)pyrimidine-2-carbonitrile (**8n**) :



Conditions derived from a previously published procedure.⁸⁰ To a solution of sodium cyanide (2 equiv., 44.7 mg, 0.912 mmol) and DABCO (0.2 equiv., 10.8 mg, 0.0912 mmol), in a mixture of DMSO (1.5 mL) and water (0.2 mL), **3h** (1 eq., 150 mg, 0.456 mmol) in DMSO (1.5 mL) was added dropwise and the reaction mixture was stirred at 50 °C 20 h. After TLC analysis showed complete conversion, the mixture was allowed to cool down to room temperature and was extracted twice with diethyl ether. The reunited organic layers were washed with brine, dried over MgSO₄ and the solvent was removed under reduced pressure. The product was purified by silica gel chromatography was performed using 75:25 Cyclohexane:Ethyl Acetate as eluant system to afford 122 mg (84% yield) of **3n** as white solid. **m.p:** 111–112 °C. **¹H NMR (400 MHz, CDCl₃) δ** 8.64 (s, 2H), 8.16 – 7.97 (m, 2H), 7.63 – 7.43 (m, 2H), 4.27 (s, 2H), 3.90 (s, 3H), 3.86 (s, 3H), 2.29 (s, 3H). **¹³C NMR (101 MHz, CDCl₃) δ** 157.79, 151.07, 150.80, 143.08, 137.17, 128.69, 127.21, 126.68, 126.19, 125.51, 125.46, 122.60, 122.58, 115.87, 62.40, 61.68, 28.33, 12.98. **HRMS (ESI)** calcd. for C₁₉H₁₈N₃O₂: 320.1394. Found: 320.1403 (MH⁺).

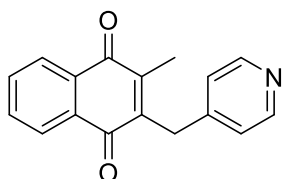
5-((1,4-dimethoxy-3-methylnaphthalen-2-yl)methyl)-2-(oxetan-3-yloxy)pyridine (**8o**)



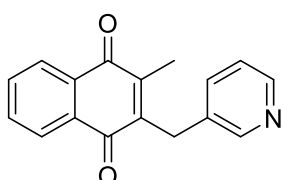
Conditions derived from a previously published procedure.⁸¹ In a flame-dried tube was added **3d** (1 eq., 200 mg, 0.642 mmol), oxetan-3-ol (2 eq., 95.2 mg, 0.0816 mL, 1.28 mmol), THF (3.5 mL) and potassium tert-butoxide (2 eq., 144 mg, 1.28 mmol). The tube was sealed and the mixture heated at 50 °C during 3 h. The mixture was diluted with water addition and extracted three times with EtOAc. The reunited organic layers were washed with brine, dried over MgSO₄ and the solvent was removed under reduced pressure. The product was purified by silica gel chromatography was performed using 80:20 Cyclohexane:Ethyl Acetate as eluant system to afford 164 mg (70% yield) of **3o** as a translucent oil. **¹H NMR (500 MHz, CDCl₃) δ** 8.15 – 8.02 (m, 2H), 7.88 (dd, J = 2.4, 0.9 Hz, 1H), 7.59 – 7.43 (m, 2H), 7.36 (dd, J = 8.5, 2.5 Hz, 1H), 6.66 (d, J = 8.4 Hz, 1H), 5.63 – 5.47 (m, 1H), 5.12 – 4.84 (m, 2H), 4.84 – 4.59 (m, 2H), 4.15 (s, 2H), 3.86 (s, 3H), 3.86 (s, 3H), 2.28 (s, 3H). **¹³C NMR (126 MHz, CDCl₃) δ** 160.91, 150.64, 150.56, 146.07, 139.24, 129.31, 128.47, 128.19, 127.30, 126.62, 126.04, 125.71, 122.55, 122.40, 110.77, 78.46, 68.98, 62.40, 61.55, 29.38, 12.76.

General procedure for the oxidative deprotection.

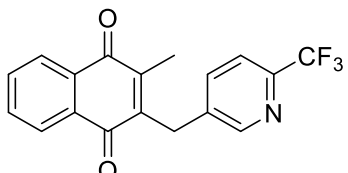
Suzuki coupling derivative **3** (1 equiv) was dissolved in stirring acetonitrile. Then, at room temperature, CAN (2.1 equiv) dissolved in water was added drop by drop (ratio ACN/H₂O 3:1, 0.05M). The mixture was stirred at room temperature during 1h. Then after TLC analysis showed complete conversion, the aqueous layer was extracted three times with dichloromethane. Combined organic layers were dried over MgSO₄ and the solvent was removed under reduced pressure. Purification by silica gel chromatography was performed using the adequate eluent.

2-methyl-3-(pyridin-4-ylmethyl)naphthalene-1,4-dione (9a)

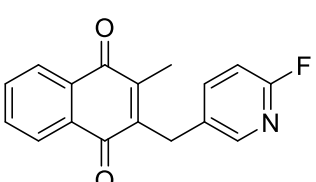
4a was not purified, yellow solid, 96% yield. **1H NMR (400 MHz, CDCl₃)** δ 8.64 (s, 2H), 8.27 – 7.96 (m, 2H), 7.87 – 7.71 (m, 2H), 7.64 (s, 2H), 4.21 (s, 2H), 2.29 (s, 3H). **13C NMR (101 MHz, CDCl₃)** δ 184.51, 184.19, 156.24, 146.37, 143.39, 141.85, 134.31, 134.16, 132.09, 131.64, 126.85, 126.79, 126.28, 33.16, 13.89.

2-methyl-3-(pyridin-3-ylmethyl)naphthalene-1,4-dione (9b)

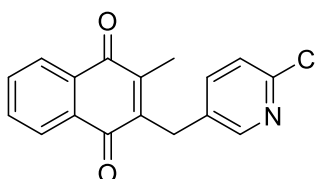
Eluant Cyclohexane:Ethyl acetate (1:1), yellow solid, 74% yield. **m.p:** 100-101°C. **1H NMR (400 MHz, CDCl₃)** δ 8.54 – 8.51 (m, 1H), 8.43 (dd, *J* = 4.8, 1.6 Hz, 1H), 8.16 – 7.97 (m, 2H), 7.70 (dd, *J* = 5.8, 3.3 Hz, 2H), 7.54 (ddd, *J* = 7.9, 2.4, 1.6 Hz, 1H), 7.18 (ddd, *J* = 7.8, 4.8, 0.9 Hz, 1H), 4.01 (s, 2H), 2.25 (s, 3H). **13C NMR (101 MHz, CDCl₃)** δ 185.16, 184.56, 150.05, 148.02, 144.83, 144.37, 136.22, 133.93, 133.78, 133.76, 132.16, 131.98, 126.61, 126.51, 123.69, 30.00, 13.44. **HRMS (ESI)** calcd. for C₁₇H₁₄NO₂: 264.1019. Found: 264.1018 (MH⁺).

2-methyl-3-((6-(trifluoromethyl)pyridin-3-yl)methyl)naphthalene-1,4-dione (9c)

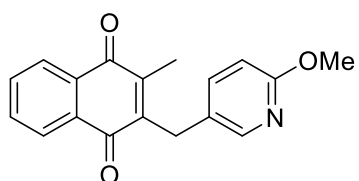
Eluant Cyclohexane:Ethyl acetate (8:2), yellow solid, 87% yield. **m.p:** 108-109°C. **1H NMR (500 MHz, CDCl₃)** δ 8.66 (d, *J* = 2.2 Hz, 1H), 8.20 – 7.97 (m, 2H), 7.89 – 7.68 (m, 3H), 7.58 (dd, *J* = 8.1, 0.8 Hz, 1H), 4.09 (s, 2H), 2.28 (s, 3H). **13C NMR (126 MHz, CDCl₃)** δ 184.92, 184.43, 150.31, 146.62 (q, *J* = 34.8 Hz), 145.23, 143.50, 137.47, 137.40, 133.99, 133.92, 132.11, 131.86, 126.66, 126.64, 121.62 (q, *J* = 279.6 Hz), 120.54 (q, *J* = 2.7 Hz), 30.00, 13.56. **19F NMR (471 MHz, CDCl₃)** δ -67.81. **HRMS (ESI)** calcd. for C₁₈H₁₃F₃NO₂: 332.0893. Found: 332.0915 (MH⁺).

2-((6-fluoropyridin-3-yl)methyl)-3-methylnaphthalene-1,4-dione (9d)

Eluant Cyclohexane:Ethyl acetate (8:2), yellow solid, 97% yield. **m.p:** 103-104°C. **1H NMR (500 MHz, CDCl₃)** δ 8.13 (d, *J* = 2.6 Hz, 1H), 8.08 (ddd, *J* = 7.4, 5.8, 3.3 Hz, 2H), 7.72 (dd, *J* = 5.8, 3.3 Hz, 2H), 7.67 (td, *J* = 8.1, 2.6 Hz, 1H), 6.84 (dd, *J* = 8.4, 3.0 Hz, 1H), 4.00 (s, 2H), 2.27 (s, 3H). **13C NMR (126 MHz, CDCl₃)** δ 185.12, 184.59, 162.61 (d, *J* = 238.4 Hz), 147.46 (d, *J* = 14.7 Hz), 144.83, 144.17, 141.52 (d, *J* = 7.8 Hz), 133.91, 133.86, 132.15, 131.95, 131.52 (d, *J* = 4.7 Hz), 126.64, 126.60, 109.63 (d, *J* = 37.5 Hz), 29.15, 13.45. **19F NMR (377 MHz, CDCl₃)** δ -70.88 (d, *J* = 7.7 Hz). **HRMS (ESI)** calcd. for C₁₇H₁₃FNO₂: 282.0925. Found: 282.0920 (MH⁺).

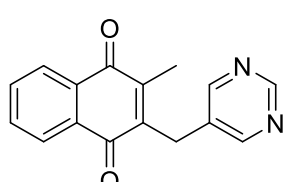
2-((6-chloropyridin-3-yl)methyl)-3-methylnaphthalene-1,4-dione (9e)

Eluant Cyclohexane:Ethyl acetate (8:2), yellow solid, 99% yield. **m.p:** 120-121°C. **1H NMR (500 MHz, CDCl₃)** δ 8.30 (d, *J* = 2.5 Hz, 1H), 8.11 – 7.96 (m, 2H), 7.75 – 7.63 (m, 2H), 7.51 (dd, *J* = 8.2, 2.6 Hz, 1H), 7.20 (d, *J* = 8.2 Hz, 1H), 3.97 (s, 2H), 2.25 (s, 3H). **13C NMR (126 MHz, CDCl₃)** δ 184.98, 184.45, 149.79, 149.75, 144.92, 143.86, 139.11, 133.88, 133.82, 132.87, 132.08, 131.86, 126.59, 126.55, 124.33, 29.30, 13.45. **HRMS (ESI)** calcd. for C₁₇H₁₃ClNO₂: 298.0629. Found: 298.0648 (MH⁺).

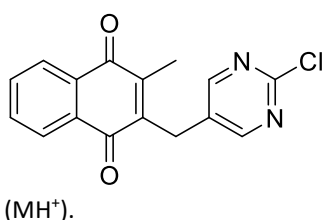
2-((6-methoxypyridin-3-yl)methyl)-3-methylnaphthalene-1,4-dione (9f)

Eluant Cyclohexane:Ethyl acetate (90:10), yellow solid, 87% yield. **m.p:** 120–121°C. **¹H NMR (400 MHz, CDCl₃) δ** 8.11 – 7.95 (m, 3H), 7.67 (dd, *J* = 5.8, 3.3 Hz, 2H), 7.50 (dd, *J* = 8.6, 2.5 Hz, 2H), 6.67 (d, *J* = 8.6 Hz, 1H), 3.91 (s, 2H), 3.88 (s, 3H), 2.24 (s, 3H). **¹³C NMR (101 MHz, CDCl₃) δ** 185.19, 184.61, 162.78, 145.90, 144.66, 144.43, 139.91, 133.70, 133.67, 132.11, 131.97, 126.66, 126.52, 126.43, 111.02, 53.79, 29.03, 13.31. **HRMS (ESI)** calcd. for C₁₈H₁₅NO₃:

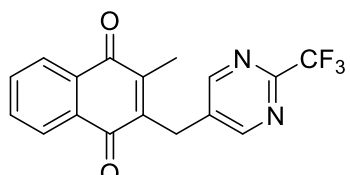
294.112470. Found: 294.112517 (MH⁺).

2-methyl-3-(pyrimidin-5-ylmethyl)naphthalene-1,4-dione (9g)

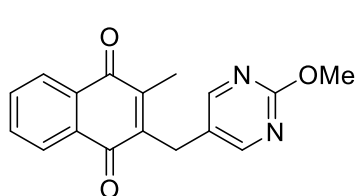
Eluant Cyclohexane:Ethyl acetate (1:1), yellow solid, 88% yield. **m.p:** 110–111°C. **¹H NMR (500 MHz, CDCl₃) δ** 9.04 (s, 1H), 8.64 (s, 2H), 8.10 – 7.98 (m, 2H), 7.76 – 7.61 (m, 2H), 3.98 (s, 2H), 2.27 (s, 3H). **¹³C NMR (126 MHz, CDCl₃) δ** 184.80, 184.28, 157.22, 157.01, 145.07, 143.18, 133.96, 133.89, 132.05, 132.01, 131.79, 126.62, 27.82, 13.53. **HRMS (ESI)** calcd. for C₁₆H₁₃N₂O₂: 265.0972. Found: 265.0982 (MH⁺).

2-((2-chloropyrimidin-5-yl)methyl)-3-methylnaphthalene-1,4-dione (9h)

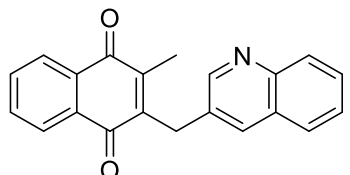
Eluant Cyclohexane:Ethyl acetate (7:3), yellow solid, 93% yield. **m.p:** 163–164°C. **¹H NMR (400 MHz, CDCl₃) δ** 8.54 (s, 2H), 8.20 – 7.92 (m, 2H), 7.85 – 7.57 (m, 2H), 3.96 (s, 2H), 2.29 (s, 3H). **¹³C NMR (101 MHz, CDCl₃) δ** 184.58, 184.14, 159.74, 159.58, 145.09, 142.64, 133.97, 133.89, 131.93, 131.63, 130.56, 126.58, 126.55, 27.06, 13.49. **HRMS (ESI)** calcd. for C₁₆H₁₂ClN₂O₂: 299.0582. Found: 299.0596 (MH⁺).

2-methyl-3-((2-(trifluoromethyl)pyrimidin-5-yl)methyl)naphthalene-1,4-dione (9i)

Eluant Cyclohexane:Ethyl acetate (8:2), yellow solid, 95% yield. **m.p:** 195–196°C. **¹H NMR (400 MHz, CDCl₃) δ** 8.82 (s, 2H), 8.25 – 8.01 (m, 2H), 7.84 – 7.65 (m, 2H), 4.08 (s, 2H), 2.32 (s, 3H). **¹³C NMR (101 MHz, CDCl₃) δ** 184.63, 184.23, 158.01, 155.31 (q, *J* = 37.1 Hz), 145.49, 142.43, 134.44, 134.19, 134.08, 132.06, 131.72, 126.77, 126.73, 119.66 (q, *J* = 275.1 Hz), 27.91, 13.68. **¹⁹F NMR (377 MHz, CDCl₃) δ** -70.23. **HRMS (ESI)** calcd. for C₁₇H₁₂F₃N₂O₂: 333.0845. Found: 333.0868 (MH⁺).

2-((2-methoxypyrimidin-5-yl)methyl)-3-methylnaphthalene-1,4-dione (9j)

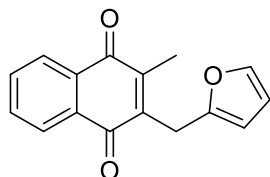
Eluant Cyclohexane:Ethyl acetate (70:30), yellow solid, 74% yield. **m.p:** 161–162°C. **¹H NMR (400 MHz, CDCl₃) δ** 8.40 (s, 2H), 8.10 – 7.96 (m, 2H), 7.67 (dd, *J* = 5.8, 3.3 Hz, 2H), 3.92 (s, 3H), 3.87 (s, 2H), 2.25 (s, 3H). **¹³C NMR (101 MHz, CDCl₃) δ** 184.91, 184.33, 164.61, 159.22, 144.51, 143.77, 133.81, 133.76, 132.01, 131.82, 126.51, 126.48, 124.86, 54.91, 26.75, 13.37. **HRMS (ESI)** calcd. for C₁₇H₁₅NO₃: 295.107719. Found: 295.108670 (MH⁺).

2-methyl-3-(quinolin-3-ylmethyl)naphthalene-1,4-dione (9k)

Eluant Cyclohexane:Ethyl acetate (1:1), yellow solid, 86% yield. **m.p:** 190–191°C. **¹H NMR (400 MHz, CDCl₃) δ** 8.87 (d, *J* = 2.2 Hz, 1H), 8.14 – 8.06 (m, 2H), 8.05 (dd, *J* = 8.5, 1.0 Hz, 1H), 7.92 (dd, *J* = 2.3, 1.0 Hz, 1H), 7.75 – 7.68 (m, 3H), 7.64 (ddd, *J* = 8.4, 6.9, 1.5 Hz, 1H), 7.49 (ddd, *J* = 8.1, 6.8, 1.2 Hz, 1H), 4.20 (s, 2H), 2.31 (s, 3H). **¹³C NMR (101 MHz, CDCl₃) δ** 185.20, 184.58, 151.69, 147.08, 144.91, 144.38, 134.76, 133.80, 133.78, 132.19, 132.02, 131.12, 129.29,

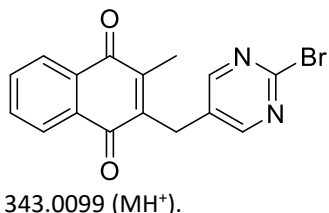
129.20, 128.14, 127.57, 126.94, 126.65, 126.54, 30.19, 13.58. **HRMS (ESI)** calcd. for C₂₁H₁₆NO₂: 314.1176. Found: 314.1177 (M⁺).

2-(furan-2-ylmethyl)-3-methylnaphthalene-1,4-dione (9l)



Eluant Cyclohexane:Ethyl acetate (98:2), orange solid, 74% yield. **m.p:** 83-84°C. **¹H NMR (400 MHz, CDCl₃)** δ 8.21 – 7.95 (m, 1H), 7.86 – 7.58 (m, 1H), 7.27 (dd, J = 1.9, 0.9 Hz, OH), 6.26 (dd, J = 3.2, 1.9 Hz, OH), 6.07 (dd, J = 3.2, 0.9 Hz, OH), 4.03 (s, 1H), 2.28 (s, 2H). **¹³C NMR (101 MHz, CDCl₃)** δ 185.34, 184.06, 151.27, 145.02, 142.41, 141.62, 133.62, 133.58, 132.21, 132.05, 126.56, 126.41, 110.55, 106.79, 25.57, 13.11.

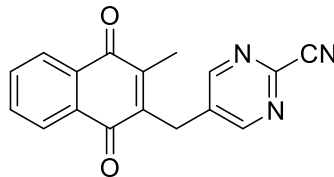
2-((2-bromopyrimidin-5-yl)methyl)-3-methylnaphthalene-1,4-dione (9m)



343.0099 (M⁺).

Eluant Cyclohexane:Ethyl acetate (75:25), yellow solid, 96% yield. **m.p:** 165-166°C. **¹H NMR (400 MHz, CDCl₃)** δ 8.48 (s, 2H), 8.11 – 8.00 (m, 2H), 7.80 – 7.60 (m, 2H), 3.94 (s, 2H), 2.28 (s, 3H). **¹³C NMR (101 MHz, CDCl₃)** δ 184.67, 184.23, 159.56, 151.26, 145.20, 142.67, 134.09, 134.00, 132.03, 131.73, 131.14, 126.69, 126.66, 27.24, 13.61. **HRMS (ESI)** calcd. for C₁₆H₁₂BrN₂O₂: 343.0077. Found: 343.0099 (M⁺).

5-((3-methyl-1,4-dioxo-1,4-dihydronaphthalen-2-yl)methyl)pyrimidine-2-carbonitrile (9n)



290.0924. Found: 290.0918 (M⁺).

Eluant Cyclohexane:Ethyl acetate (7:3), yellow solid, 87% yield. **m.p:** 179-180°C. **¹H NMR (400 MHz, CDCl₃)** δ 8.76 (s, 2H), 8.10 – 7.99 (m, 2H), 7.81 – 7.61 (m, 2H), 4.06 (s, 2H), 2.31 (s, 3H). **¹³C NMR (101 MHz, CDCl₃)** δ 184.50, 184.17, 158.11, 145.67, 143.40, 142.05, 135.19, 134.23, 134.09, 132.00, 131.62, 126.77, 126.69, 115.68, 28.20, 13.72. **HRMS (ESI)** calcd. for C₁₇H₁₂N₃O₂:

Références bibliographiques

- [1] World malaria report, **2020**, Organisation Mondiale de la Santé.
- [2] M. A. Phillips, J. N. Burrows, C. Manyando, R. H. van Huijsduijnen, W. C. Van Voorhis, T. N. C. Wells, Malaria. *Nat. Rev. Dis. Primers*, **2017**, 3, 17050.
- [3] C. A. Guerra, R. E. Howes, A. P. Patil, P. W. Gething, T. P. Van Boeckel, W. H. Temperley, C. W. Kabaria, A. J. Tatem, B. H. Manh, I. R. F. Elyazar, J. K. Baird, R. W. Snow, S. I. Hay, The International Limits and Population at Risk of *Plasmodium vivax* Transmission in 2009. *Plos Neglect. Trop. Dis.* **2011**, 4, e774.
- [4] B. Singh, L. K. Sung, A. Matusop, A. Radhakrishnan, S. S. G. Shamsul, J. Cox-Singh, A. Thomas, D. J. Conway, A large focus of naturally acquired *Plasmodium knowlesi* infections in human beings. *Lancet*, **2004**, 363, 1017–1024.
- [5] K. Marsh, S. Kinyanjui, Immune effector mechanisms in malaria. *Parasite Immunol.* **2006**, 28, 51-60.
- [6] S. Bhatt, D. J. Weiss, E. Cameron, D. Bisanzio, B. Mappin, U. Dalrymple, K. E. Battle, C. L. Moyes, A. Henry, P. A. Eckhoff, E. A. Wenger, O. Briët, M. A. Penny, T. A. Smith, A. Bennett, J. Yukich, T. P. Eisele, J. T. Griffin, C. A. Fergus, M. Lynch, F. Lindgren, J. M. Cohen, C. L. J. Murray, D. L. Smith, S. I. Hay, R. E. Cibulskis, P. W. Gething, The effect of malaria control on *Plasmodium falciparum* in Africa between 2000 and 2015. *Nature*, **2015**, 526, 207-211.
- [7] A. M. Dondorp, F. Nosten, P. Yi, D. Das, A. P. Phyo, J. Tarning, K. Lwin, F. Ariey, W. Hanpithakpong, S. J. Lee, P. Ringwald, K. Silamut, M. Imwong, K. Chotivanich, P. Lim, T. Herdman, S. S. An, S. Yeung, P. Singhasivanon, N. P. J. Day, N. Lindegardh, D. Socheat, N. J. White, Artemisinin Resistance in *Plasmodium falciparum* Malaria. *N. Engl. J. Med.* **2009**, 361, 455-467.
- [8] A. P. Phyo, S. Nkhoma, K. Stepniewska, E. A. Ashley, S. Nair, R. McGready, C. Moo, S. Al-Saai, A. M. Dondorp, K. M. Lwin, P. Singhasivanon, N. P. J. Day, N. J. White, T. J. C. Anderson, F. Nosten, Emergence of artemisinin-resistant malaria on the western border of Thailand: a longitudinal study. *Lancet*, **2012**, 379, 1960-1966.
- [9] Implications of insecticide resistance for malaria vector control, **2016**, Organisation Mondiale de la Santé.
- [10] N. J. White, S. Pukrittayakamee, T. T. Hien, M. A. Faiz, O. A. Mokuolu, A. M. Dondorp, Malaria. *Lancet*, **2014**, 383, 723-735.
- [11] A. R. Butler, S Khan, E. Ferguson, A brief history of malaria chemotherapy. *J. R. Coll. Physicians Edinb.* **2010**, 40, 172–177.
- [12] J. Achan, A. O. Talisuna, A. Erhart, A. Yeka, J. K. Tibenderana, F. N. Baliraine, P. J. Rosenthal, U. D'Alessandro, Quinine, an old anti-malarial drug in a modern world: role in the treatment of malaria. *Malar. J.* **2011**, 10, 144.
- [13] P. J. Pelletier, J. B. Caventou. *Annal. Chim. Phys.* **1820**, 15, 289–318.
- [14] R. B. Woodward, W. E. Doering, The Total Synthesis of Quinine. *J. Am. Chem. Soc.* **1945**, 67, 860–874.

- [15] S. R. Meshnick, M. J. Dobson, The History of Antimalarial Drugs. *Antimalarial Chemotherapy*, Chapitre 2, **2001**.
- [16] T. E. Wellem, C. V. Plowe, Chloroquine-Resistant Malaria. *J. Infect. Dis.* **2001**, *784*, 770-776.
- [17] D. Payne, *Parasitol. Today*, Spread of Chloroquine Resistance in *Plasmodium falciparum*, **1987**, *3*, 241-246.
- [18] R. G. Ridley, Medical need, scientific opportunity and the drive for antimalarial drugs. *Nature*, **2002**, *415*, 686-693.
- [19] K. J. Palmer, S. M. Holliday, R. N. Brogden, Mefloquine. A Review of its Antimalarial Activity, Pharmacokinetic Properties and Therapeutic Efficacy. *Drugs*, **1993**, *45*, 430-475.
- [20] P. Olliaro, C. Nevill, J. LeBras, P. Ringwald, P. Mussano, P. Garner, P. Brasseur, Systematic review of amodiaquine treatment in uncomplicated malaria *Lancet*, **1996**, *348*, 1196-1201.
- [21] a) G. K. John, N. M. Douglas, L. von Seidlein, F. Nosten, J. K. Baird, N. J. White, R. N. Price, Primaquine radical cure of *Plasmodium vivax*: a critical review of the literature. *Malar. J.* **2012**, *11*, 280; b) E. A. Ashley, J. Recht, N. J. White, Primaquine: the risks and the benefits. *Malar. J.* **2014**, *13*, 418.
- [22] Y. Tu, Artemisinin—A Gift from Traditional Chinese Medicine to the World (Nobel Lecture). *Angew.Chem. Int. Ed.* **2016**, *55*, 10210–10226.
- [23] R. T. Eastman, D. A. Fidock, Artemisinin-based combination therapies: a vital tool in efforts to eliminate malaria. *Nat. Rev. Microbiol.* **2009**, *7*, 864-874.
- [24] A. Uwimana, E. Legrand, B. H. Stokes, J.-L. Mangala Ndikumana, M. Warsame, N. Umulisa, D. Ngamije, T. Munyaneza, J.-B. Mazarati, K. Munguti, P. Campagne, A. Criscuolo, F. Ariey, M. Murindahabi, P. Ringwald, D. A. Fidock, A. Mbituyumuremyi, D. Menard, Emergence and clonal expansion of in vitro artemisinin-resistant *Plasmodium falciparum kelch13 R561H* mutant parasites in Rwanda. *Nat. Med.* **2020**, *26*, 1602-1608.
- [25] A. Hott, M. S. Tucker, D. Casandra, K. Sparks, D. E. Kyle, Fitness of artemisinin-resistant *Plasmodium falciparum* in vitro, *J. Antimicrob. Chemother.* **2015**, *70*, 2787-2796.
- [26] a) A. T. Hudson, A. W. Randall, M. Fry, C. D. Ginger, B. Hill, V. S. Latter, N. McHardy, R. B. Williams, Novel anti-malarial hydroxynaphthoquinones with potent broad spectrum anti-protozoal activity. *Parasitology*, **1985**, *90*, 45-55. b) L. G. Haile, J. F. Flaherty, ATOVAQUONE: A Review. *Ann. Pharmacother.* **1993**, *27*, 1488-1494.
- [27] K. McKeage, L. J. Scott, Atovaquone/Proguanil. A Review of its Use for the Prophylaxis of *Plasmodium falciparum*. *Malaria Drugs*, **2003**, *63*, 597-623.
- [28] G. L. Nixon, D. M. Moss, A. E. Shone, D. G. Laloo, N. Fisher, P. M. O'Neill, S. A. Ward, G. A. Biagini, Antimalarial pharmacology and therapeutics of atovaquone. *J. Antimicrob. Chemother.* **2013**, *68*, 977-985.
- [29] H. J. Painter, J. M. Morrisey, M. W. Mather, A. B. Vaidya, Specific role of mitochondrial electron transport in blood-stage *Plasmodium falciparum*. *Nature*, **2007**, *446*, 88-91.

- [30] C. D. Goodman, J. E. Siregar, V. Mollard, J. Vega-Rodríguez, D. Syafruddin, H. Matsuoka, M. Matsuzaki, T. Toyama, A. Sturm, A. Coizjnsen, M. Jacobs-Lorena, K. Kita, S. Marzuki, G. I. McFadden, Parasites resistant to the antimalarial atovaquone fail to transmit by mosquitoes *Science*, **2016**, 352, 349-353.
- [31] C. E. Pereyra, R. F. Dantas, S. B. Ferreira, L. P. Gomes, F. P. Silva-Jr, The diverse mechanisms and anticancer potential of naphthoquinones. *Cancer Cell. Int.* **2019**, 19, 207.
- [32] O. P.S. Patel, R. M. Beteck, L. J. Legoabe, Antimalarial application of quinones: A recent update. *Eur. J. Med. Chem.* **2020**, 210, 113084.
- [33] P. Sidorov, I. Desta, M. Chessé, D. Horvath, G. Marcou, A. Varnek, E. Davioud-Charvet, M. Elhabiri, Redox Polypharmacology as an Emerging Strategy to Combat Malarial Parasites *ChemMedChem*, **2016**, 11, 1339-1351.
- [34] E. Davioud-Charvet, S. Delarue, C. Biot, B. Schwöbel, C. C. Boehme, A. Müssigbrodt, L. Maes, C. Sergheraert, P. Grellier, R. H. Schirmer, K. Becker, A Prodrug Form of a *Plasmodium falciparum* Glutathione Reductase Inhibitor Conjugated with a 4-Anilinoquinoline. *J. Med. Chem.* **2001**, 44, 4268-4276.
- [35] C. Biot, H. Bauer, R. H. Schirmer, E. Davioud-Charvet, 5-Substituted Tetrazoles as Bioisosteres of Carboxylic Acids. Bioisosterism and Mechanistic Studies on Glutathione Reductase Inhibitors as Antimalarials. *J. Med. Chem.* **2004**, 47, 5972-5983.
- [36] W. Friebolin, B. Jannack, N. Wenzel, J. Furrer, T. Oeser, C. P. Sanchez, M. Lanzer, V. Yardley, K. Becker, E. Davioud-Charvet, Antimalarial Dual Drugs Based on Potent Inhibitors of Glutathione Reductase from *Plasmodium falciparum*. *J. Med. Chem.* **2008**, 51, 1260-1277.
- [37] T. Müller, L. Johann, B. Jannack, M. Brückner, D. A. Lanfranchi, D. H. Bauer, C. Sanchez, V. Yardley, C. Deregnaucourt, J. Schrével, M. Lanzer, R. H. Schirmer, E. Davioud-Charvet, Glutathione Reductase-Catalyzed Cascade of Redox Reactions To Bioactivate Potent Antimalarial 1,4-Naphthoquinones - A New Strategy to Combat Malarial Parasites. *J. Am. Chem. Soc.* **2011**, 133, 11557-11571.
- [38] K. Ehrhardt, C. Deregnaucourt, A.-A. Goetz, T. Tzanova, V. Gallo, P. Arese, B. Pradines, S. H. Adjalley, D. Bagrel, S. Blandin, M. Lanzer, E. Davioud-Charvet, The Redox Cycler Plasmodione Is a Fast-Acting Antimalarial Lead Compound with Pronounced Activity against Sexual and Early Asexual Blood-Stage Parasites. *Antimicrob. Agents Chemother.* **2016**, 60, 5146-5158.
- [39] D. A. Lanfranchi, D. Belorgey, T. Müller, H. Vezin, M. Lanzer, E. Davioud-Charvet, Exploring the trifluoromenadione core as a template to design antimalarial redox-active agents interacting with glutathione reductase. *Org. Biomol. Chem.* **2012**, 10, 4795-4806.
- [40] K Ehrhardt, E. Davioud-Charvet, H. Ke, A. B. Vaidya, M. Lanzer, M. Deponte, The Antimalarial Activities of Methylene Blue and the 1,4-Naphthoquinone 3-[4-(Trifluoromethyl)Benzyl]-Menadione Are Not Due to Inhibition of the Mitochondrial Electron Transport Chain *Antimicrob. Agents Chemother.* **2013**, 57, 2114-2120.
- [41] M. Bielitz, D. Belorgey, K. Ehrhardt, L. Johann, D. A. Lanfranchi, V. Gallo, E. Schwarzer, F. Mohring, E. Jortzik, D. L. Williams, K. Becker, P. Arese, M. Elhabiri, E. Davioud-Charvet,

- Antimalarial NADPH-Consuming Redox-Cyclers As Superior Glucose-6-Phosphate Dehydrogenase Deficiency Copycats. *Antioxid. Redox Signal.* **2015**, *22*, 1337-1352.
- [42] a) N. Jacobsen, K. Torssell, Synthesis of Naturally Occurring Quinones. Alkylation with the Silver Ion-Peroxydisulphate-Carboxylic Acid System. *Acta Chem. Scand.* **1973**, *27*, 3211-3216. b) J. Goldman, N. Jacobsen, K. Torssell, Syntheses in the Camphor Series. Alkylation of Quinones with Cycloalkyl Radicals. Attempted Syntheses of Lagopodin A and Desoxyhelicobasidin. *Acta Chem. Scand.* **1974**, *28b*, 492-500. c) J. M. Anderson, J. K. Kochi, Silver(I)-catalyzed oxidative decarboxylation of acids by peroxydisulfate. Role of silver(II). *J. Am. Chem. Soc.* **1970**, *92*, 1651–1659.
- [43] D. A. Lanfranchi, E. Cesar-Rodo, B. Bertrand, H.-H. Huang, L. Day L, L. Johann, M. Elhabiri, K. Becker, D. L. Williams, E. Davioud-Charvet, Synthesis and biological evaluation of 1,4-naphthoquinones and quinoline-5,8-diones as antimalarial and schistosomicidal agents. *Org. Biomol. Chem.* **2012**, *10*, 6375–6387.
- [44] T. J. Ritchie, S. J. F. Macdonald, R. J. Young, S. D. Pickett, The impact of aromatic ring count on compound developability: further insights by examining carbo- and hetero-aromatic and -aliphatic ring types. *Drug Discov. Today*, **2011**, *16*, 164-171.
- [45] E. Cesar Rodo, L. Feng, M. Jida, K. Ehrhardt, M. Bielitz, J. Boilevin, M. Lanzer, D. L. Williams, D. A. Lanfranchi, E. Davioud-Charvet, A Platform of Regioselective Methodologies to Access Polysubstituted 2-Methyl-1,4-naphthoquinone Derivatives: Scope and Limitations *Eur. J. Org. Chem.* **2016**, 1982–1993.
- [46] C. Morin, T. Basset, J.-C. Moutet, M. Fayolle, M. Bruckner, D. Limosin, K. Becker, E. Davioud-Charvet, The aza-analogues of 1,4-naphthoquinones are potent substrates and inhibitors of plasmoidal thioredoxin and glutathione reductases and of human erythrocyte glutathione reductase. *Org. Biomol. Chem.* **2008**, *6*, 2731-2742.
- [47] L. Feng, D. A. Lanfranchi, L. Cotos, E. Cesar-Rodo, K. Ehrhardt, A.-A. Goetz, H. Zimmermann, F. Fenaille, S. A. Blandin, E. Davioud-Charvet, Synthesis of plasmidone metabolites and ¹³C-enriched plasmidone as chemical tools for drug metabolism investigation. *Org. Biomol. Chem.* **2018**, *16*, 2647-2665.
- [48] C. O. Kangani, B. W. Day, Mild, Efficient Friedel–Crafts Acylations from Carboxylic Acids Using Cyanuric Chloride and AlCl₃. *Org. Lett.* **2008**, *10*, 2645-2648.
- [49] a) B. S. Joshi, Q. Jiang, T. Rho, S. W. Pelletier, The Synthesis of Radermachol. *J. Org. Chem.* **1994**, *59*, 8220-8232; b) M. Buccini, M. J. Piggott, A Four-Step Total Synthesis of Radermachol. *Org. Lett.* **2014**, *16*, 2490–2493.
- [50] E. Deseke, Y. Nakatani, G. Ourisson, Intrinsic Reactivities of Amino Acids towards Photoalkylation with Benzophenone – A Study Preliminary to Photolabelling of the Transmembrane Protein Glycophorin A. *Eur. J. Org. Chem.* **1998**, 243-251.
- [51] X.-L. Xu, Z. Li, Catalytic Electrophilic Alkylation of *p*-Quinones through a Redox Chain Reaction *Angew. Chem. Int. Ed.* **2017**, *56*, 8196 –8200.

- [52] G. Schäfer, J. W. Bode, Friedel–Crafts Benzylation of Activated and Deactivated Arenes. *Angew. Chem. Int. Ed.* **2011**, *50*, 10913 –10916.
- [53] V. D. Vuković, E. Richmond, E. Wolf, J. Moran, Catalytic Friedel–Crafts Reactions of Highly Electronically Deactivated Benzylic Alcohols. *Angew. Chem. Int. Ed.* **2017**, *56*, 3085 –3089.
- [54] T. Suga, S. Shimazu, Y. Ukaji, Nickel-Catalyzed Cross-Electrophile Coupling between Benzyl Alcohols and Aryl Halides Assisted by Titanium Co-reductant. *Org. Lett.* **2018**, *20*, 7846–7850.
- [55] a) D. A. Nicewicz, D. W. C. MacMillan, Merging Photoredox Catalysis with Organocatalysis: The Direct Asymmetric Alkylation of Aldehydes. *Science*, **2008**, *322*, 77–80; b) M. A. Ischay, M. E. Anzovino, J. Du, T. P. Yoon, Efficient Visible Light Photocatalysis of [2+2] Enone Cycloadditions. *J. Am. Chem. Soc.* **2008**, *130*, 12886–12887; c) J. M. R. Narayanan, J. W. Tucker, C. R. J. Stephenson, Electron-Transfer Photoredox Catalysis: Development of a Tin-Free Reductive Dehalogenation Reaction. *J. Am. Chem. Soc.* **2009**, *131*, 8756–8757.
- [56] Exemples sélectionnés: a) H.-W. Shih, M. N. Vander Wal, R. L. Grange, D. W. C. MacMillan, Enantioselective α -Benzylation of Aldehydes via Photoredox Organocatalysis. *J. Am. Chem. Soc.* **2011**, *132*, 13600–13603; b) J. Dong, X. Lyu, Z. Wang, X. Wang, H. Song, Y. Liua, Q. Wang, Visible-light-mediated Minisci C–H alkylation of heteroarenes with unactivated alkyl halides using O₂ as an oxidant. *Chem. Sci.* **2019**, *10*, 976–982; c) E. B. McLean, V. Gauchot, S. Brunen, D. J. Burns, Ai-Lan Lee, Dual copper- and photoredox-catalysed C(sp₂)–C(sp₃) coupling. *Chem. Commun.* **2019**, *55*, 4238–4241; d) G. Park, S. Y. Yi, J. Jung, E. J. Cho, Y. You, Mechanism and Applications of the Photoredox Catalytic Coupling of Benzyl Bromides. *Chem. Eur. J.* **2016**, *22*, 17790 – 17799; e) E. Arceo, I. D. Jurberg, A. Alvarez-Fernández, P. Melchiorre, Photochemical activity of a key donor–acceptor complex can drive stereoselective catalytic α -alkylation of aldehydes. *Nat. Chem.* **2013**, *5*, 750–756.
- [57] C. K. Prier, D. A. Rankic, D. W. MacMillan, Visible Light Photoredox Catalysis with Transition Metal Complexes: Applications in Organic Synthesis. *Chem. Rev.* **2013**, *113*, 5322–5363.
- [58] N. A. Romero, D. A. Nicewicz, Organic Photoredox Catalysis. *Chem. Rev.* **2016**, *116*, 10075–10166.
- [59] B. Schweitzer-Chaput, M.A. Horwitz, E. Beato, P. Melchiorre, Photochemical generation of radicals from alkyl electrophiles using a nucleophilic organic catalyst. *Nat. Chem.* **2019**, *11*, 129–135.
- [60] a) H. Görner, Photoreactions of 2-methyl-5-isopropyl-1,4-benzoquinone. *J. Photochem. Photobiol. A: Chem.* **2004**, *165*, 215–222. b) H. Görner, Photoprocesses of *p*-naphthoquinones and vitamin K₁: effects of alcohols and amines on the reactivity in solution. *Photochem. Photobiol. Sci.* **2004**, *3*, 71–78. c) H. Görner, Photoreduction of nitro-1,4-naphthoquinones in solution. *J. Photochem. Photobiol. A*. **2011**, *224*, 135–140.
- [61] S. Ohkawa, S. Terao, Z.-I. Terashita, Y. Shibouta, K. Nishikawa, Dual inhibitors of thromboxane A₂ synthase and 5-lipoxygenase with scavenging activity of active oxygen species (AOS). Synthesis of a novel series of (3-pyridylmethyl)benzoquinone derivatives. *J. Med. Chem.* **1991**, *34*, 267–276.

- [62] S.-I. Murahashi, M. Yamamura, K.-I. Yanagisawa, N. Mita, K. Hondo, Stereoselective synthesis of alkenes and alkenyl sulfides from alkenyl halides using palladium and ruthenium catalysts. *J. Org. Chem.*, **1979**, *44*, 2408-2417.
- [63] a) M. Giannerini, M. Fañanas-Mastral, B. L. Feringa, Direct catalytic cross-coupling of organolithium compounds. *Nat. Chem.* **2013**, *5*, 667-672; b) V. Hornillos, M. Giannerini, C. Vila, M. Fañanas-Mastral, B. L. Feringa, Catalytic Direct Cross-Coupling of Organolithium Compounds with Aryl Chlorides. *Org. Lett.* **2013**, *15*, 5114–5117; c) E. B. Pinxterhuis, M. Giannerini, V. Hornillos, B. L. Feringa, Fast, greener and scalable direct coupling of organolithium compounds with no additional solvents. *Nat. Commun.* **2016**, *7*, 11698.
- [64] Z. Jia, Q. Liu, X.-S. Peng, H. N. C. Wong, Iron-catalysed cross-coupling of organolithium compounds with organic halides. *Nat. Commun.* **2016**, *7*, 10614.
- [65] M. Veguillas, J. Rojas-Martín, M. Ribagorda, M. C. Carreño, Synthesis of functionalized alkyl substituted benzoquinones by Rh-catalyzed additions of boronic acids. *Org. Biomol. Chem.* **2017**, *15*, 5386–5394.
- [66] Exemples sélectionnés: a) D. N. Kursanov, Z. N. Parnes, N. M. Loim, Applications of Ionic Hydrogenation to Organic Synthesis. *Synthesis*, **1974**, *9*, 633-651; b) M. L. Yao, A. B. Pippin, G. W. Kabalka, Deoxygenation of benzylic alcohols using chloroboranes. *Tetrahedron Lett.* **2010**, *51*, 853-855; c) S. Chandrasekar, I. Karthikeyan, G. Sekar, An efficient and metal free synthesis of benzylpyridines using HI through the deoxygenation reaction. *RSC Adv.* **2015**, *5*, 58790–58797.
- [67] B. Zhu, H. Han, W.-K. Su, C. Yu, X. Jiang, Free-radical Initialized Cyclization of 2-(3-Arylpropioloyl)benzaldehydes with Toluene Derivatives: Access to Benzylated 1,4-Naphthoquinones via Copper-Catalyzed Cascade Reaction. *Adv. Synth. Catal.* **2021**, *363*, 484 – 489.
- [68] a) S. Langle, M. Abarbri, A. Duchêne, Selective double Suzuki cross-coupling reactions. Synthesis of unsymmetrical diaryl (or heteroaryl) methanes. *Tetrahedron Lett.* **2003**, *44*, 9255-9258; b) L. Chahen, H. Doucet, M. Santelli, Suzuki Cross-Coupling Reaction of Benzylic Halides with Arylboronic Acids in the Presence of a Tetraphosphine/Palladium Catalyst. *Synlett*, **2003**, *11*, 1668–1672; c) S. M. Nobre, A. L. Monteiro, Synthesis of diarylmethane derivatives from Pd-catalyzed cross-coupling reactions of benzylic halides with arylboronic acids. *Tetrahedron Lett.* **2004**, *45*, 8225–8228.
- [69] R. Kuwano, M. Yokogi, Cross-coupling of benzylic acetates with arylboronic acids: one-pot transformation of benzylic alcohols to diarylmethanes. *Chem. Commun.* **2005**, 5899–5901.
- [70] R. Kuwano, M. Yokogi, Suzuki–Miyaura Cross-Coupling of Benzylic Carbonates with Arylboronic Acids. *Org. Lett.* **2005**, *7*, 945-947.
- [71] M. McLaughlin, Suzuki–Miyaura Cross-Coupling of Benzylic Phosphates with Arylboronic Acids. *Org. Lett.* **2005**, *7*, 4875-4878.
- [72] Y.-Y. Ku, R. R. Patel, D. P. Sawick, A general, convenient and highly efficient synthesis of diarylmethanes by copper-catalyzed reaction. *Tetrahedron Lett.* **1996**, *37*, 1949-1952.

- [73] C. C. Kofink, P. Knochel, Synthesis of Functionalized Diarylmethanes via a Copper-Catalyzed Cross-Coupling of Arylmagnesium Reagents with Benzylic Phosphates. *Org. Lett.* **2006**, *8*, 4121–4124.
- [74] a) M. Amatorea, C. Gosmini, Synthesis of functionalised diarylmethanes via a cobalt-catalysed cross-coupling of arylzinc species with benzyl chlorides. *Chem. Commun.* **2008**, 5019–5021; b) R. B. Bedford, M. Huwea, M. C. Wilkinson, Iron-catalysed Negishi coupling of benzylhalides and phosphates. *Chem. Commun.* **2009**, 600–602.
- [75] a) T. Z. Nichele, A. L. Monteiro, Synthesis of diarylmethane derivatives from Stille cross-coupling reactions of benzylic halides. *Tetrahedron Lett.* **2007**, *48*, 7472–7475; b) M. Ohsumi, R. Kuwano, Palladium-catalyzed Cross-coupling of Benzylic Carbonates with Organostannanes. *Chem. Lett.* **2008**, *37*, 796–797.
- [76] N. Henry, C. Enguehard-Gueiffier, I. Thery, A. Gueiffier, One-Pot Dual Substitutions of Bromobenzyl Chloride, 2-Chloromethyl-6-halogenoimidazo[1,2-*a*]pyridine and -[1,2-*b*]pyridazine by Suzuki–Miyaura Cross-Coupling Reactions. *Eur. J. Org. Chem.* **2008**, 4824–4827.
- [77] B. H. Lipshutz, S.-K. Kim, P. Mollard, K. L. Stevens, An expeditious route to CoQ_n, vitamins K₁ and K₂, and related allylated *para*-quinones utilizing Ni(0) catalysis. *Tetrahedron*, **1998**, *54*, 1241–1253.
- [78] G. Rotthier, D. Cappoen, Q. T. Nguyen, T. A. Dang Thi, V. Mathys, V. T. Nguyen, K. Huygen, L. Maes, P. Cosb, K. A. Tehrani, Synthesis and anti-tubercular activity of N₂-arylbenzo[*g*]isoquinoline-5,10-dione-3-iminium bromides. *Org. Biomol. Chem.* **2016**, *14*, 2041–2051.
- [79] M. Schlosser, F. Cottet, Silyl-Mediated Halogen/Halogen Displacement in Pyridines and Other Heterocycles. *Eur. J. Org. Chem.* **2002**, 4181–4184.
- [80] J. Šturala, S. Boháčová, J. Chudoba, R. Metelková, R. Cibulka, Electron-Deficient Heteroarenium Salts: An Organocatalytic Tool for Activation of Hydrogen Peroxide in Oxidations. *J. Org. Chem.* **2015**, *80*, 2676–2699.
- [81] P. S. Fier, J. F. Hartwig, Synthesis and Late-Stage Functionalization of Complex Molecules through C–H Fluorination and Nucleophilic Aromatic Substitution. *J. Am. Chem. Soc.* **2014**, *136*, 10139–10147.
- [82] J. A. Bull, R. A. Croft, O. A. Davis, R. Doran, K. F. Morgan, Oxetanes: Recent Advances in Synthesis, Reactivity, and Medicinal Chemistry. *Chem. Rev.* **2016**, *116*, 12150–12233.
- [83] S. RaeppeI, F. RaeppeI, J. Suffert, Novel Exploration of the SNAr Reaction. *Synlett*, **1998**, *7*, 794–796.
- [84] R. Das, M. Kapur, Palladium-Catalyzed, *ortho*-Selective C–H Halogenation of Benzyl Nitriles, Aryl Weinreb Amides, and Anilides. *J. Org. Chem.* **2017**, *82*, 1114–1126.
- [85] P. A. Champagne, J. Pomarole, M. Thérien, Y. Benhassine, S. Beaulieu, C. Y. Legault, J. Paquin, Enabling Nucleophilic Substitution Reactions of Activated Alkyl Fluorides through Hydrogen Bonding. *Org. Lett.* **2013**, *15*, 2210–2213.

- [86] A. L. Gill, M. Frederickson, A. Cleasby, S. J. Woodhead, M. G. Carr, A. J. Woodhead, M. T. Walker, M. S. Congreve, L. A. Devine, D. Tisi, M. O'Reilly, L. C. A. Seavers, D. J. Davis, J. Curry, R. Anthony, A. Padova, C. W. Murray, R. A. E. Carr, H. Jhoti, Identification of Novel p38 α MAP Kinase Inhibitors Using Fragment-Based Lead Generation. *J. Med. Chem.* **2005**, *48*, 414-426.
- [87] L. Feng, K. Lv, M. Liu, S. Wang, J. Zhao, X. You, S. Li, J. Cao, H. Guo, Synthesis and *in vitro* antibacterial activity of gemifloxacin derivatives containing a substituted benzylxime moiety. *Eur. J. Med. Chem.* **2012**, *55*, 125-136.
- [88] Y. Miura, T. Issiki, Y. Ushitani, Y. Teki, K. Itoh, Synthesis and magnetic behaviour of polyyradical: poly(1,3-phenyleneethynylene) with π -toporegulated pendant stable aminoxy and imine N-oxide–aminoxy radicals. *J. Mater. Chem.* **1996**, *6*, 1745-1750.
- [89] D. F. J. Caputo, C. Arroniz, A. B. Durr, J. J. Mousseau, A. F. Stepan, S. J. Mansfield, E. A. Anderson, Synthesis and applications of highly functionalized 1-halo-3-substituted bicyclo[1.1.1]pentanes. *Chem. Sci.* **2018**, *9*, 5295-5300.
- [90] J. Su, Y. Zhang, M. Chen, W. Li, X. Qin, Y. Xie, L. Qin, S. Huang, M. Zhang, A Copper Halide Promoted Regioselective Halogenation of Coumarins Using *N*-Halosuccinimide as Halide Source. *Synlett.* **2019**, *30*, 630-634.
- [91] Z. She, Y. Shi, Y. Huang, Y. Cheng, F. Song, J. You. Versatile palladium-catalyzed C–H olefination of (hetero)arenes at room temperature. *ChemComm*, **2014**, *50*, 13914-13916.
- [92] A. Bunge, H.-J. Hamann, E. McCalmont, J. Liebscher, Enantioselective epoxidation of 2-substituted 1,4-naphthoquinones using *gem*-dihydroperoxides. *Tetrahedron Lett.* **2009**, *50*, 4629–4632.
- [93] M. L. Bolognesi, F. Lizzi, R. Perozzo, R. Brun, A. Cavalli, Synthesis of a small library of 2-phenoxy-1,4-naphthoquinone and 2-phenoxy-1,4-anthraquinone derivatives bearing anti-trypanosomal and anti-leishmanial activity. *Bioorg. Med. Chem. Lett.* **2008**, *18*, 2272–2276.
- [94] R. B. Smith, C. Canton, N. S. Lawrence, C. Livingstone, J. Davis, Molecular anchors—mimicking metabolic processes in thiol analysis. *New. J. Chem.* **2006**, *30*, 1718-1724.
- [95] K. Rajendra Prasad, K. Suresh Babu, R. Ranga Rao, G. Suresh, K. Rekha, J. Madhusudana Murthy, P. Usha Rani, J. Madhusudana Rao, Synthesis and insect antifeedant activity of plumbagin derivatives. *Med. Chem. Res.* **2012**, *21*, 578–583.

Résumé

Le paludisme est une maladie parasitaire tropicale touchant particulièrement les jeunes enfants en Afrique subsaharienne. La résistance aux médicaments antipaludiques s'est développée dans le monde entier depuis près de 50 ans et le besoin de nouveaux composés actifs est urgent. La plasmodione, appartenant à la série des 3-benzylménadiones, est un candidat médicament efficace agissant en interférant avec l'équilibre rédox du parasite. Cependant ses propriétés physico-chimiques sont incompatibles avec un traitement antipaludique efficace par voie orale et son mécanisme d'action est encore mal connu. Durant cette thèse nous avons développé diverses méthodes de synthèse, i) des métabolites postulés : les 3-benzoylménadiones, et ii) des analogues variés de la plasmodione. Les 3-benzoylménadiones ont été obtenues par un nouveau variant de la réaction de Friedel-Crafts clé. Cette réaction a permis également de synthétiser des sondes chimiques (pro-)ABPP pour identifier les sites d'interactions de ces métabolites avec des enzymes. Une nouvelle voie alternative de synthèse photorédox vers la série 3-benzylménadione a également été développée, permettant d'une part d'obtenir en une seule étape une plus grande variété de ces dérivés fonctionnalisés, mais aussi, grâce son mécanisme original impliquant des cascades rédox, de mieux comprendre la photoreactivité des naphtoquinones. Enfin, des analogues hétéroaromatiques de la plasmodione, avec une solubilité potentielle améliorée, ont été obtenus grâce à un couplage de Suzuki-Miyaura.

Mots-clés : médicament antipaludique, 1,4-naphtoquinone, Friedel-Crafts, (photo)rédox

Abstract

Malaria is a tropical parasitic disease that particularly affects young children in sub-Saharan Africa. Resistance to antimalarial drugs has been developing worldwide for nearly 50 years and there is an urgent need for new active compounds. Plasmodione, belonging to the 3-benzylmenadione series, is an effective drug candidate acting by interfering with the redox equilibrium of the parasite. However, its physicochemical properties are incompatible with an effective antimalarial treatment *per os* and its mechanism of action is still poorly understood. During this thesis we have developed various synthetic methods to synthesize i) the postulated metabolites: the 3-benzoylmenadiones, and ii) diverse analogues of plasmodione. The 3-benzoylmenadiones were obtained by a new variant of the key Friedel-Crafts reaction. This reaction also allowed the synthesis of (pro-)ABPP chemical probes to identify the sites of interaction of these metabolites with enzymes. A new alternative photoredox synthesis route to the 3-benzylmenadione series was also developed, allowing on the one hand to obtain in a single step a greater variety of these functionalized derivatives, but also, thanks to its original mechanism involving redox cascades, to better understand the photoreactivity of naphthoquinones. Finally, heteroaromatic analogues of plasmodione, with improved potential solubility, were obtained through a Suzuki-Miyaura coupling.

Keywords: antimalarial drug, 1,4-naphthoquinone, Friedel-Crafts, (photo)redox